frontiers | Research Topics

Natural compounds in veterinary therapeutics

Edited by
Baocheng Hao, Dongan Cui and Shuaiyu Wang

Published in
Frontiers in Veterinary Science

ISSN 1664-8714
ISBN 978-2-8325-7447-8
DOI 10.3389/978-2-8325-7447-8

Generative AI statement
Any alternative text (Alt text) provided alongside figures in the articles in this ebook has been generated by Frontiers with the support of artificial intelligence and reasonable efforts have been made to ensure accuracy, including review by the authors wherever possible. If you identify any issues, please contact us.

About Frontiers

Frontiers is more than just an open access publisher of scholarly articles: it is a pioneering approach to the world of academia, radically improving the way scholarly research is managed. The grand vision of Frontiers is a world where all people have an equal opportunity to seek, share and generate knowledge. Frontiers provides immediate and permanent online open access to all its publications, but this alone is not enough to realize our grand goals.

Frontiers journal series

The Frontiers journal series is a multi-tier and interdisciplinary set of open-access, online journals, promising a paradigm shift from the current review, selection and dissemination processes in academic publishing. All Frontiers journals are driven by researchers for researchers; therefore, they constitute a service to the scholarly community. At the same time, the *Frontiers journal series* operates on a revolutionary invention, the tiered publishing system, initially addressing specific communities of scholars, and gradually climbing up to broader public understanding, thus serving the interests of the lay society, too.

Dedication to quality

Each Frontiers article is a landmark of the highest quality, thanks to genuinely collaborative interactions between authors and review editors, who include some of the world's best academicians. Research must be certified by peers before entering a stream of knowledge that may eventually reach the public - and shape society; therefore, Frontiers only applies the most rigorous and unbiased reviews. Frontiers revolutionizes research publishing by freely delivering the most outstanding research, evaluated with no bias from both the academic and social point of view. By applying the most advanced information technologies, Frontiers is catapulting scholarly publishing into a new generation.

What are Frontiers Research Topics?

Frontiers Research Topics are very popular trademarks of the *Frontiers journals series*: they are collections of at least ten articles, all centered on a particular subject. With their unique mix of varied contributions from Original Research to Review Articles, Frontiers Research Topics unify the most influential researchers, the latest key findings and historical advances in a hot research area.

Find out more on how to host your own Frontiers Research Topic or contribute to one as an author by contacting the Frontiers editorial office: frontiersin.org/about/contact

Natural compounds in veterinary therapeutics

Topic editors

Baocheng Hao — Lanzhou Institute of Husbandry and Pharmaceutical Sciences, Chinese Academy of Agricultural Sciences, China

Dongan Cui — Lanzhou University, China

Shuaiyu Wang — China Agricultural University, China

Citation

Hao, B., Cui, D., Wang, S., eds. (2026). *Natural compounds in veterinary therapeutics*. Lausanne: Frontiers Media SA. doi: 10.3389/978-2-8325-7447-8

Table of contents

frontiers | Frontiers in Veterinary Science

TYPE Editorial
PUBLISHED 19 January 2026
DOI 10.3389/fvets.2026.1775123

OPEN ACCESS

EDITED AND REVIEWED BY
Arturo Anadón,
Complutense University of Madrid, Spain

*CORRESPONDENCE
Baocheng Hao
✉ haobaocheng@caas.cn

RECEIVED 25 December 2025
ACCEPTED 02 January 2026
PUBLISHED 19 January 2026

CITATION
Hao B, Cui D and Wang S (2026) Editorial: Natural compounds in veterinary therapeutics. *Front. Vet. Sci.* 13:1775123. doi: 10.3389/fvets.2026.1775123

Editorial: Natural compounds in veterinary therapeutics

Baocheng Hao[1,2,3]*, Dongan Cui[4] and Shuaiyu Wang[5]

[1]Key Laboratory of New Animal Drug Project of Gansu Province, Lanzhou, China, [2]Key Laboratory of Veterinary Pharmaceutical Development, Ministry of Agriculture and Rural Affairs, Lanzhou, China, [3]Lanzhou Institute of Husbandry and Pharmaceutical Sciences of Chinese Academy of Agriculture Sciences, Lanzhou, China, [4]College of Veterinary Medicine, Lanzhou University, Lanzhou, China, [5]College of Veterinary Medicine, China Agricultural University, Beijing, China

KEYWORDS

immunomodulation, intestinal health, natural compounds, pharmacologic mechanism, safety evaluations, veterinary therapeutics

Editorial on the Research Topic
Natural compounds in veterinary therapeutics

Natural compounds represent a vital source for the discovery of novel drugs (1). Amidst the shift of animal husbandry from traditional practices to large-scale intensive farming, the emergence of increased antibiotic resistance, novel diseases, and mixed infections has intensified the challenges faced by drug prophylaxis and treatment (2). In this context, the screening and discovery of new natural products with therapeutic potential, and the elucidation of their mechanisms of action, have become crucial strategies to address these challenges. A systematic review of the 14 research articles in this Research Topic clearly demonstrates the innovations of natural products in various dimensions, including animal bacterial diseases, viral diseases, intestinal health, immunomodulation, and safety evaluations, offering new solutions for disease prevention and treatment in modern animal husbandry.

In the field of animal disease prevention and treatment, natural products have exhibited remarkable antibacterial and anti-inflammatory activities. Extracts from *Eucalyptus globulus* Leaf, asiatic acid, and ursolic acid have shown significant antibacterial and anti-biofilm activity against mastitis isolates in dairy cows, particularly inhibitory effects on drug-resistant strains, providing alternative solutions to the problem of antibiotic resistance (Mezzasalma et al.). Linalool has been found to disrupt *E. coli* biofilms by dual inhibition of motility and adhesion, pointing the way for the development of anti-biofilm drugs with multi-target mechanisms. Extracts from *Pulsatilla chinensis* have effectively alleviated *Staphylococcus aureus*-induced mastitis in mice by regulating inflammatory responses and the intestinal microbiota, offering a new approach for the prevention and treatment of dairy cow mastitis (Xiang et al.).

Natural products have also shown impressive performance in antiviral and immune regulation. *Scutellaria baicalensis Georgi* extract against has demonstrated antiviral activity against Getah virus both in *vitro* and in *vivo* (Liu B. et al.); Normal butanol fraction of *Polygonum hydropiper* L. flavonoids has reduced inflammation caused by PCV2 infection in cell cultures and mouse models, providing new candidate drugs for the prevention and treatment of viral diseases (Wei et al.). *Glycyrrhiza* Polysaccharides have shown therapeutic potential against pseudorabies virus infection through immunomodulation, antioxidant activity, and restoration of the intestinal microbiota, reflecting the multifaceted and multi-pathway characteristics of natural products (Song et al.). The extract of

Gynostemma Pentaphyllum has enhanced mucosal immunity against porcine epidemic diarrhea virus, offering a new strategy for the immunoprophylaxis of intestinal virus infections.

Intestinal health is a fundamental aspect of animal health, and research into natural products in this domain is deepening. The Zengye granules have shown a good laxative effect by regulating the SCF/c-Kit pathway and the intestinal microbiota in constipated mice, providing a new option for the treatment of functional constipation (Lv et al.). The study on the gastrointestinal microbiota and serum metabolomics of subclinical mastitis in dairy cows treated with *Astragali Radix* water decoction has revealed the scientific basis for the therapeutic effects of traditional Chinese medicine through the regulation of the intestinal microecology and metabolic networks (Yan et al.).

The safety evaluation of natural products is a critical step before their application. The extract of *Stevia rebaudiana* extract has been confirmed as safe after acute, sub-chronic, genetic, and teratogenicity evaluations, providing a scientific basis for the development of feed additives (Li et al.).

Important progress has also been made in the field of antitumor research. Pseudolaric acid B induces G2/M phase arrest in canine mammary tumor cells by targeting CDK1, offering not only a new strategy for the treatment of canine mammary tumors but also a reference for human breast cancer research (Chen et al.). This study highlights the value of natural products in the era of precision medicine. Moreover, natural products have a unique advantage in the prevention and control of mycotoxin contamination. Research progress on the prevention and treatment of animal Zearalenone poisoning by natural products has provided green solutions to the issue of feed mycotoxin contamination, which is of significant importance for ensuring animal health and food safety ((Liu N. et al).

As research deepens and technology advances, natural products are certain to play an even more critical role in safeguarding animal health, promoting sustainable development in animal husbandry, and ensuring food safety (3). The guest editorial team extends its gratitude to all the reviewers for their diligent efforts in upholding the pursuit of science, advancing its frontiers, and spreading scientific knowledge. The team will continue to adhere to a scientific, rigorous, and pragmatic academic attitude, actively contributing to global scientific and technological progress.

Author contributions

BH: Writing – original draft, Writing – review & editing. DC: Writing – original draft. SW: Writing – original draft.

Conflict of interest

The author(s) declared that this work was conducted in the absence of any commercial or financial relationships that could be construed as a potential conflict of interest.

Generative AI statement

The author(s) declared that generative AI was not used in the creation of this manuscript.

Any alternative text (alt text) provided alongside figures in this article has been generated by Frontiers with the support of artificial intelligence and reasonable efforts have been made to ensure accuracy, including review by the authors wherever possible. If you identify any issues, please contact us.

Publisher's note

References

1. Vaou N, Voidarou C, Rozos G, Saldari C, Stavropoulou E, Vrioni G, et al. Unraveling nature's pharmacy: transforming medicinal plants into modern therapeutic agents. *Pharmaceutics*. (2025) 17:754. doi: 10.3390/pharmaceutics17060754

2. Zhang TF, Nickerson R, Zhang WT, Peng XT, Shang Y, Zhou YX, et al. The impacts of animal agriculture on One Health—Bacterial zoonosis, antimicrobial resistance, and beyond. *One Health*. (2024) 18:100748. doi: 10.1016/j.onehlt.2024.100748

3. He JT, Fan ZQ, Jiang Q, Yang XS, Sun JM, Pang Y, et al. Sustainable natural bio-antimicrobial: composition, bacteriostatic activity, and antibacterial strategy of *Cinnamomum camphora* essential oil. *Ind Crop Prod*. (2025) 233:121493. doi: 10.1016/j.indcrop.2025.121493

frontiers | Frontiers in Veterinary Science

TYPE Original Research
PUBLISHED 04 February 2025
DOI 10.3389/fvets.2025.1539448

OPEN ACCESS

EDITED BY
Shuaiyu Wang,
China Agricultural University, China

REVIEWED BY
Ben Dong Fu,
Jilin University, China
Yi Wu,
Yunnan Agricultural University, China

*CORRESPONDENCE
Ting-jun Hu
✉ tingjunhu@126.com

RECEIVED 04 December 2024
ACCEPTED 13 January 2025
PUBLISHED 04 February 2025

CITATION
Wei Y-h, Zhou S-m, Zhao W, Chen Q, Wang Q-h, Yu M-l, Wei Y-y and Hu T-j (2025) Normal butanol fraction of *Polygonum hydropiper* L. flavonoids reduces inflammation caused by PCV2 infections in cell and mouse models. *Front. Vet. Sci.* 12:1539448. doi: 10.3389/fvets.2025.1539448

Normal butanol fraction of *Polygonum hydropiper* L. flavonoids reduces inflammation caused by PCV2 infections in cell and mouse models

Yu-heng Wei[1], Shu-mian Zhou[1,2,3], Wen Zhao[1], Qi Chen[1], Qiu-hua Wang[1,3], Mei-ling Yu[1], Ying-yi Wei[1] and Ting-jun Hu[1,2,3]*

[1]College of Animal Science and Technology, Guangxi University, Nanning, China, [2]Guangxi Zhuang Autonomous Region Engineering Research Center of Veterinary Biologics, Nanning, China, [3]Guangxi Key Laboratory of Animal Breeding, Disease Control and Prevention, Nanning, China

Introduction: The normal butanol fraction of *Polygonum hydropiper* L. flavonoids (FNB) exhibits significant anti-inflammatory effects. This study investigated FNB's impact on inflammatory responses induced by Porcine circovirus type 2 (PCV2) in cell and mouse models.

Methods: An inflammatory model was established in RAW264.7 cells infected with varying PCV2 concentrations. And assigning both RAW264.7 cells and 108 SPF-grade KM mice to Control, PCV2, Rutin, and various dosages of FNB groups. Inflammatory factors such as Monocyte Chemoattractant Protein-1 (MCP-1), interleukin-6 (IL-6), IL-8, IL-10, Tumor Necrosis Factor-alpha (TNF-α), Reactive Oxygen Species (ROS), and Nitric Oxide (NO) were quantified using ELISA, RT-qPCR and immunohistochemistry.

Results: Results showed that a PCV2 titer of $10^{4.5}$ $TCID_{50}$/0.1 mL when applied to RAW264.7 cells effectively established an *in vitro* inflammatory model at 12 and 24 h post-infection. Following PCV2 infection, all the inflammatory factors displayed a significant increased both in culture supernatant and intracellular mRNA expression levels ($p < 0.05$ or $p < 0.01$), but these levels were reduced by FNB treatment ($p < 0.05$ or $p < 0.01$). In mouse sera post-PCV2 infection also showed elevated levels of IL-6, IL-8 IL-10, TNF-α, and MCP-1 ($p < 0.05$ or $p < 0.01$). Additionally, mRNA and protein levels for TNF-α, IL-8, IL-10, IL-6, and iNOS rose significantly in lung tissues ($p < 0.01$) but decreased with FNB treatment ($p < 0.05$ or $p < 0.01$).

Discussion: These findings suggest that FNB reduces inflammatory factor production and modulates the inflammatory response triggered by PCV2 infection, potentially enhancing host resistance against it.

KEYWORDS

porcine circovirus type 2, normal butanol fraction of *Polygonum hydropiper* L. flavonoids, inflammatory response, RAW264.7 cells, model establishment

1 Introduction

Porcine circovirus type 2 (PCV2) infections inflict marked economic damage to the pig production industry (1). It can cause immunosuppression in pigs and is associated with various inflammatory and immune-related diseases (2). Studies reported that PCV2 infection can induce the upregulation of the interleukins (ILs) IL-1β, IL-6, and IL-8. This upregulation may result in excessive inflammatory responses during initial infection stages and attract neutrophils, leading to immunosuppression. Therefore, this affects the

normal functioning of the immune response and facilitates the development of PCV2-related diseases (3). Therefore, controlling PCV2 infection and reducing the inflammatory responses it causes is critical to preventing and controlling PCV2-related diseases.

Flavonoids of *Polygonum hydropiper* L. are a class of natural active components extracted from the Polygonaceae plant *Polygonum hydropiper* L., which possess various pharmacological effects, including significant anti-inflammatory activity (4). Studies have reported that *Polygonum hydropiper* L. flavonoids have substantial anti-inflammatory effects by blocking the production of reactive oxygen species (ROS) and nitric oxide (NO) and upregulating the anti-inflammatory IL-10 while preventing the release of IL-1β, IL-6, IL-8, Tumor Necrosis Factor-alpha (TNF-α), and pro-inflammatory factors caused by LPS exposure in Mouse Mononuclear Macrophages Cells (RAW264.7 cells) (5). The RAW264.7 cell inflammation model is a major tool for studying inflammatory responses and evaluating the effectiveness of anti-inflammatory drugs (6). This model allows researchers to investigate the effects of various substances on inflammatory mediators, offering a theoretical foundation and prospective therapeutic techniques for treating inflammation-related disorders (7).

However, there have been no known cases of developing an inflammatory model of PCV2 infection in RAW264.7 cells to date. Furthermore, there is insufficient information about the modulation of PCV2-induced inflammatory responses by the normal butanol fraction of *Polygonum hydropiper* L. flavonoids (FNB). The current study evaluated the effect of FNB intervention on inflammatory responses induced by PCV2 infection in both cellular and animal models. Moreover, this study established a scientific foundation for preventing and treating animal viral infections through plant flavonoids.

2 Materials and methods

2.1 Reagents

Phosphate-buffered saline (PBS), fetal bovine serum (FBS), and high-glucose DMEM were obtained from Gibco (USA). TRIzol was from Takara Bio (Japan). The commercial ELISA kits were from NeoBioscience Technology Co., Ltd. (China) to analyze IL-10, IL-8, IL-6, Monocyte Chemoattractant Protein-1 (MCP-1), and TNF-α. The ROS Assay Kit was acquired from Applygen (China). The Chinese company Nanjing Jiancheng Bioengineering Institute provided the Nitric Oxide Assay Kit. The HiScript III RT SuperMix for qPCR (+gDNA wiper) and ChamQ Universal SYBR qPCR Master Mix were bought from Vazyme (China). The IL-10, IL-8, IL-6, TNF-α, and iNOS antibodies were acquired from Proteintech (China). The streptavidin-peroxidase (SP) immunohistochemistry (IHC) kit was purchased from Bioss (China).

2.2 FNB preparation

The *Polygonum hydropiper* L. was supplied by Tai Hua Pharmaceutical Co. Ltd. Professor Renbin Huang of Guangxi Medical University's School of Pharmacy verified the authenticity of the plant material. Tao et al.'s technique comprised the extraction and purification of the FNB in accordance with the specified protocol (5). According to the HPLC study, FNB had a total flavonoid concentration of 55.3%. Its rutin, quercetin glycoside, and quercetin concentrations were 21.9%, 8.2%, and 20.6%, respectively (5). The solution was prepared in complete DMEM, filtered using a 0.22 μm mesh, and stored at 4°C for later application.

TABLE 1 Grouping and treatment of the model establishment experiment.

Groups	Treatment	Collection
Control group	DMEM treated for 2 h	Samples were collected at 4, 8, 12, 24, and 48 h after infection
10^0 PCV2 group	10^0 PCV2 dilutions treated for 2 h	
10^{-1} PCV2 group	10^{-1} PCV2 dilutions treated for 2 h	
10^{-2} PCV2 group	10^{-2} PCV2 dilutions treated for 2 h	
10^{-3} PCV2 group	10^{-3} PCV2 dilutions treated for 2 h	

2.3 Virus and cells

PCV2 was supplied by Nanjing Agricultural University (China). Using the Reed-Muench assay, PCV2 titers were found to be $10^{4.5}$ $TCID_{50}$/0.1 mL. RAW264.7 cells were procured from the Shanghai Institute of Biochemistry and Cell Biology at the Chinese Academy of Sciences. Cells were grown in DMEM with 10% heat-inactivated FBS in an incubator at 37°C with 5% CO_2.

2.4 Cell treatment

The grouping and treatment of the model establishment experiment are shown in Table 1, with four replicates per group. RAW264.7 cells (1×10^5 cells/well) were inoculated in 12-well plates. A total of 500 μL of PCV2 dilutions at varying concentrations (MOI 1, 0.1, 0.01, and 0.001) were added to the PCV2 infection groups. At the same time, an equal volume of serum-free DMEM culture media was administered to the Control group. Following a 2-h treatment, the cells were cultured in each well with 1 mL of cell maintenance medium (DMEM culture media containing 2% fetal bovine serum) following three PBS washes. Lastly, samples were collected at various intervals.

The grouping and treatment for the experiment on the intervention effect of FNB on inflammatory responses are shown in Table 2, with 4 replicates per group. RAW264.7 cells (1×10^5 cells/well) inoculated into 12-well plates. The PCV2, FNB (high-, medium-, and low-dosage), and Rutin groups were administered $10^{4.5}$ $TCID_{50}$ of the viral solution. In contrast, the Control group was supplemented with equivalent serum-free DMEM culture media. Following a 2-h treatment, the cells underwent three washes with PBS. In the Control and PCV2 groups, 1 mL of cell

TABLE 2 Grouping and treatment for the experiment on the intervention effect of FNB on inflammatory responses.

Groups	Viral treatment	Drug treatment	Collection
Control group	DMEM treated for 2 h	2% FBS-DMEM	Samples were acquired at 4, 8, 12 and 24 hpi
PCV2 group	$10^{4.5}$ $TCID_{50}$ PCV2 treated for 2 h	2% FBS-DMEM	
Rutin40 group	$10^{4.5}$ $TCID_{50}$ PCV2 treated for 2 h	40 μg/mL Rutin	
FNB20 group	$10^{4.5}$ $TCID_{50}$ PCV2 treated for 2 h	20 μg/mL FNB	
FNB40 group	$10^{4.5}$ $TCID_{50}$ PCV2 treated for 2 h	40 μg/mL FNB	
FNB80 group	$10^{4.5}$ $TCID_{50}$ PCV2 treated for 2 h	80 μg/mL FNB	

maintenance solution (DMEM with 2% FBS) was placed in each of the wells. The FNB and the Rutin groups were each supplemented with 1 mL of DMEM containing 80, 40, and 20 μg/mL of FNB and 40 μg/mL of Rutin, respectively, and then placed in an incubator for continued culture. Subsequently, the supernatant or cells were collected from the culture medium at 4, 8, 12, and 24 h for further experiments.

2.5 Mice treatment

The animal experiment referred to Chen's research (8). A total of 108 SPF-grade KM mice, each weighing 20 ± 2 g, comprising an equal distribution of males and females, were acquired from the Animal Experiment Center of Guangxi Medical University (China). Before the experiment, the mice were acclimatized in an environment maintained at 25°C and 65% humidity for 7 days to mitigate environmental stress. Table 3 indicates that the animals were randomly allocated to several groups, namely, Control, PCV2, Rutin (100 mg/kg·BW), and FNB (25, 50, 100, 200, and 400 mg/kg·BW) groups, as well as a highest dose FNB control group (not infected with the virus). Each group contained 12 mice. Mice received daily inoculations of 1 mL PCV2 *via* intraperitoneal injection (0.3 mL/mouse), nasal drops (0.2 mL), and gavage (0.5 mL/mouse) for 3 consecutive days. FNB was gavaged into the mice from day 4 to day 6. On day 7, the animals were euthanized via asphyxiation under the guidelines established by the Guangxi University Animal Ethics Committee. Blood and lung specimens were obtained for subsequent study.

2.6 Viability of cells

The influence of FNB on RAW264.7 cell viability was assessed using the CCK8 assay. Briefly, a 96-well plate containing a Control group and 7 varying concentrations of FNB groups (12.5, 25, 50, 100, 200, 400, and 800 μg/mL), each with eight repetitions, was inoculated with 5×10^4 cells/mL at 100 μL/well. After adding 100 μL of FNB to each well, the wells were cultured for 24 h in a culture incubator. The growth medium was then taken out 2 h before the culture's end, 100 μL of serum-free DMEM with 10% CCK-8 was placed in each of the wells, and the culture was maintained for 2 h at 37°C with 5% CO_2. Lastly, a microplate reader was used to detect the OD value at 450 nm, and the CCK8 kit's instructions were followed to determine the maximum safe concentration of FNB on RAW264.7 cells.

TABLE 3 Mice treatment.

Groups	1–3 (days) all 1 mL/mouse	4–6 (days)
Control group	Physiological saline (PS, 0.9% sodium chloride solution)	PS 0.02 mL/g·BW
FNB400 group	PS	FNB 400 mg/kg·BW
PCV2 group	PCV2	PS 0.02 mL/g·BW
PCV2 + Rutin100 group	PCV2	Rutin 100 mg/kg·BW
PCV2 + FNB25 group	PCV2	FNB 25 mg/kg·BW
PCV2 + FNB50 group	PCV2	FNB 50 mg/kg·BW
PCV2 + FNB100 group	PCV2	FNB 100 mg/kg·BW
PCV2 + FNB200 group	PCV2	FNB 200 mg/kg·BW
PCV2 + FNB400 group	PCV2	FNB 400 mg/kg·BW

Mice received inoculations of either PS or PCV2 through intraperitoneal injection (0.3 mL/mouse), intranasal drops (0.2 mL), and intragastric administration (0.5 mL/mouse) daily for 3 consecutive days. On Days 4, 5, and 6, they received intragastric administration of Rutin or FNB.

TABLE 4 List of primers.

Gene name	Sequence (5′ to 3′)	Product size (bp)
β-actin	F: TTCCTTCTTGGGTATGGAAT R: GAGCAATGATCTTGATCTTC	183
IL-6	F: TAGTCCTTCCTACCCCAATTTCC R: TTGGTCCTTAGCCACTCCTTC	76
IL-8	F: GGCTTTCCACATTTGAGGACG R: CGTGGCGGTATCTCTGTCTC	77
IL-10	F: TAACTGCACCCACTTCCCAG R: AAGGCTTGGCAACCCAAGTA	89
TNF-α	F: AGCACAGAAAGCATGATCCG R: CTGATGAGAGGGAGGCCATT	107
iNOS	F: CAAGCTGAACTTGAGCGAGGA R: TTTACTCAGTGCCAGAAGCTGGA	164
MCP-1	F: CCACTCACCTGCTGCTACTCAT R: TGGTGATCCTCTTGTAGCTCTCC	76

2.7 Inflammatory cytokines detection

Following the supplier's instructions, the supernatant or serum was collected for the measurement of MCP-1, IL-10, IL-8, TNF-α, IL-6, ROS, and NO levels while employing enzyme-linked immunosorbent assay (ELISA) and related commercial assay kits.

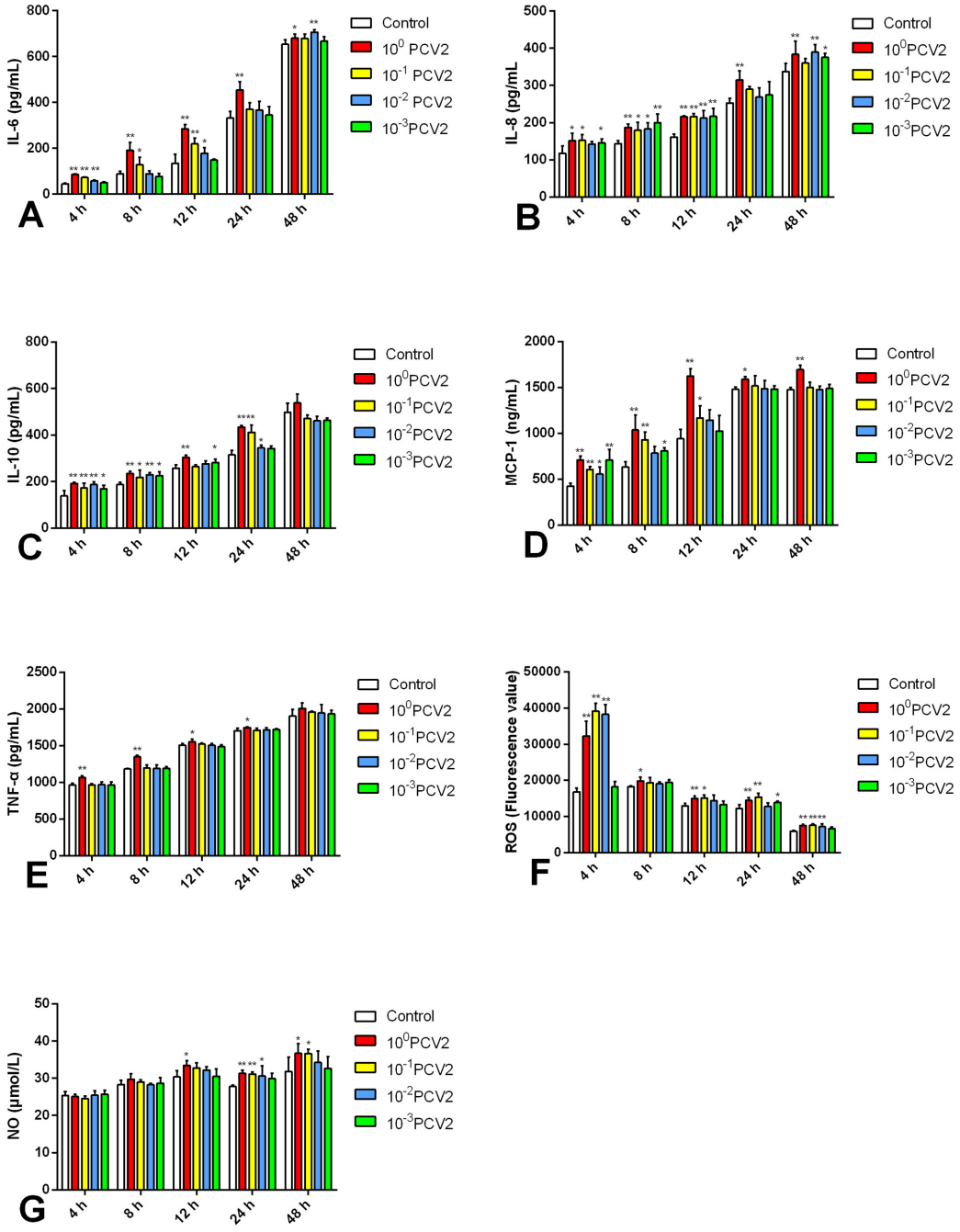

FIGURE 1
(A–G) Effects of PCV2 at different PCV2 dilutions on MCP-1, TNF-α, IL-6, IL-10, IL-8, ROS and NO level (mean ± SD, $n = 4$). $^{*}p < 0.05$, $^{**}p < 0.01$ vs. Control group.

2.8 Determination of inflammatory cytokine mRNA levels

As directed by the manufacturer, TRIzol was utilized for RNA extraction from cells and lungs. Reverse transcription was used for transcribing RNA into cDNA. Using the cDNA as the template, RT-qPCR amplification was performed through a SYRB super-mix solution and a CFX96^{TM}Real-Time PCR Detection solution (Bio-Rad, USA). Table 4 contains primer sequences for β-actin, MCP-1, TNF-α, IL-10, IL-8, IL-6, and iNOS. The relative mRNA levels, adjusted to β-actin, were determined through the comparative $2^{-\Delta\Delta ct}$ technique.

2.9 Immunohistochemistry

For the immunohistochemistry study, lung tissues preserved in 4% paraformaldehyde were embedded in paraffin wax and sliced into 3.5 μm thick pieces. The expression level of the relevant protein was then determined according to the IHC kits.

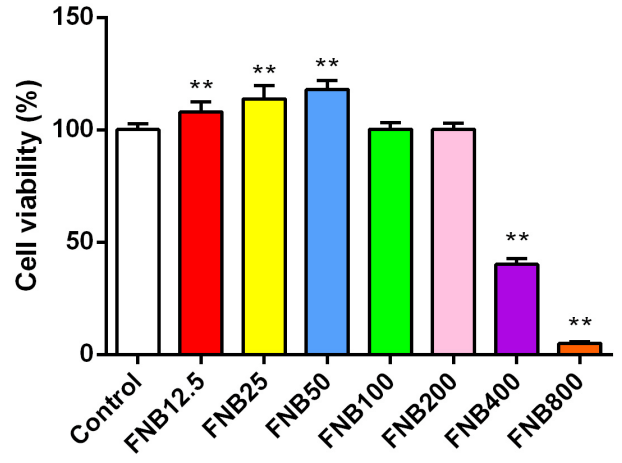

FIGURE 2
Effects of varying concentrations of FNB on RAW264.7 cell viability (mean ± SD, $n = 4$). $^{**}p < 0.01$ vs. Control group.

2.10 Statistical analysis

Data were analyzed with SPSS v.22.0, using the LSD test and one-way analysis of variance (ANOVA). Data are shown as mean ± standard deviation. $p < 0.05$ was considered statistically significant.

3 Results

3.1 Development of a PCV2-induced *in vitro* inflammation model in RAW264.7 cells

Using commercial assay kits, the concentrations of inflammatory cytokines were evaluated *in vitro* in RAW264.7 cells to develop an inflammatory model in RAW264 induced by PCV2 (Figure 1). At 12 and 24 h post-infection (hpi), all measured inflammatory cytokines showed a substantial increase ($p < 0.05$, $p < 0.01$) following infection with 10^0 PCV2 dilutions in comparison to the Control. This suggests that an *in vitro* inflammatory model can be established using 10^0 PCV2 dilutions to treat RAW264.7 cells when the PCV2 titer is $10^{4.5}$ $TCID_{50}$/0.1 mL. Therefore, we selected this condition to carry out subsequent experiments.

3.2 FNB reduces the inflammatory cytokines produced by RAW264.7 cells infected with PCV2

CCK-8 assays were utilized for measuring cell viability. At 24 h post-treatment (hpt), FNB at 12.5, 25, and 50 μg/mL elevated cell viability ($p < 0.01$; Figure 2) while FNB at 100 and 200 μg/mL had no substantial impact ($p > 0.05$). However, FNB at 400 and 800 μg/mL notably reduced viability ($p < 0.01$). Therefore, to examine their intervention effects on inflammatory responses induced by PCV2 infection, FNB concentrations of 20, 40, and 80 μg/mL were finally selected as high, medium, and low dosages, respectively.

Commercial assay kits were used to explore the intervention impacts of FNB on inflammatory cytokine levels in cells, including MCP-1, IL-8, IL-10, TNF-α, IL-6, ROS, and NO (Figure 3). The efficient development of an *in vitro* inflammatory model was demonstrated by the considerable up-regulation of all evaluated inflammatory factors induced by PCV2 infection relative to the Control ($p < 0.05$, $p < 0.01$).

At 4 or 8 hpt, the PCV2-induced increase in IL-6 and MCP-1 decreased considerably ($p < 0.01$) after exposure to 20, 40, and 80 μg/mL FNB. At 4 and 8 hpt, 40 μg/mL of FNB significantly reduced IL-10 and IL-8 levels ($p < 0.01$). TNF-α and NO levels were substantially lower than those of the PCV2 group after 8, 12, and 24 h following 20 μg/mL therapy ($p < 0.01$ or $p < 0.05$). At 4, 8, 12, and 24 h, ROS levels were significantly reduced ($p < 0.01$) by 20, 40, or 80 μg/mL FNB. An inflammatory response was triggered upon PCV2 infection, seen in raised inflammatory factor levels. Treatment with FNB significantly reduced cell TNF-α, MCP-1, IL-8, IL-6, IL-10, ROS, and NO levels, indicating that FNB could prevent inflammatory responses induced by PCV2.

3.3 FNB inhibits inflammatory cytokine mRNA levels in PCV2-infected RAW264.7 cells

Using RT-qPCR, the mRNA levels of the cytokines were further investigated. Following infection with PCV2, significant ($p < 0.01$) up-regulation of all six inflammatory factors was observed. Transcription was decreased by 40 and 80 μg/mL FNB administration, as evidenced by lower mRNA levels of MCP-1, IL-8, IL-10, IL-6, TNF-α, and iNOS at 12 hpt ($p < 0.05$, $p < 0.01$) than the PCV2 groups (Figure 4). These findings revealed that FNB could prevent PCV2 from activating genes and that PCV2 produced an inflammatory response by encouraging the expression of associated genes.

3.4 Mice infected with PCV2 had lower blood levels of inflammatory cytokines when FNB was administered

To evaluate the effects of FNB on inflammatory responses *in vivo*, we infected mice with PCV2 and treated them with FNB. The levels of IL-10, IL-6, TNF-α, MCP-1, and IL-8 in mouse sera were assessed by ELISAs. As shown in Figure 5, PCV2 infection significantly increased those inflammatory cytokines ($p < 0.05$ or $p < 0.01$). FNB administration at 100, 200, and 400 mg/kg·BW substantially decreased the increase in those inflammatory cytokines ($p < 0.05$ or $p < 0.01$).

3.5 FNB down-regulates inflammatory cytokine mrna levels in mouse lungs following PCV2 infection

We also investigated the intervention effects of FNB on PCV2 infection-induced inflammatory responses at the gene expression

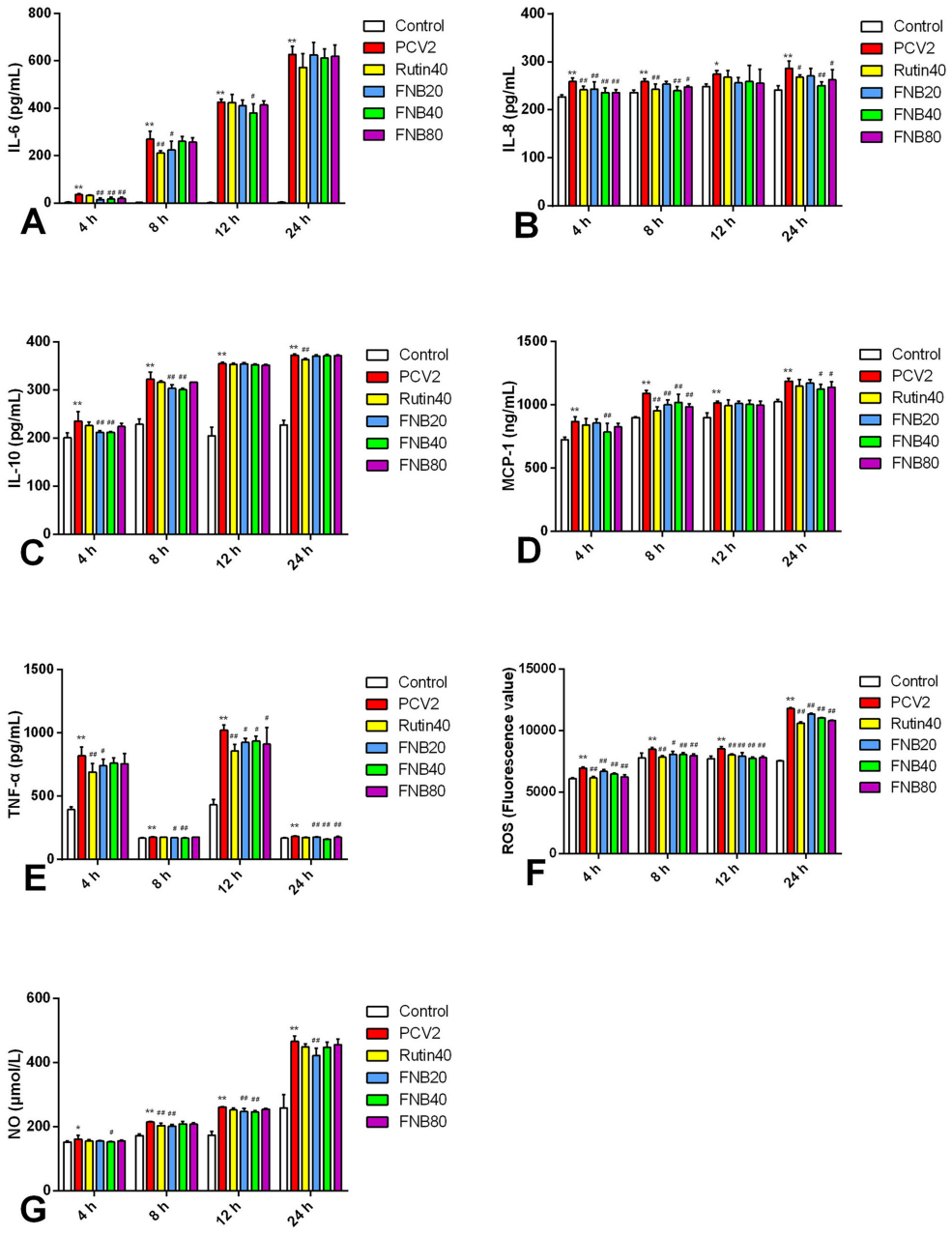

FIGURE 3
(A–G) The impact of FNB as an intervention on inflammatory cytokine levels (mean ± SD, $n = 4$). $^{*}p < 0.05$, $^{**}p < 0.01$ vs. Control group. $^{\#}p < 0.05$, $^{\#\#}p < 0.01$ vs. PCV2 group.

level. All inflammatory cytokines listed had significantly higher mRNA expression when infected with PCV2 ($p < 0.01$). Moreover, FNB was able to substantially down-regulate mRNA expression at doses of 25, 50, 100, 200, and 400 mg/kg·BW (Figure 6).

3.6 Impact of FNB on inflammatory cytokine protein expression in PCV2-infected mice lungs

Consistent with the earlier studies, we investigated the intervention effects of FNB on inflammatory responses produced by PCV2 infection using immunohistochemistry methods. The proteins IL-8, IL-10, TNF-α, IL-6, and iNOS were expressed in the lung tissues of both the PCV2 group and the Control group of mice, demonstrating a diffuse distribution in the lungs and localized expression in the cytoplasm of cells, alveolar spaces, blood vessels, and tiny bronchial epithelial cells (Figure 7A). Relative to the controls, the protein iNOS, IL-10, IL-8, TNF-α, and IL-6 expression levels in the lung tissue of PCV2-infected mice were substantially higher ($p < 0.01$). Administration of 25, 50, 100, 200, and 400 mg/kg·BW FNB markedly reduced the protein iNOS, IL-10, IL-8, TNF-α, and IL-6 expressions levels in the alveolar space, fine bronchi, and cell cytoplasm of mice ($p < 0.01$; Figure 7B).

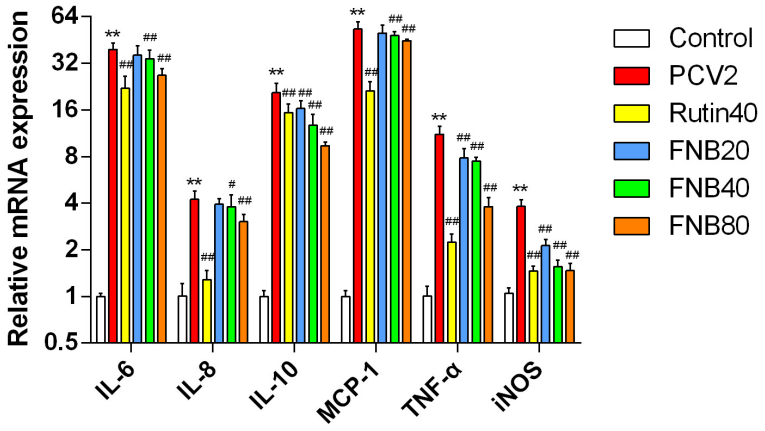

FIGURE 4
Impact of FNB on inflammatory cytokine mRNA expression levels (mean ± SD, $n = 4$). $^{**}p < 0.01$ vs. Control group. $^{\#}p < 0.05$, $^{\#\#}p < 0.01$ vs. PCV2 group.

4 Discussion

Interleukin-6 is a multifunctional cytokine essential for inflammatory responses and immunological control (9). In reports related to COVID-19, elevated levels of IL-6 are considered a predictive parameter for poor disease progression and the need for invasive oxygen support (10). IL-8 is a crucial inflammatory marker; as a chemokine, it attracts and activates neutrophils, regulates inflammatory responses, and participates in viral replication. It is reported that coronavirus porcine epidemic diarrhea virus utilizes IL-8 to facilitate viral replication by regulating Ca^{2+} flux (11). The levels of IL-8 are significantly elevated in various tumor tissues and patient serum, showing a clear correlation with patient prognosis and tumor staging (12). IL-10 is anti-inflammatory and promotes immune tolerance and regulates immune responses (13). However, in some cases, it may promote the survival of pathogens and the immune escape of tumors, and elevated IL-10 may be associated with the activity of viral infections (14). The CC chemokine family includes MCP-1, often referred to as Chemokine (CC motif) Ligand 2 (CCL2), which is essential for inflammatory reactions (15). It has been found that in COVID-19 patients, raised MCP-1 levels are associated with disease severity, and it can be used to monitor disease progression (16). One crucial pro-inflammatory cytokine necessary for apoptosis, inflammatory reactions, and immunological responses in several physiological processes is TNF-α (17). Inhibitors targeting TNF-α, such as infliximab, adalimumab, and etanercept, have been used clinically to treat multiple inflammatory diseases and have achieved significant therapeutic effects (18). ROS plays a complex and critical role in viral infections and inflammatory responses; excessive production of ROS can exacerbate inflammatory responses and enhance the replication ability of viruses (19). For example, the Porcine reproductive and respiratory syndrome virus utilizes ROS to enhance its replication (20). NO is also an important biological regulatory factor, and changes in NO levels can also serve as an inflammatory marker to determine whether an inflammatory response has occurred (21). NO levels can rise substantially in viral infections, particularly respiratory infections; in COVID-19 patients, for example, high NO levels are positively linked to disease severity (22). In this study, infection of RAW264.7 cells with PCV2 at a titer of $10^{4.5}$ $TCID_{50}$/0.1 mL for 12 and 24 h resulted in a significant increase of the levels of IL-6, IL-8, IL-10, MCP-1, TNF-α, ROS, and NO. Hence, the *in vitro* inflammatory model was established successfully.

On the other hand, studies have shown that flavonoid compounds possess significant antioxidant, anti-inflammatory, and antiviral properties. They delay the progression of viral infections by alleviating oxidative stress and inflammation by targeting pathways such as NF-κB, MAPK, ERK, and Akt (23). IFN-γ, IL-17, IL-8, IL-1β, IL-6, and TNF-α are inflammatory factors many flavonoids can decrease (24). Sargassum polysaccharide has been shown by Chen et al. to decrease TNF-α, IL-6, IL-1β, IL-8, IL-10, and MCP-1 and mRNA expression levels resulting from PCV2 infection in RAW264.7 cells (25). Chen et al. also showed that *Spatholobus suberectus Dunn*'s total flavonoids may decrease the elevated ROS and NO generation in RAW264.7 cells by PCV2 infection (26). According to a study by Ren et al., in Pseudorabies virus-infected RAW264.7 cells, the ethyl acetate fraction of flavonoids from *Polygonum hydropiper* L. can lower the levels of iNOS, NO, ROS, and other inflammatory markers (27). Ren et al. also found that the ethyl acetate flavonoid fraction from *Polygonum hydropiper* L. can inhibit increases in PCV2-induced TNF-α, IL-1β, IL-8, and NF-κB mRNA levels (28). Thus, our data are consistent with these studies, further showing the intervention impacts of FNB on PCV2-induced *in vitro* inflammatory responses.

According to Wang et al.'s *in vivo* studies, *Panax notoginseng saponins* can lower MPO and iNOS activity significantly while also lowering ROS and NO levels in the splenic lymphocytes of PCV2-infected mice (29). The total flavonoid extract from *Spatholobus suberectus Dunn* has been shown by Fu et al. to lower MPO and iNOS activity, improve thymus and spleen indices in PCV2-infected mice, alter immunological function, and lessen oxidative stress induced by viral infection (30). These findings thus support our previous research, demonstrating the impact of FNB as an intervention on PCV2-induced inflammatory reactions *in vivo*. However, the specific molecular mechanisms

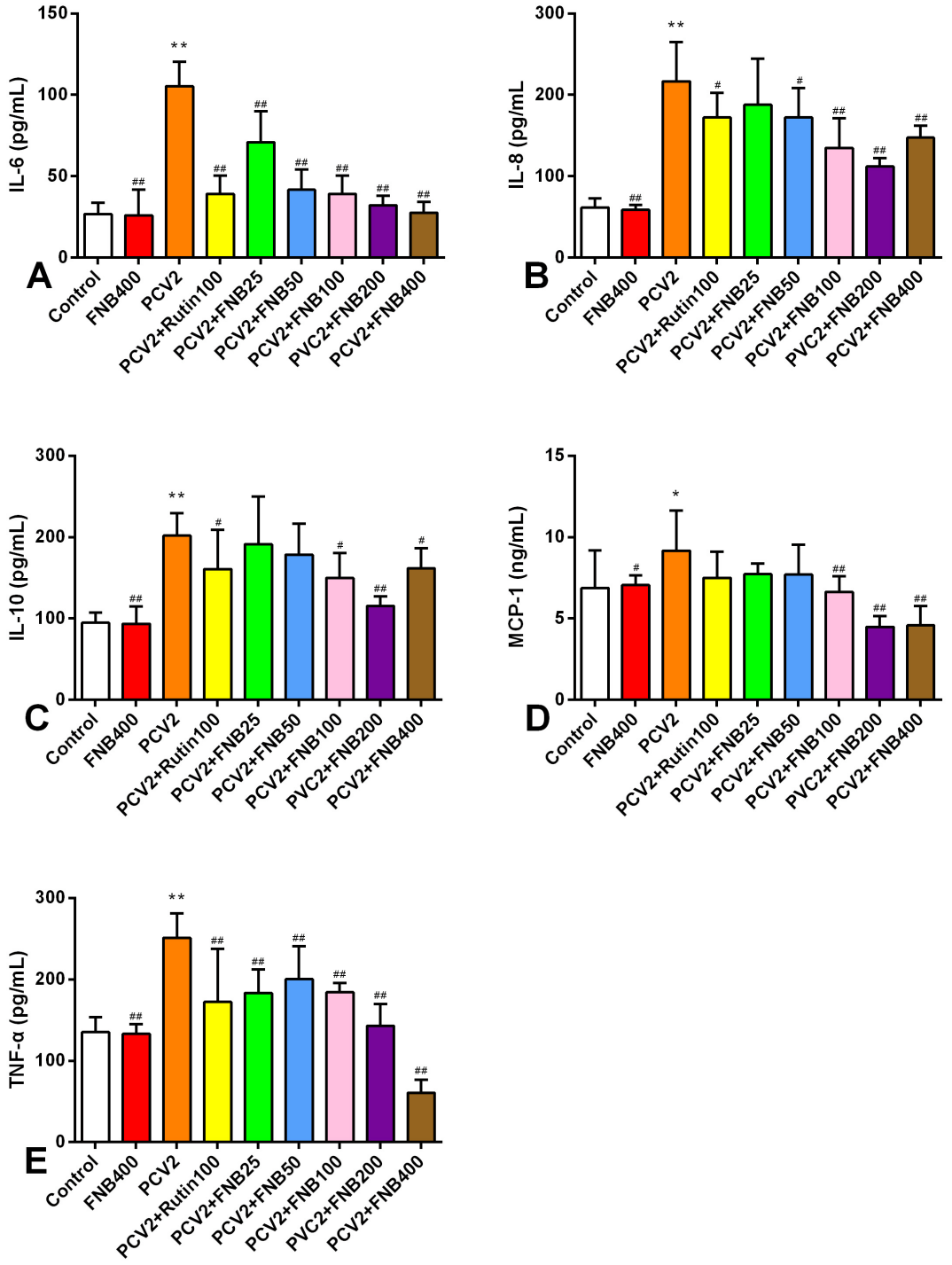

FIGURE 5
(A–E) Effects of FNB on inflammatory cytokine levels in mouse sera after PCV2 infection (mean ± SD, $n = 6$). $^{*}p < 0.05$, $^{**}p < 0.01$ vs. Control group. $^{\#}p < 0.05$, $^{\#\#}p < 0.01$ vs. PCV2 group.

underlying the intervention of FNB are still not fully understood. For instance, through which signaling pathways does FNB exert its anti-inflammatory effects, are there any non-coding RNAs involved, and what role do histone acetylation modifications play? These questions will be clarified in further studies conducted in our laboratory.

In conclusion, this study effectively created an *in vitro* PCV2 infection model in RAW264.7 cells and demonstrated that FNB could affect the inflammatory responses induced through PCV2 *in vivo* and *in vitro*. Moreover, the findings offer a foundation for the application of plant flavonoids in the prevention and management of viral infections in animals.

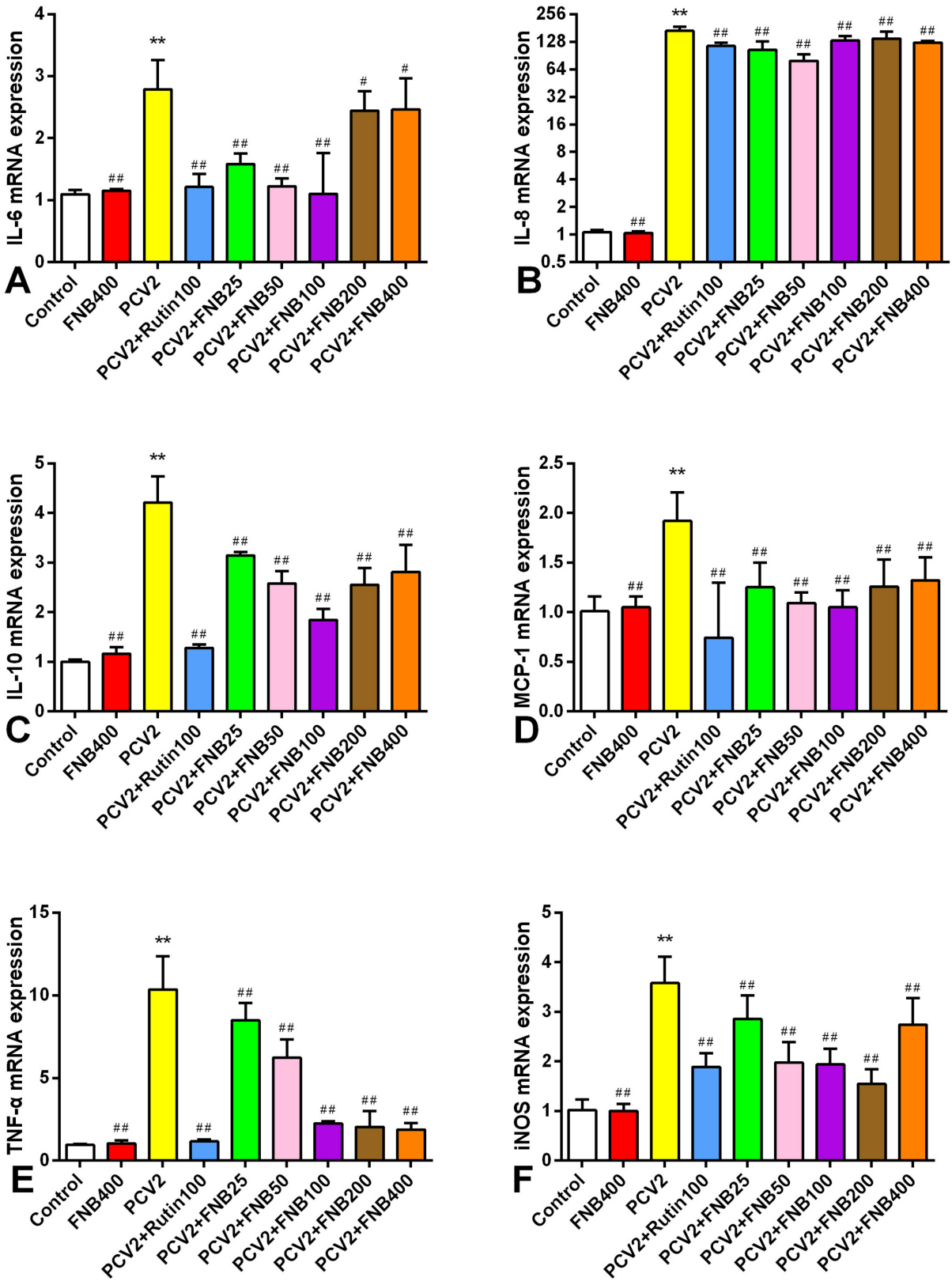

FIGURE 6
(A–F) Impact of FNB on inflammatory cytokine mRNA expression in mouse lungs following PCV2 infection (mean ± SD, $n = 6$). $^{**}p < 0.01$ vs. Control group. $^{\#\#}p < 0.01$ vs. PCV2 group.

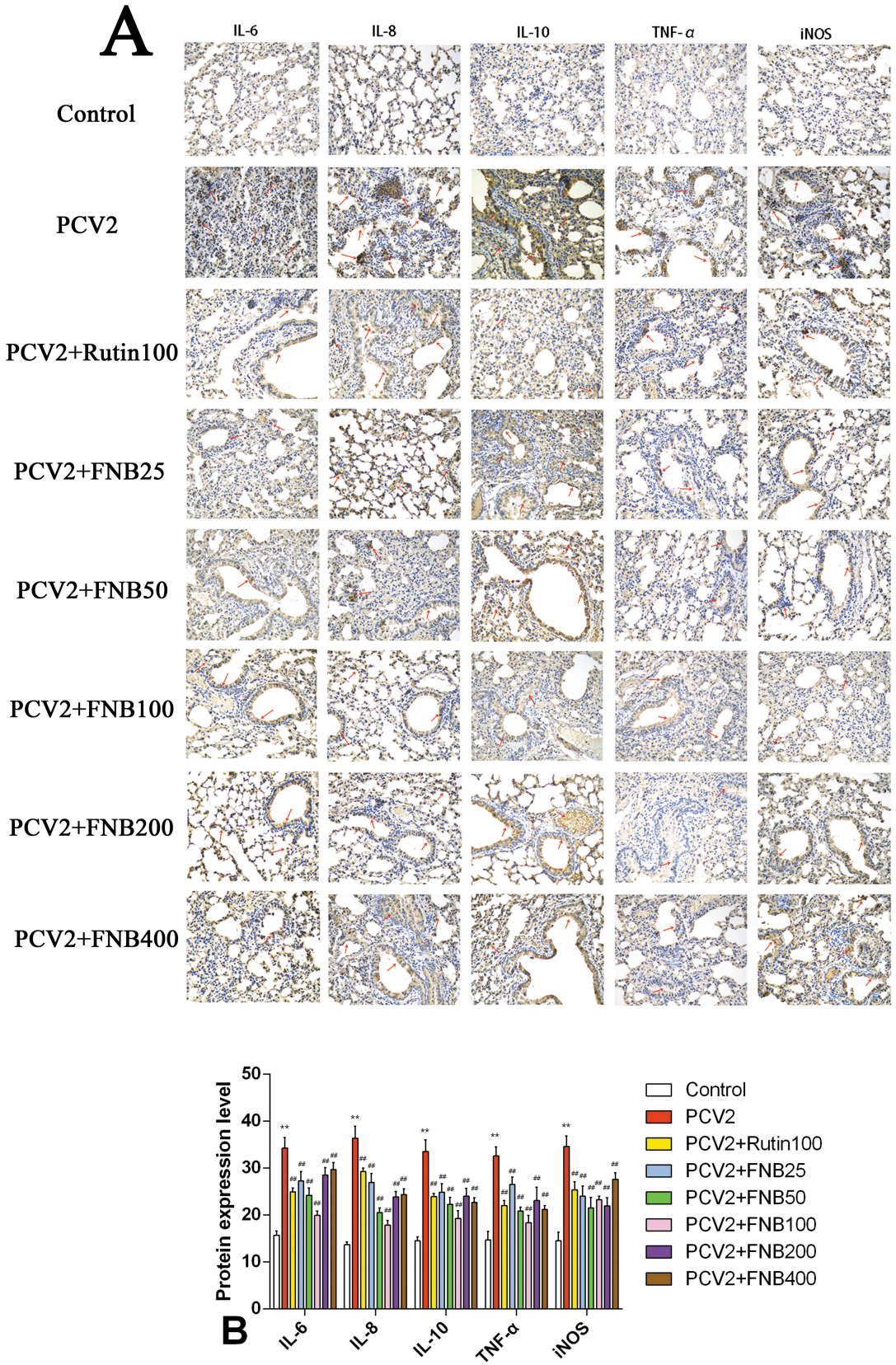

FIGURE 7
(A, B) Effects of FNB on inflammatory cytokine protein levels in mouse lungs following PCV2 infection (mean ± SD, $n = 6$). $^{**}p < 0.01$ vs. Control group. $^{\#\#}p < 0.01$ vs. PCV2 group.

Data availability statement

The original contributions presented in the study are included in the article/supplementary material, further inquiries can be directed to the corresponding author/s.

Ethics statement

Approval was obtained from the Ethics Committee of Guangxi University. The procedures used in this study adhere to the tenets of the Declaration of Helsinki. The study was conducted in accordance with the local legislation and institutional requirements.

Author contributions

Y-hW: Data curation, Writing – original draft, Conceptualization, Methodology. S-mZ: Data curation, Writing – original draft, Conceptualization, Methodology. WZ: Visualization, Writing – review & editing, Software. QC: Writing – review & editing, Investigation, Supervision. Q-hW: Formal Analysis, Writing – review & editing, Data curation. M-lY: Data curation, Resources, Writing – review & editing. Y-yW: Investigation, Validation, Writing – review & editing. T-jH: Conceptualization, Funding acquisition, Project administration, Supervision, Writing – review & editing.

Funding

The author(s) declare financial support was received for the research, authorship, and/or publication of this article. This work was funded by the National Natural Science Foundation of China (Grant No. 32072907) and the Innovation Project of Guangxi Graduate Education (Grant No. YCBZ2024068).

Acknowledgments

We thank Dr. Huang KH, a member of the College of Veterinary Medicine at Nanjing Agricultural University, for providing PCV2.

Conflict of interest

The authors declare that the research was conducted in the absence of any commercial or financial relationships that could be construed as a potential conflict of interest.

Generative AI statement

The author(s) declare that no Gen AI was used in the creation of this manuscript.

Publisher's note

All claims expressed in this article are solely those of the authors and do not necessarily represent those of their affiliated organizations, or those of the publisher, the editors and the reviewers. Any product that may be evaluated in this article, or claim that may be made by its manufacturer, is not guaranteed or endorsed by the publisher.

References

1. Guo J, Hou L, Zhou J, Wang D, Cui Y, Feng X, et al. Porcine circovirus type 2 vaccines: commercial application and research advances. *Viruses.* (2022) 14:2005. doi: 10.3390/v14092005

2. Yang X, Du Q, Wang X, Shi J, Wang T, Li P, et al. Porcine circovirus type 2 infection inhibits macrophage M1 polarization induced by other pathogens via viral capsid protein and host gC1qR protein. *Vet Microbiol.* (2023) 285:109871. doi: 10.1016/j.vetmic.2023.109871

3. Choi CY, Rho SB, Kim HS, Han J, Bae J, Lee SJ, et al. The ORF3 protein of porcine circovirus type 2 promotes secretion of IL-6 and IL-8 in porcine epithelial cells by facilitating proteasomal degradation of regulator of G protein signalling 16 through physical interaction. *J Gen Virol.* (2015) 96:1098–108. doi: 10.1099/vir.0.000046

4. Shen N, Wang T, Gan Q, Liu S, Wang L, Jin B. Plant flavonoids: classification, distribution, biosynthesis, and antioxidant activity. *Food Chem.* (2022) 383:132531. doi: 10.1016/j.foodchem.2022.132531

5. Tao J, Wei Y, Hu T. Flavonoids of *Polygonum hydropiper* L. attenuates lipopolysaccharide-induced inflammatory injury via suppressing phosphorylation in MAPKs pathways. *BMC Complement Altern Med.* (2016) 16:25. doi: 10.1186/s12906-016-1001-8

6. Li P, Hao Z, Wu J, Ma C, Xu Y, Li J, et al. Comparative proteomic analysis of polarized human THP-1 and mouse RAW2647 macrophages. *Front Immunol.* (2021) 12:700009. doi: 10.3389/fimmu.2021.700009

7. Castaneda OA, Lee SC, Ho CT, Huang TC. Macrophages in oxidative stress and models to evaluate the antioxidant function of dietary natural compounds. *J Food Drug Anal.* (2017) 25:111–8. doi: 10.1016/j.jfda.2016.11.006

8. Chen HL, Tan HL, Yang J, Song ML, Feng HY, Kuang N, et al. Inhibitory effect of polysaccharide of Sargassum weizhouense on PCV2 induced inflammation in mice by suppressing histone acetylation. *Biomed Pharmacother.* (2019) 112:108741. doi: 10.1016/j.biopha.2019.108741

9. Kaur S, Bansal Y, Kumar R, Bansal G. A panoramic review of IL-6: structure, pathophysiological roles and inhibitors. *Bioorg Med Chem.* (2020) 28:115327. doi: 10.1016/j.bmc.2020.115327

10. Kishimoto T, Kang S. IL-6 revisited: from rheumatoid arthritis to CAR T cell therapy and COVID-19. *Annu Rev Immunol.* (2022) 40:323–48. doi: 10.1146/annurev-immunol-101220-023458

11. Guo X, Feng Y, Zhao X, Qiao S, Ma Z, Li Z, et al. Coronavirus porcine epidemic diarrhea virus utilizes chemokine interleukin-8 to facilitate viral replication by regulating Ca2+ flux. *J Virol.* (2023) 97:e0029223. doi: 10.1128/jvi.00292-23

12. Bakouny Z, Choueiri TK. IL-8 and cancer prognosis on immunotherapy. *Nat Med.* (2020) 26:650–1. doi: 10.1038/s41591-020-0873-9

13. Saraiva M, Vieira P, O'Garra A. Biology and therapeutic potential of interleukin-10. *J Exp Med.* (2020) 217:e20190418. doi: 10.1084/jem.20190418

14. Alagarasu K, Kaushal H, Shinde P, Kakade M, Chaudhary U, Padbidri V, et al. *TNFA* and *IL10* polymorphisms and IL-6 and IL-10 levels influence disease severity in influenza A(H1N1)pdm09 virus infected patients. *Genes.* (2021) 12:1914. doi: 10.3390/genes12121914

15. Singh S, Anshita D, Ravichandiran V. MCP-1: function, regulation, and involvement in disease. *Int Immunopharmacol.* (2021) 101:107598. doi: 10.1016/j.intimp.2021.107598

16. Chen Y, Wang J, Liu C, Su L, Zhang D, Fan J, et al. IP-10 and MCP-1 as biomarkers associated with disease severity of COVID-19. *Mol Med.* (2020) 26:97. doi: 10.1186/s10020-020-00230-x

17. Dömling A, Li X. TNF-α: the shape of small molecules to come? *Drug Discov Today.* (2022) 27:3–7. doi: 10.1016/j.drudis.2021.06.018

18. Jang DI, Lee AH, Shin HY, Song HR, Park JH, Kang TB, et al. The role of tumor necrosis factor alpha (TNF-α) in autoimmune disease and current TNF-α inhibitors in therapeutics. *Int J Mol Sci.* (2021) 22:2719. doi: 10.3390/ijms22052719

19. Wang L, Cao Z, Wang Z, Guo J, Wen J. Reactive oxygen species associated immunoregulation post influenza virus infection. *Front Immunol.* (2022) 13:927593. doi: 10.3389/fimmu.2022.927593

20. Zhang S, Zeng L, Su B, Yang G, Wang J, Ming S, et al. The glycoprotein 5 of porcine reproductive and respiratory syndrome virus stimulates mitochondrial ROS to facilitate viral replication. *MBio.* (2023) 14:e0265123. doi: 10.1128/mbio.02651-23

21. Facchin BM, Dos Reis GO, Vieira GN, Mohr ETB, da Rosa JS, Kretzer IF, et al. Inflammatory biomarkers on an LPS-induced RAW 2647 cell model: a systematic review and meta-analysis. *Inflamm Res.* (2022) 71:741–58. doi: 10.1007/s00011-022-01584-0

22. Hussain M, Khurram Syed S, Fatima M, Shaukat S, Saadullah M, Alqahtani AM, et al. Acute respiratory distress syndrome and COVID-19: a literature review. *J Inflamm Res.* (2021) 14:7225–42. doi: 10.2147/JIR.S334043

23. Al-Khayri JM, Sahana GR, Nagella P, Joseph BV, Alessa FM, Al-Mssallem MQ. Flavonoids as potential anti-inflammatory molecules: a review. *Molecules.* (2022) 27:2901. doi: 10.3390/molecules27092901

24. Mahmoud AM, Sayed AM, Ahmed OS, Abdel-Daim MM, Hassanein EHM. The role of flavonoids in inhibiting IL-6 and inflammatory arthritis. *Curr Top Med Chem.* (2022) 22:746–68. doi: 10.2174/1568026622666220107105233

25. Chen HL, Tan HL, Yang J, Wei YY, Hu TJ. Sargassum polysaccharide inhibits inflammatory response in PCV2 infected-RAW2647 cells by regulating histone acetylation. *Carbohydr Polym.* (2018) 200:633–40. doi: 10.1016/j.carbpol.2018.06.060

26. Chen HL, Yang J, Fu YF, Meng XN, Zhao WD, Hu TJ. Effect of total flavonoids of Spatholobus suberectus Dunn on PCV2 induced oxidative stress in RAW2647 cells. *BMC Complement Altern Med.* (2017) 17:244. doi: 10.1186/s12906-017-1764-6

27. Ren CZ, Hu WY, Li JC, Xie YH, Jia NN, Shi J, et al. Ethyl acetate fraction of flavonoids from *Polygonum hydropiper* L. modulates pseudorabies virus-induced inflammation in RAW2647 cells via the nuclear factor-kappa B and mitogen-activated protein kinase pathways. *J Vet Med Sci.* (2020) 82:1781–92. doi: 10.1292/jvms.20-0263

28. Ren CZ, Hu WY, Song ML, Wei YY, Hu TJ. An ethyl acetate fraction of flavonoids from *Polygonum hydropiper* L. exhibits an anti-inflammatory activity in PCV2-infected porcine alveolar macrophages via PI3K/Akt and NF-κB pathways. *Vet Res Forum.* (2022) 13:339–47. doi: 10.30466/vrf.2021.137675.3070

29. Wang QH, Kuang N, Hu WY, Yin D, Wei YY, Hu TJ. The effect of *Panax notoginseng* saponins on oxidative stress induced by PCV2 infection in immune cells: *in vitro* and *in vivo* studies. *J Vet Sci.* (2020) 21:e61. doi: 10.4142/jvs.2020.21.e61

30. Fu YF, Jiang LH, Zhao WD, Xi-Nan M, Huang SQ, Yang J, et al. Immunomodulatory and antioxidant effects of total flavonoids of *Spatholobus suberectus* Dunn on PCV2 infected mice. *Sci Rep.* (2017) 7:8676. doi: 10.1038/s41598-017-09340-9

frontiers | Frontiers in Veterinary Science

TYPE Original Research
PUBLISHED 25 March 2025
DOI 10.3389/fvets.2025.1551501

OPEN ACCESS

EDITED BY
Baocheng Hao,
Chinese Academy of Agricultural Sciences, China

REVIEWED BY
Basavaraj S. Mathapati,
Indian Council of Medical Research (ICMR), India
Deping Song,
Jiangxi Agricultural University, China

*CORRESPONDENCE
Ling Zhu
✉ abtczl72@126.com
Zhiwen Xu
✉ abtcxzw@126.com

†These authors have contributed equally to this work and share first authorship

RECEIVED 25 December 2024
ACCEPTED 24 February 2025
PUBLISHED 25 March 2025

CITATION
Liu B, Wang Y, Shao L, Chen Y, Xu Z and Zhu L (2025) Antiviral activity of *Scutellaria baicalensis Georgi Extract* against Getah virus *in vivo* and *in vitro*. *Front. Vet. Sci.* 12:1551501. doi: 10.3389/fvets.2025.1551501

Antiviral activity of *Scutellaria baicalensis Georgi Extract* against Getah virus *in vivo* and *in vitro*

Baoling Liu[1†], Yuling Wang[1†], Lina Shao[1†], Yuanhang Chen[1], Zhiwen Xu[1,2*] and Ling Zhu[1,2*]

[1]College of Veterinary Medicine, Sichuan Agricultural University, Chengdu, China, [2]Sichuan Key Laboratory of Animal Epidemic Disease and Human Health, Sichuan Agricultural University, Chengdu, China

Introduction: The Getah virus (GETV) is a zoonotic arbovirus causing disease in humans and animals, a member of the *Alphavirus* genus. Currently, approved antiviral drugs and vaccines against alphaviruses are few available. This study aimed to investigate the anti-GETV activity of the Extract of *Scutellaria baicalensis Georgi* (ESG) *in vivo* and *in vitro*.

Methods: The cytotoxic effects of ESG on BHK-21 cells were quantitatively evaluated through the MTT assay. Quantitative analysis of viral replication was performed using qRT-PCR, while E2 protein expression was analyzed through western blotting. Furthermore, molecular docking simulations were conducted to examine the binding affinity between the principal bioactive constituents of ESG and the E2 structural proteins. Additionally, the therapeutic potential of ESG in alleviating viremia was evaluated in GETV-infected mouse models.

Results: The results showed that ESG significantly attenuated the cytopathic effects induced by GETV infection in BHK-21 cells, concurrently reducing both viral replication and E2 protein expression. Notably, ESG exhibited its most potent antiviral activity during the viral attachment and entry phases, with IC50 values of 3.69 μg/mL and 3.94 μg/mL, respectively. At a concentration of 10 μg/mL, ESG achieved 95.08% inhibition efficiency against viral attachment. Furthermore, in vivo studies revealed that ESG treatment significantly reduced the peak viral load and shortened the duration of viremia in GETV-infected mice. The main components of ESG are baicalin and baicalein, and molecular docking simulations demonstrated strong binding affinities between these compounds and the active site of GETV E2 protein, with docking scores of −6.99 kcal/mol for baicalin and −5.21 kcal/mol for baicalein.

Conclusion: The experimental findings demonstrate that ESG exhibits significant antiviral efficacy against GETV infection both *in vitro* and *in vivo*. These results indicate that ESG represents a promising therapeutic candidate for the prevention and treatment of GETV infections. Mechanistically, the antiviral activity of ESG appears to be mediated, at least in part, through the modulation of E2 protein expression.

KEYWORDS

antiviral, *Scutellaria baicalensis Georgi Extract*, Getah virus, natural compounds, traditional Chinese medicine

1 Introduction

Getah virus (GETV) belongs to the Alphavirus genus in the Togaviridae family and is a zoonotic arbovirus causing disease in humans and animals (1, 2). GETV has a broad host range, such as monkeys, birds, pigs, horses, and other mammals that may be infected, which can cause pyrexia and reproductive losses in animals. A 2015 outbreak of GETV infection occurred among Japanese racehorses sequentially to an outbreak in 2014 at

the same site (3). In 2017, an outbreak of GETV infection among pigs in China, and more than 150 pregnant sows had stillbirths or fetal mummies in this outbreak (4). GETV has brought a greater risk to the animal husbandry industry and constitutes a massive threat to public health. However, approved antiviral drugs and vaccines against alphaviruses are few available (5, 6). Currently, there are no specific treatments or drugs available for GETV infection (7). Because GETV still represents a significant threat to human and animal health worldwide, developing effective weapons against GETV remains a top priority.

Traditional Chinese Medicine (TCM) is a holistic system of healthcare that has been practiced for thousands of years. *Scutellaria baicalensis Georgi*, as one of the TCMs is a widely distributed plant has been used for heat-clearing and detoxifying. The main active components in *Scutellaria baicalensis Georgi* are flavonoids, terpenoids, and volatile oils. baicalein, baicalin, and wogonin are the essential active substances in the Extracts of *Scutellaria baicalensis Georgi* (ESG) (8). Among them, baicalin has a variety of biological functions, such as anti-bacterial, anti-inflammatory, antiviral, and anti-tumor activities (9). Relevant studies have shown that baicalin inhibits avian infectious bronchitis virus (IBV) and Porcine reproductive and respiratory syndrome virus (PRRSV) (10, 11). The findings of Moghaddam et al. showed that baicalin as the main metabolite of baicalein exerts against dengue virus activity *in vitro* (12). NIU et al. proved that baicalin effectively inhibits PRV infection (13). Although the antiviral activity of baicalin has been reported, the effect of baicalin or ESG against GETV infection remains to be investigated.

This study aimed to investigate the anti-GETV activity of the ESG *in vivo* and *in vitro*, to provide a scientific foundation for preventing and controlling GETV.

2 Materials and methods

2.1 Cell, virus, and drugs

BHK-21 cells were cultured and passaged at 37°C and 5% CO_2 and maintained in DMEM (gibco) supplemented with 10% fetal bovine serum (FBS) and antibiotic/antimycotic solution. In this study GETV SC201807 strain (GenBank number: MK693225) was used, and the virus was maintained at Sichuan Agricultural University, College of Veterinary Medicine.

Extracts of Scutellaria baicalensis Georgi (ESG, Baicalin HPLC >85%) were purchased from Baoji Fangsheng Biological Development Co., Ltd (Baoji, China). Dissolve it to 40 mg/mL with DMSO, freeze it at −20°C as stock solution and dilute to working concentration with DMEM when using.

2.2 Mice and reagents

All mice were kept in a pathogen-free environment and fed ad-lib. The procedures for care and use of animals were approved by the Ethics Committee of the Veterinary Medicine College of Sichuan Agricultural University, and all applicable institutional and governmental regulations concerning the ethical use of animals were followed.

Mouse Polyclonal Antibody to GETV E2 protein deposited in Animal Biotechnology Center, Sichuan Agricultural University, China. FITC-goat anti-mouse IgG fluorescent secondary antibody was purchased from Sangon Biotech (Shanghai) Co., Ltd (Shanghai, China).

2.3 Effect of ESG on the BHK-21 cell viability assay

The cytotoxicity of ESG on the viability of BHK-21 cells was determined using the MTT assay. The BHK-21 cells were cultured to a monolayer with a 96-well cell culture plate. The cells were treated with the ESG diluted by DMEM supplemented with 2% FBS in seven concentrations of 40, 20, 10, 5, 2.5, 1.25, and 0.625 μg/mL, and incubated at 37°C with 5% CO_2 for 48 h. Each concentration was repeated in four wells, and 0.1% DMSO and cell control were set. After 48 h, MTT solution was added to each well and the microplate was kept at 37°C for 4 h in a humidified atmosphere with 5% CO_2. Then, solubilization/stop solution was added to the wells, and the absorbance values of the wells were measured at 570 nm using a 96-well plate reader. Drug concentrations with cell viability more significant than 90% were taken as the maximum non-toxic dose (MNTD).

2.4 Determination of anti-GETV activity of ESG

A continuous treatment assay was conducted to determine the antiviral activity of ESG against any stage of the GETV life cycle. According to the method Moghaddam et al. proposed (12). BHK-21 cells were cultured to a monolayer in a 96-well cell culture plate. Then the cells were treated with low (2 μg/mL), medium (6 μg/mL), and high (10 μg/mL) doses of the ESG, and the supernatant was discarded after incubation for 5 h. The mixture of ESG and GETV (MOI = 0.1) was added to the culture plate, and the supernatant was discarded after 1 h incubation. The supernatant was washed with PBS three times, and the corresponding concentration of drug solution was added to each well. At the same time, virus control, cell control, and ribavirin (10 μg/mL) control groups were set. After incubation at 37°C with 5% CO_2 for 48 h, cytopathic effect (CPE) was observed, MTT analysis was performed, and the supernatant was collected for the following assay.

2.5 Quantitative reverse transcription-polymerase chain reaction (qRT-PCR) was used to detect the effect of ESG on virus replication

The GETV yield during the antiviral studies was evaluated by qRT-PCR assay. A total of 300 μL of supernatant collected in the previous step was taken, and the viral RNA was extracted using Trizol (Invitrogen, Beijing, China), and the cDNA was generated.

Then the amplification of the E2 encoding sequence was performed using the primers E2-F (5′-CTTGACGGTAAGGTCACGGG-3′) and E2-R (5′-GTAAGCTTCGCTAGGTCGGG-3′). The cycling parameters were 94°C for 180 s, 35 cycles of 95°C for 10 s, and 58°C for 15 s. The amplified product was verified by melting curve analysis at 58°C.

2.6 Western blotting analysis

Western Blotting (WB) assay was used to verify further the inhibitory effect of the ESG on E2 protein expression of the GETV virus. Total proteins were extracted from GETV-infected cells with protein extraction reagent (Beyotime, China) according to the manufacturer's instructions. The protein concentration was measured using the BCA kit (Thermo, USA). After being isolated using 12% SDS-PAGE, the proteins were transferred to a nitrocellulose membrane. The mouse polyclonal antibodies against GETV E2 protein (1:100) and GAPDH (1:5000) were incubated as primary antibodies, and the secondary antibodies were diluted at 1:3000 and incubated at 37°C for 1 h. Imaging was performed with the hyper signal detection of protein bands by the West Pico PLUS chemiluminescence Branch and ChemiDoc MP Bio-Rad chemiluminescence imaging system. Image J software analyzed optical density values, and changes in E2 protein expression were compared.

2.7 Time-of-addition assay

To analyze the effect of ESG on GETV, experiments were conducted with reference to previous research methods (10, 14, 15). BHK-21 cells were cultured to a monolayer with a 24-well plate, 2, 4, 6, 8, and 10 μg/mL ESG was added before (pre-treatment), during (attachment treatment), or after (entry and post-entry treatment) GETV infection (Figure 1A). For pretreatment BHK-21 cells were incubated with ESG at 37°C for 5 h, washed three times with PBS and infected with GETV (0.1 MOI) at 37°C for 1 h. For attachment treatment BHK-21 cells were incubated with ESG and GETV at 4°C for 1 h. For entry BHK-21 cells were infected with GETV (0.1 MOI) at 4°C for 1 h, washed three times with PBS and incubated with ESG at 37°C with for 1 h. For post entry treatment BHK-21 cells were infected with GETV (0.1 MOI) at 37°C for 1 h, washed three times with PBS and incubated with ESG at 37°C with 5% CO_2 until 48 h. Since the antiviral activity of ribavirin is intracellular or mainly in RNA replication, it has been used only to control this antiviral assay. All four treatment modalities were incubated in a CO_2 incubator at 37°C for up to 48 h after treatment. Cells and supernatant were collected at 48 h post-infection (hpi). Detection of virus multiplication by qRT-PCR.

2.8 Effect on viremia in mice infected with GETV

For this assay, 120 three-week-old male mice were randomly divided into four groups: A, B, C, and D. The existing GETV infection model in our laboratory showed that the LD50 of the SC201807 strain in mice is $10^{2.85}$ TCID50. Mice in groups A, B, and C were intranasally inoculated with 4 × LD50 (4 × $10^{2.85}$ TCID50) of GETV on the 3rd day of the study. Mice in group A were given ESG 3 days before GETV infection at a dose of 3 mg/mouse/day; mice in group B were given ESG on the same day as GETV; mice in group C were only infected with GETV without being given drugs; mice in group D were the negative control group, and each group was treated with individual feeding and management. The clinical symptoms of each group of mice were observed daily, and blood was collected from five mice in each group at 24 h, 48 h, 72 h, 7 days, 14 days, and 21 days after GETV infection, followed by GETV viremia testing. Table 1 shows the animal grouping and treatment plan.

2.9 Molecular docking

To investigate the interaction effects between baicalein and baicalin—the primary active components of ESG—and the E2 protein, predictive structural modeling of the E2 protein was conducted using AlphaFold 3. Subsequently, molecular docking analyses were performed to examine the binding interactions of the E2 protein with baicalein and baicalin individually, following the methodology described by Chakraborty et al. (16).

2.10 Statistical analysis

One-way analysis of variance (ANOVA) was conducted with the Graph Pad Prism 5 software; $P < 0.05$ was considered a statistically significant difference.

3 Results

3.1 Cytotoxicity of ESG on BHK-21

Cytotoxicity assay was performed to determine the non-toxic concentrations of ESG against BHK-21 cells using the MTS assay. The cells treated with 0.1% DMSO showed no cytotoxicity. The BHK-21 cell viability decreased when the drug concentration increased. At a concentration of 10 μg/mL, the viability of ESG-treated BHK-21 cells was >90% compared to vehicle control indicating that the concentration could be considered as the maximum non-toxic dose (MNTD) of ESG for BHK-21 cells (Figure 2). Therefore, 2, 4, 6, 8, and 10 μg/mL were finally selected as the working concentrations for follow-up experiments.

3.2 ESG reduces the effects of GETV on CPE and viability

To identify whether the ESG has antiviral effects, different drug concentrations were tested on GETV-infected BHK-21 cells. Observing the CPE condition under a microscope, the results showed that the cell particles in the GETV control group increased; they were rounded, and most of them fell off, with an apparent

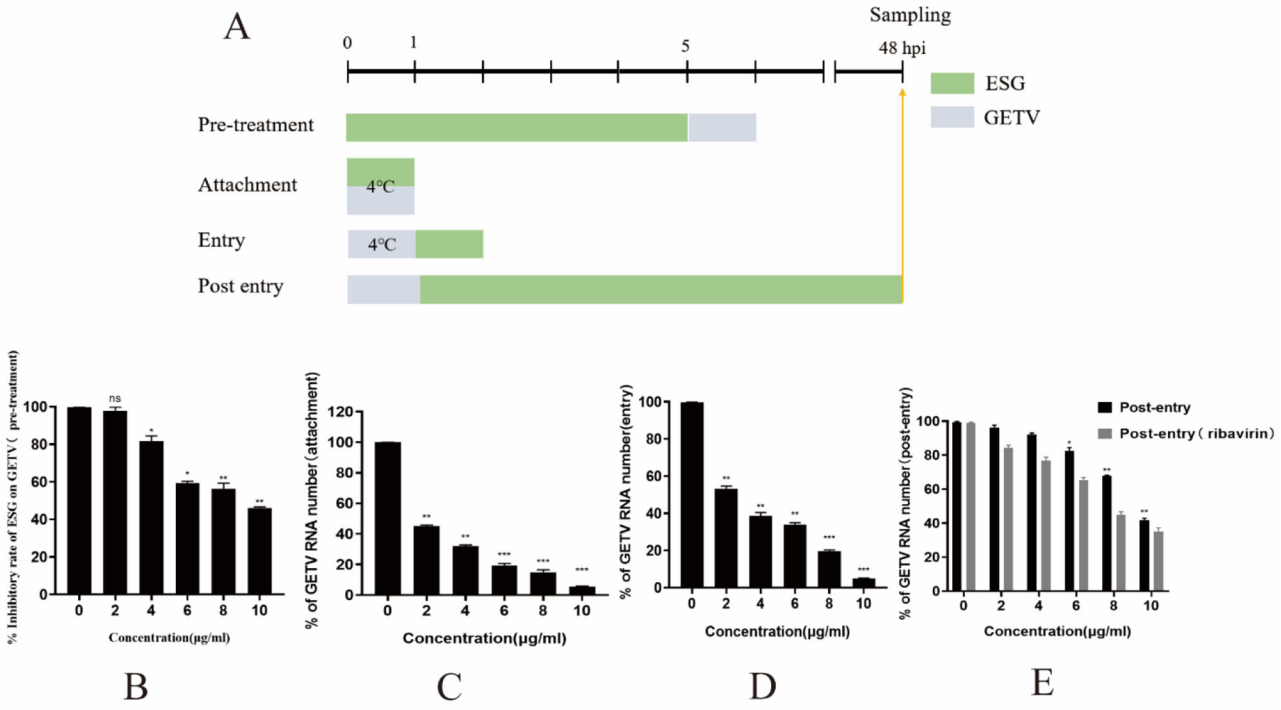

FIGURE 1
ESG inhibits GETV replication in four treatment modes. **(A)** PRRSV (0.1 MOI) was used to infect the cells for 1 h for all four treatment modes. Cells and supernatant were collected at 48 h. Except for the temperatures specifically labeled at specific times in the figure, all treatment temperatures were at 37°C. **(B–E)** GETV mRNA levels in four treatment modes. The difference was considered statistically significant when $P < 0.05$ ($^{***}P < 0.001$; $^{**}P < 0.01$; $^{*}P < 0.05$). Non-linear regression analysis was done using GraphPad Prism version 8 software.

TABLE 1 Grouping of experimental animals and treatment plan.

Treatment group	A	B	C	D
Number of mice	30	30	30	30
Dosage per mouse (mg/day)	3	3	_	_
Start time of treatment	−3	0	_	_
Way of infection	Vaccination of 4 × LD50 doses of GETV solution intranasally			

degree of CPE lesions. Compared with the virus control group, the cells in the high-dose treatment group and the ribavirin control group were similar, most of which were in an adhesive state, and the cell morphology was normal (Figure 3A). Regarding the MTT experiment and the cell survival rate, after GETV infection, the cell survival rate decreased significantly; compared with the virus infection control group, the cell viability of the groups receiving high, medium, and low doses of *Scutellaria baicalensis* extract and of the ribavirin group was significantly increased (Figure 3B), indicating that the extract significantly inhibited the pathological effect of BHK-21 cells caused by GETV.

3.3 ESG can significantly inhibit viral RNA replication

The results of the qRT-PCR showed that high, medium and low doses of ESG could inhibit viral RNA replication; an effective reduction in virus copy number could still be achieved at a drug concentration as low as 2 μg/mL (Figure 4).

3.4 ESG reduces the expression of E2 protein

Western blotting was used to determine whether ESG had an inhibitory effect on the expression of E2 protein. The WB test results showed that compared with the virus control group, as the concentration of ESG increased, the GETV E2 protein expression gradually decreased. When the drug concentration reached 10 μg/mL, the band's color was lighter. The inhibitory effect was more evident (Figure 5A). This indicates that ESG significantly inhibited the expression of E2 protein in BHK-21 cells. The optical density statistics showed that ESG significantly reduced the expression of E2 protein (Figure 5B). In this step, GAPDH was used as an internal reference to eliminate the cells' interference with the experimental results.

3.5 ESG can effectively inhibit the virus in the attachment and entry stages

According to the results of the ratio of viral gene copy numbers in the experimental group and the control group, ESG had the most potent inhibitory effect on the GETV attachment stage

(Figure 1C). When BHK-21 cells were pretreated with ESG for 5 h and then inoculated, the inhibitory effect on GETV infection was not noticeable (IC50 = 8.63 μg/mL). When the concentration was 10 μg/mL, the inhibition rate was only 53.86%. At different doses, ESG has a significant inhibitory effect on the attachment of GETV (IC50 = 3.59 μg/mL) in a dose-dependent manner. It could still be effectively inhibited when 2 μg/mL of the drug concentration. An inhibition rate reached 49.48%; when the drug concentration was 10 μg/mL, the inhibition rate advanced to 94.49%. These results indicate that the ESG has an inhibitory effect on the replication of GETV after GETV enters the cell in a dose-dependent manner. However, the drug's inhibitory effect after the virus had entered the cell (IC50 = 9.4 μg/mL) was lower than that of ribavirin (IC50 = 7.74 μg/mL) (Figure 1E). When the concentration of ESG was 10 μg/mL, the inhibition rate of the virus was still below 50%.

3.6 ESG can effectively relieve viremia in mice

The RT-qPCR method was used to analyze the whole blood samples of mice at 24 h, 48 h, 72 h, 7 days, 14 days, and 21 days after inoculation. Blood from mice in groups A, B, and C was positive for GETC from 24 h. The positivity rate in group A was 5/5 on the 7th day and decreased to 0/5 on the 14th day, whereas group B was 1/5 on the 14th day and dropped to 0/5 on the 21st day. The rate in group C was 3/5 on the 14th day and fell to 0/5 on the 21st day, whereas group D was 0/5 (Table 2). Some mice in groups A and B were negative for GETV on the 7 and 21 days. Therefore, quantitative analysis of the GETV content in the whole blood of mice was only performed at the 12th h, 24th h, 48th h, 72th h, and

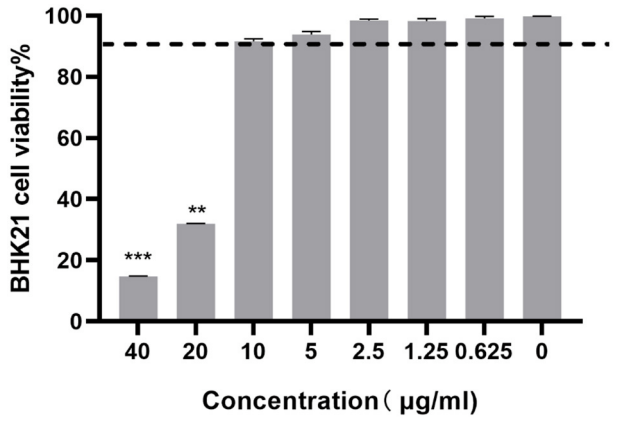

FIGURE 2
The cytotoxicity of ESG on BHK-21 cells by the MTT assay. The difference was considered statistically significant when $P < 0.05$ ($^{***}P < 0.001$; $^{**}P < 0.01$). Non-linear regression analysis was done using GraphPad Prism version 8 software.

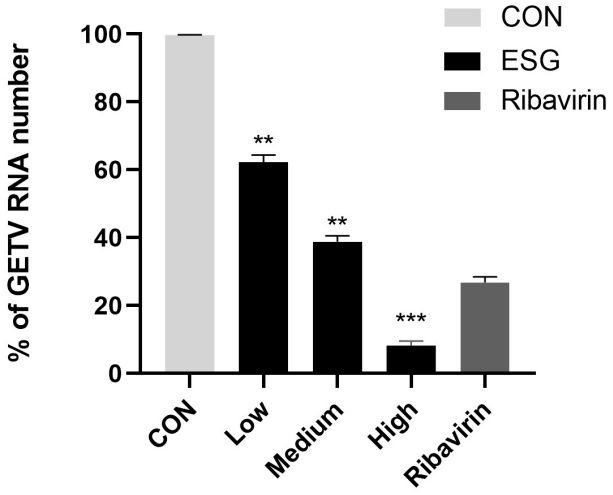

FIGURE 4
Effect of high, medium and low doses of ESG on GETV virus replication. The difference was considered statistically significant when $P < 0.05$ ($^{***}P < 0.001$; $^{**}P < 0.01$). Non-linear regression analysis was done using GraphPad Prism version 8 software.

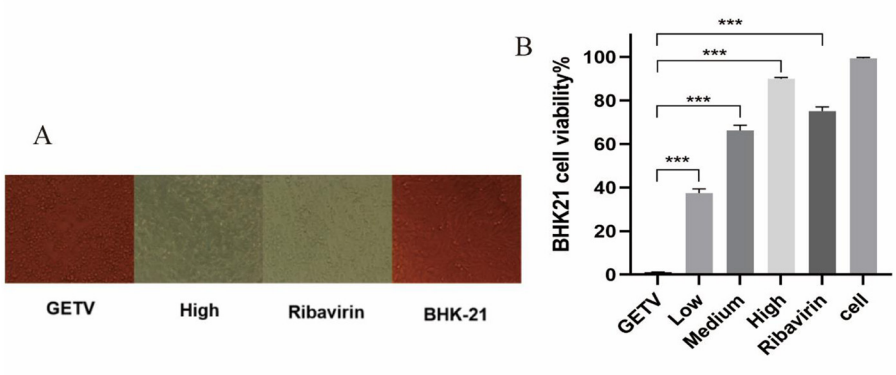

FIGURE 3
Inhibitory effects of ESG on the GETV. The difference was considered statistically significant when $P < 0.05$ ($^{***}P < 0.001$). Non-linear regression analysis was done using GraphPad Prism version 8 software. **(A)** Effect of ESG on the morphology of BHK-21 cells. **(B)** Survival rate of BHK-21 cells measured by MTT.

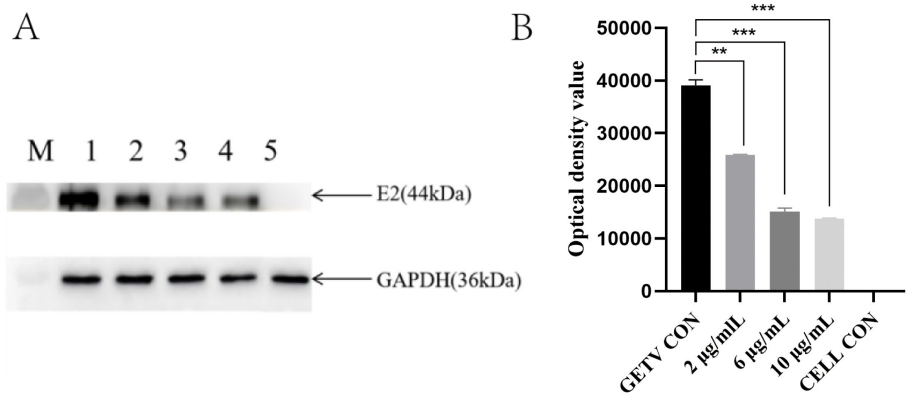

FIGURE 5
Effects of the high, medium, and low doses of ESG on GETV virus replication. **(A)** Western blot result; M, Marker; 1; GETV control; 2–4; Treat with 2, 6, 10 μg/mL ESG; 5; BHK-21 cell control. **(B)** Optical density value statistics chart. The difference was considered statistically significant when $P < 0.05$ ($^{***}P < 0.001$; $^{**}P < 0.01$). Non-linear regression analysis was done using GraphPad Prism version 8 software.

TABLE 2 GETV positive rate in mice blood.

Period	Positive rate			
	Group A	Group B	Group C	Group D
24 h	5/5	5/5	5/5	0/5
48 h	5/5	5/5	5/5	0/5
72 h	5/5	5/5	5/5	0/5
7 day	5/5	5/5	5/5	0/5
14 day	0/5	1/5	3/5	0/5
21 day	0/5	0/5	0/5	0/5

7th day (Figure 6). The virus copy number of mice in groups A, B, and C peaked at 48 h after infection and gradually decreased. The viral copy numbers in group A and group B were significantly lower than those in group C at 48 h after the virus challenge ($P < 0.05$; Figure 6).

3.7 Molecular docking

The molecular docking results showed that baicalin and baicalein bound to the active site of the E2 protein of GETV with docking scores of −6.99 and −5.21 kcal/mol (Figure 7), respectively, which demonstrated strong binding affinities between these compounds and the active site of GETV E2 protein. The inhibition of GETV by ESG may be through the regulation of the expression of E2 protein.

4 Discussion

GETV threatens public health continuously because it can infect humans and many animals. Clinically, GETV can cause fever, diarrhea, and reproductive disorders in pigs, representing significant threats to pig breeding (17). Currently, there are no effective drugs or vaccines for GETV. Therefore, it is still a challenge to prevent GETV infection and it is necessary to develop some new effective antiviral strategies or drugs to combat GETV infection.

In this study, we evaluated ESG anti-GETV activity *in vivo* and *in vitro*. We found that the mixed inoculation of ESG and GETV could effectively inhibit the virus infection, and the IC50 of GETV was 3.59 and 3.94 μg/mL, respectively. When the concentration of ESG in the adsorption process reached 10 μg/mL, it inhibited 95.08% of the GETV replication efficiency. Still, the pre-treatment and the post-entry stage inhibitory effects were not noticeable. Therefore, it is believed that ESG plays a role in the early stages of GETV infection. We suggest that ESG may act directly on the virus instead of stimulating the immune response of host cells to achieve the effect of viral suppression.

The main structural proteins of the Getah virus are Cap, E3, E2, 6K, and E1 proteins. Research on antiviral strategies against alphaviruses usually focused on the E1 and E2 proteins, which bind to cells during the endocytosis of the virus (18). In addition, E2 is also necessary for GETV budding. Western blot results showed that ESG inhibited the expression of E2 protein. The detection of E2 showed that GETV replicates and assembles successfully in the cell; therefore, ESG can also play a role in the assembly and release process of the virus in the later stages of the virus entering the cell. The results of molecular docking further confirmed that baicalin and baicalein, the main components of ESG, can bind to E2 protein, proving that E2 protein is an important target.

GETV and Chikungunya virus (CHIKV) belong to the genus Alphavirus of the Togaviridae, and ZIKV and DENV belong to the Flaviviridae. They have similar structures and are both enveloped RNA viruses of the arboviruses. Studies have shown that baicalein can inhibit the attachment of CHIKV on host cells and has a high inhibitory effect on the RNA replication process after ZIKV enters the cell; it can also significantly inhibit the ZIKV from entering the cell (15, 19). Hassandarvish et al. have shown that baicalein and baicalin affect the virus replication cycle by interacting with Dengue virus (DENV) essential proteins, such as E, NS2B-NS3, and

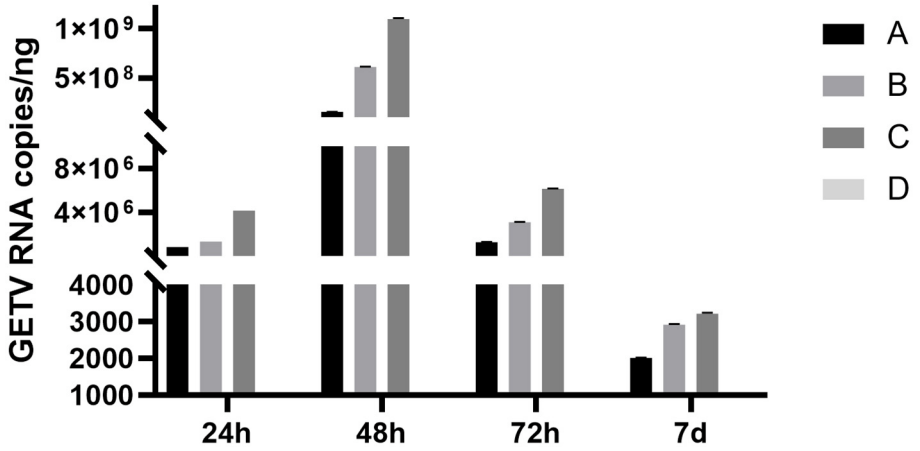

FIGURE 6
Changes in the copy numbers of the GETV in the blood of mice at different times after infection. A, B, and C denote groups A, B, and C, respectively. Mice in group A were given ESG 3 days before GETV infection at a dose of 3 mg/mouse/day; mice in group B were given ESG on the same day as GETV; mice in group C were only infected with GETV without being given drugs; mice in group D were the negative control group, and each group was treated with individual feeding and management.

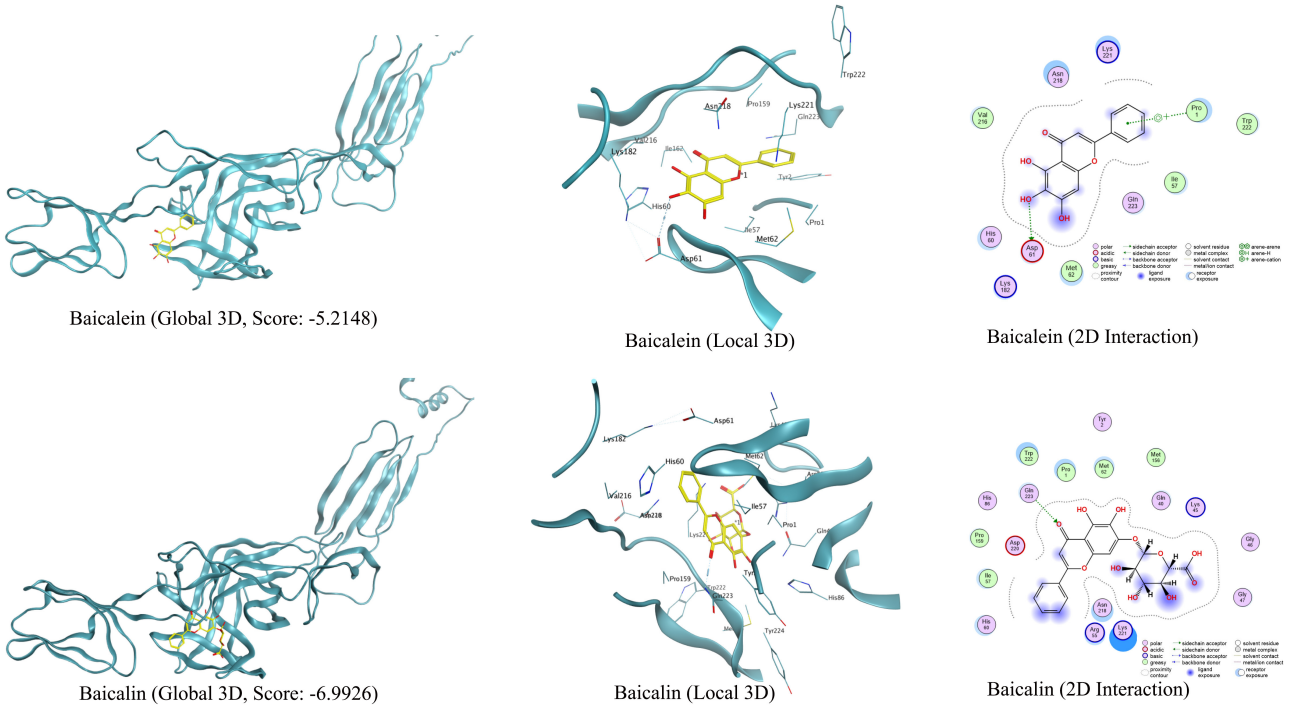

FIGURE 7
Viral target E2 protein docked with baicalin and baicalein, and their interactive residues at the active sites are shown in the images.

NS5 (20). The results of this experiment are consistent with these conclusions. The similar antiviral activity of baicalein against these viruses indicates that they may act on the same mechanism.

The antiviral experiment using ESG was carried out in mice, and ESG could effectively reduce viremia in the mouse model. It could significantly reduce the GETV load in the body within 14 days after infection and accelerate the removal of GETV. In addition, the effect of the early preventive medication is better than that of simultaneous medicines, which may be related to the particular blood concentration of the mice before GETV infection. It is suggested that ESG can be used to prevent and treat GETV. In addition, ESG can shorten the duration of GETV viremia. Our results lead us to infer that to reduce the time for the vaccine strain to carry the virus and reduce the risk of attenuated vaccine

mutation returning to strong, ESG can be used after inoculation with GETV-attenuated vaccine to facilitate the later development and application of Getah virus vaccine.

This study shows that the ESG can inhibit the attachment and entry of the virus into the cells *in vitro*, thereby inhibiting its infection of host cells. For the first time, the results show that the ESG can reduce the peak value of GETV viremia and the duration of low-level viremia in mice, and contribute to reducing the risk of virus transmission, which provides a specific reference for the prevention and control of GETV.

Data availability statement

The datasets presented in this study can be found in online repositories. The names of the repository/repositories and accession number(s) can be found in the article/supplementary material.

Ethics statement

The animal study was approved by Sichuan Agricultural University Animal Ethical and welfare Committee. The study was conducted in accordance with the local legislation and institutional requirements.

Author contributions

BL: Data curation, Writing – review & editing. YW: Validation, Writing – original draft. LS: Writing – review & editing. YC: Writing – original draft, Formal analysis, Software. ZX: Methodology, Supervision, Writing – review & editing. LZ: Supervision, Writing – review & editing.

Funding

The author(s) declare that financial support was received for the research and/or publication of this article. This work was supported by National Key Research and Development Program of China during the 14th Five-Year Plan: Research and Development of Key Technologies for the Prevention and Control of Important Diseases in Wild Animals (2024YFD1800102), the Sichuan Science and Technology Program Projects (Key R&D Projects) (No. 2023YFN0021), the Key K&D Program of Sichuan Science and Technology Plan (No. 2022YFN0007), and the National Pig Technology Innovation Center (NCTIP-MY23006).

Conflict of interest

The authors declare that the research was conducted in the absence of any commercial or financial relationships that could be construed as a potential conflict of interest.

Generative AI statement

The author(s) declare that no Gen AI was used in the creation of this manuscript.

Publisher's note

References

1. Sun Z, Wang M, Wang W, Li D, Wang J, Sui G. Getah virus capsid protein undergoes co-condensation with viral genomic RNA to facilitate virion assembly. *Int J Biol Macromol.* (2024) 265:130847. doi: 10.1016/j.ijbiomac.2024.130847

2. Wang A, Zhou F, Liu C, Gao D, Qi R, Yin Y, et al. Structure of infective Getah virus at 2.8 A resolution determined by cryo-electron microscopy. *Cell Disc.* (2022) 8:12. doi: 10.1038/s41421-022-00374-6

3. Bannai H, Ochi A, Nemoto M, Tsujimura K, Yamanaka T, Kondo T. A 2015 outbreak of Getah virus infection occurring among Japanese racehorses sequentially to an outbreak in 2014 at the same site. *BMC Vet Res.* (2016) 12:98. doi: 10.1186/s12917-016-0741-5

4. Yang T, Li R, Hu Y, Yang L, Zhao D, Du L, et al. An outbreak of Getah virus infection among pigs in China, 2017. *Transbound Emerg Dis.* (2018) 65:632–7. doi: 10.1111/tbed.12867

5. Jiao H, Yan Z, Zhai X, Yang Y, Wang N, Li X, et al. Transcriptome screening identifies TIPARP as an antiviral host factor against the Getah virus. *J Virol.* (2023) 97:591. doi: 10.1128/jvi.00591-23

6. Lu G, Chen R, Shao R, Dong N, Liu W, Li S. Getah virus: an increasing threat in China. *J Infect.* (2020) 80:350–71. doi: 10.1016/j.jinf.2019.11.016

7. Ren T, Liu M, Zhou L, Zhang L, Qin Y, Ouyang K, et al. A recombinant Getah virus expressing a GFP gene for rapid neutralization testing and antiviral drug screening assay. *Virology.* (2024) 598:110174. doi: 10.1016/j.virol.2024.110174

8. Yingrui W, Zheng L, Guoyan L, Hongjie W. Research progress of active ingredients of *Scutellaria baicalensis* in the treatment of type 2 diabetes and its complications. *Biomed Pharmacother.* (2022) 148:112690. doi: 10.1016/j.biopha.2022.112690

9. Wen Y, Wang Y, Zhao C, Zhao B, Wang J. The pharmacological efficacy of baicalin in inflammatory diseases. *Int J Mol Sci.* (2023) 24:9317. doi: 10.3390/ijms24119317

10. Chang W, Wang J, Wu F, Zhang H, Yang M. Antiviral activity and underlying mechanisms of baicalin against porcine reproductive and respiratory syndrome virus *in vitro*. *Microb Pathog.* (2024) 193:106712. doi: 10.1016/j.micpath.2024.106712

11. Feng H, Zhang K, Zhang K, Guo Z, Liu Q, Wang L, et al. Antiviral activity and underlying mechanisms of baicalin against avian infectious bronchitis virus *in vitro*. *Avian Pathol.* (2022) 51:574–89. doi: 10.1080/03079457.2022.2109453

12. Moghaddam E, Teoh BT, Sam SS, Lani R, Hassandarvish P, Chik Z, et al. Baicalin, a metabolite of baicalein with antiviral activity against dengue virus. *Sci Rep.* (2014) 4:5452. doi: 10.1038/srep05452

13. Niu Q, Zhou C, Li R, Guo J, Qiao S, Chen XX, et al. Proteomic analysis reveals the antiviral effects of baicalin on pseudorabies virus. *Int J Biol Macromol.* (2024) 277:134149. doi: 10.1016/j.ijbiomac.2024.134149

14. Farshadpour F, Gharibi S, Taherzadeh M, Amirinejad R, Taherkhani R, Habibian A, et al. Antiviral activity of Holothuria sp. a sea cucumber against herpes simplex virus type 1 (HSV-1). *Eur Rev Med Pharmacol Sci.* (2014) 18:333—7.

15. Oo A, Teoh BT, Sam SS, Bakar SA, Zandi K. Baicalein and baicalin as Zika virus inhibitors. *Arch Virol.* (2019) 164:585–93. doi: 10.1007/s00705-018-4083-4

16. Chakraborty R, Bhattacharje G, Baral J, Manna B, Mullick J, Mathapati BS, et al. *In-silico* screening and *in-vitro* assay show the antiviral effect of Indomethacin against SARS-CoV-2. *Comput Biol Med.* (2022) 147:105788. doi: 10.1016/j.compbiomed.2022.105788

17. Wu Y, Gao X, Kuang Z, Lin L, Zhang H, Yin L, et al. Isolation and pathogenicity of a highly virulent group III porcine Getah virus in China. *Front Cell Infect Microbiol.* (2024) 14:1494654. doi: 10.3389/fcimb.2024.1494654

18. Carey BD, Bakovic A, Callahan V, Narayanan A, Kehn-Hall K. New World alphavirus protein interactomes from a therapeutic perspective. *Antiviral Res.* (2019) 163:125–39. doi: 10.1016/j.antiviral.2019.01.015

19. Oo A, Rausalu K, Merits A, Higgs S, Vanlandingham D, Bakar SA, et al. Deciphering the potential of baicalin as an antiviral agent for Chikungunya virus infection. *Antiviral Res.* (2018) 150:101–11. doi: 10.1016/j.antiviral.2017.12.012

20. Hassandarvish P, Rothan HA, Rezaei S, Yusof R, Abubakar S, Zandi K. *In silico* study on baicalein and baicalin as inhibitors of dengue virus replication. *RSC Adv.* (2016) 6:31235–47. doi: 10.1039/C6RA00817H

frontiers | Frontiers in Veterinary Science

TYPE Original Research
PUBLISHED 14 May 2025
DOI 10.3389/fvets.2025.1603107

OPEN ACCESS

EDITED BY
Dongan Cui,
Lanzhou University, China

REVIEWED BY
Xuebing Wang,
Henan Agricultural University, China
Xia Lining,
Xinjiang Agricultural University, China
Panpan Liu,
Ningxia University, China

*CORRESPONDENCE
Yucheng He
heyucheng@gxu.edu.cn
Jiakang He
jkhe@gxu.edu.cn

RECEIVED 31 March 2025
ACCEPTED 28 April 2025
PUBLISHED 14 May 2025

CITATION
Xiang Y, Li Z, Liu C, Wei Z, Mo X, Zhong Y, He R, Liang Z, He Y and He J (2025) *Pulsatilla chinensis* extract alleviate *Staphylococcus aureus* induced mastitis in mice by regulating the inflammatory response and gut microbiota.
Front. Vet. Sci. 12:1603107.
doi: 10.3389/fvets.2025.1603107

Pulsatilla chinensis extract alleviate *Staphylococcus aureus* induced mastitis in mice by regulating the inflammatory response and gut microbiota

Yifei Xiang[1], Ziyang Li[1], Chengzhi Liu[1], Zhifei Wei[1], Xuelian Mo[1], Yawen Zhong[1], Ruini He[1], Zhengmin Liang[1,2,3], Yucheng He[1,2,3]* and Jiakang He[1,2,3]*

[1]College of Animal Science and Technology, Guangxi University, Nanning, China, [2]Guangxi Key Laboratory of Animal Breeding, Disease Control and Prevention, Nanning, China, [3]Guangxi Zhuang Autonomous Region Engineering Research Center of Veterinary Biologics, Nanning, China

Introduction: Subclinical mastitis (SCM) caused by *Staphylococcus aureus* (*S. aureus*) is widely prevalent in cattle herds around the world, causing huge losses to the dairy cattle farming industry and dairy product production. Currently, the use of hormones and antibacterial drugs is the most effective treatment method. However, issues such as the increase in drug resistance and residues in dairy products limit their further application. In this study, based on the response surface optimization method, *Pulsatilla chinensis* extract (PCE) was prepared from *Pulsatilla chinensis* using ethanol as the medium in a simple, efficient and low-cost way. Its functions were verified both *in vitro* and *in vivo*.

Methods and results: Through the Oxford cup method, MIC/MBC and co-culture experiments, it was demonstrated that PCE had a good inhibitory effect on the proliferation of four strains of *S. aureus in vitro*. The *in vivo* toxicity evaluation proved that PCE had high oral safety. In addition, we screened and established a mastitis model platform for lactating mice to evaluate the expected *in vivo* effects of PCE. The results showed that pre-treatment with PCE for 7 days significantly reduced the bacterial load and the levels of inflammatory factors (IL-6, IL-1β, TNF-α, MPO) in the mammary gland and blood induced by *S. aureus*, improved the pathological damage of the mammary gland tissue, and alleviated the occurrence of mastitis in mice by regulating the intestinal microbiota.

Conclusion: These results verify that PCE can be used to treat mastitis caused by *S. aureus*, and thus it is expected to become an excellent alternative to hormones and antibacterial drugs.

KEYWORDS

subclinical mastitis, *Pulsatilla chinensis* extract, *Staphylococcus aureus*, mouse mastitis model, gut microbiota

1 Introduction

Subclinical mastitis (SCM) is a major industrial bottleneck that restricts the development of the global dairy cow breeding industry and the dairy product industry (1–3). Owing to the lack of obvious symptoms, it can continuously spread among herds and is not easily detected, which consequently leads to a reduction in milk production, a decline in milk quality, culling

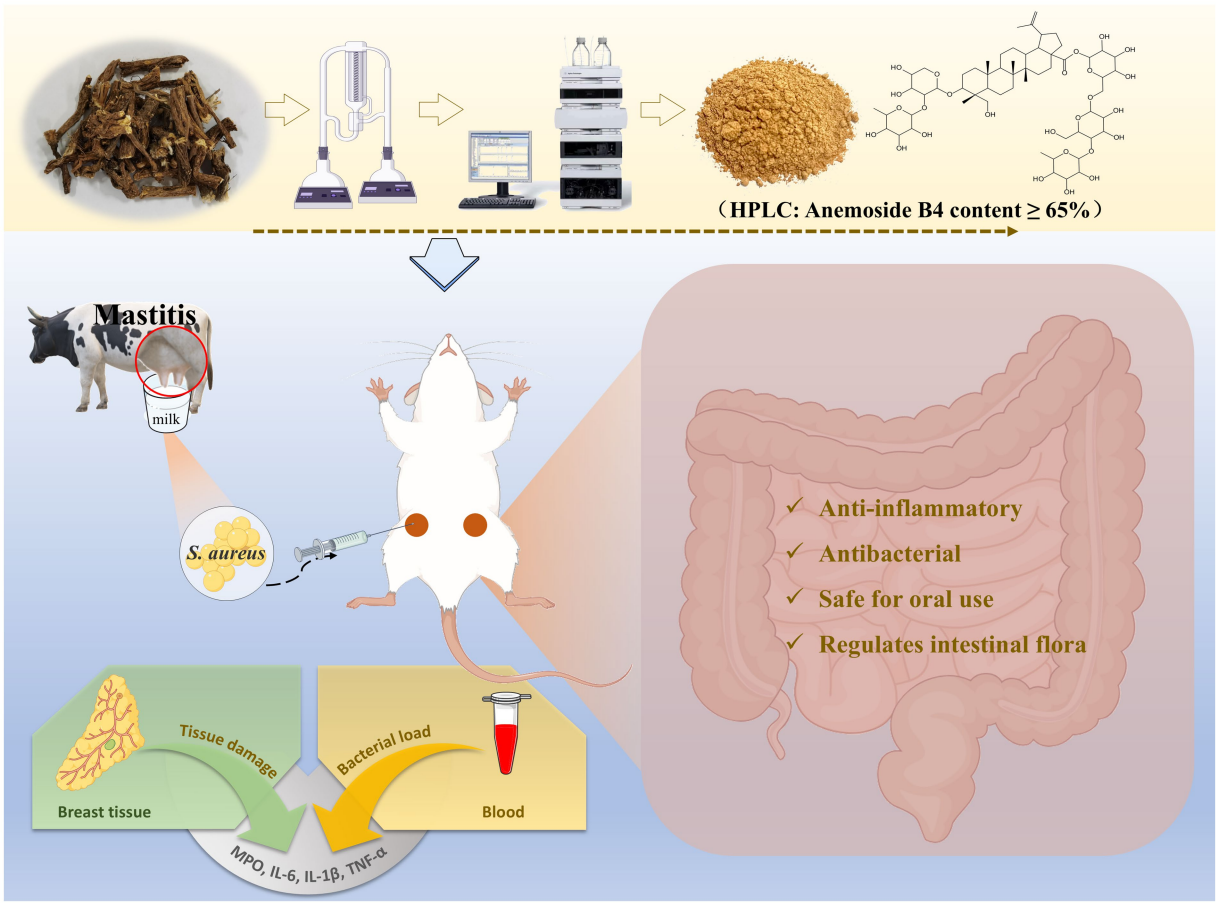

GRAPHICAL ABSTRACT

of cows, and the occurrence of secondary diseases (4). According to incomplete statistics, the economic losses caused by SCM worldwide amount to as many as 35 billion US dollars every year (5, 6).

Infection by pathogenic microorganisms is an important cause of SCM (5, 7). On the one hand, pathogenic bacteria invade the mammary gland, multiply in large numbers and launch attacks, which then trigger an outbreak of inflammation in the mammary region and even systemic inflammatory responses (8). On the other hand, an imbalance in the intestinal flora further exacerbates the difficulty in treating SCM (1, 7). *Staphylococcus aureus* (*S. aureus*) is globally recognized and the most common pathogen for SCM (9), accounting for 40% or more of the available mastitis data (10, 11). Owing to its characteristics, such as extremely high infectivity and long disease course, preventing and controlling dairy cow mastitis has always been difficult. Hormones and antibacterial drugs are the primary solutions for SCM (12). However, long-term or irrational use has led to multiple instances of drug resistance in bacteria, drug residues in milk, and imbalances in the intestinal flora (13, 14), which seriously threaten human public health (dairy products) (15, 16). Therefore, finding new strategies or substitutes for the prevention and treatment of SCM has become a major requirement for overcoming the bottleneck in the development of the dairy cow breeding industry and the dairy product industry (5).

Natural herbal medicines have gradually become important alternative strategies for disease prevention and control because of their advantages, such as high safety, low tendency to generate drug resistance, and multitarget prevention and treatment (17). The development of drugs for the prevention and treatment of dairy cow mastitis from natural medicinal resources has become a new direction for the healthy breeding of dairy cows. *Pulsatilla chinensis* has multiple pharmacological effects, such as anti-inflammatory, antioxidant, and antipathogenic effects (18). However, the antibacterial ability of *Pulsatilla chinensis* and its effect on dairy cow mastitis remain unclear.

In this study, we obtained *Pulsatilla chinensis* extract (PCE) with a relatively high content through a minimalist extraction process. We first demonstrated that PCE has a good inhibitory effect on the proliferation of *S. aureus in vitro*. Through the establishment of a mouse mastitis model during the lactation period, the antibacterial, anti-inflammatory, and mammary gland damage-alleviating effects of PCE *in vivo* were subsequently verified. Finally, the beneficial effect of PCE on the coordination of the intestinal flora was emphasized. This study provides a safer and beneficial alternative treatment strategy for the prevention and treatment of SCM and other diseases caused by *S. aureus*.

2 Materials and methods

2.1 Ethics statement

The SPF experimental KM mice were all sourced from the Laboratory Animal Center of Guangxi Medical University

(Certificate of Conformity: scxk (Gui) 2020–0003). All experiments were approved and supported by the Animal Research Ethics Committee of Guangxi University (Approval No. GXU-2022-326). All animal experiments were carried out in accordance with the "Guidelines for the Care and Use of Laboratory Animals" published by the National Institutes of Health.

2.2 Process optimization and preparation of the PCE

There is a close connection between different extraction factors and the content of the target components to be extracted. First, several portions of *Pulsatilla chinensis* medicinal materials (50 g each) were weighed in parallel. The quality of the medicinal materials was tested and confirmed to meet the requirements; that is, the content of *Anemoside B4* in the medicinal materials was ≥ 4.6%. In accordance with HPLC-SPD 20A (Shimadzu (Shanghai) Global Laboratory Consumables Co., Ltd., Shanghai, China), the following variables were investigated: extraction time (0.5 h, 1 h, 1.5 h, 2 h, 3 h), extraction time (once, twice, three times, four times, five times), ethanol volume (50, 60, 70, 80, 90%), solid–liquid ratio (1:5, 1:10, 1:15, 1:20, 1:25), extraction temperature (50°C, 60°C, 70°C, 80°C, 90°C), and particle size of the medicinal materials (whole plant, decoction pieces, 30 mesh, 50 mesh, 80 mesh). Finally, the extracted liquid was filtered and then concentrated under reduced pressure to 50 mL. After that, the content was detected by HPLC.

The three factors with the most significant influence among the above variables were screened out for the response surface methodology (RSM) experiment. The percentage of *Anemoside B4* in the extract (Y) was taken as the response value of the response surface optimization curve. Design Expert 10 was used to design the experiment. According to the 17 schemes simulated by the three factors and three levels designed in the experiment, a response surface optimization curve analysis experiment was carried out to obtain the optimal extraction process and prepare the PCE for subsequent studies.

2.3 *In vitro* investigation of the inhibitory effect of PCE on *Staphylococcus aureus*

Three *S. aureus* model strains, including CMCC (B) 26003 (National Center for Medical Culture Collections, Beijing, China), ATCC 25904, and USA 400 (feed from the Department of Veterinary Pharmacology, Jilin University, Jilin, China), and one *S. aureus* clinical isolate, GXU 2017 (isolated, identified and preserved in Guangxi Key Laboratory of Animal Breeding Disease Control and Prevention, Nanning, China), were used in this *in vitro* study, cultured at a constant temperature of 37°C for 12 h and configured into bacterial suspensions for backup.

2.3.1 Determination of the inhibition zone

Different gradients of bacterial suspensions (1×10^6, 1×10^7, and 1×10^8 CFU/mL) were prepared, and then 100 μL of each bacterial suspension was spread onto the bacterial culture plates. Four Oxford cups were placed on each plate and then injected with 100 μL of PCE solution at concentrations of 0 (control), 31.25, 125 and 500 mg/mL. The antibacterial activity was evaluated by measuring the diameter of the inhibition zone of the PCE against *S. aureus*.

2.3.2 Determination of the minimum inhibitory concentration (MIC) and minimum bactericidal concentration (MBC)

100 μL of *S. aureus* suspension (1×10^7 CFU/mL) was added to each well of a 96-well plate, followed by the addition of different concentrations of PCE solutions such that the final concentration of PCE in each well was 250, 125, 62.5, 31.25, 15.63, 7.81, 3.91, 1.95, 0.98, or 0.49 mg/mL. The plate was incubated at a constant temperature of 37°C for 24 h. The wells with clear liquid were judged as the MIC of PCE against *S. aureus*. Subsequently, 100 μL of the mixture was removed from all the clear wells and spread on culture dishes for further incubation. The lowest concentration at which almost no visible colonies grew on the culture dishes was judged as the MBC.

2.3.3 Growth curve of cocultures of PCE and *Staphylococcus aureus*

Solutions of PCE at concentrations of 1/4 MIC, 1/2 MIC, MIC, 2 MIC, and 4 MIC were cocultured with *S. aureus* (1×10^7 CFU/mL) (at 37°C, 180 rmp). Moreover, a blank control group (TSB) and a positive control group (*S. aureus* + TSB) were set up. Then, 200 μL of the coculture mixture was added at 0, 1, 2, 3, 4, 5, 6, 8, 10, and 12 h, and the optical density (OD) values were measured at 600 nm. Finally, the growth curve of the coculture of PCE and *S. aureus* was plotted on the basis of these measured OD values.

2.4 Establishment of a mouse mastitis model

Forty 7-week-old male KM mice and eighty 7-week-old female KM mice were housed in a single mouse cage at a male-to-female ratio of 1:2 and were allowed to mate freely to obtain pregnant female mice. Considering animal welfare, the experiment was carried out on the 15th day after the female mice gave birth (by which time the suckling mice had already acquired the ability to survive independently) (11).

The 80 female mice were divided into two physiological cycles, namely, the lactation period and the weaning period. For the lactation period, the maternal mice were separated from the suckling mice 3 h before the experiment (19), whereas for the weaning period, the maternal mice were separated from the suckling mice 5 days before the experiment. There were 40 female mice in each physiological cycle, and each cycle was randomly divided into a control group ($n = 8$) and four gradient *S. aureus* model groups ($n = 8$, with concentrations of 1×10^5, 1×10^6, 1×10^7, and 1×10^8 CFU/mL). Referencing the previous method and optimizing it (11), female mice were anesthetized after a 12-h fasting period. The breasts and the surrounding skin were disinfected with 75% alcohol. The mammary ducts of the fourth pair of nipples were exposed. A flat-tip microsyringe was used to inject 50 μL of *S. aureus* suspension into the mammary ducts of the mice in the model group, while the same volume of normal saline was injected into those in the Control group. Gentle massage was performed to promote the uniform distribution of the injected liquid. After 24 h, blood and mammary gland tissues were collected and stored at −80°C.

2.5 Investigation of the oral safety of PCE

Sixty 5-week-old KM mice (with an equal number of males and females) were provided with free access to water and were fed standard feed according to the standard of 10–15% body weight. Six gradient groups were randomly set up according to the dose of PCE ($n = 10$, with an equal number of females, and the experiment was carried out in separate cages), namely, 0 (Control), 1,250, 2,500, 5,000, 10,000 and 20,000 mg/kg. After a single intragastric administration, the clinical symptoms, food intake, water intake and average weight gain of the mice were continuously observed for 7 days. After the experiment, the mice were sacrificed, and pathological changes in the internal organs were observed. The aim of this study was to investigate the oral safety of PCE.

2.6 Control of mastitis in lactating mice

Sixty lactating female mice after giving birth were randomly divided into six groups, namely, the Control group ($n = 10$, continuously gavaged with sterile water for 7 days and then injected with 0.9% NaCl into the milk ducts on the 7th day), the *S. aureus* group ($n = 10$, continuously gavaged with sterile water for 7 days and then injected with 1×10^7 CFU/mL *S. aureus* suspension into the milk ducts on the 7th day), the dexamethasone (DEX) control group ($n = 10$, continuously gavaged with 5 mg/kg of DEX for 7 days and then injected with 1×10^7 CFU/mL *S. aureus* suspension into the milk ducts on the 7th day) (20, 21), and the PCE 100, 200, 400 mg/kg dose groups ($n = 10$, continuously gavaged with different doses of PCE for 7 days and then injected with 1×10^7 CFU/mL *S. aureus* suspension into the milk ducts on the 7th day). The doses of PCE were determined with reference to previous reports and preliminary experiments (22). Blood and mammary gland tissues were collected and stored at −80°C.

2.7 Bacterial load

Aseptic procedures were performed with a super clean bench. After the mice were anaesthetized, blood was collected from the eyeballs. The first 3 drops of blood were placed into an anticoagulant tube and diluted 5 times the volume of sterile normal saline. Then, 100 μL of the diluted sample was spread on nutrient agar medium. The mixture was incubated at a constant temperature of 37°C for 24 h, and the bacterial load in the blood was calculated.

Ten milligrams of mammary gland tissue was homogenized with 100 times the volume of sterilized normal saline. One hundred microlitres of the tissue homogenate was spread on nutrient agar medium. The mixture was incubated at a constant temperature of 37°C for 24 h, and the bacterial load in the mammary gland tissue was calculated.

2.8 Determination of inflammatory factors

The protocol was performed in accordance with the requirements of the instruction manual. Enzyme-linked immunosorbent assay (ELISA) kits were used to evaluate the levels of interleukin-6 (IL-6), interleukin-1β (IL-1β) and tumor necrosis factor alpha (TNF-α) in blood and mammary gland tissues (Shanghai Enzyme Linked Biotechnology Co., Ltd., Shanghai, China).

2.9 Investigation of myeloperoxidase (MPO)

In accordance with the requirements of the kit instruction manual, serum and mammary gland homogenates were collected to detect the expression level of myeloperoxidase (MPO) (NanJing JianCheng Bioengineering Institute, Nanjing, China).

2.10 Observation and scoring of mammary gland tissue pathology

The isolated mammary gland tissues were rinsed with normal saline to reduce the stagnation of milk and then placed in 10% formalin fixative for 24 h. The tissues were dehydrated with gradient ethanol and then embedded in paraffin blocks. The paraffin blocks containing the tissues were cut into slices with a thickness of 3 μm and incubated at 65°C for 4.5 h. The samples were subsequently dewaxed and rehydrated. Finally, the tissues were stained with dyes, and the slides were mounted. The prepared hematoxylin–eosin (HE)-stained pathological sections were used for histological observation and scoring of the mammary gland tissues (19).

2.11 DNA extraction and microbiomic analysis of intestinal microorganisms

The contents of the mouse caecum were collected in sterile freezing tubes, snap-frozen in liquid nitrogen and stored, and total DNA was extracted from the contents of the caecum using a DNA extraction kit (AU46111-96, BioTeke, China). Total DNA was amplified by PCR via the primers 341F/805R (341F: 5′-CCTACGGGNGGCWGCAG-3′; 805R: 5′-GACTACHVGGTATCTAATCC-3′; GACTACHVGGTATCTAATCC-3′). PCR amplification of total DNA was performed via the primers 341F/805R (341F: 5′-CCTACGGNGGCWGCAG-3′; 805R: 5′-CACTACHVGGTATCTAATCC-3′), and the resulting PCR products were purified, quantified and analyzed sequentially. Sequencing services were provided by LC-Bio Technology Co., Ltd., Hangzhou, China.

2.12 Data analysis

Each experiment was replicated in triplicate and the data derived therefrom were collected and calculated with Excel. Unless otherwise explicitly stated, all data were tested for normality distribution using GraphPad Prism 10.1.2 (GraphPad Software Inc., La Jolla, CA). In the case of normally distributed data, one-way ANOVA and Tukey's multiple comparison test were employed to analyze and compare the significance of the experimental results, followed by statistical analysis and graphing. A p-value of less than 0.05 was regarded as statistically significant.

3 Results

3.1 Optimization of the extraction process and preparation of the PCE by response surface methodology

Taking the content of *Anemoside B4* in the PCE as the standard, through a climbing test, it was found that the extraction time (Figure 1B), number of extractions (Figure 1C), and volume of ethanol (Figure 1D) had the most significant impacts on the target components in the PCE. Seventeen RSM tests were carried out on the above three factors and the content (%) of *Anemoside B4* (Tables 1, 2).

Multiple regression analysis yielded a fitting equation ($Y = 29.62 + 1.07A + 2.08B + 1.86C + 0.38AB - 0.92\,AC + 0.91\,BC - 0.79A^2 - 2.59B^2 - 1.45C^2$). In the analysis of variance, the model was extremely significant ($p < 0.01$), and the lack of fit was not significant ($p > 0.05$) (Table 3), indicating that the results were reasonable and could be used for the analysis and prediction of the PCE content under multiple factors. As seen from the *F* values (Table 3), the number of extractions and the volume of ethanol had relatively large effects on the content of *Anemoside B4* in the PCE. In the plot of residuals versus predicted values, the data points showed a random distribution (Figure 1G), and in the normal probability plot, all the points were distributed on a straight line (Figure 1H), which could accurately reflect the authenticity of the experiment. The RSM is a three-dimensional spatial surface graph composed of three factors, namely, extraction time, the number of extractions, and the volume of ethanol. The steeper the slope is, the more significant the impact (Figures 1J–L). The contour plots all showed irregular ellipses (Figures 1M–O), so the interactions among the three factors were significant.

On the basis of the results of the climbing test and RSM, the optimal extraction process for determining the PCE was determined. The content of *Anemoside B4* in the PCE extract was quantified by HPLC as 31.15 (Table 4). One kilogram of *Pulsatilla chinensis* medicinal material was added, 10 times the amount of 75% ethanol was added, hot reflux extraction was performed at 80°C for 70 min, suction filtration was carried out, and the filtrate was temporarily preserved. The filtrate was extracted three times, combined, and then concentrated under reduced pressure to 1 L. After vacuum drying (at 70°C and 0.095 Mpa), it was processed into powder to obtain 255 g of PCE. Then, 1 g of PCE was equivalent to 4 g of the original medicinal material, and the content of *Anemoside B4* in the PCE powder was measured to be 65.17%.

3.2 *In vitro* bacteriostatic capacity of the PCE

The diameter of the inhibition zone of the PCE against different *S. aureus* strains was investigated by the Oxford cup method

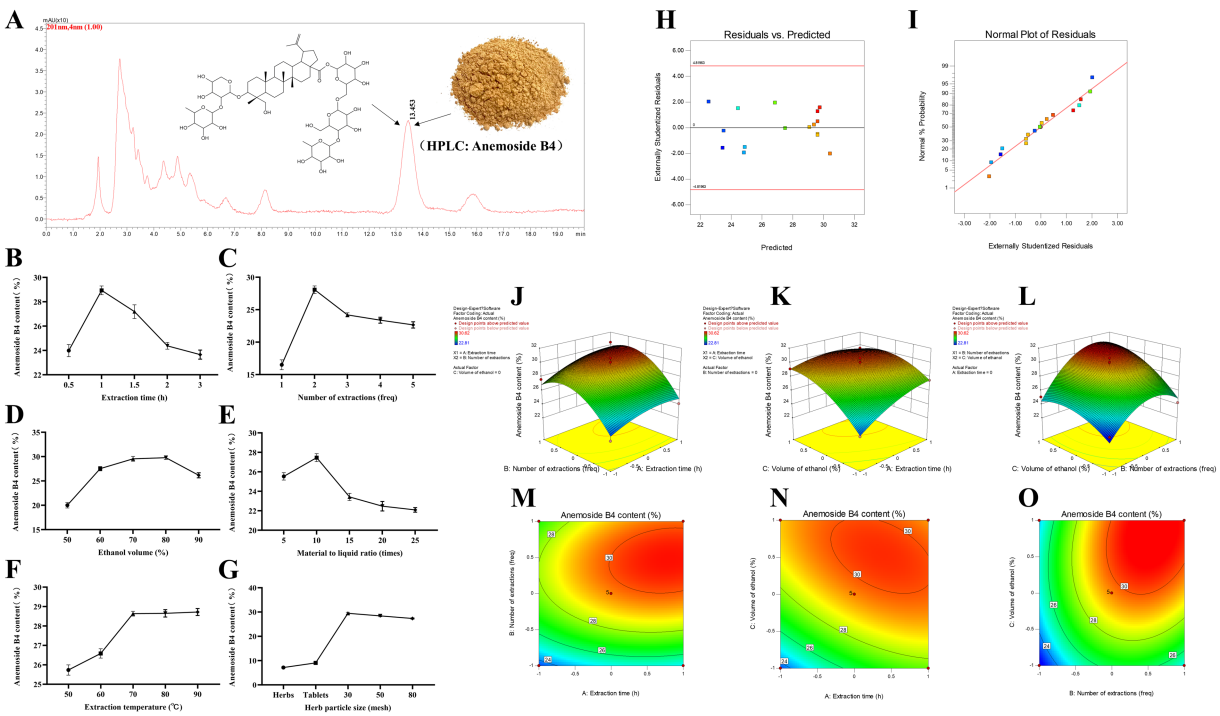

FIGURE 1
Process optimization and preparation of the PCE. **(A)** HPLC characterization and quantification. The mobile phase for HPLC was methanol and water (64:36), with isocratic elution, a flow rate of 1 mL/min, a column temperature of 30°C, an injection volume of 20 μL and a wavelength of 201 nm. **(B)** Extraction time. **(C)** Extraction times. **(D)** Ethanol volume. **(E)** Solid–liquid ratio. **(F)** Extraction temperature. **(G)** Particle size of medicinal materials. **(H)** Plot of the relationship between residuals and predicted responses. **(I)** Normal distribution plot of residuals. **(J)** Three-dimensional response surface plot of the extraction time (freq) and extraction time (h). **(K)** Three-dimensional response surface plot of ethanol volume (%) and extraction time (h). **(L)** Three-dimensional response surface plot of ethanol volume (%) and extraction time (freq). **(M)** Contour plot of extraction times (freq) and extraction times (h). **(N)** Contour plot of ethanol volume (%) and extraction time (h). **(O)** Contour plot of ethanol volume (%) and extraction time (freq).

10.3389/fvets.2025.1603107

TABLE 1 Response surface optimization test design scheme.

Level	Factors		
	A: Extraction time (h)	B: Number of extractions (freq)	C: Ethanol volume (%)
−1	0.5	1	60
0	1	2	70
1	1.5	3	80

TABLE 2 RSM multiple regression model design and results.

No.	A: Extraction time (h)	B: Number of extractions (freq)	C: Volume of ethanol (%)	*Anemoside B4* content (%)
1	0	0	0	29.19
2	−1	1	0	27.61
3	−1	0	1	29.11
4	0	1	1	29.66
5	0	0	0	30.04
6	−1	0	−1	23.41
7	0	−1	1	25.09
8	1	−1	0	24.10
9	0	0	0	29.13
10	1	0	1	29.51
11	0	0	0	30.62
12	0	1	−1	24.26
13	0	−1	−1	23.32
14	1	1	0	30.42
15	1	0	−1	27.50
16	−1	−1	0	22.81
17	0	0	0	29.13

(Figure 2A). When the concentration of *S. aureus* was 1×10^7 CFU/mL, the antibacterial effect was better, and the edge of the inhibition zone was clear. Therefore, a concentration of 1×10^7 CFU/mL was selected for subsequent studies. For the determination of the MIC and the MBC, the MIC values of PCE against *S. aureus* (1×10^7 CFU/mL) CMCC (B) 260,003, ATCC 25904, USA 400 and GXU 2017 were 31.25, 31.25, 15.625 and 62.5 mg/mL, respectively, and the MBC values were 31.25, 31.25, 31.25 and 62.5 mg/mL, respectively. The results revealed that when PCE was cocultured with *S. aureus*, it effectively inhibited the growth of different strains of *S. aureus* within 8 h (Figures 2B–E). The above results indicated that PCE exhibited favorable anti-*S. aureus* effects *in vitro*.

3.3 Establishment of a model of mastitis in *Staphylococcus aureus*-infected mice

To investigate the protective effect of PCE on mastitis, we examined mice in two physiological cycles, namely, the lactation and weaning periods, and established a mastitis model on the basis of their sensitivity to invasion by different concentrations of *S. aureus* (GXU2017) (Figure 3). Compared with those in the weaning period, the bacterial loads in both mammary gland tissues (Figure 3B) and blood (Figure 3C), which exhibited a concentration-dependent pattern, were greater in the lactating period than in the weaning period, and the bacterial load in mammary glands was much greater than that in blood. Compared with those in the control group, the expression levels of IL-6 (Figures 3D,E) and MPO (Figures 3F,G) in the serum and mammary gland tissues of lactating mice were significantly greater ($p < 0.01$). In contrast, the expression of these indicators in weaning mice was significant only under high-concentration bacterial infection. Histological analysis demonstrated that (Figure Compared with those in the weaning period), the mammary gland tissue of lactating mice presented larger-volume acini, thicker acinar walls and a more complete honeycomb structure, more pronounced inflammatory cell infiltration, acinar wall hyperplasia and more severe pathological alterations. In conclusion, an experimental surrogate model of dairy cow mastitis was established by infecting lactating mice with 1×10^7 CFU/mL *S. aureus* for 24 h.

3.4 Oral safety of the PCE

Before a drug is taken orally, its safety needs to be determined. Therefore, we conducted a 7-day oral safety evaluation. When the oral concentration of PCE was less than 20,000 mg/kg, there was no significant difference ($p > 0.05$) in water intake (Figure 4A) or weight gain (Figure 4B) between the test groups and the control group. No death or poisoning phenomenon occurred, and the mice were in a good mental state with a normal appetite and thirst. No obvious pathological changes were found in the internal organs during necropsy. In summary, PCE has excellent oral safety *in vivo*.

3.5 Protective effect of PCE against mastitis in female mice

To evaluate the effect of PCE in the mouse mastitis model, *S. aureus* was inoculated into the mammary ducts after continuous intragastric administration of PCE for 7 days (Figure 5A). Studies have shown that pretreatment with PCE (100, 200, or 400 mg/kg) can significantly reduce the excessive expression of bacteria (Figures 5B,C) and inflammatory factors (IL-6, IL-1β, TNF-α and MPO) (Figures 5D–K) in mammary gland tissues and blood ($p < 0.01$). Histological analysis revealed that the invasion of *S. aureus* into the mammary gland damaged the tissue structure of the mammary gland and induced a large number of infiltrating inflammatory cells and colloid secretions in the alveolar cavity (Figures 5L,M). In mice pretreated with PCE, the tissue structure of the mammary gland was relatively intact and clear, and only a small number of inflammatory cells adhered to the alveolar walls and around the lobular ducts. Overall, the 200 mg/kg dose had the greatest effect. These results indicate that oral administration of PCE can significantly reduce the bacterial load and inflammatory response in blood and mammary gland tissues induced by *S. aureus* and alleviate damage to mammary gland tissues.

TABLE 3 Response surface model ANOVA.

Source	Sun of squares	df	Mean square	*F* value	*p*-value Prob > *F*	Salience
Model	122.03	9	13.56	16.28	0.0007	Significant
A-Extraction time	9.22	1	9.22	11.07	0.0126	
B- Number of extractions	34.57	1	34.57	41.50	0.0004	
C-Ethanol volume	27.68	1	27.68	33.23	0.0007	
AB	0.58	1	0.58	0.69	0.4325	
AC	3.40	1	3.40	4.09	0.0829	
BC	3.29	1	3.29	3.95	0.0871	
A^2	2.65	1	2.65	3.18	0.1176	
B^2	28.32	1	28.32	34.00	0.0006	
C^2	8.80	1	8.80	10.57	0.0140	
Residual	5.83	7	0.83			
Lack of fit	3.99	3	1.33	2.89	0.1660	Not significant
Pure error	1.84	4	0.46			
Cor total	127.86	16				

TABLE 4 Process validation results.

No.	*Anemoside B4* content (%)	Average content (%)
1	31.00	
2	31.31	31.15
3	31.12	

3.6 Beneficial effects of PCE on the intestinal flora

We investigated the microbiome of the caecal contents of the mice. Principal coordinate analysis (PCoA) revealed that the microbiota structures of the CON group and the PCE group were relatively similar, while there were significant differences in the microbiota structures between the DEX group and the Model group compared with those of the CON group (Figure 6B). Therefore, it is unreasonable to simply determine whether it is beneficial or harmful to health on the basis solely of the increase or decrease in the number of amplicon sequence variants (ASVs). The number of ASVs in the gut microbiota represented only a quantitative change, as demonstrated by the greater number of ASVs in the DEX group and the Model group (Figure 6A). The species richness at the phylum level is shown in Figure 6C. *Firmicutes* and *Bacteroidota* constituted the main framework of species at the phylum level (accounting for ≥80%). *Firmicutes* are mainly involved in energy acquisition, intestinal homeostasis, nutrient absorption, and immune regulation, while *Bacteroidota* are mainly involved in food digestion, nutrient synthesis, intestinal immunity, and body metabolism. The ratio of the two is considered a key indicator of intestinal health status. They work together to maintain the balance of the intestinal microecology. An imbalance of either one may lead to intestinal dysfunction, which in turn can trigger a variety of health problems (23). A significant difference analysis at the phylum level revealed that, compared with those in the CON group, the relative abundances of *Proteobacteria*, *Deferribacterota* and *Planctomycetota* in the intestines of the Model and DEX groups were significantly greater (Figure 6D). Moreover, the PCE group presented a framework similar to that of the control group at the phylum level. Interestingly, *Planctomycetota* appeared only in the intestines of the mice in the Model group and the DEX group but not in those of the other two groups. The proportional and chord diagrams (Figure 6E) more clearly demonstrated the distribution proportions of the dominant microbiota in each group at the phylum level. In addition, through linear discriminant analysis effect size (LEfSe) analysis, significant differences in the species of the gut microbiota among the different treatment groups of mice were detected (Figures 6F,G). Notably, both the DEX group (purple) and the Model group (green) presented a large number of species with significant differences, and these differences may affect the health of the animals. A correlation clustering-labeled heatmap was used to evaluate the correlations between the gut microbiota and multiple phenotypes in mammary gland tissues (Figure 6H) and blood (Figure 6I). The abundances of *Actinobacteriota* and *Bacteroidota* were more negatively correlated with the relevant phenotypes ($p < 0.05$). Therefore, these microbiota may have inhibited the occurrence of mastitis to some extent. However, the abundances of *Firmicutes*, *Fusobacteriota* and *Proteobacteria* were more positively correlated with the relevant phenotypes ($p < 0.05$), indicating that they promoted the occurrence of mastitis. These differential results are expected to become biomarkers for the clinical diagnosis of mastitis.

4 Discussion

Although the pathogenesis of bovine mastitis has become increasingly clear (5, 24), there are still no effective preventive and control measures available at present to alleviate the spread of this disease. Current treatments are still limited to approaches such as hormone and antibacterial drug therapies, supportive (severe cases) treatments, and surgical interventions (25). Surveys have indicated that

10.3389/fvets.2025.1603107

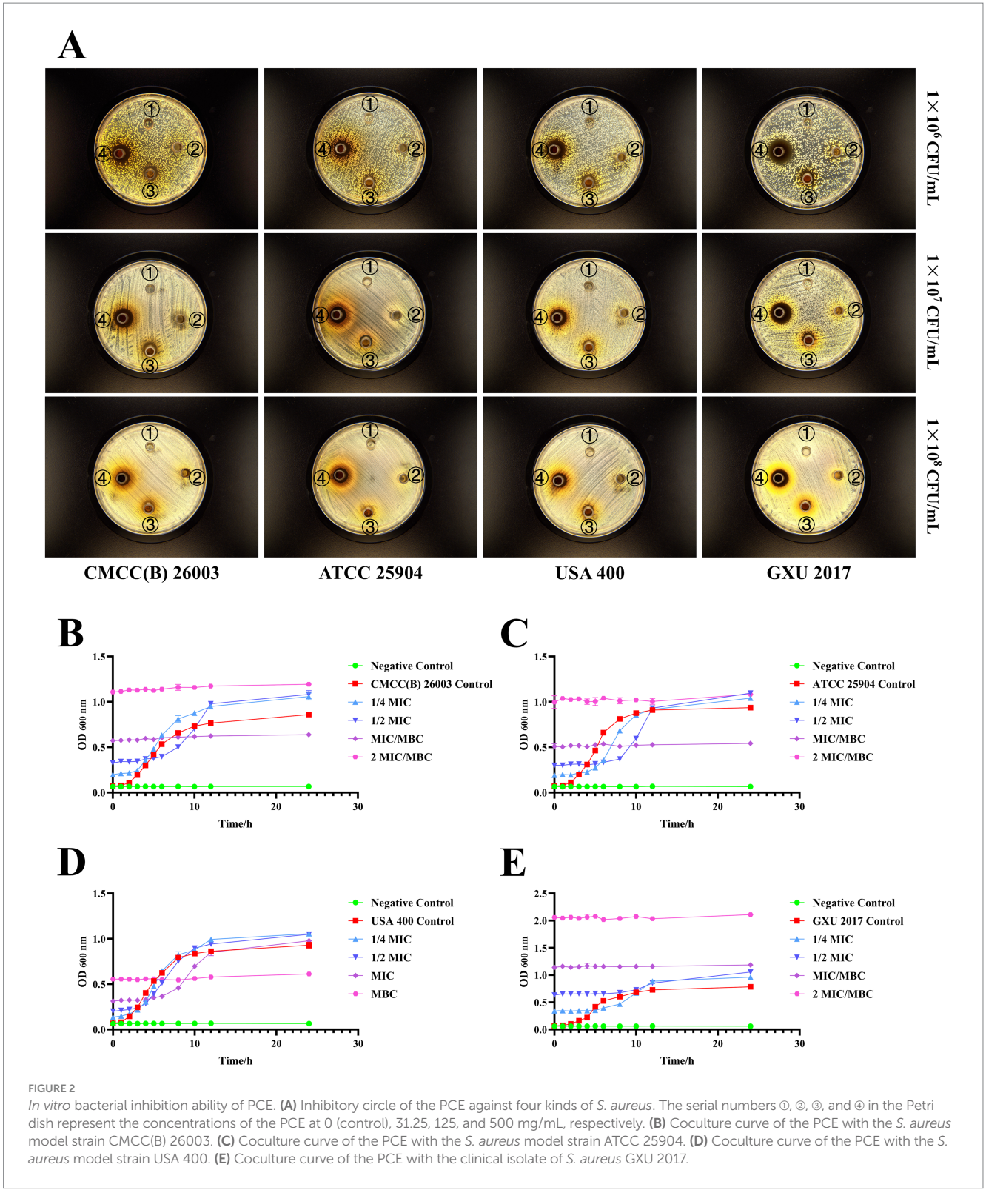

FIGURE 2
In vitro bacterial inhibition ability of PCE. **(A)** Inhibitory circle of the PCE against four kinds of *S. aureus*. The serial numbers ①, ②, ③, and ④ in the Petri dish represent the concentrations of the PCE at 0 (control), 31.25, 125, and 500 mg/mL, respectively. **(B)** Coculture curve of the PCE with the *S. aureus* model strain CMCC(B) 26003. **(C)** Coculture curve of the PCE with the *S. aureus* model strain ATCC 25904. **(D)** Coculture curve of the PCE with the *S. aureus* model strain USA 400. **(E)** Coculture curve of the PCE with the clinical isolate of *S. aureus* GXU 2017.

60–70% of all hormones and antibacterial drugs on dairy farms are used for the prevention and treatment of mastitis (5). This irrational use of drugs has promoted the emergence of multidrug resistance in bacteria, mainly *S. aureus* (26). Moreover, most chemical drugs are restricted by withdrawal periods, and the spread and infection of bacterial diseases increase significantly during the withdrawal period (27). When the withdrawal period is unstable, drug residues in milk pose a threat to human health and present hidden dangers for disease treatment (28). In the previous few years, the number of human deaths caused by drug resistance exceeded one million cases. Therefore, it has become increasingly important to search for and develop natural alternatives to address diseases with complex aetiologies (29).

10.3389/fvets.2025.1603107

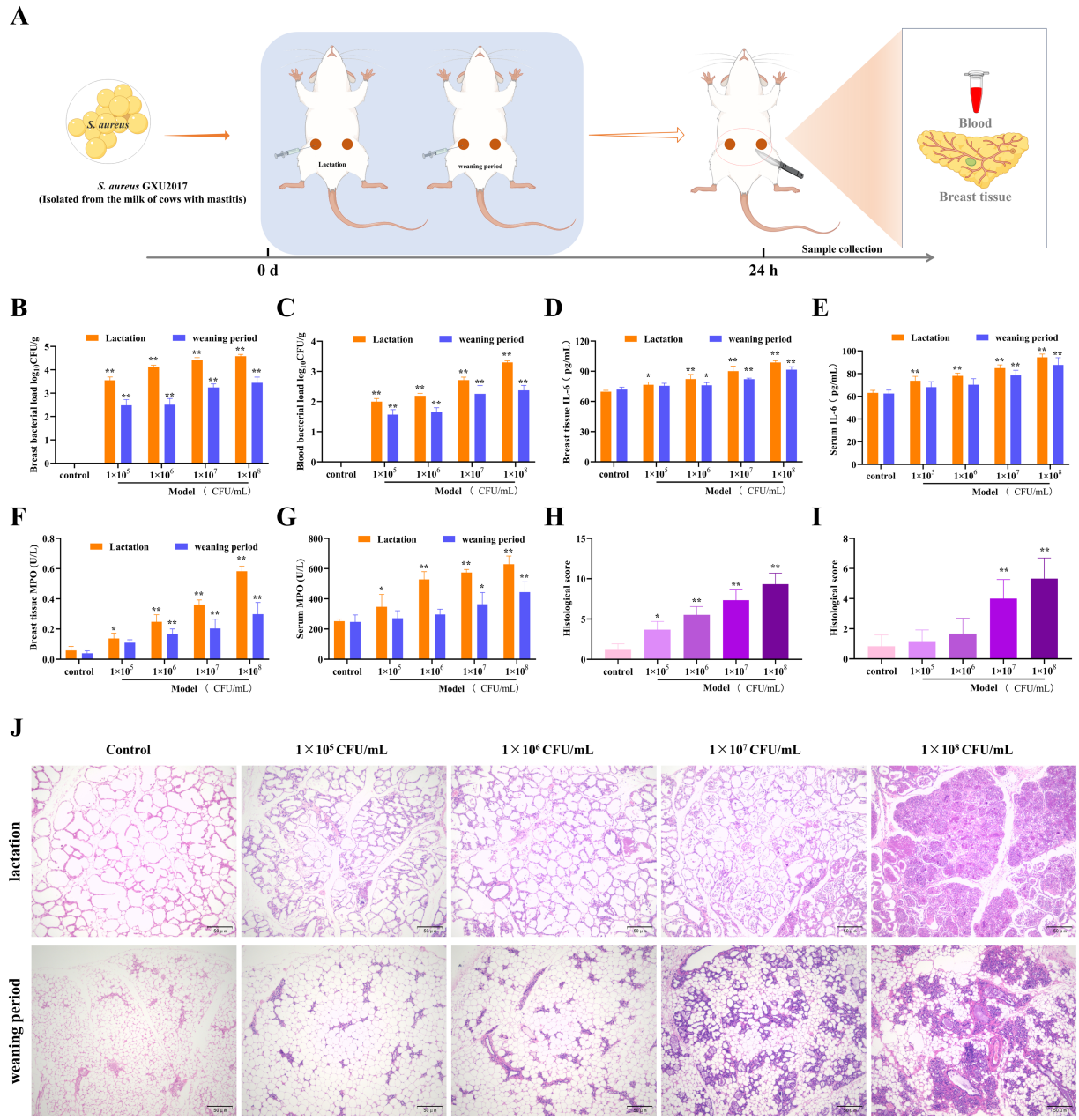

FIGURE 3
Establishment of the mouse mastitis model. **(A)** Schematic diagram of the establishment of the mouse mastitis model. **(B,C)** The load of *S. aureus* in mammary gland tissue **(B)** and blood **(C)**, 24 h after *S. aureus* infection, mice were anaesthetised and blood was collected from the eyeballs. The first three drops of blood were placed in an anticoagulant tube and diluted to obtain a whole blood dilution. In addition, 10 mg of mammary tissue was homogenized in 100 times sterile saline, and a tissue homogenate was obtained. Then, 100 μL of the whole blood dilution and tissue homogenate was coated on culture medium and incubated at 37°C for 24 h for colony counting and calculation of the bacterial load. **(D,E)** The expression of IL-6 in mammary gland tissue **(D)** and serum **(E)**. **(F,G)** The expression of MPO in mammary gland tissue **(F)** and serum **(G)**. **(H,I)** Pathological scores of mammary gland tissue of mice in the lactation period **(H)** and the weaning period **(I)**. **(J)** Pathological sections of mammary gland tissue of mice in the lactation and weaning periods (HE, ×100).

Natural plants and their active ingredients are regarded as the most suitable alternative therapies for the treatment of SCM, as they not only have remarkable efficacy but also possess characteristics such as good safety, a low propensity for drug resistance and drug residues, which are beneficial to food safety and human public health (30). *Pulsatilla chinensis* and its active ingredients are well-known natural herbal medicines that have continuously attracted our attention. Our previous studies revealed that *Anemoside B4* could prolong the survival time of mice infected with *Salmonella*, reduce the bacterial load in tissues, ameliorate the inflammatory response induced by Salmonella and alleviate intestinal damage. Moreover, *Anemoside B4* improved the colony structure and diversity of the intestinal microbiota in mice infected with Salmonella and thus restored the balance of the intestinal microbiota (31). *Anemoside B4* was the index component with the highest content in *Pulsatilla chinensis*. Therefore, optimizing the preparation process of PCE is

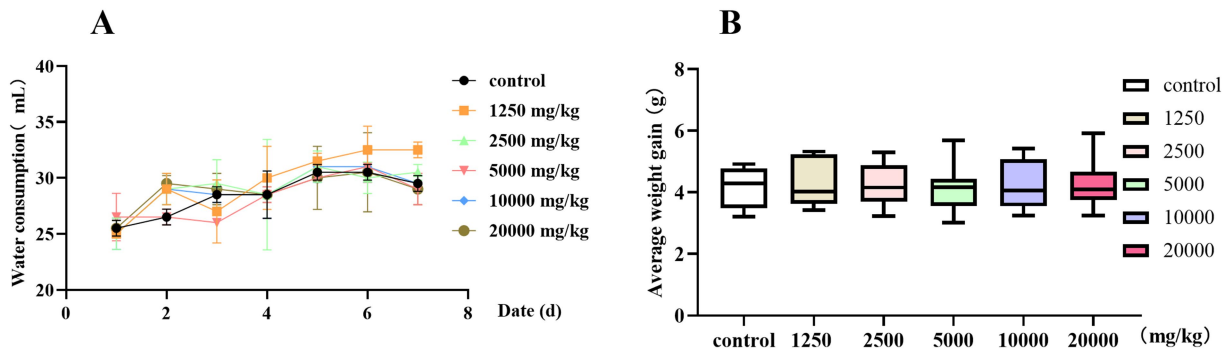

FIGURE 4
Oral safety of PCE in mice. **(A)** Litter size and water intake. **(B)** Average body weight.

conducive to increasing the content of *Anemoside B4*, which can better demonstrate its clinical application, in-depth processing and pharmacological activities. However, the research and development of veterinary drugs differ from those of human drugs. It needs to be based on economic benefits, and processes that are relatively complicated or have high extraction costs are difficult to apply in actual production (32). In this study, the heating reflux method, which has a relatively low extraction cost, was selected. On the basis of RSM optimization, PCE was finally prepared through techniques such as reflux extraction, vacuum concentration and vacuum thermal drying (Figure 1), and its pharmacological efficacy was evaluated.

Using dairy cows as experimental animals incurs relatively high costs and is not conducive to the implementation of early experiments and methodology. Therefore, research on alternative models for bovine mastitis has become more significant. In this study, we established a model of mastitis in lactating mice induced by *S. aureus*, which greatly reduced the research cost of directly using dairy cows for early clinical trials and improved animal welfare, which has drawn much attention. To gain a clearer understanding of the susceptibility to bacterial invasion under different physiological states, we conducted a comparative study on mice in two physiological cycles, namely, the lactating and weaning periods, with respect to aspects such as the bacterial load, expression of inflammatory factors, and histology. The results revealed that there were significant differences in the histological structure of the mammary gland under different physiological cycles. During the lactating period, the mammary gland was larger in size, with thicker alveolar walls and less connective tissue and adipose tissue, which was more conducive to the infection and colonization of *S. aureus*. With the subsequent invasion of the pathogen, an inflammatory storm subsequently occurs in the mammary tissue and blood. Previously, the most commonly used method was to induce a mastitis model using lipopolysaccharide (LPS) (33). However, LPS is a single commercial endotoxin, and the mastitis induced by it lacks clinical relevance. Pathogenic microorganisms obtained from the milk of cows with mastitis have greater research value. In this study, *S. aureus* (GXU 2017) isolated from the milk of cows with mastitis was used to artificially infect the mammary glands of lactating mice, and a model of mastitis in lactating mice induced by *S. aureus* was established, laying a more solid foundation for the disease model for the subsequent implementation of clinical trials.

The superiority of the PCE was subsequently investigated. *In vitro*, PCE exhibited a good inhibitory effect on the growth and reproduction of four *S. aureus* strains (including three model strains and one clinical isolate). *In vivo*, the bacterial load in the blood demonstrated that *S. aureus* could disrupt the integrity of the blood–milk barrier. After invading the blood through the mammary gland, it induces the recruitment of many neutrophils and further triggers a systemic inflammatory response. The anti-inflammatory and antibacterial effects of PCE and DEX were confirmed in this study. Both of these compounds can reduce the bacterial load in mammary tissue and blood; effectively ameliorate the high expression of inflammatory factors such as MPO, IL-1β, IL-6, and TNF-α, as well as pathological damage to the mammary tissue and blood; and verify the oral safety of PCE. The occurrence of mastitis is usually accompanied by the appearance of purulent exudates, and suppurative inflammation is closely related to the defensive response of neutrophils. The increase in neutrophils can relatively intuitively reflect the degree of damage caused by mastitis (34, 35). MPO is present in a certain proportion of neutrophils (34), and its expression level can, to some extent, reflect the degree of neutrophil infiltration and thus reflect the inflammatory situation of the animal body. Moreover, as one of the most typical messengers in the inflammation family (36, 37), the expression levels of IL-1β, IL-6, and TNF-α can be used to better evaluate the damage caused by mastitis (38).

Certainly, in bacterial diseases, the short-term curative effects of hormones and antibacterial drugs are widely recognized. However, numerous studies have already provided compelling evidence regarding the disruption of the gut microbiome by hormones and antibacterial drugs, mainly focusing on aspects such as the composition, diversity, and abundance of the gut microbiota and the reduction in the number of beneficial bacteria (39–41). This is detrimental to the physical health of animals and may serve as a trigger for the next outbreak of disease. Multiple studies have also demonstrated a correlation between the functions of the gut microbiota and mastitis (5, 42, 43). The gut microbiota is an important foundation for maintaining the stability of the gut microenvironment and preventing pathogen invasion (44, 45). Our research has shown that while PCE can effectively alleviate mastitis in mice and the inflammatory response of the body, it can also effectively improve or enhance the beneficial properties of the gut microbiota in mice. Although DEX can effectively suppress the occurrence of the inflammatory response in a short period of time,

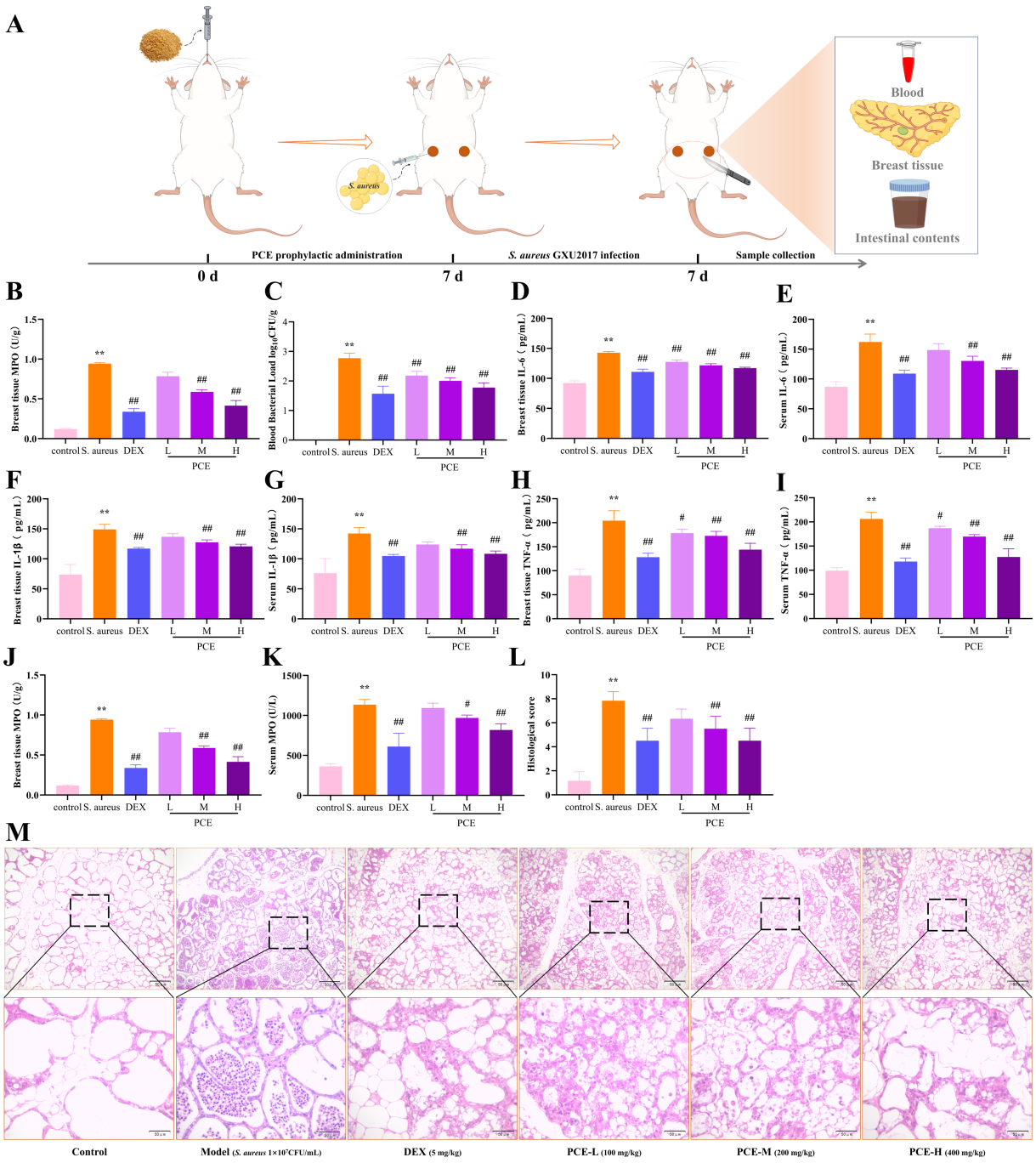

FIGURE 5
Protective effect of PCE against mastitis in female mice. **(A)** Model diagram of the experimental procedure. **(B,C)** Bacterial load in mammary tissue and blood. **(D,E)** Mammary tissue and serum IL-6 expression levels. **(F,G)** Mammary tissue and serum IL-1β expression levels. **(H,I)** Breast tissue and serum TNF-α expression levels. **(J,K)** Breast tissue and serum MPO expression levels. **(L)** Histopathological score. **(M)** Breast histological sections (HE, ×100, ×400). * and # indicate comparisons with the blank control and model groups, respectively, and $p < 0.05$ was considered statistically significant.

it is unfavorable for the gut microbiota. The long-term use of DEX may be accompanied by an imbalance in the gut microbiota and even the emergence and increase in harmful bacteria, which reflects the superiority of PCE over DEX. In the intestinal microbiota of animals, the abundances of different phyla are closely associated with the regulation of the host's inflammatory response. Actinobacteriota and Bacteroidota have been proven to maintain intestinal homeostasis through an anti-inflammatory mechanism mediated by their metabolites. In contrast, the abnormal enrichment of Firmicutes, Fusobacteriota, and Proteobacteria is significantly correlated with the formation of a pro-inflammatory microenvironment (46). The associations among the gut microbiota, mammary tissue, and blood phenotypes have enabled us to understand the beneficial aspects of *Actinobacteriota* and *Bacteroidota*, as well as the unfriendly aspects of *Firmicutes*, *Fusobacteriota*, and *Proteobacteria*. These differentially abundant

10.3389/fvets.2025.1603107

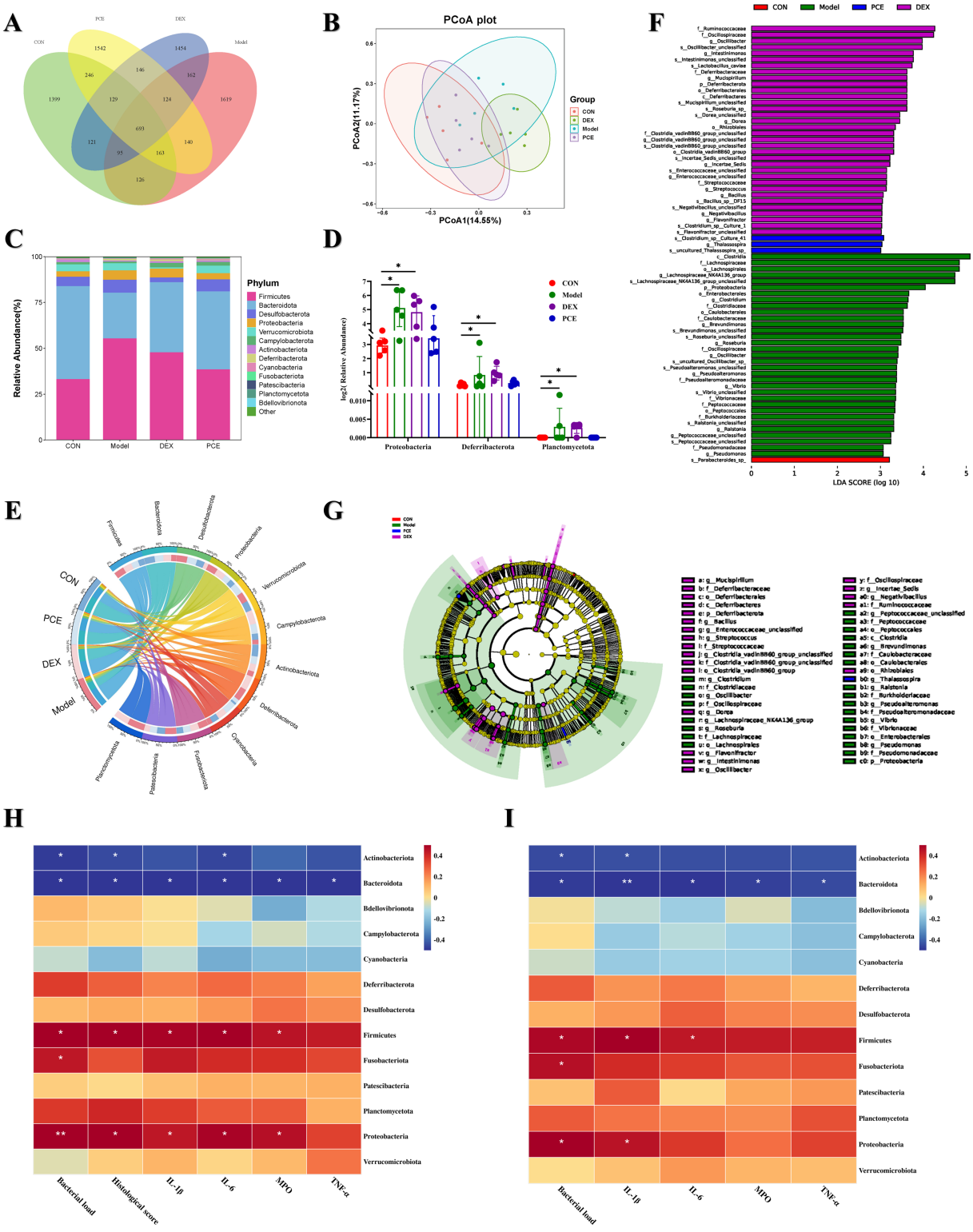

FIGURE 6
Effects of PCE on the diversity of the gut microbiota in mice. **(A)** Venn diagram of ASV analysis. **(B)** β-diversity analysis diagram (PCoA). **(C)** Stacked bar chart of the gut microbiota at the phylum level. **(D)** Diagram of significant differences in the gut microbiota at the phylum level. **(E)** Proportional and chord diagram of the gut microbiota at the phylum level (the left side shows the grouping information, and the right side shows the top 12 phyla in terms of abundance and their corresponding abundance information). The wider the width is, the greater the abundance is, and the narrower the width is, the lower the abundance is. **(F)** Distribution bar chart of linear discriminant analysis effect size (LEfSe) difference analysis of the gut microbiota ($p < 0.05$). The length of the bars represents the richness of the differential species. **(G)** Evolutionary branching diagram of LEfSe difference analysis of the gut microbiota ($p < 0.05$). The size of the nodes represents the richness of the differential species. **(H,I)** Heatmap analysis of the correlation between the gut microbiota and mammary gland tissue phenotypes **(H)** and blood phenotypes **(I)**. Red indicates a positive correlation, whereas blue indicates a negative correlation. The depth of the color is equivalent to the degree of correlation dependence. The horizontal and vertical coordinates are described previously. * and ** indicate significant differences ($p < 0.05$) and extremely significant differences ($p < 0.01$), respectively, all of which are statistically significant.

microbiota may become biomarkers for the clinical diagnosis of bovine mastitis.

5 Conclusion

In the posthormone and antibacterial drug era, we have developed an alternative, PCE, which is suitable for clinical production and application. This alternative can effectively inhibit the proliferation of *S. aureus in vitro*. On the premise of oral safety, it has proven its protective ability against *S. aureus*-induced mastitis in mice. Compared with DEX, it can suppress inflammation without disrupting the balance of the intestinal microbiota and there is no risk of drug residues. This study provides an alternative or complementary therapy to hormones and antibacterial drugs for the prevention and treatment of SCM. Of course, more in-depth research is needed to support the process from our current research to the launch of a new drug.

Data availability statement

The original contributions presented in the study are included in the article/supplementary material, further inquiries can be directed to the corresponding authors.

Ethics statement

All experiments were approved and supported by the Animal Research Ethics Committee of Guangxi University (Approval No. GXU-2022-326). The study was conducted in accordance with the local legislation and institutional requirements.

Author contributions

YX: Conceptualization, Data curation, Formal analysis, Investigation, Methodology, Software, Writing – original draft, Writing – review & editing. ZiL: Conceptualization, Investigation, Methodology, Writing – review & editing. CL: Conceptualization, Methodology, Writing – review & editing. ZW: Conceptualization, Methodology, Writing – review & editing. XM: Conceptualization, Methodology, Writing – review & editing. YZ: Conceptualization, Methodology, Writing – review & editing. RH: Conceptualization, Methodology, Writing – review & editing. ZhL: Methodology, Writing – review & editing. YH: Conceptualization, Formal analysis, Methodology, Writing – review & editing. JH: Conceptualization, Data curation, Funding acquisition, Methodology, Project administration, Resources, Supervision, Writing – review & editing.

Funding

The author(s) declare that financial support was received for the research and/or publication of this article. This work was supported by the Joint Funds of the National Natural Science Foundation of China (No. U24A20453).

Acknowledgments

The authors thank Xuming Deng for technical assistance.

Conflict of interest

The authors declare that the research was conducted in the absence of any commercial or financial relationships that could be construed as a potential conflict of interest.

Generative AI statement

The authors declare that no Gen AI was used in the creation of this manuscript.

Publisher's note

References

1. Hagner KA, Nordgren HS, Sarjokari K, Sukura A, Rajala-Schultz PJ. Role of mastitis in on-farm deaths of Finnish dairy cows. *J Dairy Sci.* (2024) 107:5962–73. doi: 10.3168/jds.2024-24405

2. Wang Y, Zhao Y, Tang X, Nan X, Jiang L, Wang H, et al. Nutrition, gastrointestinal microorganisms and metabolites in mastitis occurrence and control. *Animal Nutr.* (2024) 17:220–31. doi: 10.1016/j.aninu.2024.01.010

3. Cuccato M, Divari S, Giannuzzi D, Grange C, Moretti R, Rinaldi A, et al. Extracellular vesicle mirnome during subclinical mastitis in dairy cows. *Vet Res.* (2024) 55:112. doi: 10.1186/s13567-024-01367-x

4. Guo M, Zhang Y, Wu L, Xiong Y, Xia L, Cheng Y, et al. Development and mouse model evaluation of a new phage cocktail intended as an alternative to antibiotics for treatment of *Staphylococcus aureus*-induced bovine mastitis. *J Dairy Sci.* (2024) 107:5974–87. doi: 10.3168/jds.2024-24540

5. Hu X, He Z, Zhao C, He Y, Qiu M, Xiang K, et al. Gut/rumen-mammary gland Axis in mastitis: gut/rumen microbiota-mediated "Gastroenterogenic mastitis". *J Adv Res.* (2024) 55:159–71. doi: 10.1016/j.jare.2023.02.009

6. Puerto MA, Shepley E, Cue RI, Warner D, Dubuc JEV. The hidden cost of disease: I. Impact of the first incidence of mastitis on production and economic indicators of primiparous dairy cows. *J Dairy Sci.* (2021) 104:7932–43. doi: 10.3168/jds.2020-19584

7. Zhao C, Hu X, Bao L, Wu K, Zhao Y, Xiang K, et al. Gut dysbiosis induces the development of mastitis through a reduction in host anti-inflammatory enzyme activity by endotoxemia. *Microbiome.* (2022) 10:205. doi: 10.1186/s40168-022-01402-z

8. Javed S, McClure JA, Syed MA, Obasuyi O, Ali S, Tabassum S. Epidemiology and molecular characterization of *Staphylococcus aureus* causing bovine mastitis in water buffaloes from the Hazara division of Khyber Pakhtunkhwa, Pakistan. *PLoS One.* (2022) 17:e0268152. doi: 10.1371/journal.pone.0268152

9. Song M, Tang Q, Ding Y, Tan P, Zhang Y, Wang T, et al. *Staphylococcus aureus* and biofilms: transmission, threats, and promising strategies in animal husbandry. *J. Anim. Sci. Biotechnol.* (2024) 15:44. doi: 10.1186/s40104-024-01007-6

10. Sahreena L, Kunyan Z. Methicillin-resistant *Staphylococcus aureus*: molecular characterization, evolution, and epidemiology. *Clin Microbiol Rev.* (2018) 31:e00020–18. doi: 10.1128/CMR.00020-18

11. Pereyra E, Sacco SC, Duré A, Baravalle C, Renna MS, Andreotti CS, et al. Immune response of *Staphylococcus aureus* strains in a mouse mastitis model is linked to adaptive capacity and genotypic profiles. *Vet Microbiol*. (2017) 204:64–76. doi: 10.1016/j.vetmic.2017.04.009

12. Stevens M, Piepers S, DV S. Mastitis prevention and control practices and mastitis treatment strategies associated with the consumption of (critically important) antimicrobials on dairy herds in Flanders, Belgium. *J. Dairy Sci.* (2016) 99:2896–903. doi: 10.3168/jds.2015-10496

13. Wang H, Chen C, Chen X, Zhang J, Liu Y, Li X. PK/PD modeling to assess Rifaximin clinical dosage in a mouse model of *Staphylococcus aureus*-induced mastitis. *Front. Vet. Sci.* (2021) 8:651369. doi: 10.3389/fvets.2021.651369

14. Saleem A, Saleem Bhat S, Omonijo A, Ganai NA, Ibeagha-Awemu EM, Ahmad SM. Immunotherapy in mastitis: state of knowledge, research gaps and way forward. *Vet Q*. (2024) 44:1–23. doi: 10.1080/01652176.2024.2363626

15. Lee AS, de Lencastre H, Garau J, Kluytmans J, Malhotra-Kumar S, Peschel A. Methicillin-resistant *Staphylococcus aureus*. *Nat Rev Dis Primers*. (2018) 4:18033. doi: 10.1038/nrdp.2018.33

16. Cheung GYC, Bae JS, Otto M. Pathogenicity and virulence of *Staphylococcus aureus*. *Virulence*. (2021) 12:547–69. doi: 10.1080/21505594.2021.1878688

17. Paramasivam R, Gopal DR, Dhandapani R, Subbarayalu R, Elangovan MP, Prabhu B. Is AMR in dairy products a threat to human health? An updated review on the origin, prevention, treatment, and economic impacts of subclinical mastitis. *Infect Drug Resist*. (2023) 16:155–78. doi: 10.2147/IDR.S384776

18. Zhong J, Tan L, Chen M. Pharmacological activities and molecular mechanisms of Pulsatilla saponins. *Chin Med*. (2022) 17:59. doi: 10.1186/s13020-022-00613-8

19. Hu X, Guo J, Zhao C, Jiang P, Maimai T, Yanyi L, et al. The gut microbiota contributes to the development of *Staphylococcus aureus*-induced mastitis in mice. *ISME J*. (2020) 14:1897–910. doi: 10.1038/s41396-020-0651-1

20. Fu Y, Zhou E, Wei Z, Liang D, Wang W, Wang T, et al. Glycyrrhizin inhibits the inflammatory response in mouse mammary epithelial cells and a mouse mastitis model. *FEBS J*. (2014) 281:2543–57. doi: 10.1111/febs.12801

21. Sun WJ, Wu EY, Zhang GY, Xu BC, Chen XG, Hao KY, et al. Total flavonoids of *Abrus cantoniensis* inhibit Cd14/Tlr4/Nf-Kb/Mapk pathway expression and improve gut microbiota disorders to reduce lipopolysaccharide-induced mastitis in mice. *Front Microbiol*. (2022) 13:985529. doi: 10.3389/fmicb.2022.985529

22. Xu Q-m, Shu Z, He W-j, Chen L-y, Yang S-l, Yang G. Antitumor activity of Pulsatilla chinensis (Bunge) Regel saponins in human liver tumor 7402 cells *in vitro* and *in vivo*. *Phytomedicine*. (2012) 19:293–300. doi: 10.1016/j.phymed.2011.08.066

23. Kapoor P, Tiwari A, Sharma S, Tiwari V, Sheoran B, Ali U, et al. Effect of anthocyanins on gut health markers, Firmicutes-bacteroidetes ratio and short-chain fatty acids: a systematic review via meta-analysis. *Sci Rep*. (2023) 13:1729. doi: 10.1038/s41598-023-28764-0

24. Zhao C, Bao L, Zhao Y. A Fiber-enriched diet alleviates *Staphylococcus aureus*-induced mastitis by activating the Hdac3-mediated antimicrobial program in macrophages via butyrate production in mice. *PLoS Pathog*. (2023) 19:e1011108. doi: 10.1371/journal.ppat.1011108

25. Kwiecinski JM, Horswill AR. *Staphylococcus aureus* bloodstream infections: pathogenesis and regulatory mechanisms. *Curr Opin Microbiol*. (2020) 53:51–60. doi: 10.1016/j.mib.2020.02.005

26. Liu Y, Tong Z, Shi J, Li R, Upton M, Wang Z. Drug repurposing for next-generation combination therapies against multidrug-resistant Bacteria. *Theranostics*. (2021) 11:4910–28. doi: 10.7150/thno.56205

27. Raymond K, Hall LJ. An update on the human and animal enteric pathogen *Clostridium perfringens*. *Emerg. Microbes Infect.* (2018) 7:1–15. doi: 10.1038/s41426-018-0144-8

28. Cook MA, Wright GD. The past, present, and future of antibiotics. *Sci Transl Med*. (2022) 14:abo7793. doi: 10.1126/scitranslmed.abo7793

29. MacNair CR, Rutherford ST, Tan M-W. Alternative therapeutic strategies to treat antibiotic-resistant pathogens. *Nat Rev Microbiol*. (2024) 22:262–75. doi: 10.1038/s41579-023-00993-0

30. Abd El-Hack ME, El-Saadony MT, Salem HM, El-Tahan AM, Soliman MM, Youssef GBA, et al. Alternatives to Antibiotics for organic poultry production: types, modes of action and impacts on Bird's health and production. *Poult Sci*. (2022) 101:101696. doi: 10.1016/j.psj.2022.101696

31. Qin L. The effect of anemoside B4 on Salmonella-induced intestinal inflammation and a preliminary investigation of the mechanism. Nanning: Guangxi University (2023).

32. Zongzheng L. Therapeutic effect and application of Liquorice Chalcone an on *Clostridium Perfringens* infection. Changchun: Jilin University (2019).

33. Yu S, Liu X, Yu D, Changyong E, Yang J. Piperine protects LPS-induced mastitis by inhibiting inflammatory response. *Int Immunopharmacol*. (2020) 87:106804. doi: 10.1016/j.intimp.2020.106804

34. Zhang J, Conly J, Mcclure JA, Wu K, Zhang K. A murine skin infection model capable of differentiating the dermatopathology of community-associated MRSA strain Usa300 from other MRSA strains. *Microorganisms*. (2021) 9:287. doi: 10.3390/microorganisms9020287

35. Tang F, Fan K, Wang K, Bian C. Atractylodin attenuates lipopolysaccharide-induced acute lung injury by inhibiting NLRP3 inflammasome and TLR4 pathways. *J Pharmacol Sci*. (2018) 136:203–11. doi: 10.1016/j.jphs.2017.11.010

36. Ju X, Zhang H, Zhou Z, Chen M, Wang Q. Tumor-associated macrophages induce PD-L1 expression in gastric cancer cells through IL-6 and TNF-alpha signaling. *Exp Cell Res*. (2020) 396:112315. doi: 10.1016/j.yexcr.2020.112315

37. Xiang Y, Ji M, Wu L. Rosmarinic acid prevents cisplatin-induced liver and kidney injury by inhibiting inflammatory responses and enhancing Total antioxidant capacity, thereby activating the Nrf2 signaling pathway. *Molecules*. (2022) 27:7815. doi: 10.3390/molecules27227815

38. Massicotte-Azarniouch DHC, Jennette JC. Mechanisms of vascular damage in ANCA Vasculitis. *Semin Immunopathol*. (2022) 44:325–45. doi: 10.1007/s00281-022-00920-0

39. Angelucci F, Cechova K, Amlerova J, Antibiotics JH. Gut microbiota, and Alzheimer's disease. *J Neuroinflammation*. (2019) 16:108. doi: 10.1186/s12974-019-1494-4

40. McDonnell L, Gilkes A, Ashworth M, Rowland V, Harries TH, Armstrong D, et al. Association between Antibiotics and gut microbiome dysbiosis in children: systematic review and meta-analysis. *Gut Microbes*. (2021) 13:1–18. doi: 10.1080/19490976.2020.1870402

41. Fishbein SRS, Mahmud B, Dantas G. Antibiotic perturbations to the gut microbiome. *Nat Rev Microbiol*. (2023) 21:772–88. doi: 10.1038/s41579-023-00933-y

42. Hu J, Chen J, Xu X, Hou Q, Ren J, Yan X. Gut microbiota-derived 3-Phenylpropionic acid promotes intestinal epithelial barrier function via AhR signaling. *Microbiome*. (2023) 11:102. doi: 10.1186/s40168-023-01551-9

43. Fan L, Xia Y, Wang Y, Han D, Liu Y, Li J, et al. Gut microbiota bridges dietary nutrients and host immunity. *Sci China Life Sci*. (2023) 66:2466–514. doi: 10.1007/s11427-023-2346-1

44. Spencer JMB. Human intestinal B cells in inflammatory diseases. *Nature Rev. Gastroenterol. Hepatol.* (2023) 20:254–65. doi: 10.1038/s41575-023-00755-6

45. Seike K, Kiledal A, Fujiwara H, Henig I, Burgos da Silva M, van den Brink MRM, et al. Ambient oxygen levels regulate intestinal dysbiosis and GVHD severity after allogeneic stem cell transplantation. *Immunity*. (2023) 56:353–368.e6. doi: 10.1016/j.immuni.2023.01.007

46. Reuvers JRD, Budding AE, Marjolein VE, Stockmann HBAC, Twisk JWR, Geert K, et al. Gut proteobacteria levels and colorectal surgical infections: select trial. *Br J Surg*. (2022) 110:129–32. doi: 10.1093/bjs/znac288

frontiers | Frontiers in Veterinary Science

TYPE Original Research
PUBLISHED 14 May 2025
DOI 10.3389/fvets.2025.1565787

OPEN ACCESS

EDITED BY
Dongan Cui,
Lanzhou University, China

REVIEWED BY
Greeshma Joseph,
Silvercity Consulting, Bahrain
Dan Shao,
Chinese Academy of Agricultural Sciences, China

*CORRESPONDENCE
Costanza Spadini
✉ costanza.spadini@unipr.it

†These authors have contributed equally to this work

RECEIVED 23 January 2025
ACCEPTED 25 March 2025
PUBLISHED 14 May 2025

CITATION
Mezzasalma N, Spadini C, Spaggiari C, Annunziato G, Andreoli V, Prosperi A, Mochen L, Cavirani S, Grolli S, Taddei S, Costantino G and Cabassi CS (2025) Antibacterial and antibiofilm activity of *Eucalyptus globulus* leaf extract, asiatic acid and ursolic acid against bacteria isolated from bovine mastitis.
Front. Vet. Sci. 12:1565787.
doi: 10.3389/fvets.2025.1565787

Antibacterial and antibiofilm activity of *Eucalyptus globulus* leaf extract, asiatic acid and ursolic acid against bacteria isolated from bovine mastitis

Nicolò Mezzasalma[1†], Costanza Spadini[1*†], Chiara Spaggiari[2], Giannamaria Annunziato[2], Valentina Andreoli[1], Alice Prosperi[3], Lorenzo Mochen[1], Sandro Cavirani[1], Stefano Grolli[1], Simone Taddei[1], Gabriele Costantino[2] and Clotilde Silvia Cabassi[1]

[1]Department of Veterinary Science, University of Parma, Parma, Italy, [2]Department of Food and Drug, University of Parma, Parma, Italy, [3]Istituto Zooprofilattico Sperimentale della Lombardia e dell'Emilia-Romagna (IZSLER), Brescia, Italy

Antibiotics represent the first line therapy for bovine mastitis. However, the increasing prevalence of multidrug-resistant organisms (MDROs) highlights the need for alternative therapeutic approaches. This study evaluated the antimicrobial and antibiofilm activities of *Eucalyptus globulus* leaf extract (EGL-L), ursolic acid (UA) and asiatic acid (AA) against *Staphylococcus aureus* (SA), *Streptococcus uberis* (SU), *Streptococcus agalactiae* (SAG), and *Enterococcus* spp. (EN) isolated from bovine mastitis, 39.7% of which were MDROs. The minimal inhibitory concentration (MIC) assay demonstrated that all the compounds exhibited antimicrobial activity against the tested bacteria, including MDROs. However, EGL-L was less effective ($p < 0.001$) than UA or AA against field strains. UA was more effective against SAG and SU compared to SA ($p < 0.001$), whereas AA was more effective against SU than SA ($p < 0.001$). Conversely, EGL-L exhibited similar inhibitory effects on all bacteria. The biofilm-forming ability of the bacterial strains was also assessed, and the minimal biofilm inhibitory concentrations (MBICs) of the compounds were evaluated for moderate and strong biofilm producers. None of the compounds were able to completely inhibit biofilm formation. However, $MBIC_{80}$ values within the tested concentration range were achieved for 15 out of 32 strains with EGL-L and for 27 out of 32 strains with UA and AA. These findings highlight a promising alternative to conventional antimicrobials for AA and UA, showing potential for topical intramammary use for the control and prevention of bovine mastitis, especially because of their efficacy against biofilm formation. Future research should focus on toxicity assessments and formulation development for potential topical administration.

KEYWORDS

plant extracts, pentacyclic triterpenes, biofilm-producing organisms, multidrug-resistant organisms, MIC, minimal biofilm inhibitory concentration

Introduction

Bovine mastitis (BM) is an inflammation of the mammary gland caused by physical trauma or microorganisms that can affect the health and welfare of animals (1). In dairy cow husbandry, it is the most important cause of increased farm costs because of reduced milk production, increased medical expenses and increased animal culling (2). Contagious mastitis is caused by bacteria that recognize the udder as a primary reservoir (e.g., *Streptococcus agalactiae* and *Staphylococcus aureus*). On the other hand, environmental mastitis is commonly caused by bacteria found in the environment or fecal matter, especially under poor hygiene conditions (e.g., *Escherichia coli* or *Streptococcus uberis*) (3).

Antibiotics represent the first-line therapy for bovine mastitis, and intramammary administration (IMM) is preferred (4). However, the effectiveness of IMM therapy could be hindered by the intracellular localization of bacteria or the low lipid solubility of antimicrobial molecules, which predisposes bacteria to the emergence of antibiotic resistance, and by the ability of some bacteria to form biofilms (5). One of the key strategies for mastitis control is dry-cow therapy (DCT), which involves the intramammary administration of long-acting antimicrobial agents during the dry-off phase (6). DCT can be performed on all quarters of all drying cows (blanket DCT) or only on infected cows or quarters (selective DCT) (7). The blanket DCT was the most widely used strategy in the past to manage BMs (8). However, the worldwide increase in AMR among mastitis-associated bacteria poses significant threats to both animal and human health (9). The selective DCTs reduce antibiotic use, counteracting the spread of antimicrobial resistance. Nevertheless, a high incidence of new intramammary infections has been reported in untreated dry cows without clinical signs of mastitis (7, 10). In accordance with [Regulation (EU) 2019/6 of the European Parliament and the Council], the use of antibiotics in veterinary medicine is rigorously regulated (11). Therefore, the development of innovative approaches is imperative to achieve effective disease control while simultaneously reducing antibiotic usage.

The most investigated alternative strategies are based on probiotics, bacteriophages and animal-, plant-, and bacteria-derived antimicrobials (4). Plant derivatives, particularly plant extracts and essential oils, have been widely used in traditional medicine and have recently gained attention in veterinary medicine because of their biological properties, including antimicrobial activity (12–14). Compared with conventional antibiotics, essential oils and plant extracts offer several advantages: (i) they are classified as nonpharmaceutical compounds, (ii) they have few side effects, and (iii) their prolonged use is not associated with the development of resistance (1, 6). As these molecules act on different targets than antibiotics do, often different components of the bacterial wall, they can also be used to treat infections caused by multidrug-resistant organisms (MDROs) (6, 9). An interesting and promising product of plant origin is the extract of *Eucalyptus globulus* Labill. whose chemical composition is widely documented in the literature, along with its antibacterial and antifungal properties (15, 16). Its chemical composition, and consequently its biological properties, may vary depending on the geographical origin of collection. This variation can be influenced by environmental factors (e.g., soil composition and climate), leaf age, and genetic variations (17). Indeed, the antimicrobial effects of *Eucalyptus globulus* are primarily attributed to its phenolic compounds and pentacyclic triterpenes, which demonstrate greater efficacy against Gram-positive bacteria compared to Gram-negative bacteria. This difference in effectiveness is likely due to the protective outer membrane lipopolysaccharide layer of Gram-negative bacteria. The main active compounds specifically target cellular structures in a nonspecific manner, with proposed mechanisms including alterations in membrane permeability, loss of membrane potential, dysfunction of the proton pump, and depletion of ATP (18).

Among the most bioactive compounds of interest is the triterpene family, particularly pentacyclic triterpenes such as asiatic acid (AA), ursolic acid (UA), and their derivatives, which are known for their antibacterial properties against Gram-positive and Gram-negative bacteria (16, 19, 20). Pentacyclic triterpenes represent the most abundant group of terpenoids found in dicotyledons and serve as chemical defenses against competing plants, pathogens and herbivores. They exhibit antioxidant, antimicrobial, fungicidal and antiparasitic properties (19). As extensively reviewed in literature (19), the antibacterial activity of pentacyclic triterpenes is associated with alterations in bacterial cell structure, stimulating chemotaxis-related genes involved in host defense and affecting bacterial gene expression related to biofilm formation, peptidoglycan turnover, and cell autolysis. Additionally, the review mentioned highlights that both acids show higher antibacterial activity against Gram-positive bacteria rather than Gram-negative, probably due to the difficulty of these acids to overcome the outer membrane of Gram-negative. Consequently, there are differences in AA and UA concentrations required to inhibit bacterial growth in Gram-positive and negative bacteria. Ursolic acid is a constituent of several medicinal plants and it is known for its wide range of biological properties such as antioxidant, antibiofilm and antibacterial activities, especially against Gram-positive bacteria (20, 21). In the literature, the ability of UA to inhibit *E. coli* biofilm formation under different conditions has been described (24) influencing its transcriptome, including gene repression of *CysB* and *CysDJK* of the bacterial biosynthetic way of cysteine, which are involved in the response to oxidative stress and biofilm formation (15, 25, 26). Asiatic acid is instead known for its antimicrobial activity against both Gram-positive and Gram-negative bacteria (16, 19). However, the number of studies reporting its antibiofilm activity is lower than that reporting its activity toward UA (26).

However, few studies have focused on the antimicrobial and antibiofilm activities of AA, UA and *Eucalyptus globulus* Labill. leaves extract (EGL-L) against bacteria involved in BM.

Therefore, the present study aimed to quantify the content of AA and UA in EGL-L strains originating from Rwanda and subsequently evaluate their antimicrobial activity against both reference and field strains of *S. aureus*, *S. agalactiae*, *S. uberis* and *Enterococcus* spp. isolated during clinical and subclinical bovine mastitis. In addition, the antibiofilm activity of these alternative compounds was assessed specifically on moderate and strong biofilm-producing strains.

Materials and methods

Chemicals and reagents

Liquid chromatography–mass spectrometry (LC–MS)-grade methanol and acetonitrile were purchased from Scharlab Italia srl

(Milan, Italy); distilled water was obtained via a Milli-Q system (Millipore, Bedford, MA, USA). MS-grade ammonium acetate, acetic acid, and formic acid from Fisher Chemical (Thermo Fisher Scientific Inc., San Jose, CA, USA) were also used. Ursolic and asiatic acid <98% (HPLC) were purchased from Sigma–Aldrich (Schnelldorf, Germany).

Plant material

Leaves of *Eucalyptus globulus* (Labill., 1800) (EGL-L) were collected from eight different plants grown in the botanical garden of the INES Ruhengeri Institute of Applied Sciences, Musanze, Rwanda. Leaves were washed with tap water and air dried for 3 weeks. After drying, the leaves were ground using a grinder (particle size <800 μm).

EGL-L extract preparation

Three aliquots of *Eucalyptus* leaves (20 g each) were shredded, placed into separate hermetic flasks and subjected to hydroalcoholic maceration with 70% ethanol. A 1:10 matrix-to-solvent ratio was used. The extraction process was carried out for 72 h at room temperature (RT) with constant stirring at 100 rpm. After extraction, the extracts were filtered, and the solvent was removed via a rotary evaporator (Buchi). The resulting extracts were frozen with liquid nitrogen and then freeze-dried. The lyophilization process was conducted under vacuum conditions for 36 h at −56°C and 1 mbar (1-DL alpha Plus freeze-drier). The dried extracts were divided into different aliquots and reconstituted in EtOH:water (70,30) prior to LC–MS analysis.

HPLC–MS method for the quantification of UA and AA in EGL-L

The quantification of UA and AA in EGL-L was conducted via HPLC–MS in SIM mode. The analyses were performed in triplicate to ensure accuracy and reproducibility. Calibration curves were constructed for both compounds, which were subsequently used to determine their concentrations in the extract samples. HPLC–MS analysis was performed using a 2,695 Alliance separation system (Waters Go, Milford, MA, USA) equipped with a QuattroTM API triple quadrupole mass spectrometer with an electrospray source (Micromass, Waters, Manchester, UK). Chromatographic conditions were the following: Column XSelect®HSST3 (250 mm × 2.1 mm, 5 μm), flow rate 0.2 mL/min, column temperature 30°C, injection volume 5 μL. A gradient profile was applied using water (eluent A) and acetonitrile (eluent B) as mobile phases both acidified with 0.1% formic acid. The initial conditions were set at 100% A, after 5 min of the isocratic step, a linear change to 100% B at 8 min, and holding for 7 min before returning to initial conditions. Columns recondition was achieved over 6 min, providing a total run time of 21 min. The column was maintained at 30°C and a flow rate of 0.20 mL/min was used. MSD parameter: ESI negative, capillary voltage 2.5 kV, cone voltage 25 V, extractor voltage 2, source block temperature 120°C, desolvation temperature 350°C. Cone-gas-flow nitrogen and argon were used as collision gas. Selective ion monitoring (SIM) in negative ion mode was used. Ursolic acid was recorded as m/z 455.4 $[M-H]^-$ while asiatic acid as 487.7 $[M-H]^-$. UA and AA could not be collided into fragments when collision energy was 40 eV, or no dominant product ions were detected if collision energy was higher than 50 eV, which indicated that MRM experiment was not suitable for UA and AA quantification. Analytes concentrations in the sample were calculated from the relation within slope line obtained by linear regression analysis of this calibration curve and multiplied for their dilution factor.

Bacterial strains

The following reference strains were tested: *Staphylococcus aureus* ATCC 25923, methicillin-resistant *Staphylococcus aureus* ATCC 43300 (MRSA), *Streptococcus agalactiae* ATCC 27956, *Streptococcus uberis* ATCC 19496 and *Enterococcus faecium* ATCC 19434.

Clinical isolates of *Staphylococcus aureus* (SA; $n = 15$), *Streptococcus agalactiae* (SAG; $n = 17$), *Streptococcus uberis* (SU; $n = 18$), and *Enterococcus* spp. (EN; $n = 13$), obtained from cows with subclinical or clinical mastitis, were tested.

Clinical strains were provided by the biobanks of the Animal Infectious Disease Laboratory of the University of Parma and by the IZSLER (*Istituto Zooprofilattico Sperimentale della Lombardia e dell'Emilia-Romagna*) – Laboratory of Parma.

Bacterial strains were grown in Columbia blood agar after incubation of 24 h at 37°C. On individual colonies, Gram staining and catalase test were performed, followed by execution of API Staph® and API 20 Strep® System test (bioMérieux), as well as indicated by manufacturer (27).

Antimicrobial susceptibility testing (AST)

AST was performed via the Kirby–Bauer disk diffusion method. Owing to the intrinsic resistance of *Enterococcus* spp., testing for this genus was limited to the following antibiotics: amoxicillin/clavulanic acid (20/10 μg), ampicillin (10 μg), enrofloxacin (5 μg), erythromycin (15 μg), florfenicol (30 μg), imipenem (10 μg), marbofloxacin (5 μg), oxytetracycline (30 μg), penicillin G (10 U), rifaximin (40 μg), and vancomycin (30 μg). For the strains belonging to the *Streptococcus* genus, in addition to the abovementioned antibiotics, the following antibiotics were also tested: cefazolin (30 μg), cefquinome (30 μg), ceftiofur (30 μg), cefuroxime (30 μg), and trimethoprim/sulphamethoxazole (1.25/23.75 μg). *Staphylococcus aureus* isolates were tested with all the antibiotics listed above, except vancomycin. Additionally, they were tested with fusidic acid (10 μg), gentamicin (10 μg), kanamycin (30 μg) and lincomycin (15 μg). The interpretation of the results followed the guidelines of the Clinical and Laboratory Standards Institute (CLSI) veterinary breakpoints. When veterinary breakpoints were not available, human breakpoints were adopted (28). To assess whether the microorganism was MDR or non-MDR, the categorization proposed in the literature was adopted (29).

Bacterial inoculum

Minimal inhibitory concentration (MIC) assays were performed on both field and reference bacterial strains. The bacterial inoculum was prepared according to the CLSI standard method (30). All microbiological assays were performed within 30 min after inoculum

standardization. Briefly, for each strain, five bacterial colonies from fresh solid cultures were inoculated in sterile tubes with Müeller Hinton broth (MHB) and incubated at 37°C under aerobic conditions for 24 h for staphylococci, while streptococci and enterococci were incubated under microaerophilic conditions. After incubation, the bacterial suspension was centrifuged at 2000 rpm for 20 min at 4°C to separate the pellet containing bacteria from the supernatant. The pellet was subsequently resuspended in 10 mM phosphate buffer (PB), pH 7, to obtain an optical density (OD) of 0.08–0.13 at 600 nm in a 1 cm light path cuvette, corresponding to approximately 0.5 McFarland suspension (10^8 CFU/mL). This suspension was further diluted 1:100 in sterile MHB. Then, 50 µL of the bacterial suspension, containing 10^6 CFU/mL, was inoculated into each well to obtain a final concentration of 5×10^5 CFU/mL. The bacterial suspensions were assessed via a Biophotometer plus (Eppendorf, Hamburg, Germany) spectrophotometer at 600 nm.

MIC assay of plant extracts

The MIC assay was performed following the methods outlined in the CLSI standard methods, with minor modifications. Briefly, EGL-L, AA and UA were prepared as stock solutions in DMSO at concentrations of 200 mg/mL for EGL-L and 25.6 mg/mL for UA and AA. Serial twofold dilutions of each compound in DMSO were performed in a 96-well microtiter plate (Greiner, Milan, Italy). Then, one microliter of each diluted compound was added to the wells of the plates, followed by the addition of 50 µL of bacterial suspension containing 10^6 CFU/mL, resulting in a final bacterial concentration of 5×10^5 CFU/ml. The final dilution range for EGL-L was 2000 to 3.9 µg/mL, whereas for AA and UA, it ranged from 256 to 0.5 µg/mL. Growth and sterility controls were included for each bacterial strain and compound tested. The plates were incubated at 37°C for 24 h as described above for each bacterial strain. For each assay, three experiments were performed, with three replicates each. After incubation, the MIC was determined by visual inspection. The minimal inhibitory concentration was considered the lowest concentration able to completely inhibit bacterial growth. Furthermore, the MIC_{50} and MIC_{90} were calculated: given a graded series of MICs starting with the lowest value, MIC_{50} is the MIC value at which 50% of the isolates in a test population are inhibited (equivalent to the median MIC value), and the MIC_{90} is calculated as $n \times 0.9$, where n represents the test strains and represents the 90th percentile, as specified in the literature (31).

Bactericidal kinetic curves (BKC) evaluation

The bactericidal kinetic curves (BKC) of EGL-L, AA and UA were determined following the methods reported in literature (32). For each compound, three concentrations were selected based on their MIC values against the reference bacteria: 1 × MIC, 2 × MIC, and 4 × MIC. A growth control was also included. Each compound was subjected to serial twofold dilutions in DMSO in a 96-well microtiter plate (Greiner, Milan, Italy). Subsequently, 1 µL of each diluted solution was transferred to the respective wells, followed by the addition of 50 µL of bacterial suspension at a concentration of 10^6 CFU/mL, resulting in a final bacterial concentration of 5×10^5 CFU/mL. BKC were monitored by measuring the optical density at 620 nm using a spectrophotometer reading plates (Biophotometer Plus, Eppendorf, Hamburg, Germany). Measurements were taken at the following time points (T): 0, 0.5, 1, 2, 3, 4, 5, 6, 7, 8, 24, and 48 h.

Biofilm formation assay

The biofilm-forming ability of the reference and field strains was evaluated via methods described in the literature (33), with slight modifications. The bacterial strains were cultivated in MHB at 37°C for 24 h. After incubation, the bacterial suspension was centrifuged at 2000 rpm for 20 min at 4°C, and the supernatant was removed. The pellet was resuspended in 10 mM phosphate buffer (PB), pH 7, and adjusted spectrophotometrically to obtain a final concentration of 10^7 CFU/mL. Each well of a 96-well flat-bottomed microtiter plate was filled with 180 µL of tryptic soy broth (TSB) supplemented with 1% glucose. Thereafter, 20 µL of the previously prepared bacterial suspension was added to each well, and the plates were incubated at 37°C for 24 h. The sterility control consisted of 180 µL of TSB supplemented with 1% glucose and 20 µL of PB. Three replicates were carried out for each bacterial strain. The tests were repeated three times for each bacterial strain. After incubation, the wells were emptied and washed three times with sterile phosphate-buffered saline (PBS; pH 7.2). The residual liquid was removed by gentle flicking, and the remaining biofilm was fixed with 150 µL of methanol for 15 min. After the methanol was removed, the plates were air-dried for 2 h at room temperature. The biofilms were stained with 0.1% Hucker crystal violet (150 µL for each well) for 30 min. After staining, the crystal violet solution was removed by sequential washing with sterile deionized water. The wells were then air-dried, and 150 µL of 95% ethanol was added to each well for 30 min to solubilize the stain.

The solubilized stain was transferred to a new flat-bottomed microtiter plate, and the OD was measured at 620 nm. The biofilm-forming ability was classified on the basis of the criteria described in the literature (33, 34). Briefly, the cutoff OD (ODc) was defined as three times the standard deviation above the mean OD of the negative control, and the strains were classified as follows:

$OD \leq OD_c$ nonadherent (NA)
$OD_c < OD \leq 2\ X\ OD_c$ weakly adherent (WA)
$2\ X\ OD_c < OD \leq 4\ X\ OD_c$ moderately adherent (MA)
$4\ x\ OD_c \leq OD$ strongly adherent (StA).

Minimal inhibitory biofilm concentration assay

The minimal biofilm inhibitory concentrations (MBICs) of all the tested compounds were determined for reference and field strains classified as MA or StA. Each well of a 96-well flat-bottomed microtiter plate was filled with 178 µL of TSB supplemented with 1% glucose. Twofold dilutions of each stock solution of EGL-L, AA and UA in DMSO were prepared in a separate microtiter plate, and 2 µL of each dilution was then added to the respective wells

(Greiner, Milan, Italy). The final dilution range for EGL-L was 2000 to 3.9 µg/mL, whereas for AA and UA, it ranged from 256 to 0.5 µg/mL.

The bacterial pellet was prepared as described above, resuspended in PB and adjusted spectrophotometrically to obtain a final concentration of 10^7 CFU/mL. Thereafter, 20 µL of the bacterial suspension was added to each well. The growth control consisted of 180 µL of TSB supplemented with 1% glucose and 20 µL of bacterial suspension (10^7 CFU/mL). The sterility control was prepared with 200 µL of TSB with 1% glucose. The plates were incubated at 37°C for 24 h. Three replicates were carried out for each bacterial strain. After incubation, biofilm staining was performed as described above.

For each tested compound and concentration, the percent inhibition was calculated via the following formula:

$$OD_{inhibition} = \left(1 - OD_{GC} / OD_x\right)\%$$

where:

OD_{GC} = Mean OD of the growth control.

OD_x = Mean OD of the tested concentration.

The minimal biofilm inhibitory concentration 50 ($MBIC_{50}$) and minimal biofilm inhibitory concentration 80 ($MBIC_{80}$) values were calculated for each bacterial strain.

The $MBIC_{50}$ and $MBIC_{80}$ were defined as the minimal concentrations of compounds able to inhibit 50 and 80% of biofilm formation, respectively, compared with the negative control (31).

Statistical analysis

The data were analyzed via SPSS v29.1 software (IBM SPSS Statistics for Windows, Version 29.1; IBM Corp., Armonk, NY, USA). The variables (MICs) were checked for a normal distribution via the Kolmogorov–Smirnov normality test. Differences in MICs were subsequently assessed via the Kruskal–Wallis test. *Post hoc* analysis was performed to compare bacterial groups via pairwise comparisons of mean ranks, with Bonferroni correction.

Results

Chemical composition of the plant extracts

The quantification of UA and AA in EGL-L was conducted using HPLC-MS in SIM mode. The analyses were performed in triplicate to ensure accuracy and reproducibility. Calibration curves were constructed for both compounds (calibration range: UA from 3 to 15 µg/g; AA from 5 to 20 µg/g) and subsequently used to determine their concentrations in the extract samples (calibration equation: UA $y = 175.55x + 3002.1$, $R^2 = 0.97$; AA $y = 1157.5x + 35{,}920$, $R^2 = 0.98$). Results revealed that in 1 g of EGL-L, the concentration of UA was 16.12 ± 0.32 µg/g, while AA was present at 47.29 ± 0.13 µg/g. Chromatograms of EGL-L and the two compounds under study are shown in Figure 1. The chemical composition of *Eucalyptus globulus* Labill., particularly its ethanolic extract and volatile fraction, is well-documented in the literature. Previous studies have reported a high yield of triterpenes in ethanolic and methanolic extracts, especially oleanolic acid, betulin, and betulonic acid, along with their acetylated derivatives (35). Additionally, LC-MS analysis of ethanol-extracted *E. globulus* leaves has identified antioxidant and bioactive phytochemicals, including salicylic acid β-D-glucuronide, chlorogenic acid, epicatechin, 2″-O-galloylhyperin, isoquercitrin, isorhapontin, quercitrin, and quercetin-3-O-glucuronide (36). Given the extensive literature on *E. globulus* composition, we opted for a targeted approach, focusing solely on the identification and quantification of ursolic acid and asiatic acid. These two compounds were selected due to their well-documented biological activity and were also used as pure standards in subsequent experimental studies (22).

Antimicrobial susceptibility testing (AST)

The AST results are reported in Supplementary Tables S1–S3. The highest prevalence of MDR strains was observed in the SU group, with 14 out of 18 strains. Within this group, imipenem was the only antibiotic active against all the strains, whereas trimethoprim/sulphamethoxazole was ineffective in all the strains. In the SAG group,

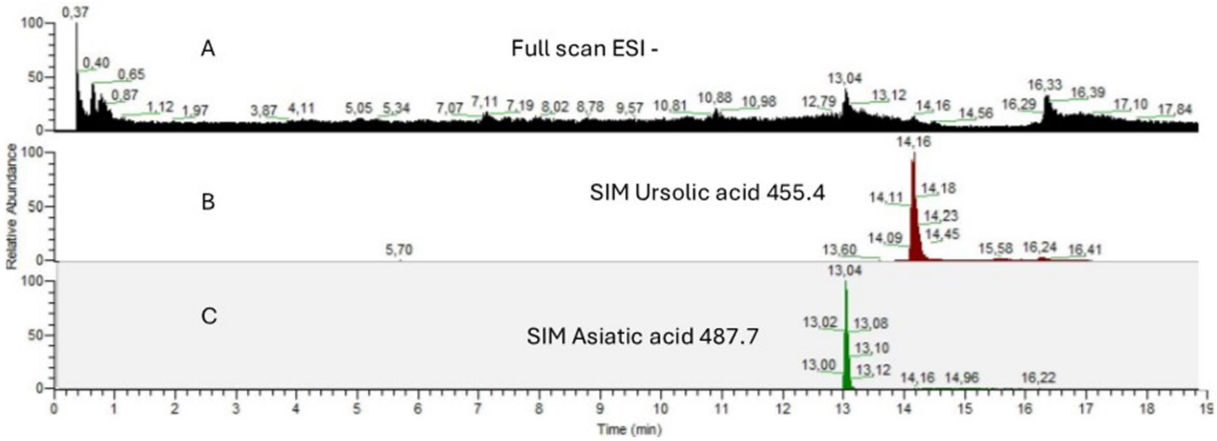

FIGURE 1
HPLC-MS chromatograms of **(A)** Full Scan in ESI negative mode of EGL-L **(B)** SIM of $[M-H]^-$ m/z 455.4 for ursolic acid **(C)** SIM of $[M-H]^-$ m/z 487.7 for asiatic acid.

none of the isolates were classified as MDR. All the SAG isolates were susceptible to cefquinome, cefuroxime, imipenem, and penicillin G but resistant to trimethoprim/sulphamethoxazole. In the EN group, only one strain was identified as MDR. This strain was susceptible to amoxicillin/clavulanic acid, florfenicol, imipenem, penicillin G and vancomycin. Notably, many EN-resistant strains resistant to ampicillin (8 out of 13) were detected. The SA group presented a greater number of MDR strains than non-MDR (10 vs. 6) strains. In particular, 3 out of 15 strains were resistant to cefoxitin, a phenotypic marker for MRSA. On the other hand, cefquinome, fusidic acid, florfenicol, imipenem and rifaximin were the most active antibiotics in this group of bacteria, with 14 out of 15 strains being susceptible to these antibiotics.

MICs of EGL, UA, and AA against reference strains

As reported in Table 1, all the compounds involved in this study showed antimicrobial activity against the reference bacterial strains. EGL-L showed the highest antimicrobial activity against SA ATCC 25923 and SU ATCC 19496, with an MIC of 250 ± 0 μg/mL, while its lowest activity was observed against SAG ATCC 27956, with an MIC of 500 ± 0 μg/mL. Ursolic acid had the lowest MIC value against SU ATCC 19496 (4 ± 0 μg/mL) and the highest MIC values against SAG ATCC 27956 and MRSA ATCC 43300, both at 24 ± 0 μg/mL. Finally, AA had the highest activity against SU ATCC 19496, with an MIC of 4 ± 0 μg/mL, and the lowest activity against MRSA ATCC 43300 and SA ATCC 25923, with an MIC of 32 ± 0 μg/mL.

MIC_{50} AND MIC_{90} of EGL-L, UA, and AA against field strains

The MIC_{50} and MIC_{90} results for EGL-L, UA and AA are reported in Table 2. The *Eucalyptus globulus* leaf extract had the highest MIC_{50} and MIC_{90} values against SA strains (500 μg/mL and 1062.50 μg/mL, respectively). An MIC_{50} value of 250 μg/mL was obtained for EGL-L against all the other bacterial groups, while the lowest MIC_{90} (500 μg/mL) was observed against the EN group. The lowest MIC_{50} and MIC_{90} values for UA were observed in the SU group (2.0 μg/mL) and SAG group (8 μg/mL), respectively. UA had the highest MIC_{50} and MIC_{90} values against the SA group (12 and 64 μg/mL, respectively). The lowest MIC_{50} and MIC_{90} values for AA were detected in the SU and SAG groups (6 and 16 μg/mL, respectively), whereas the highest MIC_{50} and MIC_{90} values were detected in the SA group (24 μg/mL and 187.50 μg/mL, respectively). Overall, the MIC_{50} and MIC_{90} values for EGL-L were significantly greater than those observed for UA and AA ($p < 0.001$). Moreover, the Kruskal–Wallis nonparametric test revealed significant differences in the median MIC values between the different bacterial groups for UA (<0.001) and AA (<0.001), whereas no significant difference was detected for EGL-L ($p = 0.056$) (Figures 2a–c). The pairwise comparison among each bacterial group revealed that for UA, the SA group was significantly different from the SU group ($p < 0.05$). For AA, the pairwise comparison revealed a significant difference between the SA group and the SU/SAG group ($p < 0.05$) (Figure 3). In Table 3 are showed the MIC average of EGL-L, UA and AA against MDR field strains of *S. aureus* and *S. uberis*.

TABLE 1 Minimal Inhibitory Concentrations (MICs) of *Eucalyptus globulus* leaves extract (EGL-L), ursolic (UA) and asiatic acids (AA) against reference bacterial strains.

Reference strains	Compounds	MIC (μg/mL)	SD
Streptococcus agalactiae ATCC 27956	EGL-L	500	0
	UA	24.0	11.30
	AA	8.00	0
Streptococcus uberis ATCC 19496	EGL-L	250	0
	UA	4.00	0
	AA	4.00	0
Enterococcus faecium ATCC 19434	EGL-L	375	176.8
	UA	10.0	8.50
	AA	8.00	0
MRSA ATCC 43300	EGL-L	375	176.8
	UA	24.0	11.30
	AA	32.0	0
Staphylococcus aureus ATCC 25923	EGL-L	250	0
	UA	12.0	5.70
	AA	32.0	0

Bactericidal kinetic curves (BKC) against reference strains

Figure 4 presents the results of BKC of EGL-L against reference bacterial strains. For *E. faecium* and *S. agalactiae*, the tested concentrations were 2000, 1,000, and 500 μg/mL, while for MRSA, *S. aureus*, and *S. uberis*, the concentrations tested were 1,000, 500, and 250 μg/mL. For *E. faecium*, all tested concentrations showed a bacteriostatic effect; however, the 2000 μg/mL concentration demonstrated the highest antimicrobial activity at all experimental time points. This concentration exhibited similar results against *S. agalactiae*. In contrast, for MRSA and *S. aureus*, all tested concentrations showed similar OD values to the growth control up to 6 h. However, during the logarithmic growth phase, a strong antimicrobial activity was observed, inhibiting bacterial growth at the remaining time points. For *S. uberis*, the 500 and 250 μg/mL concentrations showed lower OD values than the growth control throughout the experiment, while the 1,000 μg/mL concentration only exhibited this effect at 24 and 48 h.

Figure 5 shows the results of the BKC of UA against reference bacterial strains. Specifically, concentrations of 64, 32, and 16 μg/mL were tested against *S. agalactiae* and MRSA, while 32, 16, and 8 μg/mL were tested against *S. aureus*. Finally, concentrations of 16, 8, and 4 μg/mL were tested against *S. uberis* and *E. faecium*. Regarding *S. agalactiae*, all tested concentrations demonstrated bactericidal activity. In contrast, against MRSA, bactericidal effects were observed only at 64 and 32 μg/mL, while 16 μg/mL exhibited bacteriostatic activity up to 8 h. After the logarithmic phase, at 24 h, the OD values of the 16 μg/mL concentration were similar to those of the growth control, indicating bacterial growth. A similar pattern was observed against *S. aureus*, with only 32 μg/mL exhibiting bactericidal activity. In contrast, concentrations of 16 and 8 μg/mL demonstrated bacteriostatic effects up to 8 h, prior to the logarithmic phase. For

TABLE 2 Minimal Inhibitory Concentration on 50% of the strains (MIC_{50}) and Minimal Inhibitory Concentration on 90% of the strains (MIC_{90}) of *Eucalyptus globulus* leaves extract (EGL-L), ursolic (UA) and asiatic acids (AA) against field strains isolated from cows with mastitis.

Bacterial species	Compounds	MIC_{50} (μg/mL)	MIC_{90} (μg/mL)
Streptococcus agalactiae	EGL-L	250	750
	UA	4.0	8.00
	AA	8.0	16.0
Streptococcus uberis	EGL-L	250	1000
	UA	2.0	12.0
	AA	6.0	23.5
Staphylococcus aureus	EGL-L	500	1062.5
	UA	12.0	64.00
	AA	24.0	187.5
Enterococcus sp.	EGL-L	250.0	500
	UA	4.00	23.4
	AA	16.0	32.0

E. faecium, 8 and 4 μg/mL concentrations exhibited bacteriostatic effects up to 24 h, while the 16 μg/mL concentration showed a bactericidal effect. Finally, against *S. uberis*, the 16 and 8 μg/mL concentrations showed bactericidal effects.

Figure 6 displays the results of the BKC of AA against reference strains. Specifically, concentrations of 128, 64, and 32 μg/mL were tested against MRSA and *S. aureus*, while 32, 16, and 8 μg/mL were tested against *E. faecium* and *S. agalactiae*. Lastly, concentrations of 16, 8, and 4 μg/mL were tested against *S. uberis*. Asiatic acid exhibited strong antimicrobial activity with bactericidal effect against *MRSA* and *S. aureus* at all tested concentrations. In contrast, against *E. faecium* and *S. agalactiae*, bactericidal effect was observed only at 32 and 16 μg/mL, while 8 μg/mL showed a bacteriostatic effect up to 24 h. A similar pattern was observed against *S. uberis*, where 16 and 8 μg/mL showed bactericidal effects, while the 4 μg/mL concentration exhibited a bacteriostatic effect up to 24 h.

Biofilm formation of reference and field strains

The evaluation of biofilm formation by reference strains revealed that only SA ATCC 25923 was moderately adherent, whereas MRSA ATCC 43300 was strongly adherent. All the other reference strains exhibited weak adherence. For the field strains, nonbiofilm producers (nonadherent) belonged to the EN (5 out of 13; 38.5%) and SU (8 out of 18; 44.4%) groups. Weak biofilm producers were most common in the SU group (8 out of 18; 44.4%) and EN group (7 out of 13; 53.8%) but least common in the SA group (1 out of 15; 6.7%). Conversely, the SA group presented the highest proportion of moderate biofilm-producing strains (6 out of 15; 40.0%), followed by the SAG group (5 out of 17; 29.5%), SU group (2 out of 18; 11.1%) and EN group (1 out of 13; 7.7%) (Table 4).

Finally, strong biofilm-producing bacteria were found only in the SA group (8 out of 15; 53.3%) and SAG group (8 out of 17; 47.0%).

$MBIC_{50}$ and $MBIC_{80}$ of EGL, UA, and AA on moderately adherent (MA) field and reference strains

The $MBIC_{50}$ and $MBIC_{80}$ results are reported in Table 4.

For *Staphylococcus aureus* ATCC 25923, EGL-L had an $MBIC_{50}$ and $MBIC_{80}$ of 3.96 μg/mL and 7.81 μg/mL, respectively. The UA $MBIC_{50}$ and $MBIC_{80}$ values were identical (32 μg/mL). The $MBIC_{50}$ and $MBIC_{80}$ for AA were both 16 μg/mL. With respect to EGL-L, an $MBIC_{50}$ was found for all the field MA strains, except for *S. uberis* BV2 (>2000 μg/mL). The lowest $MBIC_{50}$ value was observed for *Enterococcus* sp. BV21 (7.81 μg/mL), while the highest value was found for *S. agalactiae* IZS5 and IZS12 (2000 μg/mL). Most of the MA field strains reported an $MBIC_{80}$ > 2000 μg/mL for EGL-L (9 out of 14).

Ursolic acid had the lowest $MBIC_{50}$ for *S. agalactiae* IZS5 and IZS11 (0.50 μg/mL), while the highest value was observed for *S. uberis* BV2 (256 μg/mL). An $MBIC_{80}$ of 8 μg/mL was obtained for UA on all SAG field strains identified as moderately adherent, except for *S. agalactiae* IZS4 (128 μg/mL), whereas an $MBIC_{80}$ > 256 μg/mL was reported for *S. uberis* BV2, BV16 and *S. aureus* IZS5.

Finally, AA had the lowest $MBIC_{50}$ for *S. aureus* BV16 (< 0.5 μg/mL) and the lowest $MBIC_{80}$ for *S. agalactiae* IZS10 (4 μg/mL).

$MBIC_{50}$ and $MBIC_{80}$ of EGL, UA, and AA against strongly adherent reference and field strains

The results of the $MBIC_{50}$ and $MBIC_{80}$ values for the StA reference and field strains are reported in Table 5. For MRSA ATCC 43300, the $MBIC_{50}$ and $MBIC_{80}$ values of EGL-L were 125 μg/mL and 250 μg/mL, respectively. For UA, the $MBIC_{50}$ and $MBIC_{80}$ were 32 μg/mL and 64 μg/mL, respectively. For AA, both the $MBIC_{50}$ and the $MBIC_{80}$ were 16 μg/mL. For the field strains, the lowest $MBIC_{50}$ for EGL-L was observed for *S. aureus* BV44 (3.9 μg/mL), whereas the highest was observed for *S. agalactiae* IZS13 (500 μg/mL). Notably, 8 out of 16 StA strains presented an $MBIC_{80}$ > 2000 μg/mL. Ursolic acid had the lowest $MBIC_{50}$ (0.5 μg/mL) against *S. aureus* BV44, *S. agalactiae* IZS2 and IZS6, whereas *S. aureus* BV5 and *S. agalactiae* IZS7 presented $MBIC_{80}$ values > 256 μg/mL.

For AA, the lowest $MBIC_{50}$ value (2 μg/mL) was observed for *S. aureus* BV43 and BV44 and *S. agalactiae* IZS6 and IZS8; the latter also presented the lowest $MBIC_{80}$ at the same value. The highest $MBIC_{50}$ was observed for *S. agalactiae* IZS2 (128 μg/mL). Finally, the highest $MBIC_{80}$ for AA was observed for *S. agalactiae* IZS7 (>256 μg/mL).

Discussion

Antibiotics represent the reference treatment for BM, with penicillins, aminoglycosides and tetracyclines being the most commonly used classes (7). This study assessed the susceptibility of several bacterial strains not only to antibiotics commonly used to treat BM but also to molecules classified as critically important for human health and banned in veterinary use (11). Some commonly used antibiotics, such as ampicillin, gentamicin and trimethoprim/sulphamethoxazole, were ineffective against most of the clinical strains

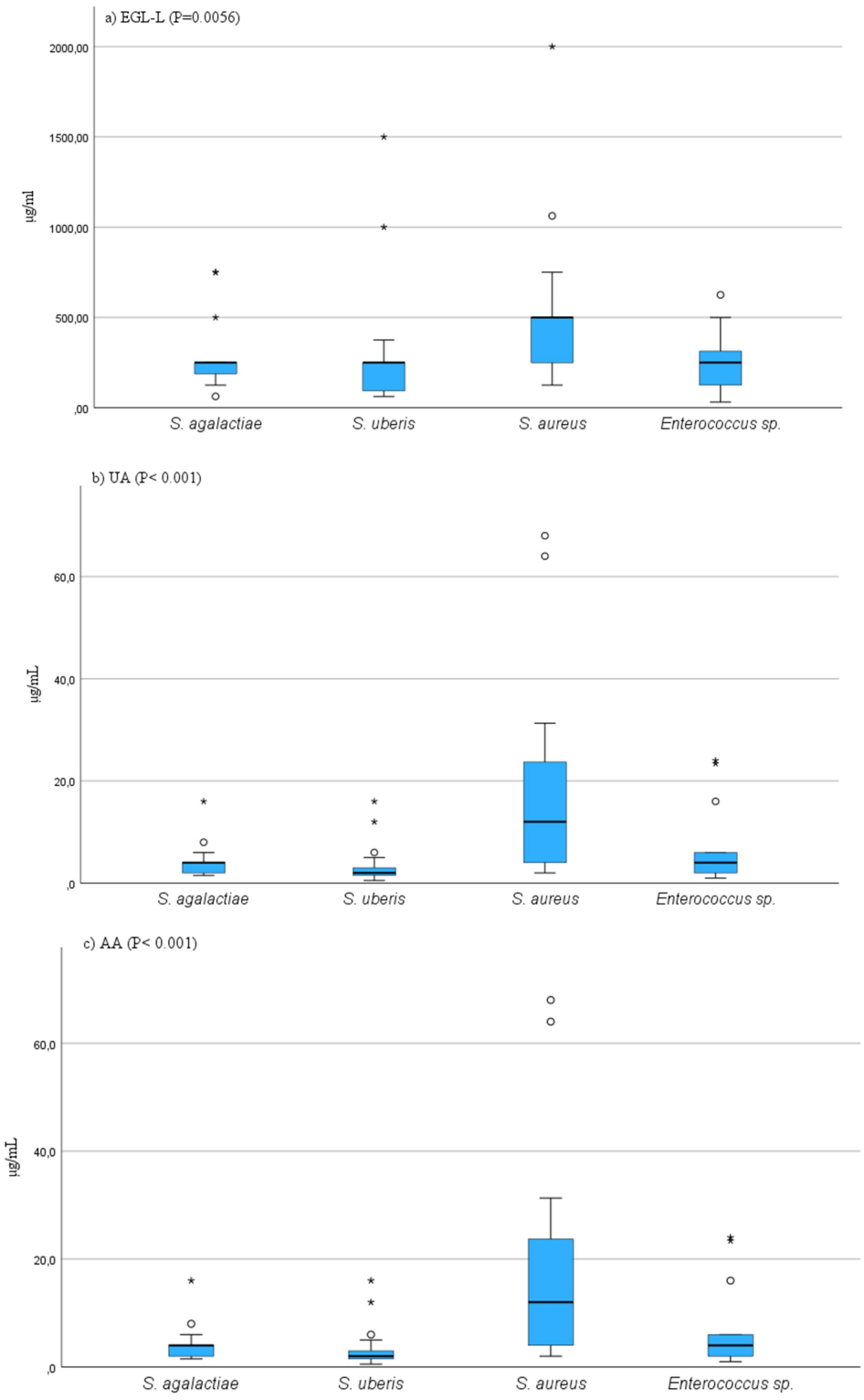

FIGURE 2
(a–c) Results of Kruscal-Wallis comparison among MIC values of field bacterial species for Eucalyptus globulus leaves extract (EGL-L), ursolic acid (UA) and asiatic acid (AA). On y-axis are showed the MIC values, on x-axis are showed bacterial species.

considered. In contrast, third-generation cephalosporins and imipenem are the most active antibiotics, although their use is restricted in veterinary clinical practice, as they belong to EMA categories A and B (37). Thirty-nine percent of the isolated strains, mainly *S. uberis* and *S. aureus*, were classified as MDROs according to the classification proposed in the literature (29). Of particular concern were *S. uberis* isolates resistant to penicillin, cephalosporins and, in one case, vancomycin. This finding was in agreement with the results reported

10.3389/fvets.2025.1565787

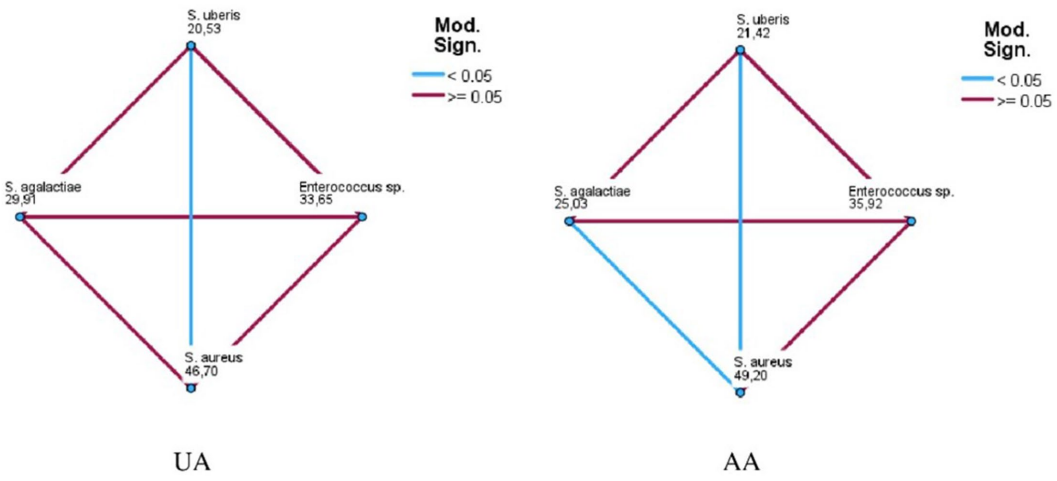

FIGURE 3
Pairwise comparison among field bacterial species for ursolic acid (UA) and asiatic acid (AA).

TABLE 3 Minimal Inhibitory Concentrations (MICs) of *Eucalyptus globulus* leaves extract (EGL-L), ursolic (UA) and asiatic acids (AA) against MDR field strains isolated from cows with mastitis.

Bacterial strains – MDR	EGL-L	UA	AA
	MIC (μg/mL) ± SD		
S. aureus MDR	618.8 ± 559.4	21.6 ± 24.4	37.2 ± 53.5
S. uberis MDR	257.2 ± 242.1	3.10 ± 4.09	15.7 ± 35.2

by other authors (38). The emergence of MDROs in veterinary medicine is of concern, as it may result in a reduction in therapeutic options for patients (39). For this reason, in recent years, researchers have focused on alternative therapeutic approaches to conventional antimicrobial agents (4). Among them, plant extracts and essential oils have shown interesting antimicrobial activity against mastitis pathogens (12). This study investigated a plant extract of *Eucalyptus globulus* leaves from Rwanda and its main pentacyclic triterpenes, AA and UA, which are well documented for their antimicrobial activity (16, 40, 41). The comparison of the results of UA and AA quantification in EGL-L and their antimicrobial activity indicates that the activity of EGL-L, even at the highest tested concentration (2000 μg/mL), is not solely due to the presence of AA and UA, given that these are present at concentrations significantly lower than their MIC values. Rather, it is also due to the synergistic activity of the phytocomplex, which is particularly rich in ursane, oleanane and lupane skeletons. Even if the MIC values of EGL-L were higher than those of AA and UA, there were no significant differences among the bacterial populations, indicating the same efficacy in all the considered bacterial groups. Conversely, for both AA and UA, different efficacy were observed among the bacterial groups. In particular, UA had significantly lower MIC values in *S. uberis* than in *S. aureus*. For AA, the same significant difference was observed between the two *Streptococcus* groups and *S. aureus*. All three tested compounds were effective against MDROs. Compared with those of conventional antibiotics, their efficacy may be due to the plurality of targets of the extract and the pentacyclic triterpenes, indicating the possibility of using these compounds to treat MDR-BM (9). These findings are consistent with the existing literature, which reports strong antimicrobial activity of UA against *S. aureus* ATCC 25923 (MIC = 8 μg/mL) and multidrug-resistant organisms (MDROs) such as MRSA (MIC = 3 μg/mL) and Vancomicin-resistant *Enterococcus* (VRE) (MIC = 4 μg/mL). Similarly, our results regarding AA align with previous research. One study evaluated its antimicrobial activity against foodborne bacterial pathogens isolated from contaminated chicken, duck, and dairy products, reporting strong activity against Gram-positive bacteria, with MIC values comparable to our findings (28 ± 2 μg/mL for *S. aureus* and 20 ± 2 μg/mL for *E. faecalis*). However, a direct comparison of the antimicrobial activity of AA and UA against Gram-negative bacteria is not feasible, as our study exclusively focused on Gram-positive bacteria isolated during bovine mastitis. Nonetheless, literature indicates that UA exhibits moderate to limited activity against *E. coli* (MIC = 50 μg/mL), *Salmonella Typhi* (MIC = 50 μg/mL), and *Pseudomonas aeruginosa* (MIC > 256 μg/mL). In contrast, AA has been reported to be more effective against foodborne bacterial strains (*E. coli* O157:H7, *S.* Typhimurium DT104, and *P. aeruginosa*), with MIC values below 40 μg/mL (16, 41).

In our study, we evaluated the BKC of EGL-L, AA, and UA against reference strains, testing three concentrations starting from their MIC values. The EGL-L extract predominantly exhibited a bacteriostatic effect at 2000 μg/mL against *E. faecium*, *S. agalactiae*, and *S. uberis*, while all tested concentrations (1,000, 500, and 250 μg/mL) showed this effect against MRSA and *S. aureus*. In contrast, UA exhibited both bactericidal and bacteriostatic effects depending on the concentration and bacterial strain. It was bactericidal against *S. uberis* (16, 8 and 4 μg/mL) and *S. agalactiae* (64, 32, and μg/mL), while only the highest concentrations showed bactericidal activity against *E. faecium* and *S. aureus*, respectively 16 and 32 μg/mL. Against MRSA, higher concentrations (64 and 32 μg/mL) were bactericidal, whereas 16 μg/mL exhibited bacteriostatic effect up to 8 h. Regarding AA, it displayed the strongest antimicrobial activity, with a bactericidal effect at all tested concentrations (128, 64, and 32 μg/mL) against MRSA and *S. aureus*. Against *E. faecium*, S. *agalactiae*, and *S. uberis*, bactericidal effects were only observed at highest concentrations, while the lowest concentrations (8 μg/mL for *E. faecium* and *S. agalactiae* and 4 μg/

10.3389/fvets.2025.1565787

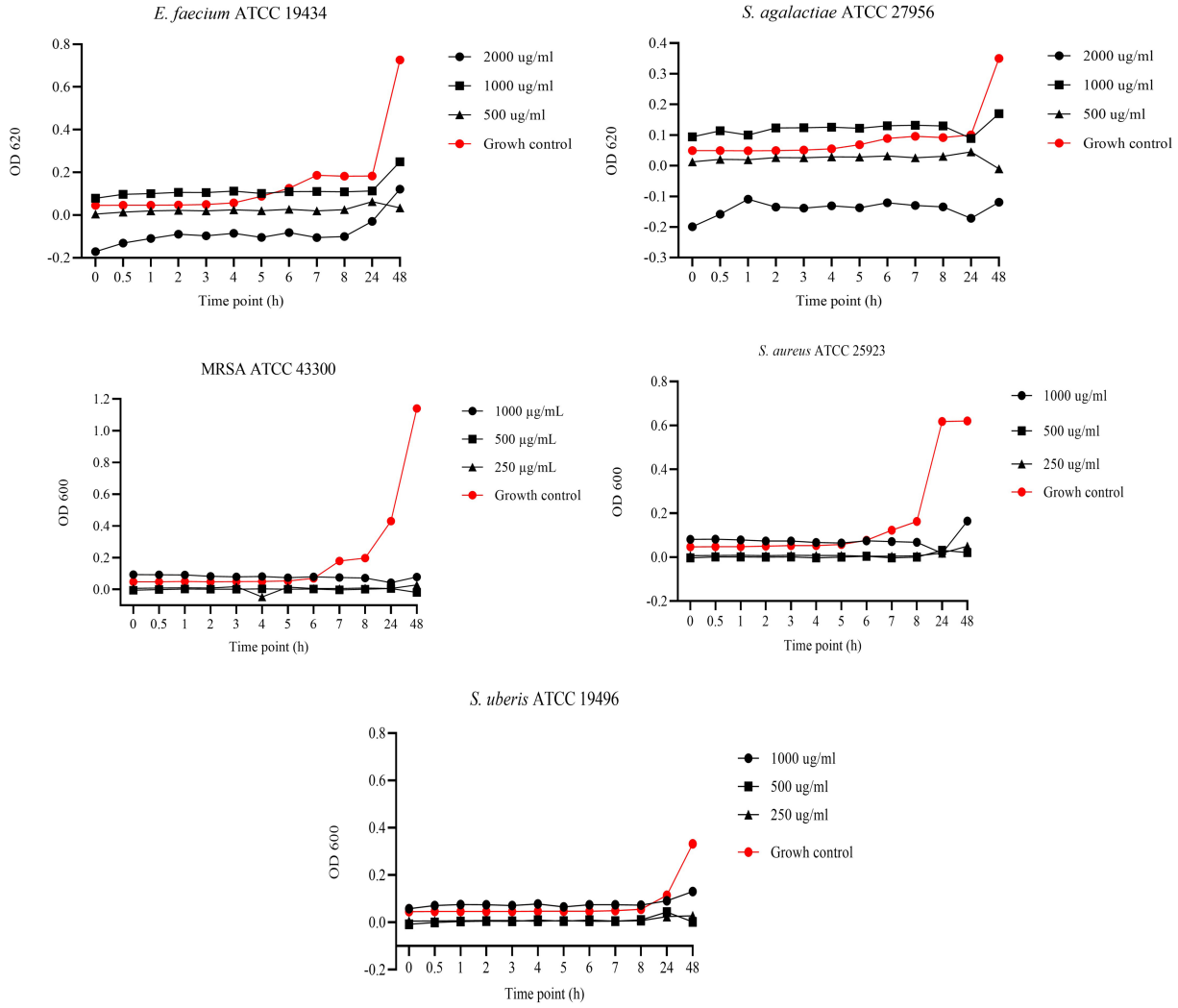

FIGURE 4
Bactericidal Kinetic Curves (BKC) of *Eucalyptus globulus* Leaves Extract (EGL-L) against tested reference bacteria. On *y* axis are reported the OD values of bacterial growth, on *x* axis the timepoint of incubation.

mL for *S. uberis*) exhibited bacteriostatic effects up to 24 h. These results indicate that EGL-L primarily exerts a bacteriostatic effect against all tested strains, while both pentacyclic triterpenes exhibited either bactericidal or bacteriostatic activity, depending on the concentration and the bacterial strain.

Biofilms act as a defense mechanism that enables bacteria to evade the immune response, resist conventional disinfectants, and reduce the effectiveness of antibiotic treatment (42). As a result, alternative strategies, including the use of plant-derived compounds aimed at either preventing biofilm formation or eradicating preformed biofilms, have been explored in recent years (40, 41). As reported in the literature (12), several compounds of plant origin have also been evaluated for their antibiofilm activity toward the main pathogens of BM. Several studies have assessed the activity of UA against biofilms formed by clinical isolates from bovine mastitis (BM). Notably, UA has been shown to effectively inhibit the formation of *Staphylococcus aureus* and *Streptococcus uberis* biofilms derived from BM at concentrations similar to those observed in this study. At concentrations of 30 and 100 µg/mL, UA inhibited 33.96 ± 3.17% and 57.40 ± 2.8% of *S. uberis* biofilm formation, respectively. For *S. aureus* from BM, UA demonstrated a stronger inhibitory effect, with 71.5 and 48.6% inhibition at concentrations of 60 µg/mL and 30 µg/mL, respectively (43, 44). In contrast, one study reports the antibiofilm activity of *Eucalyputs globulus* extract against biofilm produced solely by *S. aureus* from bovine with mastitis (5). The preliminary qualitative and quantitative assessment of the biofilm-producing ability of mastitis isolates revealed that most of our strains classified as moderate or strong biofilm producers were *S. aureus* or *S. agalactiae* species. This finding agrees with the literature (42–47), where *S. aureus* and *S. agalactiae* are indicated as the bacteria that produce the most biofilm bacteria involved in bovine mastitis. With respect to the antibiofilm activity of EGL-L, AA and UA, none of them were able to completely inhibit (99.9%) biofilm formation. However, partial inhibition, measured as the $MBIC_{50}$ or $MBIC_{80}$, was detected. The extract had an $MBIC_{80} \geq 2000$ µg/mL in more than half of the moderate and strong biofilm-producing strains. However, all the considered

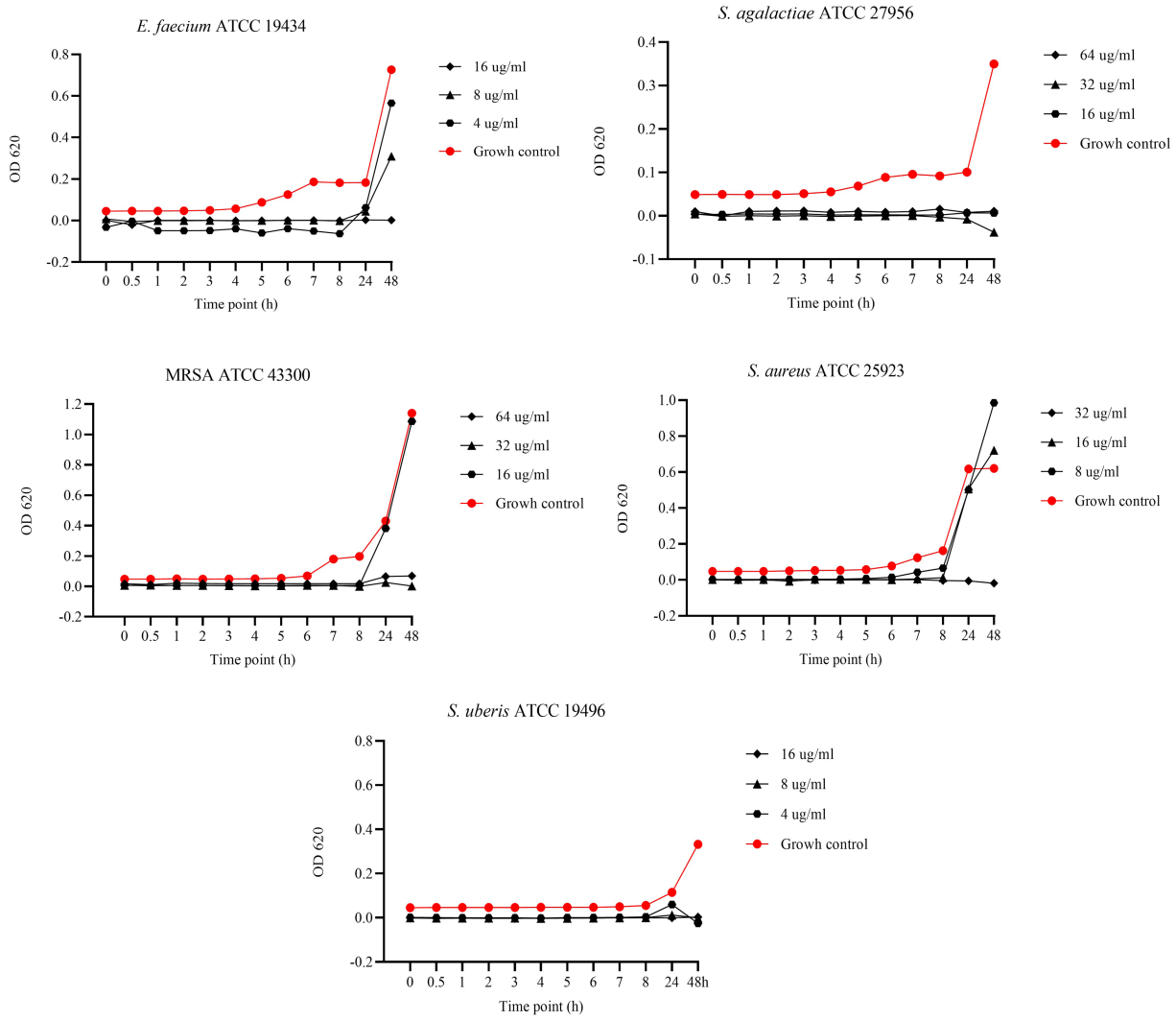

FIGURE 5
Bactericidal Kinetic Curves (BKC) of ursolic acid (UA) against tested reference bacteria. On *y* axis are reported the OD values of bacterial growth, on *x* axis the timepoint of incubation.

strains (except one) presented an $MBIC_{50} \leq 2000$ μg/mL. Another study reported the antibiofilm activity of *Eucalyptus globulus* extract, attributing its effects to a reduction in bacterial populations caused by inhibited microbial respiration, increased plasma membrane permeability, ion leakage, or the hydrophilic nature of the bacterial cell wall (48). The pentacyclic triterpenes were much more effective than the natural extract at inhibiting biofilms, since an $MBIC_{80}$ was obtained for all the tested bacteria, except for five isolates. In addition, AA had the highest antibiofilm activity, with an $MBIC_{80} \leq 32$ μg/mL for most of the tested strains. According to the literature (19), the stronger antibiofilm activity of AA than that of UA could be due to different chemical structures. This could allow AA to penetrate bacterial cells more effectively, hindering their adhesion and thereby preventing biofilm formation.

Analyzing the antimicrobial and antibiofilm activity of EGL-L, it is observed that the MIC_{90} values for *S. aureus* and *S. agalactiae*, the main biofilm-producing bacteria, are higher than the concentrations required to achieve $MBIC_{50}$, particularly against *S. aureus*. This suggests that the extract only partially inhibits biofilm formation at these concentrations. This finding is consistent with the literature, which reports that *E. globulus* extract exhibits antibiofilm activity against *S aureus* biofilms from bovine mastitis. The author reports that concentrations 8–32 times higher than the MIC are required, supporting the evidence that biofilms are 10–1,000 times more resistant than planktonic cells (5). Regarding UA, at MIC_{90}, it achieves $MBIC_{50}$ for all *S. aureus* strains and all but two *S. agalactiae* strains. However, for $MBIC_{80}$, several strains require higher concentrations. Furthermore, AA exhibits a similar behavior to UA but it is able to achieve both $MBIC_{50}$ and $MBIC_{80}$ at MIC_{90} for all *S. aureus* strains except one, while for *S. agalactiae*, it only reaches $MBIC_{50}$.

In conclusion, EGL-L only partially inhibits biofilm formation, particularly in *S. aureus*, while UA and AA demonstrate greater efficacy.

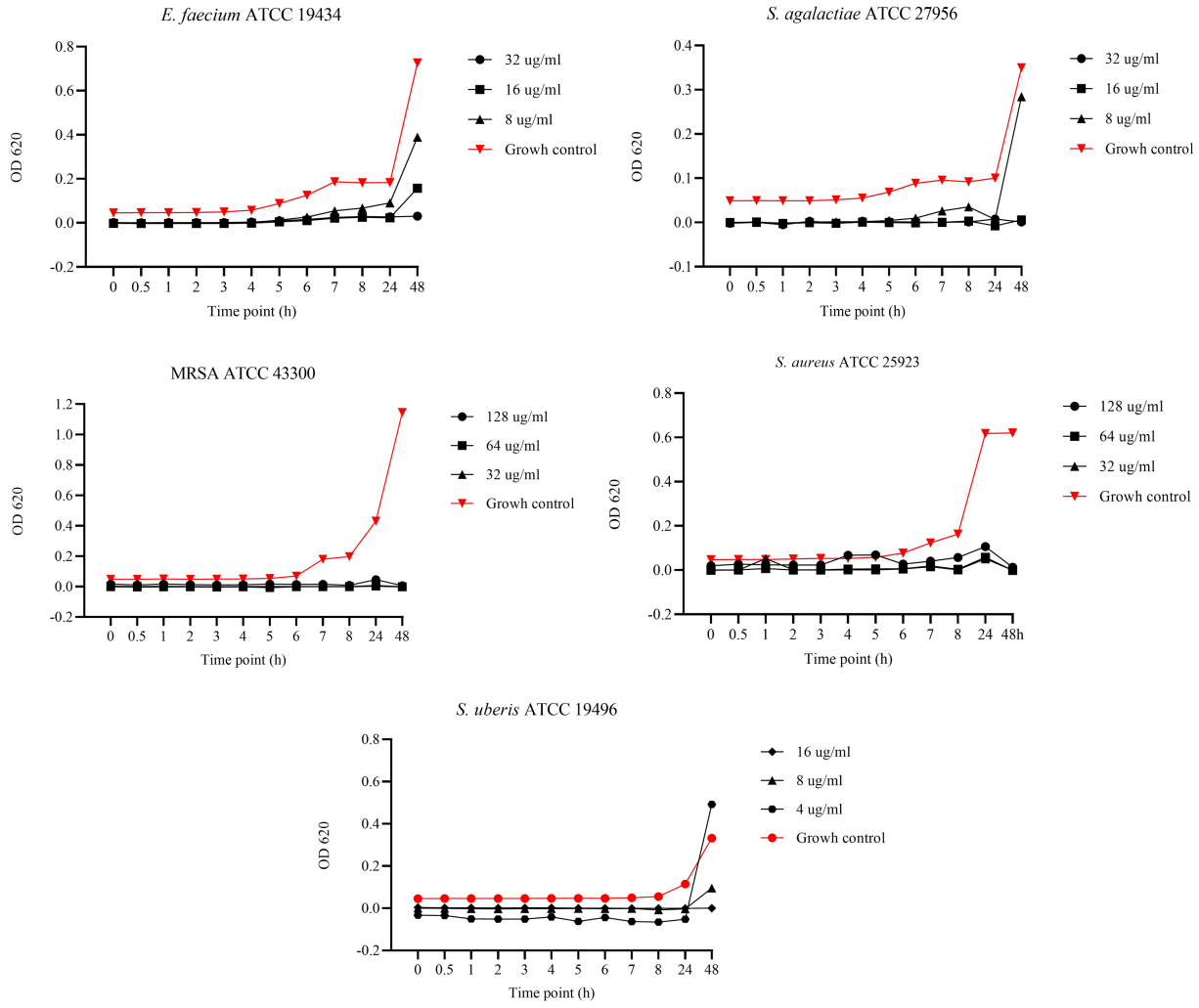

FIGURE 6
Bactericidal Kinetic Curves (BKC) of asiatic acid (AA) against tested reference bacteria. On *y* axis are reported the OD values of bacterial growth, on *x* axis the timepoint of incubation.

UA achieves $MBIC_{50}$ for nearly all strains at MIC_{90}, whereas AA appears even more active against *S. aureus*. However, for both, $MBIC_{80}$ requires higher concentrations, indicating a dose-dependent effect. These findings highlight the antibiofilm potential of UA and AA, with AA showing particularly promising results, suggesting significant prospects for future studies.

Conclusion

Bovine mastitis is the main cause of economic losses in dairy cattle farming because of the early culling of affected animals and the lack of economic income from wasting milk. Furthermore, the presence of MDROs on farms could reduce the number of therapeutic options available for treating affected animals.

In the present study, a plant extract derived from *Eucalyptus globulus* leaves was evaluated, along with its main active components AA and UA. All the tested compounds exhibited notable antimicrobial activity against MDROs. However, as expected, the pure compounds AA and UA showed lower MIC values on all field bacterial strains compared to EGL-L. Despite this, the extract demonstrated similar efficacy across all bacterial groups, possibly indicating a broader therapeutic potential compared to the two pentacyclic triterpenes, which exhibited more selective antimicrobial activity. Pentacyclic triterpenes, particularly AA, displayed promising antibiofilm activity, especially against strongly adherent field strains of bovine mastitis. These findings suggest that AA is the most promising alternative to conventional antimicrobials among the compounds tested. Asiatic acid has the potential to be used topically, intramammary, for the control and prevention of bovine mastitis, particularly due to its efficacy against biofilm formation. Future studies will be necessary to assess the *in vitro* cytotoxicity of these compounds, both on common cell lines used for screening new alternative compounds and on specific cell lines. Furthermore, *in vivo* studies and formulation development will be required to evaluate their effective topical use in the treatment of bovine mastitis.

TABLE 4 Minimal Biofilm Inhibitory Concentrations 50 and 80 ($MBIC_{50}$ and $MBIC_{80}$) of *Eucalyptus globulus* leaves extract (EGL-L), ursolic (UA), and asiatic acid (AA) against moderately adherent reference and field strains.

Moderately adherent bacteria	$MBIC_{50}$ (μg/mL)			$MBIC_{80}$ (μg/mL)		
	EGL-L	UA	AA	EGL-L	UA	AA
S. aureus ATCC 25923	3.96	32.00	16.00	7.81	32.0	16.0
S. uberis BV2	>2000	256	8.00	>2000	>256	>256
S. uberis BV16	125	4.00	4.00	>2000	>256	>256
S. agalactiae IZS4	31.25	128	4.00	1000	128	32.0
S. agalactiae IZS5	2000	0.50	2.00	>2000	8.00	32.0
S. agalactiae IZS10	500	4.00	2.00	>2000	8.00	4.00
S. agalactiae IZS11	250	0.50	4.00	>2000	8.00	8.00
S. agalactiae IZS12	2000	8.00	2.00	>2000	8.00	4.00
Enterococcus sp. BV21	7.81	65.5	4.00	>2000	256	>256
S. aureus BV16	125	1.00	< 0.50	125	32.0	32
S. aureus IZS4	15.63	16.0	16.0	62.5	32.0	16.0
S. aureus IZS5	125	16.0	16.0	>2000	>256	>256
S. aureus IZS7	15.63	32.0	16.0	>2000	256	16.0
S. aureus IZS8	62.50	16.0	16.0	62.5	16.0	16.0
S. aureus IZS9	31.25	16.0	16.0	125	16.0	16.0

TABLE 5 Minimal biofilm inhibitory concentration ($MBIC_{50}$ and $MBIC_{80}$) of *Eucalyptus globulus* leaves extract (EGL-L), ursolic (UA) and asiatic acid (AA) against strongly adherent reference and field strains.

Strongly adherent bacteria	$MBIC_{50}$ (μg/mL)			$MBIC_{80}$ (μg/mL)		
	EGL-L	UA	AA	EGL-L	UA	AA
MRSA ATCC 43300	125	32.0	16.0	250	64.0	16.0
S. aureus BV5	31.25	16.0	4.00	62.5	>256	8.00
S. aureus BV30	250	32.0	8.00	500	32.0	8.00
S. aureus BV42	7.81	4.00	4.00	7.81	0.50	4.00
S. aureus BV43	31.25	4.00	2.00	>2000	256	4.00
S. aureus BV44	3.90	0.50	2.00	62.5	8.00	4.00
S. aureus IZS2	125	32.0	16.0	>2000	256	16.0
S. aureus IZS3	62.5	32.0	16.0	>2000	64.0	16.0
S. aureus IZS6	62.5	64.0	16.0	62.5	64.0	16.0
S. agalactiae IZS2	31.25	0.50	128	500	0.50	128
S. agalactiae IZS3	125	4.00	32	125	256	32.0
S. agalactiae IZS6	125	0.50	2.00	>2000	8.00	32.0
S. agalactiae IZS7	15.63	1.00	4.00	>2000	>256	>256
S. agalactiae IZS8	31.25	1.00	2.00	125	2.00	2.00
S. agalactiae IZS13	500	16.0	8.00	>2000	16.0	8.00
S. agalactiae IZS14	7.81	4.00	8.00	>2000	4.00	8.00
S. agalactiae IZS15	62.5	4.00	8.00	>2000	8.00	8.00

Data availability statement

The raw data supporting the conclusions of this article will be made available upon request to interested researchers by the authors.

Author contributions

NM: Conceptualization, Data curation, Investigation, Methodology, Software, Writing – original draft, Writing – review & editing. CoS:

Conceptualization, Data curation, Formal analysis, Investigation, Methodology, Validation, Visualization, Writing – review & editing. ChS: Formal analysis, Investigation, Methodology, Software, Writing – review & editing. GA: Data curation, Formal analysis, Supervision, Validation, Writing – review & editing. VA: Investigation, Writing – review & editing. AP: Data curation, Investigation, Methodology, Writing – review & editing. LM: Investigation, Writing – review & editing. SC: Formal analysis, Supervision, Validation, Writing – review & editing. SG: Formal analysis, Supervision, Validation, Writing – review & editing. ST: Data curation, Formal analysis, Methodology, Software, Writing – review & editing. GC: Supervision, Validation, Writing – review & editing. CC: Project administration, Resources, Supervision, Validation, Writing – review & editing.

Funding

The author(s) declare that no financial support was received for the research and/or publication of this article.

Conflict of interest

The authors declare that the research was conducted in the absence of any commercial or financial relationships that could be construed as a potential conflict of interest.

Generative AI statement

The authors declare that no Gen AI was used in the creation of this manuscript.

Publisher's note

Supplementary material

The Supplementary material for this article can be found online at: https://www.frontiersin.org/articles/10.3389/fvets.2025.1565787/full#supplementary-material

References

1. Cheng WN, Han SG. Bovine mastitis: risk factors, therapeutic strategies, and alternative treatments — a review. *Asian Australas J Anim Sci*. (2020) 33:1699–713. doi: 10.5713/ajas.20.0156

2. Ashraf A, Imran M. Diagnosis of bovine mastitis: from laboratory to farm. *Trop Anim Health Prod*. (2018) 50:1193–202. doi: 10.1007/s11250-018-1629-0

3. Fox LK, Gay JM. Contagious mastitis. *Vet Clin North Am Food Anim Pract*. (1993) 9:475–87. doi: 10.1016/S0749-0720(15)30615-0

4. Tomanić D, Samardžija M, Kovačević Z. Alternatives to antimicrobial treatment in bovine mastitis therapy: A review. *Antibiotics*. (2023) 12:683. doi: 10.3390/antibiotics12040683

5. Gomes F, Martins N, Ferreira ICFR, Henriques M. Anti-biofilm activity of hydromethanolic plant extracts against *Staphylococcus aureus* isolates from bovine mastitis. *Heliyon*. (2019) 5:e01728. doi: 10.1016/j.heliyon.2019.e01728

6. Lopes TS, Fontoura PS, Oliveira A, Rizzo FA, Silveira S, Streck AF. Use of plant extracts and essential oils in the control of bovine mastitis. *Res Vet Sci*. (2020) 131:186–93. doi: 10.1016/j.rvsc.2020.04.025

7. Niemi RE, Hovinen M, Vilar MJ, Simojoki H, Rajala-Schultz PJ. Dry cow therapy and early lactation udder health problems—associations and risk factors. *Prev Vet Med*. (2021) 188:105268. doi: 10.1016/j.prevetmed.2021.105268

8. Kabera F, Roy JP, Afifi M, Godden S, Stryhn H, Sanchez J, et al. Comparing Blanket vs. Selective dry cow treatment approaches for elimination and prevention of intramammary infections during the dry period: A systematic review and meta-analysis. *Front Vet Sci*. (2021) 8:688450. doi: 10.3389/fvets.2021.688450

9. Mushtaq S, Shah AM, Shah A, Lone SA, Hussain A, Hassan QP, et al. Bovine mastitis: an appraisal of its alternative herbal cure. *Microb Pathog*. (2018) 114:357–61. doi: 10.1016/j.micpath.2017.12.024

10. Crispie F, Flynn J, Ross RP, Hill C, Meaney WJ. Dry cow therapy with a non-antibiotic intramammary teat seal-a review. *Ir Vet J*. (2004) 57:412–8. doi: 10.1186/2046-0481-57-7-412

11. Regulation (EU) 2019/6 of the European Parliament and of the council of 11 December 2018 on veterinary medicinal products and repealing directive 2001/82/EC. EU Commission, EURLex. (2018). Available online at: http://data.europa.eu/eli/reg/2019/6/2022-01-28 (Accessed February, 2025).

12. Caneschi A, Bardhi A, Barbarossa A, Zaghini A. Plant essential oils as a tool in the control of bovine mastitis: an update. *Molecules*. (2023) 28:3425. doi: 10.3390/molecules28083425

13. Spadini C, Iannarelli M, Carrillo Heredero AM, Montanaro SL, Mezzasalma N, Simoni M, et al. Stability of the antimicrobial activity of selected essential oils and nature identical compounds and their interaction with tween 20 against reference bacterial strains of zootechnical interest. *Ital J Anim Sci*. (2024) 23:189–99. doi: 10.1080/1828051X.2024.2304042

14. Spaggiari C, Annunziato G, Spadini C, Montanaro SL, Iannarelli M, Cabassi CS, et al. Extraction and quantification of Azelaic acid from different wheat samples (*Triticum durum* Desf.) and evaluation of their antimicrobial and antioxidant activities. *Molecules*. (2023) 28:2134. doi: 10.3390/molecules28052134

15. Singh P, Brooks JF, Ray VA, Mandel MJ, Visick KL. CysK plays a role in biofilm formation and colonization by *Vibrio fischeri*. *Appl Environ Microbiol*. (2015) 81:5223–34. doi: 10.1128/AEM.00157-15

16. Liu WH, Liu TC, Mong MC. Antibacterial effects and action modes of asiatic acid. *BioMedicine*. (2015) 5:22–9. doi: 10.7603/s40681-015-0016-7

17. Pombal S, Rodilla J, Gomes A, Silva L, Rocha P. Evaluation of the antibacterial activity of the essential oil and antioxidant activity of aqueous extracts of the *Eucalyptus globulus* Labill. leaves. *Global Adv Res J Agric Sci*. (2014) 3:2315–5094.

18. Assad U, Ahmad AA, Masood R, Muhammad N, Muhammad A, Muhammad I, et al. Phytochemical composition and in-vitro activity of ethanolic extract of *Eucalyptus globulus* leaves extract against multidrug resistanti poultry pathogens. *Cell Mol Biol*. (2021) 67:159–64. doi: 10.14715/cmb/2021.67.1.24

19. Sycz Z, Tichaczek-Goska D, Wojnicz D. Anti-planktonic and anti-biofilm properties of pentacyclic triterpenes—asiatic acid and ursolic acid as promising antibacterial future pharmaceuticals. *Biomol Ther*. (2022) 12:98. doi: 10.3390/biom12010098

20. Do Nascimento PGG, Lemos TLG, Bizerra AMC, Arriaga AMC, Ferreira DA, Santiago GMP, et al. Antibacterial and antioxidant activities of ursolic acid and derivatives. *Molecules*. (2014) 19:1317–27. doi: 10.3390/molecules19011317

21. Khedhri S, Polito F, Caputo L, Manna F, Khammassi M, Hamrouni L, et al. Chemical composition, phytotoxic and antibiofilm activity of seven eucalyptus species from Tunisia. *Molecules*. (2022):27. doi: 10.3390/molecules27238227

22. Spaggiari C, Annunziato G, Costantino G. Ursolic and oleanolic acids: two natural triterpenoids targeting antibacterial multidrug tolerance and biofilm formation. *Front Nat Prod*. (2024) 3:1456361. doi: 10.3389/fntpr.2024.1456361

23. Pereira VV, Pereira NR, Pereira RCG, Duarte LP, Takahashi JA, Silva RR. Synthesis and antimicrobial activity of ursolic acid Ester derivatives. *Chem Biodivers*. (2022) 19:e202100566. doi: 10.1002/cbdv.202100566

24. Ren D, Zuo R, Barrios AFG, Bedzyk LA, Eldridge GR, Pasmore ME, et al. Differential gene expression for investigation of *Escherichia coli* biofilm inhibition by

plant extract ursolic acid. *Appl Environ Microbiol*. (2005) 71:4022–34. doi: 10.1128/AEM.71.7.4022-4034.2005

25. Annunziato G, Spadini C, Marchetti M, Franko N, Pavone M, Iannarelli M, et al. Inhibitors of O-Acetylserine Sulfhydrylase with a cyclopropane-carboxylic acid scaffold are effective colistin adjuvants in gram negative bacteria. *Pharmaceuticals*. (2022) 15:766. doi: 10.3390/ph15060766

26. Annunziato G, Spadini C, Franko N, Storici P, Demitri N, Pieroni M, et al. Investigational studies on a hit compound cyclopropane-carboxylic acid derivative targeting O-Acetylserine Sulfhydrylase as a colistin adjuvant. *ACS Infect Dis*. (2021) 7:281–92. doi: 10.1021/acsinfecdis.0c00378

27. Carter GR, Chengap MM. Microbial diseases: A veterinarian's guide to laboratory diagnosis. Ames, IA: Iowa State University Press, (1993).

28. Clinical and Laboratory Standards Institute. Performance standards for antimicrobial susceptibility testing. CLSI document M100. Wayne, PA: CLSI (2021). 316 p.

29. Magiorakos AP, Srinivasan A, Carey RB, Carmeli Y, Falagas ME, Giske CG, et al. Multidrug-resistant, extensively drug-resistant and pandrug-resistant bacteria: an international expert proposal for interim standard definitions for acquired resistance. *Clin Microbiol Infect*. (2012) 18:268–81. doi: 10.1111/j.1469-0691.2011.03570.x

30. Clinical and Laboratory Standards Institute (CLSI). Clinical and laboratory standard institute. Methods for dilution antimicrobial susceptibility tests for bacteria that grow aerobically; approved standards – 9th edition. CLSI document M07-A9. USA: Clinical and Laboratory Standards Institute (2015).

31. Schwarz S, Silley P, Simjee S, Woodford N, van Duijkeren E, Johnson AP, et al. Assessing the antimicrobial susceptibility of bacteria obtained from animals. *Vet Microbiol*. (2010) 141:1–4. doi: 10.1016/j.vetmic.2009.12.013

32. Li WR, Shi QS, Liang Q, Xie XB, Huang XM, Ben CY. Antibacterial activity and kinetics of *Litsea cubeba* oil on *Escherichia coli*. *PLoS One*. (2014) 9:e110983. doi: 10.1371/journal.pone.0110983

33. Stepanovic S, Vukovic D, Dakic I, Savic B, Svabic-Vlahovic M. A modified microtiter-plate test for quantification of staphylococcal biofilm formation. *J Microbiol Methods*. (2000) 40:175–179.

34. Stepanović S, Vuković D, Hola V, Di Bonaventura G, Djukić S, Ćirković I, et al. Quantification of biofilm in microtiter plates: overview of testing conditions and practical recommendations for assessment of biofilm production by staphylococci. *APMIS*. (2007) 115:891–9. doi: 10.1111/j.1600-0463.2007.apm_630.x

35. Rodrigues VH, de Melo MMR, Portugal I, Silva CM. Extraction of eucalyptus leaves using solvents of distinct polarity. Cluster analysis and extracts characterization. *J Supercrit Fluids*. (2018) 135:263–74. doi: 10.1016/j.supflu.2018.01.010

36. Park JY, Kim JY, Son YG, Kang SD, Lee SW, Kim KD, et al. Characterization of chemical composition and antioxidant activity of *Eucalyptus globulus* leaves under different extraction conditions. *Appl Sci*. (2023) 13:9984. doi: 10.3390/app13179984

37. European Medicines Agency. Categorisation of antibiotics in the European Union - Answer to the request from the European Commission for updating the scientific advice on the impact on public health and animal health of the use of antibiotics in animals. (EMA/CVMP/CHMP/682198/2017). (2020). Available online at: https://www.ema.europa.eu/en/documents/report/infographic-categorisation-antibiotics-use-animals-prudent-responsible-use_en.pdf (Accessed February, 2025).

38. Awandkar SP, Kulkarni MB, Khode NV. Bacteria from bovine clinical mastitis showed multiple drug resistance. *Vet Res Commun*. (2022) 46:147–58. doi: 10.1007/s11259-021-09838-8

39. Sweeney MT, Lubbers BV, Schwarz S, Watts JL. Applying definitions for multidrug resistance, extensive drug resistance and pandrug resistance to clinically significant livestock and companion animal bacterial pathogens. *J Antimicrob Chemother*. (2018) 73:1460–3. doi: 10.1093/jac/dky043

40. Garo E, Eldridge GR, Goering MG, Pulcini EDL, Hamilton MA, Costerton JW, et al. Asiatic acid and corosolic acid enhance the susceptibility of *Pseudomonas aeruginosa* biofilms to tobramycin. *Antimicrob Agents Chemother*. (2007) 51:1813–7. doi: 10.1128/AAC.01037-06

41. Wolska KI, Grudniak AM, Fiecek B, Kraczkiewicz-Dowjat A, Kurek A. Antibacterial activity of oleanolic and ursolic acids and their derivatives. *Cent Eur J Biol*. (2010) 5:543–53. doi: 10.2478/s11535-010-0045-x

42. Kaczorek E, Małaczewska J, Wójcik R, Siwicki AK. Biofilm production and other virulence factors in streptococcus spp. isolated from clinical cases of bovine mastitis in Poland. *BMC Vet Res*. (2017) 13:1–7. doi: 10.1186/s12917-017-1322-y43

43. Jyothi JS, Putty K, Reddy YN, Dhanalakshmi K, Umair MAH. Antagonistic effect of ursolic acid on *Staphylococcal* biofilms. *Vet World*. (2018) 11:1440–4. doi: 10.14202/vetworld.2018.1440-1444

44. Greeshma AJ, Pushpa RN, Kavitha KL, Rao TS. Efficacy of resveratrol and ursolic acid on biofilm inhibition and antimicrobial resistance of *Streptococcus uberis*. *Indian J Anim Res*. (2024) 58. doi: 10.18805/IJAR.B-4697

45. Bazargani MM, Rohloff J. Antibiofilm activity of essential oils and plant extracts against Staphylococcus aureus and *Escherichia coli* biofilms. *Food Control*. (2016) 61:156–64. doi: 10.1016/j.foodcont.2015.09.036

46. Lahiri D, Dash S, Dutta R, Nag M. Elucidating the effect of anti-biofilm activity of bioactive compounds extracted from plants. *J Biosci*. (2019) 44:52. doi: 10.1007/s12038-019-9868-4

47. Mohammadian F, Rahmani HK, Bidarian B, Khoramian B. Isolation and evaluation of the efficacy of bacteriophages against multidrug-resistant (MDR), methicillin-resistant (MRSA) and biofilm-producing strains of *Staphylococcus aureus* recovered from bovine mastitis. *BMC Vet Res*. (2022) 18:406. doi: 10.1186/s12917-022-03501-3

48. Al-Taai NA, Al-Gburi NM, Khalil NK. Antibacterial and anti biofilm activity of eucalyptus plant extract Spp. *REDVET-Revista electrónica de Veterinaria*. (2022) 23:130–148.

frontiers | Frontiers in Veterinary Science

TYPE Original Research
PUBLISHED 18 June 2025
DOI 10.3389/fvets.2025.1628570

OPEN ACCESS

EDITED BY
Baocheng Hao,
Chinese Academy of Agricultural Sciences, China

REVIEWED BY
Liping Wang,
Nanjing Agricultural University, China
Xin Chen,
Yangzhou University, China

*CORRESPONDENCE
Peng Ji
✉ jip@gsau.edu.cn
Shishan Dong
✉ dongshishan@163.com

RECEIVED 14 May 2025
ACCEPTED 02 June 2025
PUBLISHED 18 June 2025

CITATION
Lv F, Li P, Wang B, Zhao M, Ji P and Dong S (2025) Laxative effect of Zengye granule by modulating the SCF/c-Kit pathway and gut microbiota in constipated mice. *Front. Vet. Sci.* 12:1628570. doi: 10.3389/fvets.2025.1628570

Laxative effect of Zengye granule by modulating the SCF/c-Kit pathway and gut microbiota in constipated mice

Fengxia Lv[1,2], Pan Li[3], Bin Wang[2,4], Menglu Zhao[4], Peng Ji[4]* and Shishan Dong[1]*

[1]College of Veterinary Medicine, Hebei Agricultural University, Baoding, China, [2]Henan Muxiang Biological Co., Ltd., Zhengzhou, China, [3]China–US (Henan) Hormel Cancer Institute, Zhengzhou, China, [4]College of Veterinary Medicine, Gansu Agricultural University, Lanzhou, China

Introduction: Zengye granule (ZYG), a traditional Chinese medicine, is listed in the Chinese Pharmacopoeia as a prescription medicine for treating various yin-deficiency diseases including inner heat, dry mouth and pharynx, and dry bound stool. However, the underlying mechanisms of its action remain unclear. This study aimed to assess the laxative effects of ZYG on diphenoxylate-induced constipation in Kunming mice and clarify the underlying mechanism of action of ZYG in treating constipation.

Methods: A model of constipation induced by diphenoxylate was developed. The laxative effect was evaluated based on the discharge time of the first black stool, fecal number, fecal weight, intestinal propulsion rate, and intestinal moisture content. Enzyme-linked immunosorbent assay was used to analyze the expression of inflammatory cytokines and neurotransmitters in serum. Histopathological analysis of colon tissues was performed using hematoxylin–eosin staining. Real-time quantitative polymerase chain reaction, immunohistochemistry, and western blotting were used to analyze the mRNA and protein expression of the stem cell factor (SCF)/c-Kit tyrosine kinase (c-Kit) signaling pathway. The composition of the mouse intestinal microbiota was determined by 16S rDNA sequencing.

Results: ZYG improved intestinal peristalsis, defecation frequency, and intestinal moisture content. ZYG decreased the abundance of *Firmicutes* at the phylum and genus levels and increased the abundance of *Bacteroidetes* at the genus level. ZYG exerted a laxative effect by modulating the SCF/c-Kit signaling pathway.

Discussion: This study provides valuable insights into laxative mechanism of ZYG and its potential veterinary application.

KEYWORDS

Zengye granule, laxative effects, diphenoxylate, constipation, stem cell factor/c-kit, gut microbiota

1 Introduction

Constipation impact patients' quality of life because it is manifested as the reduced number of defecations, laborious defecation, and dry stool knot, requiring frequent usage of osmotic and stimulant laxatives (1). It is a highly common gastrointestinal disease in sows and females during late pregnancy and lactating period (2, 3). Although osmotic and stimulant laxatives can effectively control constipation symptoms in the short term, their long-term effects are poor (4) and can increase the risk of death (5), colon cancer (6, 7), and breast cancer (8). Therefore, the development of safe drugs and therapeutic regimens for constipation is crucial.

Traditional Chinese medicines (TCMs) are used in treating diseases, and several potent biologically active components of TCM are produced after metabolism by the intestinal flora. Some TCM formulae exert therapeutic effects against constipation through multiple components, targets, and mechanisms. For instance, the Ji-Chuan decoction can reduce enteric glial cell apoptosis in mice with slow transit constipation induced by diphenoxylate administration (9); Zengye decoction (ZYD) can regulate the intestinal microbiota and change the endogenous metabolite profiles in aged constipated rats (10); Li Qi Run Chang Fang can significantly increase the relative abundance of *Lactobacillus* and enhance the symbiotic relationships between *Lactobacillus* and other intestinal flora (11); MaZiRenWan, which includes dianthrones, anthraquinone glycosides, free anthraquinones, and other polyphenols, promotes gastrointestinal motility and relieve functional constipation (12); Da-Huang-GanCao-Tang shows an effective laxative effect owing to the presence of rhein 8-*O*-*β*-D-glucopyranoside that can change the function of *Bacteroides* and metabolize the prodrug Sennoside A (13, 14); Yangyin Tongmi capsule shows mitigative effects on diphenoxylate-induced constipation by regulating the content of intestinal hormones and neurotransmitters, and expression of related proteins in the colon (15); Zhizhu decoction shows laxative effect by activating the aryl hydrocarbon receptor signaling pathway and affecting the composition of gut microbiota in transit constipation mice (16). Therefore, some TCM formulae may offer considerable therapeutic effects against constipation.

ZYD, originating from volume II of "Wenbing Tiaobian" written by Wu Jutong during the Qing dynasty (AD 1636–1912), consists of four TCMs, such as Radix Scrophulariae (*Scrophularia ningpoensis* Hemsl., Chinese name Xuanshen; XS), Radix Ophiopogonis [*Ophiopogon japonicus* (Linn. f.) Ker-Gawl., Chinese name Maidong; MD], and Radix Rehmanniae (*Rehmannia glutinosa* Libosch., Chinese name Dihuang; DH), at a ratio of 1.0:0.8:0.8 (17, 18). ZYD has been commonly used for hundreds of years to tackle moisturizing dryness, promote the production of body fluids, and treat functional constipation associated with yin deficiency (17, 18). Zengye granule (ZYG), a prescription medicine based on ZYD, is listed in the Chinese Pharmacopoeia for treating various yin-deficiency diseases including inner heat, dry mouth and pharynx, and dry bound stool (19). We have previously reported that ZYG at a dose < 10 $g{\cdot}kg^{-1}{\cdot}day^{-1}$ for 1 day or 2.5 $g{\cdot}kg^{-1}{\cdot}day^{-1}$ for 30 consecutive days had no distinct toxicity or side effects in rats (20).

In this study, we aimed to investigate the laxative effects of ZYG in a mouse model of diphenoxylate-induced constipation and the underlying mechanism.

2 Materials and methods

2.1 Materials

Compound diphenoxylate (CD, diphenoxylate 2.5 mg and 0.025 mg atropine per tablet, batch: 1803008) was purchased from Changzhou Kangpu Pharmaceutical Co., Ltd. Ma Ren pills (MRP, batch: 20200403) were obtained from Wuhan Taifu Pharmaceutical Co., Ltd. Activated carbon powder (ACP) was purchased from Fuchen Chemistry and Reagent Co., Ltd. (Tianjin, China). Sterile saline (batch: C2230518A1) was supplied by Henan Kelun Pharmaceutical Co., Ltd.

2.2 ZYG preparation

ZYG (batch: 20200301) was produced by Henan Muxiang Veterinary Pharmaceutical Co., Ltd., following standard operating procedures, and strict quality control was maintained using high-performance liquid chromatography (HPLC), as previously described (20). As described by our pervious report, the harpagoside concentration in the ZYG (batch No.: 20200301) was 105.86 μg/g by using HPLC, indicating that the ZYG was good quality (20).

2.3 Materials and ZYG preparation for oral administration

The above materials and ZYG were freshly dissolved or suspended in sterile saline before gavage. ZYG was prepared at 0.6, 0.3, and 0.15 g/mL concentrations; CD was prepared at final concentrations of 2.5 mg/mL diphenoxylate and 0.025 mg atropine suspension; ACP was prepared as a 0.1 g/mL suspension; and MRP was prepared as a 0.12 g/mL suspension. Additionally, four mixed suspensions including ZYG (three final concentrations) and ACP, and MRP (one final concentration) and ACP were prepared at final concentrations of 0.1 g/mL ACP; 0.6, 0.3, and 0.15 g/mL ZYG; and 0.12 g/mL MRP.

2.4 Animals and grouping

A total of 120 male and 120 female specific pathogen free Kunming (KM) mice (20 g ± 2 g, 4–5–week-old) were purchased from Lanzhou Veterinary Research Institute Experimental Animal Center [SCXK (Gan)2020-0002]. All mice were housed under control conditions (temperature of 20–25°C, relative humidity of 40–70%, and a 12-h light/dark cycle) with regular chow and water freely available for 1-week adaptation. The animals were cared for in accordance with the *Laboratory Animal-Guideline for Ethical Review of Animal Welfare*. The study protocol was approved by the Ethics Committee of Gansu Agricultural University and was performed in accordance with the ethical standards (ethics approval number: GSAU-Eth-VMC-2024-222).

After fasting for 12 h with free access to water, body fluid deficiency constipation model of KM mice was generated by gavage of CD at doses of 50 mg/kg diphenoxylate and 0.5 mg/kg atropine (21, 22). After 30 min, mice were randomly divided into four experimental groups ($n = 60$) for measuring fecal parameters,

activated carbon propulsion, and intestinal moisture contents, and hematologic, serum biochemical, and neurotransmitter analyses. Sixty KM mice were randomly divided into six groups (n = 10, five of each sex): control (group C), model (group M), MRP (group DC), low-dose ZYG (group ZL), medium-dose ZYG (group ZM), and high-dose ZYG (group ZH). Mice in groups C, M, and DC were orally administered (20 mL/kg) sterile saline, CD (50 mg/kg diphenoxylate and 0.5 mg/kg atropine), and 2.4 g/kg MRP, respectively, throughout the course of the study. Mice in groups ZL, ZM, and ZH were orally administered 3.0, 6.0, 12.0 g/kg (20 mL/kg) ZYG by gastric intubation, respectively. To study fecal parameters and activated carbon propulsion, mice in groups DC, ZL, ZM, and ZH were orally administered 2.0 g/kg ACP. All animals had *ad libitum* access to diet and drink.

2.5 *In vivo* laxative activity test

2.5.1 Measurement of fecal parameters

After 30 min of ZYG administration, mice in each group were individually placed in metabolic cages for 8 h. The discharge time of the first black stool, fecal number, and fecal weight within 8 h were recorded.

2.5.2 Activated carbon propulsion

Mice were euthanized 40 min after ZYG administration, and the small intestine was quickly removed. The total length of the small intestine (the distance from the pylorus to the ileocecal area) and distance traveled by activated carbon were measured. The activated carbon propulsion rate was calculated as Equation (1) (23):

$$\text{Propulsion rate} = \frac{\text{Propulsive distance}}{\text{Total small intestine length}} \times 100\% \quad (1)$$

2.5.3 Intestinal moisture content

Mice were euthanized 2 h after ZYG administration, and the small and large intestines were quickly removed. The weights of the small and large intestines were immediately recorded. Then, the intestines were dried at 90°C for 2 h. The percentage of intestinal moisture content was calculated as Equation (2) (23):

$$\text{Intestinal moisture content} = \frac{\text{Wet intestinal weight} - \text{Dry intestinal weight}}{\text{Wet intestinal weight}} \times 100\% \quad (2)$$

2.5.4 Hematological and serum biochemical analysis

After administration, mice in each group were maintained on the same diet and allowed to drink freely. General health and mortality were observed for 6 h. Immediately after the collection of red blood cells (RBC), hematological analysis was performed to evaluate RBC, white blood cell (WBC), and platelet (PLT) counts, and hemoglobin (Hb) content. For serum biochemical assay, blood samples in dry tubes were centrifuged at 3000 rpm for 15 min to separate serum. The Na^+, K^+, Cl^-, and Ca^{2+} ion concentrations were measured using a BT-2000PLUS analyzer (Biotecnica Chemistry Co., Italy).

2.5.5 Cytokine and neurotransmitter analysis

The levels of the neurotransmitters acetylcholine (Ach), nitric oxide synthase (NOS), substance P (SP), and vasoactive intestinal peptide (VIP), and those of proinflammatory cytokines interleukin (IL)-6, IL-1β, and tumor necrosis factor-alpha (TNF-α) in serum were determined using enzyme-linked immunosorbent assay kits, following the manufacturer's instructions (Shanghai Enzyme-linked Biotechnology Co., Ltd., Shanghai, China).

2.5.6 Hematoxylin–eosin (HE) staining

Colonic tissues were rinsed with normal saline, fixed in 4% paraformaldehyde, and embedded in paraffin. Paraffin-embedded tissues were dewaxed in water. They were subsequently sectioned and stained with HE (Beijing Solarbio Science & Technology Co., Ltd., Beijing, China). The sections were observed using an RX50 light microscope [Sunny Optical Technology (Group) Co., Ltd. Ningbo, China].

2.5.7 Immunohistochemical (IHC) staining

Stem cell factor (SCF) and c-Kit tyrosine kinase (c-Kit) expression was measured in fixed colon tissues by IHC staining as previously described (24). Sections were incubated with DAB (ZLI-9018 2132A0325; Beijing Zhong Shan-Golden Bridge Biological Technology Co., Ltd., Beijing, China), and images were captured using an RX50 light microscope (Sunny Optical Technology (Group) Co., Ltd.). Image Pro Plus v.6.0 was used to measure fluorescence intensity.

2.5.8 Real-time quantitative polymerase chain reaction (RTq–PCR) analysis

RTq–PCR was performed to quantify the mRNA expression of *SCF* and *c-Kit*. Total RNA from colonic tissues was extracted using TRIzol reagent, following the manufacturer's instructions, as previously described (25). The results are presented as relative expression with respect to the internal control *β-actin*.

2.5.9 Western blot analysis

Tissue samples were lysed using a radioimmunoprecipitation assay lysis buffer (Beijing Bioss Biotechnology Co., Ltd. Beijing, China) containing protease and phosphatase inhibitors, to extract proteins. Protein concentration was measured using a bicinchoninic acid protein assay kit (PC0020; Beijing Solarbio Science & Technology Co., Ltd.). Proteins were separated by 10% sodium dodecyl sulfate–polyacrylamide gel electrophoresis and transferred to a polyvinylidene difluoride membrane. The membrane was blocked with 8% skimmed milk and then incubated with primary antibodies at 4°C overnight. The membrane was then incubated with secondary antibodies for 2 h at room temperature. Finally, the membrane using AMERSHAM Image Quant 800 (Cytiva Co., Ltd. Shanghai, China). The primary antibodies (Beijing Biosynthesis Biotechnology Co., Ltd. Beijing, China), and the dilutions are as follows: c-Kit (1:100), SCF (1:200), and β-actin

(1:1000). Protein expression is presented as relative value with respect to the internal control β-actin.

2.5.10 Microbial DNA extraction and 16S rDNA gene sequencing

Genomic DNA from the microbial community was extracted using randomly selected fecal samples from each group. Gene sequencing and data analyses were performed as previously described (26).

2.6 Statistical analysis

The data are expressed as mean ± standard error. The data were compared using one-way analysis of variance followed by a *t*-test, using SPSS v.26.0 for Windows, to evaluate significant differences between groups. A *p*-value < 0.05 was considered significant.

3 Results

3.1 ZYG treatment improved symptoms of constipated mice

In this study, a constipation model was successfully induced in mice using diphenoxylate (group M). After oral administration of MRP and ZYG, the fundamental defecation indices (defecation frequency, oral-anal transit time, and fecal water content) of constipated mice significantly improved, and the constipation symptoms were alleviated.

3.1.1 Fecal parameters

The fecal parameters are shown in Table 1. All mice in group C normally defecated. However, 60% (6/10), 20% (2/10), 20% (2/10), 10% (1/10), and 20% (2/10) mice did not defecate in groups M, DC, ZL, ZM, and ZH, respectively. Compared to that of the group M, the discharge time of the first black stool significantly decreased ($p < 0.05$), and the number, weight, and moisture content of feces in groups DC, ZL, ZM, and ZH significantly increased ($p < 0.05$). Compared to that of the group DC, the discharge time of the first black stool significantly decreased ($p < 0.05$) and the feces number significantly increased ($p < 0.05$) in groups ZM and ZH. The feces weight of group ZM was significantly higher than that of group DC. Therefore, ZYG has a superior laxative effect to MRP in constipated mice.

The time of the first black stool was shorter, and the number, weight, and moisture content of feces were higher in group ZM than those in group ZL and ZH. Notably, the time of the first black stool and weight of feces were not significantly different in groups ZM and C, indicating that mice in group ZM showed normal fecal parameters. This confirmed that ZYG administration at 6.0 g/kg had the best laxative effect.

3.1.2 Activated carbon propulsion

Activated carbon propulsion is linked to the movement of the small intestine. Activated carbon propulsion of groups DC, ZL, ZM, and ZH was significantly higher ($p < 0.05$) than that of group M, and that of group ZM was significantly higher ($p < 0.05$) than that of group DC (Table 1). However, no significant differences in propulsion percentages were noticed between groups ZL and ZH. The level of activated carbon propulsion in the small intestine of mice group ZM was 63.68 ± 3.58%, which was higher than those of groups ZL and ZH. Activated carbon propulsion of group M was lowest (50.06 ± 4.26%). These results indicated that 6.0 g/kg ZYG significantly promoted peristalsis of the small intestine.

3.1.3 Intestinal moisture contents

ZYG and MRP significantly increased ($p < 0.05$) the small and large intestinal moisture contents (Table 2). Notably, the large intestinal moisture contents significantly increased ($p < 0.05$) in group ZM compared to that in group C and DC. This indicated that 6.0 g/kg ZYG showed a superior laxative effect to MRP, and the intestinal moisture contents returned to normal levels.

3.2 Effect of ZYG treatment on hematologic parameter

Mice in the DC group showed the following significant changes ($p < 0.05$): (1) an increase in WBC counts compared to those in groups M, ZM, and ZH; (2) an increase in RBC counts compared to those in groups M and ZM; and (3) an increase in Hb concentration compared to those in groups C, M, and ZM (Table 2).

Mice in the ZYG treatment groups showed the following significant changes ($p < 0.05$) in hematological parameters (Table 2): (1) an increase in Hb concentration in group ZL compared to that in group ZM; and (2) an increase in PLT counts in group ZL compared to that in groups C and M.

These results indicated that 3.0 g/kg ZYG significantly improved blood circulation and treated inflammatory disorders. Notably, 3.0 g/kg ZYG showed the best effect on hematological indicators.

TABLE 1 Fecal parameters and activated carbon propulsion of KM mice treated with ZYG.

Fecal parameter	Group C	Group M	Group DC	Group ZL	Group ZM	Group ZH
No defecation mice	0	6	2	2	1	2
Discharge time of the first black stool (min)	139.70 ± 12.75^{c}	303.50 ± 17.99^{a}	191.75 ± 23.47^{b}	170.75 ± 55.86^{bc}	155.11 ± 50.25^{c}	163.75 ± 14.49^{bc}
Feces number	28.70 ± 5.46^{a}	8.25 ± 2.36^{d}	17.38 ± 2.39^{c}	19.63 ± 5.37^{bc}	22.78 ± 3.56^{b}	20.63 ± 4.14^{bc}
Feces weight (mg)	236.2 ± 29.14^{a}	51.58 ± 17.07^{c}	173.9 ± 15.1^{b}	180.2 ± 33.7^{b}	225.0 ± 21.5^{a}	186.0 ± 18.2^{b}
Propulsion (%)	70.63 ± 2.84^{a}	50.06 ± 4.26^{d}	$60.12 \pm 3.12\%^{c}$	61.00 ± 3.28^{bc}	63.68 ± 3.58^{b}	60.85 ± 3.35^{bc}

Values are mean ± standard error ($n = 10$). The different and same superscripts in the same list indicate statistical significance ($p < 0.05$) and no statistical significance ($p > 0.05$), respectively.

TABLE 2 Intestinal moisture contents, and hematologic and serum biochemical analysis of KM mice treated with ZYG and MRP.

Parameter	Group C	Group M	Group DC	Group ZL	Group ZM	Group ZH
Intestinal moisture contents						
Large intestinal (%)	79.31 ± 1.32^{bc}	78.20 ± 2.09^{c}	79.63 ± 1.57^{b}	80.71 ± 2.05^{ab}	81.09 ± 0.98^{a}	80.54 ± 1.15^{ab}
Small intestinal (%)	78.97 ± 1.43^{ab}	77.65 ± 1.12^{c}	79.44 ± 1.61^{a}	78.90 ± 2.71^{ab}	80.22 ± 1.21^{a}	78.92 ± 0.89^{ab}
Hematology						
RBCs (10^{12}/L)	8.72 ± 0.73^{b}	8.12 ± 0.49^{c}	9.52 ± 0.76^{a}	9.27 ± 0.43^{ab}	8.74 ± 0.69^{b}	9.14 ± 0.56^{ab}
PLT (10^{9}/L)	977.10 ± 254.22^{b}	938.80 ± 382.19^{b}	1139.00 ± 368.79^{ab}	1273.60 ± 271.44^{a}	1058.60 ± 433.91^{ab}	1109.10 ± 176.80^{ab}
Hb (g/L)	141.00 ± 11.70^{bcd}	132.60 ± 8.90^{d}	155.80 ± 12.51^{a}	149.70 ± 7.10^{ab}	140.10 ± 13.09^{cd}	146.50 ± 7.85^{abc}
WBC (10^{12}/L)	3.88 ± 0.69^{a}	1.88 ± 0.80^{c}	3.23 ± 1.94^{ab}	2.40 ± 0.95^{bc}	1.85 ± 0.56^{c}	1.85 ± 0.66^{c}
Serum biochemistry						
K^+ (mmol/L)	8.38 ± 0.96	7.68 ± 0.71	8.47 ± 0.37	8.07 ± 0.76	8.33 ± 1.28	8.08 ± 1.17
Na^+ (mmol/L)	149.20 ± 2.36^{c}	151.16 ± 1.57^{b}	152.64 ± 2.35^{ab}	153.26 ± 1.54^{a}	152.85 ± 1.23^{a}	153.64 ± 1.82^{a}
Cl^- (mmol/L)	107.81 ± 5.34	109.00 ± 1.30	108.84 ± 5.73	106.84 ± 7.17	110.63 ± 1.72	106.48 ± 7.05
Ca^{2+} (mmol/L)	1.42 ± 0.07^{a}	1.28 ± 0.04^{c}	1.35 ± 0.08^{abc}	1.34 ± 0.13^{bc}	1.36 ± 0.05^{ab}	1.31 ± 0.10^{bc}
Neurotransmitter						
Ach (μg/mL)	576.74 ± 26.95^{a}	529.20 ± 24.70^{d}	553.26 ± 22.51^{b}	560.58 ± 11.54^{ab}	548.12 ± 17.03^{bc}	530.36 ± 11.51^{cd}
NOS (μmol/L)	27.93 ± 0.56^{d}	30.98 ± 1.05^{a}	29.72 ± 1.00^{b}	28.54 ± 0.72^{cd}	28.78 ± 0.75^{c}	28.89 ± 0.85^{c}
SP (ng/L)	155.62 ± 6.78^{b}	127.92 ± 5.97^{c}	162.38 ± 7.62^{a}	156.22 ± 4.31^{ab}	159.49 ± 5.03^{a}	161.15 ± 3.22^{a}
VIP (ng/L)	91.32 ± 5.66^{a}	70.42 ± 3.91^{c}	86.33 ± 2.65^{b}	89.18 ± 4.32^{ab}	93.85 ± 4.88^{a}	90.77 ± 5.12^{a}
Inflammatory cytokines						
IL-1β (pg/mL)	81.41 ± 6.54^{b}	106.18 ± 5.89^{a}	78.33 ± 7.21^{c}	83.39 ± 4.65^{b}	79.75 ± 3.29^{bc}	75.46 ± 5.18^{c}
IL-6 (pg/mL)	71.38 ± 4.63^{bc}	85.62 ± 6.85^{a}	72.17 ± 4.21^{b}	69.89 ± 3.66^{c}	73.52 ± 5.86^{b}	73.66 ± 3.71^{b}
TNF-α (pg/mL)	449.15 ± 9.21^{b}	482.19 ± 8.64^{a}	419.63 ± 8.89^{c}	428.55 ± 6.73^{c}	441.79 ± 5.28^{b}	446.32 ± 7.34^{b}

Values are mean ± standard error (n = 10). The different and same superscripts in the same list indicate statistical significance ($p < 0.05$) and no statistical significance ($p > 0.05$), respectively.

3.3 ZYG treatment improved serum biochemical parameters

3.3.1 Ion concentration

The Na^+ concentration in M and all treatment groups significantly increased ($p < 0.05$) compared to that in group C (Table 2). The Na^+ concentrations in groups ZL, ZM, and ZH, and Ca^{2+} concentration in group ZM significantly increased ($p < 0.05$), compared to those in group M. No significant differences in K^+ and Cl^- concentrations were noticed. These results indicated that ZYG significantly regulated the balance of Na^+ and Ca^{2+} electrolytes.

3.3.2 Neurotransmitter analysis

The Ach and NOS concentrations in group M significantly decreased ($p < 0.05$) and increased ($p < 0.05$), respectively, compared to those in group C (Table 2). After treatment with MRP and ZYG, the NOS concentrations in groups DC, ZL, ZM, and ZH significantly decreased ($p < 0.05$), and the Ach concentrations in groups DC, ZL, and ZM significantly increased ($p < 0.05$), compared to those in the M group. The Ach and NOS concentrations in constipated mice significantly decreased ($p < 0.05$) and increased ($p < 0.05$), respectively. Administration of MRP or ZYG significantly increased ($p < 0.05$) Ach concentration while decreasing ($p < 0.05$) concentration of NOS, showing a laxative effect.

The SP and VIP concentrations were significantly lower ($p < 0.05$) in group M than those in the other groups (Table 2). After treatment with MRP and ZYG, SP and VIP concentrations significantly increased ($p < 0.05$) compared to those in the M group ($p < 0.05$).

3.3.3 Inflammatory cytokine analysis

The concentrations of IL-1β, IL-6, and TNF-α of group M were significantly higher ($p < 0.05$) than those of group C (Table 2). After MRP or ZYG treatment, the IL-1β, IL-6, and TNF-α levels significantly decreased ($p < 0.05$). This indicated that MRP and ZYG improved the microenvironment of the body, decreased inflammatory reactions, and maintained normality.

3.4 ZYG treatment restored the intestinal mucosal barrier

Histopathological analyses of colon tissues (Figure 1) revealed the following significant findings in group M: (1) the epithelial mucosa on the tips of villi exfoliated, and mucosa were lost; (2) intercellular epithelium exhibited inflammatory cell infiltration; (3) Low number of goblet cells were observed; and (4) enteraden cells were lost. The colon organ tissues, including the mucosa, submucosa, smooth muscle layer, placenta, epithelium, and intestinal gland cells, in DC, ZL, ZM,

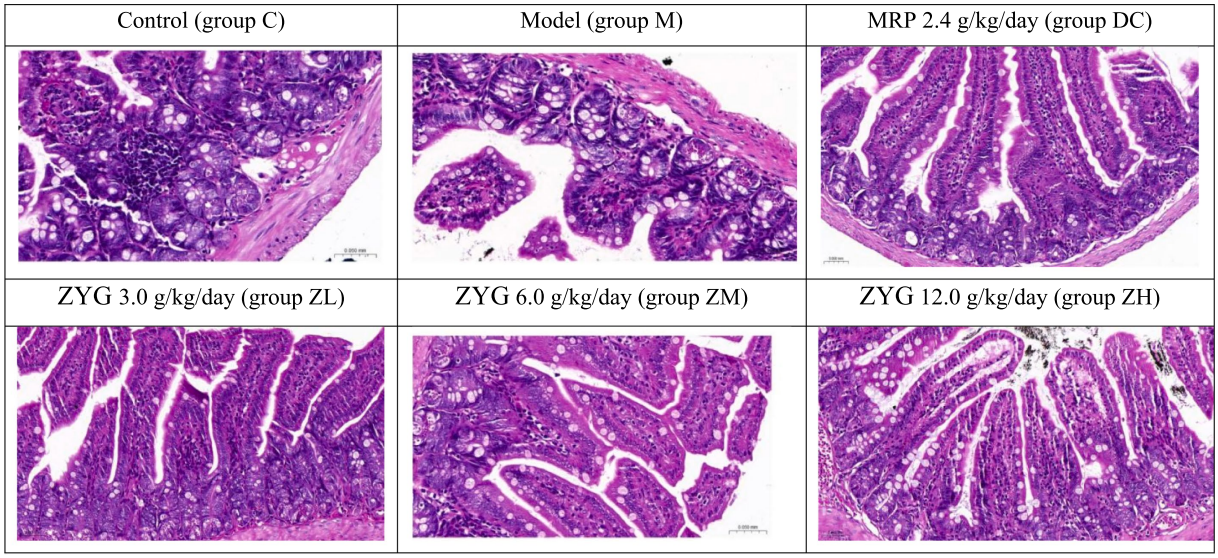

FIGURE 1
Histopathological analyses of colon tissues (HE, 400×).

and ZH groups showed no significant pathological differences in color or texture, compared with those in group C.

3.5 ZYG treatment upregulated the SCF/c-Kit signaling pathway

3.5.1 Immunohistochemistry

SCF and c-Kit were stained as brown areas, as observed by light microscopy (Figure 2A). Staining intensity, area, and distribution were higher in group C than in groups M, DC, ZL, ZM, and ZH, and those in group M were lower than those in the other groups. SCF and c-Kit levels in group M were significantly downregulated compared to those in group C (Figures 2B,C). Their levels were significantly upregulated following MRP or ZYG intervention.

3.5.2 mRNA expression

The mRNA expression of *SCF* and *c-Kit* in group M was significantly downregulated ($p < 0.001$) compared to that in group C (Figures 3A,B). After treatment with MRP or ZYG, the mRNA expression of SCF showed the following significant changes: (1) it was significantly upregulated in groups ZH ($p < 0.001$) and DC ($p < 0.05$), compared to that in group C; (2) it was significantly upregulated ($p < 0.001$) in groups ZH, compared to that in group M; and (3) it was significantly upregulated ($p < 0.001$) in group DC compared to that in group M.

After treatment with MRP or ZYG, the mRNA expression of c-Kit showed the following significant changes: (1) it was significantly downregulated ($p < 0.001$) in group ZL compared to that in group C; and (2) it was significantly upregulated ($p < 0.001$) in groups ZL, ZM, and ZH compared to that in group M.

3.5.3 Western blot analysis

SCF and c-Kit expression in group M significantly decreased ($p < 0.05$) compared to that in group C (Figures 4A–C). Mice treated with MRP or ZYG exhibited significant upregulation of SCF and c-Kit levels compared to that by mice in group M. These results indicate that the c-Kit/SCF signaling pathway was upregulated by ZYG treatment in constipated mice.

3.6 ZYG treatment modulated dysbiosis of gut microbiota

3.6.1 Assessment of sequencing data quality and alpha diversity analysis

The sequencing amount was verified to reflect diversity of the original microorganisms. Alpha diversity analyses, including Chao, Ace, Shannon, and Simpson indices, were conducted. The rarefaction curve tended to be flat with an increase in the number of sampled sequences, indicating that the sequencing amount of each sample was sufficient (Figure 5A). Statistical analysis of the alpha diversity indices showed that the diversity of the different groups showed no obvious boundaries ($p > 0.05$; Figures 5B–E).

3.6.2 Species annotation analysis

The results of species annotation analysis at the phylum and genus levels for groups C, M, and ZM are shown in Figures 6A,B. The predominant phyla in the gut microbiome of mice in these groups were *Firmicutes*, *Bacteroidota*, and *Campylobacterota*. At the phylum level, the abundances of *Firmicutes*, *Campylobacterota*, *Actinomycetota*, and *Pseudomonadota* were higher, whereas that of *Bacteroidetes* was lower in group M than in group C (Figure 6C). At the genus levels, the abundances of *Helicobacter*, *Flintibacter*, *Vescimonas*, *Desulfovibrio*, *Kineothrix*, *Acetatifactor*, and *Lacrimispora* were a higher, whereas those of *Duncaniella and Sporofaciens* were lower in group M than in group C (Figure 6D). After ZYG treatment, the phylum and genus levels were restored to those of group C. ZYG

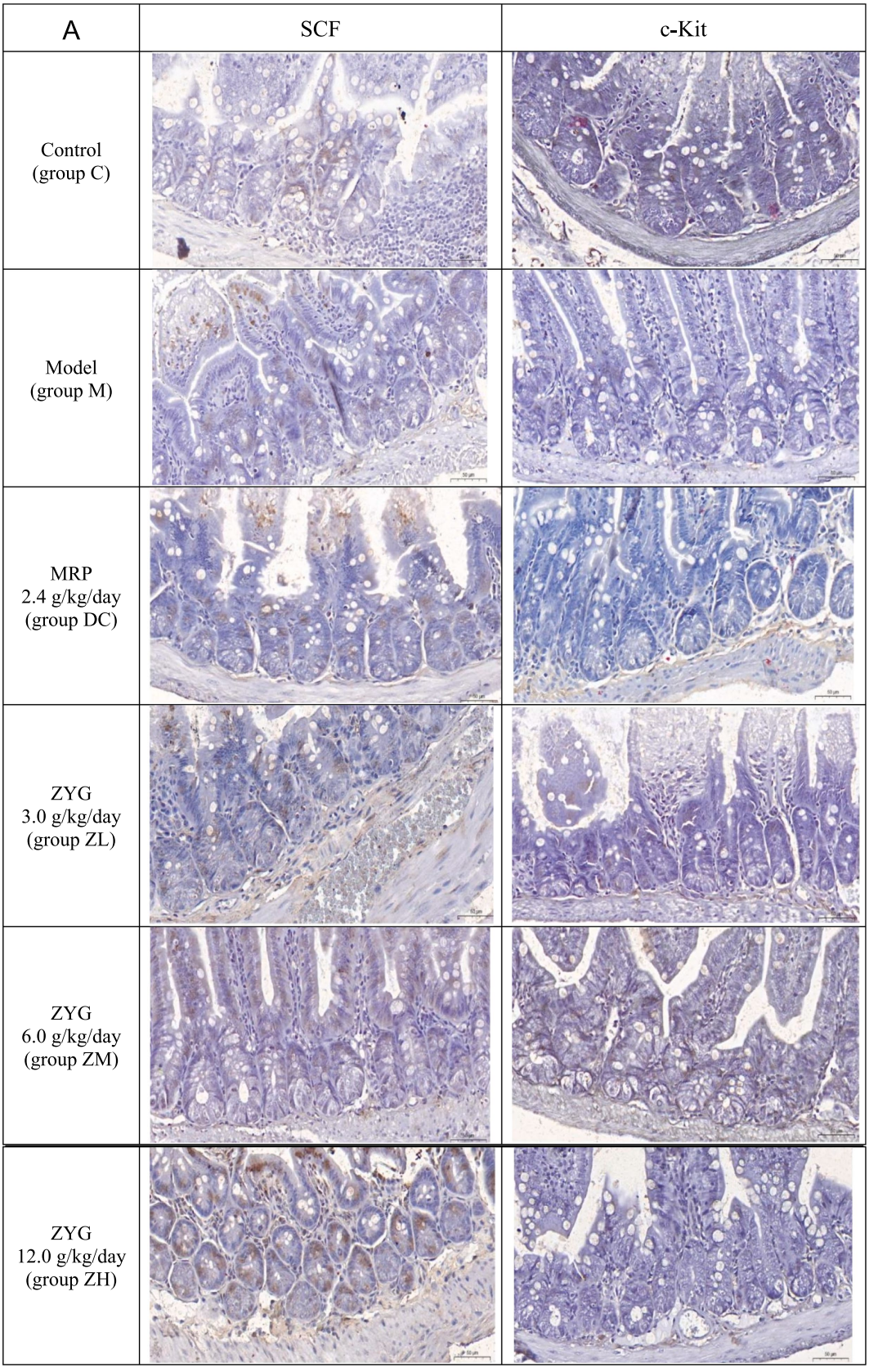

FIGURE 2 (Continued)

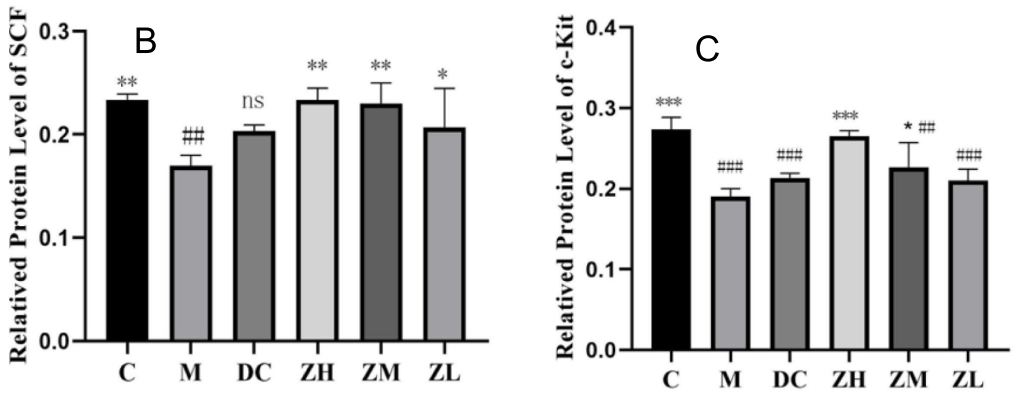

FIGURE 2
IHC analyses SCF and c-Kit (400×, **A**). Quantification of SCF **(B)** and c-Kit **(C)** levels in IHC analysis. Values are expressed as mean ± standard deviation (n = 10). The differences in SCF and c-Kit levels were analyzed using one-way analysis of variance (compared with the model group: $^{*}p < 0.05$, $^{**}p < 0.01$, $^{***}p < 0.001$; compared with the blank group: $^{\#\#}p < 0.01$, $^{\#\#\#}p < 0.001$).

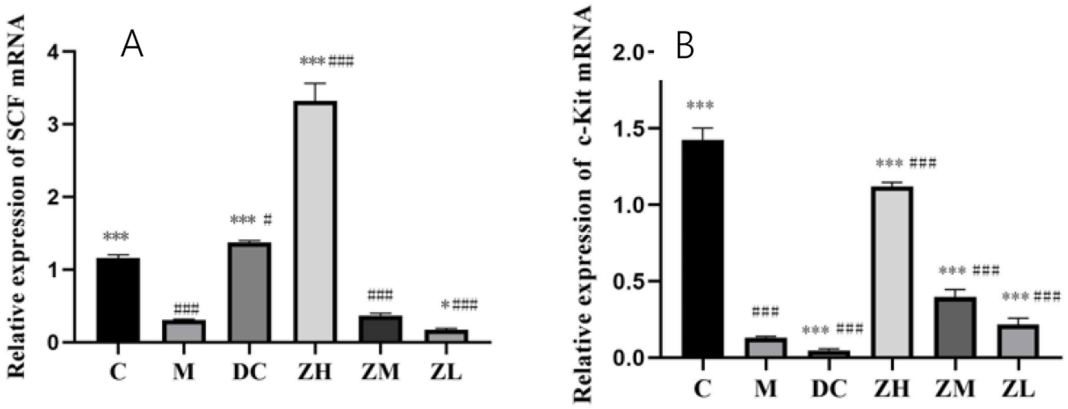

FIGURE 3
SCF **(A)** and c-Kit **(B)** mRNA expression after MRP and ZYG intervention. Values are expressed as mean ± standard deviation (n = 10). The differences in SCF and c-Kit levels were analyzed using one-way analysis of variance (compared with the model group: $^{*}p < 0.05$, $^{***}p < 0.001$; compared with the blank group: $^{\#}p < 0.05$, $^{\#\#\#}p < 0.001$).

effectively restored the gut microbiota composition of constipated mice to the levels similar to those of group C.

3.6.3 Analysis of significantly altered microbiota

Linear discriminant analysis Effect Size was used to detect species that significantly differed among groups. The linear discriminant analysis scoring plot showed significant abundances of 22 microbes at the genus level in groups C, M, and ZM (Figure 7A). In group C, the significantly dominant gut microbiota was *Roseburia*. In group M, the significantly dominant gut microbiotas were *Clostridiumsensustricto*, *Mycobacteriales*, *Clostridiaceae*, *Segatella*, *Faecalibaculum*, *Corynebacteriaceae*, and *Corynebacterium*. In group ZM, the significantly dominant gut microbiotas were *Porphyromonadaceae*, *Parabacteroides*, *Actinobacteria*, *Flavimobilis*, *Jonesiacea*, *Pseudochrobactrum*, *Brucellaceae*, *Hyphomicrobiales*, *Leuconostocaceae*, *Weissella*, *Alcaligenaceae*, *Globicatella*, *Betaproteobacteria*, and *Burkholderiales*.

3.6.4 Functional prediction of differential microbes

To study the specific functions of the gut microbiota, PICRUSt was used to predict the metabolic function profiles of ZYG at the genus level (Figures 7B–D). These differential microbes were highly related to nucleotide and amino acid metabolism, glycan biosynthesis and metabolism, energy metabolism, cell motility, growth, and death, immune and endocrine systems, carbohydrate and lipid metabolism, and digestive system.

4 Discussion

ZYD is a classic TCM formula comprising XS, SD, and MD, which can increase fluid and moistening dryness. XS is used as a "monarch drug" for nourishing Yin, and SD and MD are used as "ministerial drug" in this formula.

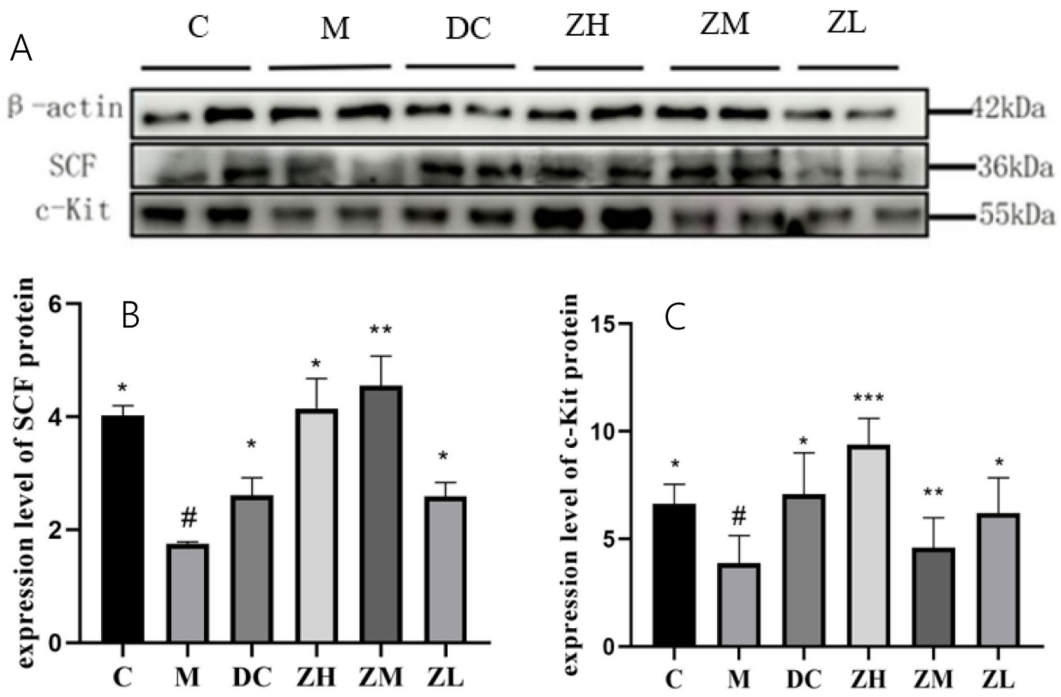

FIGURE 4
Western blot analysis of SCF and c-Kit expression **(A)** and quantitative analysis **(B,C)**. Values were expressed as mean ± standard deviation (n = 10). The differences in SCF and c-Kit levels were analyzed using one-way analysis of variance (compared with the model group: $^{*}p < 0.05$, $^{**}p < 0.01$, $^{***}p < 0.001$; compared with the blank group: $^{\#}p < 0.05$, $^{\#\#}p < 0.01$, $^{\#\#\#}p < 0.001$).

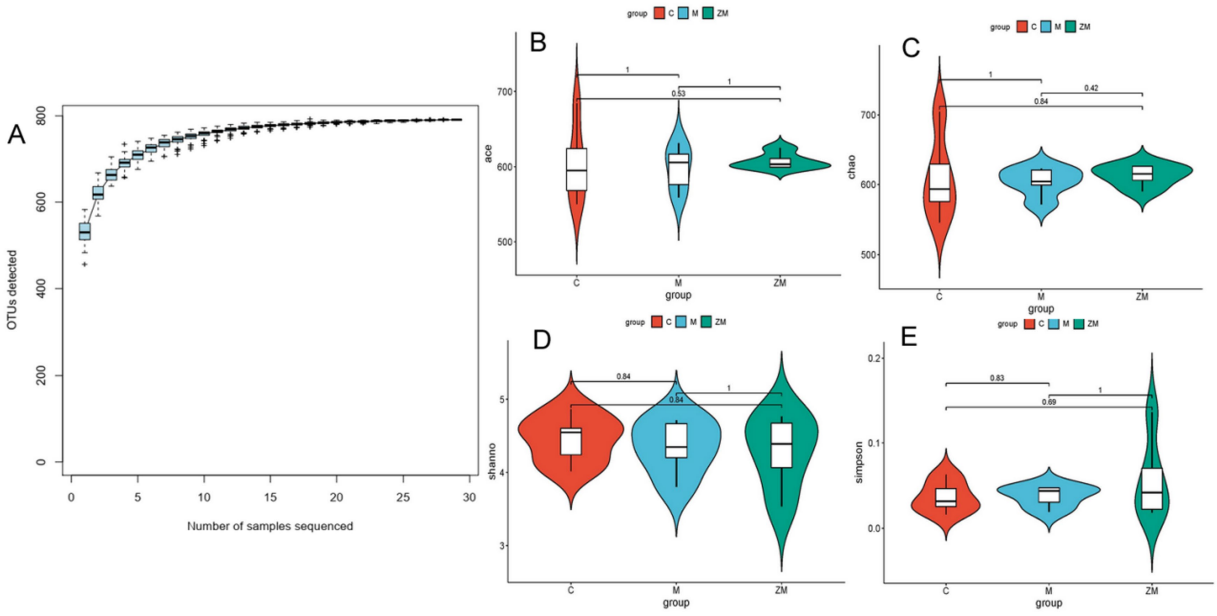

FIGURE 5
Accumulation curve of gut microbiota species **(A)**. Indices of ace **(B)**, Chao **(C)**, Shannon **(D)**, and Simpson **(E)**.

Constipation is characterized by infrequent bowel movements, and difficulty during or incompletion of defecation, which is caused by decreased peristaltic ability of the small intestine (4). Additionally, the reduction in peristalsis of the intestinal smooth muscle can increase water absorption, leading to reduced stool moisture and dry stools. The intestinal propulsive rate, quantity, and water content of feces are key indices of constipation, which are used to evaluate the laxative effect of drugs (27). The diphenoxylate-induced constipation model has been widely used to study the efficacy and mechanism of laxatives, which result in fluid deficiency and reduce the moisture

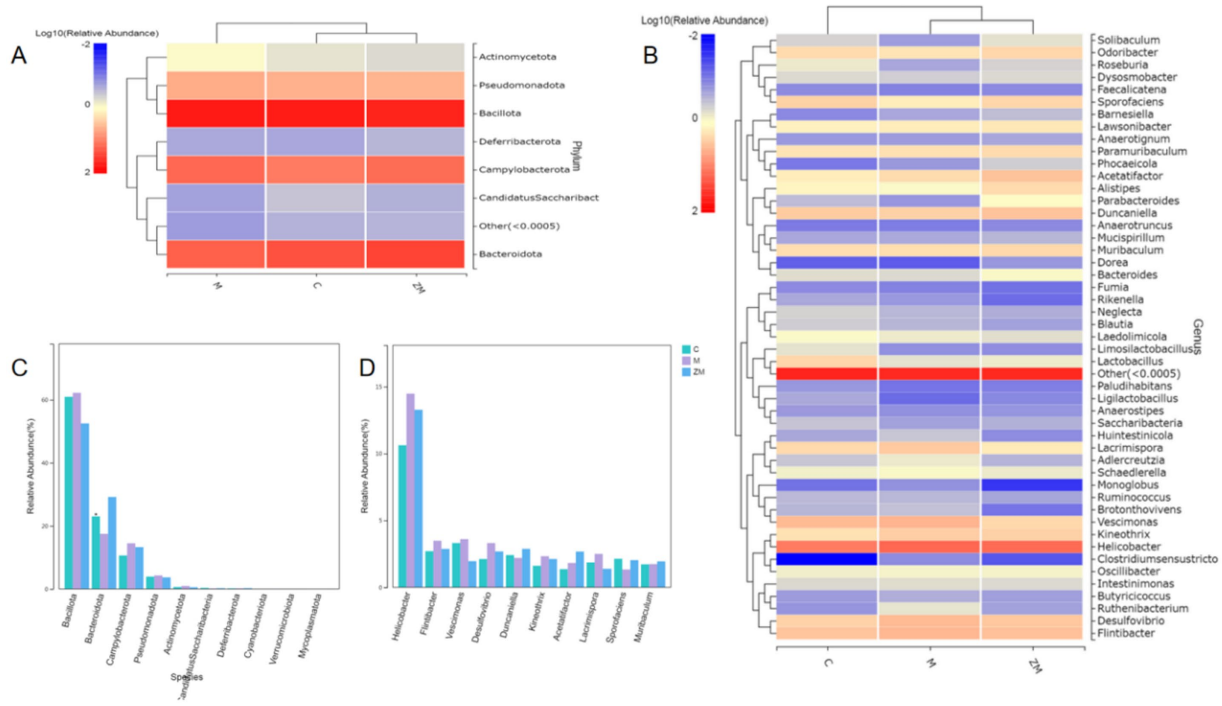

FIGURE 6
Taxonomic composition analysis of gut microbiota at the phylum and genus levels **(A)**. Phylum- and genus-level abundance distribution heatmap **(B)**. Comparison of microbial communities with differences at the phylum level **(C)**. Comparison of microbial communities with differences at the genus level **(D)**.

content of the intestine and feces. MRP is a TCM formula comprising six Chinese herbs including Semen cannabis, Rhubarb, Apricot kernel, *Magnolia officinalis*, *Paeonia lactiflora* Pall, and Fructus aurantii immaturus (28). MRP is commonly used to treat chronic constipation by regulating the intestinal flora, improving intestinal movement, and alleviating constipation symptoms (29, 30). In the present study, MRP was used as a positive control for assessing the potential of ZYG as a therapeutic drug for treating constipation. ZYG restored normal fecal parameters in constipated mice and significantly promoted the peristaltic ability of the small intestine. Notably, 6.0 g/kg ZYG offered more effective constipation therapy than did 2.4 g/kg MRP. Consumption of dietary fiber (2), probiotics (3, 31), inulin and isomalto-oligosaccharide (32), and sugarcane bagasse (33) can relieve constipation in sows. Therefore, further studies are necessary to evaluate the therapeutic effects of ZYG in constipated sows.

Hematological parameters can serve as supporting evidence of renal function. In this study, the hematological parameters significantly increased by ZYG treatment, indicating that ZYG could restore normal renal function in constipated mice.

The enteric nervous system (ENS) is at the core of the regulatory control and defensive functions of the digestive tract, which is jointly constituted by excitatory and inhibitory nerves (34, 35). Neural signals pass between distinct gut regions for coordinating digestive activity using a wide range of chemical messengers. Ach, an excitatory neurotransmitter in the ENS, can directly activate specific receptors on the membrane of gastrointestinal smooth muscle and gland cells, and promote intestinal peristalsis (36, 37). SP, an excitatory neurotransmitter, can activate Ach and induce smooth muscle contractions, thereby acting as a regulator of Ach (38). In contrast, VIP, an inhibitory neurotransmitter, exhibits a strong vasodilatory effect, specifically by inhibiting the tone of intestinal muscles (39, 40). Excessive NOS production in the ENS typically inhibits intestinal contractions, thereby contributing to constipation (41). ZYG treatment effectively improved constipation symptoms by significantly regulating the expression of Ach, NOS, SP, and VIP in constipated mice.

Serum inflammatory cytokine levels positively correlate with the severity of constipation, which can increase intestinal permeability and lead to impaired intestinal mucosal barrier function (42). We noticed that ZYG treatment decreased the levels of IL-1β, IL-6, and TNF-α, reduced colonic inflammation, maintained the colonic structure, and alleviated histopathological deterioration in constipated mice.

The abundance of beneficial bacteria and levels of pathogenic bacteria or conditioned pathogens in the intestine are reduced and increased, respectively, by constipation, which can cause displacement of intestinal bacteria, leading to the release of several inflammatory factors (11). *Bacteroidetes* and *Firmicutes* are the most abundant phyla in the gut microbiota, and the ratio of *Firmicutes* to *Bacteroidetes* (F/B) is an index for evaluating intestinal health. An increased F/B ratio can lead to an increased risk of intestinal diseases (43–45). ZYD can reduce the levels of harmful bacteria and increase the abundance of beneficial bacteria (10). We noticed that ZYG significantly increased the phylum level of *Bacteroidetes*, indicating that the F/B ratio significantly increased and reduced the amounts of harmful metabolites in the body. ZYG effectively restored constipated mice to normalcy by regulating the expression of several neurotransmitters, inflammatory cytokines, and the gut microbiota.

The proliferation of interstitial cells of Cajal (ICC) is regulated by c-Kit and SCF, which are closely related to gastrointestinal motility (46, 47). Therefore, modulating ICC by targeting the SCF/c-Kit signaling pathway may be a potential therapy for constipation. Some

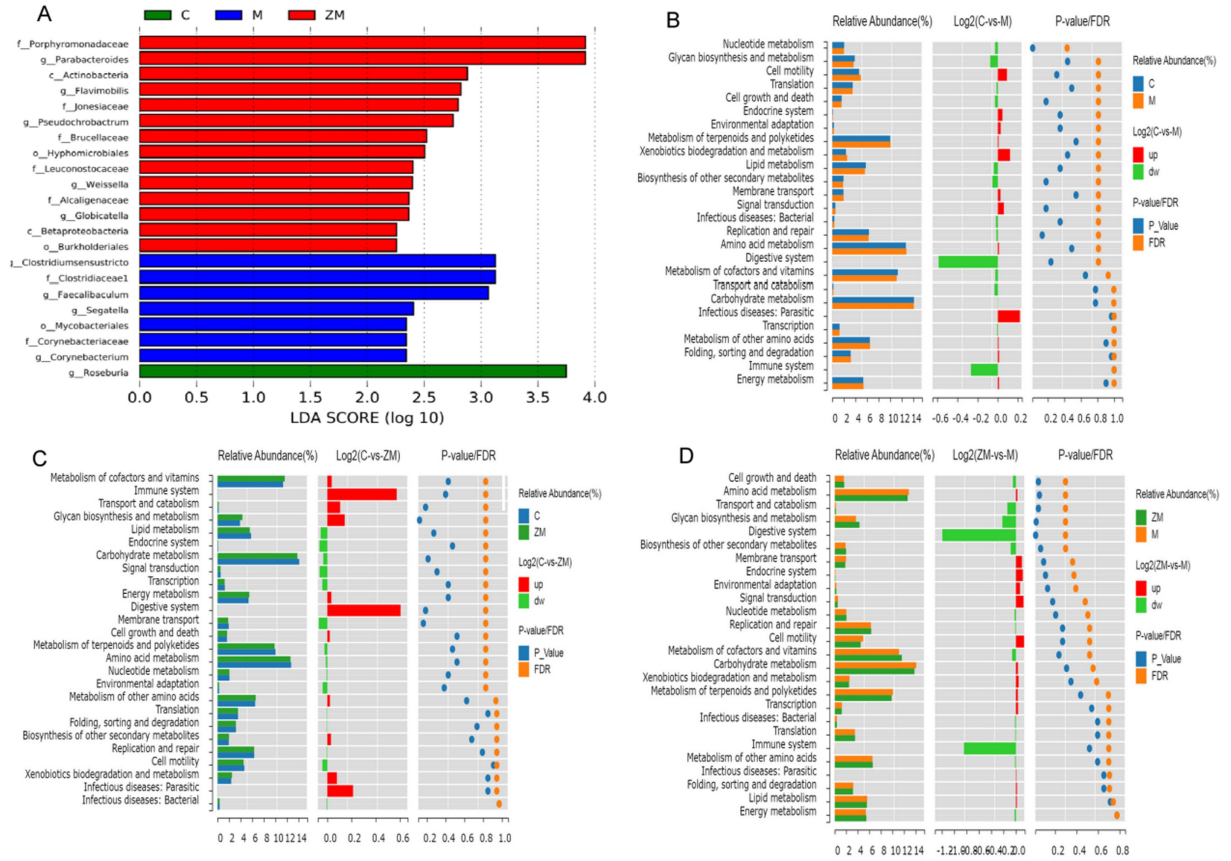

FIGURE 7
Linear discriminant analysis Effect Size analysis of gut microbiota: linear discriminant analysis histogram **(A)**. PICRUSt functional prediction analysis of DC and M **(B)**, DC and ZM **(C)**, and M and ZM **(D)** groups.

TCMs and their formulae, such as *Cistanche deserticola* (48), *Prunus persica* (L.) Batsch blossom (25), and Qi Lang (49), can promote ICC proliferation by targeting the SCF/c-Kit signaling pathway for relieving constipation. Our study showed that ZYG promoted intestinal motility in diphenoxylate-induced constipated mice by significantly upregulating mRNA and protein expression of SCF and c-Kit.

In summary, ZYG shows excellent therapeutic effect in alleviating constipation in diphenoxylate-treated mice. It is necessary to evaluate the therapeutic effect of ZYG in constipated model sows. Therefore, this study provides a scientific basis for the veterinary clinical application of ZYG for treating constipation in sows.

Data availability statement

The original contributions presented in the study are included in the article/Supplementary material, further inquiries can be directed to the corresponding authors.

Ethics statement

The animal study was approved by Ethics Committee of Gansu Agricultural University. The study was conducted in accordance with the local legislation and institutional requirements.

Author contributions

FL: Formal analysis, Methodology, Writing – original draft, Investigation, Writing – review & editing. PL: Formal analysis, Software, Writing – original draft. BW: Methodology, Writing – original draft, Validation. MZ: Supervision, Data curation, Writing – original draft. PJ: Writing – review & editing, Supervision, Resources. SD: Writing – review & editing, Conceptualization.

Funding

The author(s) declare that financial support was received for the research and/or publication of this article. This work was supported by the Key Research and Development Project of Henan Province (grant number 221111111600).

Conflict of interest

FL, BW were employed by Henan Muxiang Biological Co., Ltd.

The remaining authors declare that the research was conducted in the absence of any commercial or financial relationships that could be construed as a potential conflict of interest.

Generative AI statement

The authors declare that no Gen AI was used in the creation of this manuscript.

Publisher's note

All claims expressed in this article are solely those of the authors and do not necessarily represent those of their affiliated organizations, or those of the publisher, the editors and the reviewers. Any product that may be evaluated in this article, or claim that may be made by its manufacturer, is not guaranteed or endorsed by the publisher.

Supplementary material

The Supplementary material for this article can be found online at: https://www.frontiersin.org/articles/10.3389/fvets.2025.1628570/full#supplementary-material

References

1. Xu SM, Bai LP, Lu JG, Dong QJ, Cao B. Study on medication rules of traditional chinese medicine in treating constipation through data mining and network pharmacology. *Biomed Res Int*. (2022) 2022:6733851. doi: 10.1155/2022/6733851

2. Lu D, Pi Y, Ye H, Wu Y, Bai Y, Lian S, et al. Consumption of dietary fiber with different physicochemical properties during late pregnancy alters the gut microbiota and relieves constipation in sow model. *Nutrients*. (2022) 14:2511. doi: 10.3390/nu14122511

3. Ma T, Huang W, Li Y, Jin H, Kwik LY, Sun Z, et al. Probiotics alleviate constipation and inflammation in late gestating and lactating sows. *NPJ Biofilms Microb*. (2023) 9:70. doi: 10.1038/s41522-023-00434-z

4. Wang L, Wu F, Hong Y, Shen L, Zhao L, Lin X. Research progress in the treatment of slow transit constipation by traditional Chinese medicine. *J Ethnopharmacol*. (2022) 290:115075. doi: 10.1016/j.jep.2022.115075

5. Stark ME. Challenging problems presenting as constipation. *Am J Gastroenterol*. (1999) 94:567–74. doi: 10.1111/j.1572-0241.1999.00917.x

6. Rao SS, Rattanakovit K, Patcharatrakul T. Diagnosis and management of chronic constipation in adults. *Nat Rev Gastroenterol Hepatol*. (2016) 13:295–305. doi: 10.1038/nrgastro.2016.53

7. Sonnenberg A, Müller AD. Constipation and cathartics as risk factors of colorectal cancer: a meta-analysis. *Pharmacology*. (1993) 47:224–33.

8. Nellesen D, Yee K, Chawla A, Lewis BE, Carson RT. A systematic review of the economic and humanistic burden of illness in irritable bowel syndrome and chronic constipation. *J Manag Care Pharm*. (2013) 19:755–64. doi: 10.18553/jmcp.2013.19.9.755

9. Wang XM, Lv LX, Qin YS, Zhang YZ, Yang N, Wu S, et al. Ji-Chuan decoction ameliorates slow transit constipation via regulation of intestinal glial cell apoptosis. *World J Gastroenterol*. (2022) 28:5007–22. doi: 10.3748/wjg.v28.i34.5007

10. Liu D, Lin L, Lin Y, Zhong Y, Zhang S, Liu W, et al. Zengye decoction induces alterations to metabolically active gut microbiota in aged constipated rats. *Biomed Pharmacother*. (2019) 109:1361–71. doi: 10.1016/j.biopha.2018.11.013

11. Li S, He Y, Zhang H, Zheng R, Xu R, Liu Q, et al. Formulation of traditional Chinese medicine and its application on intestinal flora of constipated rats. *Microb Cell Factories*. (2020) 19:212. doi: 10.1186/s12934-020-01473-3

12. Ma Q, Wang CZ, Sawadogo WR, Bian ZX, Yuan CS. Herbal medicines for constipation and phytochemical comparison of active components. *Am J Chin Med*. (2022) 50:723–32. doi: 10.1142/S0192415X2250029X

13. Takayama K, Tabuchi N, Fukunaga M, Okamura N. Rhein 8-O-β-D-glucopyranoside elicited the purgative action of daiokanzoto (Da-Huang-Gan-Cao-Tang), despite dysbiosis by ampicillin. *Biol Pharm Bull*. (2016) 39:378–83. doi: 10.1248/bpb.b15-00815

14. Takayama K, Takahara C, Tabuchi N, Okamura N. Daiokanzoto (Da-Huang-Gan-Cao-Tang) is an effective laxative in gut microbiota associated with constipation. *Sci Rep*. (2019) 9:3833. doi: 10.1038/s41598-019-40278-2

15. Liu S, Sui D, Fu W, Yu X, Li Y, Wu X, et al. Laxative effects of Yangyin Tongmi capsule on a model of diphenoxylate-induced constipation in mice. *Evid Based Complement Alternat Med*. (2020) 2020:1471824. doi: 10.1155/2020/1471824

16. Wen Y, Zhan Y, Tang S, Liu F, Wu R, Kong P, et al. Zhizhu decoction alleviates slow transit constipation by regulating aryl hydrocarbon receptor through gut microbiota. *Pharm Biol*. (2023) 61:111–24. doi: 10.1080/13880209.2022.2157020

17. Li CY, Wu SL, Sun LX, Yan TT, Wang Y. Protective effect of Zengye decoction (增液汤) on submandibular glands in nonobese diabetic mice. *Chin J Integr Med*. (2019) 25:45–50. doi: 10.1007/s11655-014-1981-5

18. Zeng Y, Peng X, Wang Y, Hou L, Ma W, Yang P. Therapeutic effect of modified zengye decoction on primary Sjogren's syndrome and its effect on plasma exosomal proteins. *Front Pharmacol*. (2022) 13:930638. doi: 10.3389/fphar.2022.930638

19. Chinese Pharmacopoeia Commission. Chin. Pharmacopoeia. 2020. Beijing: China Medical Science Press (2020). 1853 p.

20. Lv F, Li P, Yuan N, Liu L, Wang B, Zhang C, et al. Toxicological safety evaluation of zengye granule through acute and 30-day toxicity studies in rats. *J Ethnopharmacol*. (2024) 318:116884. doi: 10.1016/j.jep.2023.116884

21. Zhu F, Xu S, Zhang Y, Chen F, Ji J, Xie G. Total glucosides of paeony promote intestinal motility in slow transit constipation rats through amelioration of interstitial cells of Cajal. *PLoS One*. (2016) 11:e0160398. doi: 10.1371/journal.pone.0160398

22. Xu J, Zhou X, Chen C, Deng Q, Huang Q, Yang J, et al. Laxative effects of partially defatted flaxseed meal on normal and experimental constipated mice. *BMC Complement Altern Med*. (2012) 12:14. doi: 10.1186/1472-6882-12-14

23. Xie Y, Zhan X, Tu J, Xu K, Sun X, Liu C, et al. *Atractylodes* oil alleviates diarrhea-predominant irritable bowel syndrome by regulating intestinal inflammation and intestinal barrier via SCF/c-kit and MLCK/MLC2 pathways. *J Ethnopharmacol*. (2021) 272:113925. doi: 10.1016/j.jep.2021.113925

24. Qian W, Li W, Chen X, Cui L, Liu X, Yao J, et al. Exploring the mechanism of Xingpi capsule in diarrhea predominant-irritable bowel syndrome treatment based on multiomics technology. *Phytomedicine*. (2023) 111:154653. doi: 10.1016/j.phymed.2023.154653

25. Liang S, He Z, Liang Z, Wang K, Du B, Guo R, et al. *Prunus persica* (L.) Batsch blossom soluble dietary fiber synergia polyphenol improving loperamide-induced constipation in mice via regulating stem cell factor/C-kit, NF-κB signaling pathway and gut microbiota. *Food Res Int*. (2024) 192:114761. doi: 10.1016/j.foodres.2024.114761

26. Zhang CE, Yu XH, Cui YT, Wang HJ, Chen X, Ma XJ, et al. Shengjiang Xiexin decoction ameliorates antibiotic-associated diarrhea by altering the gut microbiota and intestinal metabolic homeostasis. *Phytomedicine*. (2023) 113:154737. doi: 10.1016/j.phymed.2023.154737

27. Gibson GR, Probert HM, Loo JV, Rastall RA, Roberfroid MB. Dietary modulation of the human colonic microbiota: updating the concept of prebiotics. *Nutr Res Rev*. (2004) 17:259–75. doi: 10.1079/NRR200479

28. Zhan Y, Tang X, Xu H, Tang S. Maren pills improve constipation via regulating AQP3 and NF-κB signaling pathway in slow transit constipation in vitro and in vivo. *Evid Based Complement Alternat Med*. (2020) 2020:9837384. doi: 10.1155/2020/9837384

29. Zhan Y, Wen Y, Du LJ, Wang XX, Tan XY, Kong PF, et al. Effects of Maren pills on the intestinal microflora and short-chain fatty acid profile in drug-induced slow transit constipation model rats. *Front Pharmacol*. (2022) 13:804723. doi: 10.3389/fphar.2022.804723

30. Wang K, Qiu H, Chen F, Cai P, Qi F. Considering traditional Chinese medicine as adjunct therapy in the management of chronic constipation by regulating intestinal flora. *Biosci Trends*. (2024) 18:127–40. doi: 10.5582/bst.2024.01036

31. Li F, Wu D, Ma K, Wei T, Wu J, Zhou S, et al. Effect of dietary supplementation of *Bacillus subtilis* QST 713 on constipation, reproductive performance and offspring growth performance of sows. *Anim Reprod Sci*. (2025) 274:107785. doi: 10.1016/j.anireprosci.2025.107785

32. Yu X, Fu C, Cui Z, Chen G, Xu Y, Yang C. Inulin and isomalto-oligosaccharide alleviate constipation and improve reproductive performance by modulating motility-related hormones, short-chain fatty acids, and feces microflora in pregnant sows. *J Anim Sci*. (2021) 99:skab257. doi: 10.1093/jas/skab257

33. Huang RH, Zhang BB, Wang J, Zhao W, Huang YX, Liu Y, et al. Effect of dietary sugarcane bagasse on reproductive performance, constipation, and gut microbiota of gestational sows. *Animals (Basel)*. (2024) 14:2523. doi: 10.3390/ani14172523

34. Furness JB. The enteric nervous system and neurogastroenterology. *Nat Rev Gastroenterol Hepatol*. (2012) 9:286–94. doi: 10.1038/nrgastro.2012.32

35. Sharkey KA, Mawe GM. The enteric nervous system. *Physiol Rev*. (2023) 103:1487–564. doi: 10.1152/physrev.00018.2022

36. Gao CC, Li GW, Wang TT, Gao L, Wang FF, Shang HW, et al. Rhubarb extract relieves constipation by stimulating mucus production in the colon and altering the intestinal flora. *Biomed Pharmacother*. (2021) 138:111479. doi: 10.1016/j.biopha.2021.111479

37. Wu H, Chen Y, Huang B, Yu Y, Zhao S, Liu J, et al. *Aster tataricus* alleviates constipation by antagonizing the binding of acetylcholine to muscarinic receptor and inhibiting Ca^{2+} influx. *Biomed Pharmacother*. (2021) 133:111005. doi: 10.1016/j.biopha.2020.111005

38. Koon HW, Zhao D, Xu H, Bowe C, Moss A, Moyer MP, et al. Substance P-mediated expression of the pro-angiogenic factor CCN1 modulates the course of colitis. *Am J Pathol*. (2008) 173:400–10. doi: 10.2353/ajpath.2008.080222

39. Iwasaki M, Akiba Y, Kaunitz JD. Recent advances in vasoactive intestinal peptide physiology and pathophysiology: focus on the gastrointestinal system. *F1000Res*. (2019) 8:F1000 Faculty Rev-1629. doi: 10.12688/f1000research.18039.1

40. Wen Y, Zhan Y, Li J, Xu L, Huang C, Wu R, et al. Zhi zhu ma ren pill relieves constipation in mice through endoplasmic reticulum stress-mediated apoptosis. *Am J Transl Res*. (2024) 16:5829–45. doi: 10.62347/YLIE1988

41. Cortesini C, Cianchi F, Infantino A, Lise M. Nitric oxide synthase and VIP distribution in enteric nervous system in idiopathic chronic constipation. *Dig Dis Sci*. (1995) 40:2450–5. doi: 10.1007/BF02063253

42. Fan Q, Gao Y, Zhou Y, Wu J, Wang H, Dong Y, et al. *Weizmannia coagulans* BC99 relieves constipation symptoms by regulating inflammatory, neurotransmitter, and lipid metabolic pathways: a randomized, double-blind, placebo-controlled trial. *Food Secur*. (2025) 14:654. doi: 10.3390/foods14040654

43. Zhao G, Zhang R, Huang F, Dong L, Liu L, Jia X, et al. Hydrolyzed bound phenolics from rice bran alleviate hyperlipidemia and improve gut microbiota dysbiosis in high-fat-diet fed mice. *Nutrients*. (2022) 14:1277. doi: 10.3390/nu14061277

44. Banaszak M, Górna I, Woźniak D, Przysławski J, Drzymała-Czyż S. Association between gut dysbiosis and the occurrence of SIBO, LIBO, SIFO and IMO. *Microorganisms*. (2023) 11:573. doi: 10.3390/microorganisms11030573

45. Perna S, Alalwan TA, Alaali Z, Alnashaba T, Gasparri C, Infantino V, et al. The role of glutamine in the complex interaction between gut microbiota and health: a narrative review. *Int J Mol Sci*. (2019) 20:5232. doi: 10.3390/ijms20205232

46. Foong D, Zhou J, Zarrouk A, Ho V, O'Connor MD. Understanding the biology of human interstitial cells of Cajal in gastrointestinal motility. *Int J Mol Sci*. (2020) 21:4540. doi: 10.3390/ijms21124540

47. Li H, Cao W, Zhang XB, Zhang XX, Gu C, Gu LM, et al. Atractylenolide-1 alleviates gastroparesis in diabetic rats by activating the stem cell factor/c-kit signaling pathway. *Mol Med Rep*. (2021) 24:691. doi: 10.3892/mmr.2021.12331

48. Zhang X, Zheng FJ, Zhang Z. Therapeutic effect of *Cistanche deserticola* on defecation in senile constipation rat model through stem cell factor/C-kit signaling pathway. *World J Gastroenterol*. (2021) 27:5392–403. doi: 10.3748/wjg.v27.i32.5392

49. Li J, Fu Y, Wang Y, Zheng Y, Zhang K, Li Y. Qi Lang formula relieves constipation via targeting SCF/c-kit signaling pathway: an integrated study of network pharmacology and experimental validation. *Heliyon*. (2024) 10:e31860. doi: 10.1016/j.heliyon.2024.e31860

10.3389/fvets.2025.1628570

Glossary

TCM - Traditional Chinese medicine

ZYD - Zengye decoction

XS - Radix Scrophulariae

MD - Radix Ophiopogonis

DH - Radix Rehmanniae

ZYG - Zengye granule

CD - Compound diphenoxylate

MRP - Ma Ren pills

ACP - Activated carbon powder

HPLC - High-performance liquid chromatography

KM - Kunming mice

RBC - Red blood cell

WBC - White blood cell

PLT - Platelet count

Hb - Hemoglobin

Ach - Acetylcholine

NOS - Nitric oxide synthase

SP - Substance P

VIP - Vasoactive intestinal peptide

IL - Cytokines interleukin

TNF-α - Tumor necrosis factor-alpha

HE - Hematoxylin–eosin

IHC - Immunohistochemistry

SCF - Stem Cell Factor

c-Kit - c-Kit tyrosine kinase

RTq–PCR - Quantitative real-time polymerase chain reaction

ENS - Enteric nervous system

ICC - Interstitial cells of Cajal

frontiers | Frontiers in Veterinary Science

TYPE Original Research
PUBLISHED 23 July 2025
DOI 10.3389/fvets.2025.1645372

OPEN ACCESS

EDITED BY
Baocheng Hao,
Chinese Academy of Agricultural Sciences, China

REVIEWED BY
Jianzhong Wang,
Shanxi Agricultural University, China
Osmar Antonio Jaramillo-Morales,
University of Guanajuato, Mexico

*CORRESPONDENCE
Shoujun Li
shoujunli@scau.edu.cn

†These authors have contributed equally to this work

RECEIVED 11 June 2025
ACCEPTED 07 July 2025
PUBLISHED 23 July 2025

CITATION
Ji J, Ma Y, Wan S, Ding X, Wang J, Zhong Y, Song Y, Zhao J, Su Z, Jia K and Li S (2025) Pharmacokinetics and safety evaluation of anemoside B4 in healthy Beagle dogs. *Front. Vet. Sci.* 12:1645372. doi: 10.3389/fvets.2025.1645372

Pharmacokinetics and safety evaluation of anemoside B4 in healthy Beagle dogs

Jinzhao Ji[1,2†], Yuqiao Ma[1,2†], Shaobing Wan[1,2], Xiaoqing Ding[1,2], Jingyu Wang[1,2], Yongcheng Zhong[1,2], Yangyang Song[3], Junqing Zhao[3], Zhetong Su[3], Kun Jia[1,2] and Shoujun Li[1,2*]

[1]College of Veterinary Medicine, South China Agricultural University, Guangzhou, China, [2]Guangdong Technological Engineering Research Center for Pet, Guangzhou, China, [3]Guangxi Innovate Pharmaceutical Co., Ltd., Liuzhou, Guangxi, China

Background: Anemoside B4 (AB4), a pentacyclic triterpenoid saponin extracted from the traditional Chinese medicinal herb *Pulsatilla chinensis*, has shown anti-inflammatory and immunomodulatory effects in both preclinical and clinical studies. However, pharmacokinetic and safety data in dogs remain limited. This study aimed to evaluate the pharmacokinetics, bioavailability, and safety of AB4 in healthy Beagle dogs.

Methods: In the single-dose pharmacokinetic study, 40 dogs received subcutaneous AB4 at 10, 20, or 40 mg/kg, or an intravenous bolus at 20 mg/kg. Plasma concentrations were measured using a validated HPLC–MS/MS method to determine pharmacokinetic parameters, bioavailability, dose proportionality, and sex-related differences. In the repeated-dose study, 10 dogs received 20 mg/kg subcutaneously once daily for 7 consecutive days to evaluate drug accumulation and fluctuation. In the target animal safety study, 32 dogs were randomly assigned to receive 1× (20 mg/kg), 3× (60 mg/kg), or 5× (100 mg/kg) doses of AB4, and saline as a control, via daily subcutaneous injection for 7 days. Routine clinical examinations, hematology, serum biochemistry, gross necropsy, and histopathology were assessed.

Result: AB4 exhibited rapid elimination, high absolute bioavailability, and dose-proportional pharmacokinetics in the 10–40 mg/kg range. No evidence of accumulation after repeated dosing. Within the dose range of 20–100 mg/kg, AB4 demonstrated good safety, with no observable toxicity or adverse effects. No significant effects were observed on physiological parameters. Histopathological analysis revealed no consistent or target-organ specific lesions.

Discussion: These findings provide fundamental pharmacokinetic and safety data to support the rational clinical use of AB4 in veterinary medicine and lay the groundwork for future clinical applications.

KEYWORDS

anemoside B4, pharmacokinetics, safety, dog, veterinary medicine

1 Introduction

Pulsatilla chinensis is a traditional Chinese medicinal herb that has been widely used in classical medicine for its antipyretic and detoxifying properties according to TCM theory (1, 2). In recent years, multiple triterpenoid saponins have been isolated from *P. chinensis*, among which anemoside B4 (AB4) is the most abundant (3, 4). AB4 belongs to the class of pentacyclic triterpenoid saponins (PTS) and exhibits various pharmacological effects, including immunomodulatory, anti-inflammatory, and anti-tumor activities (5–7). Owing to its low

production cost and simple extraction process, AB4 has attracted increasing attention in veterinary medicine research.

Several studies have demonstrated the therapeutic potential of AB4 in inflammatory-related diseases, such as Colitis, enteritis, Acute gouty arthritis, and pneumonia (8–12). However, despite the expanding body of fundamental research, pharmacokinetic and safety data in target animal species remain scarce, particularly in dogs. Understanding the pharmacokinetic behavior and safety profile of AB4 is essential for guiding its rational clinical use, especially with regard to administration strategies, risk of drug accumulation, and the establishment of safe dosage ranges.

Pharmacokinetics, which studies the absorption, distribution, metabolism, and excretion (ADME) of drugs, plays a vital role in determining both efficacy and safety (13). As a PTS compound, AB4 is highly polar and exhibits poor membrane permeability. After oral administration, it is mainly absorbed via passive diffusion, with only a small portion absorbed actively (14, 15). AB4 has been reported to exhibit low systemic exposure and marked first-pass effects following oral administration (16). Following intravenous injection, AB4 is primarily distributed in the kidneys, followed by the lungs (17). Studies have shown that AB4 undergoes extensive hepatic metabolism, including deglycosylation, oxidation, dehydrogenation, reduction, sulfation, hydration, acetylation, and glucuronidation (18). These metabolites are mainly excreted via bile and feces, while the unmetabolized AB4 is primarily eliminated through urine (17).

In preclinical safety assessments, repeated intraperitoneal injection of AB4 at 2.5 g/kg daily for 14 days in mice did not induce adverse effects on survival, locomotor activity, or liver and kidney function (19). *In vitro* experiments also showed that AB4, at concentrations up to 200 μmol/L (approximately 244.276 μg/mL), had no significant impact on cell viability (20). Furthermore, long-term oral administration of AB4 at doses of 100 and 200 mg/kg for 38 days did not result in decreased peripheral lymphocyte counts or increased neutrophil counts in mice, nor were any obvious adverse effects or behavioral abnormalities observed, suggesting that AB4 is well tolerated under experimental conditions (21).

Although a number of preclinical studies have been conducted, further comprehensive evaluation of the pharmacokinetics and safety of AB4 in dogs is still needed. This study aims to elucidate the absorption, distribution, metabolism, and excretion of AB4 in healthy dogs, thereby providing a foundation for optimizing clinical dosing regimens. In addition, by conducting a target animal safety test, the study aims to assess the safe dosage range and potential toxicity of AB4 in dogs to ensure its safe clinical application.

2 Materials and methods

2.1 Medication and reagents

Anemoside B4 (AB4, purity: 96.4%) was purchased from the National Institutes for Food and Drug Control (Beijing, China). The investigational drug, AB4 for injection (purity: 94.2%) was provided by Guangxi Innovate Pharmaceutical Co., Ltd. (Guangxi, China). Normal saline for injection was obtained from HFQ Co., Ltd. (Jiangsu, China). All reagents and solvents used were of analytical or HPLC grade.

2.2 LC-MS/MS instrumentation and conditions

The HPLC-MS/MS analysis was performed using a SHIMADZU LCMS-8045 system (Shimadzu Corporation, Kyoto, Japan) equipped with a ZORBAX Eclipse Plus C18 column (2.1 × 50 mm, 1.8 μm; Agilent Technologies, USA). The mobile phase consisted of solvent A (ultrapure water) and solvent B (acetonitrile containing 0.1% formic acid). The gradient elution conditions are summarized in Table 1.

2.3 Method validation

The method was evaluated in terms of specificity, linearity, accuracy, precision, recovery, matrix effect, and stability, in accordance with standard bioanalytical guidelines (ICH M10, 2022).

2.4 Dogs

Healthy Beagle dogs (9–11 months old) purchased from Zhenhe Laboratory Animal Co., Ltd. (Fuzhou, China) were used in this study. All procedures were approved by the Animal Clinical Research Ethics Committee of the Veterinary Drug Evaluation Center, South China Agricultural University (Approval No. 2023E007). Before the study, dogs underwent a 7-day acclimation. During the study, dogs were fed a standardized diet with daily intake calculated based on resting energy requirement (RER) and maintenance energy requirement (MER) to ensure nutritional balance and appropriate caloric intake. Water was freely available.

2.5 Grouping and drug administration

In the single-dose pharmacokinetic (PK) study, 40 Beagle dogs (equal numbers of males and females) were randomly assigned into four parallel groups: low-dose (10 mg/kg), medium-dose (20 mg/kg), high-dose (40 mg/kg), and intravenous (20 mg/kg). AB4 was administered as a single subcutaneous injection in the dorsal neck

TABLE 1 Gradient elution conditions for LC-MS/MS analysis of AB4 in canine plasma.

Time (min)	Flow rate (mL/min)	Mobile phase A (%)	Mobile phase B (%)
1.00	0.30	75	25
1.50		10	90
2.50		10	90
2.60		75	25
5.50		75	25

Mass spectrometric detection was performed in MRM mode using an ESI source. The analyte AB4 was quantified using transitions m/z 1219.50 → 749.20 (quantifier, CE 55 V, Q3 pre-bias 36 V) and 1219.50 → 468.90 (qualifier, CE 41 V, Q3 pre-bias 23 V), with a Q1 pre-bias of 34 V and a dwell time of 100 ms. Instrument parameters included nebulizing gas flow 3 L/min, heating gas flow 10 L/min, interface temperature 300°C, drying gas flow 10 L/min, and desolvation temperature 526°C.

or intravenously into the cephalic vein; In the multiple-dose PK study, 10 dogs (five males and five females) received 20 mg/kg AB4 once daily (8:00 a.m.) by subcutaneous injection for 7 consecutive days.

In the safety study, 40 dogs (equal numbers of males and females) were randomized into four groups: low-dose (20 mg/kg), medium-dose (60 mg/kg), high-dose (100 mg/kg), and a saline control group (0 mg/kg). AB4 was administered subcutaneously once daily (8:00 a.m.) for 7 days at 24-h intervals.

All AB4 solutions were prepared at a concentration of 48 mg/mL, and the administered volume was adjusted according to body weight and dosing requirements. Detailed dosing information is provided in the Supplementary materials 7–9.

2.6 Sample collection and processing

In the single-dose pharmacokinetic (PK) study, a blank blood sample was collected before dosing. After administration, 2 mL blood samples were collected from the cephalic vein at 5, 10, 15, 30, and 45 min, and at 1, 2, 3, 3.5, 4, 6, 9, 12, 16, 24, 36, and 48 h.

In the multiple-dose PK study, a pre-dose blood sample was collected before the first administration, followed by sampling at the same time points as the single-dose study. Additional trough samples were collected within 5 min before each daily administration. On days 2 to 6, samples were collected at 3, 3.25, 3.5, 3.75, and 4 h. After the final dose, samples were taken at the same time points as the single-dose group, with additional collections at 60 and 72 h.

Plasma was separated by centrifugation at 4000 rpm for 10 min. Subsequently, 300 µL of plasma was mixed with 900 µL of methanol, vortexed for 3 min, and centrifuged at 14,000 rpm for 10 min at 4°C. The resulting supernatant was filtered through a 0.22 µm PTFE membrane and subjected to LC–MS/MS analysis.

In the safety study, blood was collected from the cephalic vein for hematology, serum biochemistry. According to the AVMA Guidelines for the Euthanasia of Animals (2020 Edition), dogs were rapidly administered propofol intravenously at a dose of 10 mg/kg. After confirming deep anesthesia, bilateral axillary vessels were incised for exsanguination, ensuring a painless procedure. Following euthanasia, major organs were collected, weighed for organ coefficient calculation, then fixed in 10% neutral-buffered formalin, and prepared for histopathological examination using H&E staining.

2.7 Pharmacokinetic analysis

Plasma concentration–time data were analyzed using non-compartmental analysis (NCA) in Phoenix WinNonlin software (Certara, USA) (22). Pharmacokinetic Parameters were compared between male and female dogs within each dose group to assess sex-based differences. Bioavailability was calculated based on AUC comparison between IV bolus and SC groups. Dose linearity for key PK parameters (C_{max}, AUC_{0-t}, and $AUC_{0-\infty}$) was assessed using the power model approach.

2.8 Safety assessment procedures

Safety assessments were conducted on Days 0 (D0), 4 (D4), 7 (D7), and 14 (D14). Blood samples were collected for laboratory testing, including hematology and serum biochemistry. Local tolerance at the injection site was also monitored. Body weight was recorded on D0 and D14 (after fasting). On D14, gross anatomical examinations and organ weight measurements were performed in the control and high-dose groups. Throughout the study, dogs were monitored for clinical signs and adverse events (AEs).

2.9 Statistical analysis

Statistical analyses were conducted using SPSS software (version 25.0; IBM, Armonk, NY, USA), with a two-sided significance level of $\alpha = 0.05$.

In the pharmacokinetic study, continuous variables were tested for normality and homogeneity of variance. Normally distributed data with equal variances were analyzed using independent samples t-tests; those with unequal variances were analyzed using Welch's ANOVA. Non-normally distributed data were assessed using the Mann–Whitney U test.

In the safety study, normally distributed data are presented as mean ± SD and analyzed using one-way ANOVA, followed by Dunnett's test or Tamhane's T2 test depending on variance equality. Non-normally distributed data are expressed as median (P25, P75) and analyzed using the Wilcoxon rank-sum test. Categorical data are shown as frequency and percentage (n, %) and compared using the chi-square or Fisher's exact test. Paired data were evaluated using the paired t-test or Wilcoxon signed-rank test.

3 Result

3.1 Method validation

The HPLC–MS/MS method established for AB4 quantification in Beagle dog plasma demonstrated acceptable selectivity, sensitivity, accuracy, and reproducibility. No significant endogenous interference or system carryover was observed. The method showed good linearity over 0.2–20 µg/mL ($R^2 > 0.99$). Precision and accuracy were within ±15% (±20% for Lower Limit of Quantification), and recovery exceeded 80%. Dilution integrity and stability under various conditions (freeze–thaw, short−/long-term storage, post-preparative) were confirmed. Detailed validation data are provided in the Supplementary materials 1–6, 36–37.

3.2 Pharmacokinetics after single dose administration

At baseline, no statistically significant differences in body weight were observed among groups ($F = 0.397$, $p = 0.756$). Pharmacokinetic parameters of AB4 were analyzed using a

non-compartmental model. Following single-dose administration, AB4 exhibited a short elimination half-life ($t_1/_2 \approx 3$–4 h), a high clearance rate, and a moderate apparent volume of distribution ($V_d/F < 300$ mL/kg), indicating rapid elimination and limited tissue distribution. Moreover, AB4 showed high absolute bioavailability.

Sex-based comparisons revealed statistically significant differences in terminal elimination rate constant(λ_z) and $t_1/_2$ in the low-dose subcutaneous group: λ_z was $0.23 \pm 0.02\ h^{-1}$ in females and $0.20 \pm 0.02\ h^{-1}$ in males ($t = -2.361$, $p = 0.046$), while $t_1/_2$ was 3.08 ± 0.22 h vs. 3.48 ± 0.22 h, respectively ($t = 2.374$, $p = 0.045$). In the intravenous group, only steady-state volume of distribution (V_{ss}) showed a significant difference (164 ± 9 mL/kg in females vs. 207 ± 30 mL/kg in males; $F = 8.935$, $p = 0.033$). No other pharmacokinetic parameters showed statistically significant sex differences ($p > 0.05$).

Detailed pharmacokinetic parameters are summarized in Table 2, and mean plasma concentration-time profiles are illustrated in Figure 1.

3.3 Evaluation of dose proportionality

Dose proportionality of AB4 was assessed in Beagle dogs following single subcutaneous administration at 10, 20, and 40 mg/kg. After normalization by body weight, the systemic exposure parameters(C_{max}, AUC_{0-t}, and $AUC_{0-\infty}$)increased approximately in proportion to the dose (1:2:4), indicating a dose-proportional relationship.

A power model analysis was performed to further evaluate linear pharmacokinetics. The estimated exponents (β) for C_{max}, AUC_{0-t}, and $AUC_{0-\infty}$ were 0.9417, 1.032, and 1.027, respectively, all of which are close to 1. These results indicated that AB4 exhibits linear pharmacokinetic behavior over 10-40 mg/kg dose range in dogs.

Dose proportionality and fitted curves of systemic exposure are presented in Table 3. Linear regression plots based on the power function model for key pharmacokinetic parameters are shown in Figure 2.

3.4 Pharmacokinetics after multiple dose administration

Following repeated subcutaneous administration of AB4 at 20 mg/kg once daily for 7 days, the mean steady-state trough concentration ($C_{ss\text{-}min}$) was 1.35 ± 0.51 μg/mL, and the mean steady-state average concentration ($C_{ss\text{-}avg}$) was 19.61 ± 5.27 μg/mL. The degree of fluctuation (DF) was 2.52 ± 0.42.

The accumulation ratios estimated by three different methods were as follows: R (based on the terminal elimination rate constant) was 1.03 ± 0.01, R_{AUC} was 1.22 ± 0.52, and R_{Cmax} was 1.16 ± 0.18. These results indicate that AB4 exhibits no significant accumulation in dogs under the tested dosing regimen. The concentration-time curve of AB4 in dogs after multiple dosing is presented in Figure 3, and pharmacokinetic parameters following repeated subcutaneous administration ($n = 10$) are summarized in Table 4.

3.5 Clinical observations

At baseline, body weight in the 5 × dose group was significantly lower than the saline control group ($p = 0.008$), while no significant differences were observed in other treatment groups ($p > 0.05$). During the entire observation period (Days 0–14), Dogs in treatment and

TABLE 2 Pharmacokinetic parameters of AB4 in canine plasma following single-dose administration ($\bar{X}$, $n = 10$).

Parameters	Unit	Subcutaneous injection			Intravenous bolus injection
		10 mg/kg	20 mg/kg	40 mg/kg	20 mg/kg
C_{max}	μg/mL	22.33 ± 2.99	52.63 ± 21.27	84.28 ± 25.50	NA
C_0	μg/mL	NA	NA	NA	198.30 ± 19.95
t_{max}	h	4.00 ± 0.75	4.95 ± 1.12	4.30 ± 0.95	NA
MRT_{0-t}	h	6.79 ± 0.34	8.10 ± 1.48	8.29 ± 0.62	3.74 ± 0.46
$MRT_{0-\infty}$	h	7.03 ± 0.39	8.30 ± 1.49	8.39 ± 0.60	3.91 ± 0.51
$t_{1/2}$	h	3.28 ± 0.32*	3.57 ± 0.61	3.53 ± 0.50	3.34 ± 0.54
λ_z	1/h	0.21 ± 0.02*	0.20 ± 0.03	0.20 ± 0.03	0.21 ± 0.04
AUC_{0-t}	h·μg/mL	194.0 ± 23.3	461.8 ± 130.1	829.2 ± 239.0	427.7 ± 76.3
$AUC_{0-\infty}$	h·μg/mL	196.2 ± 23.6	465.3 ± 129.7	831.9 ± 238.6	430.7 ± 76.5
V_d/F	mL/kg	245 ± 45	233 ± 59	257 ± 56	NA
CL/F	mL/h/kg	51.7 ± 6.5	46.3 ± 13.6	50.5 ± 9.9	NA
V_{ss}	mL/kg	NA	NA	NA	185 ± 31*
CL	mL/h/kg	NA	NA	NA	48.1 ± 10.5
F	%	90.72#	107.97	96.94#	NA

"NA" indicates not applicable or statistical analysis required.
"*" indicates a statistically significant difference between females and males within the same group ($p < 0.05$).
"#" indicates that dose normalization was applied.

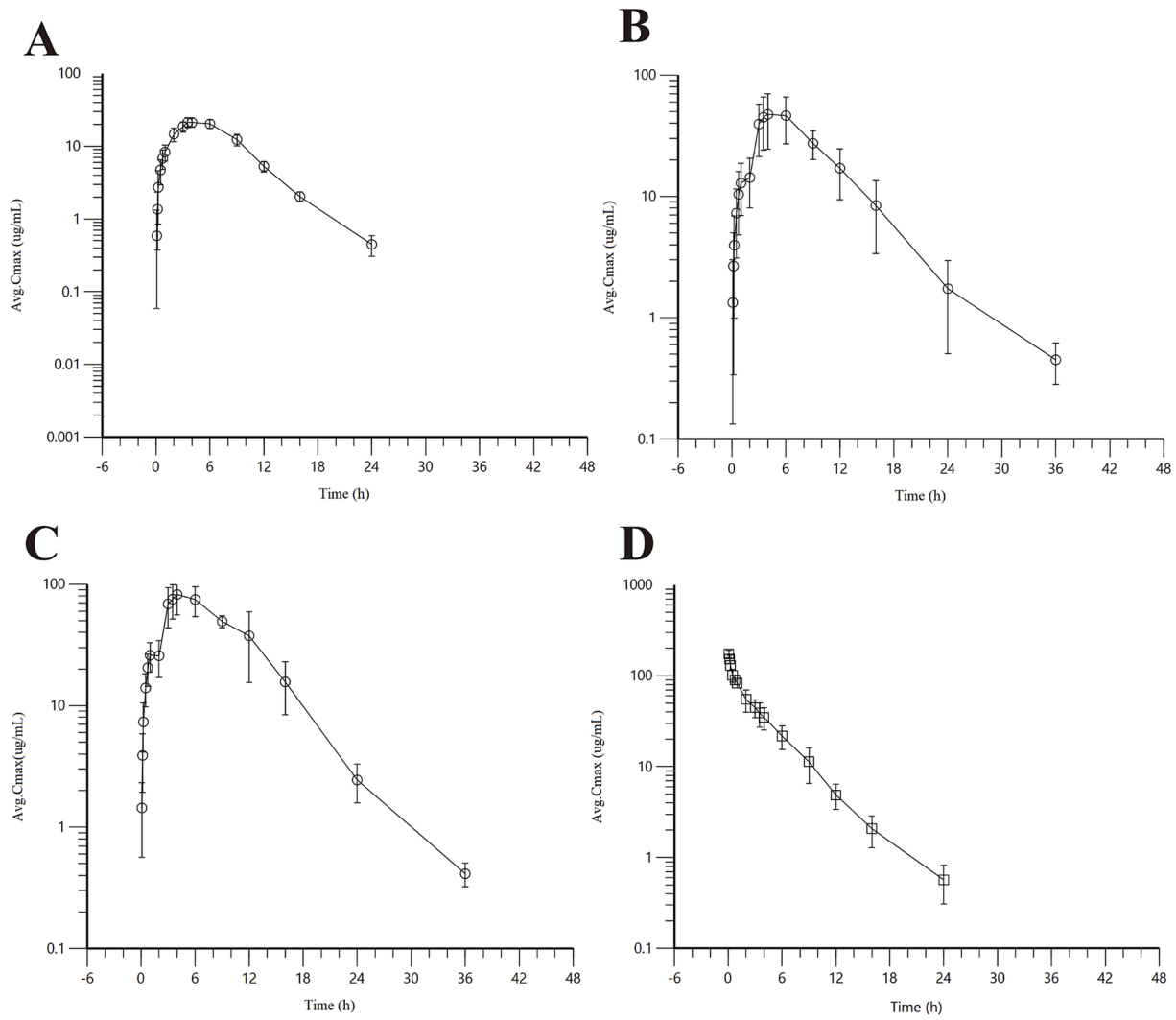

FIGURE 1
Concentration-time curve of AB4 in dogs after single dose. **(A)** Low-dose subcutaneous injection group (10 mg/kg); **(B)** midium-dose subcutaneous injection group (20 mg/kg); **(C)** High-dose subcutaneous injection group (40 mg/kg); **(D)** Intravenous bolus injection (20 mg/kg).

TABLE 3 Dose proportionality of systemic exposure and fitted curves.

Parameters	Dose-proportionality of systemic exposure	Regression equation	Correlation coefficient (R^2)
C_{max}	1:2.36:3.77	$C_{max} = 0.2429 \cdot Dose^{0.9417}$	$R^2 = 0.7832$
AUC_{0-t}	1:2.41:4.22	$AUC_{0-t} = 1.706 \cdot Dose^{1.032}$	$R^2 = 0.8760$
$AUC_{0-\infty}$	1:2.41:4.19	$AUC_{0-\infty} = 1.747 \cdot Dose^{1.027}$	$R^2 = 0.8764$

control groups maintained stable vital signs. Body temperature, respiratory rate, and heart rate remained within normal physiological ranges, with no signs of fever, hypothermia, tachypnea, or arrhythmia. Food and water intake were normal, with no cases of anorexia or polydipsia. Fecal and urinary characteristics appeared normal. Dogs were alert and active, with bright eyes and responsive behavior. Mucous membranes were moist and pink, and the skin on the lips and nose remained normal. No injection site reactions (e.g., erythema, edema, pain, or pruritus) were observed, apart from mild bleeding due to needle puncture. No significant differences in body weight gain were observed between groups ($p > 0.05$), indicating no treatment-related effects. No adverse events or mortality occurred during the study. Injection site manifestations are provided in the Supplementary material 38.

3.6 Blood hematology and serum biochemistry

Hematological results showed that during the administration period, red blood cell parameters, platelet counts, and white blood cell

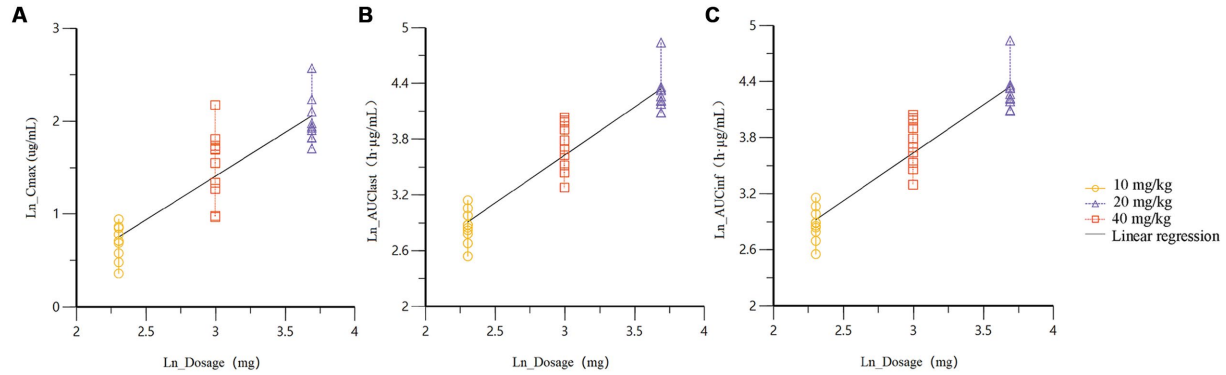

FIGURE 2
Linear regression plots of the power function model for key pharmacokinetic parameters **(A)** C_{max}; **(B)** AUC_{0-t}; **(C)** $AUC_{0-\infty}$.

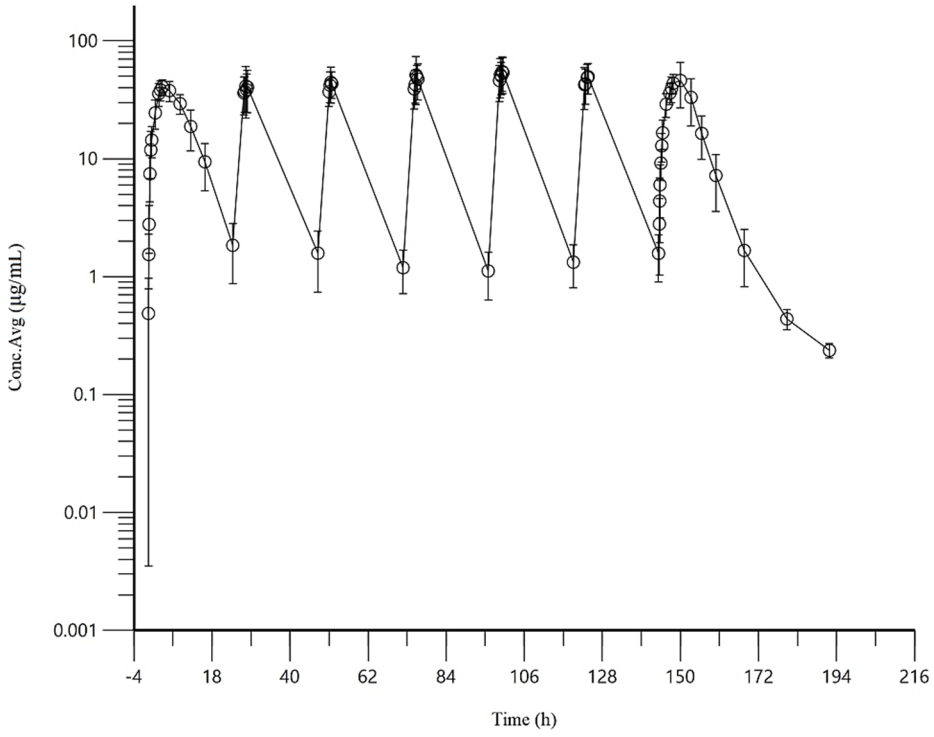

FIGURE 3
Concentration-time curve of AB4 in dogs after multiple doses (20 mg/kg). "NA" indicates not applicable or statistical analysis required.

counts in dogs remained within normal ranges, with no statistically significant differences compared to the saline control group. On Day 14 (seven days after drug withdrawal), statistically significant differences in neutrophil (NEUT) and total white blood cell (WBC) counts were observed between the treatment groups and the control group.

Serum biochemistry results indicated that serum markers of liver function (AST, ALT, ALP, GGT, and TBIL) remained within reference ranges, with no statistically significant differences from the control group on any test day. Renal function parameters (CREA and UREA) showed minor statistical differences at isolated time points, however, all values remained within physiological ranges and did not persist throughout the study. Indicators of protein metabolism (TP, ALB, GLOB) and lipid/glucose metabolism (TG, GLU, TC) were also within reference ranges. Although some intergroup differences were observed at certain time points, no trends related to drug intervention were identified, and the variations were primarily attributed to individual differences among animals. No significant effects were observed on muscle function (CK) or on calcium and phosphorus levels.

These findings indicated that AB4 administered at doses of 20–100 mg/kg did not induce clinically significant effects on hematological or serum biochemical profiles in dogs. All data are detailed in Supplementary materials 12–35.

TABLE 4 Pharmacokinetic parameters of AB4 in dogs following multiple dose administration ($\overline{X}$, n = 10).

Parameters	Unit	Dosing Schedule	
		Initial administration	Continuous administration for 7 days
λ_z	h^{-1}	0.17 ± 0.05	0.16 ± 0.03
$t_{1/2}$	h	4.29 ± 1.07	4.39 ± 0.76
t_{max}	h	4.3 ± 0.92	4.8 ± 1.74
$C_{ss\text{-}min}$	μg/mL	NA	1.35 ± 0.51
$C_{ss\text{-}avg}$	μg/mL	NA	19.61 ± 5.27
$C_{ss\text{-}max}$	μg/mL	NA	51.05 ± 18.61
C_{max}	μg/mL	42.66 ± 7.01	NA
$AUC_{0\text{-}t}$	h·μg/mL	403.2 ± 82.6	482.0 ± 133.8
$AUC_{0\text{-}\infty}$	h·μg/mL	466.8 ± 119.0	485.1 ± 133.0
AUC_{ss}	h·μg/mL	NA	470.6 ± 126.5
V_d/F	mL/kg	267 ± 35	NA
V_{ss}/F	mL/kg	NA	280 ± 58
CL/F	mL/h/kg	45.4 ± 11.7	NA
CL_{ss}/F	mL/h/kg	NA	45.6 ± 23.1
$MRT_{0\text{-}\infty}$	h	9.02 ± 1.36	8.21 ± 0.89
$R_{\lambda z}$		NA	1.03 ± 0.01
R_{AUC}		NA	1.22 ± 0.52
R_{Cmax}		NA	1.16 ± 0.18
DF		NA	2.52 ± 0.42

"NA" indicates not applicable or statistical analysis required.

3.7 Necropsy and histopathological examination

Gross necropsy findings in the 5 × dose group revealed no visible abnormalities in the heart, liver, spleen, lungs, kidneys, thymus, pancreas, gastrointestinal tract, and lymph nodes. All examined organs exhibited normal color, intact serosal surfaces, and well-defined margins, with no signs of hemorrhage, ulceration, necrosis, or other gross lesions. No apparent differences were noted compared to the saline control group.

Organ coefficient analysis showed no statistically significant differences ($p > 0.05$) in the weights of major organs (heart, liver, spleen, lungs, and kidneys) between the 5 × dose group and the saline control group. These results indicated that AB4 administration did not cause hypertrophy, atrophy, or abnormal enlargement of the major organs. Detailed results are presented in Table 5.

Histopathological changes observed in the 5 × dose group, diffuse hepatic vacuolar degeneration, lymphoid follicle hyperplasia in the renal cortex (1/8, 12.5%), splenic nodule edema with loosely arranged lymphocytes, intestinal villus edema, lymph node edema (1/8, 12.5%), and congestion of hepatic vessels and sinusoids (1/8, 12.5%) were observed. In the saline control group, focal pulmonary interstitial hyperplasia (1/8, 12.5%), decreased lymphocytes in the splenic red pulp, proteinaceous exudate in renal tubules accompanied by epithelial necrosis, and pancreatic edema (1/8, 12.5%) were noted. These histopathological findings did not exhibit consistency or directional trends and were determined to be incidental or attributable to individual variation. There was no statistically significant difference in the incidence of lesions between the two groups ($p > 0.05$). Detailed results are presented in Table 6. Representative histopathological sections are shown in Figures 4, 5, and additional sections are provided in the Supplementary material 39.

TABLE 5 Results of organ coefficient measurement (Unit: /, $\overline{X}\pm$SD, n = 8).

Group	Organ name				
	Heart	Liver	Spleen	Lungs	Kidneys
5 × dose group	0.84 ± 0.13	3.09 ± 0.30	0.26 ± 0.02	0.91 ± 0.13	0.52 ± 0.08
Saline control group	0.94 ± 0.04	2.81 ± 0.29	0.30 ± 0.05	0.94 ± 0.13	0.48 ± 0.07
t	−2.08	1.902	−1.983	−0.468	0.975
p value	0.069	0.078	0.067	0.647	0.346

TABLE 6 Incidence of tissue lesions in dogs.

Group	Dogs exhibiting tissue lesions		Z	p value
	Frequency count (n = 8)	Frequency (%)		
5 × dose group	3	37.5	−0.522	0.602
Saline control group	2	25.0		

4 Discussion

To date, most publicly available pharmacokinetic data on AB4 have been obtained from rodent models, with a lack of corresponding PK and safety data in dogs (23–25). This study presents a comprehensive and detailed characterization of the pharmacokinetic profile of AB4 in healthy dogs following both single and repeated subcutaneous administration, and systematically evaluates its safety. The findings provide a predictive framework for developing rational dosing strategies in clinical veterinary settings.

Following a single subcutaneous injection, AB4 exhibited limited distribution, rapid elimination, and high bioavailability, with linear pharmacokinetics. At the low dose level (10 mg/kg), statistically significant differences in λ_z and $t_{1/2}$ were observed between male and female dogs ($p < 0.05$), whereas no such differences were noted at the medium and high dose levels. This phenomenon may be attributed to AB4's strong plasma protein binding capacity (binding rate >80%)

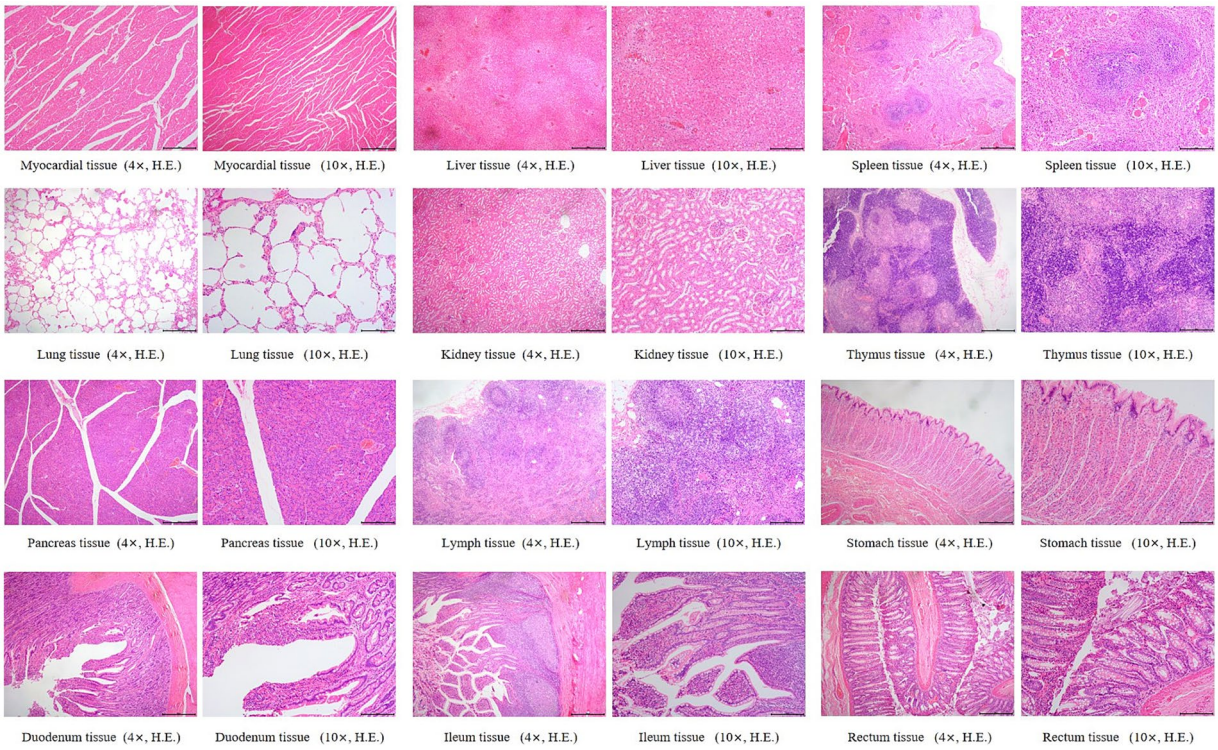

FIGURE 4
Histopathological sections of dogs in the 5 × dose group. "4×": Microscopic images were captured using a 4 × objective lens, scale bar = 500 μm; "10×": Microscopic images were captured using a 10 × objective lens, scale bar = 200 μm.

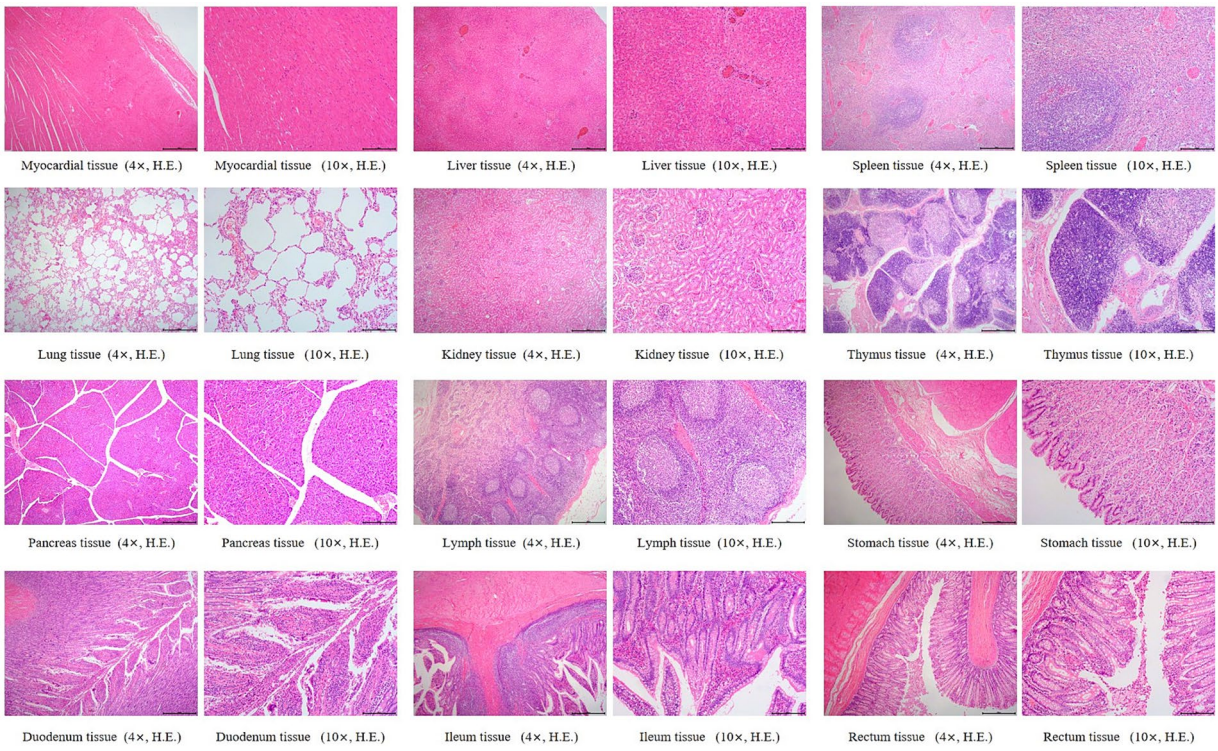

FIGURE 5
Histopathological sections of dogs in the saline control group. "4×": Microscopic images were captured using a 4 × objective lens, scale bar = 500 μm; "10×": Microscopic images were captured using a 10 × objective lens, scale bar = 200 μm.

(26). It has been reported that α_1-acid glycoprotein (AAG), a major binding protein for basic drugs, is typically more abundant in males (27). At lower plasma concentrations, variations in protein binding can substantially affect the free drug fraction. As the administered dose increases, binding sites become saturated, diminishing the influence of plasma proteins and thereby reducing sex-related difference. In this study, although λ_z and $t_{1/2}$ ($p = 0.045$) in the low-dose group were statistically significant, their p-values approached the 0.05 threshold. To further assess the robustness of these findings, the Mann–Whitney U test-a nonparametric test with broader applicability-was employed, revealing no significant sex differences for λ_z ($U = 21$, $p = 0.76$) or $t_{1/2}$ ($U = 3.5$, $p = 0.59$). Given that no sex differences were observed in other PK parameters or in the medium- and high-dose groups, these results are considered marginally significant and of limited clinical relevance.

Under repeated subcutaneous administration at 20 mg/kg for seven consecutive days, AB4 demonstrated an accumulation ratio <2 and a degree of fluctuation between 1 and 3, indicating no significant accumulation and moderate plasma concentration variability. Although repeated administration led to a slight increase in $t_{1/2}$ and volume of distribution compared to single dosing, the differences were not statistically significant, suggesting that AB4 maintains a stable pharmacokinetic profile upon multiple dosing. However, the mean peak-to-trough concentration ratio at steady state was relatively high. Based on these pharmacokinetic findings, it is recommended that clinical dosing strategies be adjusted accordingly: For acute or severe cases, an increased initial dose or more frequent dosing may be warranted to rapidly achieve therapeutic plasma levels. Conversely, for milder cases or during recovery, a reduced dose with increased dosing frequency may help lower drug burden and improve treatment precision.

In the safety study, a high dose of 100 mg/kg was employed without inducing abnormalities in liver or kidney function or histopathological alterations. Combined with the PK findings, which indicate rapid elimination and no evidence of drug accumulation after 7 days of administration, the data further support the safety of AB4. Throughout the study period, no antibiotics were administered. Although subcutaneous injections and blood sampling could induce minor inflammatory responses, NEUT and WBC levels in the treatment groups remained within normal limits and exhibited minimal fluctuation, which may reflect the anti-inflammatory properties of AB4 (28, 29). In contrast, the saline control group exhibited greater variability in NEUT and WBC levels, with values significantly higher on Day 14 compared to some treatment groups.

Body weight in all groups showed a significant increase on Day 14 compared with baseline (Day 0), and the extent of weight gain was consistent with the expected growth pattern for Beagle dogs of this age, with no evidence of drug-induced weight loss or growth suppression, further supporting the favorable tolerability of AB4. Detailed results are provided in the Supplementary material 10.

In current veterinary practice, treatment of inflammatory diseases such as pneumonia commonly relies on glucocorticoids, which can lead to adverse effects including immunosuppression, gastrointestinal bleeding, and osteoporosis when used long term (30, 31). Compared with glucocorticoids, AB4 appears to offer a more favorable safety profile, making it a promising candidate for long-term anti-inflammatory therapy.

Future studies should focus on elucidating the tissue distribution and metabolic pathways of AB4 in target organs, particularly the lungs and kidneys. These investigations will provide critical insights into its therapeutic mechanisms and the potential risk of organ-specific accumulation. Additionally, further pharmacodynamic (PD) studies are warranted to establish a comprehensive PK/PD model. This model would enable more precise characterization of AB4's *in vivo* disposition and therapeutic effects, facilitating accurate predictions of drug concentrations and efficacy under various dosing regimens. Collectively, these studies will inform optimized treatment strategies and reinforce the scientific foundation for AB4's future application in veterinary medicine.

5 Conclusion

This study provides a detailed pharmacokinetic and safety evaluation of AB4 in dogs. Following subcutaneous administration, AB4 exhibited limited distribution, rapid elimination, high absolute bioavailability, and linear pharmacokinetic characteristics, with no evident accumulation after repeated dosing. Within the dose range of 20–100 mg/kg, AB4 demonstrated good safety, with no observable toxicity or adverse effects. These pharmacokinetic and safety data may inform future veterinary applications and contribute to rational dose optimization in subsequent clinical studies.

Data availability statement

The original contributions presented in the study are included in the article/Supplementary material, further inquiries can be directed to the corresponding author.

Ethics statement

The animal study was approved by South China Agricultural University Animal Clinical Research Ethics Committee. The study was conducted in accordance with the local legislation and institutional requirements.

Author contributions

JJ: Conceptualization, Writing – review & editing, Writing – original draft, Methodology, Formal analysis. YM: Formal analysis, Writing – original draft, Data curation, Validation, Methodology. SW: Data curation, Software, Writing – original draft. XD: Visualization, Investigation, Writing – original draft. JW: Visualization, Writing – original draft, Investigation. YZ: Visualization, Writing – original draft, Investigation. YS: Conceptualization, Supervision, Writing – original draft. JZ: Writing – original draft, Conceptualization, Supervision. ZS: Writing – original draft, Conceptualization, Supervision. KJ: Validation, Conceptualization, Writing – original draft, Project administration. SL: Writing – review & editing, Funding acquisition, Resources, Project administration, Conceptualization.

Funding

The author(s) declare that financial support was received for the research and/or publication of this article. This study was supported by the Pharmacokinetics and Safety Evaluation of anemoside B4 in Dogs Project (5500-H231026).

Acknowledgments

We thank the Experimental Animal Center of South China Agricultural University for providing the experimental facilities and conditions for this study.

Conflict of interest

YS, JZ, and ZS were employed by Guangxi Innovate Pharmaceutical Co., Ltd.

The remaining authors declare that the research was conducted in the absence of any commercial or financial relationships that could be construed as a potential conflict of interest.

Generative AI statement

The authors declare that no Gen AI was used in the creation of this manuscript.

Publisher's note

All claims expressed in this article are solely those of the authors and do not necessarily represent those of their affiliated organizations, or those of the publisher, the editors and the reviewers. Any product that may be evaluated in this article, or claim that may be made by its manufacturer, is not guaranteed or endorsed by the publisher.

Supplementary material

The Supplementary material for this article can be found online at: https://www.frontiersin.org/articles/10.3389/fvets.2025.1645372/full#supplementary-material

References

1. Li H, Wang L, Zhang X, Xia W, Zhou X, Sui H, et al. *Pulsatilla chinensis* (Bge.) regel: a systematic review on anticancer of its pharmacological properties, clinical researches and pharmacokinetic studies. *Front Oncol*. (2022) 12:888075. doi: 10.3389/fonc.2022.888075

2. Leng D. A comprehensive review on botany, phytochemistry, traditional uses, pharmacology, analytical methods, processing methods, pharmacokinetics and toxicity of *Pulsatilla chinensis*. *Altern Ther Health Med*. (2024) 30:374–80.

3. Li YH, Zou M, Han Q, Deng LR, Weinshilboum RM. Therapeutic potential of triterpenoid saponin anemoside B4 from *Pulsatilla chinensis*. *Pharmacol Res*. (2020) 160:105079. doi: 10.1016/j.phrs.2020.105079

4. Zhang T, Zhang J, Chen F, Liu A, Jiang J, Yan Z, et al. Qualitative and quantitative analysis of triterpenoids in different tissues of *Pulsatilla chinensis*. *J Pharm Biomed Anal*. (2023) 234:115528. doi: 10.1016/j.jpba.2023.115528

5. Li X, Zhou X, Liu J, Zhang J, Feng Y, Wang F, et al. Liposomal co-delivery of PD-L1 siRNA/Anemoside B4 for enhanced combinational immunotherapeutic effect. *ACS Appl Mater Interfaces*. (2022) 14:28439–54. doi: 10.1021/acsami.2c01123

6. Zhang Y, Zha Z, Shen W, Li D, Kang N, Chen Z, et al. Anemoside B4 ameliorates TNBS-induced colitis through S100A9/MAPK/NF-kappaB signaling pathway. *Chin Med*. (2021). 16:11. doi: 10.13422/j.cnki.syfjx.2017180071

7. He L, Zhang Y, Kang N, Wang Y, Zhang Z, Zha Z, et al. Anemoside B4 attenuates nephrotoxicity of cisplatin without reducing anti-tumor activity of cisplatin. *Phytomedicine*. (2019) 56:136–46. doi: 10.1016/j.phymed.2018.10.035

8. Tian X, Li J, Liu S, Dong Q, Fu Y, Luo R, et al. Anemoside B4 attenuates necrotic enteritis of laying hens induced by *Clostridium perfringens* via inhibiting NF-κB and PI3K/Akt/mTOR signalling pathways. *Heliyon*. (2024) 10:e33161. doi: 10.1016/j.heliyon.2024.e33161

9. Ji J, Ding X, Liu C, Dai L, Yu J, Li L, et al. Efficacy and safety of anemoside B4 in canine pneumonia treatment: a prospective, randomized controlled trial. *Front Vet Sci*. (2025) 12:1530318. doi: 10.3389/fvets.2025.1530318

10. Ni X, Wang Q, Ning Y, Liu J, Su Q, Lv S, et al. Anemoside B4 targets NEK7 to inhibit NLRP3 inflammasome activation and alleviate MSU-induced acute gouty arthritis by modulating the NF-κB signaling pathway. *Phytomedicine*. (2025) 138:156407. doi: 10.1016/j.phymed.2025.156407

11. Lv L, Li Q, Wang K, Zhao J, Deng K, Zhang R, et al. Discovery of a new anti-inflammatory agent from Anemoside B4 derivatives and its therapeutic effect on colitis by targeting pyruvate carboxylase. *J Med Chem*. (2024) 67:7385–405. doi: 10.1021/acs.jmedchem.4c00222

12. Liang QH, Li QR, Chen Z, Lv LJ, Lin Y, Jiang HL, et al. Anemoside B4, a new pyruvate carboxylase inhibitor, alleviates colitis by reprogramming macrophage function. *Inflamm Res*. (2024) 73:345–62. doi: 10.1007/s00011-023-01840-x

13. Mager DE. Quantitative structure-pharmacokinetic/pharmacodynamic relationships. *Adv Drug Deliv Rev*. (2006) 58:1326–56. doi: 10.1016/j.addr.2006.08.002

14. Jeong DW, Kim YH, Kim HH, Ji HY, Yoo SD, Choi WR, et al. Dose-linear pharmacokinetics of oleanolic acid after intravenous and oral administration in rats. *Biopharm Drug Dispos*. (2007) 28:51–7. doi: 10.1002/bdd.530

15. Liu H, Yang J, Du F, Gao X, Ma X, Huang Y, et al. Absorption and disposition of ginsenosides after oral administration of *Panax notoginseng* extract to rats. *Drug Metab Dispos*. (2009) 37:2290–8. doi: 10.1124/dmd.109.029819

16. Guo X, Xie Y, Lian S, Li Z, Gao Y, Xu Z, et al. A sensitive HPLC–MS/MS method for the simultaneous determination of anemoside B4, anemoside A3 and 23-hydroxybetulinic acid: application to the pharmacokinetics and liver distribution of *Pulsatilla chinensis* saponins. *Biomed Chromatogr*. (2018). 32:e4124. doi: 10.1002/bmc.4124

17. He M, Ouyang H, He M, Tan T, Li J, Zhang X, et al. Application of a liquid chromatography–tandem mass spectrometry method to the pharmacokinetics, tissue distribution and excretion in the study of anemoside B4, a novel antiviral agent candidate, in rats. *Biomed Chromatogr*. (2017) 31: e3914. doi: 10.1002/bmc.3914

18. Wan JY, Zhang YZ, Yuan JB, Yang FQ, Chen Y, Zhou LD, et al. Biotransformation and metabolic profile of anemoside B4 with rat small and large intestine microflora by ultra-performance liquid chromatography–quadrupole time-of-flight tandem mass spectrometry. *Biomed Chromatogr*. (2017) 31:e3873. doi: 10.1002/bmc.3873

19. Kang N, Shen W, Zhang Y, Su Z, Yang S, Liu Y, et al. Anti-inflammatory and immune-modulatory properties of anemoside B4 isolated from *Pulsatilla chinensis* in vivo. *Phytomedicine*. (2019) 64:152934. doi: 10.1016/j.phymed.2019.152934

20. Xiao M, Luo R, Liang Q, Jiang H, Liu Y, Xu G, et al. Anemoside B4 inhibits SARS-CoV-2 replication in vitro and in vivo. *Chinese Herbal Med*. (2024) 16:106–12. doi: 10.1016/j.chmed.2023.09.005

21. Zou M, Chen FJ, Deng LR, Han Q, Huang CY, Shen SS, et al. Anemoside B4 ameliorates experimental autoimmune encephalomyelitis in mice by modulating inflammatory responses and the gut microbiota. *Eur J Pharmacol*. (2022) 931:175185. doi: 10.1016/j.ejphar.2022.175185

22. Gabrielsson J, Weiner D. Non-compartmental analysis. *Methods Mol Biol*: (2012) 929. 377–89. doi: 10.1007/978-1-62703-050-2_16

23. Ye Y, Xue M, Tian X, Gao H, Hu P, Wang L, et al. Pharmacokinetic and metabolite profile of orally administered anemoside B4 in rats with an improved exposure in formulations of rectal suppository. *J Ethnopharmacol*. (2023) 315:116694. doi: 10.1016/j.jep.2023.116694

24. Yang L, Meng X, Yu X, Kuang H. Simultaneous determination of anemoside B4, phellodendrine, berberine, palmatine, obakunone, esculin, esculetin in rat plasma by UPLC-ESI-MS/MS and its application to a comparative pharmacokinetic study in normal and ulcerative colitis rats. *J Pharm Biomed Anal*. (2017) 134:43–52. doi: 10.1016/j.jpba.2016.11.021

25. Tian X, Xu Z, Chen M, Hu P, Liu F, Sun Z, et al. Simultaneous determination of eight bioactive compounds by LC-MS/MS and its application to the pharmacokinetics, liver first-pass effect, liver and brain distribution of orally administrated Gouteng-

Baitouweng (GB) in rats. *J Chromatogr B Analyt Technol Biomed Life Sci*. (2018) 1084:122–31. doi: 10.1016/j.jchromb.2018.03.013

26. Jia J, Hui O, He M-Y, He doi: 10.13422/j.cnki.syfjx.2017180071M-Z, Q J-M, F Y-L, et al. Investigation of rat plasma protein binding characteristics of Anemoside B4 by high-throughput equilibrium dialysis combined with UPLC-MS/MS technique. *Zhongguo Shiyan Fangji Xue Zazhi*. (2017) 23:71–74.

27. Kishino S, Nomura A, Itoh S, Nakagawa T, Takekuma Y, Sugawara M, et al. Age- and gender-related differences in carbohydrate concentrations of alpha1-acid glycoprotein variants and the effects of glycoforms on their drug-binding capacities. *Eur J Clin Pharmacol*. (2002) 58:621–8. doi: 10.1007/s00228-002-0530-x

28. He J, Yuan R, Cui X, Cui Y, Han S, Wang QQ, et al. Anemoside B4 protects against *Klebsiella pneumoniae*- and influenza virus FM1-induced pneumonia via the TLR4/Myd88 signaling pathway in mice. *Chin Med*. (2020) 15:68. doi: 10.1186/s13020-020-00350-w

29. Lu T, Wang Q, Zhao M, Wang J, Guo Q. Research progress on pharmacological actions and molecular mechanisms of Anemoside B4. *Pharmacol Res*. (2023) 7:100251. doi: 10.1016/j.prmcm.2023.100251

30. Oray M, Abu SK, Ebrahimiadib N, Meese H, Foster CS. Long-term side effects of glucocorticoids. *Expert Opin Drug Saf*. (2016) 15:457–65. doi: 10.1517/14740338.2016.1140743

31. Peng B, Li J, Chen M, Yang X, Hao M, Wu F, et al. Clinical value of glucocorticoids for severe community-acquired pneumonia: a systematic review and meta-analysis based on randomized controlled trials. *Medicine*. (2023) 102:e36047. doi: 10.1097/MD.0000000000036047

frontiers | Frontiers in Veterinary Science

TYPE Original Research
PUBLISHED 18 August 2025
DOI 10.3389/fvets.2025.1611467

OPEN ACCESS

EDITED BY
Shuaiyu Wang,
China Agricultural University, China

REVIEWED BY
Hongxu Du,
Southwest University, China
Ruonan Bo,
Yangzhou University, China
Patipan Hnokaew,
Chiang Mai University, Thailand

*CORRESPONDENCE
Yanming Wei
✉ weiym@gsau.edu.cn
Peng Ji
✉ jip@gsau.edu.cn

RECEIVED 14 April 2025
ACCEPTED 17 July 2025
PUBLISHED 18 August 2025

CITATION
Yan J, Zhou K, Ma T, Ji P and Wei Y (2025) Gastrointestinal flora and serum metabolomic elucidation of *Astragali Radix* water decoction intervention in subclinical bovine mastitis. *Front. Vet. Sci.* 12:1611467. doi: 10.3389/fvets.2025.1611467

Gastrointestinal flora and serum metabolomic elucidation of *Astragali Radix* water decoction intervention in subclinical bovine mastitis

Jianpeng Yan[1,2], Ke Zhou[1], Ting Ma[1], Peng Ji[1]* and Yanming Wei[1]*

[1]Tranditional Chinese Veterinary Medicine Laboratory, College of Veterinary Medicine, Gansu Agricultural University, Lanzhou, China, [2]Lanzhou Center for Animal Disease Prevention & Control, Lanzhou, China

Background: This study addresses the global challenge of subclinical bovine mastitis (SCBM) in dairy cows, a prevalent disease causing substantial economic losses, by investigating the mechanistic basis of *Astragali Radix*, a traditional herbal remedy with empirically validated efficacy but incompletely understood modes of action.

Methods: Initially, the active components of *Astragali Radix* were identified using LC-MS/MS. Dose-response trials were conducted in Holstein cows ($n = 24$ SCBM cases; $n = 6$ healthy controls), along with multi-omics integration, including 16S rRNA sequencing for rumen/feces microbiota and UHPLC-MS metabolomics for serum analysis. The therapeutic effects of Astragali Radix water decoction (ARWD) on milk production, inflammatory markers, immune parameters, and oxidative stress were systematically evaluated.

Results: ARWD administration dose-dependently improved milk yield and protein content while reducing somatic cell counts. Serum pro-inflammatory cytokines (TNF-α, IL-6, IL-1β) decreased, contrasting with increases in immunoglobulins (IgA, IgM, IgG) and enhanced superoxide dismutase activity. Microbiota restructuring featured ruminal enrichment of Bifidobacterium and fecal dominance of Rikenellaceae_RC9_gut_group, coupled with suppression of pro-inflammatory taxa (e.g., Christensenellaceae_R-7_group). Metabolomic analysis identified four ARWD-responsive biomarkers, notably Spirotaccagenin and Pelanin, operating through linoleic acid metabolism and phospholipase D signaling pathways. Strong correlations linked microbial shifts to improved lactation parameters and reduced inflammation.

Conclusion: The findings establish that ARWD alleviates SCBM through coordinated microbiota remodeling and metabolic reprogramming, specifically enhancing antioxidant defenses, restoring mammary barrier integrity, and modulating immune-inflammation crosstalk, with optimal efficacy at 0.4 $g \cdot kg^{-1} \cdot d^{-1}$ dosage. This mechanistic validation positions ARWD as a scientifically grounded, eco-friendly alternative for sustainable mastitis management, reconciling therapeutic effectiveness with agricultural economic priorities.

KEYWORDS

Astragali Radix, subclinical bovine mastitis, phytochemical untargeted metabolomics, metabolomics, 16S rRNA

1 Introduction

In recent years, subclinical bovine mastitis (SCBM) has emerged as a significant issue in the dairy industry, second only to clinical mastitis. This condition has a profound impact on milk yield and quality, negatively affecting overall herd health and ultimately reducing the profitability of dairy farms (1). Veterinary experts agree that controlling somatic cell count (SCC) is crucial for sustainable dairy production. SCBM is characterized by the gradual onset, high contagion rates, and increased SCC levels in milk, often going unnoticed until it causes considerable economic losses (2). Therefore, it is vital to implement preventive measures during the SCBM phase to ensure the health of bovine mammary glands. While traditional antibiotic treatments are commonly employed, they can adversely affect milk quality and pose risks to human health due to the potential for antimicrobial resistance, highlighting the urgent need for sustainable alternatives (3).

According to traditional Chinese veterinary medicine (TCVM), deficiencies in qi and blood contribute to the development of SCBM, increasing cows' susceptibility to bacterial colonization in the mammary tissues. Key pathogens involved include *Staphylococcus aureus* and *Streptococcus agalactiae*, which take advantage of weakened immune states to establish persistent infections (4).

The mammary gland serves as an essential component of the immune system, employing intricate mechanisms to protect against bacterial infections, which are vital for managing infections. Recent research indicates that the gastrointestinal microbiota, often called the "second genome," significantly contributes to the immune defenses of the mammary gland through interactions along the gut-mammary axis (5). This microbial community is crucial for the immune system, particularly in identifying pathogens within the mammary glands and regulating inflammation.

The gut-immune axis has emerged as a significant area of research, with compelling evidence indicating a bidirectional communication between gut microbiota and host immunity (6). An imbalance in gut microbiota is linked to various health problems, including infections and inflammatory diseases. In dairy cows, changes in gut microbiota composition can heighten the risk of mastitis, even in subclinical cases (7). This microbial dysregulation impacts the production of immunomodulatory metabolites, such as short-chain fatty acids (SCFAs), which plays a crucial role in regulating the immune system throughout the body (8). In this regard, herbal medicines have shown promising immunomodulatory properties without adverse effects. For instance, *Astragali Radix*, a prominent herb known for boosting qi, has been found to modulate immune responses and affect gut microbiota. Experimental studies indicate that this herb promotes the growth of beneficial bacteria like *Lactobacillus* and *Bifidobacterium* while inhibiting harmful pathogens such as *Escherichia* and *Salmonella* (9). Additionally, bioactive compounds found in Astragalus, including polysaccharides and saponins, significantly enhance macrophage phagocytosis, promote the maturation of dendritic cells, and stimulate T-lymphocyte proliferation (10). Moreover, advanced technologies like high-throughput 16S rRNA gene sequencing and metabolomics are shedding light on the interactions between traditional Chinese medicine (TCM), gut microbiota, and immune function. By influencing microbial communities and regulating metabolic pathways, these innovative methods help clarify the mechanisms underlying TCM interventions (11, 12).

This study explored the therapeutic effectiveness and underlying mechanisms of *Astragali Radix* water decoction (ARWD) in treating bovine SCBM by utilizing fecal 16S rRNA sequencing and serum untargeted metabolomics. Additionally, the research identified the bioactive components of ARWD decoction through LC-MS/MS analysis. The findings provide a scientific foundation for clinical application of ARWD in SCBM prevention and control within veterinary practice.

Abbreviations: ARWD, Astragali Radix water decoction; SCBM, subclinical bovine mastitis; SCC, somatic cell count; TCVM, traditional Chinese veterinary medicine; SCFAs. short-chain fatty acids; TCM, traditional Chinese medicine; MDA, malondialdehyde; SOD, superoxide dismutase; MPO, myeloperoxidase; LDH, lactate dehydrogenase; IgA, immunoglobulin A; IgG, immunoglobulin G; IgM, immunoglobulin M; IL-2, interleukin-2; IL-1β, interleukin-1β; TNF-α, tumor necrosis factor α; AR_H, Astragali Radix water decoction high-dose; AR_M, Astragali Radix water decoction medium-dose; AR_L, Astragali Radix water low-dose; MOD, model group; NC, negative controls; TS, total milk solids; MUN, milk urea nitrogen; OTUs, operational taxonomic units; LPS, lipopolysaccharide; PCA, principal component analysis.

2 Materials and methods

2.1 Materials and reagents

Astragali Radix was purchased from Lanzhou Yellow River medicine market. Origin: Liupanshan Region, China. The following kits were used in this study: malondialdehyde (MDA) test kit (catalog No. YJ016824), superoxide dismutase (SOD) test kit (catalog No. YJ036559), myeloperoxidase (MPO) test kit (catalog No. YJ300741), lactate dehydrogenase (LDH) test kit (catalog No. YJ520026), immunoglobulin A (IgA) ELISA kit (catalog No. YJ542063), immunoglobulin G (IgG) ELISA kit (catalog No. YJ330698), immunoglobulin M (IgM) ELISA kit (catalog No. YJ627279), Interleukin-2 (IL-2) ELISA kit (catalog No. YJ002498), interleukin-1 β (IL-1 β) ELISA kit (catalog No. YJ064295), interleukin-6 (IL-6) ELISA kit (catalog No. YJ064296) and tumor necrosis factor α (TNF- α) ELISA kit (catalog No. YJ077389), all the above were purchased from Shanghai Meilian Biotechnology Company.

2.2 Preparation of ARWD

Astragali Radix were mixed with distilled water at a 1:10 (w/v) ratio. The mixture was vigorously boiled, then simmered at low heat for 30 min and filtered through four-layer sterile gauze. The residue underwent re-extraction with an 8-fold volume of distilled water following identical boiling/simmering conditions, followed by gauze filtration. Both filtrates were combined for subsequent experiments.

TABLE 1 Chemical composition of TMR.

Ingredient	Content (%)	Nutrient composition	Content (%)
Corn silage	56.5	Dry matter	47.4
Brewing grain	14.6	Neutral detergent fiber	31.1
Alfalfa hey	2.4	Crude protein	16.5
Oat grass	1.6	Ether extract	3.5
Concentrate feed	24.9	rumen undegradable protein	33.4

The concentrate feed is composed of corn (53.2%), soybean meal (32.9%), cottonseed (5%), fat (2.2%), salt (0.8%), and premix (5.9%).

2.3 Experimental animals and grouping

All experimental cows were obtained from the Gansu Holstein Dairy Cattle Breeding Center and selected as multiparous, mid-lactation individuals (3–9 years old) with comparable body weights. The animals were fed mixed ration (TMR) three times a day at 8:00, 16:00, and 21.30 respectively (Table 1). Mammary health was assessed via SCC and clinical mastitis evaluation. Based on established criteria (13, 14), cows with SCC $<$ 200,000 cells/ml were considered healthy, while those with SCC $>$ 200,000 cells/ml without clinical symptoms were diagnosed with SCBM. Untreated positive cows with SCBM for 3–5 days ($n = 24$) were randomly assigned to four experimental groups ($n = 6$ per group): *Astragali Radix* water decoction High-dose group (0.4 $g{\cdot}kg^{-1}{\cdot}d^{-1}$, AR_H), *Astragali Radix* water decoction Medium-dose group (0.2 $g{\cdot}kg^{-1}{\cdot}d^{-1}$, AR_M), *Astragali Radix* water decoction Low-dose group (0.1 $g{\cdot}kg^{-1}{\cdot}d^{-1}$, AR_L). Model group: untreated SCBM controls (MOD). Six additional healthy cows received equivalent volumes of water as negative controls (NC). All ARWD treatments were administered orally via force-feeding for seven consecutive days. Sample Collection: 5 ml of blood were collected from each cow through the tail vein 1 h after feeding on the morning of day 8. The blood samples were then centrifuged at 3,000 r/min for 15 min at 4°C to separate the serum. Rumen fluid was extracted by inserting a rumen sampler via the mouth into the rumen and using a syringe. The first two tubes of rumen fluid were discarded to prevent salivary contamination. Approximately 150 ml of rumen fluid was sampled from each cow. Fecal samples were collected from the rectum using sterile long-arm gloves, 3 h after feeding, and placed in sterile, sealed plastic bags. Fecal and rumen fluid samples were immediately snap frozen in liquid nitrogen and stored at −80°C. Milk samples were collected and transported on ice for somatic cell count (SCC) analysis and milk composition testing.

2.4 LC-MS/MS analysis of ARWD samples

The LC-MS/MS analysis was performed using a UHPLC-Q Exactive system (Thermo Scientific) equipped with a UPLC BEH C18 column (2.1 × 100 mm i.d., 1.7 μm). The mobile phase consisted of (A) 2% acetonitrile containing 0.1% formic acid and (B) acetonitrile with 0.1% formic acid. Full-scan MS data were acquired in both positive and negative ionization modes over a mass range of 70–1,050 m/z at a resolution of 70,000. Data processing, including peak alignment, extraction, and quantification, was conducted using Compound Discoverer QI v3.0 (WatersCorporation, Milford, USA) software. Metabolite identification was achieved by matching accurate mass and MS/MS spectra against the Majorbio Bio-Pharm Technology Co., Ltd (Shanghai, China) database with (mass accuracy threshold of $<$10 ppm).

2.5 Milk yield statistical analysis

Milking was performed using rotary milking parlors pre- and post-treatment, with individual milk yields recorded for each cow.

2.6 Somatic cell count and milk composition analysis

SCC and milk composition parameters [fat, protein, lactose, total milk solids (TS), milk urea nitrogen (MUN)] were analyzed using a CombiFoss^{TM} 7 analyzer (Foss Analytical, Denmark).

2.7 Detection of serum oxidative stress markers

The biochemical test kit was used to measure the levels of LDH, MPO, MDA, and SOD in serum. All experimental procedures were strictly conducted according to the manufacturer's instructions for the reagents.

2.8 Detection of serum inflammatory cytokines

The levels of IL-1β, IL-6, IL-2, and TNF-α in serum were measured using ELISA test kits. All experimental procedures were strictly carried out according to the instructions provided by the manufacturer for the reagents.

2.9 Detection of serum immunoglobulin

The levels of IgA, IgM, and IgG in serum were measured using biochemical test kits. All experimental procedures were strictly followed according to the instructions provided by the manufacturer for the reagents.

2.10 Rumen and fecal microbiota analysis

After drug administration, rumen fluid and rectal content were collected and stored at −80°C. According to the manufacturer's

instructions, total microbial genomic DNA was extracted from 18 gastric juice samples and 18 fecal samples using the E.Z.N.A.® soil DNA Kit (Omega Bio-tek, Norcross, GA, U.S.). The mass and concentration of DNA were determined by 1.0% agarose gel electrophoresis and NanoDrop2000 spectrophotometer (Thermo Scientific, United States), and were stored at −80°C for further use. The hypervariable region V3–V4 of the bacterial 16S rRNA gene were amplified with primer pairs 338F (5′-ACTCCTACGGGAGGCAGCAG3′) and 806R (5′-GGACTACHVGGGTWTCTAAT3′) by T100 Thermal Cycler PCR thermocycler (BIO-RAD, USA). The PCR reaction mixture included 4 μl of 5 × Fast Pfu buffer, 2 μl of 2.5 mm dNTPs, 0.8 μl (5 μm) for each primer, 0.4 μl of Fast Pfu polymerase, 10 ng of template DNA, and ddH2O up to a final volume of 20 μl. The PCR amplification cycle conditions are as follows: initial denaturation at 95°C for 3 min, denaturation at 95°C for 30 s, annealing at 55°C for 30 s, extension at 72°C for 45 s, single extension at 72°C for 10 min, and conclusion of 27 cycles at 4°C. The PCR product was extracted from 2% agarose gel and purified using the PCR Clean-Up Kit (Yuhua, Shanghai, China) according to manufacturer's instructions and quantified using Qubit 4.0 (Thermo Fisher Scientific, USA), and the purified amplifiers were aggregated in equal molar amounts. 2 × 300 bp paired-end sequencing was performed on the Illumina Nextseq2000 platform (Illumina, San Diego, USA) according to the standard protocols by Majorbio Bio-Pharm Technology Co., Ltd. (Shanghai, China).

2.11 Serum untargeted metabolomics analysis

Serum samples from blank control, model, and astragalus intervention groups (n = 6/group) were extracted with methanol:acetonitrile (1:1, v/v). After ultrasonication (5°C, 40 kHz, 30 min) and incubation (−20°C, 30 min), supernatants were collected by centrifugation (13,000 g, 4°C, 15 min), dried under nitrogen, and reconstituted in acetonitrile:water (1:1, v/v). Quality control (QC) samples were processed identically.

Metabolites were analyzed using UHPLC-Q Exactive Focus MS (Thermo Fisher) with an ACQUITY UPLC HSS T3 column (100 × 2.1 mm, 1.8 μm). Mobile phases: (A) 95% water/5% acetonitrile (0.1% formic acid); (B) 47.5% acetonitrile/47.5% isopropanol/5% water (0.1% formic acid). Flow rate: 0.40 ml/min, injection volume: 5 μl, column temperature: 40°C. MS parameters: ±3.50 kV spray voltage, 325°C capillary temperature, full scan at 81–1,000 m/z (70,000 resolution), HCD fragmentation (30 eV).

Raw data were processed in Progenesis QI v3.0 for peak alignment. Metabolites were identified by matching MS/MS spectra against HMDB, Metlin, and Majorbio Bio-Pharm Technology Co., Ltd. (Shanghai, China) in-house databases (MS error <10 ppm, spectral score filtering). Differential metabolites underwent pathway enrichment analysis ($P < 0.05$).

2.12 Correlation analysis

Spearman's rank correlation analysis was performed to investigate relationships between differential metabolites and gut microbiota among NC, MOD, and AR_H groups. Additionally, pairwise correlations were analyzed between metabolites/gastrointestinal microbiota and dairy parameters (SCC, milk yield, milk composition), inflammatory factors, immune/antioxidant indices.

2.13 Statistical analysis

Gastrointestinal flora alpha diversity was statistically determined using the Kruskal–Wallis test, and beta-diversity was statistically determined using the ANOSIM test. Statistical analyses were performed using one-way ANOVA in GraphPad Prism 8 (GraphPad Software), with significance levels defined as $P < 0.05$ (significant), $P < 0.01$ (highly significant), and $P > 0.05$ (not significant).

3 Results

3.1 LC-MS/MS analysis of ARWD

Total ion chromatograms were acquired in both positive and negative ion modes. As shown in Figure 1, well-resolved peaks with uniform distribution were observed under the current analytical conditions. Qualitative analysis was performed by matching the mass spectrometry data matrix (retention time, m/z, and peak intensity) against the MJBIOTCM database. Nine compounds were identified, including flavonoids, steroids, and their derivatives (Table 2).

3.2 Effects of ARWD on milk yield in SCBM cows

Analysis of milk yield before and after oral administrations revealed significant intergroup differences. Pretreatment milk yield in the MOD group was significantly lower than the NC group ($P < 0.01$). Post-intervention, all ARWD treated groups (AR_L, AR_M, AR_H) exhibited increased milk yields compared to baseline levels. Notably, the AR_H group showed marked improvement vs. the MOD group ($P < 0.01$), approaching NC group values. AR_L and AR_M groups demonstrated moderate milk yield increases post-treatment, though these changes lacked statistical significance ($P > 0.05$) (Figure 2).

3.3 Effects of ARWD on SCC and milk composition in SCBM cows

Post-treatment SCC analysis demonstrated significant reduction in the AR_H group vs. baseline ($P < 0.01$) and MOD

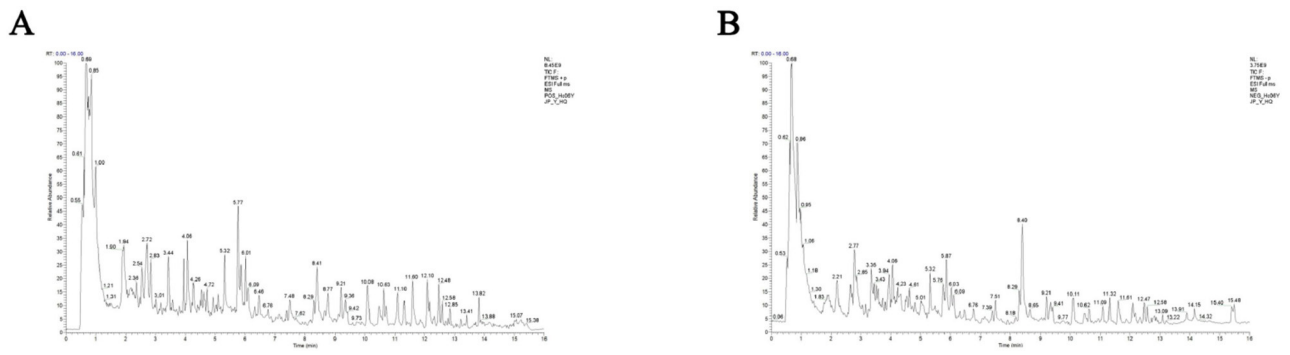

FIGURE 1
LC-MS/MS total ion chromatograms of ARWD in positive and negative ion modes. **(A)** Positive ion mode (POS); **(B)** negative ion mode (NEG).

TABLE 2 Identification results of Astragalus samples by LC-MS/MS analysis.

Item	Compound name	Retention time (min)	Y_HQ	[M/Z]	Error (ppm)
1	Astragaloside III	9.3573	1,824, 771.43	802.4935	−1.5223
2	Astragaloside VI	8.6389	1,118, 351.30	964.5454	−2.2808
3	Ononin	5.3179	25,164, 078.81	431.1329	−1.7787
4	Calycosin-7-O-β-D-glucoside	4.0636	9,787, 917.63	491.1199	0.8519
5	Astragaloside II	10.6241	12,801, 642.07	871.4708	1.3701
6	Calycosin	5.8688	14,925, 299.13	283.0612	−0.0517
7	Astragaloside IV	8.2492	132, 954.70	829.4596	0.6632
8	Formononetin	8.4049	19,202, 627.74	267.0663	−0.1162
9	Isoastragaloside IV	9.3646	745, 646.04	819.4311	1.0494

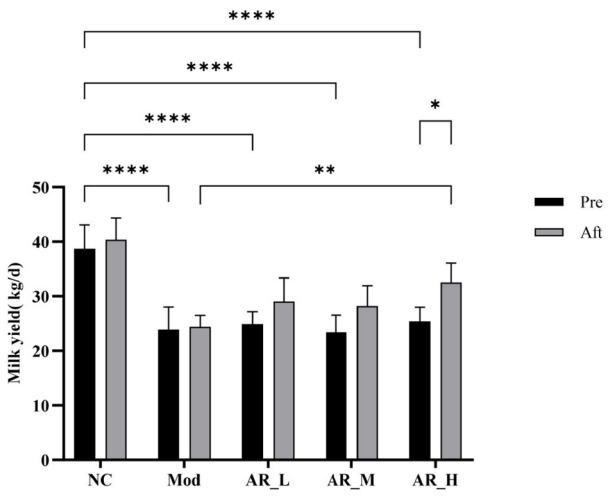

FIGURE 2
Milk yield changes. Differences between the two groups are indicated by (*), $^{*}P < 0.05$, $^{**}P < 0.01$, $^{***}P < 0.001$, $^{****}P < 0.0001$.

group ($P < 0.01$). The AR_M group showed moderate SCC decrease compared to MOD ($P < 0.05$), while AR_L exhibited no significant change (Figure 3A).

Milk fat content analysis showed that after ARWD intervention, the fat content in the AR_H group was significantly higher than that in the MOD group ($P < 0.01$). Compared with before treatment, the fat content in the AR_H, AR_M, and AR_L groups increased after ARWD intervention, but the increase was not significant (Figure 3B).

Milk protein content analysis indicated that the protein levels in the AR_H group after treatment were significantly lower than before treatment ($P < 0.05$). Compared with the MOD group, the protein contents in the AR_H, AR_M, and AR_L groups were all lower than those in the MOD group and lower than before administration (Figure 3C).

Lactose, Total Solids, and Milk Urea Nitrogen analysis revealed that no statistically significant differences in lactose, total solids (TS), or milk urea nitrogen (MUN) were detected among experimental groups relative to NC ($P > 0.05$). Slight increases in lactose and TS were observed in AR_H and AR_M groups, though these trends did not reach statistical significance (Figures 3D–F).

3.4 Effects of ARWD on serum inflammatory cytokines in SCBM cows

As shown in Figure 4, IL-6 expression in the AR_H group was significantly reduced post-intervention compared to pre-treatment

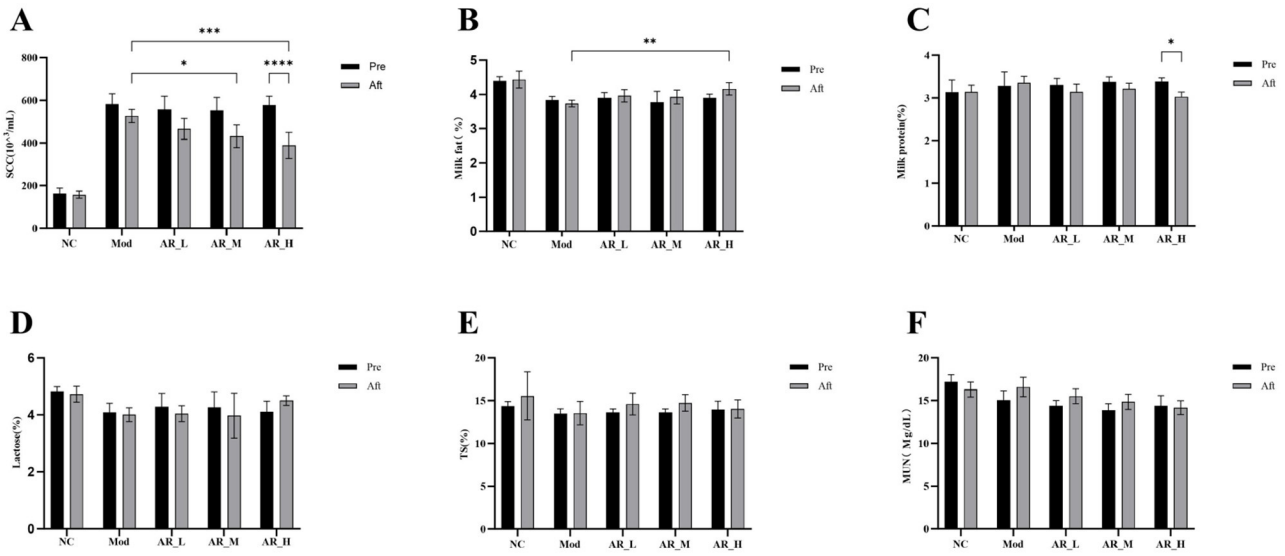

FIGURE 3
Changes of the somatic cells and milk components. **(A)** SCC; **(B)** milk fat; **(C)** milk protein; **(D)** latctose; **(E)** TS; **(F)** MUN. The differences between the two groups are indicated by (*), $^{*}P < 0.05$, $^{**}P < 0.01$, $^{***}P < 0.001$, $^{****}P < 0.0001$.

($P < 0.01$). Similarly, IL-1β levels showed marked reduction in AR_H vs. both pre-treatment ($P < 0.05$) and MOD group ($P < 0.05$). TNF-α expression in AR_H group was significantly lower than MOD group ($P < 0.05$). In contrast, AR_M and AR_L groups exhibited no significant alterations in IL-6, IL-1β, or TNF-α levels compared to NC or MOD groups ($P > 0.05$). IL-2 expression remained unchanged across all experimental phases (Figure 4).

3.5 Effects of ARWD on oxidative stress in SCBM cows

Post-intervention analysis revealed significant increases in SOD activity ($P < 0.01$) and marked reductions in MDA ($P < 0.01$), LDH ($P < 0.05$), and MPO ($P < 0.05$) levels in the AR_H group. Notably, AR_H group MPO levels were significantly lower than MOD group ($P < 0.01$). No significant differences were observed between AR_M and AR_L groups (Figure 5). These findings demonstrate that Astragalus supplementation, particularly at high doses, significantly enhanced antioxidant capacity and alleviated oxidative stress, while lower doses exhibited moderate effects.

3.6 Effects of ARWD on immunoglobulins in SCBM cows

ARWD exerted significant modulatory effects on the immunoglobulin profiles in experimental groups. In the AR_H group, post-treatment levels of IgA, IgG, and IgM were significantly elevated compared to pre-treatment ($P < 0.05$). Furthermore, AR_H exhibited marked increases in IgM and IgG vs. the MOD group ($P < 0.05$). In contrast, AR_M and AR_L groups demonstrated no significant alterations in immunoglobulin levels relative to MOD ($P > 0.05$) (Figure 6). These findings indicate that high-dose Astragalus supplementation enhanced immune function through immunoglobulin modulation, while medium- and low-dose groups showed marginal efficacy.

3.7 Effects of ARWD on rumen and gut microbiota in SCBM cows

3.7.1 Rumen fluid microbiota sequencing

A total of 4, 323 valid 16S rRNA sequences were obtained from 18 rumen fluid samples. Clustering analysis of non-redundant sequences at 97% similarity threshold identified 2,058 operational taxonomic units (OTUs). Rarefaction curves approached saturation with increasing sequencing depth, indicating adequate sequencing coverage (Figure 7A).

3.7.2 Rumen microbiota Alpha diversity analysis

No significant differences in Ace, Chao, Coverage, Shannon, Simpson, or Sobs indices were observed between Astragalus-treated and MOD groups ($P > 0.05$). However, downward trends in Shannon and Sobs indices were noted in the intervention group (Figures 7B, C). These results suggest potential modulatory effects of ARWD on rumen microbial richness and diversity in SCBM cows, though statistical significance was not achieved.

3.7.3 Rumen fluid microbial composition at phylum and genus levels

Analysis of 18 rumen fluid samples revealed distinct microbial compositions at phylum and genus levels. Phylum-level composition identified 15 phyla. Firmicutes dominated across groups (62.5% in NC, 74.8% in MOD, 73.5% in AR_H group), followed by Bacteroidota (16.0%, 15.3%, 14.2%) and Actinobacteriota (17.2%, 5.4%, 7.4%). Minor phyla including Patescibacteria and Spirochaetota showed substantially lower

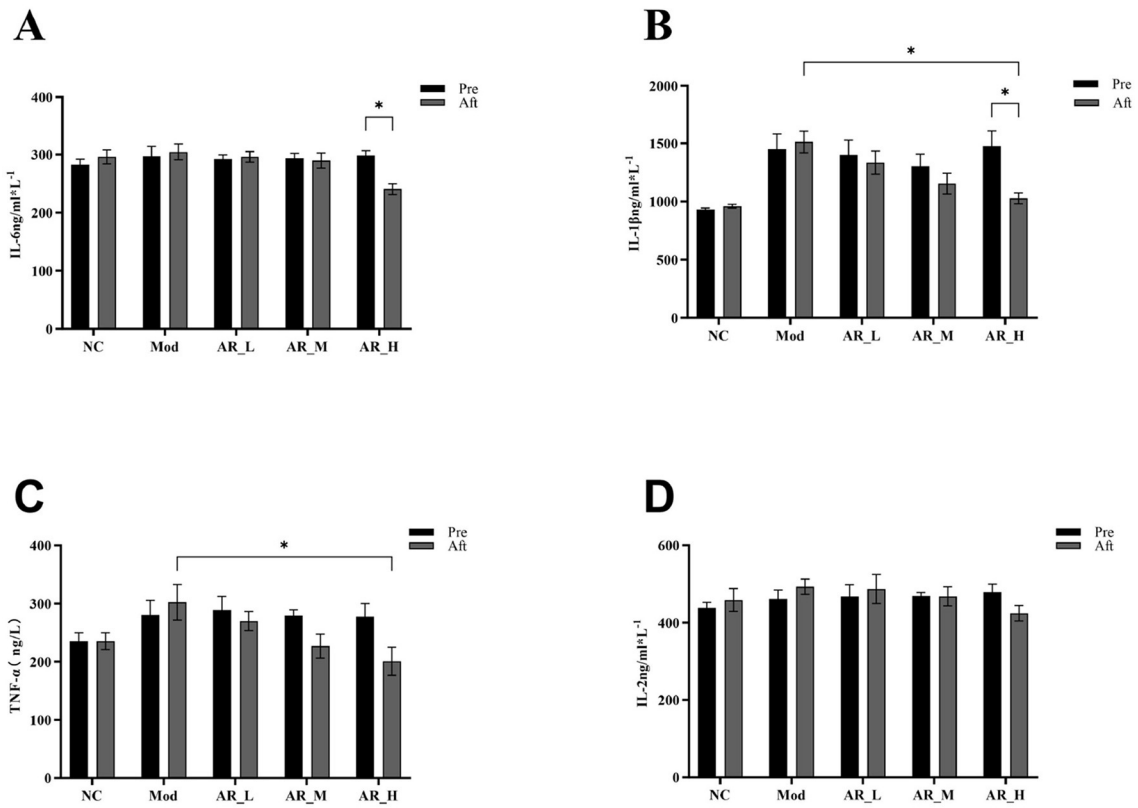

FIGURE 4
Changes of the serum inflammatory cytokines. **(A)** IL-6; **(B)** IL-1β; **(C)** TNF-α; **(D)** IL-2. The differences between the two groups are indicated by (*), $^{*}P < 0.05$.

abundances (<2% collectively) (Figure 7D). Genus-level analysis detected 294 genera. Dominant genera in NC included *UCG-005* (16.2%), *Bifidobacterium* (16.6%), *Romboutsia* (3.1%), and *Paeniclostridium* (2.8%). MOD group exhibited altered profiles: *UCG-005* (20.8%), *Bifidobacterium* (4.6%), *Romboutsia* (3.0%), and *Paeniclostridium* (1.9%). Astragalus intervention induced notable compositional shifts vs. MOD group: increased abundances of *Bifidobacterium* (6.8%), *Romboutsia* (5.3%), and *Paeniclostridium* (4.0%), with reduced *UCG-005* (17.9%) (Figure 7E). These phylum- and genus-level microbial restructuring patterns suggest potential mechanistic links to Astragalus' therapeutic effects on SCBM in dairy cows.

3.7.4 Rumen microbiota β-diversity analysis

Bray-Curtis distance-based PCoA and NMDS analyses revealed partial separation of microbial communities among groups. The AR_H group exhibited distinct clustering from the MOD group, with closer proximity to the NC group, suggesting partial restoration of rumen microbiota structure in SCBM cows (Figures 7F, G). However, limited effects were observed on fecal microbiota β-diversity indices.

3.7.5 LEfSe analysis of rumen microbiota

LEfSe analysis with linear discriminant analysis (LDA) revealed significant microbial shifts between the MOD and AR_H groups ($P < 0.05$, Figure 7H). Compared to the MOD group, the AR_H group showed significant enrichment in beneficial genera such as *Clostridium_sensu_stricto_1* ($P = 0.016$), *Turicibacter* ($P = 0.037$), *Erysipelotrichaceae_UCG-008* ($P = 0.028$), and fiber-degrading taxa including *Cellulosilyticum* ($P = 0.004$) *Clostridium_sensu_stricto_6* ($P = 0.036$) *hoa5-07d05_gut_group* ($P = 0.007$). Conversely, *Blautia* ($P = 0.006$), *Ruminococcus_gauvreauii_group* ($P = 0.016$), *Roseburia* ($P = 0.004$) and other inflammation-associated genera, and *Brevibacillus* ($P = 0.028$), *Pseudobutyrivibrio* ($P = 0.006$), *Marvinbryantia* ($P = 0.006$) and other Potential pathobionts were significantly reduced. These microbiota alterations suggest that ARWD may alleviate SCBM by modulating microbial communities linked to immune regulation and metabolic balance.

3.7.6 Fecal microbiota sequencing

A total of 5,216 high-quality 16S rRNA sequences were obtained from 18 fecal samples. Clustering at 97% similarity threshold yielded 2, 290 OTUs. The rarefaction curve plateaued with increasing sequencing depth (Figure 8A), confirming adequate sampling coverage to capture microbial diversity.

3.7.7 Fecal microbiota Alpha diversity

Alpha diversity indices (Ace, Chao, Shannon, Simpson, Sobs, and Coverage) showed increased trends in the AR_H group

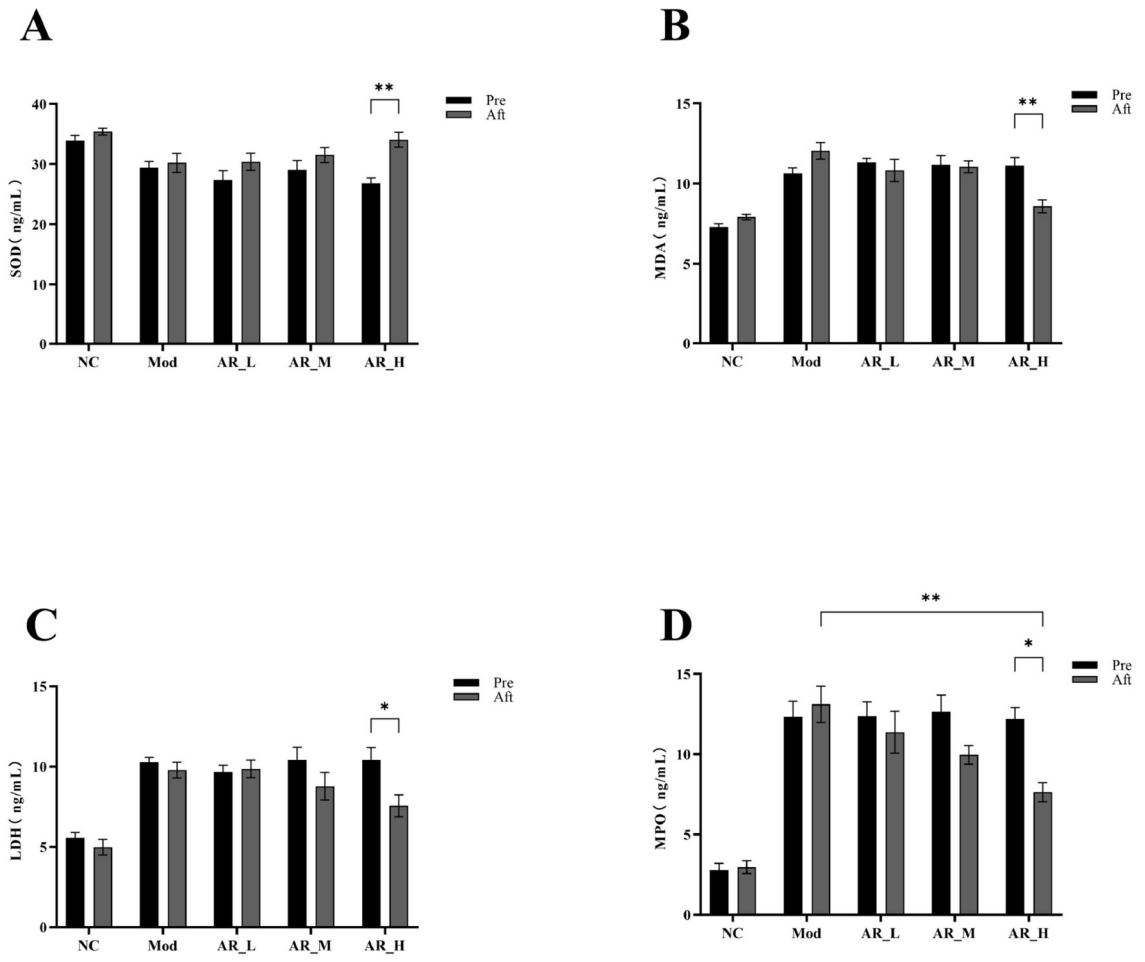

FIGURE 5
Changes of the serum oxidative stress markers. **(A)** SOD; **(B)** MDA; **(C)** LDH; **(D)** MPO. The differences between the two groups are indicated by (*), $^{*}P < 0.05$, $^{**}P < 0.01$.

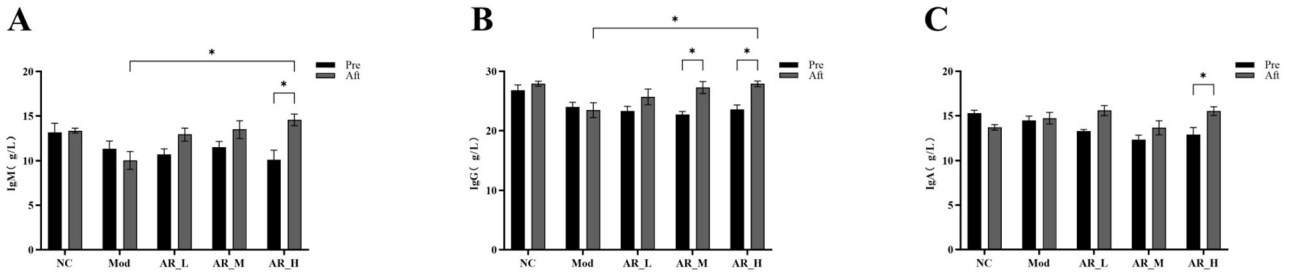

FIGURE 6
Changes of the serum Immunoglobulin. **(A)** IgM; **(B)** IgG; **(C)** IgA. The differences between the two groups are indicated by (*), $^{*}P < 0.05$.

compared to MOD, though without statistical significance ($P > 0.05$, Figures 8B–G). This non-significant elevation in richness (Ace/Chao) and evenness (Shannon/Simpson) suggests a potential but modest modulatory effect of Astragalus intervention on microbial community structure in SCBM cows.

3.7.8 Fecal microbial composition at phylum and genus levels

Taxonomic classification using the RDP classifier and Bayesian algorithm identified 19 phyla and 320 genera across 18 fecal samples. Phylum-level analysis revealed dominant taxa across groups: Firmicutes: 50.1% (NC), 54.7% (MOD), 44.7% (AR_H).

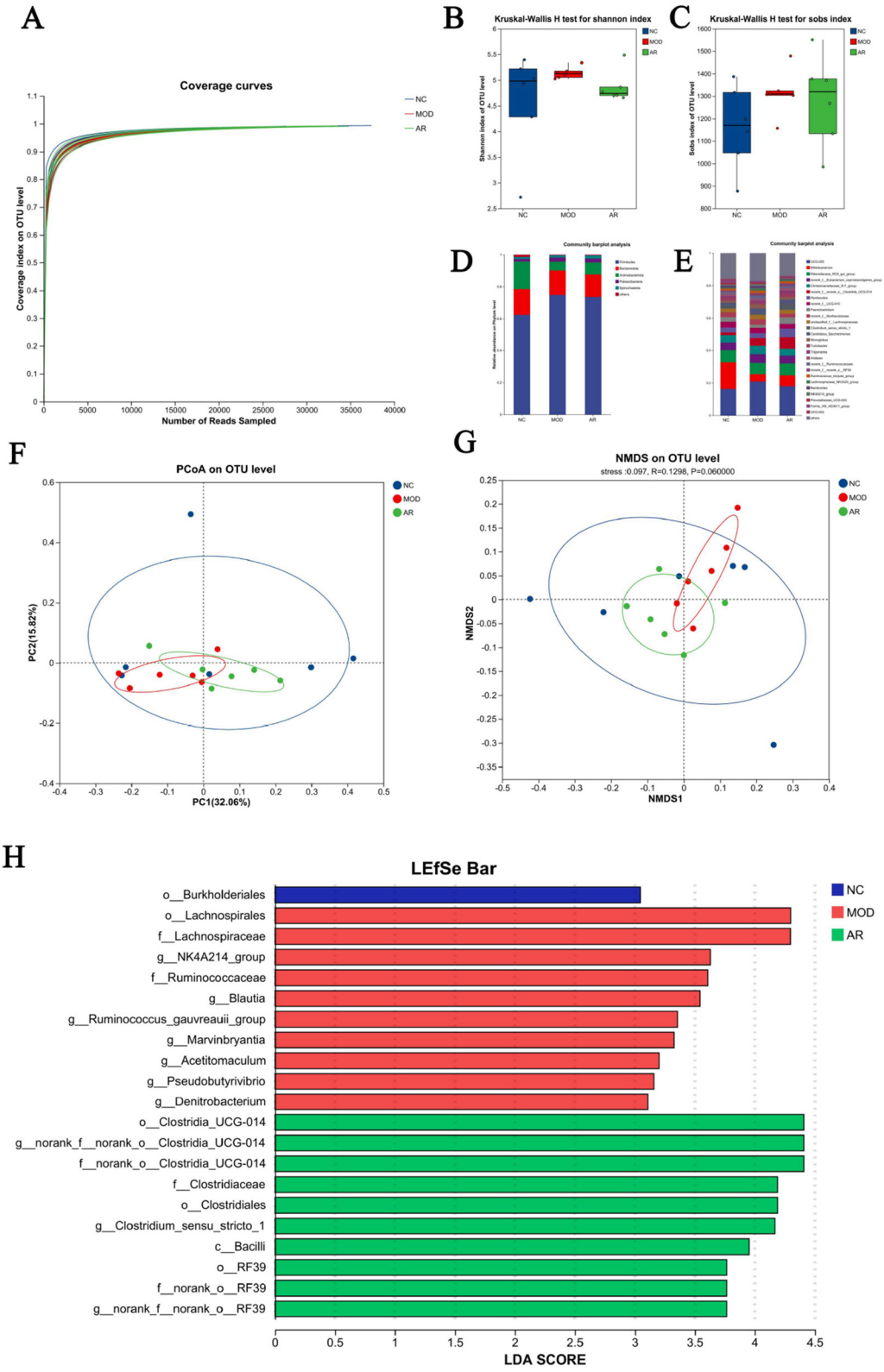

FIGURE 7
Diversity of the rumen bacterial flora. **(A)** Microbial species rarefaction curve; **(B)** Shannon; **(C)** Sobs; **(D)** phylum level; **(E)** genus levels; **(F)** PCoA; **(G)** NMDS; **(H)** LDA.

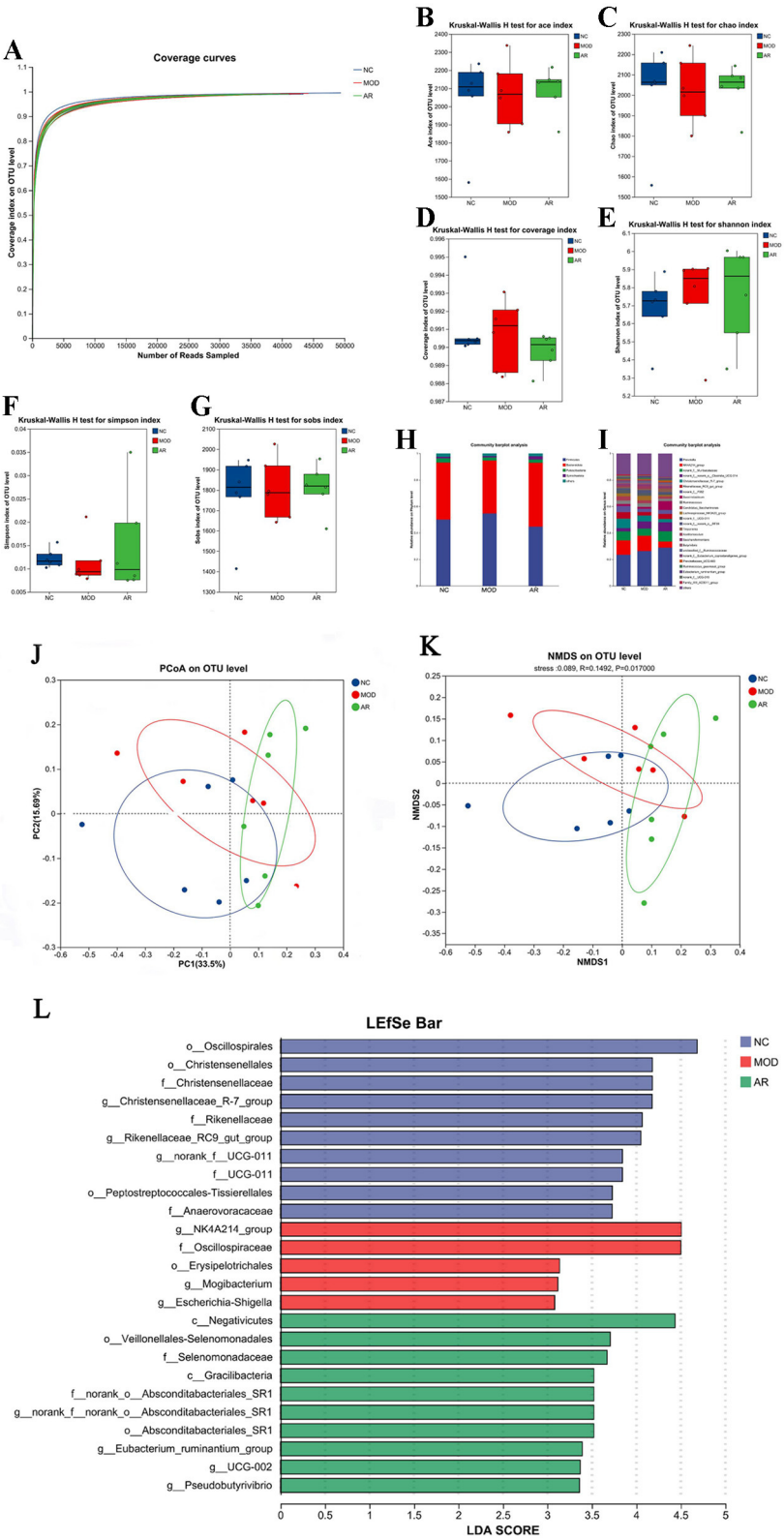

FIGURE 8
Diversity of the fecal microflora. **(A)** Feces microbial species rarefaction curve; **(B)** ACE; **(C)** Chao; **(D)** coverage; **(E)** Shannon; **(F)** Simpson; **(G)** Sobs;**(H)** phylum level; **(I)** genus levels; **(J)** NMDS; **(K)** PCoA; **(L)**LDA.

Bacteroidota: 43.1% (NC), 39.95% (MOD), 48.25% (AR_H). Minor phyla: Patescibacteria (3.2%, 2.3%, 2.5%) and Spirochaetota (1.2%, 1.04%, 2.5%) (Figure 8H). Genus-level profiling demonstrated group-specific dominance: *NK4A214_group*: 10.94% (NC), 11.52% (MOD), 4.57% (AR_H). *Christensenellaceae_R-7_group*: 7.13% (NC), 4.49% (MOD), 2.5% (AR_H). Functional shifts: *Succiniclasticum* increased to 6.69% in AR_H (vs. 1.44% in MOD), while *Ruminococcus_gauvreauii_group* declined to 0.68% (vs. 1.27% in MOD) (Figure 8I). These results highlight distinct fecal microbiota restructuring at both taxonomic levels following Astragalus intervention in SCBM cows.

3.7.9 Fecal microbiota Beta-diversity analysis

Beta-diversity analysis based on Bray-Curtis distance revealed partial compositional shifts among NC, MOD, and AR_H groups. PCoA and NMDS plots demonstrated distinct clustering of AR_H group from MOD, with a convergence trend toward CON (Figures 8J, K). These findings suggest *Astragalus* intervention partially restored microbial richness and diversity in SCBM cows, though its effects on β-diversity metrics remained statistically non-significant, indicating limited structural reorganization of the fecal microbiota community.

3.7.10 LEfSe analysis of fecal microbiota across groups

LEfSe analysis with LDA identified significant microbial biomarkers between MOD and AR_H groups ($P < 0.05$, Figure 8L). Compared to MOD, the AR_H group exhibited enrichment of fiber-degrading genera (e.g., *Treponema*, $P = 0.037$; *Selenomonas*, $P = 0.01$) and metabolic regulators (*Anaerovibrio*, $P = 0.025$), alongside suppression of mastitis-associated taxa (*Ruminococcus_gauvreauii_group*, $P = 0.037$; *Corynebacterium*, $P = 0.007$). Notably, opportunistic pathogens (*Brevibacillus*, $P = 0.002$) and inflammation-linked genera (*Roseburia*, $P = 0.037$) were reduced. These findings highlight Astragalus-induced remodeling of gut microbiota, potentially mediating systemic anti-inflammatory effects via the gut-mammary axis in SCBM cows.

3.8 Identification of serum characteristic metabolites and analysis of related metabolic pathways in cows with SCBM

Orthogonal partial least squares-discriminant analysis (OPLS-DA) was employed to investigate metabolic disparities. As shown in Figure 9A, score plots in both positive and negative ion modes revealed distinct clustering patterns among groups (NC, MOD, and AR_H), with tight intra-group sample aggregation, indicating significant intergroup differences ($P < 0.05$) and robust data reproducibility. Differential metabolites were screened using criteria of variable importance in projection (VIP) > 1.0 and $P < 0.05$, identifying 270 metabolites between MOD and NC groups and 198 metabolites between AR_H and MOD groups (Figures 9B, C). The OPLS-DA/PLS-DA models, validated by seven-fold cross-validation, highlighted metabolites critical for group classification via VIP analysis.

MOD vs. NC comparisons showed 24 significantly downregulated and 6 upregulated metabolites. In AR_H vs. MOD, 15 metabolites were downregulated and 15 upregulated. Notably, MOD exhibited marked reductions in *3, 7-dihydroxy-12-oxocholanoic acid*, *pelanin*, and *6-formylpterin* compared to NC ($P < 0.05$), while AR_H restored these metabolites to near-normal levels ($P < 0.05$). Pathway analysis identified five dysregulated pathways in MOD vs. NC: *linoleic acid metabolism* ($P = 0.003$), *choline metabolism in cancer* ($P = 0.007$), *retrograde endocannabinoid signaling* ($P = 0.012$), *cAMP signaling pathway* ($P = 0.018$), *and phospholipase D signaling* ($P = 0.023$). AR_H significantly restored these pathways (Figure 9D), suggesting its therapeutic role in modulating lipid-associated inflammation and cellular signaling cascades in SCBM.

3.9 Correlation analysis between serum metabolites and gastrointestinal microbiota

In this study, seven differential metabolites significantly associated with rumen microbiota ($R > 0.5$, $P < 0.05$) were identified (Figure 10A). Among them, betaine exhibited a positive correlation with *norank_f__norank_o__WCHB1-41*, cyclohexane with *Christensenellaceae_R-7_group*, and 3-guanidinopropanoate with *Rikenellaceae_RC9_gut_group*, suggesting that these metabolites may promote or be linked to the abundance or activity of these bacterial taxa. Conversely, PC (17:0/0:0) and indoxyl showed negative correlations with *Christensenellaceae_R-7_group*, lauryldiet with *norank_f__F082*, and betaine with *norank_f__Muribaculaceae*, indicating potential inhibitory effects on the growth or function of these microbial populations. These findings highlight the complex interactions between distinct metabolites and rumen microbiota, which may play a pivotal role in modulating host rumen microbial communities and providing a foundation for further exploration of underlying mechanisms.

Four differential metabolites displayed strong correlations with fecal microbiota ($R > 0.5$, $P < 0.05$) (Figure 10B). Specifically, PC (17:0/0:0) was positively correlated with *norank_f__norank_o__RF39*, whereas p-tolyl sulfate showed a negative correlation with *NK4A214_group*, taurohyocholate with *Bifidobacterium*, and lysoPC (16:1(9Z)/0:0) with *unclassified_c__Clostridia*. These results suggest that these metabolites may influence the composition and activity of fecal microbiota, underscoring the potential role in regulating the fecal microbial dynamics.

3.10 Correlation analysis between gastrointestinal microbiota and SCC, milk yield, milk composition, and serum parameters

Spearman correlation analysis was performed to evaluate the associations between the relative abundance of gastrointestinal microbiota at the genus level and 18 metrics, including SCC, milk yield, milk composition, and serum parameters.

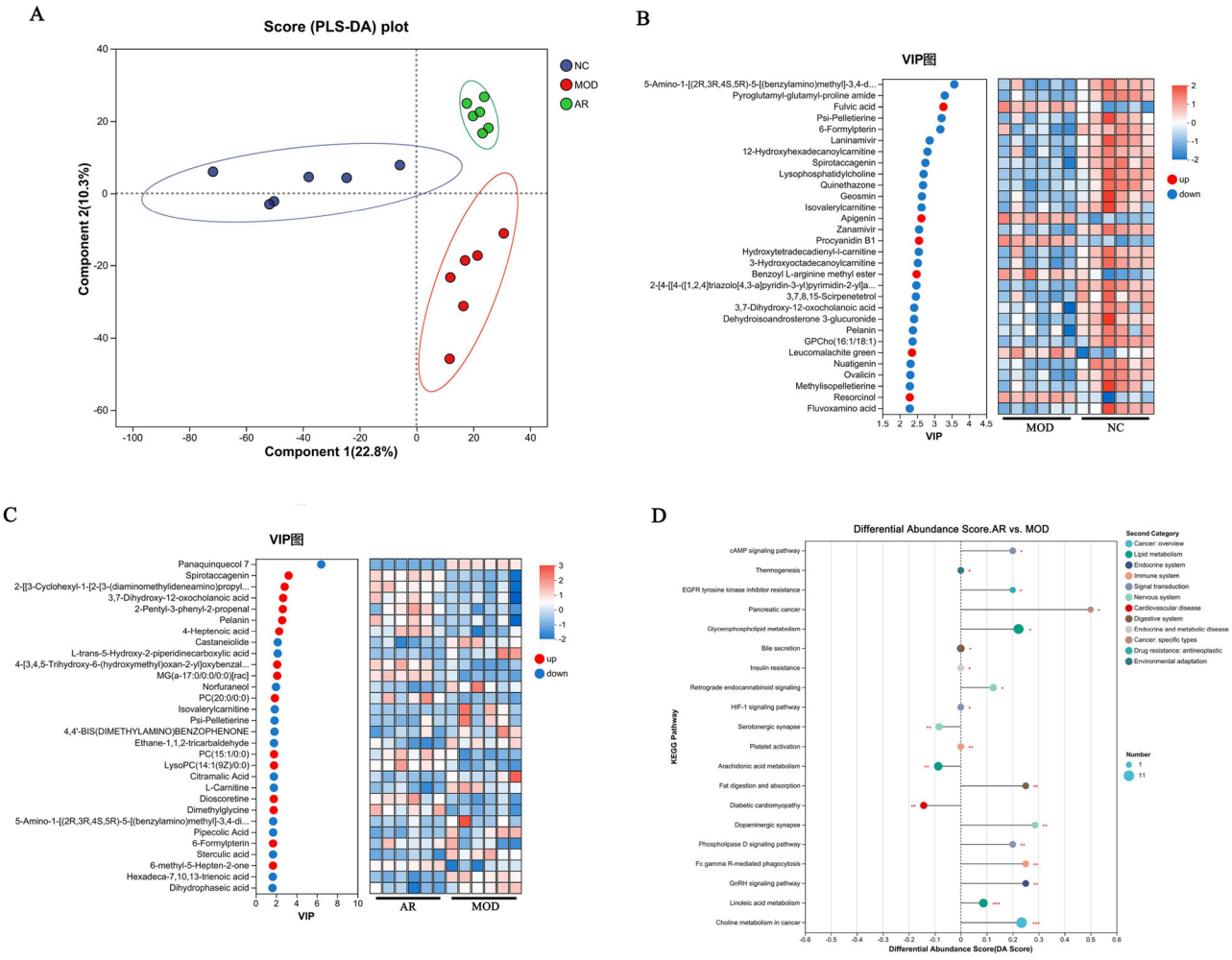

FIGURE 9
Effects of AR_H on the serum metabolites. **(A)** PLS-DA score plot; **(B)** heatmap of MOD vs. NC; **(C)** heatmap of AR vs. MOD; **(D)** KEGG pathway enrichment analysis.

As illustrated in Figure 11A, 29 OTUs displayed significant correlations with at least one metric. Notably, *Acetitomaculum*, *Ruminococcus_gauvreauii_group*, *Pseudobutyrivibrio*, *norank_f__norank_o__RF39*, and *Monoglobus* in the rumen showed significant positive correlations with SCC, whereas *UCG-014* exhibited a negative correlation with SCC ($P < 0.05$), suggesting its potential protective role. Conversely, *Pseudobutyrivibrio* and *Ruminococcus_gauvreauii_group* were negatively correlated with milk yield, indicating detrimental associations with lactation performance.

Key correlations with inflammatory markers were also observed: *Lachnospiraceae_NK4A136_group*, *Balautia*, *unclassified_f_Lachnospiraceae*, and *Dorea* displayed positive correlations with TNF-α, while *Balautia*, *NK4A214_group*, *Bacteroides*, and *unclassified_f_Oscillospirales* were positively correlated with IL-6 ($P < 0.05$), highlighting their involvement in inflammatory responses. Intriguingly, *Acetitomaculum* and *Ruminococcus_gauvreauii_group* showed positive correlations with IL-1β, LDH, and MPO—markers of inflammation and cellular damage—but negative correlations with SOD, lactose, IgG, and milk fat ($P < 0.05$), linking these genera to oxidative stress and milk quality deterioration. These findings reveal significant associations between specific rumen microbial taxa and critical clinical/biochemical parameters, identifying potential microbial targets for improving host health and productivity.

In the fecal microbiota (Figure 11B), *Eubacterium_ruminantium_group* was positively correlated with SCC, whereas *Rikenellaceae_RC9_gut_group*, *norank_f__norank_o__WCHB1-41*, *norank_f__F082*, and *Veillonellaceae_UCG-001* exhibited negative correlations with SCC ($P < 0.05$), implying potential anti-inflammatory properties. Notably, *norank_f__UGG-010*, *norank_f__norank_o__WCHB1-41*, and *Rikenellaceae_RC9_gut_group* demonstrated positive correlations with milk yield, highlighting their potential role in yield enhancement. *Norank_f__norank_o__RF39* and *Eubacterium_ruminantium_group* were positively correlated with LDH, linking them to tissue damage and inflammatory states. Additionally, genera such as *Eubacterium_nodatum_group*, *Eubacterium_hallii_group*, *norank_f__Eubacterium_coprostanoligenes_group*,

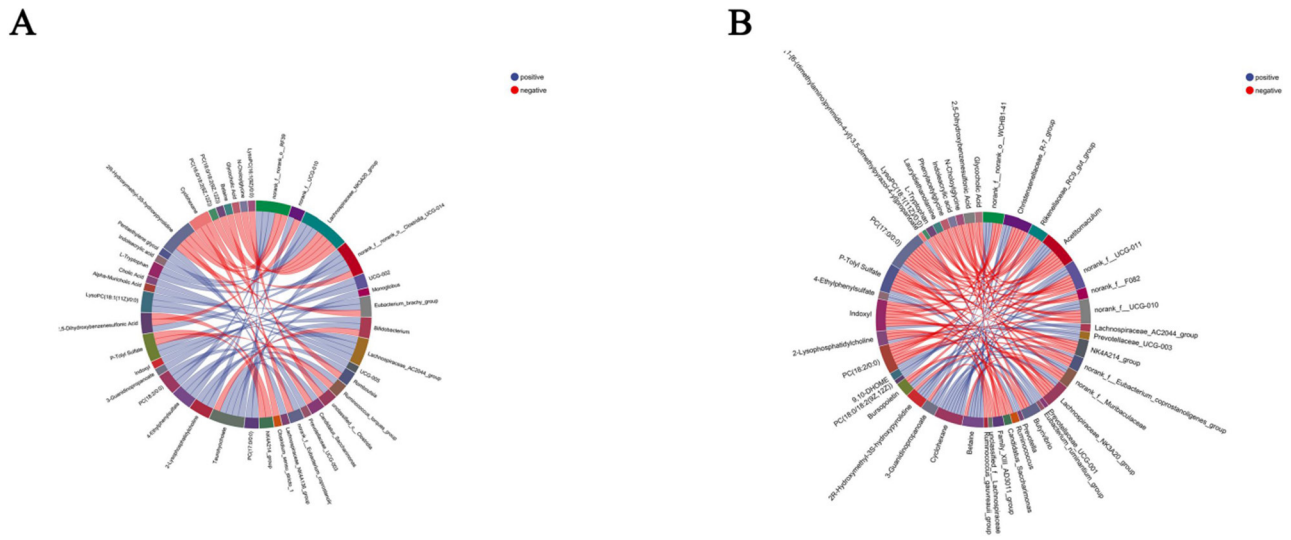

FIGURE 10
Correlation analysis results between serum differential metabolites and gastrointestinal microbiota. **(A)** Serum differential metabolites-rumen microbiota correlation; **(B)** serum differential metabolites-intestinal microbiota correlation. Red and blue lines indicate positive and negative correlations, respectively.

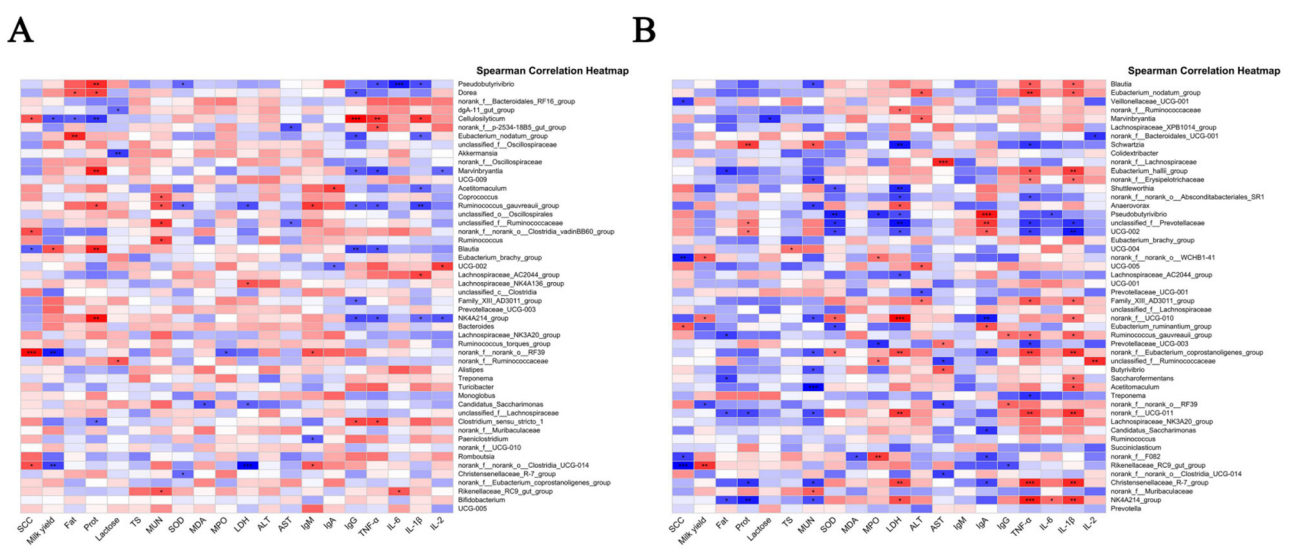

FIGURE 11
Correlation analysis results between gastrointestinal microbiota and clinical parameters. **(A)** Correlation between rumen microbiota and clinical parameters; **(B)** correlation between intestinal microbiota and clinical parameters. Red and blue colors indicate positive and negative correlations, respectively.

norank_f__UCG-011, *Christensenellaceae_R-7_group*, and *NK4A214_group* showed positive correlations with TNF-α ($P < 0.05$), emphasizing their participation in systemic inflammation.

The therapeutic efficacy of ARWD in SCBM might largely stem from its ability to modulate gastrointestinal microbiota, particularly by influencing microbial taxa associated with inflammation, milk production, and systemic health. These results underscore the pivotal role of gastrointestinal microbiota in both the pathophysiology and treatment of SCBM.

3.11 Correlation analysis between serum metabolites and SCC, milk yield, milk composition, and serum parameters

Correlation analysis between serum metabolites (AR_H vs. MOD) and clinical indicators, milk composition, and serum parameters (Figure 12) revealed significant changes in metabolite levels associated with SCC, serum parameters, and milk composition following ARWD intervention. Notably, serum *D-fructose* exhibited positive correlations with SCC, LDH,

and MDA, but negative correlations with milk yield, fat, and lactose ($P < 0.05$), suggesting its association with inflammation and impaired milk quality. Furthermore, metabolites such as *6-oxopiperidine-2-carboxylic acid*, *2, 3-dihydroxybenzoic acid*, *L-carnitine*, *decanedioic acid*, and *(3S, 5R, 6R, 7E)-3, 5, 6-trihydroxy-7-megastigmen-9-one* showed significant positive correlations with SCC, MDA, and MPO, but negative correlations with milk yield, fat, lactose, and IgG ($P < 0.05$), implicating their roles in inflammatory responses, oxidative stress, and immune dysfunction. Conversely, *PE (20:1/0:0)* demonstrated a negative correlation with TNF-α and IL-6 ($P < 0.05$), highlighting the potential anti-inflammatory properties.

These results indicate that AR_H effectively modulates serum metabolites, reduces SCC, alleviates inflammation and oxidative stress, and improves milk yield and immune function. Taken together, these results highlight *Astragali Radix* as a promising traditional herbal formulation for the treatment of SCBM in dairy cows.

4 Discussion

SCBM in dairy cows remains a critical health challenge requiring urgent resolution in modern livestock farming. With increasing antibiotic resistance and evolving veterinary drug regulations, there is a pressing need to develop greener and healthier alternatives (15). In this study, untargeted metabolomic was employed to analyze the bioactive components of ARWD and integrated serum metabolomics with 16S rRNA sequencing were used to elucidate the therapeutic mechanism on SCBM of ARWD.

To clarify the bioactive basis of ARWD in treating bovine mastitis, LC-MS/MS analysis identified nine active compounds, including *Astragalosides* III, VI, and IV, ononin, formononetin, and their derivatives. These compounds were found to exhibit anti-inflammatory, antioxidant, and immunomodulatory properties. Notably, *Astragaloside* III demonstrated significant anti-inflammatory activity by reducing inflammatory responses and accumulating in immune organs such as the thymus and spleen, highlighting its immunomodulatory potential (16). Furthermore, *Astragaloside polysaccharides* and *Astragaloside* IV markedly suppressed the expression of pro-inflammatory cytokines and apoptosis in lipopolysaccharide (LPS)-induced bovine mammary epithelial cell models, underscoring their pivotal role in mitigating mastitis (17). Other components, such as *ononin* and *formononetin*, also showed therapeutic promise. *Ononin* reduced ROS generation and inhibited pro-inflammatory factors, suggesting broad applications in anti-inflammatory and anticancer therapies (18). Similarly, *formononetin* alleviated LPS-induced mastitis symptoms by enhancing the integrity of the lactation barrier and suppressing AhR-Src signaling pathway activation (19). Additionally, bioactin A demonstrated robust anti-inflammatory and immune-enhancing properties, further supporting its development as a therapeutic agent for mastitis (20).

SCC serves as a critical biomarker for assessing udder health in dairy cows, where significant elevation in SCC levels typically indicates mastitis. The increase in SCC is primarily attributed to immune cell infiltration into mammary tissues, triggering inflammatory responses. Studies have shown that mastitis pathogenesis involves LPS and pathogenic microorganisms stimulating the release of pro-inflammatory cytokines such as IL-1β and TNF-α, leading to inflammatory damage in mammary tissues and marked increases in SCC (21, 22). Elevated SCC levels are often associated with impaired mammary barrier function, resulting in sustained pathogenic stimulation and exacerbated inflammation. Clinical studies further reveal significant differences in lactation performance between cows with varying SCC levels (23). In healthy cows, milk proteins predominantly comprise casein, whey proteins, and minor non-protein nitrogen components. During mastitis, inflammatory mediators disrupt mammary epithelial cell function and increase barrier permeability, causing an imbalance in protein composition and reduced total protein content. Notably, the proportion of casein declines significantly, while concentrations of whey proteins such as lactoferrin and lactoglobulin rise substantially. These shifts likely reflect the activation of mammary immune defenses, which enhance the secretion of whey proteins, particularly antimicrobial proteins, to combat infection (24, 25).

Mastitis-induced changes in osmotic gradients facilitate the leakage of plasma proteins such as albumin and fibrinogen into milk, further altering milk protein composition and potentially compromising dairy processing quality. Studies also indicate that cows with elevated SCC levels typically have lower milk protein content, which is associated with the metabolic burden of inflammation as well as physical damage and functional decline in mammary tissues (25).

The development of bovine mastitis is closely associated with the overexpression of pro-inflammatory cytokines, particularly IL-1β, IL-6, and TNF-α, which play pivotal roles in inflammatory cascades (26). IL-1β acts as a critical initiator of inflammatory responses by activating NF-κB and MAPK signaling pathways, thereby inducing the release of other pro-inflammatory cytokines and significantly enhancing neutrophil migration into mammary tissues, exacerbating tissue damage (27). Elevated IL-1β levels in milk from mastitic cows correlate positively with increased SCC (26). IL-6, a key mediator of acute-phase responses, enhances antimicrobial defenses by stimulating lactoferrin and C-reactive protein production. However, its role in increasing vascular permeability may also promote inflammatory dissemination (28). Prolonged IL-6 overexpression further impairs mammary barrier function and is strongly associated with reduced lactose secretion. TNF-α, another central regulator of pro-inflammatory responses, induces apoptosis and oxidative stress, aggravating mammary tissue lesions (29). Our findings demonstrate that ARWD significantly reduces IL-1β, IL-6, and TNF-α expression levels in milk from mastitic cows. These results suggest that ARWD alleviates mammary inflammation and tissue damage by disrupting cytokine-triggered inflammatory cascades. Consistent with this, Khan et al. (30) reported that certain natural plant-derived bioactive compounds regulate mastitis-associated cytokines. By suppressing the overexpression of pro-inflammatory cytokines, ARWD effectively mitigates mastitis symptoms, preserves mammary tissue integrity, and improves lactation performance in dairy cows.

The onset of bovine mastitis is accompanied by exacerbated oxidative stress, characterized by dysregulated levels of oxidative

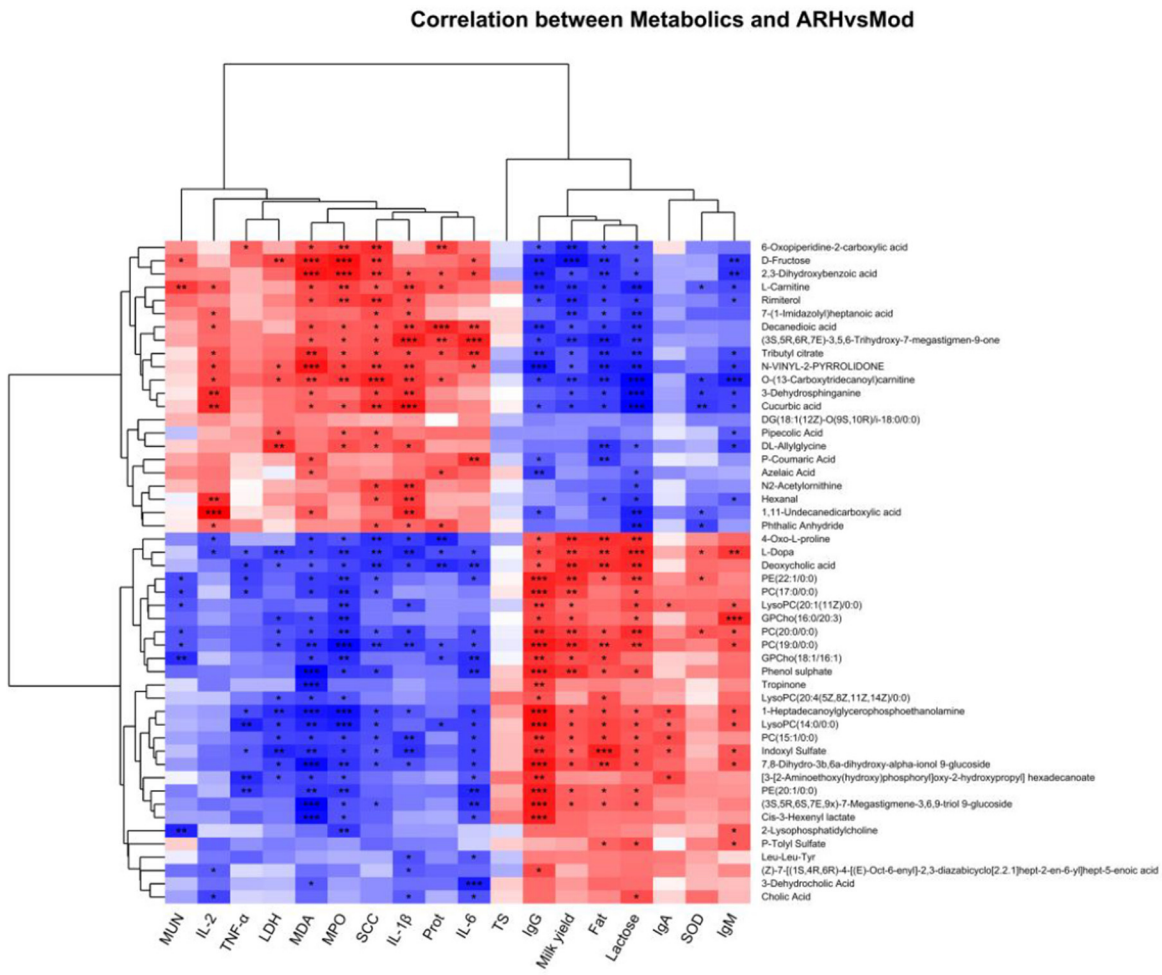

FIGURE 12
Correlation analysis results between serum metabolites and clinical parameters. Red and green colors indicate positive and negative correlations, respectively; *P* values are denoted as * <0.05, ** <0.01, *** <0.001.

biomarkers such as MPO, LDH, SOD, and MDA. MPO, a key oxidative enzyme released by neutrophils, reflects the intensity of inflammatory responses and neutrophil hyperactivation. Elevated MPO activity is recognized as a marker of inflammatory severity in mastitic cows (31, 32). LDH, an indicator of cellular damage, increases significantly during mastitis due to inflammation and necrosis in mammary tissues, signifying impaired tissue metabolism and compromised mammary barrier integrity (33). Concurrently, reduced SOD activity—a critical antioxidant enzyme counteracting oxidative stress—leads to free radical accumulation, aggravating tissue damage. MDA, a lipid peroxidation byproduct, exhibits elevated concentrations indicative of oxidative membrane damage (34). Our results demonstrate that ARWD significantly reduced MPO and LDH activities in mastitis models while elevating SOD levels and reducing MDA concentrations. These findings highlight ARWD's efficacy in mitigating oxidative stress-induced tissue damage, underscoring its potential as a therapeutic agent for bovine mastitis.

The pathogenesis of bovine mastitis is accompanied by immune system activation (35), with immunoglobulins IgM, IgG, and IgA playing critical roles in mammary immune defense. During mastitis, LPS translocation from the rumen to the bloodstream enhances pro-inflammatory cytokine release and elevates serum immunoglobulin levels (36). IgM, the primary antibody in the initial immune response, rapidly recognizes mastitis-associated pathogens and facilitates pathogen clearance by activating the complement system. IgG, the predominant antibody in bovine mammary immunity, provides protection by neutralizing pathogen toxins and enhancing phagocyte functionality. The marked increase in milk IgG levels during mastitis reflects sustained immune responses to mammary infections (28). Additionally, IgA, a key component of local mucosal immunity, prevents pathogen adhesion to mammary epithelial cells, thereby reducing tissue damage. Studies indicate that elevated IgA levels in bovine milk strengthen local immune barriers and enhance protective functions (28). In this study, ARWD significantly elevated serum IgM, IgG, and IgA levels in mastitic cows, indicating its dual role in augmenting systemic primary immune responses and suppressing inflammatory progression via improved local mammary immunity. These findings align with reports by

Khan et al. (30), who demonstrated that certain herbal components effectively upregulate immunoglobulin expression linked to bovine mammary immunity. Collectively, this underscores the protective effects and theoretical rationale for using traditional Chinese medicine in mastitis management.

The rumen microbiota plays a pivotal role in both the development and therapeutic management of bovine mastitis by modulating systemic immune functions during inflammatory responses (29, 37). Our study revealed significant shifts in microbial diversity within the rumen and intestines of mastitic cows, with ARWD intervention promoting a restorative trend in microbiota composition. Notably, key genera such as *Turicibacter, Cellulosilyticum, Brevibacillus, Roseburia,* and *Saccharofermentans* were implicated in these dynamics.

Turicibacter is a strictly anaerobic, Gram-positive, rod-shaped bacterium typically abundant in the gut and rumen of healthy animals. It critically maintains microbial balance, supports host metabolic health, and regulates immune functions (38). *Cellulosilyticum* is a cellulolytic genus essential for degrading plant fibers in the rumen, producing volatile fatty acids (VFAs) vital for energy metabolism. Mastitis-induced reductions in its abundance impair energy homeostasis and compromise immune defenses (39). *Brevibacillus* is a Gram-positive, spore-forming, thermotolerant genus within the Bacillaceae family, exhibiting aerobic/facultative anaerobic traits. Brevibacillus strains demonstrate resistance to 67% of tested antibiotics, suggesting potential interference with mastitis treatment (40). *Roseburia* is a strictly anaerobic, Gram-positive genus prevalent in mammalian intestines. Zhao et al. (41) reported that citrus flavonoid extracts reduce its abundance, improving inflammatory and immune-metabolic functions in cows. *Saccharofermentans* is an acid-producing bacterium critical for mammary barrier integrity. Its depletion correlates with metabolic dysregulation and reduced milk protein levels in lactating cows (42). Our findings demonstrate that ARWD significantly restored the abundance of beneficial rumen microbiota, particularly *Turicibacter* and *Cellulosilyticum*. These results suggest that ARWD alleviates mastitis by rebalancing rumen microbiota and enhancing metabolic functions, thereby mitigating inflammation and supporting mammary health.

The onset of bovine mastitis is frequently accompanied by significant gut microbiota disruption, which not only alters microbial diversity but also directly impacts host immunometabolic and inflammatory responses. Our study identified marked changes in the abundance of *Roseburia*, *Treponema*, *Selenomonas*, *Prevotellaceae_UCG-004*, *Corynebacterium*, *Staphylococcus*, *Microbacterium*, and *Eubacterium_nodatum_group* in the gut microbiota of mastitic cows. *Roseburia*, a primary producer of short-chain fatty acids (SCFAs) via butyrate metabolism, plays a pivotal role in maintaining intestinal barrier integrity and suppressing systemic inflammation. Its depletion in mastitic cows is strongly associated with exacerbated immune dysfunction (41). Conversely, *Treponema*, a Gram-negative spirochete linked to chronic inflammation and tissue damage, exhibited elevated abundance, potentially exacerbating mastitis through lipopolysaccharide (LPS)-mediated immune hyperactivation (43). Similarly, increased *Selenomonas* (a Gram-negative genus involved in metabolic regulation) abundance may disrupt metabolic homeostasis and inflammatory control, aggravating mammary tissue injury (44). *Prevotellaceae_UCG-004*, enriched in high-fiber diets, was modulated by dietary calcium propionate to improve energy metabolism and hypocalcemia (45). Pathogenic roles were observed for Corynebacterium (46) and *Staphylococcus/Microbacterium* (47) with Astragalus supplementation specifically inhibiting *Microbacterium* to exert anti-inflammatory effects. Notably, *Eubacterium_nodatum_group*, a Gram-positive anaerobic commensal linked to metabolic regulation, showed reduced abundance in *Astragalus*-treated buffalo with mastitis, suggesting its role in microbiota-driven therapeutic modulation (39). These findings underscore the potential of *Astragalus* to alleviate mastitis by restoring gut microbiota balance and targeting pathogenic taxa, highlighting its dual role in metabolic and immune regulation.

ARWD significantly increased the abundance of the gut microbiota genus *Roseburia* while reducing *Treponema* and *Selenomonas* levels, suggesting its ability to alleviate mastitis by restoring gut microbial equilibrium, suppressing pro-inflammatory bacteria, and improving systemic immune-metabolic homeostasis. These findings highlight ARWD potential to mitigate clinical manifestations of bovine mastitis.

Serum metabolomics identified four key differential metabolites in cows with SCBM: *spirotaccagenin*, *3, 7-dihydroxy-12-oxocholanoic acid*, *pelanin*, and *6-formylpterin*. These metabolites were linked to dysregulated pathways, including *linoleic acid metabolism*, *choline metabolism in cancer*, *retrograde endocannabinoid signaling*, *cAMP signaling*, and *phospholipase D signaling*, which collectively influence inflammatory responses, oxidative stress, and immune regulation. Spirotaccagenin is a steroidal compound hypothesized to exert anti-inflammatory and immunostimulatory effects via downstream steroidal glycosides, which modulate cell proliferation and antimicrobial activity (48, 49). 3,7-Dihydroxy-12-oxocholanoic acid is a bile acid derivative critical for lipid digestion and absorption, with potential roles in gut microbiota modulation and immune function (50). Pelanin is an anthocyanin derivative renowned for its antioxidant and anti-inflammatory properties, attenuating chronic inflammation via inhibition of NF-κB and STAT1/3 signaling pathways (51). 6-Formylpterin: Suppresses lipopolysaccharide (LPS)-induced nitric oxide (NO) production in macrophages, demonstrating anti-inflammatory potential (52). Pathway analysis revealed that linoleic acid metabolism—a dual modulator of pro- and anti-inflammatory responses through its role as a precursor for arachidonic acid—enhances bacterial clearance in macrophages, suggesting lipid-mediated immune defense (53). Similarly, the *phospholipase D* signaling pathway regulates cellular stress and inflammation during mastitis by modulating secondary messengers involved in proliferation and anti-apoptosis (54, 55). ARWD significantly elevated these metabolites and restored pathway activity, particularly in *linoleic acid* metabolism, thereby enhancing anti-inflammatory and antioxidant capacity. These findings elucidate ARWD molecular mechanisms in SCBM management, emphasizing its dual role in microbiota restoration and metabolic reprogramming to combat inflammation and oxidative stress.

5 Conclusion

ARWD effectively mitigates SCBM by modulating rumen-gut microbiota interactions and regulating linoleic acid metabolism and phospholipase D signaling. This intervention significantly reduced pro-inflammatory cytokines (IL-1β, TNF-α), enhanced immunoglobulins (IgM/IgG/IgA), and improved antioxidant capacity, achieving dual therapeutic benefits of lowered somatic cell counts and increased milk yield. These findings highlight ARWD's multi-target anti-inflammatory and antioxidant mechanisms, offering a sustainable alternative to antibiotics for mastitis management.

Data availability statement

The data presented in the study is deposited in the https://www.ncbi.nlm.nih.gov/ repository, accession number: SRP589200 and SRP589088.

Ethics statement

The animal study was approved by Animal Ethics Committee of Gansu Agricultural University (GSAU-Eth-VMC-2021-020). The study was conducted in accordance with the local legislation and institutional requirements.

Author contributions

JY: Data curation, Investigation, Methodology, Validation, Visualization, Writing – original draft, Writing – review & editing, Formal analysis. KZ: Data curation, Investigation, Methodology, Project administration, Validation, Writing – review & editing. TM: Methodology, Validation, Formal analysis, Software, Writing – review & editing. PJ: Project administration, Conceptualization, Funding acquisition, Resources, Supervision, Writing – review & editing. YW: Funding acquisition, Project administration, Resources, Supervision, Conceptualization, Writing – review & editing.

Funding

The author(s) declare that financial support was received for the research and/or publication of this article. This research was supported by the National Natural Science Foundation of China (grant number: U21A20262), the Science and Technology Plan of Gansu Province (24ZDNA001), 2025 Project for Outstanding Graduate Students in Science and Technology of Gansu Province (No. 25CXZX-76).

Acknowledgments

We thank all authors for their contributions and support.

Conflict of interest

The authors declare that the research was conducted in the absence of any commercial or financial relationships that could be construed as a potential conflict of interest.

The author(s) declared that they were an editorial board member of Frontiers, at the time of submission. This had no impact on the peer review process and the final decision.

Generative AI statement

The author(s) declare that no Gen AI was used in the creation of this manuscript.

Publisher's note

References

1. Pakrashi A, Ryan C, Gueret C, Berry DP, Corcoran M, Keane MT, et al. Early detection of subclinical mastitis in lactating dairy cows using cow-level features. *J Dairy Sci.* (2023) 106:4978–90. doi: 10.3168/jds.2022-22803

2. Cavero D, Tölle KH, Rave G, Buxadé C, Krieter J. Analysing serial data for mastitis detection by means of local regression. *Livest Sci.* (2007) 110:101–10. doi: 10.1016/j.livsci.2006.10.006

3. Sindhu S, Saini T, Rawat HK, Chahar M, Grover A, Ahmad S, et al. Beyond conventional antibiotics approaches: global perspectives on alternative therapeutics including herbal prevention, and proactive management strategies in bovine mastitis. *Microb Pathog.* (2024) 196:106989. doi: 10.1016/j.micpath.2024.106989

4. Bittante G, Amalfitano N, Bergamaschi M, Patel N, Haddi ML, Benabid H, et al. Composition and aptitude for cheese-making of milk from cows, buffaloes, goats, sheep, dromedary camels, and donkeys. *J Dairy Sci.* (2022) 105:2132–52. doi: 10.3168/jds.2021-20961

5. Belkaid Y, Harrison OJ. Homeostatic immunity and the microbiota. *Immunity.* (2017) 46:562–76. doi: 10.1016/j.immuni.2017.04.008

6. Wiertsema SP, van Bergenhenegouwen J, Garssen J, Knippels LMJ. The interplay between the gut microbiome and the immune system in the context of infectious diseases throughout life and the role of nutrition in optimizing treatment strategies. *Nutrients.* (2021) 13:886. doi: 10.3390/nu13030886

7. Derakhshani H, Fehr KB, Sepehri S, Francoz D, De Buck J, Barkema HW, et al. Invited review: Microbiota of the bovine udder: contributing factors and potential implications for udder health and mastitis susceptibility. *J Dairy Sci.* (2018) 101:10605–25. doi: 10.3168/jds.2018-14860

8. Silva YP, Bernardi A, Frozza RL. The role of short-chain fatty acids from gut microbiota in gut-brain communication. *Front Endocrinol.* (2020) 11:25. doi: 10.3389/fendo.2020.00025

9. Che Y, Li L, Kong M, Geng Y, Wang D, Li B, et al. Dietary supplementation of Astragalus flavonoids regulates intestinal immunology and the gut microbiota to

improve growth performance and intestinal health in weaned piglets. *Front Immunol.* (2024) 15:1459342. doi: 10.3389/fimmu.2024.1459342

10. Li CX, Liu Y, Zhang YZ, Li JC, Lai J. Astragalus polysaccharide: a review of its immunomodulatory effect. *Arch Pharm Res.* (2022) 45:367–89. doi: 10.1007/s12272-022-01393-3

11. Kim J, Zhang S, Zhu Y, Wang R, Wang J. Amelioration of colitis progression by ginseng-derived exosome-like nanoparticles through suppression of inflammatory cytokines. *J Ginseng Res.* (2023) 47:627–37. doi: 10.1016/j.jgr.2023.01.004

12. Tian S, Zheng N, Zu X, Wu G, Zhong J, Zhang J, et al. Integrated hepatic single-cell RNA sequencing and untargeted metabolomics reveals the immune and metabolic modulation of Qing-Fei-Pai-Du decoction in mice with coronavirus-induced pneumonia. *Phytomedicine.* (2022) 97:153922. doi: 10.1016/j.phymed.2021.153922

13. Ma C, Sun Z, Zeng B, Huang S, Zhao J, Zhang Y, et al. Cow-to-mouse fecal transplantations suggest intestinal microbiome as one cause of mastitis. *Microbiome.* (2018) 6:200. doi: 10.1186/s40168-018-0578-1

14. Hiitiö H, Vakkamäki J, Simojoki H, Autio T, Junnila J, Pelkonen S, et al. Prevalence of subclinical mastitis in Finnish dairy cows: changes during recent decades and impact of cow and herd factors. *Acta Vet Scand.* (2017) 59:22. doi: 10.1186/s13028-017-0288-x

15. Cheng WN, Han SG. Bovine mastitis: risk factors, therapeutic strategies, and alternative treatments - a review. *Asian-Australas J Anim Sci.* (2020) 33:1699–713. doi: 10.5713/ajas.20.0156

16. Liu XH, Guo L, Yang YL, Hu F, Chen XY, Feng SL. Development and validation of a rapid and simple UPLC-ESI-MS method for pharmacokinetics and tissue distribution of Astragaloside III in rats. *J Chromatogr Sci.* (2016) 54:811–8. doi: 10.1093/chromsci/bmw021

17. Jiaqi F, Fang J, Yusi L, Xuezhang Z. Effects of astragalus polysaccharide and astragaloside IV on lipopolysaccharides-induced inflammation of bovine mammary epithelial cells. *J South China Agric Univ.* (2022) 43:16–28. doi: 10.7671/j.issn.1001-411X.202106034

18. Bhuia MS, Aktar MA, Chowdhury R, Ferdous J, Rahman MA, Hasan MSA, et al. Therapeutic potentials of ononin with mechanistic insights: a comprehensive review. *Food Biosci.* (2023) 56:103302. doi: 10.1016/j.fbio.2023.103302

19. Xiang K, Shen P, Gao Z, Liu Z, Hu X, Liu B, et al. Formononetin protects LPS-induced mastitis through suppressing inflammation and enhancing blood-milk barrier integrity via AhR-induced Src inactivation. *Front Immunol.* (2022) 13. doi: 10.3389/fimmu.2022.814319

20. Yuan Z, Li F, Zhang W, Wei Y, Hua Y. Exploring the potential role of Sophora alopecuroides L. in inflammation of bovine mammary epithelial cells induced by lipoteichoic acid based on network pharmacology and experimental validation. *Comb Chem High Throughput Screen.* (2024). doi: 10.2174/0113862073313036240829070704

21. Li K, Zhang L, Xue J, Yang X, Dong X, Sha L, et al. Dietary inulin alleviates diverse stages of type 2 diabetes mellitus via anti-inflammation and modulating gut microbiota in db/db mice. *Food Funct.* (2019) 10:1915–27. doi: 10.1039/C8FO02265H

22. Zhao XH, Gong JM, Zhou S, Liu CJ, Qu MR. The effect of starch, inulin, and degradable protein on ruminal fermentation and microbial growth in rumen simulation technique. *Ital J Anim Sci.* (2016) 13:3123. doi: 10.4081/ijas.2014.3121

23. Schepers AJ, Lam TJ, Schukken YH, Wilmink JB, Hanekamp WJ. Estimation of variance components for somatic cell counts to determine thresholds for uninfected quarters. *J Dairy Sci.* (1997) 80:1833–40. doi: 10.3168/jds.S0022-0302(97)76118-6

24. Ma C, Zhao J, Xi X, Ding J, Wang H, Zhang H, et al. Bovine mastitis may be associated with the deprivation of gut Lactobacillus. *Benef Microbes.* (2016) 7:95–102. doi: 10.3920/BM2015.0048

25. Vojinovic D, Radjabzadeh D, Kurilshikov A, Amin N, Wijmenga C, Franke L, et al. Relationship between gut microbiota and circulating metabolites in population-based cohorts. *Nat Commun.* (2019) 10:5813. doi: 10.1038/s41467-019-13721-1

26. Bannerman DD, Paape MJ, Lee JW, Zhao X, Hope JC, Rainard P. Escherichia coli and Staphylococcus aureus elicit differential innate immune responses following intramammary infection. *Clin Diagn Lab Immunol.* (2004) 11:463–72. doi: 10.1128/CDLI.11.3.463-472.2004

27. He X, Wei Z, Zhou E, Chen L, Kou J, Wang J, et al. Baicalein attenuates inflammatory responses by suppressing TLR4 mediated NF-κB and MAPK signaling pathways in LPS-induced mastitis in mice. *Int Immunopharmacol.* (2015) 28:470–6. doi: 10.1016/j.intimp.2015.07.012

28. Gabay C, Kushner I. Acute-phase proteins and other systemic responses to inflammation. *N Engl J Med.* (1999) 340:448–54. doi: 10.1056/NEJM199902113400607

29. Hu X, Li S, Mu R, Guo J, Zhao C, Cao Y, et al. The rumen microbiota contributes to the development of mastitis in dairy cows. *Microbiol Spectr.* (2022) 10:e0251221. doi: 10.1128/spectrum.02512-21

30. Khan W, Khan SA, Khan FA, Khan S, Ullah I, Shah A, et al. Therapeutic potential of natural products and antibiotics against bovine mastitis pathogen of cows and buffaloes. *Vet Med.* (2023) 68:271–80. doi: 10.17221/80/2022-VETMED

31. Raulo SM, Sorsa T, Tervahartiala T, Latvanen T, Pirilä E, Hirvonen J, et al. Increase in milk metalloproteinase activity and vascular permeability in bovine endotoxin-induced and naturally occurring Escherichia coli mastitis. *Vet Immunol Immunopathol.* (2002) 85:137–45. doi: 10.1016/S0165-2427(01)00423-8

32. Liu Y, Jiang Y, Yang Y, Wang H, Ye J, Liu D, et al. Houttuynia essential oil and its self-microemulsion preparation protect against LPS-induced murine mastitis by restoring the blood-milk barrier and inhibiting inflammation. *Front Immunol.* (2022) 13:842189. doi: 10.3389/fimmu.2022.842189

33. Wall SK, Wellnitz O, Hernández-Castellano LE, Ahmadpour A, Bruckmaier RM. Supraphysiological oxytocin increases the transfer of immunoglobulins and other blood components to milk during lipopolysaccharide- and lipoteichoic acid-induced mastitis in dairy cows. *J Dairy Sci.* (2016) 99:9165–73. doi: 10.3168/jds.2016-11548

34. Özkan H, Keçeli HH, Kaya U, Dalkiran S, Yüksel M, Tek E, et al. Considering potential roles of selected MicroRNAs in evaluating subclinical mastitis and Milk quality in California mastitis test (+) and infected bovine milk. *Anim Sci J.* (2024) 95:e13959. doi: 10.1111/asj.13959

35. Sordillo LM, Streicher KL. Mammary gland immunity and mastitis susceptibility. *J Mammary Gland Biol Neoplasia.* (2002) 7:135–46. doi: 10.1023/A:1020347818725

36. Dong G, Liu S, Wu Y, Lei C, Zhou J, Zhang S. Diet-induced bacterial immunogens in the gastrointestinal tract of dairy cows: impacts on immunity and metabolism. *Acta Vet Scand.* (2011) 53:48. doi: 10.1186/1751-0147-53-48

37. Xu Q, Qiao Q, Gao Y, Hou J, Hu M, Du Y, et al. Gut microbiota and their role in health and metabolic disease of dairy cow. *Front Nutr.* (2021) 8:701511. doi: 10.3389/fnut.2021.701511

38. Tan YJ, Koh SP, Khoizirah S, Rozaihan M, Manthan J, Khirrol NAW, et al. Genomic mapping milk microbiota from healthy, sub-clinical and clinical mastitis of Jersey Friesian cattle in a Malaysian farm. *Food Res.* (2023) 56:103302. doi: 10.26656/fr.2017.6(S4).006

39. Chen X, An M, Zhang W, Li K, Kulyar MF, Duan K, et al. Integrated bacteria-fungi diversity analysis reveals the gut microbial changes in buffalo with mastitis. *Front Vet Sci.* (2022) 9:918541. doi: 10.3389/fvets.2022.918541

40. Gutiérrez-Chávez AJ, Martínez-Ortega EA, Valencia-Posadas M, León-Galván MF, de la Fuente-Salcido NM, Bideshi DK, et al. Potential use of Bacillus thuringiensis bacteriocins to control antibiotic-resistant bacteria associated with mastitis in dairy goats. *Folia Microbiol.* (2016) 61:11–9. doi: 10.1007/s12223-015-0404-0

41. Zhao Y, Yu S, Li L, Zhao H, Li Y, Jiang L, et al. Feeding citrus flavonoid extracts decreases bacterial endotoxin and systemic inflammation and improves immunometabolic status by modulating hindgut microbiome and metabolome in lactating dairy cows. *Anim Nutr.* (2023) 13:386–400. doi: 10.1016/j.aninu.2023.03.007

42. Li M, Zhong H, Li M, Zheng N, Wang J, Zhao S. Contribution of ruminal bacteriome to the individual variation of nitrogen utilization efficiency of dairy cows. *Front Microbiol.* (2022) 13:815225. doi: 10.3389/fmicb.2022.815225

43. Jin W, Xue C, Liu J, Yin Y, Zhu W, Mao S. Effects of disodium fumarate on in vitro rumen fermentation, the production of lipopolysaccharide and biogenic amines, and the rumen bacterial community. *Curr Microbiol.* (2017) 74:1337–42. doi: 10.1007/s00284-017-1322-y

44. Xie T, Kong F, Wang W, Wang Y, Yang H, Cao Z, et al. In vitro and in vivo studies of soybean peptides on milk production, rumen fermentation, ruminal bacterial community, and blood parameters in lactating dairy cows. *Front Vet Sci.* (2022) 9:911958. doi: 10.3389/fvets.2022.911958

45. Zhang F, Zhao Y, Wang Y, Wang H, Nan X, Guo Y, et al. Dietary supplementation with calcium propionate could beneficially alter rectal microbial composition of early lactation dairy cows. *Front Vet Sci.* (2022) 9:940216. doi: 10.3389/fvets.2022.940216

46. Johnstone KJ, Robson J, Cherian SG, Wan Sai Cheong J, Kerr K, Bligh JF. Cystic neutrophilic granulomatous mastitis associated with Corynebacterium including Corynebacterium kroppenstedtii. *Pathology.* (2017) 49:405–12. doi: 10.1016/j.pathol.2017.01.006

47. Gryaznova MV, Syromyatnikov MY, Dvoretskaya YD, Solodskikh SA, Klimov NT, Mikhalev VI, et al. Microbiota of cow's milk with udder pathologies. *Microorganisms.* (2021) 9:1974. doi: 10.3390/microorganisms9091974

48. Nguyen DH, Bruguière A, Miyamoto T, Dias AMM, Bellaye P-S, Collin B, et al. Steroidal glycosides from Yucca rostrata and Dracaena braunii and their cytotoxic and antimicrobial evaluation. *Biochem Syst Ecol.* (2024) 113:104791. doi: 10.1016/j.bse.2024.104791

49. da Silva Leite JM, Barros Araújo CB, Alves LP, Bezerra Pereira MR, Guedes GG, de Carvalho Moreira LMC, et al. Trends and application of analytical methods for the identification and quantification of dexamethasone in drug delivery system. *Curr Pharm Anal.* (2023) 19:1–19. doi: 10.2174/1573412918666221004122046

50. Vítek L, Haluzík M. The role of bile acids in metabolic regulation. *J Endocrinol.* (2016) 228:R85–96. doi: 10.1530/JOE-15-0469

51. Lee HH, Lee SG, Shin JS, Lee HY, Yoon K, Ji YW, et al. p-coumaroyl anthocyanin mixture isolated from tuber epidermis of solanum tuberosum attenuates reactive oxygen species and pro-inflammatory mediators by suppressing NF-κB and STAT1/3 signaling in LPS-induced RAW2647 macrophages. *Biol Pharm Bull.* (2017) 40:1894–902. doi: 10.1248/bpb.b17-00362

52. Mori H, Arai T, Hirota K, Ishii H, Endo N, Makino K, et al. Effects of 6-formylpterin, a xanthine oxidase inhibitor and a superoxide scavenger, on production of nitric oxide in RAW 2647 macrophages. *Biochim Biophys Acta*. (2000) 1474:93–9. doi: 10.1016/S0304-4165(99)00210-X

53. Yan B, Fung K, Ye S, Lai PM, Wei YX, Sze KH, et al. Linoleic acid metabolism activation in macrophages promotes the clearing of intracellular Staphylococcus aureus. *Chem Sci*. (2022) 13:12445–60. doi: 10.1039/D2SC04307F

54. Nabih AM, Hussein HA, El-Wakeel SA, Abd El-Razik KA, Gomaa AM. Corynebacterium pseudotuberculosis mastitis in Egyptian dairy goats. *Vet World*. (2018) 11:1574–80. doi: 10.14202/vetworld.2018.1574-1580

55. Corl CM, Gandy JC, Sordillo LM. Platelet activating factor production and proinflammatory gene expression in endotoxin-challenged bovine mammary endothelial cells. *J Dairy Sci*. (2008) 91:3067–78. doi: 10.3168/jds.2008-1066

frontiers | Frontiers in Veterinary Science

TYPE Original Research
PUBLISHED 22 August 2025
DOI 10.3389/fvets.2025.1636663

OPEN ACCESS

EDITED BY
Dongan Cui,
Lanzhou University, China

REVIEWED BY
Yun Peng Fan,
Northwest A&F University, China
Quanxi Wang,
Fujian Agriculture and Forestry University, China

*CORRESPONDENCE
Shanshan Xie
✉ xiess@henau.edu.cn
Bo Tang
✉ hawktb@163.com
Shuaiyu Wang
✉ wangshuaiyu2016@cau.edu.cn

†These authors have contributed equally to this work and share first authorship

RECEIVED 28 May 2025
ACCEPTED 08 August 2025
PUBLISHED 22 August 2025

CITATION
Zhang Y, Tang R, Liu Y, Hao Z, Fan K, Xie S, Tang B and Wang S (2025) Immunoenhancing effects of Gynostemma Pentaphyllum Extract on mucosal immunity against porcine epidemic diarrhea virus.
Front. Vet. Sci. 12:1636663.
doi: 10.3389/fvets.2025.1636663

Immunoenhancing effects of Gynostemma Pentaphyllum Extract on mucosal immunity against porcine epidemic diarrhea virus

Yanxiang Zhang[1†], Ruihan Tang[1,2†], Yuanqing Liu[1], Zhihui Hao[1,3,4], Kai Fan[1], Shanshan Xie[5]*, Bo Tang[6]* and Shuaiyu Wang[1,3,4]*

[1]College of Veterinary Medicine, China Agricultural University, Beijing, China, [2]Agricultural College, Hubei Three Gorges Polytechnic, Yichang, China, [3]Innovation Center of Chinese Veterinary Medicine, China Agricultural University, Beijing, China, [4]Key Biology Laboratory of Chinese Veterinary Medicine, Ministry of Agriculture and Rural Affairs, Beijing, China, [5]College of Veterinary Medicine, Henan Agricultural University, Zhengzhou, China, [6]Beijing Biopharmaceutical Technology Center, Zhaofenghua Biotechnology Co., Ltd. (Nanjing), Beijing, China

Introduction: This study investigated the mucosal immunoadjuvant effects of Gynostemma Pentaphyllum Extract (Gynostemma P.E), the bioactive constituents of *Gynostemma pentaphyllum*, against porcine epidemic diarrhea virus (PEDV).
Methods: Twenty-four mice were randomly divided into four groups: a negative control group (intranasal administration of antigen only), a Gynostemma P.E-antigen mixture test group (intranasal administration), and two positive control groups (intramuscular injection of antigen or inactivated homemade vaccine, respectively). Fourteen days post booster immunization, spleen samples were collected to assess splenic lymphocyte proliferation activity. Intestinal segments were harvested for histological evaluation; duodenal intraepithelial lymphocytes (IELs) and IgA-positive cell numbers were quantified via H&E staining and immunohistochemistry (IHC). Serum and mucosal lavage fluid were analyzed for specific IgG and secretory IgA (sIgA) antibody levels.
Results: The results demonstrated that Gynostemma P.E significantly promoted immune organ development, enhanced splenic lymphocyte proliferation ($p < 0.05$), and elevated serum IgG and nasal mucosal sIgA antibody levels ($p < 0.05$).
Discussion: This study presents an innovative approach that integrates bioactive compounds from traditional Chinese medicine with intranasal mucosal immunization, offering new perspectives for combating gastrointestinal infections in veterinary medicine, and demonstrates that Gynostemma P.E significantly enhance PEDV-specific mucosal immunity in mice, providing a foundation for developing safer and more effective PEDV vaccines (and other veterinary vaccines), data supporting Gynostemma P.E as mucosal immunoadjuvants, and a theoretical framework for future clinical trials.

KEYWORDS

Gynostemma Pentaphyllum Extract, porcine epidemic diarrhea virus, mucosal immunity, antibody level, veterinary vaccine

1 Introduction

Porcine epidemic diarrhea (PED), caused by porcine epidemic diarrhea virus (PEDV), is an acute enteric disease affecting pigs of all ages (1). The disease is particularly devastating to neonatal piglets, with mortality rates reaching 80–100% (2). Although inactivated and live-attenuated vaccines are currently available, effective control remains challenging due to

PEDV's high mutation rate, frequent co-infections with other pathogens, and potential recombination with transmissible gastroenteritis virus (TGEV) (3). These factors contribute to its persistent threat to China's swine industry.

PEDV transmission occurs primarily through fecal-oral routes, indirect contact with contaminated fomites, and fecal-nasal exposure (4), all of which involve mucosal invasion. Therefore, enhancing mucosal immunity represents a critical strategy for infection prevention. While numerous mucosal adjuvants exist, few simultaneously meet the following essential criteria: (1) high safety profile, (2) capacity to induce potent immune responses with long-lasting memory, and (3) stability under varied storage conditions. Active components from traditional Chinese medicine have demonstrated significant immunomodulatory effects with excellent safety and stability profiles (5, 6), making them ideal candidates for immune modulation. Their prospects as adjuvants to enhance both the magnitude and durability of influenza vaccine responses are highly promising (7).

Gynostemma pentaphyllum is a traditional Chinese medicinal herb with a broad pharmacological profile. Previous studies have shown that both its total saponins and polysaccharides exert antiviral and immunopotentiating effects in animals, and evidence has indicated that gypenosides possess adjuvant activity in modulating cellular and humoral immunity (8–10). Recent work has also demonstrated the immune-enhancing effects of ginseng stem-leaf saponins against PEDV (11), yet no reports have described the use of intranasal gypenosides to boost intestinal mucosal immunity against PED.

Starting from the goal of "how to elevate intestinal mucosal immunity in swine herds," the present study selected Gynostemma P.E as the test agent. Mice were intranasally immunized with inactivated PEDV antigen combined with Gynostemma P.E, and the impact on mucosal immunity was assessed. Measurements of nasal wash IgA levels, splenic lymphocyte proliferation, and intestinal mucosal immune parameters preliminarily confirmed that intranasal co-delivery of Gynostemma P.E with antigen significantly enhanced PEDV-specific mucosal responses. These findings offer a reference for improving the efficacy of PED and other veterinary vaccines and provide an experimental basis for the clinical application of Gynostemma P.E.

2 Materials and methods

2.1 Instruments, drugs, and reagents

The following equipment was used: MJ-78A autoclave (Shanghai Shiduke Instrument Equipment Co., Ltd), BBXW-20 ice maker (Beijing Boxiang Xingwang Technology Co., Ltd), D3024R centrifuge (SCILOGEX), microplate reader and vortex mixer (BIO-RAD). Gynostemma P.E (Catalog No. E3343) was purchased from Selleck Chemicals (United States). PED inactivated antigen and inactivated vaccine (inactivated antigen mixed with ISA 201 adjuvant at a 9:11 volume ratio) were kindly provided by Zhaofenghua (Nanjing) Biological Technology Co., Ltd. Mouse PEDV-IgG and IgA ELISA kits were obtained from Shanghai Jianglai Biotechnology Co., Ltd. CCK8 kit and DAB chromogen were purchased from Beijing Solarbio Science & Technology Co., Ltd. Goat anti-mouse IgA polyclonal antibody and HRP-conjugated rabbit anti-goat IgG antibody were acquired from Abcam (UK).

2.2 Preparation of Gynostemma P.E and vaccine

The purchased Gynostemma P.E (powder form, derived from the whole plant of *Gynostemma pentaphyllum*) was homogenized with inactivated antigen in phosphate-buffered saline (PBS) to formulate a vaccine solution. This solution contained 1 μL of antigen and 100 μg of the botanical extract per mouse, with a final immunization volume of 10 μL per mouse, and was freshly prepared before each administration.

2.3 Experimental animals and group immunization

Twenty-four healthy male Balb/c mice (6–8 weeks old, 20 ± 2 g) were purchased from Vital River Laboratory Animal Technology Co., Ltd. [Production license: SYXK (Jing) 2019–0025]. After 7 days of acclimatization, mice were randomly divided into 4 groups ($n = 6$): Group A (negative control) received a mixture of normal saline and inactivated antigen via intranasal administration. Group B (Gynostemma P.E + Ag) received a mixture of Gynostemma P.E and inactivated antigen via intranasal administration. Group C (Positive Control 1) and Group D (Positive Control 2) also received PED inactivated antigen and PED inactivated vaccine (containing ISA 201 adjuvant) respectively via intramuscular injection. All mice were immunized through the above routes on days 1 and 21. Each immunization delivered 100 μL of inactivated antigen with $TCID_{50}$ of $10^{7.5}$ per mouse. Samples were collected 14 days after the second immunization.

2.4 Sample collection and processing

Given that preliminary experiments showed no significantly higher antibody levels in any test groups compared to the control group two weeks after the first immunization, and that the extract began to exert adjuvant effects two weeks after the second immunization, serum and mucosal lavage samples were collected two weeks after the second immunization in studies using Gynostemma P.E as an adjuvant.

Serum samples were obtained via retro-orbital plexus puncture or enucleation. Mice were sacrificed by cervical dislocation, and nasal lavage fluid was collected by injecting ice-cold PBS into the trachea (100 μL collected from nostrils). Duodenal mucosa was homogenized and centrifuged. Thymus and spleen were weighed, and intestinal segments (5 cm) were either fixed in 4% paraformaldehyde or flash-frozen in liquid nitrogen for storage at −80 °C.

2.5 Specific IgG and IgA antibody titers measurement

Serum IgG and mucosal IgA levels in nasal lavage/intestinal homogenate were determined by ELISA. Absorbance at 450 nm was measured using a microplate reader, with antibody concentrations calculated against standard curves.

2.6 Splenocyte proliferation assay

Splenocytes were isolated by mechanical dissociation, filtration and centrifugation. Cells (3 replicates/sample) were cultured with ConA in 96-well plates, and proliferation was assessed using CCK8 kit. Stimulation Index (SI) was calculated as: SI = OD ConA-treated/OD untreated (12).

2.7 Histological analysis

Intestinal segments were paraffin-embedded, sectioned, and stained with hematoxylin–eosin (HE). Intraepithelial lymphocytes (IELs) were counted under light microscopy (10 villi/sample, scoring system: 0 = none; 1 = 1–5; 2 = 6–10; 3 = 11–15; 4 = 16–20; 5 > 20 cells/villus). For immunohistochemistry (IHC), sections were dewaxed, incubated with HRP-conjugated secondary antibody, developed with DAB, and counterstained with hematoxylin.

2.8 Statistical analysis

All data are presented as mean ± SD. Statistical analysis was performed using Excel and GraphPad Prism. $p < 0.05$ was considered statistically significant, while $p < 0.01$ indicated highly significant differences.

3 Results

3.1 Increased serum IgG and nasal mucosal sIgA antibodies by gypenoside treatment

As shown in Figure 1 serum IgG antibody levelsSerum IgG antibody levels, the serum IgG antibody levels in mice immunized intranasally with Gynostemma P.E combined with antigen were significantly higher than those in the antigen-only intranasal negative control group ($p < 0.05$), but showed no significant difference compared with the positive control groups (antigen injection or vaccine injection). Analysis of nasal lavage fluid IgA levels (Figure 2) revealed that the intranasal immunization group with Gynostemma P.E and antigen exhibited significantly elevated IgA titers compared to both the negative control group and the antigen injection group ($p < 0.05$), while no statistically significant difference was observed versus the vaccine injection group. Furthermore, duodenal mucosal supernatant IgA assays (Figure 3) demonstrated that the gypenoside-antigen intranasal group achieved markedly higher IgA antibody levels than the antigen-only intranasal control and antigen injection groups ($p < 0.05$), with no significant difference compared to the vaccine injection group.

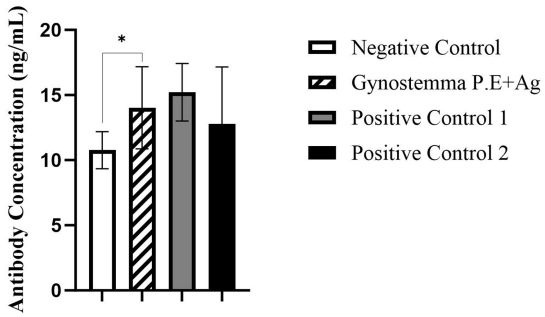

FIGURE 1
Serum IgG antibody levels. * indicates a statistically significant difference between groups ($p < 0.05$). Negative control: intranasal saline treatment; positive control 1: antigen injection group; positive control 2: vaccine injection group.

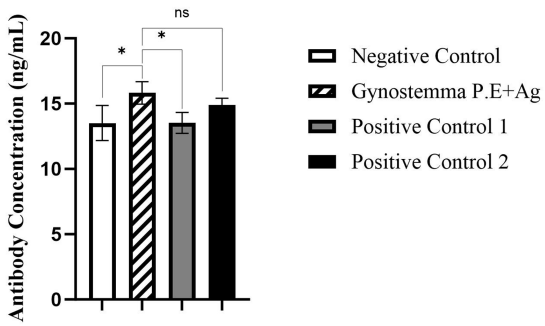

FIGURE 2
Detection of IgA antibody levels in nasal lavage fluid. * indicates a statistically significant difference between groups ($p < 0.05$); ns indicates no significant difference ($p > 0.05$).

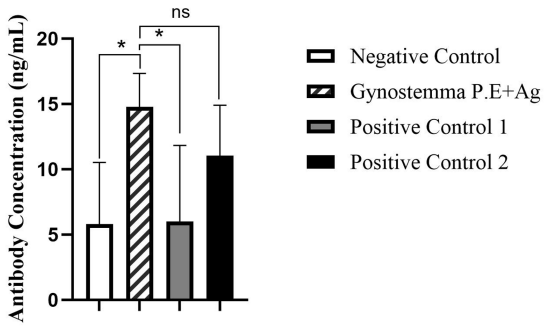

FIGURE 3
Measurement of IgA antibody levels in duodenal homogenate. * indicates a statistically significant difference between groups ($p < 0.05$); ns indicates no significant difference ($p > 0.05$).

3.2 Gynostemma P.E significantly enhanced splenic lymphocyte proliferation in mice

Two weeks after secondary immunization, spleens were aseptically harvested and lymphocyte proliferation was assessed by CCK-8 assay. The gypenoside plus intranasal antigen group exhibited a robust splenic lymphocyte proliferative response (Figure 4). Notably, the stimulation index (SI) in this group was significantly higher than that in both the antigen injection and vaccine injection positive control groups ($p < 0.01$). Moreover, compared with the intranasal antigen

negative control group, the gypenoside plus antigen group showed a significantly increased SI value (*$p < 0.05$).

3.3 Higher intraepithelial lymphocytes (IELs) within the duodenum epithelium after gypenoside stimulation

H&E staining revealed round, densely stained nuclei (Figure 5, black arrows indicate IELs). Ten well-oriented intestinal villi per group were randomly selected for IEL counting. As shown in Figure 6, the gypenoside plus intranasal antigen group had significantly higher IEL counts than the antigen injection group ($p < 0.05$), but no significant differences were observed compared with the intranasal antigen group or vaccine injection group.

3.4 Gypenoside increased IgA-positive cells in intestinal mucosa

IgA-positive cells (indicated by black arrows in Figure 7) were predominantly localized in the lamina propria of intestinal mucosa, with cytoplasmic brown staining. Semi-quantitative analysis using the MOD value (ratio of IOD to Area) revealed that the gypenoside plus intranasal

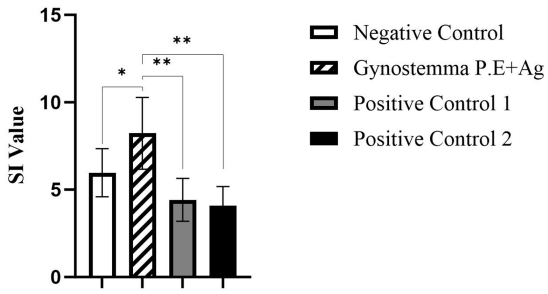

FIGURE 4
Effect of gypenoside on splenic lymphocyte stimulation index (SI). * indicates significant difference ($p < 0.05$); ** indicates highly significant difference ($p < 0.01$).

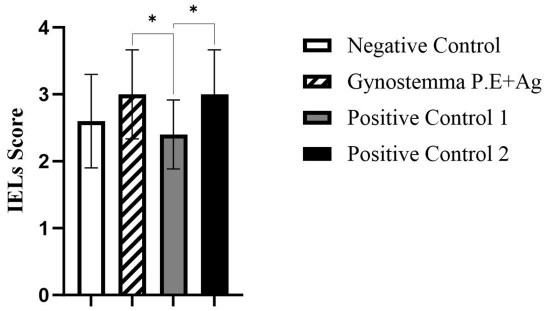

FIGURE 6
H&E staining analysis of IELs. * indicates a statistically significant difference between groups ($p < 0.05$).

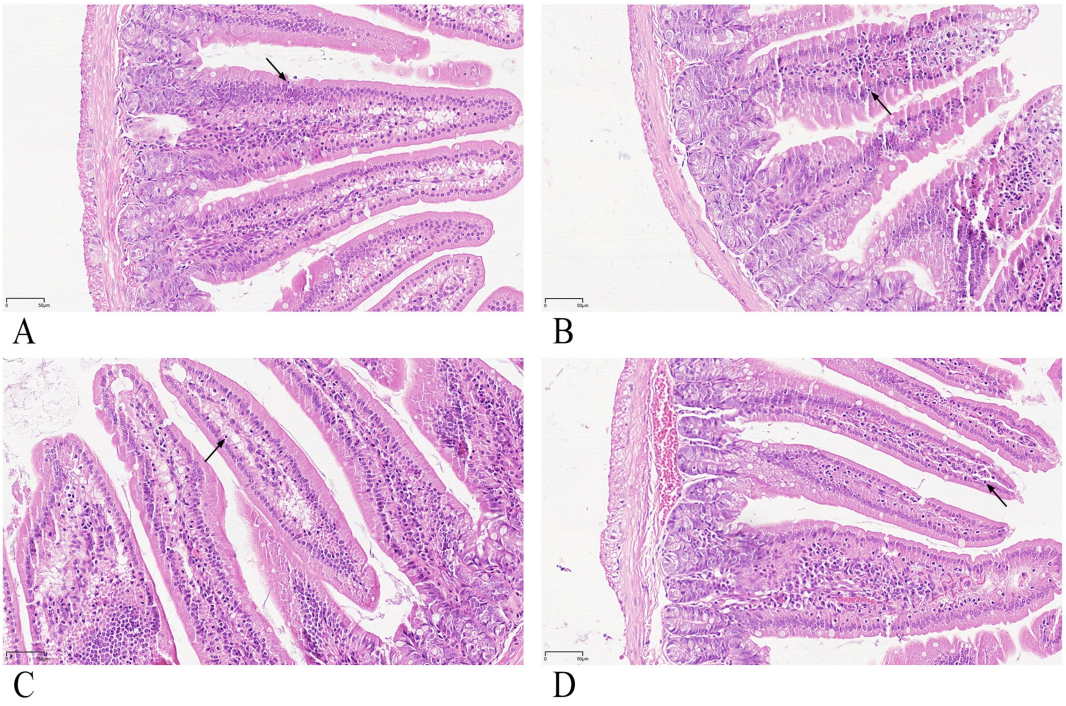

FIGURE 5
(A–D) Histological section of duodenum (H&E staining, 400×). **(A)** Intranasal antigen group (negative control). **(B)** Gynostemma P.E plus intranasal antigen group. **(C)** Antigen injection group (positive control 1). **(D)** Vaccine injection group (positive control 2). Black arrows indicate intraepithelial lymphocytes.

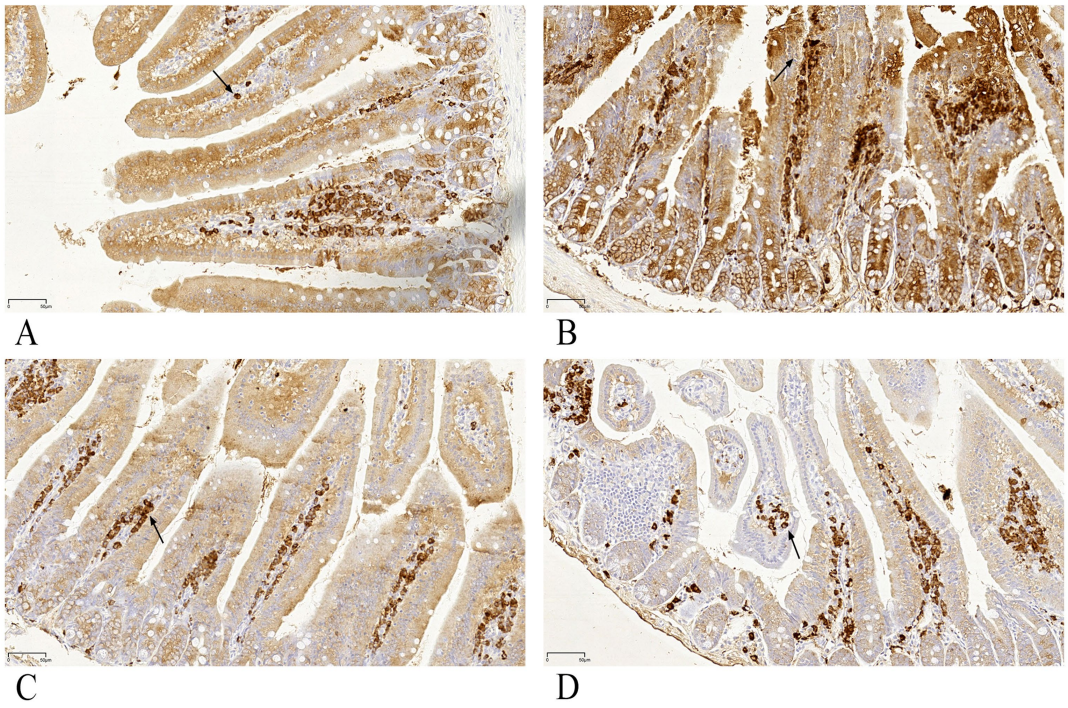

FIGURE 7
(A–D) Histological section of duodenum (immunohistochemical staining 400x). **(A)** Intranasal antigen group (negative control). **(B)** Gynostemma P.E plus intranasal antigen group. **(C)** Antigen injection group (positive control 1). **(D)** Vaccine injection group (positive control 2). Black arrows indicate intraepithelial lymphocytes.

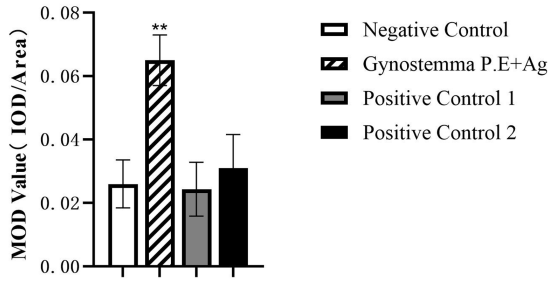

FIGURE 8
Immunohistochemical analysis of duodenum. ** indicates highly significant difference ($p < 0.01$).

antigen group exhibited a highly significant increase in IgA-positive cell numbers compared to the control group ($p < 0.01$, Figure 8).

4 Discussion

Porcine epidemic diarrhea (PED) is highly contagious and often breaks out successively in adjacent pig farms, causing catastrophic impacts on the region (13, 14). Studies report that mice inoculated with PEDV develop pathological changes including pulmonary inflammation and intestinal villous atrophy (15). Intramuscular injection of inactivated vaccine elevates antibody levels (16). Research demonstrated that intranasal inoculation of PEDV induces typical gastrointestinal symptoms in piglets. Compared to other routes, intranasal inoculation exhibits a longer incubation period, indicating viral transmission from nasal epithelium to the gastrointestinal tract (17). Current studies focus on antigen delivery mechanisms and intranasal immunization to enhance mucosal/systemic immunity (18, 19). Thus, intranasal inoculation serves as a reliable mucosal route for PEDV, further supporting airborne transmission. Additionally, as a key hub of mammalian mucosal immunity, intestinal epithelium acts as a real-time monitoring platform for systemic immunity, displaying distant infections (e.g., nasal mucosa) (20). Notably, PEDV primarily targets small intestinal epithelium. These collective findings provide the theoretical basis for this study's use of nasal mucosal inoculation to enhance intestinal mucosal immunity.

This study evaluates the immunoenhancing effects of Gynostemma P.E on mucosal immunity against PEDV as a vaccine adjuvant. The experimental design followed the principle of equivalent inactivated antigen inoculation, and compared the efficacy differences among various immunization routes, as well as the effects of the extract on immune cell proliferation, specific antibody production, and intestinal mucosal immune responses. Groups A (negative control) and B (Gynostemma P.E + Ag) both received intranasal immunization, enabling direct comparison to reveal the immunoenhancement effect of Gynostemma P.E. Groups C (positive control 1) and D (positive control 2) both received intramuscular injection (representing conventional inactivated vaccination), allowing comparison to confirm ISA201 adjuvant efficacy. Groups A and C both received inactivated antigen alone (without adjuvants), permitting comparison of the intrinsic effects of the two immunization routes. Therefore, comparison between Groups B and D directly evaluates the novel

GP-adjuvanted intranasal vaccine versus the current optimal conventional vaccination regimen (D Group). This design simultaneously validates both the adjuvant effect of Gynostemma P.E and the superiority of intranasal mucosal immunization.

In this study, the GP + antigen intranasal group showed significantly higher serum IgG levels than the negative control group ($p < 0.05$), higher nasal wash and duodenal homogenates IgA levels than all other groups except the vaccine injection group ($p < 0.05$). This indicates Gynostemma P.E can not only potentiate the immunogenicity of the intranasal route by activating mucosal immunity to promote local IgA secretion, but also significantly enhance systemic humoral immune responses and IgG production, thereby enhancing antigen-specific antibody responses. Although the precise mechanism requires further investigation, these findings provide important experimental evidence for the feasibility of needle-free immunization strategies.

The spleen as a critical immune organ contains abundant lymphoid tissue, including various immune cells. Upon initial antigen stimulation, antigen-presenting cells (APCs) present antigens and activate cellular and humoral immunity, while generating memory T cells and memory B cells. Upon re-exposure to the same antigen, these memory cells rapidly proliferate to achieve a swift immune response. Studies suggest that Gynostemma P.E enhance immune organ function by activating splenic lymphocyte proliferation or macrophage activation (21). As an early and easily quantifiable immune indicator, splenocyte proliferation exhibits high stability in cellular immunity evaluation and often correlates positively with final protective efficacy (22). To further understand the host's immune status, this study measured splenocyte proliferation activity (SI value). Results demonstrated that intranasal co-administration of Gynostemma P.E and antigen significantly increased splenocyte proliferative activity compared to all control groups ($p < 0.05$). These results suggest that Gynostemma P.E may promote immune organ development, enhance T lymphocyte activation, and activate APCs or directly stimulate T cells to enter the cell cycle and proliferate. This process establishes the foundation for subsequent specific immune responses, thereby enhancing systemic immune competence.

Intraepithelial lymphocytes (IELs) and lamina propria lymphocytes in the small intestine constitute the effector sites of the gut mucosal immune system. IELs play a crucial role in mediating immune tolerance and regulation, demonstrating significant potential in immune surveillance (23–26). HE staining showed the number of duodenal IELs in the Gynostemma P.E + Ag intranasal group differed significantly only from the antigen injection group, suggesting Gynostemma P.E may enhance intestinal mucosal barrier function. The minimal difference from the vaccine injection group was possibly due to the complex functional interplay of IELs and the influence of adjuvants in the vaccine. Further research on cytokine production may clarify the reasons behind IEL population changes. IHC detection revealed significantly increased IgA + cell density (MOD value) in the lamina propria ($p < 0.01$), confirming that Gynostemma P.E promotes local immune cell recruitment and antibody secretion—potentially through regulation of cytokine networks like IL-5 and IL-6.

In conclusion, this study preliminarily demonstrates that Gynostemma P.E significantly enhances mucosal immunity induced by PEDV inactivated antigen while achieving comparable effects with higher safety. The results further clarify Gynostemma P.E's immunoenhancing properties, providing a basis for its use in improving animal mucosal immunity, enhancing PED and other veterinary vaccines, and developing novel needle-free PED vaccine adjuvants. Future research is needed to focus on its active components and molecular mechanisms to facilitate clinical applications.

Data availability statement

The original contributions presented in the study are included in the article/supplementary material, further inquiries can be directed to the corresponding authors.

Ethics statement

The animal study was approved by Ethics Committee of China Agricultural University. The study was conducted in accordance with the local legislation and institutional requirements.

Author contributions

YZ: Conceptualization, Methodology, Writing – original draft, Data curation. RT: Methodology, Data curation, Writing – original draft, Conceptualization. YL: Visualization, Software, Writing – original draft. ZH: Investigation, Writing – review & editing, Supervision. KF: Writing – review & editing. SX: Writing – review & editing, Resources, Data curation, Funding acquisition. BT: Investigation, Writing – review & editing, Validation. SW: Supervision, Project administration, Funding acquisition, Conceptualization, Writing – review & editing.

Funding

The author(s) declare that financial support was received for the research and/or publication of this article. This work was funded by the National Key Research and Development Program of China (grant no. 2022YFD1801101-2) (China Agricultural University, SW) and the High-Level Talent Special Support Fund (no. 111/30501434) (Henan Agricultural University, SX).

Acknowledgments

We thank Zhaofenghua (Nanjing) Biological Technology Co., Ltd., for providing PED antigen and inactivated vaccine.

Conflict of interest

BT was employed by Zhaofenghua Biotechnology Co., Ltd. (Nanjing).

The remaining authors declare that the research was conducted in the absence of any commercial or financial relationships that could be construed as a potential conflict of interest.

Generative AI statement

The author(s) declare that no Gen AI was used in the creation of this manuscript.

Any alternative text (alt text) provided alongside figures in this article has been generated by Frontiers with the support of artificial intelligence and reasonable efforts have been made to ensure accuracy, including review by the authors wherever possible. If you identify any issues, please contact us.

Publisher's note

References

1. Zhao DH. Establishment and Application of an Indirect ELISA Method for Detection of IgA against Porcine Epidemic Diarrhea Virus. China (LZ): Chinese Academy of Agricultural Sciences (2020).

2. Yang LM, Wang JH, Xu MG, Wang H, Zhang XJ, Liu WJ, et al. Preparation and immunogenicity evaluation of an mRNA vaccine against porcine epidemic diarrhea. *Chin J Biotechnol*. (2023) 39:2624–33. doi: 10.13345/j.cjb.220853

3. Guo JH, Lai YN, Yang ZX, Song WB, Zhou JW, Zhuang L, et al. Coinfection and nonrandom recombination drive the evolution of swine enteric coronaviruses. *Emerg Microbes Infect*. (2024) 13:2332653. doi: 10.1080/22221751.2024.2332653

4. Jung K, Saif JL, Wang QH. Porcine epidemic diarrhea virus (PEDV): an update on etiology, transmission, pathogenesis, and prevention and control. *Virus Res*. (2020) 286:198045. doi: 10.1016/j.virusres.2020.198045

5. Zhang YZ, Chen YW, Zhou J, Wang X, Ma LR, Li JN, et al. Porcine epidemic diarrhea virus: an updated overview of virus epidemiology, virulence variation patterns and virus–host interactions. *Viruses*. (2022) 14:2434. doi: 10.3390/v14112434

6. Lin CM, Saif JL, Marthaler D, Wang QH. Evolution, antigenicity and pathogenicity of global porcine epidemic diarrhea virus strains. *Virus Res*. (2016) 226:20–39. doi: 10.1016/j.virusres.2016.05.023

7. Zhang Y, Li XY, Li HY, Wu XX, Dong YZ, Zhao J. Application and prospect of natural active ingredients of traditional Chinese medicine in immunological adjuvant for influenza vaccine. *Zhongguo Zhong Yao Za Zhi*. (2023) 48:5985–92. doi: 10.19540/j.cnki.cjcmm.20230823.602

8. Yang GH, Zhang JL, Wang SH, Wang J, Wang J, Zhu YH, et al. Gypenoside inhibits bovine viral diarrhea virus replicationby interfering with viral attachment and internalization and activating apoptosis of infected cells. *Viruses*. (2021) 13:1810. doi: 10.3390/v13091810

9. Li Q, Chen YM, Wang XY, Zhang YF, Cao HJ, Wang C, et al. Research progress on the chemical composition and pharmacological effects of Gynostemma. *J Liaoning Univ Tradit Chin Med*. (2025) 27:104–12. doi: 10.13194/j.issn.1673-842X.2025.03.019

10. Yu Y, Wang DQ, Abula SD, Hu YL, Zhao XJ, Huang Y, et al. The immunological adjuvant activity of gypenosides liposome against Newcastle disease vaccine. *Int J Biol Macromol*. (2013) 60:116–21. doi: 10.1016/j.ijbiomac.2013.05.024

11. Su F, Xu LH, Xue Y, Xu W, Li JX, Yu B, et al. Immune enhancement of nanoparticle-encapsulated ginseng stem-leaf Saponins on porcine epidemic diarrhea virus vaccine in mice. *Vaccine*. (2022) 10:1810. doi: 10.3390/vaccines10111810

12. Xu GP, He YF, Jiang P, Zhao XH, Chen CW. Evaluation of the immunizing effects of adjuvant of alcohol extract of *Polygonatum sibiricum* F. On mice. *J Anhui Agric Univ*. (2024) 51:604–9. doi: 10.13610/j.cnki.1672-352x.20240830.011

13. Guo JH, Fang LR, Ye X, Chen JY, Xu SE, Zhu XY, et al. Evolutionary and genotypic analyses of global porcine epidemic diarrhea virus strains. *Transbound Emerg Dis*. (2019) 66:111–8. doi: 10.1111/tbed.12991

14. Dong B, Dai AL, Li XH, Yang XY. The four of structural genes sequences of a porcine epidemic diarrhea virus from domestic piglet in Fujian, China. *Virol J*. (2020) 17:79. doi: 10.1186/s12985-020-01345-7

15. Feng ZH, Zhao H, Li ZL, Lin MH, Huang WL, Liu CC, et al. The infectivity and pathogenicity characteristics of a recombinant porcine epidemic diarrhea virus, CHFJFQ. *Viruses*. (2025) 17:401. doi: 10.3390/v17030401

16. Li XW, Zhang BZ, Zhang DS, Liu SD, Ren J. The construction of recombinant *Lactobacillus casei* vaccine of PEDV and its immune responses in mice. *BMC Vet Res*. (2021) 17:184. doi: 10.1186/s12917-021-02885-y

17. Li YC, Wu QX, Huang LL, Yuan C, Wang JL, Yang Q. An alternative pathway of enteric PEDV dissemination from nasal cavity to intestinal mucosa in swine. *Nat Commun*. (2018) 9:3811. doi: 10.1038/s41467-018-06056-w

18. Deng K, Huang ZQ, Jing B, Zhu L, Feng YM, Jiang Q, et al. Mucoadhesive chitosan-catechol as an efficient vaccine delivery system for intranasal immunization. *Int J Biol Macromol*. (2024) 273:133008. doi: 10.1016/j.ijbiomac.2024.133008

19. Hartwell LB, Melo BM, Xiao P, Lemnios AA, Li N, Chang HJ, et al. Intranasal vaccination with lipid-conjugated immunogens promotes antigen transmucosal uptake to drive mucosal and systemic immunity. *Sci Transl Med*. (2022) 14:eabn1413. doi: 10.1126/scitranslmed.abn1413

20. Allaire MJ, Crowley MS, Law TH, Chang YS, Ko JH, Vallance AB. The intestinal epithelium: central coordinator of mucosal immunity. *Trends Immunol*. (2018) 39:677–96. doi: 10.1016/j.it.2018.04.002

21. Zhu X, Tao LJ, Liu HY, Yang GQ. Effects of fermented feed on growth performance, immune organ indices, serum biochemical parameters, cecal odorous compound production, and the microbiota community in broilers. *Poult Sci*. (2023) 102:102629. doi: 10.1016/j.psj.2023.102629

22. Lee SY, Park SY, Park HJ. Immuno-enhancing effects of *Galium aparine* L. in cyclophosphamide-induced immunosuppressed animal models. *Nutrients*. (2024) 16:597. doi: 10.3390/nu16050597

23. Ma HT, Qiu Y, Yang H. Intestinal intraepithelial lymphocytes: maintainers of intestinal immune tolerance and regulators of intestinal immunity. *J Leukoc Biol*. (2021) 109:339–47. doi: 10.1002/JLB.3RU0220-111

24. Lockhart A, Mucida D, Bilate AM. Intraepithelial lymphocytes of the intestine. *Annu Rev Immunol*. (2024) 42:289–316. doi: 10.1146/annurev-immunol-090222-100246

25. Gui YY, Cheng H, Zhou JY, Xu H, Han JJ, Zhang DF. Development and function of natural TCR$^+$ CD8αα$^+$ intraepithelial lymphocytes. *Front Immunol*. (2022) 13:1059042. doi: 10.3389/fimmu.2022.1059042

26. Zhang HH, Hu YM, Liu DD, Liu Z, Xie NX, Liu SH, et al. The histone demethylase Kdm 6b regulates the maturation and cytotoxicity of TCRαβ$^+$ CD8αα$^+$ intestinal intraepithelial lymphocytes. *Cell Death Differ*. (2022) 29:1349–63. doi: 10.1038/s41418-021-00921-w

frontiers | Frontiers in Veterinary Science

TYPE Original Research
PUBLISHED 04 September 2025
DOI 10.3389/fvets.2025.1646665

OPEN ACCESS

EDITED BY
Baocheng Hao,
Chinese Academy of Agricultural Sciences, China

REVIEWED BY
Julio César Morales-Medina,
National Polytechnic Institute of Mexico (CINVESTAV), Mexico
Zhen Yang,
Chinese Academy of Agricultural Sciences, China
Jianhai Zhang,
Shanxi Agricultural University, China

*CORRESPONDENCE
Shusheng Tang
✉ tssfi@cau.edu.cn

RECEIVED 13 June 2025
ACCEPTED 18 August 2025
PUBLISHED 04 September 2025

CITATION
Li Y, Zhu L, He D, Fang L, Li Y and Tang S (2025) *Stevia rebaudiana* extract (main components: chlorogenic acid and its analogues) as a new safe feed additive: evaluation of acute toxicity, sub chronic toxicity, genotoxicity, and teratogenicity. *Front. Vet. Sci.* 12:1646665. doi: 10.3389/fvets.2025.1646665

Stevia rebaudiana extract (main components: chlorogenic acid and its analogues) as a new safe feed additive: evaluation of acute toxicity, sub chronic toxicity, genotoxicity, and teratogenicity

Yuting Li[1], Liping Zhu[2], Dongsheng He[2], Ling Fang[2], Yajing Li[2] and Shusheng Tang[1]*

[1]National Key Laboratory of Veterinary Public Health and Safety, College of Veterinary Medicine, China Agricultural University, Beijing, China, [2]Zhucheng Haotian Pharm Co., Ltd, Zhucheng, China

Introduction: *Stevia rebaudiana* extract (SREC), primarily composed of chlorogenic acid and its analogues, is a promising feed additive with potential benefits for livestock performance, gut health, and antioxidant capacity. However, its safety evaluation has not been comprehensively studied.
Methods: The safety of SREC was assessed through a series of tests, including acute oral toxicity in mice and rats, a 90-day subchronic toxicity test in rats, genotoxicity assays (Ames test, mouse bone marrow micronucleus test, and mouse sperm abnormality test), and teratogenicity evaluation in pregnant rats.
Results: The acute oral toxicity test indicated that the LD_{50} of SREC in mice and rats was greater than 5,000 mg/kg body weight. In the 90-day subchronic toxicity test, SREC was non-toxic at doses up to 50,000 mg/kg in feed. The Ames test showed no mutagenic effects on *Salmonella typhimurium strains* TA_{97}, TA_{98}, TA_{100}, and TA_{102}. No genotoxicity was observed in the mouse bone marrow micronucleus test or the sperm abnormality test, with no significant differences compared to controls ($p > 0.05$). Similarly, no teratogenic effects were found in pregnant rats, with normal embryonic development across treatment and control groups.
Discussion: SREC exhibited low toxicity in both acute and subchronic tests, and no evidence of genotoxicity or teratogenicity was observed. These findings suggest that SREC is safe as a potential feed additive and provide valuable reference data for its safety evaluation.

KEYWORDS

***Stevia rebaudiana* extract, oral acute toxicit, sub chronic toxicity, genotoxicity, teratogenicity**

Introduction

In recent years, the rapid development of the livestock (1) and poultry farming industry, alongside advances in feed technology, has led to the widespread use of antibiotics and growth promoters in commercial compound and complete feeds (2) to enhance growth performance and prevent diseases. However, the excessive use of antibiotics resulted in the emergence of

antibiotic-resistant bacteria, posing serious threats to both animal health and human health through the food chain, which in turn compromises the effectiveness of clinical antibiotics (3). Consequently, many countries and regions have restricted or banned the use of antibiotic growth promoters in animal husbandry, accelerating the shift toward natural, safe, and effective alternatives (4–6). The demand for plant-derived feed additives with functional properties continues to grow.

Stevia rebaudiana (7) is traditionally cultivated for its sweet-tasting compounds. In addition to the well-known steviosides, stevia leaves are also rich in chlorogenic acid (CGA) and its analogues (8), which are phenolic compounds with a wide range of biological activities, including antioxidant (9), anti-inflammatory (10), antimicrobial (11), antitumor (12), antihyperuricemic (13), immunoregulatory, and anti-fatigue (14) effects. Leveraging these properties, we developed a CGA-rich extract from stevia leaves, hereafter referred to as SREC, with a CGA content of approximately 43%. Unlike conventional stevia sweeteners, SREC is specifically formulated to enhance the functional benefits of CGA and its analogues. Given its demonstrated bioactivities, SREC represents a valuable alternative to antibiotic growth promoters in livestock and poultry farming, with the potential to improve animal health.

However, despite its promising bioactivity, toxicological studies on SREC are limited, particularly in the context of its use as a feed additive. Establishing the toxicological safety of SREC is a critical prerequisite for its approval and application in animal nutrition. Without sufficient toxicity data, the use of SREC will face regulatory and safety challenges, hindering its practical implementation. Therefore, the present study aims to conduct a comprehensive toxicological evaluation of SREC, including assessments of acute oral toxicity, sub-chronic toxicity, genotoxicity (Ames test, mouse bone marrow micronucleus test, and mouse sperm abnormality test), and teratogenicity. These findings will provide essential scientific evidence to support the safe and effective integration of SREC into livestock feed and promote its development as a natural alternative to antibiotic growth promoters.

Materials and methods

SREC (containing 43.3% total chlorogenic acid), was provided by Zhucheng Haotian Pharm Co., Ltd. Sodium azide (NaN_3, 99.9%) and dicofol (98.1%) were purchased from Sigma Aldrich, USA. 2-Aminofluorene (2-AF, 98%) was obtained from Alfa Aesar, UK. Formaldehyde (37–40%) was purchased from Tianjin Damao Chemical Reagent Factory, China. Potassium hydroxide was sourced from Shantou Xilong Chemical Factory Co., Ltd., China. Eosin and alizarin red were obtained from Beijing Chemical Reagent Company, China. Hematoxylin was purchased from Beijing JiuZhou Bolein Biotechnology Co., Ltd., China. Paraffin was obtained from Leica Biosystems.

The following chemicals were all purchased from Sinopharm Chemical Reagent Co., Ltd., Beijing, China: potassium dihydrogen phosphate, disodium hydrogen phosphate, methanol, glycerol, Giemsa stain, cedarwood oil, ammonium phosphate, citric acid, dipotassium phosphate, magnesium sulfate heptahydrate, sodium chloride, potassium chloride, sodium hydroxide, hydrochloric acid, sodium dihydrogen phosphate, D-biotin, L-histidine, glucose, glucose-6-phosphate, coenzyme II, agar powder, nutrient agar, nutrient broth, glacial acetic acid, glycerin, chloral hydrate, neutral gum, xylene, anhydrous ethanol, and aqueous eosin.

Blood biochemical test reagents, including serum albumin (Alb), alanine aminotransferase (ALT), aspartate aminotransferase (AST), blood urea nitrogen (BUN), total cholesterol (TCH), creatinine (Cr), glucose (Glu), and total protein (TP), were purchased from Shanghai Kehua Bio-engineering Co., Ltd.

Animals and care

SD rats and ICR mice (both female and male) of SPF grade were purchased from SBF (Beijing) Biotechnology Co., Ltd. The SD rats had body weights ranging from 180 to 220 g, and the ICR mice had body weights ranging from 18 to 22 g. All SD rats and ICR mice were housed for 7 days at the Animal Drug Safety Evaluation Center of the Ministry of Agriculture (Beijing) to acclimate to the standard laboratory conditions of room temperature (20–26 °C), relative humidity (50–65%), and artificial lighting (12-h light/dark cycle). During the entire experimental period, all SD rats and ICR mice were provided with sufficient standard rodent chow and water, and were allowed to eat and drink freely. All facilities were maintained to prevent contamination from exogenous factors, ensuring cleanliness throughout the feeding and experimental process. The experimental protocols involving animals were approved by the Institutional Animal Care and Use Committee of China Agricultural University, adhering to ethical standards for the humane treatment of animals (Animal Ethics Approval No. AW80804202-2-1).

Acute oral toxicity study

Our preliminary study indicated that a single oral dose of SREC at levels of 512, 1,600 and 5,000 mg/kg · body weight (bw) did not cause any toxic effects when administered to both rats and mice during the preliminary phase. Based on these results, a dose of 5,000 mg/kg·bw was selected for further testing, following the principles of the OECD Test Guideline 425 (15) (Up-and-Down Procedure), which allows for testing doses up to 5,000 mg/kg·bw to determine the toxicological limit dose (16, 17). For the formal test, 30 rats and 30 mice were used, with the rats and mice each randomly divided into 3 groups of 10 animals each (5 males and 5 females per group). The test substance was prepared as a suspension in 1% carboxymethyl cellulose sodium and administered orally. All animals were observed for general behavior, toxic symptoms, and mortality over a period of 7 days. If any deaths occurred after 4 days of administration, the observation period was extended to 14 days, and if necessary, up to 28 days. Necropsies were performed on any deceased animals, and the results were documented. At the end of the experiment, surviving animals underwent gross necropsy, with observations recorded for mortality rate, clinical symptoms, body weight changes, and general examination results throughout the observation period.

Sub chronic toxicity study

Eighty rats, aged 4–5 weeks and weighing 70–90 g, were randomly divided into four groups, each comprising 20 rats (10 males and 10 females). The rats were fed diets containing SREC at dosages of 0 mg/kg feed (negative control: NC), 2,000 mg/kg feed (low dose),

10,000 mg/kg feed (medium dose), and 50,000 mg/kg feed (high dose). The feed, sourced from Xiaoshuyoutai Biotechnology Co., Ltd., was thoroughly mixed with the SREC and pelleted. Over a period of 90 days, the health status of both control and experimental groups was monitored daily, assessing clinical signs of toxicity such as changes in behavior, physical appearance, and mortality (18). Food intake and body weight recorded every 5 days at a consistent time to minimize variability. On day 45 and 90, five male and five female rats from each group were randomly selected for hematological and biochemical analysis. Blood samples were collected via abdominal aorta under anesthesia, followed by immediate euthanasia for organ collection and then followed by weighing and dissection. Hematological parameters, including hemoglobin (HGB), red blood cells (RBC), white blood cells (WBC), platelets (PLT), hematocrit (HCT), eosinophils (EOS), basophils (BAS), neutrophils (NEU), monocytes (MO), and lymphocytes (LYM), were measured using a HEMAVET 950FS hematology analyzer (Drew Scientific). Biochemical parameters such as albumin (Alb), alanine aminotransferase (ALT), aspartate aminotransferase (AST), blood urea nitrogen (BUN), total cholesterol (TCH), creatinine (Cr), glucose (Gl), total protein (TP), and triglycerides (TG) were measured using the ELLIPSE automated biochemistry analyzer (Vital Scientific) with specific reagent kits. Fresh organs were collected for organ coefficient calculation and histopathological examination. Organs, including liver, spleen, lung, heart, kidney, and intestine, were stained with hematoxylin and eosin (HE) for pathological observation (19).

Salmonella reverse mutation (Ames) test

Following the method described by Hayashi et al. (20), a bacterial reverse mutation assay was performed to determine the genotoxic potential of SREC. Salmonella typhimurium strains (21) TA_{97}, TA_{98}, TA_{100}, and TA_{102}, obtained from the National Key Laboratory of Veterinary Public Health Safety, China Agricultural University, were used. Toxicity and solubility (precipitation) of SREC were assessed on all strains (22). Experimental setup: negative control (NC) and positive controls (PC): 2-aminoanthracene (2-AF, 10.0 μg/100 μL) for strains with S9-mix, dexon (50.0 μg/100 μL) for strains without S9-mix, and sodium azide (NaN_3, 1.5 μg/100 μL) for strain TA_{100} without S9-mix. Dose groups: 30 μg/plate, 6 μg/plate, 1.2 μg/plate, 0.24 μg/plate, 0.048 μg/plate, negative control (Dimethyl sulfoxide), and positive control. Test Procedure: 0.1 mL of test substance (dissolved in Dimethyl sulfoxide), 0.1 mL of overnight bacterial culture, and 0.5 mL of S9-mix or phosphate buffer were mixed with 2 mL of molten top agar and poured onto minimal glucose agar plates. Plates were incubated at 37 ± 2 °C for 48–72 h, and revertant colonies were counted. Mutagenicity was indicated by a doubling of revertant colonies compared to the control or a dose-dependent increase. Each treatment was done in duplicate.

Micronucleus test on bone marrow cells of mice

The *in vivo* genotoxic potential (23) of SREC was evaluated using the bone marrow micronucleus test in ICR mice, based on the method described by Hayashi et al. (24). A total of 80 ICR mice (40 males and 40 females) were divided into five groups of 16 mice each (8 males and 8 females per group). Three dose groups were established: 5,000, 2,500, and 1,250 mg/kg·bw. Preliminary toxicity tests showed that the highest dose of 5,000 mg/kg·bw did not induce any clinical signs of toxicity, aligning with the OECD Test Guideline 474 for genotoxicity testing which allows for such dosing if no severe toxicity is observed (25). The SREC was dissolved in a 1% CMC-Na solution and administered by oral gavage once daily for two consecutive days. The negative control group received 1% CMC-Na solution, while the positive control group received cyclophosphamide (40 mg/kg·bw) via intragastric administration 24 h before sacrifice. Observations were conducted at 0.5, 2.5, 5, and 24 h after the first dose, and at 0.5, 2.5, and 24 h after the second dose to detect any toxic effects and treatment-related discomfort. After the final treatment, the mice were euthanized using CO_2 gas.

Bone marrow preparations were made according to the method of Schmid (26). Micronuclei were identified as small round or oval bodies, approximately 1/5 to 1/20 the diameter of polychromatic erythrocytes (PCE). For each animal, the number of micronucleated cells in 1,000 PCEs was counted, and the ratio of PCE to normochromatic erythrocytes (NCE) was scored in every 200 erythrocytes to assess the toxic effects of the extract on bone marrow cells and hematopoiesis.

Sperm abnormality test in mice

Fifty 6-8-week-old rats were randomly divided into five groups. The experimental groups received SREC at 1,250, 2,500, and 5,000 mg/kg·bw (1 mL/100 g·bw). The positive control group (PC) received cyclophosphamide at 40 mg/kg·bw, and the negative control group (NC) received a 1% CMC-Na solution (1 mL/100 g·bw). All substances were administered by gavage once daily for 5 days, prepared as suspensions in a 1% CMC-Na solution. Sperm abnormality tests are conducted in accordance with standard methods (27). On the 35th day after the first treatment, five mice from each group were randomly selected. After euthanasia, both epididymides were isolated, placed in 2 mL of saline, and dissected. The saline containing sperm was aspirated, agitated, and allowed to stand for 5 min. The mixture was then filtered to remove tissue debris, and two drops of filtrate were placed on a slide for each mouse, creating four slides per mouse. The slides were air-dried, fixed with methanol for 10 min, stained with 2% eosin for 50 min, rinsed with water, and air-dried.

Teratogenicity test in rats: reproductive and embryotoxicity test design

A total of 120 rats, aged 7–8 weeks, were used in this study, including 80 females (weighing 220–250 g) and 40 males (weighing 250–300 g). The male-to-female ratio was set at 1:2 per cage. Female rats with sperm present in their vaginal smears were identified as newly "pregnant" rats (minimum of 12) and then these pregnant rats were randomly divided into four groups. SREC was prepared as a suspension in a 1% CMC-Na solution. The experimental groups received SREC at doses of 312.5 mg/kg·bw (low dose), 1,250 mg/kg·bw (medium dose), and 5,000 mg/kg·bw (high dose) by gavage (1 mL/100 g·bw). The negative control group (PC) received 1% CMC-Na solution (1 mL/100 g·bw). All pregnant rats were treated continuously for 10 days, from the 7th to the 16th day of gestation. On the 20th day of gestation, the rats were dissected to assess reproductive function indicators, embryonic development indicators, and fetal malformation indicators (28, 29).

Statistical analysis

Data were analyzed using GraphPad Prism version 9.0 (GraphPad Software, San Diego, CA, USA). All values are expressed as the mean

± standard deviation (SD). Statistical comparisons between groups were performed, with a p-value of < 0.05 considered statistically significant.

Results

Acute oral toxicity

During the 14-day observation period, no clinical symptoms or toxic deaths were observed in either male or female rats and mice treated with SREC. At the scheduled necropsy, no abnormal pathological findings were detected in the lungs, spleen, heart, liver, kidneys, or gastrointestinal tract of rats (both sexes) administered 5,000 mg/kg body weight of SREC.

Sub chronic toxicity study

Throughout the 90-day study, rats in all dose groups (2,000–50,000 mg/kg feed) and the negative control group exhibited no abnormal clinical signs, including changes in behavior, appearance, excreta, or skin. Feed intake, water consumption, and body weight gain remained stable, with no significant differences among groups (Figures 1, 2 and Supplementary Figure S1).

Hematological evaluations on Days 45 and 90 revealed no dose-related changes in parameters such as hemoglobin (HGB), red blood cell count (RBC), and white blood cell count (WBC); all values remained within normal physiological ranges (Table 1 and Supplementary Table S1). Similarly, biochemical parameters—including albumin (Alb), AST, total cholesterol (TCH), creatinine (Cr), glucose (Glu), triglycerides (TG), total protein (TP), and blood urea nitrogen (BUN)—were unaffected (Table 2). A statistically significant increase in ALT levels ($p < 0.05$) was observed in high-dose females; however, values remained within normal limits, suggesting no clinical relevance.

Organ coefficient measurements and histopathological analyses of major organs (heart, liver, kidneys, spleen, lungs, gastrointestinal tract, testes, and ovaries) showed no treatment-related abnormalities at either time point (Table 3, Figure 3, Supplementary Table S3, and Supplementary Figure S2). No signs of hemorrhage, edema, inflammation, or tissue damage were detected.

Taken together, these results indicate that dietary administration of SREC at doses up to 50,000 mg/kg feed for 90 days produced no observable subchronic toxicity in rats.

3. Salmonella reverse mutation (Ames) test

The mutagenic potential of SREC was evaluated using the Ames test, a widely accepted method for assessing genetic toxicity. Results from two independent experiments using *Salmonella typhimurium* strains TA_{97}, TA_{98}, TA_{100}, and TA_{102} are presented in Figure 4 and Supplementary Figure S3. As shown in Figures 4a,b, all strains exhibited normal bacterial lawn morphology. The positive controls were valid, producing a significant increase ($p < 0.05$) in revertant colonies—exceeding four times the number observed in the negative control.

SREC was tested at concentrations ranging from 0.048 to 30 μg/plate under both S9-activated and non-activated conditions. At all doses, the number of revertant colonies remained statistically comparable to that of the negative control group ($p > 0.05$), indicating no mutagenic effect.

Therefore, SREC was considered non-mutagenic under the conditions of the Ames test.

Micronucleus test on bone marrow cells of mice

The micronucleus assay was conducted to evaluate potential chromosomal damage. Results of the bone marrow micronucleus test in female and male mice are presented in Table 4. As shown, the frequency of micronucleated erythrocytes in the positive control group was significantly higher than in the negative control group ($p < 0.01$). No significant differences in micronucleus frequency were observed between any SREC-treated group and the negative control in either sex ($p > 0.05$). The ratio of polychromatic erythrocytes (PCE) to mature erythrocytes (RBC) remained within the normal range across all groups. These findings indicate that SREC did not induce

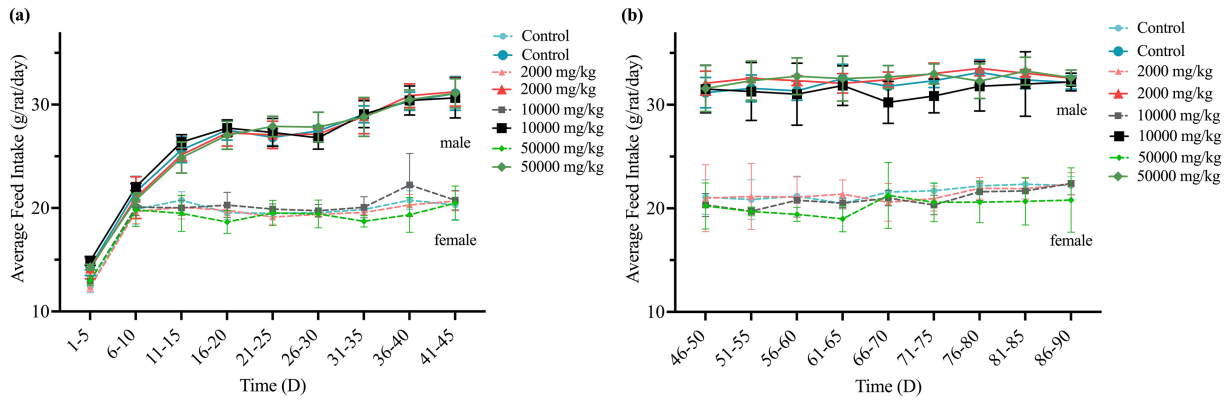

FIGURE 1
Effect of SREC on average feed intake of rats in the 90-day feeding study, as follows: **(a)** 1–45 days feed intake, **(b)** 46–90 days feed intake.

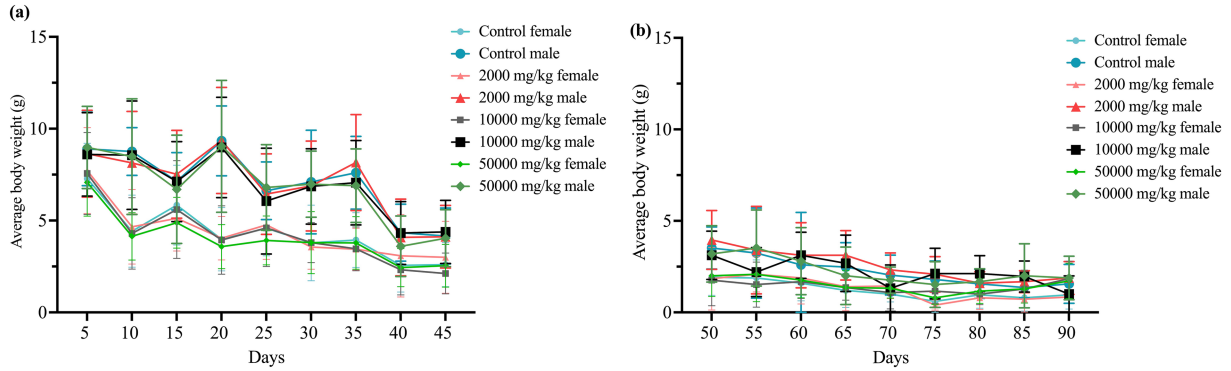

FIGURE 2
Effect of SREC on average body weight of rats in the 90-day feeding study, as follows: **(a)** 1–45 days body weight, and **(b)** 50–90 days body weight.

micronucleus formation in bone marrow cells at doses of 1,250–5,000 mg/kg·bw.

Sperm abnormality test in mice

The sperm abnormality assay was conducted to assess potential germ cell genetic toxicity. Sperm abnormality rates for each experimental group are presented in Table 5, with the distribution of specific malformations shown in Supplementary Figure S4. As indicated in Table 5, the sperm abnormality rate in the positive control group was significantly higher than that in the negative control group ($p < 0.01$). In contrast, no significant increase in sperm abnormalities was observed in SREC-treated mice compared to the negative control ($p > 0.05$), indicating that SREC had no significant effect on sperm morphology at doses of 1,250–5,000 mg/kg·bw.

Teratogenicity test in rats: reproductive and embryotoxicity

Throughout the study period, no clinical signs of toxicity or mortality were observed in pregnant rats administered SREC at doses of 312.5, 1,250, or 5,000 mg/kg·bw, nor in those in the negative control group. As shown in Figure 5, maternal weight gain did not differ significantly among treatment groups compared to controls ($p > 0.05$), indicating that SREC did not adversely affect maternal health within the tested dose range.

On gestation Day 20, dams were sacrificed, and reproductive parameters—including ovarian weight, number of corpora lutea, implantation sites, uterine weight, and number of live fetuses—were evaluated (Table 6). Fetal outcomes such as live birth rate, stillbirth rate, resorption rate, placental weight, fetal weight, body length, and tail length were also assessed (Tables 6, 7). Across all treatment groups, no statistically significant differences were found in reproductive or fetal developmental parameters compared to controls ($p > 0.05$).

Malformation assessments—including external, skeletal, and visceral examinations—revealed no adverse effects attributable to SREC. No external anomalies were observed in any group (Table S5). Skeletal analysis showed mild ossification delays in both treated and control fetuses, primarily involving the sternum and limb bones, with no significant differences in skeletal malformation rates (Supplementary Table S6 and Figure 6). No visceral abnormalities were detected (Supplementary Table S7).

Taken together, these findings demonstrate that SREC does not induce maternal toxicity, reproductive toxicity, embryotoxicity, or teratogenic effects in rats at doses up to 5,000 mg/kg·bw, as evidenced by normal reproductive performance, fetal development, and morphological integrity across all examined endpoints.

Discussion

The long history of herbal medicine suggests that traditional herbs are generally regarded as non-toxic and clinically effective. However, the safety of these herbal substances remains insufficiently studied. SREC, renowned for its potent antioxidant and anti-inflammatory properties, has shown promising benefits in improving growth performance and boosting health across various animal species. Nevertheless, the potential systemic toxicity of SREC has not been comprehensively evaluated. Therefore, this study aimed to fill this gap by conducting a full toxicological evaluation of SREC, including assessments of acute oral toxicity, sub-chronic toxicity, genotoxicity, and teratogenicity.

In terms of acute toxicity, SREC was assessed by administering 5,000 mg/kg·bw to rats and mice over a 14-day observation period (30). No clinical symptoms or toxic deaths were observed, and no abnormal findings were recorded during necropsy. These findings confirm the absence of acute toxicity and align with findings from similar studies on other plant-based feed additives. For example, an acute toxicity study on *Campomanesia velutina* aqueous extract found no significant toxic effects at doses up to 1,200 mg/kg·bw in mice, with only transient symptoms, such as diarrhea, abdominal cramps, and tremors, observed at the highest dose (17). Similarly, the hydroalcoholic extract of *Withania somnifera* roots, when administered at doses up to 2,000 mg/kg·bw in an acute toxicity test, did not cause any toxic symptoms, mortality, or behavioral changes in rats during the 14-day observation period (16). The findings from this study reinforce the conclusion that SREC exhibits no acute toxic potential at high dose.

Following the acute toxicity evaluation, a 90-day subchronic toxicity study was conducted using dietary SREC at doses ranging

TABLE 1 Feeding SREC for 90 days: effects on hematological parameters in SD rats.

Groups (mg/kg) feed	HGB(g/L)		RBC (10^{12}/L)		WBC (10^9/L)		PLT (10^9/L)		HCT (%)		EOS (10^9/L)		BAS (10^9/L)		NEU(10^9/L)		MO (10^9/L)		LYM(10^9/L)	
	♀	♂	♀	♂	♀	♂	♀	♂	♀	♂	♀	♂	♀	♂	♀	♂	♀	♂	♀	♂
50,000	166.80 ± 4.55*	168.80 ± 12.36	7.49 ± 0.18	8.30 ± 0.61	6.85 ± 1.49	12.10 ± 2.60*	874.80 ± 71.63	763.401 ± 84.37	50.04 ± 1.71*	50.24 ± 3.96	0.06 ± 0.02	0.05 ± 0.04	0 ± 0	0.01 ± 0.01	1.79 ± 0.37*	4.24 ± 0.92	0.51 ± 0.12*	1.15 ± 0.29*	4.50 ± 1.03	6.64 ± 1.95
10,000	142.20 ± 13.14	151.20 ± 18.82	6.97 ± 0.54	7.85 ± 0.71	7.40 ± 3.36	10.28 ± 0.74*	732.40 ± 72.68	694.60 ± 107.90	45.22 ± 3.50	45.98 ± 4.53	0.04 ± 0.02	0.02 ± 0.02	0 ± 0	0 ± 0	2.76 ± 1.60	3.37 ± 0.33	0.62 ± 0.43	0.68 ± 0.23	3.98 ± 1.46	6.19 ± 0.37
2000	150.80 ± 10.66	165.60 ± 6.77	7.87 ± 0.40	8.72 ± 0.53	5.66 ± 1.77	7.32 ± 1.12	740.20 ± 48.15	619.80 ± 103.39	46.80 ± 3.22	47.81 ± 2.07	0.03 ± 0.02	0.02 ± 0.02	0 ± 0	0 ± 0	1.93 ± 0.68	2.52 ± 0.42	0.37 ± 0.15	0.55 ± 0.10	3.32 ± 1.09	4.23 ± 1.05
NC	155.20 ± 7.16	153.60 ± 9.40	7.80 ± 0.59	8.43 ± 0.68	5.96 ± 0.71	7.01 ± 1.93	784.00 ± 81.41	791.20 ± 77.48	45.48 ± 1.96	45.08 ± 3.04	0.06 ± 0.03	0.06 ± 0.06	0 ± 0	0.01 ± 0.01	2.48 ± 0.41	3.54 ± 1.38	0.32 ± 0.08	0.42 ± 0.18	3.11 ± 0.46	2.99 ± 0.68

*Significantly different from the NC group ($p < 0.05$). ♀-female, ♂-male.

TABLE 2 Effects of SREC on blood biochemical parameters in SD rats after 90 days of feeding.

Groups (mg/kg) feed	Alb (g/L)		ALT (U/L)		AST (U/L)		TCH (mmol/L)		Cr (μmoL/L)		Glu (mmol/L)		TG (mmol/L)		TP (g/L)		BUN (mmol/L)	
	♀	♂	♀	♂	♀	♂	♀	♂	♀	♂	♀	♂	♀	♂	♀	♂	♀	♂
5,000	42.80 ± 1.46	40.38 ± 1.81	44.40 ± 8.17*	54.20 ± 10.94	99.40 ± 13.11	102.20 ± 11.67	2.33 ± 0.19	2.19 ± 0.33	32.26 ± 4.37	32.04 ± 7.33	8.00 ± 1.08	8.43 ± 2.48	0.62 ± 0.11	1.26 ± 0.49	67.84 ± 2.94	66.78 ± 4.43	5.75 ± 1.22	5.79 ± 0.57
1,250	42.60 ± 3.05	39.50 ± 1.22*	41.20 ± 1.92	52.40 ± 6.43	94.80 ± 11.14	118.20 ± 21.46	2.12 ± 0.21	1.91 ± 0.20	29.08 ± 13.32	34.25 ± 4.37	8.49 ± 2.82	7.76 ± 2.57	0.68 ± 0.36	0.78 ± 0.28	68.32 ± 5.37	65.14 ± 2.45	6.47 ± 1.18	5.26 ± 0.39
312.5	44.04 ± 2.14	40.50 ± 1.36	49.40 ± 10.36	54.80 ± 7.79	102.60 ± 24.56	121.00 ± 37.66	2.11 ± 0.41	1.88 ± 0.47	36.35 ± 1.47	30.52 ± 13.82	7.70 ± 1.10	9.81 ± 2.59	0.56 ± 0.23	0.55 ± 0.20	70.58 ± 5.49	66.96 ± 3.41	6.02 ± 5.91	6.30 ± 0.74
NC	44.76 ± 2.45	41.38 ± 0.68	46.40 ± 3.91	60.00 ± 5.96	108.00 ± 13.17	108.20 ± 15.02	2.24 ± 0.21	1.66 ± 0.53	40.08 ± 3.93	33.84 ± 5.07	7.32 ± 1.47	7.82 ± 1.06	0.59 ± 0.11	0.72 ± 0.38	72.50 ± 4.61	66.40 ± 2.06	6.00 ± 1.10	5.71 ± 1.10

*Significantly different from the NC group ($p < 0.05$). ♀-female, ♂-male.

10.3389/fvets.2025.1646665

10.3389/fvets.2025.1646665

TABLE 3 Effect of SREC on organ coefficient of rats after feeding for 90 days.

Groups (mg/kg feed)	Liver		Kidney		Spleen		Gastrointestinal		Lung		Heart		Testicle	Ovary
	♀	♂	♀	♂	♀	♂	♀	♂	♀	♂	♀	♂	♂	
5,000	3.61 ± 0.33	3.40 ± 0.18	0.59 ± 0.02	0.62 ± 0.04	0.22 ± 0.04	0.20 ± 0.02	9.99 ± 0.54	7.66 ± 1.14	0.69 ± 0.06	0.57 ± 0.24	0.32 ± 0.06	0.29 ± 0.03	0.74 ± 0.05	0.04 ± 0.01
1,250	3.82 ± 0.78	3.43 ± 0.47	0.64 ± 0.06	0.64 ± 0.08	0.23 ± 0.04	0.20 ± 0.02	9.60 ± 1.91	7.35 ± 0.10	0.73 ± 0.18	0.51 ± 0.05	0.34 ± 0.05	0.32 ± 0.02	0.73 ± 0.06	0.04 ± 0.01
312.5	3.60 ± 0.34	3.11 ± 0.45	0.66 ± 0.07	0.63 ± 0.10	0.21 ± 0.02	0.18 ± 0.02	8.61 ± 0.70	6.90 ± 0.93	0.61 ± 0.14	0.58 ± 0.15	0.33 ± 0.02	0.30 ± 0.04	0.64 ± 0.11	0.04 ± 0.01
NC	3.27 ± 0.41	3.05 ± 0.23	0.61 ± 0.03	0.58 ± 0.07	0.20 ± 0.01	0.18 ± 0.03	9.29 ± 1.27	6.77 ± 0.62	0.66 ± 0.16	0.58 ± 0.07	0.31 ± 0.02	0.31 ± 0.05	0.65 ± 0.14	0.05 ± 0.01

Organ coefficient = organ weight/body weight × 100%. The data were compared with the same sex of control group. *Significantly different from the NC group ($p < 0.05$). ♀-female, ♂-male.

from 2,000 to 50,000 mg/kg feed. No significant changes in behavior, feed intake, or body weight were observed, and there were no abnormalities detected in organ system toxicity evaluations, including the heart, liver, kidneys, and gastrointestinal tract. Hematological and biochemical parameters remained within normal physiological ranges, with no dose-dependent effects.

These observations are consistent with previous findings on other plant-based feed additives. For example, an investigation of *Arecae semen* aqueous extract showed that at doses up to 4,500 mg/kg feed, no significant changes were observed in biochemical parameters or organ weights in rats, although some mild signs of toxicity, including weight loss and changes in liver and testis organ weights, were observed in the high-dose group (31). Similarly, a study on marigold flavonoids from marigold inflorescence residue, administered at doses up to 50,000 mg/kg feed for 90 days, showed no significant adverse effects on body weight or organ function (18). In contrast, the sub-chronic toxicity study on *Nityanand Rasa* (NR) (19), an Ayurvedic herbo-metallic formulation, showed mild liver and kidney toxicity at high doses of 600 mg/kg feed. These comparisons collectively suggest that SREC may have a broader safety margin than some other plant-based formulations, especially at higher doses.

To further assess genetic safety, SREC was evaluated using the Ames test, micronucleus assay, and sperm morphology test, and it did not induce any statistically significant abnormalities in any of these assays (32–34). This consistent lack of genotoxic responses across multiple endpoints provides robust evidence for the genetic safety of SREC (35). These findings are consistent with other studies of herbal extracts. For instance, a study on marigold flavonoids, extracted from marigold inflorescence residue, showed no evidence of genotoxicity in the Ames test, sperm aberration test, or *in vivo* micronucleus test at doses up to 5,000 mg/kg·bw (18). Similarly, a study on *Agrimonia* and *Filipendula* species plant extracts demonstrated no mutagenic or genotoxic effects in both the Ames test and micronucleus assay, supporting the non-genotoxic potential of these herbal extracts (23). By contrast, Metolcarb, an insecticide, produced strong genotoxicity responses, including increased mutagenic revertants and chromosomal damage in various test systems. These comparisons further emphasize the favorable genetic safety profile of SREC.

In addition to systemic and genetic toxicity, potential reproductive and developmental toxicity of SREC was assessed via a teratogenicity study (36). This evaluation was designed to detect potential effects on fertility, fetal development, and neonatal outcomes (37). In the teratogenicity study, no significant effects were observed on reproductive function, fetal development, or birth outcomes at doses ranging from 312.5 to 5,000 mg/kg·bw. There were no significant differences in reproductive indicators such as ovarian weight, implantation number, and live birth rates between the treated groups and the negative control group. Similarly, fetal growth and development indicators, including placental weight, fetal weight, body length, and tail length, remained unaffected. These outcomes strongly support the absence of teratogenic effects, indicating that SREC is unlikely to impair reproductive performance or fetal health. Therefore, its application in breeding animal diets appears to be safe and without detrimental effects on progeny development.

Despite these positive results, several limitations should be acknowledged. The 90-day duration and limited sample size may not fully capture the potential long-term effects of SREC. Future studies should consider extended exposure periods and larger populations to

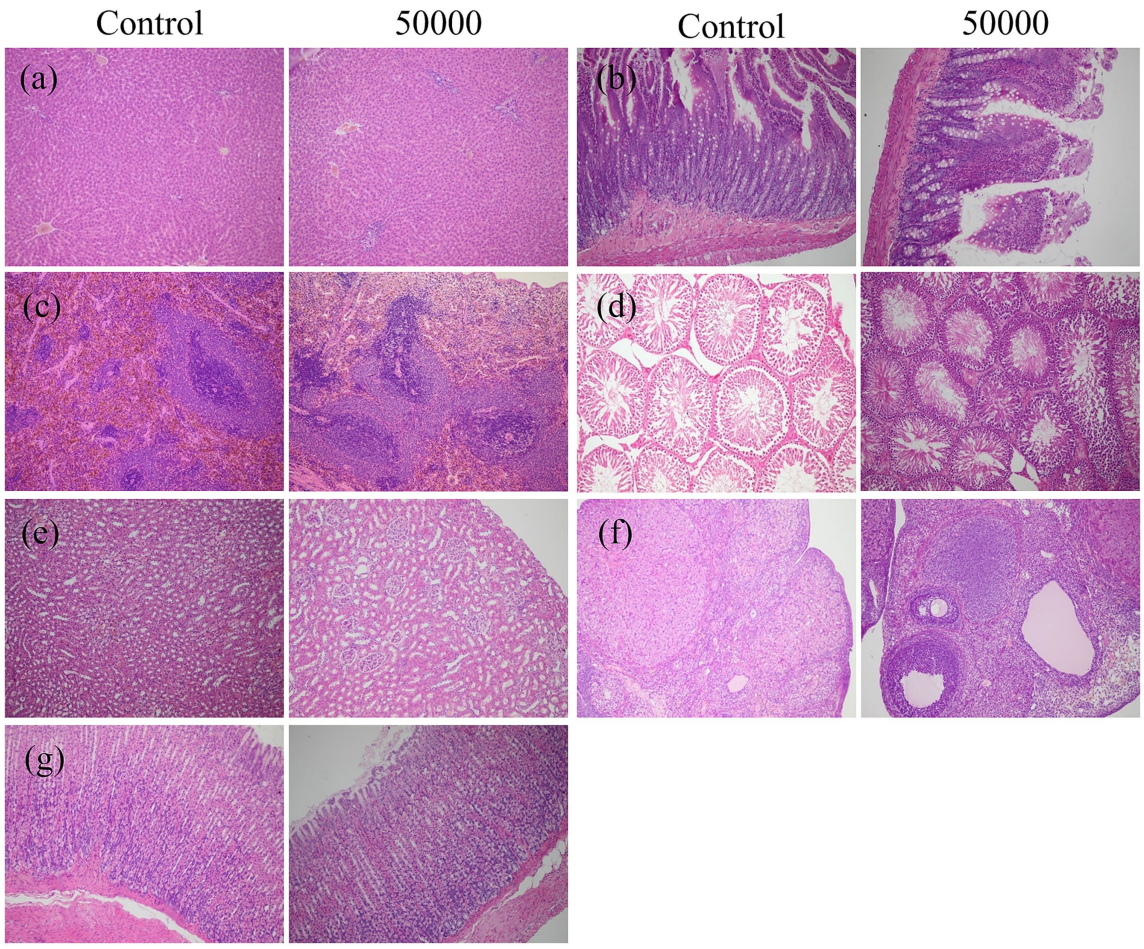

FIGURE 3
Effect of SREC on the histopathological change in rats after feeding for 90 days (female and male were similar, only the control group and the high-dose group were included); **(a)** liver; **(b)** intestine; **(c)** spleen; **(d)** testis; **(e)** kidney; **(f)** ovary; **(g)** stomach (All images taken at ×20 magnification).

validate these findings. Additionally, the current genotoxicity and teratogenicity assessments only represent specific toxicological endpoints. Additional evaluations involving neurotoxicity, endocrine-disrupting potential, and immunotoxicity would be beneficial to comprehensively characterize the safety profile of SREC.

In summary, this study provides foundational evidence supporting the safety of SREC, demonstrating no acute, sub-chronic, genotoxic, or teratogenic toxicity. These findings support its potential use as a safe and effective natural feed additive. However, further research is necessary to elucidate the mechanisms of action of its bioactive components, particularly chlorogenic acid and its derivatives—especially in relation to immune modulation, cellular signaling, and gut microbiota composition. Moreover, long-term safety assessments across multiple species and production contexts are essential. Given its favorable characteristics, SREC deserves further investigation as a potential substitute for antibiotic growth promoters in livestock farming (38, 39).

Conclusion

This study provides a comprehensive assessment of the safety profile of SREC, utilizing various *in vivo* and *in vitro* tests. The acute oral toxicity test demonstrated that SREC is well-tolerated, with no adverse effects or mortality at doses up to 5,000 mg/kg·bw (LD_{50} > 5,000 mg/kg·bw). The 90-day repeated dose oral toxicity study confirmed the safety of SREC at doses up to 50,000 mg/kg feed, with no significant changes in vital signs, behavior, hematological or biochemical indices, immune function, or organ health. Additionally, genotoxicity assessments, including the Ames test, mouse bone marrow micronucleus assay, and sperm morphology test, showed that SREC does not exhibit genotoxic properties. Teratogenicity testing on pregnant rats revealed no significant teratogenic effects, with no observed differences in embryonic development compared to the negative control group.

These findings collectively support the safety of SREC as a promising natural feed additive for livestock and poultry. However, while the results are encouraging, several limitations in this study must be acknowledged. The sample size and the duration of exposure were limited, and while no adverse effects were observed in the experimental animals, further studies with larger sample sizes and longer durations are needed to more comprehensively evaluate the long-term safety and efficacy of SREC. Additionally, future research should include testing in other animal models and under varying environmental conditions to confirm the generalizability of these results.

10.3389/fvets.2025.1646665

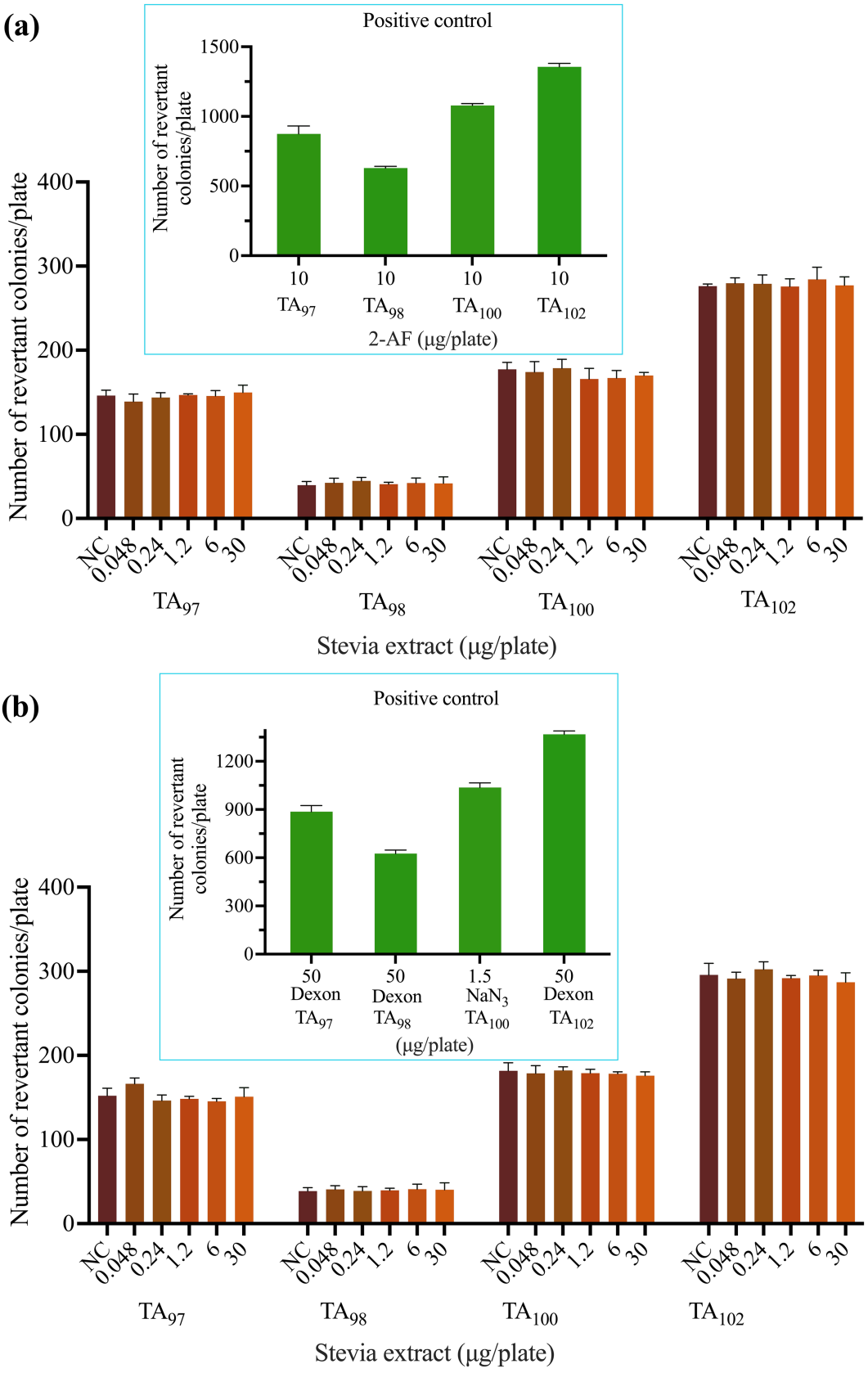

FIGURE 4
Effect of SREC on bacterial reverse mutation assay (Ames test). **(a)** With (+ S9 mix) and **(b)** without (– S9 mix) metabolic activation. 2-AF: 2-aminofluorene. Dexon: Fenaminosulf. NaN_3: Sodium azide. NC: negative control.

TABLE 4 The results of the micronucleus test on mouse bone marrow cells using SREC.

Groups (mg/kg·bw)	PCE/RBC ratio		MN/1000 PCE (%)		Significance of difference
	♂	♀	♂	♀	
5,000	0.99 ± 0.10	0.97 ± 0.08	5.17 ± 2.37	4.14 ± 2.39	$p > 0.05$
2,500	0.96 ± 0.05	1.00 ± 0.06	4.54 ± 1.92	5.18 ± 2.25	$p > 0.05$
1,250	1.01 ± 0.09	0.97 ± 0.06	4.78 ± 1.61	5.48 ± 2.01	$p > 0.05$
NC	0.97 ± 0.08	0.99 ± 0.05	5.15 ± 1.98	4.95 ± 1.85	-
PC	0.78 ± 0.08	0.87 ± 0.14	21.06 ± 4.63	19.89 ± 7.29	$p < 0.01$**

The data were compared with the negative control group, *Significantly different from the NC group ($p < 0.05$), **Significantly different from the NC group ($p < 0.01$). ♀-female, ♂-male.

TABLE 5 Results of sperm malformation test in mice with SREC (sperm malformation rate).

Groups (mg/kg·bw)	Malformed sperm count	Malformed sperm count (%)	Significance of difference
5,000	152	3.03 ± 0.65	$p > 0.05$
2,500	139	2.78 ± 0.79	$p > 0.05$
1,250	145	2.90 ± 0.74	$p > 0.05$
NC	133	2.66 ± 0.68	--
PC	312	6.24 ± 0.90	$p < 0.01$**

The number of mice in each dose group was 5 and the sperm count was 5,000; the data were compared with the negative control group, *Significantly different from the NC group ($p < 0.05$), **Significantly different from the NC group ($p < 0.01$).

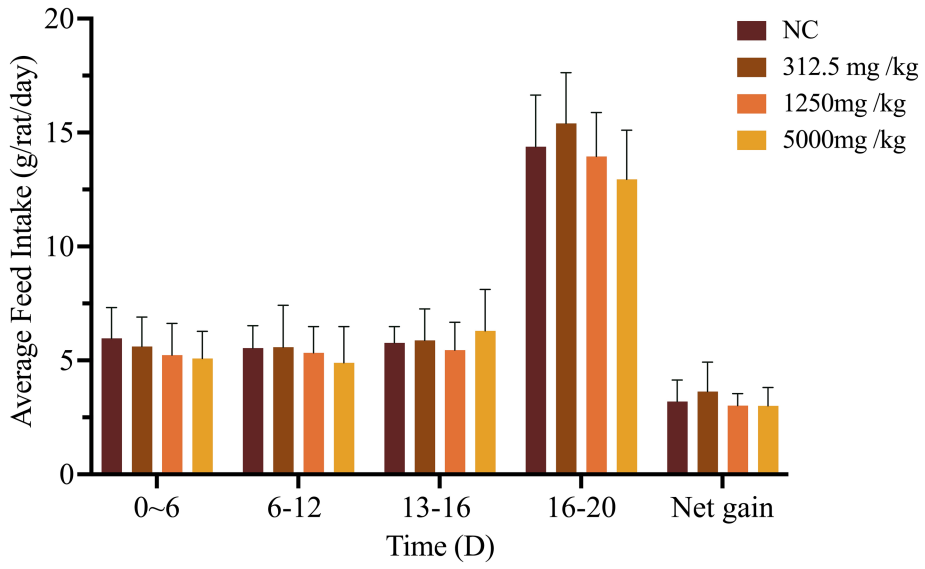

FIGURE 5
Effects of SREC on daily weight gain in pregnant rats. Net weight gain = gestational mouse weight gain − litter weight. *Significantly different from the NC at $p < 0.05$, **Significantly different from the NC at $p < 0.01$.

TABLE 6 Effects of SREC on reproductive function in rats.

Groups (mg/kg·bw)	Ovarian weight(g)	Corpus luteum number	Average number of plants	Uterine weight (g)	Average number of live births
5,000	0.18 ± 0.02	16.08 ± 3.15	14.08 ± 2.47	6.91 ± 0.59	14.00 ± 2.30
1,250	0.18 ± 0.03	16.92 ± 1.68	13.67 ± 1.30	7.51 ± 0.53	13.58 ± 1.38
312.5	0.21 ± 0.02	17.33 ± 1.07	14.25 ± 1.54	7.05 ± 0.40	14.67 ± 1.83
NC	0.19 ± 0.05	17.08 ± 1.83	15.17 ± 1.64	7.56 ± 0.65	15.33 ± 1.92

The data in the table are the average of 12 pregnant rats in each group.

TABLE 7 Effects of SREC on embryonic development of rats.

Groups (mg/kg·bw)	Number of live births	Placental weight (g)	Fetal rat weight (g)	Fetal length (cm)	Fetal tail length (cm)
5,000	168	0.52 ± 0.02	3.68 ± 0.09	3.67 ± 0.06	1.21 ± 0.05
1,250	163	0.51 ± 0.02	3.65 ± 0.05	3.67 ± 0.02	1.21 ± 0.04
312.5	171	0.52 ± 0.01	3.64 ± 0.07	3.67 ± 0.03	1.22 ± 0.02
NC	182	0.51 ± 0.02	3.68 ± 0.06	3.68 ± 0.04	1.22 ± 0.05

The data in the table are the average of 12 pregnant rats in each group. *Significantly different from the NC group ($p < 0.05$), **Significantly different from the NC group ($p < 0.01$).

FIGURE 6
Effect of plant soot on skeletal malformations in rats.

In conclusion, SREC demonstrates a favorable safety profile and holds significant potential as a sustainable alternative to traditional antibiotics in animal feed. Further research is necessary to fully establish its long-term safety and efficacy across a broader range of applications.

Data availability statement

The dataset generated and analyzed during the current study is available from the corresponding author on reasonable request. There are Requests to access the datasets should be directed to lytingm@163.com.

Ethics statement

The animal study was approved by China Agricultural University Laboratory Animal Welfare and Animal Experimental Ethical. The study was conducted in accordance with the local legislation and institutional requirements.

Author contributions

YuL: Formal analysis, Visualization, Investigation, Data curation, Methodology, Writing – original draft. LZ: Data curation, Resources, Validation, Writing – review & editing. DH: Data curation, Writing – review & editing, Validation. LF: Supervision, Writing – review & editing, Resources. YaL: Supervision, Writing – review & editing, Formal analysis. ST: Data curation, Writing – original draft, Funding acquisition, Supervision, Visualization, Conceptualization, Resources, Writing – review & editing, Project administration.

Funding

The author(s) declare that financial support was received for the research and/or publication of this article. This work was supported by the National Natural Science Foundation of China (Grant No. 32473083).

Conflict of interest

LZ, DH, LF, and YL were employed by Zhucheng Haotian Pharm Co., Ltd.

The remaining authors declare that the research was conducted in the absence of any commercial or financial relationships that could be construed as a potential conflict of interest.

Generative AI statement

The author(s) declare that no Generative AI was used in the creation of this manuscript.

Any alternative text (alt text) provided alongside figures in this article has been generated by Frontiers with the support of artificial intelligence and reasonable efforts have been made to ensure accuracy, including review by the authors wherever possible. If you identify any issues, please contact us.

Publisher's note

All claims expressed in this article are solely those of the authors and do not necessarily represent those of their affiliated organizations, or those of the publisher, the editors and the reviewers. Any product that may be evaluated in this article, or claim that may be made by its manufacturer, is not guaranteed or endorsed by the publisher.

Supplementary material

The Supplementary material for this article can be found online at: https://www.frontiersin.org/articles/10.3389/fvets.2025.1646665/full#supplementary-material

References

1. Hu Y, Cheng H, Tao S. Environmental and human health challenges of industrial livestock and poultry farming in China and their mitigation. *Environ Int*. (2017) 107:111–30. doi: 10.1016/j.envint.2017.07.003

2. Zou A, Nadeau K, Xiong X, Wang PW, Copeland JK, Lee JY, et al. Systematic profiling of the chicken gut microbiome reveals dietary supplementation with antibiotics alters expression of multiple microbial pathways with minimal impact on community structure. *Microbiome*. (2022) 10:127. doi: 10.1186/s40168-022-01319-7

3. Hassell JM, Ward MJ, Muloi D, Bettridge JM, Robinson TP, Kariuki S, et al. Clinically relevant antimicrobial resistance at the wildlife-livestock-human interface in Nairobi: an epidemiological study. *Lancet Planet Health*. (2019) 3:e259–69. doi: 10.1016/S2542-5196(19)30083-X

4. Fangueiro JF, de Carvalho NM, Antunes F, Mota IF, Pintado ME, Madureira AR, et al. Lignin from sugarcane bagasse as a prebiotic additive for poultry feed. *Int J Biol Macromol*. (2023) 239:124262. doi: 10.1016/j.ijbiomac.2023.124262

5. Gao J, Yang Z, Zhao C, Tang X, Jiang Q, Yin Y. A comprehensive review on natural phenolic compounds as alternatives to in-feed antibiotics. *Sci China Life Sci*. (2023) 66:1518–34. doi: 10.1007/s11427-022-2246-4

6. Abd El-Hack ME, de Oliveira MC, Attia YA, Kamal M, Almohmadi NH, Youssef IM, et al. The efficacy of polyphenols as an antioxidant agent: an updated review. *Int J Biol Macromol*. (2023) 250:126525. doi: 10.1016/j.ijbiomac.2023.126525

7. Ahmad U, Ahmad RS, Arshad MS, Mushtaq Z, Hussain SM, Hameed A. Antihyperlipidemic efficacy of aqueous extract of *Stevia rebaudiana* Bertoni in albino rats. *Lipids Health Dis*. (2018) 17:175. doi: 10.1186/s12944-018-0810-9

8. Karakose H, Jaiswal R, Kuhnert N. Characterization and quantification of hydroxycinnamate derivatives in *Stevia rebaudiana* leaves by LC-MSn. *J Agric Food Chem*. (2011) 59:10143–50. doi: 10.1021/jf202185m

9. Ji L, Jiang P, Lu B, Sheng Y, Wang X, Wang Z. Chlorogenic acid, a dietary polyphenol, protects acetaminophen-induced liver injury and its mechanism. *J Nutr Biochem*. (2013) 24:1911–9. doi: 10.1016/j.jnutbio.2013.05.007

10. Rakshit S, Mandal L, Pal BC, Bagchi J, Biswas N, Chaudhuri J, et al. Involvement of ROS in chlorogenic acid-induced apoptosis of Bcr-Abl+ CML cells. *Biochem Pharmacol*. (2010) 80:1662–75. doi: 10.1016/j.bcp.2010.08.013

11. Lou Z, Wang H, Rao S, Sun J, Ma C, Li J. P-coumaric acid kills bacteria through dual damage mechanisms. *Food Control*. (2012) 25:550–4. doi: 10.1016/j.foodcont.2011.11.022

12. Sarnataro C, Spanghero M. In vitro rumen fermentation of feed substrates added with chestnut tannins or an extract from *Stevia rebaudiana* Bertoni. *Anim Nutr*. (2020) 6:54–60. doi: 10.1016/j.aninu.2019.11.009

13. Mehmood A, Zhao L, Ishaq M, Xin W, Zhao L, Wang C, et al. Anti-hyperuricemic potential of stevia (*Stevia rebaudiana* Bertoni) residue extract in hyperuricemic mice. *Food Funct*. (2020) 11:6387–406. doi: 10.1039/C9FO02246E

14. Koubaa M, Rosello-Soto E, Sic Zlabur J, Rezek Jambrak A, Brncic M, Grimi N, et al. Current and new insights in the sustainable and green recovery of nutritionally valuable compounds from *Stevia rebaudiana* Bertoni. *J Agric Food Chem*. (2015) 63:6835–46. doi: 10.1021/acs.jafc.5b01994

15. OECD Test no. 425: Acute Oral toxicity: Up-and-down procedure (2022)

16. Prabu PC, Panchapakesan S, Raj CD. Acute and sub-acute oral toxicity assessment of the hydroalcoholic extract of *Withania somnifera* roots in Wistar rats. *Phytother Res*. (2013) 27:1169–78. doi: 10.1002/ptr.4854

17. Araujo MC, Barcellos NM, Vieira PM, Gouveia TM, Guerra MO, Peters VM, et al. Acute and sub chronic toxicity study of aqueous extract from the leaves and branches of *Campomanesia velutina* (Cambess) O. Berg. *J Ethnopharmacol*. (2017) 201:17–25. doi: 10.1016/j.jep.2017.02.043

18. Wu D, Wu J, Cheng X, Qian J, Du R, Tang S, et al. Safety assessment of marigold flavonoids from marigold inflorescence residue. *J Ethnopharmacol*. (2022) 297:115520. doi: 10.1016/j.jep.2022.115520

19. Kshirsagar SR, Kumari M, Bajad SM, Kumar MJM, Saxena S, Kumari SI. Assessment of sub-chronic oral toxicity of Nityanand rasa: an ayurvedic herbo-metallic formulation. *J Ethnopharmacol*. (2023) 312:116494. doi: 10.1016/j.jep.2023.116494

20. Lee MY, Sc, Kim JY, Shin HK. Genotoxicity evaluation of Guibi-tang extract using an in vitro bacterial reverse mutation assay, chromosome aberration assay, and in vivo micronucleus test. *BMC Complement Altern Med*. (2014) 1:14.215

21. Mortelmans K, Zeiger E. The ames *Salmonella*: microsome mutagenicity assay. *Mutat Res*. (2000) 455:29–60. doi: 10.1016/s0027-5107(00)00064-6

22. Liman R, Akyil D, Eren Y, Konuk M. Testing of the mutagenicity and genotoxicity of metolcarb by using both Ames/Salmonella and Allium test. *Chemosphere*. (2010) 80:1056–61. doi: 10.1016/j.chemosphere.2010.05.011

23. Pukalskiene M, Slapsyte G, Dedonyte V, Lazutka JR, Mierauskiene J, Venskutonis PR. Genotoxicity and antioxidant activity of five Agrimonia and Filipendula species plant extracts evaluated by comet and micronucleus assays in human lymphocytes and Ames Salmonella/microsome test. *Food Chem Toxicol*. (2018) 113:303–13. doi: 10.1016/j.fct.2017.12.031

24. Hayashi M. The micronucleus test-most widely used in vivo genotoxicity test. *Genes Environ*. (2016) 38:18. doi: 10.1186/s41021-016-0044-x

25. OECD. Test no. 474: Mammalian erythrocyte micronucleus test (2016)

26. Macgregor JT, Tucker JD, Ziderman II, Wehr CM, Friedman M. Non-clastogenicity in mouse bone marrow of fructose/lysine and other sugar/amino acid browning products with in vitro genotoxicity. *Food Chem Toxicol*. (1989) 27:715–21. doi: 10.1016/0278-6915(89)90076-8

27. Kumar SN, Arghya B, Imam RS, Kshama D, Salma K. Hyrdoalcoholic root bark extract of Salacia oblonga prevented Mitomycin-C induced sperm abnormality in Wistar rats. *Pharmacogn Mag*. (2009) 5:254–49.

28. Prooije AE S-v, Waalkens-Berendsen DH, Bär A. Embryotoxicity and teratogenicity study with Erythritol in rats. *Regul Toxicol Pharmacol*. (1996) 24:S232–6. doi: 10.1006/rtph.1996.0103

29. Rodrigues NER, Oliveira A, Lima SMA, Nunes DM, Albuquerque PBS, da Cunha M, et al. Effect of the aqueous extract of *Chrysobalanus icaco* leaves on maternal reproductive outcomes and fetal development in Wistar rats. *Curr Issues Mol Biol*. (2023) 45:7617–29. doi: 10.3390/cimb45090479

30. Shi SR, Gu H, Chang LL, Wang ZY, Tong HB, Zou JM. Safety evaluation of daidzein in laying hens: part I. Effects on laying performance, clinical blood parameters, and organs development. *Food Chem Toxicol*. (2013) 55:684–8. doi: 10.1016/j.fct.2013.01.009

31. Lin Q, Jia Z, Xu X, Xu S, Han T, Gao Y, et al. Sub-chronic toxicity study of arecae semen aqueous extract in Wistar rats. *J Ethnopharmacol*. (2018) 215:176–83. doi: 10.1016/j.jep.2017.08.031

32. Feng J, Li X, Manzi HP, Kiki C, Lin L, Hong J, et al. Chlorination of microcystin-LR in natural water: kinetics, transformation products, and genotoxicity. *J Environ Manag*. (2023) 338:117774. doi: 10.1016/j.jenvman.2023.117774

33. Kamiya H, Makino T, Suzuki T, Kobayashi M, Matsuoka I. Mutations induced by 8-oxo-7,8-dihydroguanine in WRN- and DNA polymerase lambda-double knockdown cells. *Mutagenesis*. (2018) 33:301–10. doi: 10.1093/mutage/gey024

34. Kaleeswaran S, Sriram P, Prabhu D, Chinnathambi, Vijayakumar, Mathuram LN. Anti- and pro-mutagenic effects of silymarin in the Ames bacterial reverse mutation assay. *Phytother Res*. (2009) 23:1378–84. doi: 10.1002/ptr.2772

35. Kristien Mortelmans EZ. The Ames Salmonella:microsome mutagenicity assay. *Mutation Res*. (2000) 455:29–60.

36. Wiesner J, Ziemann C, Hintz M, Reichenberg A, Ortmann R, Schlitzer M, et al. FR-900098, an antimalarial development candidate that inhibits the non-mevalonate isoprenoid biosynthesis pathway, shows no evidence of acute toxicity and genotoxicity. *Virulence*. (2016) 7:718–28. doi: 10.1080/21505594.2016.1195537

37. Greek R, Shanks N, Rice MJ. The history and implications of testing thalidomide on animals. *J Philos Sci Law*. (2011) 11:33. doi: 10.2174/156652401766617033116231 5

38. Sa S, Seol Y, Lee AW, Heo Y, Kim HJ, Park CJ. Teratogenicity of D-allulose. *Toxicol Rep*. (2022) 9:821–4. doi: 10.1016/j.toxrep.2022.03.028

39. Dong Z, Tang SS, Ma XL, Tan B, Tang ZS, Li CH, et al. Acute, chronic, and genotoxic studies on the protopine total alkaloids of the *Macleaya cordata* (Willd.) R. Br. In rodents. *Front Pharmacol*. (2022) 13:987800. doi: 10.3389/fphar.2022.987800

frontiers | Frontiers in Veterinary Science

TYPE Original Research
PUBLISHED 09 October 2025
DOI 10.3389/fvets.2025.1644200

OPEN ACCESS

EDITED BY
Baocheng Hao,
Chinese Academy of Agricultural Sciences, China

REVIEWED BY
Zhaoyan Lin,
China Agricultural University, China
Yougang Zhong,
China Agricultural University, China

*CORRESPONDENCE
Shanshan Xie
✉ xiess@henau.edu.cn
Qingda Meng
✉ qingdameng@henau.edu.cn

†These authors have contributed equally to this work

RECEIVED 10 June 2025
ACCEPTED 24 September 2025
PUBLISHED 09 October 2025

CITATION
Chen M, Han H, Qin M, Li H, Lu Q, Huang X, Meng Q and Xie S (2025) Pseudolaric acid B induces G2/M phase arrest in canine mammary tumor cells by targeting CDK1. *Front. Vet. Sci.* 12:1644200. doi: 10.3389/fvets.2025.1644200

Pseudolaric acid B induces G2/M phase arrest in canine mammary tumor cells by targeting CDK1

Mengjuan Chen[1,2†], Hui Han[1,2†], Mengke Qin[1,2], Huixin Li[1,2], Qiqi Lu[1,2], Xin Huang[1,2], Qingda Meng[1,2*] and Shanshan Xie[1,2*]

[1]College of Veterinary Medicine, Henan Agricultural University, Zhengzhou, China, [2]Research Center for Organoids, College of Veterinary Medicine, Henan Agricultural University, Zhengzhou, China

Introduction: Current management of canine mammary tumors (CMTs) remains reliant on surgical resection and chemotherapy. However, these strategies are often limited by high recurrence rates and systemic toxicity. Addressing these limitations requires urgent development of safer and more effective therapeutics. Pseudolaric acid B (PAB), a bioactive compound extracted from the roots of the *Pseudolarix kaempferi* Gord., has garnered attention for its broad-spectrum antitumor activity and favorable pharmacokinetic profile, and it has shown promise in inhibiting the growth of a variety of tumors, including breast cancer. The aim of this study was to investigate the anticancer effects of PAB on canine mammary tumor U27 cells and its underlying mechanisms.
Methods and results: *In vitro* analyses demonstrated that PAB dose dependently reduced cell viability, suppressed cell proliferation, and triggered caspase-mediated apoptosis. Transcriptomic profiling of PAB-treated tumor cells revealed significant enrichment of differentially expressed genes in pathways such as gap junction, cell cycle, and cellular senescence. Mechanistically, CDK1 suppression by PAB, achieved through binding that diminishes its expression and stability, induced G2/M phase arrest and halted mitotic progression. While these findings suggest the potential of PAB as a candidate for canine mammary tumor treatment, further investigations are warranted to delineate its precise *in vivo* targeting specificity and pharmacodynamic interactions.
Discussion: These findings not only expand the translational applicability of PAB in veterinary oncology but also identify CDK1 as a potential therapeutic vulnerability for combinatorial treatment strategies in CMTs.

KEYWORDS

canine mammary tumor, Pseudolaric acid B, CDK1, cell cycle, cell apoptosis

1 Introduction

Canine mammary tumors (CMTs) rank as the second most prevalent malignant neoplasms following skin tumors in dogs, and represent a substantial threat to canine health (1). Surgical resection remains the primary therapeutic intervention for CMTs (2). However, even after complete excision, residual tumor microenvironment components may contribute to disease recurrence. CMTs share remarkable pathological and molecular similarities with human breast cancer, particularly in terms of molecular pathogenesis and metastatic behavior (3), making them a highly relevant translational model for anticancer drug development. Although chemotherapy and targeted therapies have improved overall survival and reduced mortality in human breast cancer patients (4), approximately 30% eventually develop therapeutic resistance, compounded by substantial drug-related adverse effects. These limitations underscore an urgent unmet clinical need for the identification of novel, more effective, and safer therapeutic targets, pharmacological agents, and bioactive compounds.

Naturally derived small-molecule compounds with well-defined structures and demonstrated therapeutic efficacies, have long been regarded as promising candidates for anti-cancer drug development (5, 6). Pseudolaric acid B (PAB), an acid isolated from the root of *Pseudolarix kaempferi* Gorden, has broad-spectrum biological properties, with potent anti-fungal, anti-virus, anti-angiogenic, and anti-fertility activities (7–9). Furthermore, PAB exerts anti-tumor efficacy against various malignancies, particularly cervical, gastric, and breast cancers (10–12). Mechanistic studies reveal that PAB induces G2/M phase cell cycle arrest and subsequent apoptosis through modulating the ROS-triggered AMPK/mTOR, PI3K/AKT, ERK1/2 and Wnt signaling pathways (7, 10, 12). However, the direct molecular target(s) of PAB in breast cancer cells and its precise mechanism of action remains to be fully elucidated.

CDK1 (Cyclin-Dependent Kinase 1), a member of Cyclin dependent kinases (CDKs) family, is a highly conserved Ser/Thr protein kinase (13). CDK1, one of the most extensively characterized cell cycle regulators, serves as the master kinase coordinating critical proliferation pathways (14, 15). Its complex with Cyclin B1 constitutes the essential driver of mitotic entry, predominantly controlling the G2/M transition and representing CDK indispensable for mammalian cell cycle progression (16). Studies have reported that abnormal expression and activity changes of CDK1 can promote tumorigenesis and immune escape of breast cancer through a variety of mechanisms (17–19). The deubiquitinating enzyme YOD1 constitutes a key tumorigenic driver in triple-negative breast cancer by stabilizing CDK1 (20). Selective targeting of CDK1, rather than CDK4/6 or CDK2, may exert lethal effects on MYC-dependent breast cancer cells (21). Furthermore, CDK1 exerts extracyclic oncogenic functions through substrate phosphorylation. Its targeting of USP29 stabilizes the TWIST1 transcription factor, consequently promoting EMT, cancer stemness, chemoresistance, and metastasis in triple-negative breast cancer (TNBC) (20). These findings highlight the critical role of CDK1 in breast cancer progression and its therapeutic potential in breast cancer subtypes.

Based on the above, this study systematically explored the anti-tumor effects of PAB in canine mammary tumor through *in vitro* experiments. Transcriptome sequencing analysis further elucidated the underlying mechanism of PAB and identified CDK1 as a potential therapeutic target. Our results validated that PAB suppressed cancer cell proliferation via cell cycle arrest at the G2/M phase in CMT-U27 cells, which is mechanistically linked to the downregulation of CDK1. Consequently, this research evaluated the anti-cancer effect and molecular mechanism of PAB in canine mammary cancer, providing an effective, low-toxicity drug and a new therapeutic strategy for the clinical treatment of breast cancer.

2 Materials and methods

2.1 Cell culture and drug treatment

Canine mammary tumor U27 cells were obtained from OriCell (Guangzhou, China), and cultured in RPMI 1640 medium (#10491, Solarbio, Beijing, China) supplemented with 10% fetal bovine serum (FBS) (#FBSST-01033-500, Oricell, Guangzhou, China), 1% penicillin–streptomycin (P/S) (#P1400, Solarbio, Beijing, China) at 37 °C in 5% CO_2. Pseudolaric acid B, PAB (10 mM in DMSO) (#HY-N6939, MedChemExpress, USA) and Ro-3306 (10 mM) (#HY-12529, MCE, Shanghai, China) were diluted with RPMI 1640 culture medium to final concentrations of 0.625, 1.25, 2.5, 5, 10, and 20 μM. U27 cells were seeded in 96-well plates at a density 1×10^4 cells/well. After reaching 70–80% confluency, cells were treated with different concentrations of the drug or an equal volume of DMSO (vehicle control) for 24 h prior to harvesting.

2.2 Cell viability assay

CCK-8 (Cell Counting Kit-8) assay was performed to evaluate the cell viability. After 24 h drug treatment, 10 μL of CCK-8 reagent (#C0038, Beyotime, Shanghai, China) was added to each well, followed by incubation at 37 °C for 2 h. Absorbance at 450 nm was then measured using a microplate reader (Biotek, VT, USA).

2.3 Crystal violet cell proliferation assay

U27 cells were inoculated into 96-well plates, drug-treated for 24 h and washed with PBS. Next, cells were fixed with 100% methanol and stained with 0.1% crystal violet (Biyuntian Biotechnology Co., Ltd., Shanghai, China) for 30 min in dark. Images were captured with microscope (Sunny Optical Technology Co., Ltd., Ningbo, China). After solubilizing in 10% acetic acid, absorbance at 570 nm (OD570) was then measured using a microplate reader (Biotek, VT, USA).

2.4 Annexin V-FITC/PI double staining assay

Apoptosis was analyzed using an Annexin V-FITC/PI staining kit (#KTA0002, Abbkine, Wuhan, China). Cells treated with PAB were collected and washed with cold PBS. Subsequently, the cells incubated with Annexin V-FITC and PI for 15 min at room temperature under dark conditions. Apoptotic cells were analyzed using BD FACSCelesta™ flow cytometry (Becton, Dickinson and Company, NJ, USA), and the data were processed using FlowJo™ V10 software.

2.5 Western blot analysis

Canine mammary tumor U27 cells were seeded into 6-well plates at a density of 1×10^6 cells per well. Following seeding, cells were treated with PAB or an equivalent concentration of DMSO (vehicle control) and incubated for 24 h. The cells were lysed using RIPA buffer (Epizyme, #PC101) with protease inhibitor cocktail and the concentration was determined with the BCA kit (Epizyme, #ZJ102). Protein samples were separated on 10% acrylamide SDS-PAGE gel and the protein bands were transferred to PVDF membrane (Millipore, Bedford, MA, USA). Subsequently, 5% fat-free milk was blocked at room temperature for 1 h, and the PVDF membrane was incubated with the primary antibody overnight at 4 °C. Then washed with 1 × PBST, the membrane was incubated with secondary antibody at room temperature for 1 h. Finally, the signals were detected using an ECL reagent and captured

with the amersham imagequant 800 imaging system (Cytiva, USA). *β*-actin (#GB11001-100, Servicebio, Wuhan, China) was used as an internal control. Antibodies against the following proteins were used in the experiments: Caspase 3 (#9662), Caspase 9 (#9502), Bax (#2772) and Bcl-2 (#2876), which were obtained from Cell Signaling Technology (MA, USA), CDK1 (#Ab095719) obtained from Aladdin (Shanghai, China). All the above antibody dilutions are 1:1000.

2.6 RNA sequencing analysis of PAB-treated canine mammary tumor U27 cells

RNA sequencing was performed by Majorbio (Shanghai, China). Canine mammary tumor U27 cells were seeded into 24-well plates at a density of 1×10^5 cells per well. Following seeding, cells were treated with 2.5 μM PAB or an equivalent concentration of DMSO (vehicle control) and incubated for 24 h. Then cells were collected, and total RNA was extracted using the Trizol reagent kit (Vazyme, #PC101) according to the manufacturer 's protocol. The concentration and purity of the extracted RNA were detected by Nanodrop2000 (Thermo Fisher Scientific, MA, USA), the integrity of RNA was detected by agarose gel electrophoresis, and the RQN value was determined by Agilent5300 (Agilent Technologies, CA, USA). Total RNA samples were subjected to poly (A) mRNA enrichment using Oligo (dT) magnetic beads. The purified mRNA was fragmented in optimized cleavage buffer followed by double-stranded cDNA synthesis using SuperScript double-stranded cDNA synthesis kit (Invitrogen, CA, USA). Following cDNA synthesis, terminal modification steps including end-repair, phosphorylation, and 'A' base addition were performed in accordance with standardized Illumina's library construction protocol. And polymerase chain reaction (PCR) amplified. The resulting cDNA libraries were sequenced using Illumina NovaSeq 6,000 by Majorbio Bio-pharm Technology Co., Ltd. (Shanghai, China). The data was processed via the online platform of Majorbio Cloud Platform.[1]

2.7 Real-time quantitative PCR (RT-qPCR) validation of DEGs

Canine mammary tumor U27 cells were seeded in 24-well plates at 1×10^5 cells/well. After overnight attachment, cells were treated with 2.5 μM PAB or vehicle control (equivalent DMSO concentration) for 24 h. Total RNA was extracted using the Trizol reagent (Vazyme, #PC101) and reverse transcriptase reaction was performed with HiScript II Q RT SuperMix for qPCR (Vazyme, #R223-01) according to the manufacturer's recommendations. The cDNA was diluted 1:5 in nuclease-free ddH2O. Real-time PCR was conducted with SYBR Green qPCR Master Mix (Vazyme, #Q321) on a Bio-Rad CFX96 Touch™ Real-Time PCR Detection System. *GAPDH* gene was used as an internal control. All primers employed for qPCR experiments are detailed in Table 1.

TABLE 1 List of primers.

Gene name	Sequence (5′ to 3′)	Product size (bp)
FOS	F: CAAGCGGAGACAGACCAACT	105
	R: GTGAGCTGCCAGGATGAACT	
NR4A1	F: TAAGGGCTTCTTCAAGCGCA	145
	R: TTCCTTCACCATGCCTACGG	
GAPDH	F: GTCCCCACCCCCAATGTATC	128
	R: GTGTAGCCCAGGATGCCTTT	
CDK1	F: TCCATCCCTCCTGGTCAGTT	173
	R: GCAAGGCCAAAATCAGCCAA	
PLK1	F: AGAACCCAATGTCTGAGCGG	115
	R: GCATTGACGCTGTGTAGCTG	
BIRC5	F: ACCGCGTCTCTACGTTCAAG	114
	R: CCAAGTCTGGCTCGTTCTCA	
CDCA5	F: AAAGAGGCTTGGGTTCCCTG	95
	R: AGTGTCCAGCATCTTCCTGC	
RB1	F: CTCTCACCTCCTGCATTGCT	104
	R: ATCCGTGCACTCCTGTTCTG	
P53	F: GAGTTCGTGACCGAGGTTGT	116
	R: TTGGCCCGCAAATTTCCTTC	

2.8 Molecular docking analysis

The three-dimensional structure of PAB was derived from PubChem database,[2] while the crystal structure of CDK1 was sourced from Protein Data Bank (PDB ID: 5LQF), The docking experiment between PAB and CDK1 was then performed using the Autodock Vina program, analyzing the binding energy between the ligand and the protein. The interactions were visualized using Pymol software.

2.9 Cell cycle analysis

For cell cycle analysis, the PAB-treated cells were collected, and fixed by 4% paraformaldehyde at room temperature. After treated with 0.2% Triton X-100 for 5 min, cells were washed with PBS, and incubated with DAPI (#C0065, Solarbio, Beijing, China) for 5 min in the dark. Then, BD FACSCelestaTM flow cytometry (Becton, Dickinson and Company, NJ, USA) was used for detecting.

2.10 Cellular thermal shift assay (CETSA)

In this procedure, U27 cells were exposed to PAB (2.5 μM) for 24 h before resuspended in PBS containing protease inhibitors (#HY-K0010, MCE, Shanghai, China). Both vehicle control and PAB-treated cells were systematically allocated into six experimental groups, with each group exposed to a defined thermal gradient ranging from 42 °C

1 www.majorbio.com

2 https://pubchem.ncbi.nlm.nih.gov/

to 67 °C at 5 °C intervals. Following a 3-min incubation at each temperature, cells were lysed by freeze–thaw cycles in liquid nitrogen. The supernatant collected after centrifugation was mixed with protein loading buffer (#LT101S, Epizyme, Shanghai, China) and boiled for 10 min prior to analysis by SDS-PAGE to quantify CDK1 protein expression and evaluate its thermal stability under PAB treatment.

2.11 Statistical analysis

All analyses were repeated in triplicate, and the data were expressed as mean ± standard deviation (SD). The measurement results were conducted statistical analysis using GraphPad Prism software. Differences between two groups were analyzed by student's t-test, and differences between three or more groups were analyzed by one-way ANOVA. Statistical details are provided in the respective figure legends. Differences with $p < 0.05$ were regarded as statistically significant.

3 Results

3.1 PAB suppresses the viability and proliferation of canine mammary tumor cells

To validate the functional effects of PAB (Figure 1A) in U27 cells, we treated them with varying concentrations of PAB (0, 0.625, 1.25, 2.5, 5, 10, and 20 μM) and investigated multiple biological processes, including proliferation and viability. We began with an LDH analysis to evaluate the toxic effects of PAB on U27 cells (Figure 1B). The results showed a highly significant cytotoxic effect ($p < 0.001$) in both low- and high-dose PAB-treated groups compared to the control group, indicating a significant loss of membrane integrity. We then assessed the impact of PAB on U27 cell viability using the CCK-8 assay. As expected, PAB suppressed U27 cell viability ($p < 0.001$), with higher concentrations of PAB significantly reducing cell viability (Figure 1C). Furthermore, crystal violet cell proliferation assay demonstrated that PAB could inhibit U27 cell proliferation ($p < 0.001$), with higher concentrations of PAB showing greater inhibition than lower concentrations (Figure 1D). The statistical results, presented in Figure 1E, show that PAB inhibited the proliferation of canine mammary tumor cells in a dose-dependent manner. Additionally, we observed that PAB exposure induced morphological alterations in U27 cells, characterized by a distinct rounding phenotype (Figure 1F). These results suggested that PAB effectively inhibits the viability and proliferation of canine mammary tumor cells.

3.2 PAB triggers apoptosis in canine mammary tumor cells via caspase activation

The induction of cancer cell death represents a fundamental objective of antineoplastic therapy, with apoptosis serving as a key mechanism for tumor suppression (22). We examined the apoptosis-inducing effects of PAB on U27 cells through flow cytometry and Western blot analysis. Flow cytometry revealed a significant increase in apoptotic tumor cells following PAB treatment ($p < 0.001$) (Figures 2A,B). To further confirm the pro-apoptotic effect of PAB on U27 cells, we analyzed changes in apoptotic marker protein expression (Figures 2C–G). Results showed downregulation of the inactive Caspase-9 precursor (pro-caspase-9) and significant increase in its cleaved, active form ($p < 0.001$). Processed caspase-3 fragment expressions were also elevated significantly ($p < 0.001$). Notably, dose-dependent upregulation of Bax ($p < 0.001$), a pro-apoptotic Bcl-2 family protein, occurred only at higher PAB concentrations (5–10 μM). Additionally, the ratio of Bcl2/Bax was downregulated after PAB treatment, indicating that the apoptotic pathway was activated. These results provide consistent evidence for the pro-apoptotic properties of PAB in U27 cells through caspase cascade activation and Bax modulation.

3.3 PAB alters the transcriptional landscape of canine mammary tumor cells

To systematically investigate PAB's molecular mechanism of action, we conducted whole-transcriptome analysis of U27 cells following PAB or vehicle (DMSO) treatment. Principal component analysis (PCA) demonstrated clear separation between treatment groups and tight clustering of biological replicates, indicating robust experimental reproducibility and significant transcriptomic changes induced by PAB (Figure 3A). Comparative transcriptomic profiling identified 899 differentially expressed genes (DEGs) ($p < 0.05$, $|\log2 FC| > 1.5$), comprising 349 up-regulated and 560 down-regulated transcripts (Figures 3B–D).

3.4 Functional enrichment of DEGs in PAB-treated canine mammary tumor cells

Enrichment analysis was conducted separately for DEGs to further explore the functions of DEGs. The top 20 Gene Ontologies (GO) and the Kyoto Encyclopedia of Genes and Genomes (KEGG) pathways that were significantly enriched in each group were selected for presentation. GO term enrichment results showed that the DEGs were mainly enriched in catalytic activity, binding, cellular anatomical entity, cellular process, and biological regulation (Figure 4A). In addition, according to KEGG analysis, DEGs indicated significant enrichment in gap junction, cell cycle, cellular senescence, IL-17 signaling pathway, protein digestion and absorption (Figure 4B).

To identify potential protein targets of PAB, we performed protein–protein interaction (PPI) network analysis of DEGs, showing that *ELOVL7*, *PCNA*, *CREBBP*, *MED1*, *SNAP23*, and *CDK1* were hub genes (Figure 4C). By integrating the GTEx and TCGA databases, we analyzed the expression differences of these hub genes between human breast cancer patients and normal populations. Our analysis revealed that CDK1 gene was significantly upregulated, suggesting its potential role in breast cancer pathogenesis (Supplementary Figure S1). Notably, both RNA-seq and RT-qPCR analyses consistently demonstrated significant downregulation of CDK1 mRNA expression following PAB treatment (Figure 4D), which strongly suggests that CDK1 plays a crucial role in mediating PAB's anti-tumor effects. To validate the RNA-seq results, we randomly selected three DEGs for RT-qPCR verification. The expression patterns of these genes were

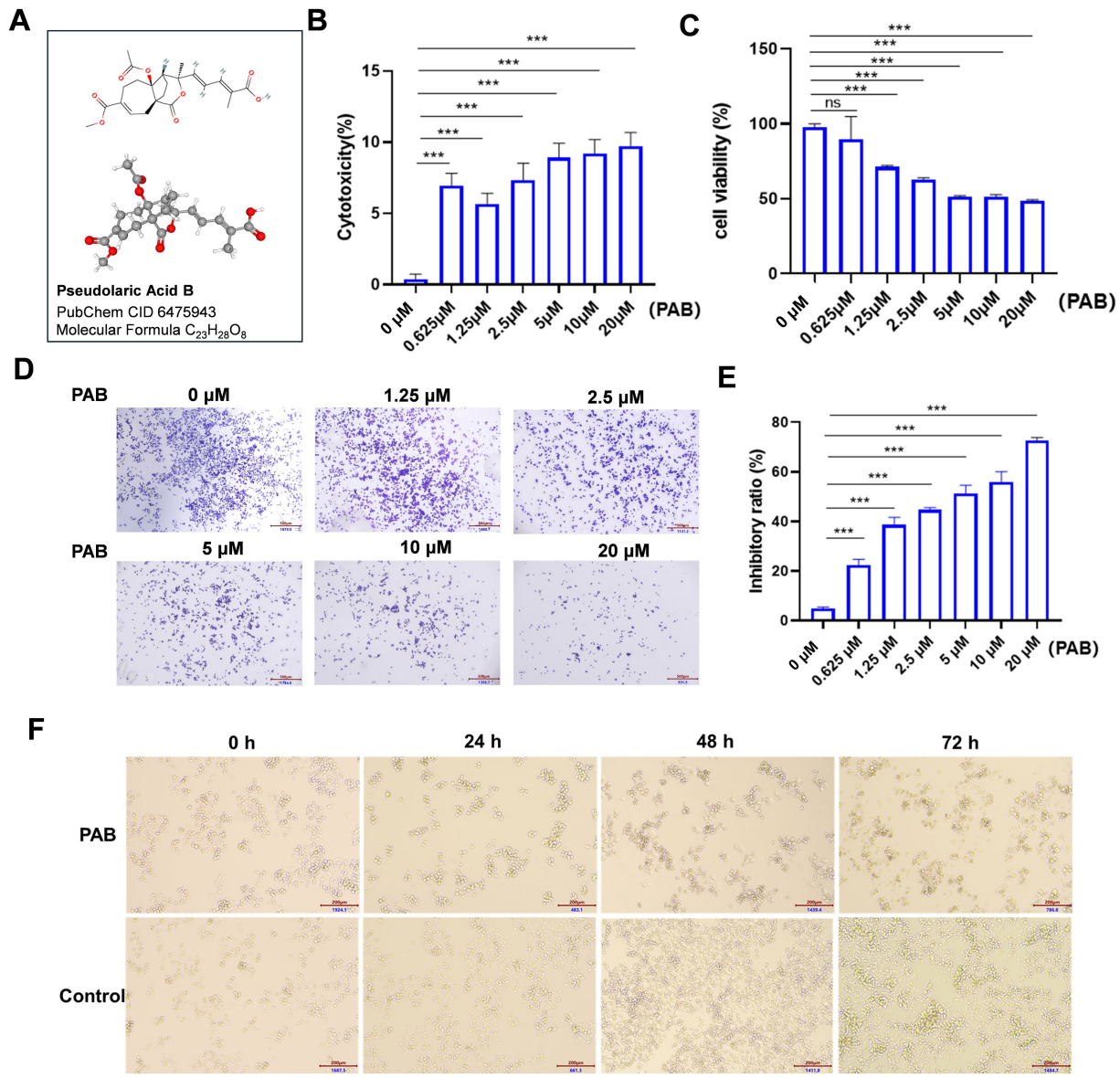

FIGURE 1
PAB inhibited the proliferation and viability in canine mammary tumor U27 cells. **(A)** Chemical structure of PAB. **(B,C)** Canine mammary tumor U27 cells were exposed to different concentrations of PAB (0, 0.625, 1.25, 2.5, 5, 10 or 20 μM) for 24 h, LDH activity **(B)** in the supernatant was quantified using a colorimetric assay by measuring absorbance at 490 nm and the cell viability **(C)** of canine mammary tumor U27 cells was detected by CCK-8 assay. **(D)** Representative images of the proliferative ability of canine mammary tumor U27 cells treated with PAB (0, 0.625, 1.25, 2.5, 5, 10 or 20 μM) via crystal violet cell proliferation assay. **(E)** Quantitative analysis of cells stained with crystal violet. Values represent mean ± SD of three biological replicates. **(F)** Representative images of morphological changes of U27 cells after PAB exposure at varying time points. DMSO-treated control cells maintained normal morphology and PAB-treated (2.5 μM) cells exhibited significant rounding. Scale bar: 200 μm. Unpaired two-tailed Student's *t*-test or one-way ANOVA was performed. ***$p < 0.001$, **$p < 0.01$, *$p < 0.05$, ns, not significant.

fully consistent with the RNA-seq data (Figure 4D), confirming the reliability and reproducibility of our transcriptome analysis.

3.5 PAB induces G2/M cell cycle arrest through CDK1 targeting

Considering the important role of CDK1 in the development and progression of multiple cancers and that PAB can significantly regulate CDK1 (23), this phenomenon was subsequently investigated in depth. Molecular docking results showed that PAB was able to bind to HIS120 (2.2 Å), ARG123 (3.1 Å), LYS311 (2.8 Å), TYR175 (3.1 Å), SER167 (2.8 Å), and TYR175 (2.9 Å) of CDK1 (Figure 5A). And the calculated binding energy between PAB and CDK1 is −7.7 kJ/mol. This energetically favorable interaction was associated with significant biological effects, as evidenced by Western blot analysis showing a marked reduction in CDK1 protein levels following PAB treatment (Figure 5B). CETSA demonstrated compound-protein interactions via temperature-induced

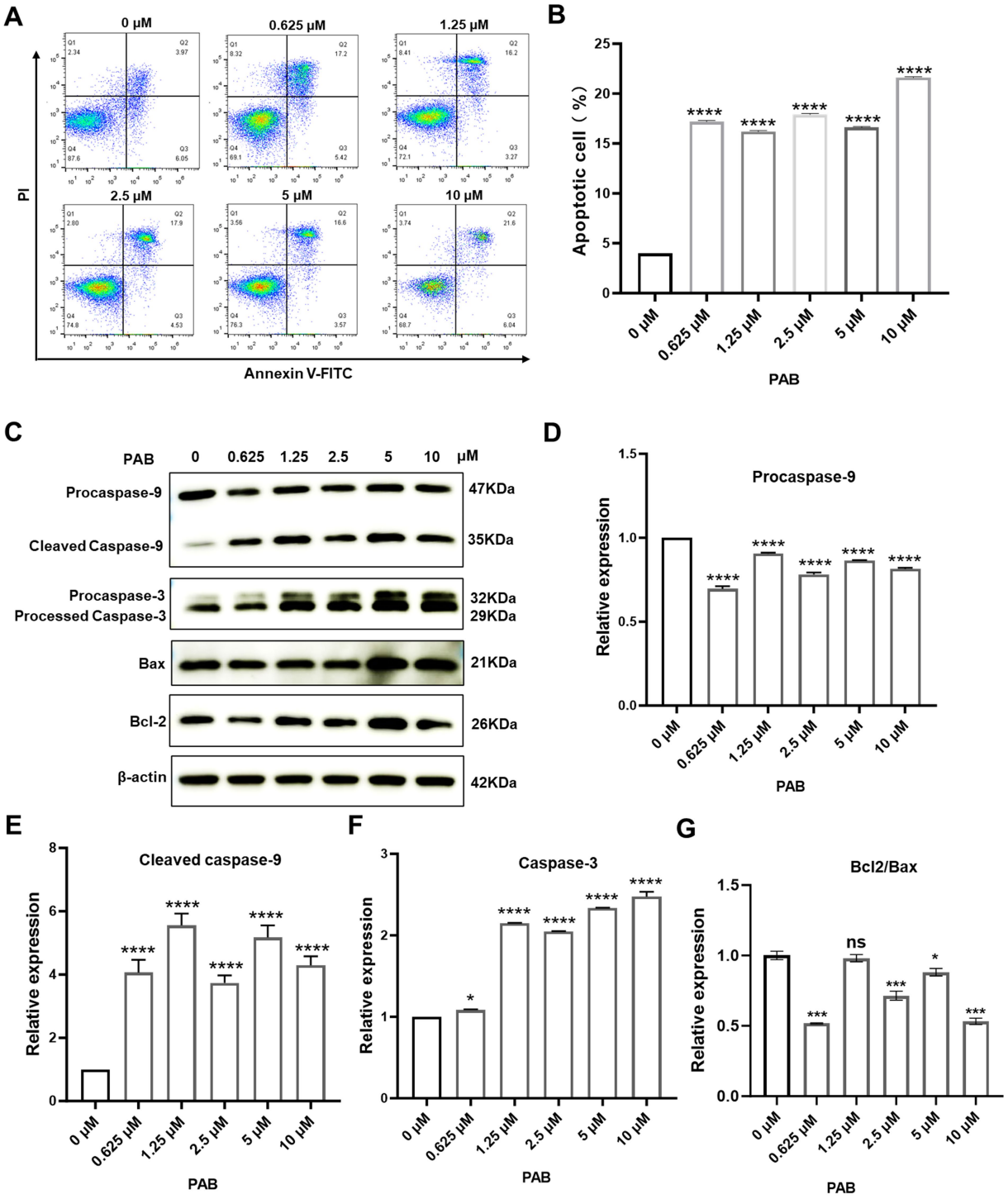

FIGURE 2
PAB triggered apoptosis through caspase activation in canine mammary tumor cells. **(A)** Flow cytometry was performed to determine the percentage of apoptotic canine mammary tumor U27 cells after 24 h of treatment with PAB (0, 0.625, 1.25, 2.5, 5 or 10 μM). **(B)** Quantitative analysis of late (end-stage) apoptotic cells (Q2). Data are presented as the percentage of apoptotic cells relative to the total population. **(C–G)** Western blot analysis **(C)** was conducted to evaluate apoptotic markers (procaspase-9, cleaved caspase-9, caspase-3, Bax and Bcl2) in canine mammary tumor U27 cells treated with PAB (0, 0.625, 1.25, 2.5, 5 or 10 μM) for 24 h. **(D–G)** Quantitative results of protein expression. β-Actin served as an internal reference and quantitative analysis of band intensities was performed using ImageJ software. Values represent mean ± SD of three biological replicates. Unpaired two-tailed Student's *t*-test or one-way ANOVA was performed. ****$p < 0.0001$, ***$p < 0.001$, **$p < 0.01$, *$p < 0.05$, ns, not significant.

denaturation, confirming PAB binding to CDK1, which promoted thermal destabilization and degradation of CDK1 at elevated temperatures (52–67 °C) (Figures 5C,D). The concurrent demonstration of both computational binding and functional downregulation strongly supports CDK1 as a potential binding site of PAB in canine mammary tumor cells.

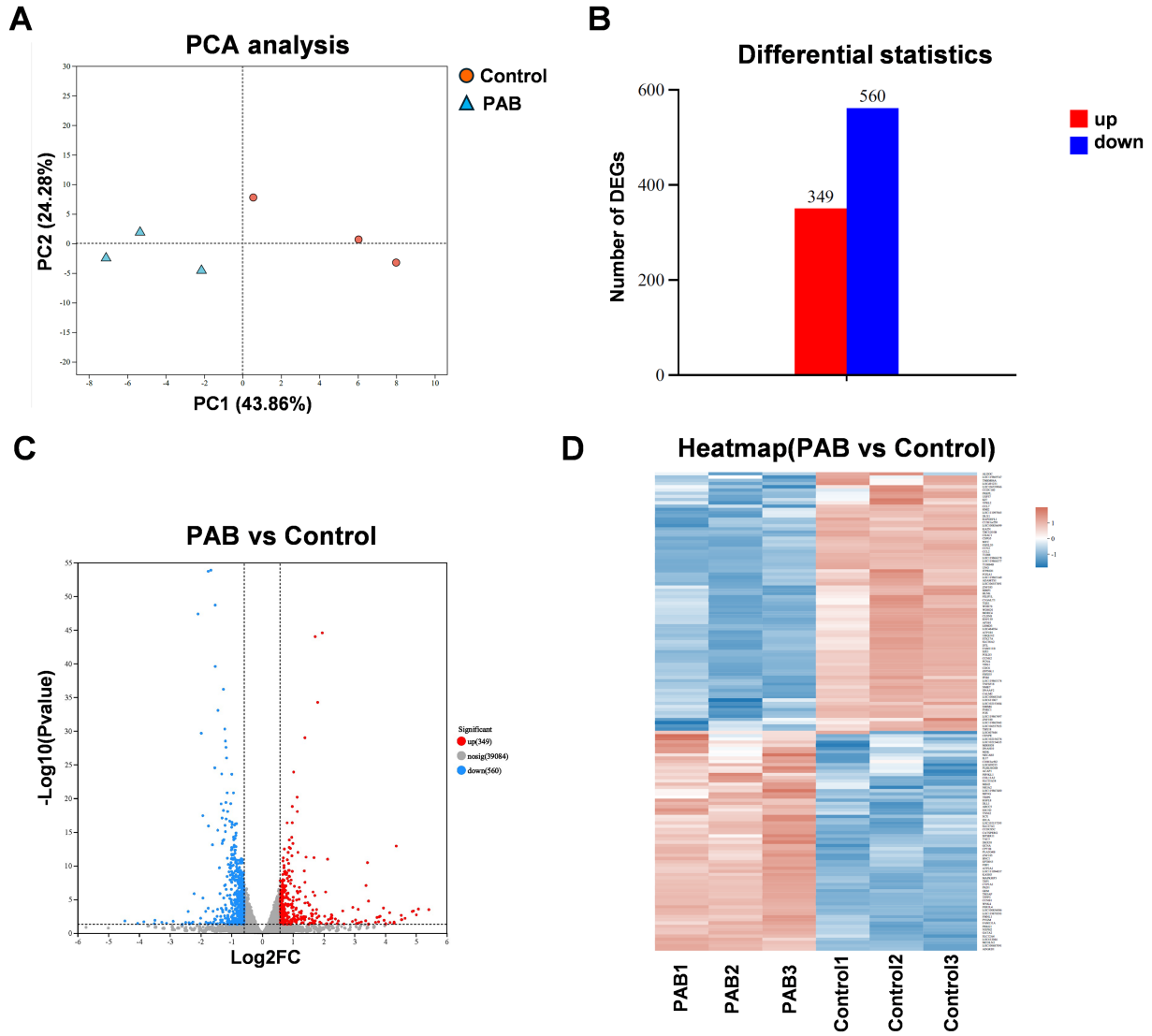

FIGURE 3
Different expression analysis in genes of canine mammary tumor cells treated with PAB. Canine mammary tumor U27 cells were seeded in 6-well plates and treated with PAB (2.5 μM) or an equivalent concentration of DMSO (vehicle control) for 24 h (n = 3). **(A)** PCA score plot of the transcriptomics. **(B)** Number of differentially expressed genes (DEGs) upregulated and downregulated. **(C)** Volcano plot showing DEGs of RNA-seq data. **(D)** The heatmap displayed the upregulated DEGs and downregulated DEGs ranked by fold change.

To further explore the properties of PAB-CDK1 interaction, we compared the effects of the CDK1 inhibitor Ro-3306 with those of PAB on canine mammary tumor cells. Similar to PAB, Ro-3306 significantly inhibited cell viability at elevated concentrations (Figure 5E). Furthermore, quantification of CDK1-dependent downstream gene expression revealed that PAB produced comparable suppressive effects to Ro-3306 (Figures 5F–J). Given CDK1's pivotal role in controlling G2/M phase transition, whether PAB-mediated CDK1 downregulation affects cell cycle progression in U27 cells was investigated. Flow cytometric analysis revealed a dose-dependent accumulation of cells in G2/M phase following PAB treatment (66.0% at 1.25 μM vs. 35.7% in control, Figures 5K–M). This cell cycle blockade correlated with the observed reduction in CDK1 protein levels, strongly suggesting that PAB's anti-tumor activity is mediated, at least in part, through CDK1-related inhibition of G2/M progression.

4 Discussion

Canine mammary tumors, predominantly affecting female dogs, represent the most prevalent neoplastic condition in this population. While the majority of canine mammary tumors exhibit benign biological behavior, approximately 50% of malignant canine neoplasms are attributed to mammary malignancies (24). Surgical resection remains the gold standard for canine mammary carcinoma treatment. While conventional chemotherapeutics (e.g., cyclophosphamide, 5-fluorouracil, doxorubicin) adapted from human breast cancer protocols have been employed in veterinary practice (25, 26). Their efficacy is often limited by dose-limiting toxicities, drug resistance, and high recurrence rates (27). Given the unlimited proliferative potential of cancer cells, the main strategy of cancer treatment is to induce cancer cell death and inhibit tumor proliferation (28). Studies have

10.3389/fvets.2025.1644200

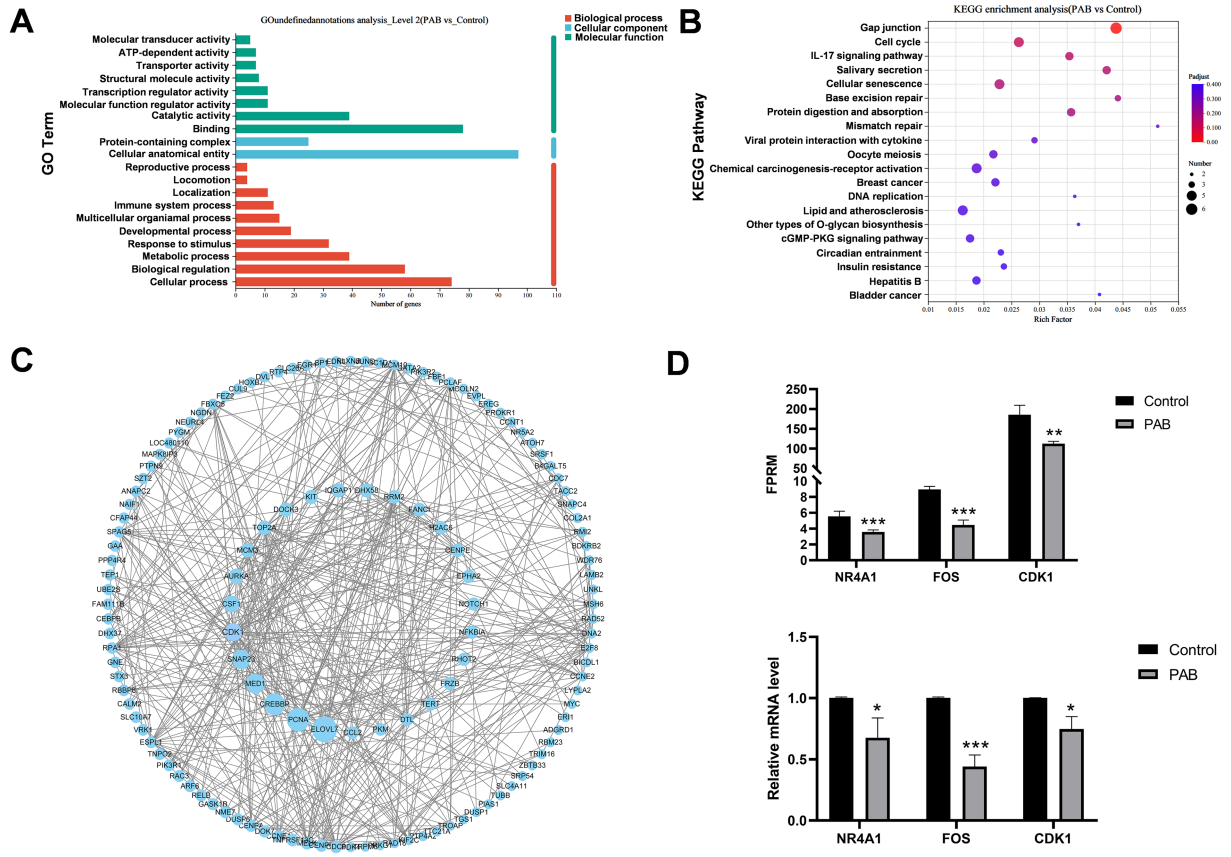

FIGURE 4
Functional enrichment analysis of DEGs in canine mammary tumor cells treated with PAB. Canine mammary tumor U27 cells were seeded in 6-well plates and treated with PAB (2.5 μM) or an equivalent concentration of DMSO (vehicle control) for 24 h (n = 3). **(A)** GO enrichment analysis of DEGs. **(B)** KEGG enrichment analysis of DEGs. The size of the dots represents the number of differential genes, and the intensity of the color represents the level of significance (the redder the color, the smaller the p-value) **(C)** PPI analysis of DEGs was performed using Cytoscape software. DEGs are arranged according to the betweenness centrality. The larger betweenness centrality, the larger the circle. **(D)** Validation of DEGs expression using RT-qPCR. *GAPDH* gene as a standardized internal reference. N = 3 for each group. Values represent mean ± SD of three biological replicates. Unpaired two-tailed Student's t-test was performed. ***p < 0.001, **p < 0.01, *p < 0.05, ns, not significant. FPRM, Fragments Per Kilobase of exon model per Million mapped fragments.

shown that PAB exerts antitumor effects through multiple pathways, including significant inhibition tumor cell growth, induction tumor cell apoptosis, and inhibition tumor invasion and migration (29). However, the molecular mechanisms of PAB in cancer remain largely unexplored. Here, the anti-tumor bioactivity of PAB was investigated *in vitro*, and PAB altered the morphology of canine mammary tumor U27 cells, inhibited cell proliferation and promoted apoptosis. The target and mechanisms of PAB action were preliminarily predicted by RNA-seq and computational simulation analysis. These findings highlight PAB's potential as a selective therapeutic agent for canine mammary cancer, while simultaneously providing novel conceptual frameworks for advancing anticancer drug development from natural product-derived anticancer agents in veterinary oncology.

The anti-cancer activity of PAB has been studied in several cancer types. In esophageal squamous cell carcinoma, PAB could inhibit cancer cell proliferation, invasion and angiogenesis by regulating CD147 (29). In melanoma cells, PAB induces apoptosis through p53 and Bax/Bcl-2 pathways. There are also reports showing PAB may induce apoptosis dependent on the AKT/mTOR, NF-κB, p38, caspase pathways (10, 30, 31). The present study found that PAB promoted apoptosis in canine mammary tumor cells and increased the expression of Bax, caspase-3, cleaved-caspase-9, and processed-caspase-3, and that the high catalytic activity of cysteine asparaginase-3 is a common initiator of apoptotic cell death. It has been previously shown that in response to stimulation by pro-apoptotic factors, Bax proteins migrate from the cytoplasm to the outer mitochondrial membrane, altering the permeability of the outer mitochondrial membrane and facilitating the mitochondrial release of Cyt-c (32). The release of Cyt-c results in the formation of an apoptotic vesicle complex by binding Cyt-c to Apaf-1, procaspase-9 and dATP. The dimeric complex activates first caspase-9 and then caspase-3, and these activations lead to apoptosis (33, 34). These findings support the hypothesis that PAB-induced apoptosis in canine mammary cancer involves the mitochondrial pathway, though further mechanistic investigation is warranted.

To further explore the underlying mechanisms of PAB in canine mammary cancer, we performed transcriptomic sequencing. The results suggested that PAB-treated canine mammary tumor cells were involved in multiple cellular functions, including gap junction, cell cycle, cellular senescence, mismatch repair. Gap junctions are a unique form of cellular connectivity that contribute to cancer cell invasion, increase

10.3389/fvets.2025.1644200

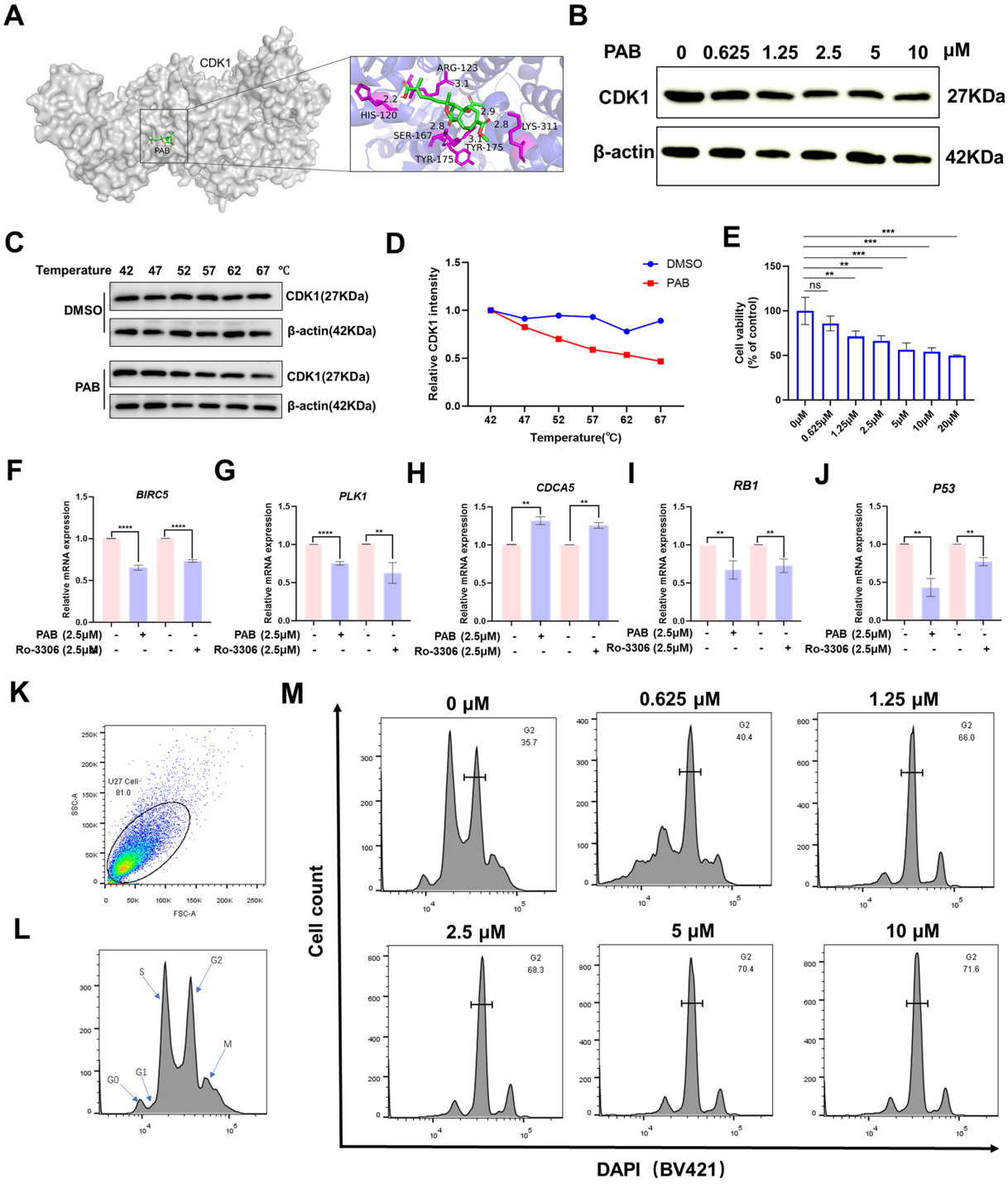

FIGURE 5
PAB induced G2/M cell cycle arrest by modulation of CDK1. **(A)** Molecular docking computer simulation predicts the binding site of PAB and CDK1 protein. **(B)** Western blot analysis of CDK1 protein expression under different concentrations (0, 0.625, 1.25, 2.5, 5 or 10 μM) for 24 h of PAB-treated canine mammary tumor U27 cells. β-Actin served as an internal reference and quantitative analysis of band intensities was performed using ImageJ software. **(C,D)** Representative western blot images of PAB (2.5 μM) and CDK1 from the CETSA (U27 cells, at 42 to 67 °C) and quantitatively analyzed using Image J software (n = 3). **(E)** Canine mammary tumor U27 cells were exposed to different concentrations of Ro-0036 (0, 0.625, 1.25, 2.5, 5, 10 or 20 μM) for 24 h, the cell viability of canine mammary tumor U27 cells was detected by CCK-8 assay. **(F–J)** CDK1 downstream target genes (*BIRC5*, *PLK1*, *CDCA5*, *RB1*, *P53*) mRNA expression levels were assayed after PAB or Ro-3306 treatment of U27 canine mammary tumor cells. Unpaired two-tailed Student's t-test or one-way ANOVA was performed. **(K–M)** The cell cycle distribution of PAB-treated (0, 0.625, 1.25, 2.5, 5 or 10 μM) canine mammary tumor U27 cells for 12 h was determined by flow cytometry using DAPI staining.

nutrient supply and waste removal within the tumor, and interact with immune cells to evade detection (35, 36). Studies have shown that PAB treatment induces L929 cell cycle blocking and induces cell aging in mouse fibrosarcoma (37). Similarly, our study found that the differential

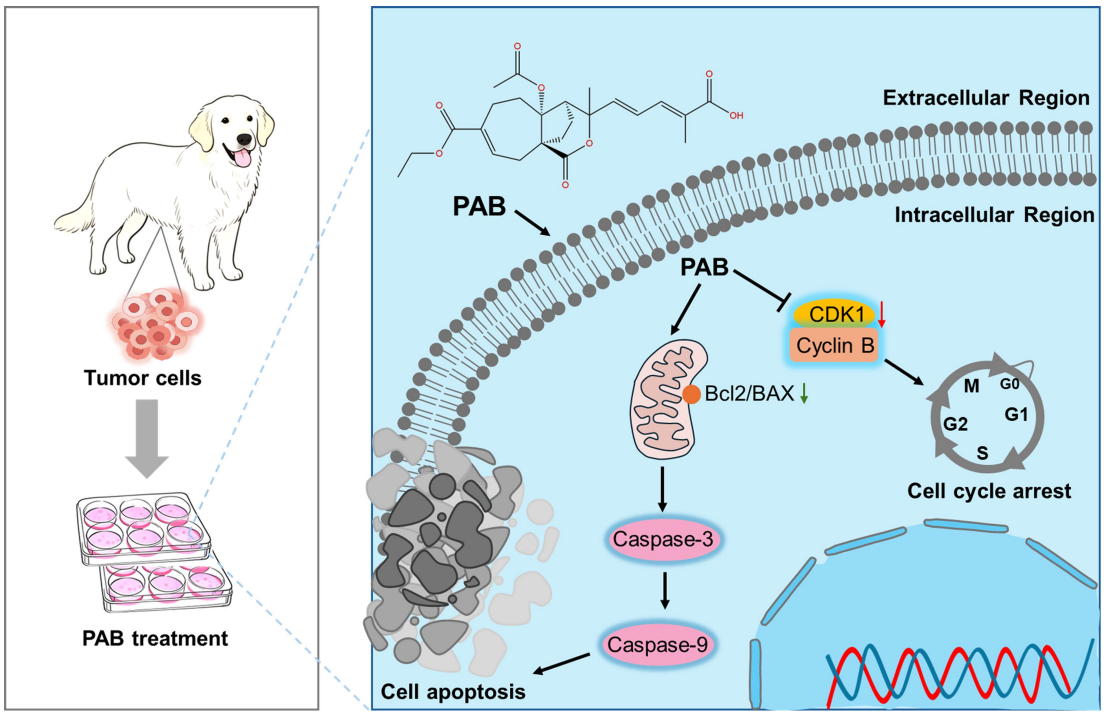

FIGURE 6
Schematic illustration of the molecular mechanism of PAB against canine mammary tumor *via* promoting tumor apoptosis and cell cycle blockade.

expression genes of canine mammary tumor cells after PAB treatment were significantly enriched in the cell cycle and cell aging signaling pathways. Breast carcinogenesis commonly arises from functional alterations or genetic mutations in key regulatory proteins, resulting in abnormal activation or suppression of critical signaling cascades (38). Subsequent PPI analysis of differential genes identified CDK1 as a key PAB target, with this protein playing a pivotal role in cell cycle regulation. Its expression was significantly upregulated in tumor tissue, while the expression was significantly downregulated after PAB treatment.

Previous studies have reported PAB as a cell cycle inhibitor, while CDK1 is a key mediator regulating the G2/M transition (8). PAB treatment induced cell cycle arrest at the G2/M phase in this study. Molecular docking analysis and CETSA results revealed the binding of PAB to CDK1 promoted the degradation of CDK1, reducing the thermal stability of CDK1, further supporting CDK1 as a potential functional target of PAB. Consistent with the phenomenon that senescence and cell death spontaneously occur during or following mitotic arrest in both normal and cancer cells, RNA sequencing identified that differentially expressed genes were predominantly enriched in cell cycle progression and cellular senescence signaling pathways (39). Our findings collectively reveal that PAB triggers cell cycle arrest by targeting CDK1, thereby inducing cellular senescence and apoptosis. This mechanism underscores the therapeutic potential of PAB in modulating cell fate through CDK1-dependent pathways.

In summary, as a natural product-derived agent, PAB demonstrates distinct advantages over conventional chemotherapeutics by addressing critical limitations such as drug resistance and systemic toxicity through its multi-target mechanisms. Our data suggested CDK1-dependent cell cycle arrest as the central mechanism driving PAB-induced senescence and mitochondrial apoptosis (Figure 6). The compound's ability to simultaneously target proliferative signaling and activate intrinsic apoptotic pathways addresses critical challenges in veterinary oncology, particularly tumor recurrence and chemoresistance. While these findings highlight the translational potential of PAB, certain limitations must be addressed, including *in vivo* validation of CDK1 targeting efficacy and pharmacokinetic optimization in future studies. Furthermore, comparative studies across species may elucidate conserved mechanisms to bridge veterinary and human anticancer drug development. This work not only advances natural product-based therapeutics for CMTs but also establishes a paradigm for mechanism-driven drug discovery in companion animal cancers.

Data availability statement

Sequence data that support the findings of this study have been deposited in the National Center for Biotechnology Information with the primary accession code PRJNA1290691.

Ethics statement

Ethical approval was not required for the studies on animals in accordance with the local legislation and institutional requirements because only commercially available established cell lines were used.

Author contributions

MC: Data curation, Methodology, Visualization, Writing – original draft. HH: Investigation, Methodology, Writing – review & editing. MQ: Investigation, Visualization, Writing – review &

editing. HL: Investigation, Visualization, Writing – review & editing. QL: Investigation, Visualization, Writing – review & editing. XH: Investigation, Visualization, Writing – review & editing. QM: Conceptualization, Funding acquisition, Supervision, Writing – original draft, Writing – review & editing. SX: Supervision, Validation, Writing – review & editing.

Funding

The author(s) declare that financial support was received for the research and/or publication of this article. This work was supported by the National Natural Science Foundation of China (Grant No. 32502996) to SX; the Ministry of Human Resources and Social Security of China (Grant No. 109-23XM0447) to QM; and the High-level Talent Support Program of Henan Agricultural University (Grant Nos. 111-30501275 and 111-30501434) to QM and SX.

Conflict of interest

The authors declare that the research was conducted in the absence of any commercial or financial relationships that could be construed as a potential conflict of interest.

Generative AI statement

The authors declare that no Gen AI was used in the creation of this manuscript.

Any alternative text (alt text) provided alongside figures in this article has been generated by Frontiers with the support of artificial intelligence and reasonable efforts have been made to ensure accuracy, including review by the authors wherever possible. If you identify any issues, please contact us.

Publisher's note

Supplementary material

The Supplementary material for this article can be found online at: https://www.frontiersin.org/articles/10.3389/fvets.2025.1644200/full#supplementary-material

References

1. Pinho SS, Carvalho S, Cabral J, Reis CA, Gärtner F. Canine tumors: a spontaneous animal model of human carcinogenesis. *Transl Res*. (2012) 159:165–72. doi: 10.1016/j.trsl.2011.11.005

2. Kaszak I, Witkowska-Piłaszewicz O, Domrazek K, Jurka P. The novel diagnostic techniques and biomarkers of canine mammary tumors. *Vet Sci*. (2022) 9:526. doi: 10.3390/vetsci9100526

3. Kim T-M, Yang IS, Seung B-J, Lee S, Kim D, Ha Y-J, et al. Cross-species oncogenic signatures of breast cancer in canine mammary tumors. *Nat Commun*. (2020) 11:3616. doi: 10.1038/s41467-020-17458-0

4. Choong GM, Cullen GD, O'Sullivan CC. Evolving standards of care and new challenges in the management of HER2-positive breast cancer. *CA Cancer J Clin*. (2020) 70:355–74. doi: 10.3322/caac.21634

5. Miao Q, Deng W-Q, Lyu W-Y, Sun Z-T, Fan S-R, Qi M, et al. Erianin inhibits the growth and metastasis through autophagy-dependent ferroptosis in KRASG13D colorectal cancer. *Free Radic Biol Med*. (2023) 204:301–12. doi: 10.1016/j.freeradbiomed.2023.05.008

6. Ma Z, Xiang X, Li S, Xie P, Gong Q, Goh B-C, et al. Targeting hypoxia-inducible factor-1, for cancer treatment: recent advances in developing small-molecule inhibitors from natural compounds. *Semin Cancer Biol*. (2022) 80:379–90. doi: 10.1016/j.semcancer.2020.09.011

7. Luo D, He F, Liu J, Dong X, Fang M, Liang Y, et al. Pseudolaric acid B suppresses NSCLC progression through the ROS/AMPK/mTOR/autophagy signalling pathway. *Biomed Pharmacother*. (2024) 175:116614. doi: 10.1016/j.biopha.2024.116614

8. Chiu P, Leung LT, Ko BCB. Pseudolaric acids: isolation, bioactivity and synthetic studies. *Nat Prod Rep*. (2010) 27:1066–83. doi: 10.1039/b906520m

9. Liu M-L, Sun D, Li T, Chen H. A systematic review of the immune-regulating and anticancer activities of Pseudolaric acid B. *Front Pharmacol*. (2017) 8:394. doi: 10.3389/fphar.2017.00394

10. Wang D, Xin Y, Tian Y, Li W, Sun D, Yang Y. Pseudolaric acid B inhibits gastric cancer cell metastasis in vitro and in haematogenous dissemination model through PI3K/AKT, ERK1/2 and mitochondria-mediated apoptosis pathways. *Exp Cell Res*. (2017) 352:34–44. doi: 10.1016/j.yexcr.2017.01.012

11. Yu J, Cui Q, Jiang Y, Yang W, Tashiro S, Onodera S, et al. Pseudolaric acid B induces apoptosis, senescence, and mitotic arrest in human breast cancer MCF-7. *Acta Pharmacol Sin*. (2007) 28:1975–83. doi: 10.1111/j.1745-7254.2007.00706.x

12. Guan D, Li C, Lv X, Yang Y. Pseudolaric acid B inhibits PAX2 expression through Wnt signaling and induces BAX expression, therefore promoting apoptosis in HeLa cervical cancer cells. *J Gynecol Oncol*. (2019) 30:e77. doi: 10.3802/jgo.2019.30.e77

13. Zeng K, Li W, Wang Y, Zhang Z, Zhang L, Zhang W, et al. Inhibition of CDK1 overcomes Oxaliplatin resistance by regulating ACSL4-mediated Ferroptosis in colorectal Cancer. *Adv Sci*. (2023) 10:2301088. doi: 10.1002/advs.202301088

14. Truman AW, Kristjansdottir K, Wolfgeher D, Hasin N, Polier S, Zhang H, et al. CDK-dependent Hsp70 phosphorylation controls G1 cyclin abundance and cell-cycle progression. *Cell*. (2012) 151:1308–18. doi: 10.1016/j.cell.2012.10.051

15. Mohamed TMA, Ang Y-S, Radzinsky E, Zhou P, Huang Y, Elfenbein A, et al. Regulation of cell cycle to stimulate adult cardiomyocyte proliferation and cardiac regeneration. *Cell*. (2018) 173:104–116.e12. doi: 10.1016/j.cell.2018.02.014

16. Santamaría D, Barrière C, Cerqueira A, Hunt S, Tardy C, Newton K, et al. Cdk1 is sufficient to drive the mammalian cell cycle. *Nature*. (2007) 448:811–5. doi: 10.1038/nature06046

17. He J, Gao R, Yang J, Li F, Fu Y, Cui J, et al. NCAPD2 promotes breast cancer progression through E2F1 transcriptional regulation of CDK1. *Cancer Sci*. (2023) 114:896–907. doi: 10.1111/cas.15347

18. Zhou Y, Han C, Li D, Yu Z, Li F, Li F, et al. Cyclin-dependent kinase 11(p110) (CDK11(p110)) is crucial for human breast cancer cell proliferation and growth. *Sci Rep*. (2015) 5:10433. doi: 10.1038/srep10433

19. Wang Q, Bode AM, Zhang T. Targeting CDK1 in cancer: mechanisms and implications. *Npj Precis Oncol*. (2023) 7:58–14. doi: 10.1038/s41698-023-00407-7

20. Han Z, Jia Q, Zhang J, Chen M, Wang L, Tong K, et al. Deubiquitylase YOD1 regulates CDK1 stability and drives triple-negative breast cancer tumorigenesis. *J Exp Clin Cancer Res*. (2023) 42:228. doi: 10.1186/s13046-023-02781-3

21. Kang J, Sergio CM, Sutherland RL, Musgrove EA. Targeting cyclin-dependent kinase 1 (CDK1) but not CDK4/6 or CDK2 is selectively lethal to MYC-dependent human breast cancer cells. *BMC Cancer*. (2014) 14:32. doi: 10.1186/1471-2407-14-32

22. Nosalova N, Huniadi M, Horňáková Ľ, Valenčáková A, Horňák S, Nagoos K, et al. Canine mammary tumors: classification, biomarkers, traditional and personalized therapies. *Int J Mol Sci*. (2024) 25:2891. doi: 10.3390/ijms25052891

23. Xie B, Wang S, Jiang N, Li JJ. Cyclin B1/CDK1-regulated mitochondrial bioenergetics in cell cycle progression and tumor resistancecyclin B1/CDK1. *Cancer Lett*. (2019) 443:56–66. doi: 10.1016/j.canlet.2018.11.019

24. Ferreira T, da Costa RMG, Dias F, Gama A, Gaspar VM, Mano JF, et al. Exploring the role of microRNAs as diagnostic and prognostic biomarkers in canine mammary tumors. *GeroScience*. (2024) 46:6641–57. doi: 10.1007/s11357-024-01260-7

25. Sorenmo K. Canine mammary gland tumors. *Vet Clin North Am Small Anim Pract*. (2003) 33:573–96. doi: 10.1016/s0195-5616(03)00020-2

26. Huang Y-Y, Chen C-H, Hsu C-H, Kuo T-Y, Liu C-C, Liao AT-C, et al. Inhibiting autophagy potentiates the antitumor efficacy of *Euphorbia royleana* for canine mammary gland tumors. *BMC Vet Res*. (2020) 16:193. doi: 10.1186/s12917-020-02408-1

27. Wu C-C, Chang C-Y, Chou P-Y, Chan X-Y, Huang C-C, Yang Y, et al. Multiplexed immunoassay for a serum autoantibody biomarker panel in diagnostic and prognostic prediction of canine mammary tumors. *Vet Q*. (2025) 45:1–12. doi: 10.1080/01652176.2024.2435978

28. Li J, Liu S, Chen J, Wang H, Feng X, Jia C, et al. Uncovering the underlying mechanism of yuanhuacine against colorectal cancer by transcriptomics and experimental investigations. *Phytomedicine*. (2025) 140:156570. doi: 10.1016/j.phymed.2025.156570

29. Yin Z, Cai H, Wang Z, Jiang Y. Pseudolaric acid B inhibits proliferation, invasion, and angiogenesis in esophageal squamous cell carcinoma through regulating CD147. *Drug Des Devel Ther*. (2020) 14:4561–73. doi: 10.2147/DDDT.S269915

30. Wen C, Chen J, Zhang D, Wang H, Che J, Qin Q, et al. Pseudolaric acid B induces mitotic arrest and apoptosis in both 5-fluorouracil-sensitive and -resistant colorectal cancer cells. *Cancer Lett*. (2016) 383:295–308. doi: 10.1016/j.canlet.2016.09.007

31. Tong J, Yin S, Dong Y, Guo X, Fan L, Ye M, et al. Pseudolaric acid B induces caspase-dependent apoptosis and autophagic cell death in prostate cancer cells. *Phytother Res*. (2013) 27:885–91. doi: 10.1002/ptr.4808

32. Ashkenazi A, Fairbrother WJ, Leverson JD, Souers AJ. From basic apoptosis discoveries to advanced selective BCL-2 family inhibitors. *Nat Rev Drug Discov*. (2017) 16:273–84. doi: 10.1038/nrd.2016.253

33. Saito M, Korsmeyer SJ, Schlesinger PH. BAX-dependent transport of cytochrome c reconstituted in pure liposomes. *Nat Cell Biol*. (2000) 2:553–5. doi: 10.1038/35019596

34. Zhu ZJ, Teng M, Li HZ, Zheng LP, Liu JL, Yao Y, et al. Virus-encoded miR-155 ortholog in Marek's disease virus promotes cell proliferation via suppressing apoptosis by targeting tumor suppressor WWOX. *Vet Microbiol*. (2021) 252:108919. doi: 10.1016/j.vetmic.2020.108919

35. Ruch R. Gap junctions and Connexins in Cancer formation, progression, and therapy. *Cancer*. (2020) 12:3307. doi: 10.3390/cancers12113307

36. Dong H, Pei Q, Ren J, Zhang Y, Wei X, Shen A, et al. Cholesterol-dependent Nsp5-endosomes co-trafficking to lysosomes facilitates porcine reproductive and respiratory syndrome virus replication by activating autophagy. *Vet Microbiol*. (2025) 305:110507. doi: 10.1016/j.vetmic.2025.110507

37. Yu J h, Liu C y, Zheng G b, Zhang LY, Yan M h, Zhang W y, et al. Pseudolaric acid B induced cell cycle arrest, autophagy and senescence in murine fibrosarcoma l929 cell. *Int J Med Sci*. (2013) 10:707–18. doi: 10.7150/ijms.5726

38. Mei C, Liu Y, Liu Z, Zhi Y, Jiang Z, Lyu X, et al. Dysregulated signaling pathways in canine mammary tumor and human triple negative breast cancer: advances and potential therapeutic targets. *Int J Mol Sci*. (2024) 26:145. doi: 10.3390/ijms26010145

39. Jiang L, Wen C, He Q, Sun Y, Wang J, Lan X, et al. *Pseudolaric acid B* induces mitotic arrest and apoptosis in both imatinib-sensitive and -resistant chronic myeloid leukaemia cells. *Eur J Pharmacol*. (2020) 876:173064. doi: 10.1016/j.ejphar.2020.173064

frontiers | Frontiers in Veterinary Science

TYPE Original Research
PUBLISHED 17 October 2025
DOI 10.3389/fvets.2025.1679013

OPEN ACCESS

EDITED BY
Shuaiyu Wang,
China Agricultural University, China

REVIEWED BY
Spase Stojanov,
Institut Jožef Stefan (IJS), Slovenia
Yun Ji,
China Agricultural University, China
Mohib Kakar,
Beijing Institute of Technology, China

*CORRESPONDENCE
Xianghua Shu
✉ ynndsxh@ynau.edu.cn

†These authors have contributed equally to this work

RECEIVED 04 August 2025
ACCEPTED 22 September 2025
PUBLISHED 17 October 2025

CITATION
Song C, Wei Q, Shen H, Zhang X, Pan D, Zhang Z, Zhang Y, Yang S and Shu X (2025) Therapeutic potential of *Glycyrrhiza* polysaccharides in pseudorabies virus infection: immune modulation, antioxidant activity, and gut microbiota restoration. *Front. Vet. Sci.* 12:1679013. doi: 10.3389/fvets.2025.1679013

Therapeutic potential of *Glycyrrhiza* polysaccharides in pseudorabies virus infection: immune modulation, antioxidant activity, and gut microbiota restoration

Chunlian Song[1†], Qianfei Wei[1†], Hong Shen[2], Xue Zhang[1], Deng Pan[1], Zhihui Zhang[1], Ying Zhang[1], Shanhai Yang[3] and Xianghua Shu[1*]

[1]The Yunnan Key Laboratory of Veterinary Etiological Biology, College of Veterinary Medicine, Yunnan Agricultural University, Kunming, China, [2]Tacheng Animal Husbandry and Veterinary Station, Tacheng, China, [3]Mangshi Animal Husbandry Station, Mangshi, China

Aim of the study: This study aimed to evaluate the protective effects of *Glycyrrhiza* polysaccharides (GPs) on Pseudorabies virus (PRV)-infected mice and elucidate their mechanisms of action, with a focus on intestinal immunity, oxidative stress, mucosal barrier function, and gut microbiota composition.
Materials and methods: GPs were extracted via hot water extraction and ethanol precipitation. Seventy-two SPF-grade male mice were randomly divided into six groups and treated with different doses of GPs or *Astragalus* polysaccharides (APS), followed by PRV challenge. Clinical parameters, inflammatory cytokines (TNF-α, IL-6, IL-4, IL-10), oxidative stress markers (SOD, CAT, MDA), histopathology, tight junction protein expression (Occludin, ZO-1), sIgA levels, intestinal permeability, viral load, and gut microbiota profiles were assessed.
Results: GP administration significantly alleviated PRV-induced symptoms, reduced mortality and disease activity index, and improved food intake. Medium and high doses notably downregulated TNF-α and IL-6, while upregulating IL-4 and IL-10. Antioxidant activities (SOD, CAT) were enhanced, and MDA levels were decreased. Histological analyses showed recovery from villus atrophy and goblet cell loss. GPs improved tight junction integrity, elevated sIgA, reduced gut permeability and viral burden. Microbiota analysis revealed increased α-diversity, enrichment of *Lactobacillus* and *Bacteroides*, and suppression of potential pathogens. Functional predictions suggested GPs influenced immunity- and metabolism-related microbial pathways.
Conclusion: GPs exert protective effects against PRV-induced intestinal injury by modulating immune and oxidative responses, enhancing mucosal barrier integrity, and rebalancing gut microbiota. These findings support the potential of GPs as a therapeutic agent for viral enteric diseases. To our knowledge, this is the first study to demonstrate the protective role of GPs against PRV infection *in vivo*. These findings expand current understanding of the antiviral potential of plant-derived polysaccharides and highlight GPs as a promising candidate for the development of novel polysaccharide-based therapeutics for viral enteric diseases.

KEYWORDS

Glycyrrhiza polysaccharides, pseudorabies virus, gut microbiota, intestinal barrier, oxidative stress, immune regulation

1 Introduction

Pseudorabies (PR), also known as Aujeszky's disease, is a highly contagious disease caused by the pseudorabies virus (PRV) (1). PRV is a globally distributed virus that primarily infects pigs, cattle, sheep, mice, and rabbits, among other animals. Among these, pigs serve as the reservoir host, and both infected and virus-carrying pigs are major sources of transmission. The virus is also capable of infecting various wild and carnivorous animals. Clinically, the infection is characterized by distinctive symptoms, most notably intense pruritus (itching) (2). Research shows that PRV infection can cause necrotizing enteritis and disrupt the gut microbiota, ultimately leading to intestinal homeostasis imbalance. Changes in the intestinal environment further exacerbate the destruction of the microbiota, resulting in increased inflammation (3). Currently, attenuated live vaccines, such as Bartha K61, are widely used worldwide to prevent PRV infection in pigs. However, increasing evidence shows that these vaccines do not provide complete protection against the new PRV variants that have emerged since the end of 2011 (4). Therefore, identifying diverse and effective therapeutic approaches has become a crucial strategy to address the threats posed by PRV variants.

Natural products, particularly plant-derived polysaccharides, have attracted increasing attention as alternative or complementary antiviral strategies due to their immunomodulatory and gut microbiota-regulating properties (5). Notably, the use of traditional Chinese medicine polysaccharides for the treatment of PRV-induced viral enteritis represents a highly innovative approach, highlighting their potential as novel therapeutic agents in this context. Among them, *Glycyrrhiza* (*Glycyrrhiza* spp.), an important medicinal herb in traditional Chinese medicine, represents a promising candidate. Polysaccharides are one of the main bioactive components of *Glycyrrhiza*, Studies have shown that *Glycyrrhiza* Polysaccharides (GPs) has biological activities such as immune regulation (6) and antioxidant (7), antitumor (8), antiviral (9), and antibacterial (10) properties. GPs effectively alleviates LPS-induced acute colitis and promotes gut health by downregulating inflammatory cytokines (such as TNF-α, IL-1β, and IL-6), enhancing the expression of tight junction proteins, improving intestinal barrier function, and modulating gut microbiota composition by increasing beneficial bacteria (such as *Lactobacillus*, *Bacteroides*, and *Akkermansia*) while suppressing pathogenic bacteria (11). Wangdi Song (12) found that low molecular weight GPs effectively alleviates cyclophosphamide-induced intestinal barrier damage and gut microbiota imbalance by repairing intestinal structure, increasing goblet cell number and mucus secretion, improving Th1/Th2 balance, and enhancing levels of short-chain fatty acids (SCFAs) and beneficial gut bacteria. However, its mechanism of action in viral enteritis, especially in models induced by PRV, remains unclear. Previous studies have demonstrated that plant-derived extracts can also exert prebiotic effects by modulating the gut microbiota (13, 14). For example, water extract from *Abies alba* wood has been shown to promote the growth of *Lactobacillus paracasei*, *L. acidophilus*, *L. rhamnosus*, *L. gasseri*, *L. crispatus*, and *L. bulgaricus* without affecting lignan metabolism, suggesting that plant-derived bioactive compounds may exert health benefits by improving the gut microbial environment (15). *Coix seed* polysaccharide (CSP) alleviates DSS-induced ulcerative colitis by reducing weight loss, lowering inflammatory cytokines, restoring intestinal barrier integrity, and modulating gut microbiota and beneficial metabolites such as 3-hydroxybutyrate (16). However, despite these advances, direct evidence linking PRV-induced enteritis with TCM interventions, particularly GPs, remains limited. Specifically, it is unclear whether GPs can directly mitigate PRV-induced intestinal injury by modulating immune responses, oxidative stress, mucosal barrier integrity, and gut microbiota composition.

This study aims to evaluate the protective effects and underlying mechanisms of GPs against PRV-induced infection in mice, with a focus on its therapeutic potential in viral enteritis. Specifically, the study seeks to determine whether GPs exerts its effects through modulation of immune responses, attenuation of oxidative stress, restoration of intestinal barrier integrity, and regulation of gut microbiota. The findings are expected to provide a theoretical foundation for the development and application of traditional Chinese medicine polysaccharides in the prevention and treatment of viral intestinal diseases.

2 Materials and methods

2.1 Materials and reagents

The *Glycyrrhiza* used in this study was purchased from the Yunnan Traditional Chinese Medicine Market and identified as *Glycyrrhiza uralensis* roots by the Department of Veterinary Traditional Chinese Medicine at Yunnan Agricultural University. Seventy-two SPF-grade male Kunming mice (5–6 weeks old, 22 ± 3 g) were obtained from Yunnan University (license number SCXK (Dian) K2015-0002). The PRV-XD-F3 virus strain was supplied by the Yunnan Academy of Animal Science and Veterinary Medicine.

2.2 Extraction and purification of polysaccharides

GPs were extracted using a water extraction–alcohol precipitation method. Briefly, 500 g of *Glycyrrhiza* root powder was refluxed with 95% ethanol at 60 °C under reduced pressure three times (4 h each) to remove pigments and lipid-soluble impurities. The dried residue was used for polysaccharide extraction. The residue was mixed with distilled water at a material-to-liquid ratio of 1:25, subjected to ultrasonic treatment at 70 °C (300 W, 20 min), and subsequently extracted at 75 °C for 6 h. The extract was filtered, concentrated to 300 mL, cooled, and precipitated with 1,500 mL of 95% ethanol for 24 h. The precipitate obtained after centrifugation (4,000 rpm, 10 min) was collected as crude GPs and stored at −20 °C. Crude polysaccharides were deproteinized using the Sevag method (chloroform:n-butanol = 4:1), concentrated under reduced pressure,

and freeze-dried at −80 °C for 72 h to yield purified GPs powder. Polysaccharide content was determined by the phenol–sulfuric acid method using a glucose calibration curve.

2.3 Infection of PRV in BHK-21 cells and determination of viral titer

BHK-21 cells were cultured in DMEM supplemented with 10% fetal bovine serum and antibiotics (100 μg/mL streptomycin and 100 IU/mL penicillin) at 37 °C in a 5% CO_2 incubator. One milliliter of PRV viral stock was inoculated onto confluent BHK-21 cells and allowed to adsorb for 2 h. After removal of the viral inoculum, maintenance medium was added for continued culture until approximately 90% cytopathic effect (CPE) was observed. The infected cells were subjected to three freeze–thaw cycles at −80 °C, followed by centrifugation at 12,000 rpm for 15 min at 4 °C. The supernatant containing virus was aliquoted and stored at −80 °C. For $TCID_{50}$ determination, the virus stock was serially diluted 10-fold in maintenance medium and inoculated onto BHK-21 cells in 96-well plates (100 μL per well) with eight replicates per dilution and blank controls. CPE was monitored, and the $TCID_{50}$ was calculated using the Reed-Muench method.

2.4 Animal feeding and model establishment

Seventy-two SPF-grade, 8-week-old male Kunming mice were acclimated for 1 week and randomly divided into six groups (n = 12): normal control (CON), PRV infection model (PRV), high-dose GPs (GPH, 400 mg/kg), medium-dose GPs (GPM, 200 mg/kg), low-dose GPs (GPL, 100 mg/kg), and positive control with APS (200 mg/kg) (11). The treatment groups received oral administration for 14 consecutive days. Subsequently, PRV infection was induced by intraperitoneal injection of 30 μL PRV suspension ($10^{5.6}$ $TCID_{50}$/0.1 mL) (Figure 1A). Body weight, food intake, and clinical symptoms were monitored daily. On day 3 post-infection, mice were euthanized by CO_2 asphyxiation in accordance with AVMA guidelines, and death was confirmed before tissue collection. Mortality was recorded, and survival curves were generated. Blood samples were collected for serum separation. The colon was dissected and measured, while colon contents, duodenum, and colon segments (~5 cm) were harvested. Portions of tissues were fixed in 4% paraformaldehyde, mucosa was scraped for centrifugation, and the remaining tissues were wrapped in foil. All samples were snap-frozen in liquid nitrogen and stored at −80 °C for subsequent analyses.

2.5 Disease activity index scoring

Starting from the establishment of the PRV infection model, the mice were assessed daily at fixed times for mental state, motor ability, food intake, and fur condition, and their body weight was measured. Stool characteristics and occult blood were also observed. The Disease Activity Index (DAI) was calculated by summing the scores of percentage body weight loss, stool consistency, and presence of occult blood to comprehensively reflect the severity of disease activity. The scoring criteria were as follows: no weight change, normal stool, and no occult blood scored 0 points; 1–5% weight loss, softer stool, and light blue occult blood scored 1 point; 6–10% weight loss, loose stool, and obvious blue occult blood scored 2 points; 11–15% weight loss,

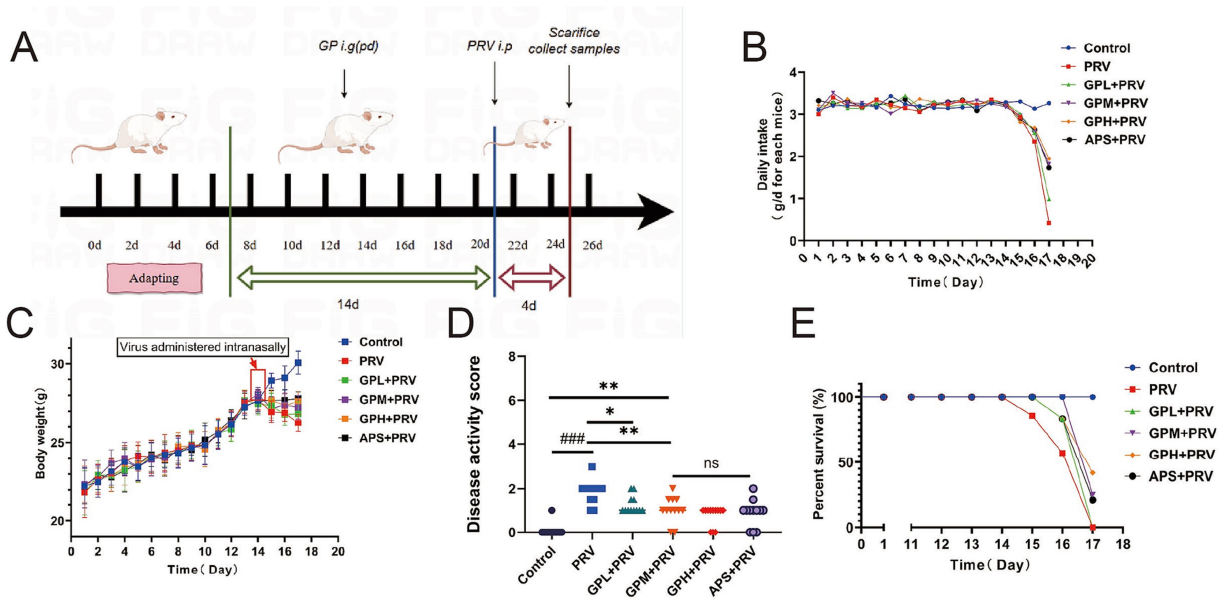

FIGURE 1
GPs alleviate clinical symptoms and improve survival in PRV-infected mice. **(A)** Experimental design. **(B)** Daily food intake per cage to per animal. **(C)** Body weight changes over time. Body weight gain was suppressed in the PRV group, whereas GPs treatment improved weight maintenance. **(D)** Disease activity index (DAI) score. **(E)** Survival curves. All data are presented as mean ± SD (n = 12). ###p < 0.001 vs. control group; p < 0.05, *p < 0.01 vs. PRV group; ns, not significant.

mucus-like stool, and large amounts of dark blue occult blood scored 3 points; weight loss over 15%, watery stool, and visible blood in stool scored 4 points. The DAI scoring was performed in a blinded manner by two independent observers to ensure objectivity and reliability. A total of $n = 12$ mice were included in each group.

2.6 Enzyme-linked immunosorbent assay

The levels of TNF-α, IL-6, IL-4, and IL-10 in mouse serum were measured using enzyme-linked immunosorbent assay (ELISA) according to the instructions provided with the ELISA kits (batch numbers: Ml002095, Ml002293, Ml002149, Ml037873) from Shanghai Enzyme-linked Biotechnology Co., Ltd. Serum levels of superoxide dismutase (SOD), catalase (CAT), and malondialdehyde (MDA) were also detected by ELISA using corresponding kits (batch numbers: Ml001998, Ml037752, Ml002001) from the same company. All experiments were conducted under strictly controlled conditions to ensure data accuracy and reproducibility.

2.7 Hematoxylin and eosin analysis

Duodenal and colonic tissues were fixed in 4% paraformaldehyde for 72 h, then cut into tissue blocks approximately 3 mm thick and rinsed under running water for 20 min. The tissues were dehydrated through a graded ethanol series (75, 85, 95, 100%) and cleared with xylene before being embedded in paraffin. Sections were cut at a thickness of 5 μm, floated on a 40 °C water bath, and dried. After deparaffinization using xylene and graded ethanol, the sections were stained with hematoxylin for 5 min, differentiated in acid alcohol for 3–5 s, blued, and then counterstained with eosin for 30 s. The sections were then dehydrated again through graded ethanol and xylene, and mounted with neutral resin (China National Pharmaceutical Group Chemical Reagents Co., Ltd., batch number 10004160). Microscopic observation was performed using a SOPTOP ICX41 microscope (Sunny Instrument), and images were captured. Using Image Viewer software, villus height, crypt depth, and mucosal thickness were measured to evaluate the pathological effects of PRV infection on intestinal tissue.

2.8 Periodic acid–Schiff analysis

Paraffin sections were baked in an oven at 65 °C for 30 min, followed by deparaffinization in xylene twice for 15 min each. The sections were then rehydrated through a graded ethanol series (100, 95, 85, 75%) and rinsed twice in distilled water for 5 min each. The sections were treated with periodic acid solution (China National Pharmaceutical Group Chemical Reagents Co., Ltd., batch number 10004160) for 8 min, rinsed under running water for 5 min, dried, and stained with Schiff's reagent (Sigma-Aldrich, batch number S5133) in the dark for 15 min, followed by washing for 10 min. Subsequently, the sections were counterstained with hematoxylin for 2 min and blued in PBS for 3 min. The sections were dehydrated through a graded ethanol series (75, 85, 95, 100%, 5 min each) and cleared twice in xylene for 10 min each, then mounted with neutral resin. Images were captured under a microscope (Sunny Instrument, SOPTOP ICX41), and ImageJ software was used to quantitatively analyze the proportion of goblet cells in at least five fields of view in the duodenum and colon to assess changes in intestinal mucus secretion.

2.9 Immunofluorescence analysis

Paraffin-embedded intestinal tissue sections were first deparaffinized in xylene and rehydrated through a graded ethanol series. Antigen retrieval was performed using pH 6.0 citrate buffer in a microwave (boiled on high for 5 min, then medium heat for 3 min, followed by natural cooling). Sections were then incubated in 3% hydrogen peroxide solution for 15 min in the dark to block endogenous peroxidase activity. After blocking with 5% BSA for 15 min, the sections were incubated overnight at 4 °C in a humid chamber with primary antibodies against ZO-1 (Proteintech, Cat# 21773-1-AP) or Occludin (Proteintech, Cat# 27260-1-AP). The next day, sections were washed three times with PBS and incubated with HRP-labeled secondary antibody (Servicebio, Cat# G23303) at room temperature in the dark for 50 min. Subsequently, TYR570 fluorescent dye (red, Servicebio, Cat# G1223-570) and TYR520 fluorescent dye (green, Servicebio, Cat# G1223-520) were applied for 10 min, followed by nuclear counterstaining with DAPI (Servicebio, Cat# G1012). Finally, sections were mounted with antifade mounting medium (Servicebio, Cat# G1401) and observed under a multichannel fluorescence microscope (Nikon Eclipse C1, Japan). Fluorescence intensities of ZO-1 and Occludin were quantified using ImageJ software (NIH, USA) to compare tight junction protein expression differences among treatment groups.

2.10 Extraction of nucleic acids from intestinal tissue

Mouse intestinal tissues were taken from a − 80 °C freezer, and 0.1 g of tissue was weighed and ground in liquid nitrogen. Then, 25 mg of the ground tissue was mixed with 180 μL Buffer GL, 20 μL Proteinase K, and 10 μL RNase A (TaKaRa DNA Extraction Kit, Takara, Cat# D3350) and lysed in a 56 °C water bath for 10 min. Next, 200 μL Buffer GB and 200 μL of 100% ethanol were added and mixed thoroughly before transferring the mixture to a spin column and centrifuging at 12,000 rpm for 2 min. The column was washed sequentially with 500 μL Buffer WA and 700 μL Buffer WB twice. Finally, DNA was eluted with 35 μL of ddH_2O. The concentration of the extracted DNA was measured using a NanoDrop spectrophotometer and stored at −20 °C for later use.

2.11 Determination of intestinal viral load

Primers and TaqMan probe were designed targeting the PRV gE gene. The forward primer sequence was 5'-CTACAGCGAGAG CGACAACGA-3′, the reverse primer sequence was 5'-CGACAGC GAGCAGATGACCA-3′, and the probe sequence was 5'-HEX-CACA CGGCCACGTCGCCACCTG-BHQ1-3′. The qPCR reaction system (20 μL) contained 10 μL Premix Ex Taq (Takara, Cat# RR420A), 0.5 μL each of forward and reverse primers (10 μM), 0.5 μL probe

(5 μM), 2 μL DNA template, and 6.5 μL ddH_2O. PCR cycling conditions were initial denaturation at 95 °C for 3 min, followed by 40 cycles of 95 °C for 15 s, 60 °C for 45 s, and 55.3 °C for 30 s. Viral load was calculated based on the standard curve: $y = -2.395x + 37.091$ ($R^2 = 0.993$).

2.12 RT-qPCR detection of intestinal tight junction protein mRNA expression

Total RNA was extracted from intestinal tissues using a Jifan fully automated nucleic acid extractor and magnetic bead kit, and cDNA was synthesized with TransScript One-Step gDNA Removal and cDNA Synthesis SuperMix (TransGen Biotech, Cat# AT311). Specific primers targeting ZO-1 (forward 5'-CTGGACAGCGAAGA CCACAT-3′, reverse 5'-TGCTGGTGAAGTTGGTGTTG-3′, product length 153 bp) and Occludin (forward 5'-TCACCTTGGTTCGCT CTGTC-3′, reverse 5'-AGCAGGGTGTCCTGAGAAAG-3′, product length 168 bp) were used, with *β*-actin as the internal reference gene (forward 5'-GAGATTGGCATGGCTTTATTTG-3′, reverse 5'-ACTG CTGTCACCTTCACCGTT-3′, product length 127 bp). qPCR reactions were carried out in a 25 μL system containing 12.5 μL SYBR Premix Ex Taq II (Takara, Cat# RR820A), 2 μL cDNA, 1 μL of each primer, and 8.5 μL ddH_2O. The thermal cycling protocol included initial denaturation at 95 °C for 30 s, followed by 40 cycles of 95 °C for 5 s and 60 °C for 30 s. Product specificity was confirmed by melting curve analysis, and relative expression levels of target genes were calculated using the $2^{-\Delta\Delta Ct}$ method.

2.13 Western blotting

Protein expression levels of ZO-1, Occludin, and *β*-actin were detected by Western blot. Tissue samples were lysed using RIPA lysis buffer (Beyotime, #P0013B) supplemented with PMSF (Beyotime, #ST506) and protease inhibitor cocktail (Thermo Fisher, Halt™, #78430). Tissues were ground in liquid nitrogen, and cells were scraped using a sterile cell scraper (Corning) to assist lysis. Lysates were incubated on ice and centrifuged at 12,000 rpm for 15 min at 4 °C to collect the supernatant. Protein concentration was determined using the BCA assay (Thermo Fisher Scientific, #23225): a BSA standard curve was generated, BCA working reagent was added to each well, and absorbance was measured at 562 nm using a microplate reader (BioTek, Synergy H1). Equal amounts of protein were mixed with loading buffer (5 × SDS loading buffer, Beyotime, #P0015L), denatured at 95 °C for 5 min, and resolved on SDS-PAGE gels (10% or 12%, Bio-Rad Mini-PROTEAN system). Proteins were transferred onto PVDF membranes (Millipore, Immobilon-P, #IPVH00010) using a wet transfer system (Bio-Rad, Mini Trans-Blot Cell). Membranes were blocked with 5% non-fat milk in TBST for 1 h at room temperature, followed by incubation with primary antibodies anti-ZO-1 (Proteintech, Wuhan Sanying, Cat# 21773-1-AP, rabbit, 1:1000, 230 kDa), anti-Occludin (Affinity, Cat# DF7504, rabbit, 1:1000, 59 kDa), and anti-*β*-actin (Servicebio, Cat# GB15003, rabbit, 1:5000, 42 kDa) at 4 °C overnight. After washing with TBST, membranes were incubated with HRP-conjugated secondary antibodies (Servicebio, Cat# GB23303, 1:3000) for 1 h at room temperature. Chemiluminescent signals were developed using an ECL substrate (Thermo Scientific, #32106), and images were captured with a gel imaging system (Bio-Rad, ChemiDoc MP).

2.14 16S rRNA gene sequencing analysis of mouse gut microbiota

To evaluate the regulatory effect of GPs on the gut microbiota of mice, colon contents from each group were collected. Microbial genomic DNA was extracted using the QIAGEN DNeasy PowerSoil Kit (QIAGEN, Cat# 12888). The V3–V4 region of the 16S rRNA gene was amplified using primers 341F (5'-CCTAYGGGRBGCASCAG-3′) and 806R (5'-GGACTACNNGGGTATCTAAT-3′) with TransStart FastPfu DNA Polymerase (TransGen Biotech, Cat# AP221). The PCR products were verified by 2% agarose gel electrophoresis and purified using the AxyPrep DNA Gel Extraction Kit (Axygen, Cat# AP-GX-500). DNA concentration was measured with Qubit 4.0 (Thermo Fisher). Libraries were constructed using the Illumina TruSeq Nano DNA LT Library Prep Kit (Cat# FC-121-4001) and, after quality control with the KAPA Library Quantification Kit (Roche, Cat# KK4824), paired-end sequencing (PE250) was performed on the Illumina NovaSeq 6,000 platform. Sequencing data were quality controlled using Cutadapt (v1.9.1) to remove low-quality and low-abundance sequences, resulting in high-quality amplicon sequence variants (ASVs). Alpha diversity (e.g., Shannon, Chao1) and beta diversity (e.g., PCoA) analyses were conducted using QIIME2 (v2020.2) to systematically assess the effects of GPs on the composition and diversity of the gut microbiota.

2.15 Statistical analysis

All data represent at least three independent experiments. Normally distributed data with equal variance are expressed as means ± SD and analyzed by one-way ANOVA using GraphPad Prism 10.0, with two-group comparisons by unpaired two-tailed Student's *t*-test. Non-normal or unequal variance data were analyzed by Kruskal–Wallis test, followed by pairwise comparisons if significant. $p < 0.05$ was considered statistically significant, $p < 0.01$ highly significant, and $p < 0.001$ extremely significant. Quantitative results from immunofluorescence and PAS staining were measured using ImageJ. Additional details are provided in figure legends.

3 Results

3.1 GPs alleviate clinical symptoms and improve survival in PRV-infected mice

Table 1 shows that GPs were successfully extracted from *glycyrrhiza* powder using the Sevag method, with a yield of 3.57 ± 0.07% and a purity of 71.32 ± 1.35% (Table 2), indicating that the extraction process is simple, environmentally friendly, and cost-effective. During the gavage period (days 1–14), body weight steadily increased in all groups, with no significant differences in food intake ($p > 0.05$) (Figures 1B,C). After PRV infection, both body weight and food intake decreased in all groups except the CON, with the PRV group showing the most pronounced reduction ($p < 0.01$). On day 17, food intake in the PRV decreased by

TABLE 1 Rate of GPs obtained (X ± s, n = 5).

Extraction batch	Initial weight of *Glycyrrhiza* (g)	Weight of GPs (g)	Extraction yield (%)	Average extraction yield	RSD (%)
1	200	7.14	3.57	3.57 ± 0.07	0.02
2	200	6.89	3.45		
3	200	7.25	3.63		
4	200	6.88	3.44		
5	200	7.13	3.57		

TABLE 2 Polysaccharide content in *Glycyrrhiza* (X ± s, n = 5).

Extraction batch	Polysaccharide content (%)	Average content (%)	RSD (%)
1	69.36	71.32 ± 1.35	0.02
2	73.74		
3	75.36		
4	68.57		
5	69.56		

86.8% compared to CON, whereas the decreases in the GPL, GPM, GPH, and APS groups were 69.9, 44.2, 40.5, and 46.9%, respectively. Among these, the GPM and GPH groups showed the smallest reductions, consistent with their relatively higher body weights, which were only 6.5 and 4.5% lower than CON, respectively. These results indicate that GPs alleviated PRV-induced anorexia and weight loss in a dose-dependent manner. Consistently, DAI scores were significantly elevated in the PRV group ($p < 0.05$), whereas GPs treatment markedly reduced DAI in a dose-dependent manner (Figure 1D). Mortality analysis further confirmed the protective effects: the mortality rate was 58.33% in the PRV group, which decreased to 41.67, 25.00, and 25.00% in the GPL, GPM, and GPH, respectively, and 33.33% in the APS group, while no deaths occurred in the CON (Figure 1E).

3.2 GPs alleviate PRV-induced inflammation and oxidative stress in mice

PRV infection markedly disrupted the balance of inflammatory cytokines and oxidative stress in mice. Compared with the CON, the PRV group exhibited significantly elevated serum TNF-α and IL-6 levels ($p < 0.001$) and markedly reduced IL-10 and IL-4 levels ($p < 0.01$) (Figures 2A–D). Treatment with GPs, particularly at GPM and GPH doses, significantly suppressed the elevation of pro-inflammatory cytokines and restored anti-inflammatory cytokine levels toward those observed in the CON ($p < 0.05$), indicating potent anti-inflammatory regulatory effects. Similarly, the PRV group displayed pronounced oxidative stress, as evidenced by significantly higher MDA levels ($p < 0.001$) and reduced SOD and CAT activities compared with the CON ($p < 0.001$) (Figures 2E–G). In contrast, GPs intervention significantly enhanced SOD and CAT activities ($p < 0.01$) and decreased MDA levels ($p < 0.001$) relative to the PRV group, with values approaching those of the CON. Taken together, these results demonstrate that GPs effectively alleviated PRV-induced inflammatory imbalance and oxidative stress, exhibiting a dose-dependent protective effect (Supplementary Figure 1).

3.3 GPs exhibit dose-dependent protective effects against small intestinal injury in PRV-infected mice

Histopathological examination revealed that PRV infection caused severe intestinal injury in mice. In small intestinal sections (Figures 3A,F), marked villus atrophy, epithelial shedding, and extensive infiltration of inflammatory cells were observed. Compared with the CON, mice in the PRV group exhibited significantly reduced intestinal wall thickness (Figure 3B), small intestinal villus height (Figure 3C), crypt depth (Figure 3D), mucosal thickness (Figure 3E), and goblet cell area proportion (Figure 3G) ($p < 0.01$), indicating that PRV infection resulted in intestinal structural damage and impairment of the mucosal barrier. Relative to the PR, intervention with GPs, particularly at GPM and GPH doses, significantly ameliorated these pathological alterations. In the GPs-treated groups, villus height and mucosal thickness were markedly increased (Figures 3C,E), while crypt depth and goblet cell proportion were also significantly elevated (Figures 3D,G) ($p < 0.05$). Further comparison with the CON showed that the intestinal morphology of the GPH was closest to normal, with villus and mucosal structures nearly restored to the control level, suggesting a strong dose-dependent protective effect. The APS also exhibited partial improvement; however, its efficacy remained inferior to that of the GPH group when compared with the CON. Overall, the protective effect of GPs against PRV-induced intestinal injury exhibited a clear dose-dependent pattern (Supplementary Figure 2).

3.4 Dose-dependent protective effect of GPs on colonic structural damage in PRV-infected mice

Histopathological examination showed that PRV infection markedly damaged the colonic structure of mice. In the CON, the intestinal tissue structure was intact, with moderate intestinal wall thickness, and normal villus height and mucosal thickness (Figures 4A–C,E). In contrast, the PRV exhibited a significantly thinner intestinal wall (Figures 4B, $p < 0.001$), markedly reduced villus height (Figure 4C, $p < 0.01$), shortened colonic length (Figure 4D, $p < 0.001$), decreased mucosal thickness (Figure 4E, $p < 0.001$), and a significantly reduced goblet cell area proportion (Figures 4F,H, $p < 0.001$). In addition, villus atrophy and epithelial shedding were observed in tissue sections (Figures 4A,G, red arrows), indicating that PRV infection severely disrupted intestinal architecture and impaired mucosal barrier function. GPs intervention significantly ameliorated PRV-induced intestinal injury. The GPL group showed partial recovery in intestinal parameters, but

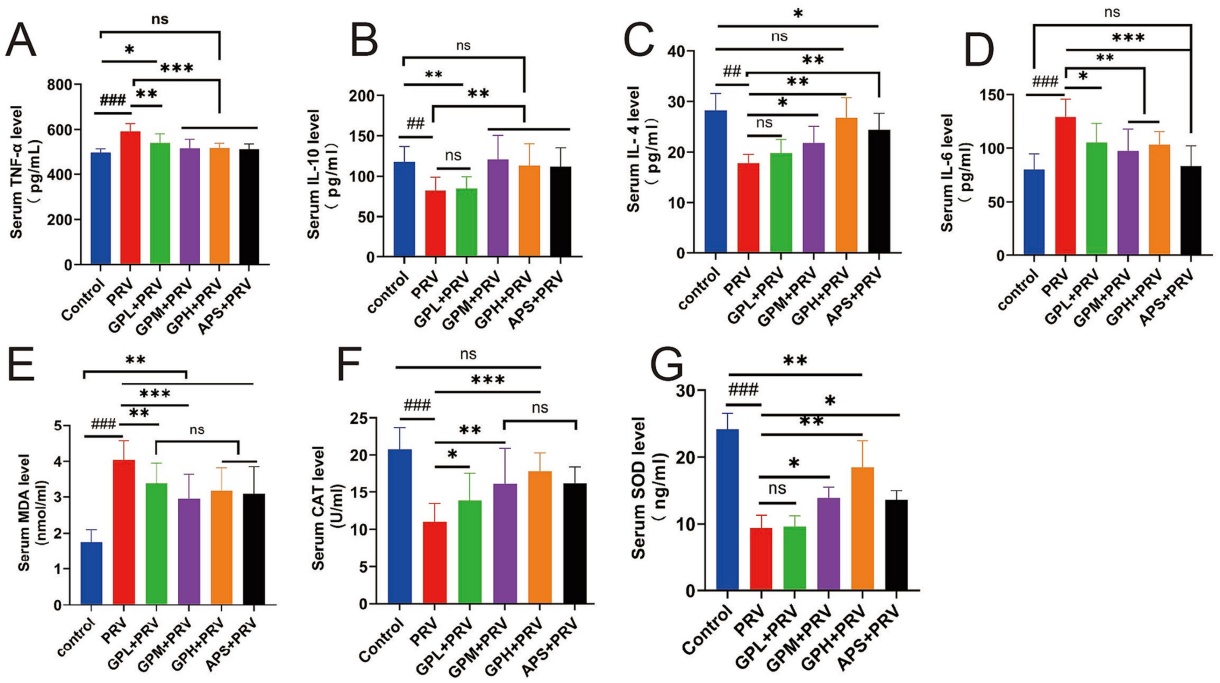

FIGURE 2
GPs alleviate PRV-induced inflammation and oxidative stress in mice. **(A–D)** Serum inflammatory cytokines: **(A)** TNF-α; **(B)** IL-10; **(C)** IL-4; **(D)** IL-6. **(E–G)** Serum oxidative stress markers: **(E)** MDA; **(F)** CAT; **(G)** SOD. Data are presented as mean ± SD (n = 12). ###$p < 0.001$, ##$p < 0.01$ vs. CON; $p < 0.05$, *$p < 0.01$, **$p < 0.001$ vs. PRV group; ns, not significant.

the effects were not significant. In contrast, both the GPM and GPH exhibited significant increases in intestinal wall thickness, colonic villus height, and mucosal thickness (Figures 4B,C,E, $p < 0.05$), as well as significant improvements in colonic length and goblet cell area proportion (Figures 4D,F,H, $p < 0.05$), indicating a dose-dependent protective effect. Further comparison with the CON revealed that the intestinal morphology in the GPH was most similar to normal, with villus and mucosal structures nearly restored to control levels, and no significant differences were observed in several parameters compared with the CON (Figures 4B,D,F,G) ($p > 0.05$). In contrast, the GPM showed partial but incomplete recovery, whereas the APS exhibited limited improvement and remained significantly different from the CON, highlighting the superior protective efficacy of GPs, particularly at high doses. Moreover, gross morphological observation of the mouse intestine (Figure 4G) further supported these findings: compared with the CON, the intestines in the PRV were visibly shorter and thinner, whereas GPs treatment, especially in the GPH, partially restored intestinal length and morphology toward normal. Taken together, these results demonstrate that the protective effect of GPs against PRV-induced colonic injury was dose dependent, with the strongest efficacy observed in the GPH (Supplementary Figure 3).

3.5 GPs enhance the intestinal barrier by upregulating the expression of tight junction proteins

As shown in Figure 5, PRV infection markedly impaired intestinal barrier function in mice. Compared with the CON, mice in the PRV group exhibited significantly increased intestinal permeability, with elevated serum D-lactic acid and DAO levels (Figures 5A,B, $p < 0.01$), and markedly decreased intestinal sIgA levels (Figure 5C, $p < 0.05$). In addition, the relative mRNA expression of the tight junction proteins Occludin and ZO-1 was significantly reduced (Figures 5E,F, $p < 0.001$). Consistently, immunofluorescence staining (Figures 5G,H) and Western blot analysis (Figures 5I–K) also revealed marked decreases in Occludin and ZO-1 protein levels ($p < 0.001$), indicating that PRV infection severely disrupted the intestinal tight junction structure. Compared with the CON, drug-treated groups showed partial improvement in serum D-lactic acid, DAO, sIgA, as well as Occludin and ZO-1 mRNA and protein expression levels ($p > 0.05$). In contrast, both the GPM and GPH groups, as well as the APS group, exhibited significant restoration: serum D-lactic acid and intestinal sIgA levels were nearly comparable to those of the CON ($p > 0.05$), and Occludin and ZO-1 mRNA and protein expression were markedly upregulated ($p < 0.05$), with no significant differences relative to the CON. Immunofluorescence results further showed that intestinal tight junction structures were almost restored to normal, suggesting a dose-dependent protective effect of GPs. Moreover, WB results confirmed that the APS group also showed improvement in Occludin and ZO-1 protein expression, although the extent of recovery remained inferior to that of the GPH group. Overall, while the APS group performed better than the PRV group, most parameters remained lower than those of the CON, and the protective efficacy was slightly weaker than that of GPH. Although the results of Western blot analysis (Figures 5I–K) showed weaker correlations, the overall trend remained consistent, supporting the conclusion that PRV infection severely disrupted the intestinal tight junction structure (Supplementary Figures 4, 5). Collectively, GPs intervention significantly ameliorated PRV-induced intestinal barrier damage in

10.3389/fvets.2025.1679013

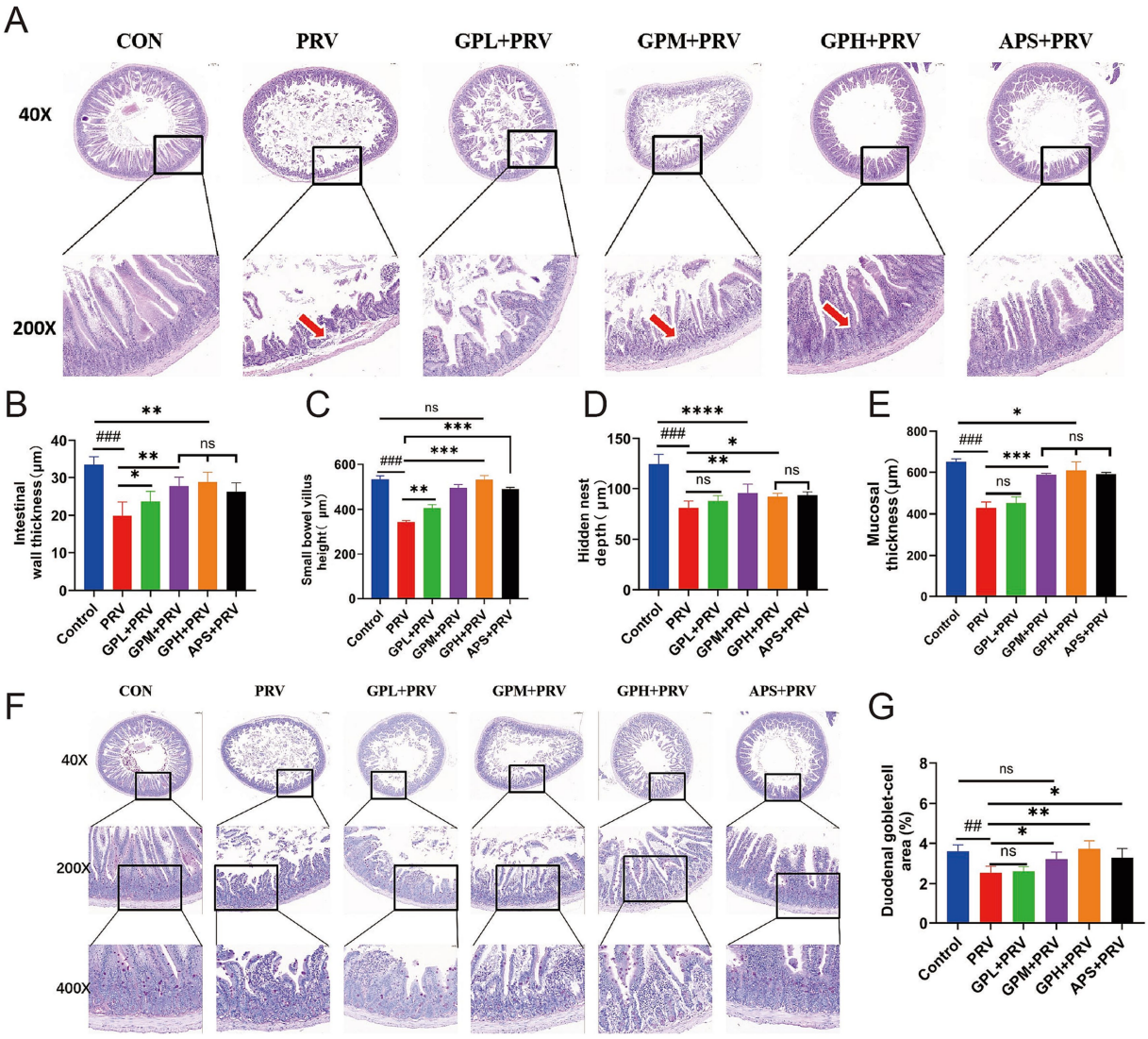

FIGURE 3
GPs exhibit dose-dependent protective effects against small intestinal injury in PRV-infected mice. **(A)** Representative H&E-stained images of the small intestine at 40 × and 200 × magnifications in CON, PRV, GPL, GPM, GPH, and APS. Red arrows indicate villus damage. **(B)** Intestinal wall thickness. **(C)** Small bowel villus height. **(D)** Hidden nest depth. **(E)** Mucosal thickness. **(F)** H&E-stained sections of the duodenum at 40×, 200×, and 400 × magnifications. **(G)** Goblet cell area in the duodenum (percentage of total tissue area). Data are presented as mean ± SD (n = 9). $p < 0.001$ vs. CON; *$p < 0.05$, **$p < 0.01$, ***$p < 0.001$ vs. PRV; ns, not significant.

mice, with the GPH group showing the most pronounced protective effect and exhibiting minimal differences compared with the CON.

3.6 GPs modulated the composition of the gut microbiota in mice infected with PRV

PRV infection profoundly disrupted the intestinal microbiota in mice. α-diversity analysis (Figures 6A–D) revealed significantly reduced microbial richness and diversity, as indicated by decreased Shannon, Simpson, Chao1, and ACE indices compared with the CON group. The Venn diagram (Figure 6E) showed that PRV mice shared fewer core OTUs with CON, while GPM and GPH groups exhibited greater overlap, suggesting partial restoration of the core community. Taxonomic profiling (Figures 6F,G) demonstrated notable alterations in microbial structure, with an abnormal Firmicutes/Bacteroidetes ratio, decreased Lactobacillus and Bacteroides, and increased Prevotella in the PRV group; these changes were reversed following GPs treatment. β-diversity analysis (Figure 6H) further confirmed distinct clustering between PRV and CON, with microbial communities of GPM and GPH clustering more closely with the controls. LEfSe analysis (Figures 6I,J) revealed enrichment of pro-inflammatory taxa in the PRV group, whereas beneficial taxa such as Lactobacillus were enriched in GPs-treated groups. Functional prediction (Figure 6) indicated suppression of pathways related to carbohydrate, amino acid, and energy metabolism by PRV, while GPs restored these processes, particularly those involved in ribosomal activity, DNA replication, and transcription. Collectively, these findings indicate that GPs intervention effectively alleviated PRV-induced dysbiosis by reshaping microbial composition and restoring functional capacity, thereby promoting intestinal microecological balance.

10.3389/fvets.2025.1679013

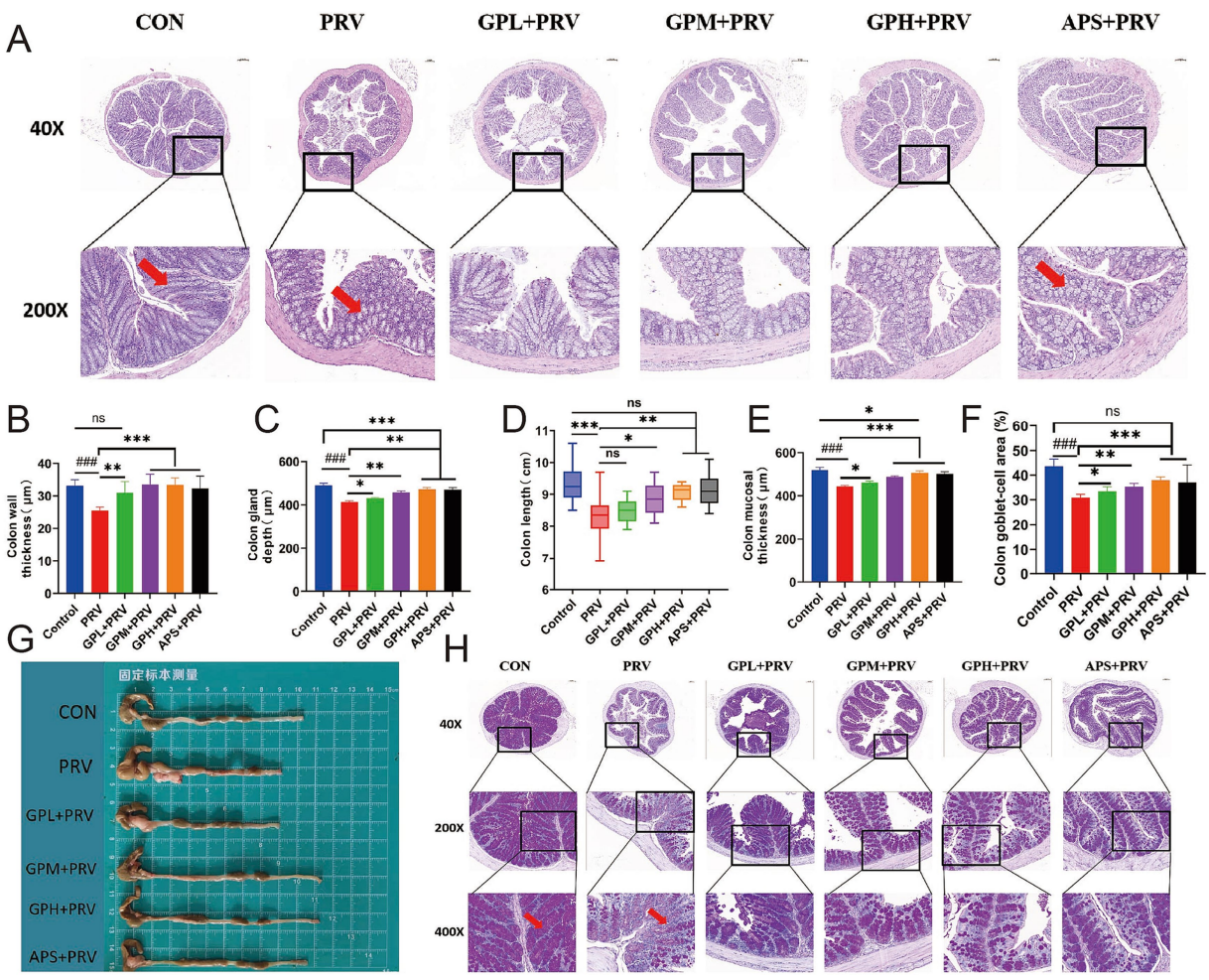

FIGURE 4
Dose-dependent Protective Effect of GPs on Colonic Structural Damage in PRV-Infected Mice. **(A)** H&E-stained colon sections at 40 × and 200 × magnifications. Red arrows indicate mucosal damage. **(B)** Colon wall thickness. **(C)** Colon gland (crypt) depth. **(D)** Colon length(cm). **(E)** Colon Mucosal thickness. **(F)** Colon Goblet cell area (% of total colon tissue). **(G)** Gross images of isolated colon tissues from each group. **(H)** H&E-stained sections at 40×, 200×, and 400 × magnifications. Red arrows indicate goblet cell loss. Data are presented as mean ± SD (n = 9). $p < 0.001$ vs. CON; *$p < 0.05$, **$p < 0.01$, ***$p < 0.001$ vs. PRV; ns, not significant.

4 Discussion

This study systematically investigated the protective effects of GPs against PRV infection in mice from multiple perspectives, including clinical symptoms, biochemical markers, intestinal histomorphology, mucosal barrier function, and gut microbiota composition. The results demonstrated that GPs significantly alleviated a series of pathophysiological changes induced by PRV infection, such as weight loss, increased mortality, cytokine storm, oxidative stress, intestinal barrier disruption, and gut microbiota dysbiosis, in a dose-dependent manner. These findings not only provide new experimental evidence for the antiviral potential of GPs but also lay a theoretical foundation for exploring the multi-target mechanisms of natural compounds in antiviral therapy.

Viral infections often trigger intense inflammatory responses, especially neurotropic viruses such as PRV, which can rapidly activate the innate immune system and induce the massive release of pro-inflammatory cytokines, resulting in a cytokine storm that causes tissue damage and even death (17). In the present study, PRV infection significantly upregulated serum levels of TNF-α and IL-6, indicating a strong systemic inflammatory response. Treatment with GPs led to a marked decrease in these pro-inflammatory cytokines, accompanied by increased expression of anti-inflammatory cytokines IL-4 and IL-10, suggesting that GPs exerts a regulatory effect on immune homeostasis. Previous studies have indicated that GPs can promote the release of anti-inflammatory cytokines while inhibiting the synthesis and release of pro-inflammatory mediators (12), thereby enhancing host resistance. Our *in vivo* findings further support this mechanism. Notably, the cytokine regulation pattern observed here—namely the suppression of TNF-α/IL-6 and the elevation of IL-4/IL-10—is consistent with earlier reports, but our data extend these findings by demonstrating that such effects also occur in the context of PRV infection, highlighting the relevance of GPs in viral neuroinflammation. Oxidative stress is a key pathological process often accompanying viral infections. PRV can induce oxidative damage by activating mitochondrial ROS production and suppressing antioxidant defense systems, leading to lipid peroxidation and apoptosis (18). In our study, PRV-infected mice exhibited significantly

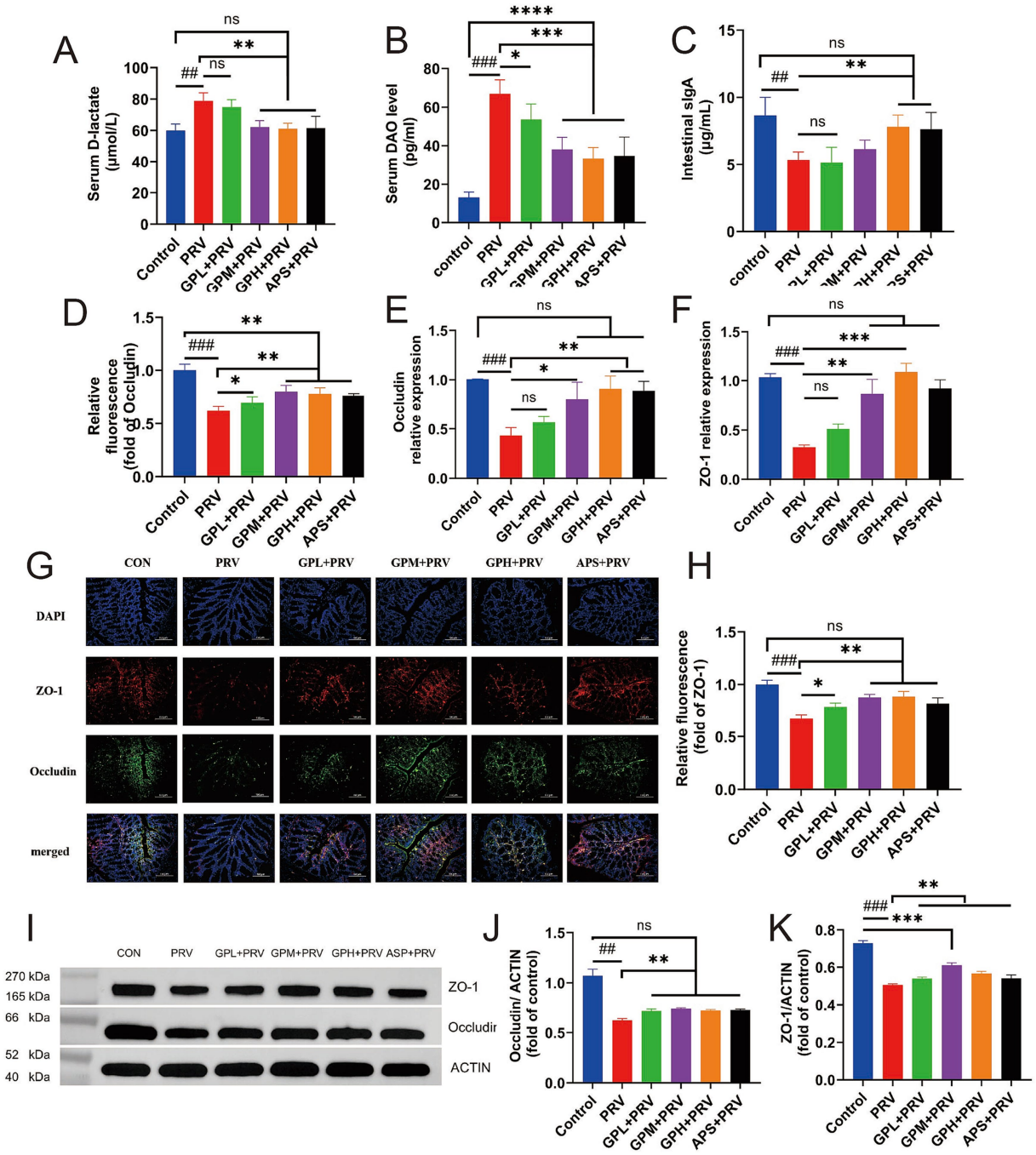

FIGURE 5
GPs enhance the intestinal barrier by upregulating the expression of tight junction proteins. **(A–C)** Serum levels of D-lactate **(A)**, DAO **(B)**, and intestinal SIgA **(C)** were measured to assess intestinal permeability and immune response (n = 12). **(D–F)** Relative fluorescence intensity **(D)**, mRNA expression of occludin **(E)**, and mRNA expression of ZO-1 **(F)** in intestinal tissues were evaluated. **(G)** Representative immunofluorescence images showing ZO-1 (red), occludin (green), and nuclei (DAPI, blue) in intestinal sections (n = 5). Scale bar = 20 μm. **(H)** Quantification of relative fluorescence intensity of ZO-1 based on immunofluorescence in **(G)** (n = 5). **(I)** Representative Western blot images for ZO-1 and occludin expression. ACTIN was used as a loading control. **(J,K)** Quantification of occludin **(J)** and ZO-1 **(K)** protein levels normalized to ACTIN. Data are presented as mean ± SD. *p < 0.05, **p < 0.01, ***p < 0.001 vs. PRV group; $^{\#}p$ < 0.05, $^{\#\#}p$ < 0.01, $^{\#\#\#}p$ < 0.001 vs. CON; ns, not significant.

increased levels of malondialdehyde (MDA), alongside reduced activities of antioxidant enzymes such as SOD and CAT, indicating a classic oxidative injury state. GPs treatment effectively lowered MDA levels and restored antioxidant enzyme activities, highlighting its strong antioxidant protective potential. This antioxidant response is in line with previous findings that GPs can scavenge free radicals and enhance enzymatic defenses; however, our results demonstrate a particularly pronounced recovery of SOD and CAT activities under PRV challenge, suggesting that GPs may exert stronger protective effects in viral oxidative injury models compared to non-viral settings.

10.3389/fvets.2025.1679013

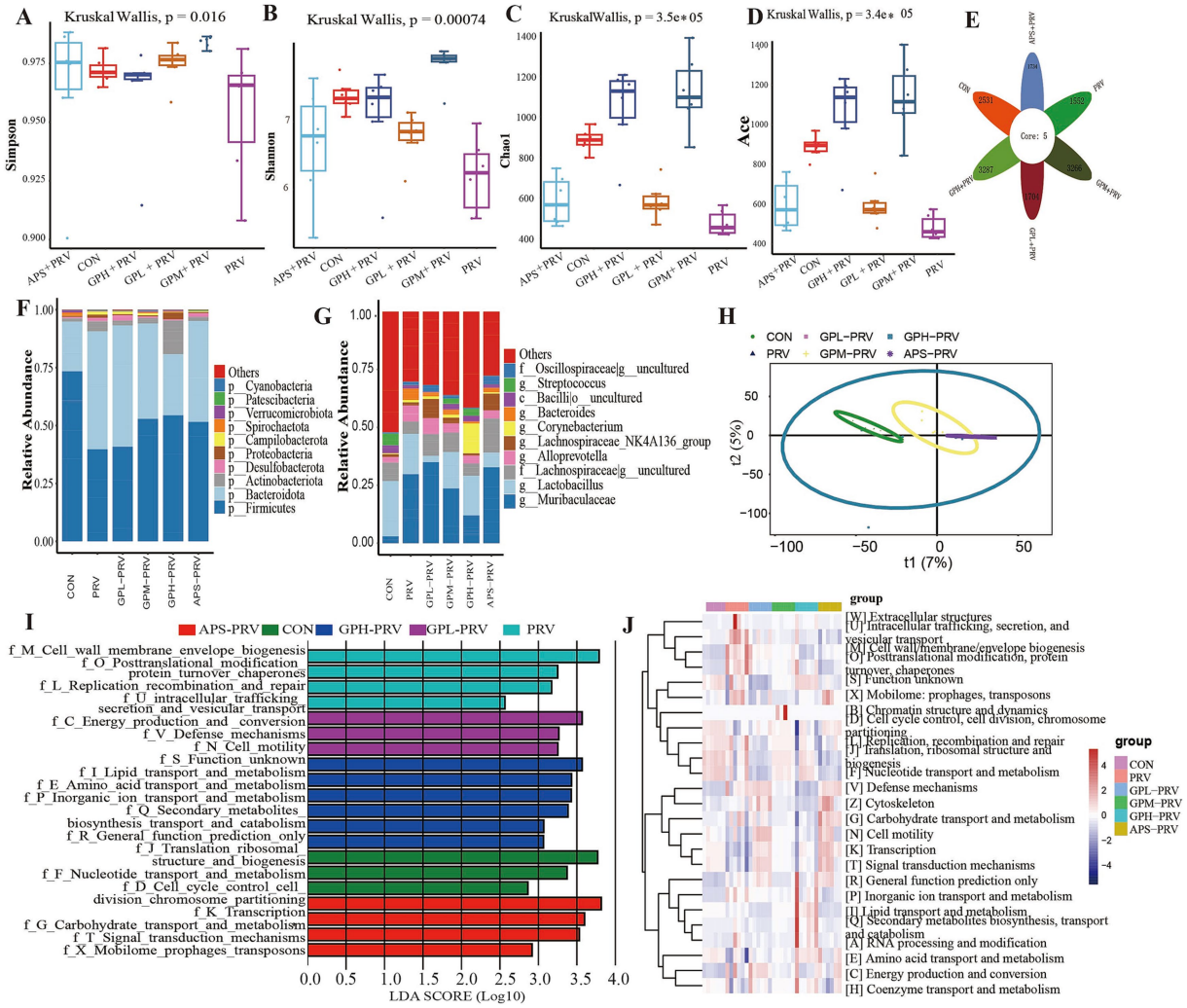

FIGURE 6
GPs modulated the composition of the gut microbiota in mice infected with PRV. **(A–D)** Alpha diversity indices: Shannon, Simpson, Chao1, ACE. (p = 0.00074, p = 0.0016, $p = 3.5 \times 10^{-5}$, $p = 3.4 \times 10^{-5}$) **(E)** Venn diagram of shared OTUs. **(F)** Relative abundance at the phylum level. **(G)** Relative abundance at the genus level. **(H)** Principal Coordinate Analysis (PCoA). **(I)** LDA scores of significantly different taxa. **(J)** Heatmap of predicted functional pathways. n = 6, $p < 0.05$, $p < 0.01$, $p < 0.001$; ns not significant.

Mechanistically, neurotropic viral infections such as PRV are known to activate the (19) pathway, driving the transcription of pro-inflammatory cytokines (e.g., TNF-α, IL-6) (20), while excessive ROS production further amplifies inflammation (21). At the same time, activation of the Nrf2–HO-1 pathway is a canonical defense that counteracts oxidative damage (22), and MAPK signaling (p38, JNK, ERK) integrates inflammatory and oxidative cues to regulate cytokine production (22). Prior studies have shown that GPs can suppress NF-κB activation, enhance Nrf2–HO-1 signaling, and modulate MAPK activity, thereby reducing inflammation and restoring redox balance (23, 24). In line with our findings, this suggests that GPs may protect against PRV-induced pathology by simultaneously down-regulating NF-κB, up-regulating Nrf2–HO-1, and fine-tuning MAPK signaling, ultimately breaking the vicious cycle between inflammation and oxidative stress.

Although PRV is primarily characterized by neurotropism, recent studies have shown that it can invade the central nervous system via both the blood–brain barrier (25) and the intestinal barrier (26), especially in immunocompromised hosts. As one of the body's most crucial immune barriers, the integrity of the intestinal epithelium plays a key role in limiting systemic viral dissemination (27). In this study, PRV infection led to notable structural abnormalities in the intestinal mucosa, including villus atrophy, crypt hyperplasia, and goblet cell disorganization, indicating substantial epithelial damage. More importantly, the expression of tight junction proteins such as Occludin and ZO-1 was significantly reduced, accompanied by elevated serum levels of DAO and D-lactate, as well as reduced sIgA secretion — all suggesting increased intestinal permeability and impaired barrier function. GPs treatment significantly ameliorated both histological and molecular indicators of intestinal damage, indicating its potential to restore barrier integrity after viral injury. The mechanisms may include promoting epithelial regeneration, maintaining mucosal immune homeostasis, and upregulating tight junction protein expression. Further research is needed to elucidate

the specific signaling pathways through which GPs facilitates epithelial repair, providing direction for future studies.

The gut microbiota plays a pivotal role in maintaining host immune homeostasis, and its structural diversity and functional integrity are crucial in resisting viral infections (28). Previous studies have shown that PRV infection can disrupt microbial composition, promoting the overgrowth of opportunistic pathogens and exacerbating CNS injury through the microbiota–immune–brain axis (27). In the current study, PRV infection led to reduced α-diversity of gut microbiota, with a decline in beneficial bacteria such as *Lactobacillus*, and an increased abundance of potential pathogens such as *Prevotella* and *Staphylococcus*, indicating significant dysbiosis. GPs intervention notably restored microbial diversity and increased the relative abundance of beneficial bacteria, suggesting a strong probiotic effect. Importantly, these microbial shifts are functionally relevant to host immunity. For instance, *Lactobacillus* and *Bacteroides* are major producers of SCFAs, which can suppress pro-inflammatory cytokine production and promote regulatory T cell differentiation (29–31), thereby alleviating excessive inflammation. In contrast, *Prevotella* enrichment has been associated with Th17 cell activation and chronic inflammation, potentially aggravating viral pathogenesis (32, 33). Further PICRUSt functional prediction analysis showed that GPs treatment restored pathways related to fatty acid synthesis and amino acid metabolism. This may indirectly regulate host immunity and barrier function by modulating the profile of metabolic products such as SCFAs and tryptophan metabolites (34). It should be emphasized, however, that these findings regarding SCFAs functions were primarily based on PICRUSt functional predictions rather than direct observations of typical SCFA-producing taxa. This limitation highlights the need for future studies combining targeted metabolomics with inflammatory and oxidative markers to validate the proposed "microbiota–metabolite–immune" axis. Taken together, these effects suggest that GPs may maintain intestinal homeostasis via the microbiota–metabolite axis, supporting its potential as a functional prebiotic.

Despite the comprehensive insights gained in this study, some limitations remain. Firstly, the focus was mainly on *in vivo* observations, without thoroughly investigating whether GPs directly interferes with the PRV replication cycle. Future studies should integrate virological assays, such as viral titers and protein expression analyses, to evaluate the direct antiviral potential of GPs. Secondly, the current model utilized mice, which differ immunologically from pigs, the natural host of PRV. Further validation in pig models is essential to assess the efficacy and safety of GPs in a clinically relevant context. In addition, more translational barriers should be considered, including the oral bioavailability, metabolic stability, and practical feasibility of GPs administration in real-world settings. Finally, GPs is a complex mixture of polysaccharides with undefined active components. Future studies should aim to identify its key functional monomers or structural domains through structure–activity relationship analyses, laying a foundation for the development of standardized antiviral therapeutics. Given that PRV primarily threatens pigs, it is also worth discussing the potential application of GPs in veterinary practice, for instance as a feed additive for preventive intervention, to enhance the practical value of these findings.

5 Conclusion

GPs treatment significantly reduced PRV-induced mortality, alleviated clinical symptoms, and improved intestinal morphology in infected mice. These protective effects were associated with downregulation of pro-inflammatory cytokines (TNF-α, IL-6), upregulation of anti-inflammatory cytokines (IL-4, IL-10), enhancement of antioxidant enzyme activities (SOD, CAT), restoration of tight junction proteins (Occludin, ZO-1), and elevation of mucosal sIgA levels. Moreover, GPs decreased viral burden and reshaped gut microbiota by increasing beneficial genera such as *Lactobacillus* and *Bacteroides* while suppressing potential pathogens. Collectively, these findings provide mechanistic evidence that GPs protect against PRV-induced intestinal injury through coordinated regulation of immunity, oxidative stress, barrier integrity, and microbial homeostasis, supporting their potential as a natural therapeutic agent for viral enteric diseases.

Data availability statement

The sequencing data generated in this study have been deposited in the Genome Sequence Archive (GSA) under accession number CRA027930, and are publicly available at https://ngdc.cncb.ac.cn/gsa/browse/CRA027930.

Ethics statement

The animal study was approved by Yunnan University (license number SCXK (Dian) 82 K2015-0002). The study was conducted in accordance with the local legislation and institutional requirements.

Author contributions

CS: Project administration, Writing – review & editing. QW: Writing – original draft. HS: Writing – original draft. XZ: Writing – original draft. DP: Writing – review & editing. ZZ: Writing – review & editing. YZ: Writing – review & editing. SY: Formal analysis, Methodology, Writing – original draft. XS: Funding acquisition, Writing – review & editing.

Funding

The author(s) declare that financial support was received for the research and/or publication of this article. This study was jointly supported by the Yunnan Joint International R&D Center of Veterinary Public Health (202403AP140033). Yunnan Key Laboratory of Veterinary Etiological Biology (Grant No: 202449CE340019) and the Yunnan Province Rural Revitalization Science and Technology Special Project "Yunnan Province Weixin County Recycling Agriculture Science and Technology Mission" (Grant No. 202304BI090011).

Acknowledgments

We sincerely thank the members of our laboratory and colleagues for their help and constructive discussions during the course of this research.

Conflict of interest

The authors declare that the research was conducted in the absence of any commercial or financial relationships that could be construed as a potential conflict of interest.

Generative AI statement

The authors declare that no Gen AI was used in the creation of this manuscript.

Any alternative text (alt text) provided alongside figures in this article has been generated by Frontiers with the support of artificial intelligence and reasonable efforts have been made to ensure accuracy, including review by the authors wherever possible. If you identify any issues, please contact us.

Publisher's note

All claims expressed in this article are solely those of the authors and do not necessarily represent those of their affiliated organizations, or those of the publisher, the editors and the reviewers. Any product that may be evaluated in this article, or claim that may be made by its manufacturer, is not guaranteed or endorsed by the publisher.

Supplementary material

The Supplementary material for this article can be found online at: https://www.frontiersin.org/articles/10.3389/fvets.2025.1679013/full#supplementary-material

References

1. Wang C, Li L, Zhai X, Chang H, Liu H. Evasion of the antiviral innate immunity by PRV. *Int J Mol Sci*. (2024) 25:140. doi: 10.3390/ijms252313140

2. Zhang T, Liu Y, Chen Y, Wang A, Feng H, Wei Q, et al. A single dose glycoprotein D-based subunit vaccine against pseudorabies virus infection. *Vaccine*. (2020) 38:6153–61. doi: 10.1016/j.vaccine.2020.07.025

3. Lama Tamang R, Juritsch AF, Ahmad R, Salomon JD, Dhawan P, Ramer-Tait AE, et al. The diet-microbiota axis: a key regulator of intestinal permeability in human health and disease. *Tissue Barriers*. (2023) 11:2077069. doi: 10.1080/21688370.2022.2077069

4. Nie Z, Zhu S, Wu L, Sun R, Shu J, He Y, et al. Progress on innate immune evasion and live attenuated vaccine of pseudorabies virus. *Front Microbiol*. (2023) 14:1138016. doi: 10.3389/fmicb.2023.1138016

5. Yu Y, Shen M, Song Q, Xie J. Biological activities and pharmaceutical applications of polysaccharide from natural resources: a review. *Carbohydr Polym*. (2018) 183:91–101. doi: 10.1016/j.carbpol.2017.12.009

6. Song W, Zhang T, Wang Y, Xue S, Zhang Y, Zhang G. Glycyrrhiza uralensis polysaccharide modulates characteristic Bacteria and metabolites, improving the immune function of healthy mice. *Nutrients*. (2025) 17:225. doi: 10.3390/nu17020225

7. Mutaillifu P, Bobakulov K, Abuduwaili A, Huojiaaihemaiti H, Nuerxiati R, Aisa HA, et al. Structural characterization and antioxidant activities of a water soluble polysaccharide isolated from *Glycyrrhiza glabra*. *Int J Biol Macromol*. (2020) 144:751–9. doi: 10.1016/j.ijbiomac.2019.11.245

8. Shen H, Zeng G, Sun B, Cai X, Bi L, Tang G, et al. A polysaccharide from Glycyrrhiza inflata licorice inhibits proliferation of human oral cancer cells by inducing apoptosis via mitochondrial pathway. *Tumour Biol*. (2015) 36:4825–31. doi: 10.1007/s13277-015-3135-6

9. Yang Y, Liu Y, Lou R, Lei Y, Li G, Xu Z, et al. Glycyrrhiza polysaccharides inhibits PRRSV replication. *Virol J*. (2023) 20:140. doi: 10.1186/s12985-023-02052-9

10. Wittschier N, Faller G, Hensel A. Aqueous extracts and polysaccharides from liquorice roots (*Glycyrrhiza glabra* L.) inhibit adhesion of *Helicobacter pylori* to human gastric mucosa. *J Ethnopharmacol*. (2009) 125:218–23. doi: 10.1016/j.jep.2009.07.009

11. Wei X, Li N, Wu X, Cao G, Qiao H, Wang J, et al. The preventive effect of Glycyrrhiza polysaccharide on lipopolysaccharide-induced acute colitis in mice by modulating gut microbial communities. *Int J Biol Macromol*. (2023) 239:124199. doi: 10.1016/j.ijbiomac.2023.124199

12. Song W, Wang Y, Li G, Xue S, Zhang G, Dang Y, et al. Modulating the gut microbiota is involved in the effect of low-molecular-weight Glycyrrhiza polysaccharide on immune function. *Gut Microbes*. (2023) 15:2276814. doi: 10.1080/19490976.2023.2276814

13. Ran X, Li Y, Guo W, Li K, Guo W, Wang X, et al. Angelica sinensis polysaccharide alleviates *Staphylococcus aureus*-induced mastitis by regulating the intestinal Flora and gut metabolites. *J Agric Food Chem*. (2024) 72:24504–17. doi: 10.1021/acs.jafc.4c06094

14. Chen Y, Ma H, Liang J, Sun C, Wang D, Chen K, et al. Hepatoprotective potential of four fruit extracts rich in different structural flavonoids against alcohol-induced liver injury via gut microbiota-liver axis. *Food Chem*. (2024) 460:140460. doi: 10.1016/j.foodchem.2024.140460

15. Stojanov S, Ravnikar M, Berlec A, Kreft S. Interaction between silver fir (*Abies alba*) wood water extract and lactobacilli. *Pharmazie*. (2021) 76:614–7. doi: 10.1691/ph.2021.1794

16. Ji ZH, Xie WY, Wu HY, Yuan B. Coix seed polysaccharide mitigates ulcerative colitis in mice through the modulation of gut microbiota and improvement of intestinal metabolism balance. *J Agric Food Chem*. (2025) 73:11067–79. doi: 10.1021/acs.jafc.5c02458

17. Zhang Y, Shu X, Zhang Y, Song C, Wu Y, Cui K, et al. Astrocyte-derived MMP-9 is a key mediator of pseudorabies virus penetration of the blood-brain barrier and tight junction disruption. *Vet Res*. (2025) 56:72. doi: 10.1186/s13567-025-01486-z

18. Zhou Q, Shi D, Tang YD, Zhang L, Hu B, Zheng C, et al. Pseudorabies virus gM and its homologous proteins in herpesviruses induce mitochondria-related apoptosis involved in viral pathogenicity. *PLoS Pathog*. (2024) 20:e1012146. doi: 10.1371/journal.ppat.1012146

19. Zhou Q, Zhang L, Lin Q, Liu H, Ye G, Liu X, et al. Pseudorabies virus infection activates the TLR-NF-κB Axis and AIM2 Inflammasome to enhance inflammatory responses in mice. *J Virol*. (2023) 97:e0000323. doi: 10.1128/jvi.00003-23

20. Zhang X, Xie J, Gao M, Yan Z, Chen L, Wei S, et al. Pseudorabies virus ICP0 abolishes tumor necrosis factor alpha-induced NF-κB activation by degrading P65. *Viruses*. (2022) 14:954. doi: 10.3390/v14050954

21. Chen A, Huang H, Fang S, Hang Q. ROS: a "booster" for chronic inflammation and tumor metastasis. *Biochim Biophys Acta Rev Cancer*. (2024) 1879:189175. doi: 10.1016/j.bbcan.2024.189175

22. Ding X, Jian T, Wu Y, Zuo Y, Li J, Lv H, et al. Ellagic acid ameliorates oxidative stress and insulin resistance in high glucose-treated HepG2 cells via miR-223/keap1-Nrf2 pathway. *Biomed Pharmacother*. (2019) 110:85–94. doi: 10.1016/j.biopha.2018.11.018

23. Niu P, Zhang X, Zhang G, Jing R, Qiao Y, Zhou X, et al. A polysaccharide from Glycyrrhiza uralensis attenuates myocardial fibrosis via modulating the MAPK/PI3K/AKT signaling pathway. *Int J Biol Macromol*. (2025) 286:138207. doi: 10.1016/j.ijbiomac.2024.138207

24. Gao N, Li Y, Zhang L, Zhang Y, Wang X. The administration of *Glycyrrhiza* polysaccharides mitigates liver injury in mice caused by mancozeb via the Keap1-Nrf2/NF-κB pathway. *Food Chem Toxicol*. (2025) 195:115088. doi: 10.1016/j.fct.2024.115088

25. Wang Y, Zhang X, Ma X, Zhang K, Li S, Wang X, et al. Study on the kinetic model, thermodynamic and physicochemical properties of Glycyrrhiza polysaccharide by ultrasonic assisted extraction. *Ultrason Sonochem*. (2019) 51:249–57. doi: 10.1016/j.ultsonch.2018.10.012

26. Zhang C, Liu Y, Chen S, Qiao Y, Zheng Y, Xu M, et al. Effects of intranasal pseudorabies virus AH02LA infection on microbial community and immune status in the ileum and Colon of piglets. *Viruses*. (2019) 11:518. doi: 10.3390/v11060518

27. Zhuang M, Zhang X, Cai J. Microbiota-gut-brain axis: interplay between microbiota, barrier function and lymphatic system. *Gut Microbes*. (2024) 16:2387800. doi: 10.1080/19490976.2024.2387800

28. Ancona G, Alagna L, Alteri C, Palomba E, Tonizzo A, Pastena A, et al. Gut and airway microbiota dysbiosis and their role in COVID-19 and long-COVID. *Front Immunol*. (2023) 14:1080043. doi: 10.3389/fimmu.2023.1080043

29. Yuan M, Chang L, Gao P, Li J, Lu X, Hua M, et al. Synbiotics containing sea buckthorn polysaccharides ameliorate DSS-induced colitis in mice via regulating Th17/Treg homeostasis through intestinal microbiota and their production of BA metabolites and SCFAs. *Int J Biol Macromol*. (2024) 276:133794. doi: 10.1016/j.ijbiomac.2024.133794

30. Yan Y, Lei Y, Qu Y, Fan Z, Zhang T, Xu Y, et al. *Bacteroides uniformis*-induced perturbations in colonic microbiota and bile acid levels inhibit TH17 differentiation and ameliorate colitis developments. *NPJ Biofilms Microbiomes*. (2023) 9:56. doi: 10.1038/s41522-023-00420-5

31. Mann ER, Lam YK, Uhlig HH. Short-chain fatty acids: linking diet, the microbiome and immunity. *Nat Rev Immunol*. (2024) 24:577–95. doi: 10.1038/s41577-024-01014-8

32. Larsen JM. The immune response to Prevotella bacteria in chronic inflammatory disease. *Immunology*. (2017) 151:363–74. doi: 10.1111/imm.12760

33. Huang Y, Tang J, Cai Z, Zhou K, Chang L, Bai Y, et al. Prevotella induces the production of Th17 cells in the Colon of mice. *J Immunol Res*. (2020) 2020:1–14. doi: 10.1155/2020/9607328

34. Wu Y, Sun J, Xie W, Xue S, Li X, Guo J, et al. Immunomodulation of *Glycyrrhiza* polysaccharides in vivo based on microbiome and metabolomics approaches. *Foods*. (2025) 14:874. doi: 10.3390/foods14050874

Glossary

GPs - *Glycyrrhiza* Polysaccharides

PRV - Pseudorabies Virus

APS - *Astragalus* Polysaccharides

TNF-α - Tumor Necrosis Factor-alpha

IL-6 - Interleukin-6

IL-4 - Interleukin-4

IL-10 - Interleukin-10

SOD - Superoxide Dismutase

CAT - Catalase

MDA - Malondialdehyde

ZO-1 - Zonula Occludens-1

sIgA - Secretory Immunoglobulin A

DAO - Diamine Oxidase

DAI - Disease Activity Index

qPCR - Quantitative Polymerase Chain Reaction

RT-qPCR - Reverse Transcription qPCR

BHK-21 - Baby Hamster Kidney-21

SPF - Specific Pathogen Free

CPE - Cytopathic Effect

$TCID_{50}$ - 50% Tissue Culture Infectious Dose

ELISA - Enzyme-Linked Immunosorbent Assay

H&E - Hematoxylin and Eosin

PAS - Periodic Acid-Schiff

HRP - Horseradish Peroxidase

DAPI - 4′,6-diamidino-2-phenylindole

PVDF - Polyvinylidene Fluoride

BCA - Bicinchoninic Acid

SDS-PAGE - Sodium Dodecyl Sulfate Polyacrylamide Gel Electrophoresis

ECL - Enhanced Chemiluminescence

ASV - Amplicon Sequence Variant

OTU - Operational Taxonomic Unit

LEfSe - Linear Discriminant Analysis Effect Size

PCoA - Principal Coordinate Analysis

NMDS - Non-metric Multidimensional Scaling

PICRUSt - Phylogenetic Investigation of Communities by Reconstruction of Unobserved States

KEGG - Kyoto Encyclopedia of Genes and Genomes.

frontiers | Frontiers in Veterinary Science

TYPE Review
PUBLISHED 21 November 2025
DOI 10.3389/fvets.2025.1710151

OPEN ACCESS

EDITED BY
Baocheng Hao,
Chinese Academy of Agricultural Sciences, China

REVIEWED BY
Hao Lu,
Northwest A&F University, China
Zhao-ying Liu,
Hunan Agricultural University, China

*CORRESPONDENCE
Guangliang Shi
✉ shiguangliang@neau.edu.cn

RECEIVED 21 September 2025
ACCEPTED 03 November 2025
PUBLISHED 21 November 2025

CITATION
Liu N, Zhang Q, Piao Y, Sun C and Shi G (2025) Research progress on the prevention and treatment of zearalenone poisoning in animals using natural products. *Front. Vet. Sci.* 12:1710151. doi: 10.3389/fvets.2025.1710151

Research progress on the prevention and treatment of zearalenone poisoning in animals using natural products

Nannan Liu[1], Qi Zhang[2,3,4], Yulan Piao[1], Chenghe Sun[1] and Guangliang Shi[2,3,4]*

[1]Jilin Agricultural Science and Technology College, Jilin, China, [2]College of Veterinary Medicine, Northeast Agricultural University, Harbin, China, [3]Heilongjiang Provincial Key Laboratory of Pathogenic Mechanism for Animal Disease and Comparative Medicine, Harbin, China, [4]Institute of Chinese Veterinary Medicine, Northeast Agricultural University, Harbin, China

Zearalenone (ZEA) is a non-steroidal estrogenic mycotoxin produced by Fusarium fungi, widely present in cereal feeds such as corn, barley, wheat, and sorghum. It not only impacts agricultural production and feed safety but also poses a serious threat to animal health. Extensive research demonstrates that natural products can effectively mitigate the toxic effects of zearalenone. This paper reviews zearalenone's physicochemical properties and toxicological effects, with a focus on advances in the research on reducing zearalenone toxicity through plant, microbial, and mineral-derived natural products. The aim is to provide theoretical references for developing more efficient and safer zearalenone detoxification agents.

KEYWORDS

zearalenone, toxicity, natural products, detoxification methods, bee pollen

1 Introduction

Zearalenone (ZEA), also known as F-2 toxin, is a non-steroidal estrogenic mycotoxin produced by Fusarium graminearum fungi. It is one of the top three mycotoxins in animal feed globally (1). Grain feeds such as wheat and corn are susceptible to contamination by zearalenone and other toxins during production, processing, and transportation. Furthermore, ZEA exhibits chemical stability, produces numerous metabolites, and persists for extended periods. The Food and Agriculture Organization of the United Nations (FAO) estimates that approximately 25% of the world's grain production is contaminated with mycotoxins (2). Based on ZEA monitoring data from China between 2004 and 2024, Wang et al. (3) Comprehensively analyzed ZEA contamination levels in Chinese feed and raw materials. International comparisons indicate that China's zearalenone contamination levels exceed those in Europe.

The phenol-dihydroxy lactone structure of ZEA resembles that of estrogen. When animals consume ZEA-contaminated grain feed, it undergoes metabolic conversion within the body and is transported via the bloodstream throughout the system. There, it binds to estrogen receptors, triggering various pathological processes including estrogenic effects, oxidative stress, apoptosis, and inflammation. This leads to multi-organ damage affecting the uterus, testes, liver, kidneys, and spleen. Affected animals exhibit symptoms including prolonged estrus cycles, miscarriages, testicular atrophy, and poor sperm quality (4–7), causing substantial economic losses in livestock farming and feed processing industries. Currently, ZEA detoxification methods face limitations such as low efficacy, high costs, and significant toxicity (8–10).

In recent years, extensive research has focused on the antagonistic effects of natural plant extracts, microorganisms and their metabolites, and mineral materials against ZEA. Natural products, with their advantages of high safety, wide availability, and diverse mechanisms of action, have gradually become a hotspot in ZEA detoxification research. For example, a variety of bioactive substances found in natural plants, such as flavonoids, polysaccharides, and polyphenols, can successfully lessen the harm that ZEA does to organs, including the kidneys, liver, testes, and uterus. This is accomplished by scavenging reactive oxygen species, blocking inflammatory and apoptotic signaling pathways, and counteracting the estrogen-like actions of ZEA (11–14). This review systematically outlines the physicochemical properties, toxicity mechanisms, and mitigation methods of ZEA, with a focus on summarizing research progress in natural medicines for zearalenone mitigation. It aims to provide a theoretical foundation for the innovation of ZEA pollution prevention and control technologies and the industrial application of natural mitigants, thereby contributing to the improvement of food security and public health safeguards.

2 Zearalenone

2.1 Physicochemical properties of zearalenone

ZEA, chemically named 6-(10-hydroxy-6-oxo-undec-2-enyl)β-resorcylic acid lactone, has the molecular formula $C_{18}H_{22}O_5$. Its molecule contains two phenolic hydroxyl groups and one lactone ring, belonging to the β-resorcylic acid lactone class of compounds. Its chemical structure is shown in Figure 1 (15). ZEA exhibits stable chemical properties with a well-defined melting point. The pure compound melts at 164–165 °C and gradually decomposes when heated above 200 °C. Its toxicity is difficult to destroy through high-temperature treatment. At room temperature, its structure remains stable. Although hydrolysis occurs under alkaline conditions, its structure can be restored by lowering the pH. ZEA is readily soluble in polar organic solvents such as methanol, ethanol, acetone, and chloroform, but poorly soluble in water (Table 1).

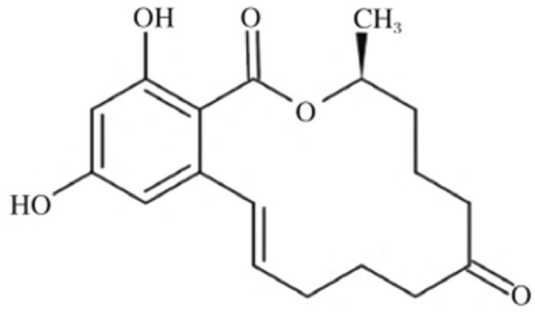

FIGURE 1
Chemical formula of zearalenone in corn. Reproduced with permission from Wu et al. (15).

2.2 Toxic effects of zearalenone

2.2.1 Reproductive toxicity

The reproductive organs are the primary target sites for ZEA toxicity. ZEA, structurally similar to estrogen, can competitively bind to estrogen receptors within the body, thereby disrupting the normal synthesis of steroid hormones such as estradiol, testosterone, and progesterone (16). When sows ingest ZEA-contaminated feed, it readily damages reproductive organs such as the uterus and ovaries, manifesting clinical symptoms including vulvar swelling, mammary gland redness and swelling, estrus cycle disruption, and abortion (17). Gilt sows are particularly sensitive to ZEA; estrogen poisoning can occur when feed contains ZEA levels exceeding 1 mg/kg (18). Research proved that ZEA can cause abnormal follicular development in laying hens, characterized by increased stromal cell numbers, vacuolation-induced edema, accompanied by congestion, hemorrhage, oocyte retraction, and separation of the granulosa and theca membranes (19, 20). At concentrations exceeding 5 mg/kg, ZEA leads to reduced egg production, heightened inflammation, impaired ovarian function, and disrupted sex hormone secretion (21). ZEA activates the phosphorylation of AMPK in endometrial epithelial cells. This process modulates TSC2 and Rheb, affecting mTOR phosphorylation levels and subsequently inducing autophagy. Concurrently, it upregulates the expression of proliferative genes PCNA and BCl_2 while downregulating the apoptotic gene Bax. After promoting proliferation of endometrial epithelial cells, this ultimately leads to thickening of the endometrium and myometrium, increased density of uterine glands, and induces uterine hypertrophy (22) (Table 2; Figure 2).

ZEA poisoning can also cause male animals to exhibit symptoms such as decreased sperm production and quality. Testicular interstitial cells are the primary site for testosterone synthesis in males. Studies indicate that ZEA significantly damages mitochondria in porcine testicular interstitial cells, inducing apoptosis through the PI3K-AKT signaling pathway mediated by mitochondria, which regulates the Bcl-2 protein family (23). ZEA induces mitochondrial morphological abnormalities and functional disorders, leading to mtDNA leakage into the cytoplasm. Free mtDNA acts as a damage-associated molecular pattern (DAMP), activating the endoplasmic reticulum transmembrane protein STING, which in turn triggers the NF-κB signaling pathway. This pathway not only upregulates inflammatory factor expression but also induces pyroptosis by regulating NLRP3 inflammasomes, resulting in damage to testicular and mouse testicular supporting cells (24). In both *in vivo* and *in vitro* studies of ZEA-induced male goat reproductive dysfunction, ZEA caused significant declines in sperm quality, disruption of seminiferous tubules, and impaired structure of goat testicular interstitial supporting cells along with blood-testis barrier function. Concurrently, supporting cells exhibited numerous vacuoles and excessive endoplasmic reticulum swelling (25) (Figure 3).

2.2.2 Genotoxicity

Extensive research indicates that ZEA exhibits genotoxicity, capable of inducing chromosomal aberrations, DNA damage, and gene mutations (26). In aquatic models, treating zebrafish embryos with 350–950 μg/L ZEA until 96 h post-fertilization (hpf) resulted in a highly significant increase in comet assay olive tail moments (OTM). Extensive apoptotic cells appeared in brain regions, accompanied by oxidative stress and DNA damage, with injury severity positively correlated with ZEA concentration and exposure

TABLE 1 Mitigating effects of natural products on ZEA and their applications.

Types of natural products	Representative substance	Primary mechanism of action	Experimental model/ effect(s)	References
Plant-derived Flavonoids	Rutin, Quercetin, Soy Isoflavones	1. Antioxidant: Scavenges ROS and enhances SOD and GSH-Px activity. 2. Anti-apoptotic/Anti-inflammatory: Regulates Bax/Bcl-2 balance and inhibits NF-κB pathway. 3. Anti-endocrine disruption: Competitively binds to estrogen receptors.	Alleviating ZEA damage to porcine endometrial cells, mouse liver, and male reproductive systems.	(44–58)
Plant-derived polysaccharides	Astragalus polysaccharides, nettle polysaccharides	1. Antioxidant Effects: Enhances SOD and GSH-Px activity while reducing MDA levels. 2. Immunomodulation: Inhibits ERS and apoptosis pathways (Bax/Caspase-3). 3. Signal Pathway Regulation: Involves pathways such as PI3K-Akt and glutathione metabolism.	Protects porcine testicular supporting cells and avian thymus cells, alleviating oxidative damage to the liver and kidneys.	(57–63)
Plant-derived Polyphenols	Proanthocyanidins, Curcumin, Resveratrol	1. Antioxidant: Activates the Nrf2/ARE pathway, upregulating the expression of HO-1 and other genes. 2. Anti-inflammatory: Inhibits NLRP3 inflammasome and NF-κB pathways. 3. Regulates the microbiota-organ axis: For example, curcumin modulates the "gut microbiota-testicular axis."	Reduce the toxicity of ZEA in mouse intestinal, liver, and testicular tissues, as well as in porcine kidney cells.	(62–70)
Microbial Source	*Bacillus cereus*, Meyerozyma caribbica, Lactic Acid Bacteria Consortium (LBC-4)	1. Secreting Degradative Enzymes: For instance, Bacillus belerensis produces CotA laccase and Prx peroxidase reductase, efficiently degrading ZEA into low-toxicity products under high-temperature, alkaline conditions. 2. Adsorption and biodegradation: For example, functional groups on the cell surface of Meyerozyma caribbica adsorb ZEA, while intracellular enzymes (laccase, peroxidase) biotransform it. The lactic acid bacteria Consortium (LBC-4) can degrade ZEA into less toxic derivatives.	1. Bacillus baileyensis exhibits an in vitro degradation rate of over 91% for ZEA, with significantly reduced estrogenic activity in the degradation products. 2. At a concentration of 1×10^8 cells/mL, Meyerozyma caribbica achieves an 80.3% degradation rate for ZEA. 3. The lactic acid bacteria Consortium (LBC-4) exhibits optimal attenuation effects at 37 °C and pH 7–8.	(70–78)
Mineral Source	Montmorillonite, Activated Carbon	Physical adsorption: Adsorption of ZEA molecules through charge interactions and pore structure.	Adsorption efficiency is limited, and desorption occurs; it may indiscriminately adsorb nutrients, resulting in restricted applications.	(78–81)
Bee-derived Products	Honey, Bee Pollen, Propolis	Antioxidant, Anti-inflammatory, Immunomodulatory: Rich in polyphenols, flavonoids; enhances antioxidant enzymes (SOD, CAT, GSH-Px); modulates immune function.	Honey: protects against liver injury, improves semen quality. Bee Pollen/Propolis: enhances total antioxidant capacity, immune cell activity, and antibody production in broilers.	(81–84)

duration (27). In rat primary testicular supporting cells, ZEA induced DNA damage and inhibited cell proliferation by activating the P-ATM → p53 → p21 signaling pathway, revealing its detrimental effects on male germ cell genetic material (28). Furthermore, in human breast cancer MCF7 cells, ZEA significantly elevated 5-methylcytosine levels and upregulated the expression of metabolism-related genes such as DNMT1, MGMT, IGF1, and HK2. However, it had no significant effect on DNA methylation or related gene expression in human normal breast epithelial MCF10F cells, suggesting that its genotoxicity exhibits cell specificity (29).

2.2.3 Immunotoxicity

The vast majority of immune cells express estrogen receptors on their surfaces. When ZEA binds to these receptors, it disrupts the normal functioning of the body's immune system. The immune system comprises three major components: immune molecules, immune cells, and immune organs. *In vitro* experiments with chicken spleen lymphocytes showed that after 48 h of exposure to 25 μg/mL ZEA, IL-2 mRNA levels increased while IL-6 and IFN-γ levels decreased significantly, indicating that ZEA infection may interfere with cytokine secretion in chicken spleen lymphocytes (30). Literature reports indicate

TABLE 2 Mechanisms and application prospects of natural products in countering ZEA toxicity.

Action dimension	Core strategy	Representative natural products	Specific mechanisms and targets	Advantages	Limitations and challenges
Source Elimination	Biological Degradation	*Bacillus velezensis*, *Bacillus amyloliquefaciens*	Secretes enzymes (e.g., CotA laccase, Prx peroxiredoxin) to directly break down ZEA into low-toxicity products (e.g., C17H24O4)	Efficient and specific; removes the toxin at its root; functions under broad conditions (thermostable, alkali-tolerant)	Environmental stability of strains/enzymes; long-term safety of degradation products requires comprehensive evaluation; industrial production costs
In Vivo Antagonism	Receptor Competition	Soy Isoflavones	Competitively binds to estrogen receptors (ERα/ERβ), blocking ZEA's estrogen-like effects	Direct mechanism; significant protective effects on the reproductive system; additional nutritional benefits	Efficacy depends on dose ratio; may produce complex estrogenic regulatory effects at high doses
	Signaling Pathway Regulation	Curcumin, Resveratrol, Proanthocyanidins, *Potentilla anserina* Polysaccharide	Activates antioxidant pathways (e.g., Nrf2/ARE, SIRT1/FOXO1); inhibits inflammation/apoptosis pathways (e.g., NF-κB, JNK)	Multi-target, comprehensive benefits; simultaneously alleviates oxidative stress, inflammation, and apoptosis	Complex composition makes mechanism studies difficult; potentially low absorption and bioavailability
Physical Protection	Adsorption	Montmorillonite, Activated Carbon	Non-specific physical adsorption via layered structure and high surface area, reducing intestinal absorption of ZEA	Low cost; easy to use; suitable for preliminary management of acute poisoning	Low adsorption efficiency for ZEA; risk of desorption; non-selectively adsorbs nutrients (vitamins, minerals)
Systemic Repair	Antioxidation/ Immunoregulation	Astragalus Polysaccharide, Honey, Bee Pollen, Propolis	Enhances activity of endogenous antioxidant enzymes (e.g., SOD, GSH-Px); protects immune organs (thymus, spleen); modulates cytokine secretion	Boosts the body's innate resistance; multiple functions (nutrition, antioxidation, immunity); high safety profile	Relatively slow onset; effects are indirect; quality and source of bee products can vary greatly
Ecological Intervention	Gut Microbiota Modulation	Lactic Acid Bacteria, Curcumin	Maintains gut microbiota balance (e.g., increases Lactobacillus abundance); repairs intestinal barrier; may confer indirect protection via the "gut-liver axis" or "gut-testis axis"	Focuses on holistic health; may reduce intestinal absorption and reabsorption of ZEA	Mechanistic research is still in early stages; effects show individual variability

that in experiments where ZEA induces porcine spleen damage, ZEA upregulates the expression and synthesis of pro-inflammatory cytokines such as TNF-α and IL-8, activates the JNK pathway, and inhibits p38/MAPK and NF-κB, thereby disrupting immune homeostasis (31). Liang et al. (32) found that ZEA significantly inhibited mouse thymic epithelial cell proliferation in a dose- and time-dependent manner. Furthermore, literature reports indicate that ZEA and its metabolites can also affect intestinal and humoral immunity, such as altering intestinal mucosal IgA levels and inhibiting lymphocyte proliferation, with metabolites often exhibiting greater toxicity than ZEA itself (33).

2.2.4 Cytotoxicity

ZEA exerts cytotoxic effects on multiple cell types. It induces oxidative stress and activates apoptotic signaling pathways, leading to oxidative damage, apoptosis, or abnormal proliferation in various cells. In germ cells, ZEA upregulates ERS marker proteins such as GRP78, CHOP, and PERK in porcine endometrial epithelial cells (PECs), activates the JNK pathway, promotes β-catenin nuclear translocation, blocks G1 phase progression, and inhibits Bax and Caspase3, thereby inducing abnormal cell proliferation (34). In porcine trophoblast cells (pTr), ZEA activates the PERK-eIF2α-ATF4-CHOP and MAPK pathways, inhibits PI3K/AKT, elevates ROS and Ca^{2+}, disrupts mitochondrial membrane potential, and induces autophagic apoptosis (35). In porcine endometrial stromal cells (ESCs), ZEA activates the ASK1-JNK pathway via the endoplasmic reticulum stress (ERS), elevates nuclear p-JNK, upregulates Bax and Caspase3/9 while downregulating Bcl-2, thereby intensifying apoptosis (36). In immune cells, 1–25 μg/mL ZEA inhibited LPS-activated mouse splenic lymphocyte proliferation with inhibition rates ranging from 5.62 to 88.17% over 24–72 h. It concurrently induced DNA fragmentation, with apoptosis rates increasing to 33.15% at higher concentrations (37).

2.2.5 Hepatotoxicity and nephrotoxicity

As the primary organs for ZEA metabolism and excretion in the body, the liver and kidneys are key targets for its toxicity. Regarding hepatotoxicity, studies have demonstrated that ZEA treatment of primary support cells for 24 h promotes intracellular ROS production, reduces cell viability and antioxidant enzyme activity, and causes a decrease in mitochondrial membrane potential. Concurrently, it induces activation of the Caspase-dependent apoptosis pathway and enhances autophagy activity (38), indicating that its hepatotoxic mechanism is closely related to oxidative stress (39, 40). The kidney serves as a secondary metabolic organ and is one of the primary target organs for zearalenone. After multiple enterohepatic circulations *in vivo*, zearalenone is filtered by the kidneys and ultimately excreted in urine. Specific effects include inducing glomerular atrophy, tubular epithelial cell degeneration, and proteinuria. In renal toxicity studies, female Wistar rats administered 40 mg/kg ZEA via gavage for one week exhibited significantly reduced kidney weight, markedly elevated serum blood urea nitrogen (BUN) and uric acid (UA) levels, significantly decreased creatinine (CRE), along with increased malondialdehyde (MDA) in kidney tissue. Along with marked decreases in antioxidant enzyme activities such as superoxide dismutase (SOD), catalase (CAT), and glutathione peroxidase (GSH-px). Pathological lesions observed included renal vascular congestion, tubular dilatation, interstitial congestion, scattered cellular degeneration and necrosis, and glomerular cavity dilatation (41). Further mechanistic studies revealed that in porcine kidney epithelial cells (PK-15), ZEA induces apoptosis by activating ROS-mediated mitochondrial apoptosis pathways, upregulating pro-apoptotic proteins such as Bax and Caspase-3, and downregulating the anti-apoptotic protein Bcl-2 (42). Moreover, after ZEA enters the animal body, the liver can metabolize this toxin into two isomers: α-zearalenol (α-ZOL) and β-zearalenol (β-ZOL). The metabolite α-Zearalenol (α-ZOL) exhibits even greater cellular toxicity than ZEA itself, suggesting its metabolic activation process plays a critical role in liver and kidney toxicity (43).

2.3 Species-specific characteristics of ZEA toxicity

ZEA is a common mycotoxin that exerts toxic effects on various animal species. Pigs, chickens, cattle, and other animals are exposed to this toxin through consumption of ZEA-contaminated feed. Significant differences exist in ZEA sensitivity across species, primarily manifested in exposure routes, toxic doses, and typical clinical symptoms. Pigs are the most susceptible species to ZEA. Even trace amounts of ZEA in feed—as low as 0.1–0.15 mg/kg—can induce reproductive tract inflammation in sows. The maximum allowable levels of ZEA in feed for piglets and growing-finishing pigs are 0.1 mg/kg and 0.5 mg/kg, respectively. Typical clinical symptoms in pigs are concentrated in the reproductive system. For example, weaned gilts may exhibit vulvar hypertrophy and ovarian atrophy, while adult sows may experience infertility and pseudopregnancy. Boars may show testicular atrophy, sperm abnormalities, and reduced libido (4). In contrast, poultry and ruminants demonstrate higher tolerance. High ZEA doses (≥5 mg/kg) impair laying hen production performance and disrupt reproductive hormone secretion. At ZEA levels exceeding 5 mg/kg, laying hens exhibit significantly reduced average egg weight, markedly decreased blood luteinizing hormone (LH) levels, and markedly elevated progesterone levels, with these changes exhibiting a dose-dependent effect (44). Cattle, however, possess rumen microorganisms that partially degrade ZEA, resulting in a higher toxic threshold and atypical clinical symptoms. The primary potential impact is a slight reduction in reproductive performance. Case reports indicate that when corn zearalenone levels in feed reach 200 mg/kg, growing cattle exhibit toxic symptoms such as restlessness, reddened vaginal mucosa, and swollen labia (45).

These differences primarily stem from interspecies variations in metabolic pathways: pigs convert ZEA into the more toxic α-zearalenol, whereas poultry and ruminants produce less toxic metabolites. Therefore, subsequent research on natural product detoxification strategies for ZEA must account for species specificity: For swine, focus should be placed on developing formulations that block ZEA's estrogen-like activity and promote excretion. For poultry and cattle, emphasis should shift toward additives that protect intestinal health and enhance overall production performance, enabling precise and effective detoxification interventions.

3 Research on natural products for ZEA attenuation

3.1 Plant-derived natural products

3.1.1 Flavonoids

Upon entering the animal body, ZEA can cause structural damage and functional impairment in multiple organs and tissues through various pathways, including oxidative stress, apoptosis, inflammatory responses, and endocrine disruption. In recent years, flavonoid natural medicines have garnered significant attention in ZEA poisoning research due to their wide availability, low toxicity, and multifaceted biological activities. Their detoxifying effects primarily achieve ZEA poisoning mitigation through multi-pathway, multi-target interventions.

Regarding the alleviation of oxidative damage, ZEA induces the production of large amounts of reactive oxygen species (ROS) upon entering the body. When ROS generation exceeds clearance, it triggers lipid peroxidation reactions, producing harmful substances such as malondialdehyde (MDA). Concurrently, it inhibits the activity of antioxidant enzymes like superoxide dismutase (SOD) and glutathione peroxidase (GSH-Px), disrupting the body's oxidative stress balance and causing oxidative damage to tissues like the uterus, liver, and spleen. Flavonoid-based natural medicines such as hyperoside, quercetin, rutin, and silymarin effectively address this issue. On one hand, they directly react with ROS to eliminate them, reducing ROS attacks on cells. On the other hand, they activate the body's own antioxidant enzyme system, enhancing the activity and expression levels of antioxidants like SOD and GSH-Px, thereby strengthening the body's ROS clearance capacity. Through these dual mechanisms, flavonoids significantly reduce the production of lipid peroxidation byproducts like malondialdehyde (MDA), maintain oxidative stress equilibrium, and mitigate ZEA-induced oxidative damage across multiple tissues and organs. These effects have been validated in various animal models and cellular experiments (46–51).

In inhibiting apoptosis and inflammatory responses, ZEA causes harm to the body by activating the apoptosis pathway. ZEA promotes the activation of Caspase family proteins while regulating the

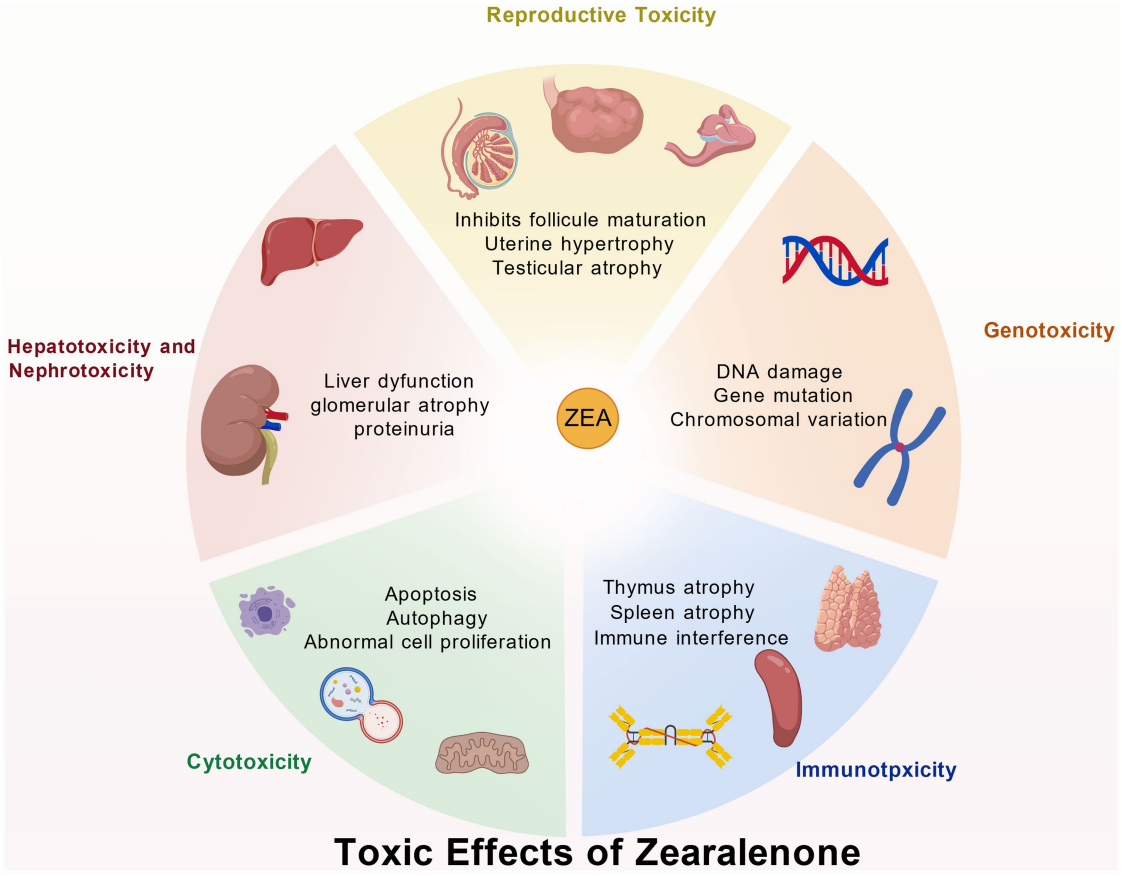

FIGURE 2
Toxic effects of zearalenone. Created with BioGDP.com.

expression of apoptosis-related proteins, leading to the upregulation of pro-apoptotic protein Bax and the downregulation of anti-apoptotic protein Bcl-2. This disrupts the balance of apoptosis, resulting in massive cell death in tissues. Additionally, ZEA induces the release of inflammatory mediators such as tumor necrosis factor-α (TNF-α) and interleukin-6 (IL-6), activating inflammatory signaling pathways like nuclear factor-κB (NF-κB) to trigger inflammatory damage. Flavonoid compounds like rutin and baicalin exhibit significant inhibitory effects against these mechanisms. Studies indicate that these compounds restore apoptotic balance by downregulating apoptosis-related proteins like Bax and Caspase-3 while upregulating Bcl-2 expression, thereby inhibiting excessive cell death (52, 53). For example, in a chick liver injury model established with 2.5 mg/kg ZEA, chicks were simultaneously administered 20 mg/kg, 40 mg/kg, or 80 mg/kg baicalin via oral gavage for one week. Immunohistochemical analysis revealed that baicalin dose-dependently reduced ZEA-induced hepatocyte apoptosis in chicks. Specifically, the 80 mg/kg baicalin group exhibited no significant difference in hepatocyte apoptosis compared to the blank control group, with virtually no discernible hepatocyte apoptosis observed (Xu Jingnan, 2022). In a ZEA-induced porcine endometrial stromal cell injury model, rutin was demonstrated to further enhance apoptosis inhibition by activating the nuclear factor E2-related factor 2 (Nrf2) signaling pathway (54). Treatment of porcine ESCs with 52.03 μM ZEA significantly increased the apoptosis rate. The addition of 25 μM rutin significantly reduced ZEA-induced apoptosis in porcine ESCs ($p < 0.01$). When Nrf2 was pre-silenced (si-Nrf2), ZEA-induced apoptosis further increased, and the addition of 25 μM rutin significantly suppressed this enhanced apoptotic effect (Z + N + R group vs. Z + N group, $p < 0.01$) (Chen et al., 2025). Concurrently, these flavonoids inhibit the activation of inflammatory signaling pathways such as NF-κB, reducing the secretion of inflammatory mediators like TNF-α and IL-6. This effectively alleviates inflammatory states in tissues like the liver and mitigates ZEA-induced inflammatory damage (55). In a model inducing porcine renal epithelial cell damage, quercetin targets CaSR to inhibit the CaSR/CaMKII pathway, regulating calcium homeostasis and maintaining mitochondrial dynamics stability, thereby preventing ZEA-induced apoptosis (56).

Regarding antagonizing endocrine-disrupting effects, ZEA exhibits estrogen-like activity by competitively binding to estrogen receptor alpha (ERα) and estrogen receptor beta (ERβ) in animals. This interferes with normal hormonal signaling pathways, leading to reproductive endocrine disorders and subsequent reproductive system abnormalities in animals, such as abnormal follicle development in sows and reduced sperm quality in boars. Flavonoid compounds like soy isoflavones demonstrate unique advantages in this context. They compete with ZEA for estrogen receptor binding sites. Due to their stronger binding affinity, they reduce ZEA's receptor occupancy, thereby diminishing its estrogenic effects. Simultaneously, soy isoflavones regulate estrogen receptor expression levels, restoring

10.3389/fvets.2025.1710151

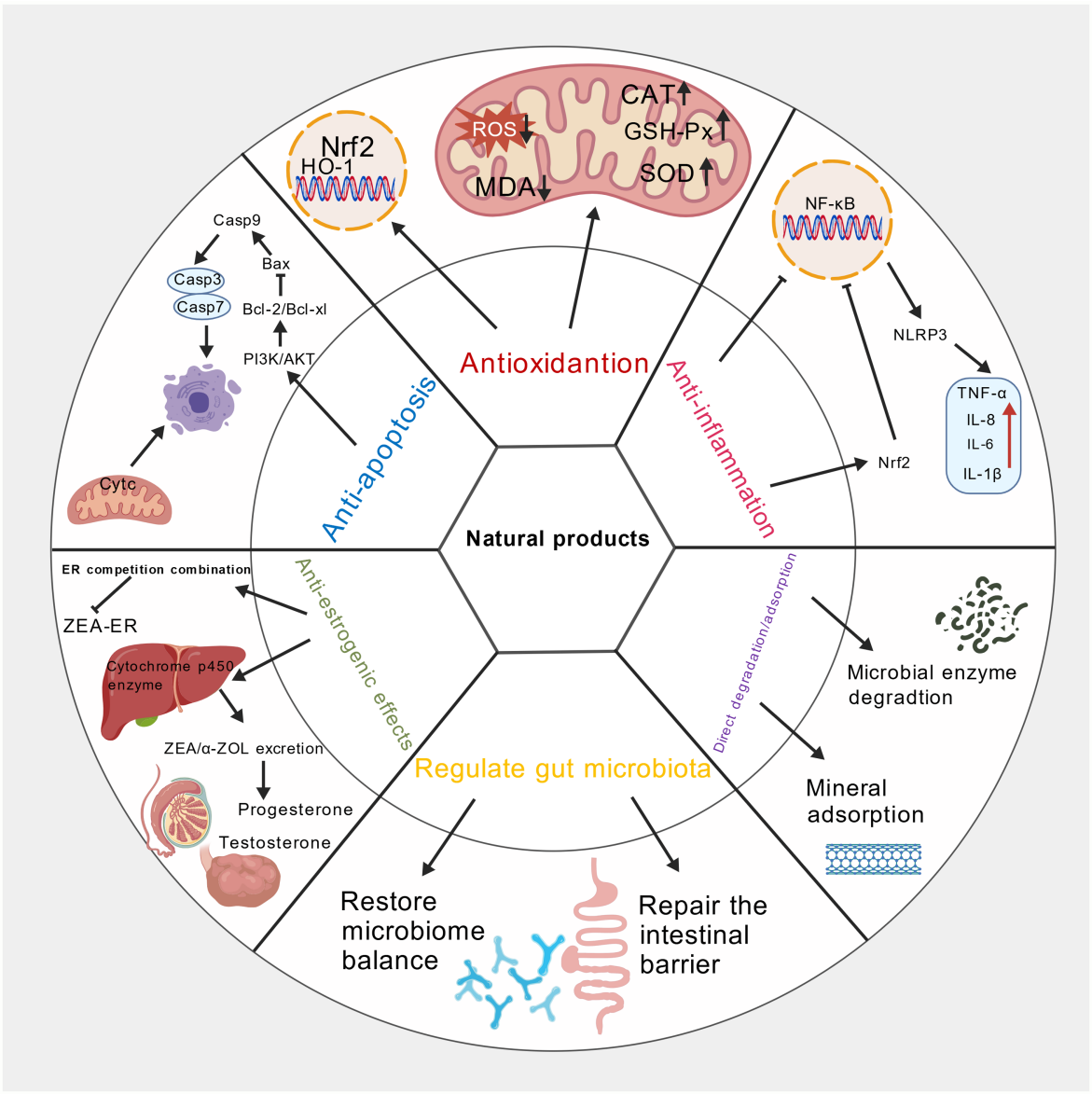

FIGURE 3
Mechanism diagram of natural products alleviating zearalenone toxicity. Created with BioGDP.com.

normal hormone signaling pathways and maintaining reproductive endocrine balance (57). Furthermore, Practical application studies reveal that supplementing sow diets with soy isoflavones not only antagonizes ZEA's estrogenic effects but may also accelerate the biotransformation and degradation of ZEA and its metabolites within the body by regulating the activity of relevant metabolic enzymes in tissues such as the liver. This approach reduces ZEA residues in the liver and muscle tissues of gilts during puberty and post-puberty, thereby mitigating the persistent harm caused by ZEA to animal organisms (58).

In summary, flavonoid-based natural medicines significantly mitigate ZEA toxicity through multiple mechanisms, including alleviating oxidative damage, inhibiting apoptosis and inflammatory responses, and antagonizing endocrine disruption. As research continues to advance, the application prospects of flavonoid-based natural medicines in alleviating ZEA poisoning will become increasingly broad, providing important research directions and potential solutions for addressing livestock production and food safety issues caused by ZEA contamination.

3.1.2 Polysaccharides

Polysaccharide-based natural medicines, characterized by their wide availability, high biocompatibility, minimal toxicity, and multifaceted biological activities, including antioxidant, immunomodulatory, and anti-inflammatory effects, have emerged as a significant research focus for alleviating ZEA poisoning. These substances exert protective effects through multidimensional and multitranslational pathways by precisely targeting key pathological stages of ZEA poisoning, offering novel strategies for its prevention and control.

Polysaccharides from diverse sources demonstrate unique advantages in mitigating ZEA-induced oxidative stress and

apoptosis. *Pteridium aquilinum* polysaccharide (PAP-1b) exhibited significant protective effects in studies targeting testicular supporting cells of Changbai pigs (59). As critical cells maintaining spermatogenesis, testicular supporting cells are highly susceptible to ZEA toxicity. PAP-1b enhances cellular ROS scavenging capacity by boosting the activity of antioxidant enzymes such as superoxide dismutase (SOD) and glutathione peroxidase (GSH-Px). Concurrently, it reduces levels of the lipid peroxidation product malondialdehyde (MDA) and the cellular damage marker lactate dehydrogenase (LDH), effectively mitigating ZEA-induced oxidative damage. Further studies revealed that PAP-1b also modulates apoptosis-related molecules to restore the Bax/Bcl-2 ratio and mitochondrial membrane potential, thereby inhibiting apoptosis. Its protective effects are closely associated with the PI3K-Akt signaling pathway and glutathione metabolism pathway. Key molecules in these pathways, GPX1 and SELENOK, play central roles in mediating PAP-1b's detoxification effects. For example, a porcine testicular supporting cell damage model was established using 100 μM ZEA. After 4 h of pretreatment with 150 μg/mL Pteridium polysaccharide (PAP-1b), cells were cultured continuously for 48 h. flow cytometry analysis revealed significantly elevated apoptosis rates in the ZEA-treated group alone, whereas the PAP-1b-treated group exhibited significantly reduced apoptosis rates compared to the ZEA group ($p < 0.05$), with apoptosis levels approaching those of the blank control group (Shi et al., 2025).

Regarding the repair of ZEA-induced immune suppression, the thymus, as a central immune organ, is a critical site for T lymphocyte differentiation and maturation. ZEA can impair immune function by inducing thymocyte apoptosis. Astragalus polysaccharides (APS) significantly protect chicken thymocytes by downregulating the expression of endoplasmic reticulum stress-related genes such as ATF4, ATF6, and CRP78, as well as pro-apoptotic genes like Bax and Caspase-3, while simultaneously upregulating the expression of the anti-apoptotic gene Bcl-2, thereby inhibiting ZEA-induced thymocyte apoptosis. At a concentration of 200 μg/mL, APS exhibited optimal protective effects on thymocytes, effectively restoring thymic tissue morphology, enhancing immune cell activity, repairing ZEA-induced immune suppression, and strengthening the body's antitoxic capacity (60).

Beyond the aforementioned polysaccharides, substances such as Poria cocos polysaccharide (PCP), *Lycium barbarum* polysaccharide (LBP), and selenium-chitosan also demonstrate promising potential in alleviating ZEA toxicity (61–63). PCP alleviates ZEA-induced oxidative damage across multiple tissues by elevating antioxidant enzyme activity (SOD, GPx) in mouse liver and kidney tissues, reducing MDA levels, and maintaining normal organ physiological functions. LBP specifically protects against ZEA-induced renal injury by inhibiting ZEA-induced mitochondrial apoptosis and autophagy in mouse kidneys. It reduces pathological damage and fibrosis in renal tissue by downregulating pro-apoptotic and autophagy-related molecules, thereby preserving renal filtration and metabolic functions. Selenium-chitosan, a conjugate of selenium and chitosan, demonstrated superior protective effects in a porcine endometrial epithelial cell injury model. It significantly downregulates ZEA-induced expression of genes, including JNK, ASK1, c-Jun, MKK4, and p53 by reducing intracellular ROS levels. By modulating the JNK/SAPK signaling pathway, it effectively mitigates ZEA-induced cell cycle arrest, mitochondrial damage, and apoptosis, offering a novel strategy for protecting endometrial function and reducing reproductive disorders in livestock and poultry.

In summary, polysaccharide-based natural medicines exert detoxification effects through multiple pathways, including enhancing antioxidant capacity, precisely regulating signaling pathways, and inhibiting apoptosis. Their mechanisms of action cover several key pathological stages of ZEA poisoning. These findings not only enrich the theoretical framework for ZEA poisoning prevention and control but also provide crucial experimental evidence for developing safe and effective natural anti-ZEA toxins. This research holds significant practical and applied value for promoting the healthy development of livestock and poultry farming and ensuring food safety.

3.1.3 Polyphenols

ZEA is a common mycotoxin that damages the liver, reproductive system, and intestines. Polyphenolic natural medicines possess antioxidant, anti-inflammatory, and cell signaling pathway-modulating properties, enabling detoxification through multiple pathways. Proanthocyanidins (PCs) are internationally recognized as potent natural antioxidants and are widely used in ZEA detoxification research. Their protective effects primarily arise from regulating pathways associated with oxidative stress and apoptosis. In the mouse intestinal epithelial cell (MODE-K) model, ZEA activates the endoplasmic reticulum stress (ERS)-apoptosis pathway by upregulating ERS-related mRNA and protein expression, including CHOP, GRP78, JNK, and Caspase-12. Simultaneously reducing anti-apoptotic protein Bcl-2 levels and increasing pro-apoptotic protein Bax levels to induce apoptosis. It also inhibits superoxide dismutase (SOD) and glutathione peroxidase (GSH-Px) activity, decreases glutathione (GSH) content, and increases malondialdehyde (MDA) production, leading to oxidative damage. Conversely, PCs at concentrations of 5–15 μg/mL significantly reversed these changes by reducing apoptosis rates, restoring antioxidant enzyme activity and GSH content, inhibiting MDA elevation, and downregulating the expression of molecules associated with the ERS apoptosis pathway. This mechanism involves suppressing ERS-induced apoptosis pathways and alleviating oxidative stress (64). In mouse testicular supporting cells (TM4 cells), ZEA disrupts the Nrf2/ARE signaling pathway, downregulating mRNA and protein expression of Nrf2 and its downstream target genes HO-1, NQO1, GSH-Px, and γ-GCS, thereby weakening cellular antioxidant capacity. PCs (2.5–10 μg/mL) can activate the Nrf2/ARE pathway, upregulate the expression of the aforementioned antioxidant genes and proteins, enhance SOD and GSH-Px activity, reduce MDA accumulation, and decrease lactate dehydrogenase (LDH) release, thereby mitigating ZEA-induced cellular oxidative damage and apoptosis. The protective effect is optimal at a concentration of 5 μg/mL (65).

Curcumin (CUR), an extract from the ginger family, exhibits antioxidant, anti-inflammatory, and gut microbiota-modulating effects, demonstrating protective actions against ZEA-induced damage to the liver, kidneys, and reproductive system. In a mouse liver injury model, ZEA (40 mg/kg) induced hepatocyte edema, mitochondrial vacuolation, elevated serum AST and ALT activity, increased ROS and MDA levels in liver tissue, decreased SOD, CAT, and GSH-Px activity, activated the NLRP3 inflammasome, and upregulated NLRP3, Caspase-1p20 protein, and IL-1β expression. Conversely, 150 mg/kg curcumin mitigated hepatic pathological

damage through dual antioxidant and anti-inflammatory actions, restoring antioxidant enzyme activity, reducing ROS and MDA levels, inhibiting NLRP3 inflammasome activation and IL-1β release, and alleviating hepatic oxidative stress and inflammatory responses (66). In porcine kidney epithelial cells (PK-15 cells), ZEA (36.55 μg/mL) induces cellular oxidative stress, increases ROS and MDA production, and decreases SOD and CAT activity. Curcumin (6.25–25 μmol/L) activates the SIRT1/FOXO1 signaling pathway, upregulates SIRT1 protein expression, and reduces FOXO1 acetylation. This promotes mRNA and protein expression of downstream antioxidant enzymes Mn-SOD and CAT, scavenges ROS, reduces lipid peroxidation, and alleviates ZEA-induced oxidative damage in renal cells (42). Furthermore, in a male mouse model of reproductive damage, ZEA (40 mg/kg) disrupts gut microbiota balance by decreasing Lactobacillus abundance while increasing Prevotella and Bacteroides abundance. This activates the IL-17A-TNF-α signaling pathway in testes, reducing testosterone secretion, decreasing sperm survival rates, and increasing deformity rates. Curcumin at 200 mg/kg modulates gut microbiota structure, restores beneficial bacterial abundance, inhibits IL-17A pathway activation, elevates testosterone levels, and improves sperm quality. Its protective effects are associated with the regulation of the "gut microbiota-testicular axis" (67).

Resveratrol (RSV) is a natural polyphenolic antioxidant primarily found in plants such as grapes and *Polygonum cuspidatum*. RSV can reduce ZEA toxicity through multiple pathways. Regarding liver protection, in a ZEA-induced liver injury mouse model, RSV alleviated pathological damage, restored antioxidant enzyme activity, inhibited NF-κB nuclear translocation and inflammatory factor release, demonstrating optimal protective effects (68). In mouse testicular supporting cells, RSV activates the PI3K/Akt pathway, promotes Akt phosphorylation, thereby driving Nrf2 nuclear translocation and upregulating HO-1 expression. This enhances cellular antioxidant capacity, reduces ROS production, and inhibits apoptosis-related proteins (Caspase-3, PARP cleavage) while increasing the Bax/Bcl-2 ratio, thus preventing cell death (69). Regarding intestinal protection, ZEA disrupts the intestinal barrier in mice. A 100 mg/kg RSV dose restores intestinal structure and barrier function by activating the Nrf2 pathway and inhibiting the NF-κB pathway to alleviate damage (70).

In summary, polyphenolic natural compounds mitigate ZEA toxicity through multi-targeted, multi-pathway mechanisms, including regulating oxidative stress-related pathways, inhibiting inflammatory pathways, and improving gut microbiota dysbiosis. Different polyphenolic compounds exhibit distinct target profiles: proanthocyanidins and resveratrol primarily regulate intracellular antioxidant and apoptosis pathways, while curcumin combines antioxidant, anti-inflammatory, and gut microbiota-modulating effects. These findings provide theoretical foundations for ZEA poisoning prevention and treatment, laying the groundwork for polyphenolic applications in animal husbandry.

3.2 Microbial-derived natural products

3.2.1 Bacillus species

Bacillus species demonstrate exceptional performance in mitigating zearalenone toxicity due to their potent degradation capabilities and environmental adaptability. For instance, the Bacillus paeiliosus strain PA26-7 efficiently degrades zearalenone by secreting extracellular enzymes. This strain degrades zearalenone under a wide range of conditions: initial medium pH 4.0–8.0 and cultivation temperatures 25–60 °C. The degradation products exhibit lower cytotoxicity and estrogenic activity compared to zearalenone (71). Additionally, the *Bacillus velezensis* strain B.26 is particularly noteworthy. Studies indicate that this strain can degrade 91.64% of ZEA within 24 h at 70 °C and pH 10.0 (72). This high degradation efficiency is primarily attributed to its secreted CotA laccase and Prx peroxidoreductase. Through genomic mining and molecular cloning techniques, researchers successfully isolated and recombinantly expressed these two enzymes. CotA enzyme achieved over 91% degradation of ZEA within 6 h at 70 °C and pH 8.0, with its activity significantly enhanced by adding ions such as Na^+ and Cu^{2+}. Prx enzyme reached a degradation rate of 59.74% for ZEA within 6 h at 70 °C and pH 11.0. This indicates that both enzymes exhibit high degradation efficiency under both high-temperature and alkaline conditions. Their degradation products are low-toxicity compounds C17H24O4 and C12H16O4, without generating high-risk estrogen metabolites such as α-ZEL, thereby ensuring the safety of the degradation process.

Bacillus degradation enzymes show broad application prospects for mitigating zearalenone toxicity. These enzymes not only demonstrate high degradation efficiency under laboratory conditions but are also considered to possess significant potential for application in the food and feed industries due to their environmental friendliness and safety. With further technological optimization and commercialization, these degradative enzymes are expected to become powerful tools for degrading and removing mycotoxin contamination. Additionally, the *Bacillus amyloliquefaciens* strain XJ-140 was screened for its high-efficiency ZEA degradation capability, degrading 93.75% of ZEA (2 μg/mL) within 24 h of incubation. This degradation primarily occurs via extracellular enzymes, supplemented by cell wall adsorption (73).

3.2.2 Yeast

Yeast exhibits significant potential for degrading ZEA in corn. Recent studies have revealed unique mechanisms and high efficiency in ZEA degradation by various yeast strains. For instance, the Tibetan yeast strain *Saccharomyces cerevisiae* KAB68 demonstrates outstanding ZEA degradation capabilities. At a culture density of 1×10^8 cells/mL, this strain achieved an 80.3% degradation rate for ZEA. Studies indicate that this yeast strain removes ZEA through a dual mechanism involving adsorption and intracellular biodegradation (74). This dual-action mechanism not only enhances degradation efficiency but also ensures the environmental friendliness of the degradation process.

The mechanism of yeast-mediated ZEA degradation primarily involves adsorption and biotransformation. During adsorption, functional groups on the yeast cell surface—such as O–H, N–H, C═O, and C–O—bind to ZEA molecules, thereby reducing their free concentration in solution (75). During biotransformation, yeast secretes specific enzymes like laccase and peroxidase to degrade ZEA into less toxic metabolites. For instance, Pichia pastoris has been engineered to express zearalenone-degrading enzymes, which efficiently break down ZEA during fermentation (76). Additionally,

components of the yeast cell wall participate in the adsorption of ZEA, further enhancing its degradation capacity.

These studies not only elucidate the molecular mechanisms by which yeast degrades ZEA but also provide a theoretical basis for developing yeast-based bio-detoxifiers. Future research should focus on further optimizing degradation conditions for yeast to enhance its efficiency and stability in practical applications, as well as identifying additional yeast strains with high degradation capacity.

3.2.3 Lactic acid bacteria

Lactic acid bacteria have garnered increasing attention in recent years for their role in degrading zearalenone (ZEA) due to their widespread application and safety profile in the food industry. Research indicates that lactic acid bacteria reduce ZEA toxicity through two primary mechanisms: adsorption and biotransformation. For instance, current research demonstrates that the novel lactic acid bacteria strain LBC-4 can degrade ZEA into less toxic derivatives, with optimal detoxification occurring at 37 °C and pH 7–8 (77). In animal studies, Lactobacillus significantly reduced ZEA's toxic effects on rat blood, liver, kidneys, and uterus, while aiding in the restoration of normal physiological and biochemical parameters (78).

Although lactic acid bacteria show great potential for ZEA detoxification, further research is needed on their biodegradation mechanisms, the toxicity of degradation products, and microbial safety for animals.

3.3 Mineral-based natural products

Research on mineral-based natural products for reducing zearalenone toxicity has primarily focused on activated carbon and montmorillonite. As a natural mineral adsorbent, montmorillonite exhibits adsorption properties toward zearalenone. It can adsorb various mycotoxins, thereby reducing their levels in feed. First, most mineral adsorbents exhibit poor adsorption efficiency for ZEA. Experimental results indicate that the adsorption rate of sodium-based montmorillonite ZEA is only 4%, suggesting certain limitations in the physical adsorption method. This is attributed to ZEA's weakly polar groups and low electrophilicity, making charge-based adsorption difficult (79). Second, when using montmorillonite as an adsorbent, desorption of zearalenone must be considered. Research indicates that montmorillonite exhibits good adsorption of zearalenone under acidic conditions at pH 3. However, desorption of adsorbed zearalenone occurs at both pH 3 and pH 5, with particularly pronounced desorption observed at pH 5 (80). This implies that in practical applications, relying solely on montmorillonite's adsorption capacity may not fully eliminate zearalenone, necessitating comprehensive consideration of both adsorption and desorption phenomena. Additionally, activated carbon—a highly porous, insoluble powder with a large specific surface area—exhibits strong adsorption capacity but non-selectively binds feed nutrients, potentially causing adverse effects in animals. For instance, adding 2.5% or 5.0% montmorillonite to pig diets resulted in liver damage (81). Mineral-based natural products like montmorillonite and activated carbon show potential for reducing zearalenone toxicity, but limitations include restricted adsorption capacity, desorption issues, and indiscriminate nutrient binding. In production practice, the selection and optimization of adsorbent usage protocols should be based on factors such as feed pH, animal digestive physiology, and the type and concentration of zearalenone in the feed. This approach ensures more effective zearalenone removal, safeguarding feed safety and animal health.

3.4 Bee-derived natural products

ZEA primarily exhibits toxic effects including reproductive toxicity, immunosuppression, and liver damage. These effects not only disrupt normal physiological functions in animals but also lead to reduced livestock production efficiency and economic losses. Bee-derived natural products are substances formed through fermentation when bees collect raw materials such as plant pollen and nectar and combine them with their own secretions. Core categories include bee pollen, honey, and propolis, while other components with potential bioactivity encompass beeswax and royal jelly (82). Recent domestic and international studies confirm that bee-derived natural products are rich in bioactive substances such as polyphenols, flavonoids, polysaccharides, amino acids, vitamins, and minerals. They exhibit multiple pharmacological effects including antioxidant, anti-inflammatory, immunomodulatory, and hepatoprotective/nephroprotective properties (83, 84). This provides scientific rationale for their potential to antagonize ZEA toxicity and positions them as an emerging direction in ZEA detoxification research.

From the perspective of the correlation between chemical composition and pharmacological effects, the detoxification potential of bee-derived natural products is closely related to their unique composition. Bee pollen, a granular substance formed when bees collect pollen grains from plant anthers and mix them with their own secretions, contains core active components such as flavonoids (e.g., rutin, quercetin), polyphenols, and polysaccharides. Among these, flavonoids can scavenge excess reactive oxygen species (ROS), activate the antioxidant pathway via nuclear factor E2-related factor 2 (Nrf2), enhance the activity of antioxidant enzymes such as superoxide dismutase (SOD) and glutathione peroxidase (GSH-Px), and simultaneously inhibit the production of malondialdehyde (MDA), a lipid peroxidation product. This mechanism closely aligns with the previously described pathway by which plant-derived flavonoids (e.g., soy isoflavones) antagonize ZEA-induced oxidative damage. Regarding immune regulation, the polysaccharides in bee pollen promote T-lymphocyte and B-lymphocyte proliferation, elevate immunoglobulin (IgA, IgM) secretion levels, and enhance leukocyte activity, thereby repairing damage to immune organs. This is crucial for mitigating ZEA-induced immunosuppression. Research confirms that adding 2–3% bee pollen to broiler feed significantly alleviates thymus and spleen atrophy caused by ZEA (5 mg/kg) and reverses the decline in peripheral blood cytokine levels (e.g., IL-2, IFN-γ). This effect is mediated by activating the PI3K-Akt signaling pathway and suppressing excessive NF-κB inflammatory pathway activation, directly supporting the detoxification value of "bee pollen" highlighted in the keywords (84).

Honey, as the most extensively studied category among natural apicultural products, primarily consists of glucose and fructose (accounting for approximately 60–80%), alongside phenolic acids

(such as caffeic acid and chlorogenic acid), flavonoids (including apigenin and kaempferol), and enzymes (like sucrase and catalase) (85, 86). These components confer honey with significant antioxidant and hepatoprotective activities: In a mouse model of alcoholic liver injury, 15 g/kg of red eucalyptus honey alleviated hepatic edema and inflammatory infiltration by upregulating mRNA and protein expression of CAT, SOD, and GSH-Px, while reducing serum alanine aminotransferase (ALT) and aspartate aminotransferase (AST) activity (85). In ZEA-induced liver injury, phenolic acids in honey mitigated hepatocyte apoptosis by inhibiting NLRP3 inflammasome activation, reducing proinflammatory factor release (e.g., IL-1β), and enhancing mitochondrial membrane potential stability. This mechanism synergized with curcumin's antagonism of ZEA hepatotoxicity. Furthermore, in studies on boar semen preservation, adding 10% buckwheat honey increased SOD and CAT activity in semen, reduced ROS accumulation, and improved sperm motility and survival rate (86). This finding suggests honey may mitigate ZEA-induced damage to male germ cells through antioxidant pathways, providing direction for future research.

Propolis is a resinous substance collected by bees from plant buds and tree bark, processed by mixing with their own secretions. Its primary active components include flavonoids (e.g., morin, pinobanksin), terpenoids, and phenolic esters (e.g., phenethyl caffeate). Modern pharmacological studies confirm propolis exhibits broad-spectrum antibacterial, anti-inflammatory, and immune-enhancing effects: On one hand, its flavonoid compounds competitively bind estrogen receptors (ERα/ERβ), reducing ZEA's binding efficiency to these receptors and thereby attenuating its estrogen-like effects—a mechanism similar to how soy isoflavones antagonize ZEA's reproductive toxicity. On the other hand, phenethyl caffeate in propolis can inhibit JNK signaling pathway activation, reduce the release of pro-inflammatory factors TNF-α and IL-6, and repair ZEA-damaged immune organs. In broiler chicken trials, supplementing feed with 0.1–0.2% propolis significantly enhanced total antioxidant capacity (T-AOC) in ZEA-exposed chickens, promoted spleen lymphocyte proliferation and antibody production, and synergistically improved ZEA-induced immunosuppression with bee pollen (84).

Overall, bee-derived natural products alleviate ZEA toxicity through multiple mechanisms—including antioxidant, anti-inflammatory, immunomodulatory, and endocrine-disrupting effects—due to their multi-component, multi-target characteristics. These effects complement the detoxification mechanisms of plant- and microbe-derived natural products. However, current research has limitations: First, the mechanisms of bee-derived natural products are primarily studied at the whole-animal or cellular level, with their active components (e.g., bee pollen flavonoids, propolis terpenoids) and direct interactions with ZEA (e.g., molecular docking, enzyme activity regulation) yet to be fully elucidated. Second, bee product quality is significantly influenced by plant sources and harvesting seasons, lacking standardized extraction and application protocols. Future research should integrate metabolomics and proteomics to decipher the key bioactive components and signaling pathways through which bee-derived natural products antagonize ZEA toxicity. Concurrently, establishing quality control standards for bee-derived detoxifiers will provide scientific support for their industrial application in preventing and controlling ZEA contamination within the livestock industry.

4 Summary and prospects

ZEA contamination is a complex global issue in agriculture and food safety, posing a multi-organ, multi-dimensional threat to animal health. This review demonstrates that relying on a single method is insufficient for effective mitigation. Natural products, due to their diverse mechanisms of action, offer an ideal solution for building a multi-layered, comprehensive defense system against toxicity. From microbial enzymes that degrade ZEA at the source, to plant active compounds that antagonize its effects *in vivo*, and to polysaccharides and bee products that systemically enhance the body's antioxidant and immune capacity, various natural strategies have their own focus and work synergistically.

Current research has progressed from simple efficacy observation to the exploration of molecular mechanisms, revealing the central role of key signaling pathways such as Nrf2, NF-κB, and ERS in the detoxification process. However, challenges remain: most studies are still at the experimental stage, far from large-scale clinical application; the safety and stability of microbial agents, the bioavailability of plant extracts, the selectivity of mineral adsorbents, and the standardization of bee products urgently need to be resolved.

Future research should concentrate on the following directions: First, deepen the investigation of the molecular mechanisms underlying natural product detoxification. Utilize modern biotechnologies such as gene editing and proteomics to further elucidate their target sites and signaling pathways, providing more precise targets for developing novel detoxifiers. Second, optimize the extraction, purification, and formulation processes of natural products to enhance their stability and bioavailability, developing natural detoxifier products suitable for different animal species and farming environments. Third, strengthen ecotoxicological research on microbial degradation of ZEA to assess its long-term impacts in natural environments, ensuring the safety and sustainability of microbial degradation technologies. Fourth, conduct large-scale field trials to validate the efficacy and safety of natural detoxifiers in practical aquaculture settings, advancing their industrial application. Additionally, international cooperation and exchange should be enhanced to integrate global resources in jointly addressing ZEA pollution, thereby contributing to food security and public health.

Author contributions

NL: Writing – original draft. QZ: Writing – original draft. YP: Writing – review & editing. CS: Writing – review & editing. GS: Writing – original draft.

Funding

The author(s) declare that financial support was received for the research and/or publication of this article. This research was funded by Jilin Province science and technology development Project (grant number 20240601087RC).

Acknowledgments

Image sources created with BioGDP.com.

Conflict of interest

The authors declare that the research was conducted in the absence of any commercial or financial relationships that could be construed as a potential conflict of interest.

Generative AI statement

The authors declare that no Gen AI was used in the creation of this manuscript.

Any alternative text (alt text) provided alongside figures in this article has been generated by Frontiers with the support of artificial intelligence and reasonable efforts have been made to ensure accuracy, including review by the authors wherever possible. If you identify any issues, please contact us.

Publisher's note

References

1. Gruber-Dorninger C, Jenkins T, Schatzmayr G. Global mycotoxin occurrence in feed: a ten-year survey. *Toxins*. (2019) 11:375. doi: 10.3390/toxins11070375

2. Marin S, Ramos AJ, Cano-Sancho G, Sanchis V. Mycotoxins: occurrence, toxicology, and exposure assessment. *Food Chem Toxicol.* (2013) 60:218–37. doi: 10.1016/j.fct.2013.07.047

3. Wang XY, Lou X, Du JH, Bai YJ, Fan ZH, Liao CS. Study on the contamination of zearalenone in feeds and feed raw materials in China. In proceedings of the 28th academic symposium of the veterinary pathology branch of the Chinese Association of Animal Science and Veterinary Medicine, the 27th academic symposium of the animal pathophysiology professional Committee of the Chinese Association of pathophysiology, the 7th academic symposium of the experimental pathology professional Committee of the Chinese Association for laboratory animal sciences, and the 6th academic symposium of the veterinary pathologist branch of the Chinese veterinary association. Henan: Henan University of Science and Technology (2025). doi: 10.26914/c.cnkihy.2025.035296

4. Xu WJ, Wei WJ, Chen XG, Zhang ZQ, Liu YM, Lü QX. Research progress on the hazards of zearalenone to pigs and its prevention and control. *Feed Res.* (2024) 47:166–71. doi: 10.13557/j.cnki.issn1002-2813.2024.05.031

5. Jia R, Ma Q, Fan Y, Ji C, Zhang J, Liu T, et al. The toxic effects of combined aflatoxins and zearalenone in naturally contaminated diets on laying performance, egg quality, and mycotoxin residues in eggs of layers, and the protective effect of *Bacillus subtilis* biodegradation product. *Food Chem Toxicol.* (2016) 90:142–50. doi: 10.1016/j.fct.2016.02.010

6. Li HM. Clinical symptoms, laboratory examination, prevention, and treatment of zearalenone poisoning in pigs. *Modern Anim. Husbandry Sci. Technol.* (2017) 10:98–137. doi: 10.19369/j.cnki.2095-9737.2017.10.090

7. Feng YQ, Zhao AH, Wang JJ, Tian Y, Yan ZH, Dri M, et al. Oxidative stress as a plausible mechanism for zearalenone to induce genome toxicity. *Gene*. (2022) 829:146511. doi: 10.1016/j.gene.2022.146511

8. Xue LL, Zhang PZ, Yang XJ, Fan SW, Li W. Research progress on contamination status and biological detoxification of zearalenone in corn and its by-products. *Anim Husb Vet Med.* (2024) 56:145–51.

9. Qi L, Li Y, Luo X, Wang R, Zheng R, Wang L, et al. Detoxification of zearalenone and ochratoxin a by ozone and quality evaluation of ozonised corn. *Food Addit Contam Part A Chem Anal Control Expo Risk Assess*. (2016) 33:1700–10. doi: 10.1080/19440049.2016.1232863

10. Feng XL, Zhou YH, Li LA, Jiao XL. Research progress on the hazards of zearalenone and the detoxification effect of physical adsorbents. *Modern Agric. Sci. Technol.* (2021) 21:133–5. doi: 10.3969/j.issn.1007-5739.2021.21.048

11. Gao G, Jiang H, Lin H, Yang H, Wang K. Asiaticoside ameliorates uterine injury induced by zearalenone in mice by reversing endometrial barrier disruption, oxidative stress, and apoptosis. *Rep. Biol. Endocrinol.* (2024) 22:118. doi: 10.1186/s12958-024-01288-6

12. Sun PX, Yin LL, Meng G, Sun SX, Zhang YY, Shi YX, et al. Research progress on the elimination of zearalenone by plant extracts. *Feed Res.* (2023) 46:158–64. doi: 10.13557/j.cnki.issn1002-2813.2023.16.030

13. Jing S, Liu C, Zheng J, Dong Z, Guo N. Toxicity of zearalenone and its nutritional intervention by natural products. *Food Funct*. (2022) 13:10374–400. doi: 10.1039/D2FO01545E

14. Salem IB, Boussabbeh M, Neffati F, Najjar MF, Abid-Essefi S, Bacha H. Zearalenone-induced changes in biochemical parameters, oxidative stress and apoptosis in cardiac tissue: protective role of crocin. *Hum Exp Toxicol.* (2016) 35:623–34. doi: 10.1177/0960327115597467

15. Wu FY, Yang XY, Li JL, Chen BJ. Research progress on reproductive toxicity of zearalenone to sows. *Acta Vet Zootech Sin*. (2020) 51:227–33. doi: 10.11843/j.issn.0366-6964.2020.02.003

16. Kowalska K, Habrowska-Górczyńska DE, Piastowska-Ciesielska AW. Zearalenone as an endocrine disruptor in humans. *Environ Toxicol Pharmacol*. (2016) 48:141–9. doi: 10.1016/j.etap.2016.10.015

17. Wang H. Epidemiological characteristics, clinical manifestations, prevention and treatment of zearalenone poisoning in pigs. *Modern Animal Husb. Sci. Technol.* (2019) 47:90–1. doi: 10.19369/j.cnki.2095-9737.2019.04.046

18. Xiao ZJ. Zearalenone poisoning and reproductive disorders in pigs. *China Anim Husb Vet Med.* (2005) 32:45–6. doi: 10.3969/j.issn.1671-7236.2005.02.018

19. Yuan T, Li J, Wang Y, Li M, Yang A, Ren C, et al. Effects of zearalenone on production performance, egg quality, ovarian function and gut microbiota of laying hens. *Toxins*. (2022) 14:653. doi: 10.3390/toxins14100653

20. Zhang WL, Li QF, Luo Y, Zhang XD, Yang H, Deng H. Effects of zearalenone on production performance, ovarian tissue structure and ERα expression in laying hens. *China Poultry*. (2021) 43:30–5. doi: 10.16372/j.issn.1004-6364.2021.08.006

21. Ling AR, Guo JL, Guo WB, Yang JH, Zhao ZH. Effects of zearalenone on production performance, blood indicators and reproductive hormone levels in laying hens. *Acta Agric Shanghai*. (2019) 35:100–6. doi: 10.15955/j.issn1000-3924.2019.04.18

22. Yang L, Liao W, Dong J, Chen X, Huang L, Yang W, et al. Zearalenone promotes uterine hypertrophy through AMPK/mTOR mediated autophagy. *Toxins*. (2024) 16:73. doi: 10.3390/toxins16020073

23. Lü YM. Study on zearalenone-induced apoptosis of porcine Leydig cells via mitochondria-mediated PI3K-AKT signaling pathway [master's thesis]. Shenyang: Shenyang Agricultural University (2023).

24. Liu P, Zheng H, Gu Y, Xu Z, Zou H, Gu J, et al. Zearalenone toxin induces pyroptosis by activating mitochondrial DNA-STING-NFκB axis in testis and TM4 cell damage. *Chem Biol Interact*. (2025) 418:111618. doi: 10.1016/j.cbi.2025.111618

25. Liu T, Liu G, Xu Y, Huang Y, Zhang Y, Wu Y, et al. Zearalenone induces blood-testis barrier damage through endoplasmic reticulum stress-mediated paraptosis of Sertoli cells in goats. *Int J Mol Sci*. (2023) 25:553. doi: 10.3390/ijms25010553

26. Li RF, Wu J, Yuan LY, Wu Y, Yuan H. Research progress on genotoxicity of zearalenone. *Shanghai J Anim Husband Vet Med.* (2009) 6:26–7. doi: 10.3969/j.issn.10007725.2009.06.011

27. Muthulakshmi S, Maharajan K, Habibi HR, Kadirvelu K, Venkataramana M. Zearalenone induced embryo and neurotoxicity in zebrafish model (*Danio rerio*): role of oxidative stress revealed by a multi biomarker study. *Chemosphere*. (2018) 198:111–21. doi: 10.1016/j.chemosphere.2018.01.141

28. Cai PR, Wang BJ, Feng NN, Wang L, Li Q, Zou H, et al. Study on DNA damage of rat Sertoli cells induced by zearalenone. *Chin Vet Sci*. (2018) 48:1201–6. doi: 10.16656/j.issn.1673-4696.2018.0176

29. Karaman EF, Ozden S. Alterations in global DNA methylation and metabolism-related genes caused by zearalenone in MCF7 and MCF10F cells. *Mycotoxin Res*. (2019) 35:309–20. doi: 10.1007/s12550-019-00358-8

30. Wang YC, Deng JL, Xu SW, Peng X, Zuo ZC, Cui HM, et al. Effects of zearalenone on IL-2, IL-6, and IFN-γ mRNA levels in the splenic lymphocytes of chickens. *Sci World J.* (2012) 2012:567327. doi: 10.1100/2012/567327

31. Pistol GC, Braicu C, Motiu M, Gras MA, Marin DE, Stancu M, et al. Zearalenone mycotoxin affects immune mediators, MAPK signalling molecules, nuclear receptors and genome-wide gene expression in pig spleen. *PLoS One*. (2015) 10:e0127503. doi: 10.1371/journal.pone.0127503

32. Liang ZS, Xu LN, Ma YJ, Deng XB, Li Y, Fan XL, et al. Toxic effect of zearalenone on mouse thymic epithelial cells. *Chin J Vet Sci*. (2009) 29:894–7. doi: 10.16303/j.cnki.1005-4545.2009.07.019

33. Bulgaru CV, Marin DE, Pistol GC, Taranu I. Zearalenone and the immune response. *Toxins*. (2021) 13:248. doi: 10.3390/toxins13040248

34. Song TT. Study on the mechanism of zearalenone-induced uterine hypertrophy in weaned piglets [master's thesis]. Tai'an: Shandong Agricultural University (2020).

35. Bai J, Li J, Liu N, Jia H, Si X, Zhou Y, et al. Zearalenone induces apoptosis and autophagy by regulating endoplasmic reticulum stress signalling in porcine trophectoderm cells. *Anim Nutr*. (2022) 12:186–99. doi: 10.1016/j.aninu.2022.08.016

36. Zhao J, Hai S, Chen J, Ma L, Rahman SU, Zhao C, et al. Zearalenone induces apoptosis in porcine endometrial stromal cells through JNK Signaling pathway based on endoplasmic reticulum stress. *Toxins*. (2022) 14:758. doi: 10.3390/toxins14110758

37. Ma YJ, Xu LN, Li YG, Fan XL, Liang ZS, Deng XB. Effect of zearalenone on apoptosis of splenic lymphocytes in mice. *J Domestic Anim Ecol*. (2009) 30:52–6. doi: 10.3969/j.issn.1673-1182.2009.01.013

38. Liu X, Xi H, Han S, Zhang H, Hu J. Zearalenone induces oxidative stress and autophagy in goat Sertoli cells. *Ecotoxicol Environ Saf*. (2023) 252:114571. doi: 10.1016/j.ecoenv.2023.114571

39. Wu J, Li J, Wu Y, Yang M, Chen Y, Wang N, et al. Betulinic acid mitigates zearalenone-induced liver injury by ERS/MAPK/Nrf2 signaling pathways in mice. *Food Chem Toxicol Int J Res Assoc*. (2023) 177:113811. doi: 10.1016/j.fct.2023.113811

40. Han JX, He JB, Gao F, Yang SH, Liang TT, Dong S, et al. Protective effect of proanthocyanidins against zearalenone-induced oxidative damage to liver and kidney in mice. *China Anim Husb Vet Med*. (2016) 43:402–6. doi: 10.16431/j.cnki.1671-7236.2016.02.017

41. Ben Taheur F, Mansour C, Skhiri SS, Chaaban H, Jridi M, Fakhfakh N, et al. Kefir mitigates renal damage caused by zearalenone in female wistar rats by reducing oxidative stress. *Toxicon Off J Int Soc Toxinol*. (2024) 243:107743. doi: 10.1016/j.toxicon.2024.107743

42. Cui HJ, Lu CT, Pan LQ, Hu H, Zhong PY, Zhu JY, et al. Curcumin alleviates zearalenone-induced oxidative damage in porcine renal epithelial cells via the SIRT1/FOXO1 pathway. *Sci Agric Sin*. (2023) 56:1007–18. doi: 10.3864/j.issn.0578-1752.2023.05.015

43. Tatay E, Espín S, García-Fernández AJ, Ruiz MJ. Oxidative damage and disturbance of antioxidant capacity by zearalenone and its metabolites in human cells. *Toxicol Vitro Int J Pub Assoc BIBRA*. (2017) 45:334–9. doi: 10.1016/j.tiv.2017.04.026

44. Ning CM, An JX, Zhao Y, Yang Y. Toxic effects of zearalenone on animal reproductive performance and its mechanism. *Chin J Anim Nutr*. (2023) 35:2166–74. doi: 10.12418/CJAN2023.204

45. Lang XZ. Case analysis of zearalenone mycotoxicosis in replacement heifers. *Shandong J Anim Sci Vet Med*. (2017) 38:96–7. doi: 10.16431/j.cnki.1671-7236.2024.01.044

46. Zhu W, Ge M, Li X, Wang J, Wang P, Tai T, et al. Hyperoside attenuates zearalenone-induced spleen injury by suppressing oxidative stress and inhibiting apoptosis in mice. *Int Immunopharmacol*. (2022) 102:108408. doi: 10.1016/j.intimp.2021.108408

47. Zhu YD, Yang Q, Wang XF, Liu XW, Jiang GJ. Mitigative effect of three traditional Chinese medicine components on zearalenone-induced liver injury in mice. *China Anim Husb Vet Med*. (2024) 51:434–42.

48. Chen PD. Study on the mechanism of quercetin alleviating zearalenone-induced PNH/HL-059 cell injury [master's thesis]. Jilin: Jilin University (2025).

49. Wang C, Chen C, Wang M, Rahman SU, Wei B, Ding H, et al. Rutin attenuates zearalenone-induced ferroptosis of endometrial stromal cells in piglets through the p53 signaling pathway. *Ecotoxicol Environ Saf*. (2025) 290:117546. doi: 10.1016/j.ecoenv.2024.117546

50. Zhang QQ, Wang YN, Tang Y, Su X, Zhang JY, Huang SM, et al. Mitigative effect of rutin on zearalenone-induced reproductive organ injury in female mice. *Chin J Anim Sci*. (2023) 59:278–84. doi: 10.19556/j.0258-7033.20220414-03

51. Gao X, Xiao ZH, Liu M, Zhang NY, Khalil MM, Gu CQ, et al. Dietary silymarin supplementation alleviates zearalenone-induced hepatotoxicity and reproductive toxicity in rats. *J Nutr*. (2018) 148:1209–16. doi: 10.1093/jn/nxy114

52. Sayed H, Zhang Q, Tang Y, Wang Y, Guo Y, Zhang J, et al. Alleviative effect of rutin on zearalenone-induced reproductive toxicity in male mice by preventing spermatogenic cell apoptosis and modulating gene expression in the hypothalamic-pituitary-gonadal Axis. *Toxins*. (2024) 16:121. doi: 10.3390/toxins16030121

53. Xu JN. Observation and study on the protective effect of baicalin against zearalenone-induced liver injury in chicks [master's thesis]. Foshan: Foshan University of Science and Technology (2022).

54. Chen C, Wang C, Jiang H, Wang M, Rahman SU, Chen C, et al. Rutin alleviates zearalenone-induced endoplasmic reticulum stress and mitochondrial pathway apoptosis in porcine endometrial stromal cells by promoting the expression of Nrf2. *Toxins*. (2024) 17:7. doi: 10.3390/toxins17010007

55. Wang Y, Wang Q, Wang G, Zhang Q, Guo Y, Su X, et al. Rutin, a natural flavonoid glycoside, ameliorates zearalenone induced liver inflammation via inhibiting lipopolysaccharide gut leakage and NF-κB signaling pathway in mice. *Food Chem Toxicol Int J Pub Br Ind Biol Res Assoc*. (2024) 191:114887. doi: 10.1016/j.fct.2024.114887

56. Chen S, Xu T, Xu A, Chu J, Luo D, Shi G, et al. Quercetin alleviates zearalenone-induced apoptosis and necroptosis of porcine renal epithelial cells by inhibiting CaSR/CaMKII signaling pathway. *Food Chem Toxicol Int J Pub British Ind Biol Res Assoc*. (2023) 182:114184. doi: 10.1016/j.fct.2023.114184

57. Wang DF, Zhang NY, Peng YZ, Qi DS. Interaction of zearalenone and soybean isoflavone in diets on the growth performance, organ development and serum parameters in prepubertal gilts. *J Anim Physiol Anim Nutr*. (2012) 96:939–46. doi: 10.1111/j.1439-0396.2011.01212.x

58. Wang DF, Zhou HL, Hou GY, Qi DS, Zhang NY. Soybean isoflavone reduces the residue of zearalenone in the muscle and liver of prepubertal gilts. *Animal*. (2013) 7:699–703. doi: 10.1017/S1751731112002066

59. Shi HX. Mechanism of *potentilla anserina* polysaccharide alleviating zearalenone-induced oxidative stress in porcine Sertoli cells [doctoral dissertation]. Lanzhou: Gansu Agricultural University (2025).

60. Hu H, Xu ZK, Zhang KZ, Lu CT, Zhou JY, Cui HJ, et al. Protective effect of astragalus polysaccharide against zearalenone-induced apoptosis of chicken thymus cells. *Heilongjiang Anim Sci Vet Med*. (2022) 10:109–14. doi: 10.13881/j.cnki.hljxmsy.2021.08.0383

61. Dai D. J., Li H., Zhang Y. J., Zhu S. X., Huang J. S., Kang W. C. (2024). "Mitigative effect of poria cocos polysaccharide on zearalenone-induced toxicity in mice," in *Proceedings of the 11th National Toxicology Congress of Chinese Society of Toxicology* (229–230). College of Animal Science and Technology, Guangxi University.

62. Chen HM. Effect of *lycium barbarum* polysaccharide on zearalenone-induced renal mitochondrial apoptosis and autophagy in mice [master's thesis]. Guangzhou: South China Agricultural University (2021).

63. Wang H, She F, Chen F, Li K, Qin S. Selenium-chitosan protects porcine endometrial epithelial cells from zearalenone-induced apoptosis via the JNK/SAPK Signaling pathway. *Biol Trace Elem Res*. (2024) 202:2075–84. doi: 10.1007/s12011-023-03816-8

64. Long M, Chen X, Wang N, Wang M, Pan J, Tong J, et al. Proanthocyanidins protect epithelial cells from zearalenone-induced apoptosis via inhibition of endoplasmic reticulum stress-induced apoptosis pathways in mouse small intestines. *Molecules*. (2018) 23:1508. doi: 10.3390/molecules23071508

65. Shi W. Protective effect of proanthocyanidins against zearalenone-induced oxidative damage in mouse testicular Sertoli cells [master's thesis]. Shenyang: Shenyang Agricultural University (2017).

66. Song C, Fu CQ, Huangfu HP, Zhang AG, Wang YK, Shi DM, et al. Effect of curcumin on zearalenone-induced hepatic oxidative stress and NLRP3 inflammasome activation in mice. *Chin J Vet Sci*. (2023) 43:1898–904. doi: 10.16303/j.cnki.1005-4545.2023.09.15

67. Peng B, Guo S, Niu J, Guo Y, Wang Z, Zhang W. Curcumin attenuates zearalenone-induced reproductive damage in mice by modulating the gut microbe-testis Axis. *Foods*. (2025) 14:2703. doi: 10.3390/foods14152703

68. Zhu GS. Protective effect of resveratrol against zearalenone-induced hepatic oxidative damage and inflammation in mice [master's thesis]. Yangzhou: Yangzhou University (2022).

69. She JJ, Feng NN, Zheng H, Liu SS, Zou H, Gu JH, et al. Protective effect of resveratrol against zearalenone-induced oxidative damage and apoptosis in TM4 cells. *Chin Vet Sci*. (2020) 50:1453–60. doi: 10.16656/j.issn.1673-4696.2020.0170

70. Xia S, Yan C, Gu J, Yuan Y, Zou H, Liu Z, et al. Resveratrol alleviates zearalenone-induced intestinal dysfunction in mice through the NF-κB/Nrf2/HO-1 signalling pathway. *Foods*. (2024) 13:1217. doi: 10.3390/foods13081217

71. Deng FR, Chen JH, Jia SH, Yao CY, Li RJ, Deng YQ, et al. Screening and performance evaluation of a zearalenone-degrading bacterial isolate PA26-7. *Microbiol. China*. (2023) 50:3404–16. doi: 10.13344/j.microbiol.china.221078

72. Wei Z, Zhang X, Shi L, Jin J, Yang B, Xing F. Functional characterization and mechanism of two zearalenone-degrading enzymes from *Bacillus velezensis* B.26. *J Agric Food Chem*. (2025) 73:14629–40. doi: 10.1021/acs.jafc.5c03232

73. Xue LL, Zhang PZ, Yang XJ, Fan SW, Li W. Screening, identification, and degradation efficacy evaluation of zearalenone-degrading bacteria. *J. Northwest A&F Univ*. (2025) 53:13–22. doi: 10.13207/j.cnki.jnwafu.2025.01.002

74. Xu ZL, Chen YB, Meng KL, Yang CXY, Jiang DD, Jiang DS, et al. Research on the degradation efficacy and mechanism of zearalenone by Tibetan yeast *Meyerozyma caribbica* 68. *Guangdong Agric Sci*. (2025) 22:1–15.

75. Jing S, Lan X, Liu Y, Sun C, Ye H, Wang J, et al. Microbe-mediated removal of zearalenone using yeast strain *Rhodotorula dairenensis* isolated from the gut microbiome of zearalenone-treated mice. *J Agric Food Chem*. (2025) 73:9320–36. doi: 10.1021/acs.jafc.4c11881

76. Wang Y, Wang Y, Jiang J, Zhao Y, Xing F, Zhou L. Sheng wu gong cheng xue bao. *Chin J Biotechnol*. (2020) 36:372–80. doi: 10.13345/j.cjb.190150

77. Murtaza B, Wang L, Li X, Ali A, Haq SU, Ji-bin L, et al. Novel *lactobacillus* consortium for effective zearalenone adsorption and biodegradation. *Int Biodeterior Biodegrad*. (2024) 194:105889. doi: 10.1016/J.IBIOD.2024.105889

78. Ali SA, Ibrahim HJ, Ali MN, Ali KM, Shahad HH, Rusul NK. Bioremediation of zearalenone by using *Lactobacillus acidophilus* in albino rats bodies (in vivo). *J Contemp Med Sci*. (2015) 1:21–5. doi: 10.22317/jcms.v1i1.12

79. Zeng L, Yan CJ, Chen G, Yu CC. Study on the adsorption properties of different silicate mineral materials for mycotoxins. *Chin J Anim Sci*. (2011) 47:64–6.

80. Liang XW, Li FD, Zhang JM, Ma YP, Zhao QY, Gao HL. Study on the adsorption of montmorillonite and attapulgite to mycotoxins. *Chin Anim Husb Vet Med*. (2014) 41:133–8.

81. Elliott CT, Connolly L, Kolawole O. Potential adverse effects on animal health and performance caused by the addition of mineral adsorbents to feeds to reduce mycotoxin exposure. *Mycotoxin Res*. (2020) 36:115–26. doi: 10.1007/s12550-019-00375-7

82. Anjos O, Miguel MDG. Unveiling the chemistry and bioactivity of bee products and their derivatives. *Foods*. (2025) 14:3058. doi: 10.3390/foods14173058

83. Wang HZ, Wang JZ, Wang CP. Research progress of bee products in promoting human health. *Apic China*. (2022) 73:52–5. doi: 10.3969/j.issn.0412-4367.2022.02.024

84. Al-Kahtani SN, Alaqil AA, Abbas AO. Modulation of antioxidant Defense, immune response, and growth performance by inclusion of Propolis and bee pollen into broiler diets. *Anim MDPI*. (2022) 12:1658. doi: 10.3390/ani12131658

85. Wang JY, Lin WK, Tao CL. Protective effect of jarrah honey against acute alcoholic liver injury in mice. *Biol Chem Eng*. (2024) 10:111–5. doi: 10.3969/j.issn.2096-0387.2024.02.022

86. Lan Q, Xie Y, Pan J, Chen Q, Xiao T, Fang S. The antibacterial and antioxidant roles of buckwheat honey (BH) in liquid preservation of boar semen. *Biomed Res Int*. (2021) 2021:5573237. doi: 10.1155/2021/5573237

frontiers | Frontiers in Veterinary Science

TYPE Original Research
PUBLISHED 17 December 2025
DOI 10.3389/fvets.2025.1716637

OPEN ACCESS

EDITED BY
Baocheng Hao,
Chinese Academy of Agricultural Sciences, China

REVIEWED BY
Adelijiang Wusiman,
Xinjiang Agricultural University, China
Mostafa Gouda,
National Research Centre, Egypt

*CORRESPONDENCE
Irfan Baboo
✉ irfan@cuvas.edu.pk
Valiollah Palangi
✉ valiollah.palangi@neu.edu.tr

RECEIVED 30 September 2025
REVISED 17 November 2025
ACCEPTED 21 November 2025
PUBLISHED 17 December 2025

CITATION
Shafiq A, Baboo I, Farooq Z, Majeed H and Palangi V (2025) Development and evaluation of clove oil nanoemulsion-based topical cream for anti-inflammatory activity in mice. *Front. Vet. Sci.* 12:1716637. doi: 10.3389/fvets.2025.1716637

Development and evaluation of clove oil nanoemulsion-based topical cream for anti-inflammatory activity in mice

Ahsan Shafiq[1], Irfan Baboo[1]*, Zahid Farooq[1], Hamid Majeed[2] and Valiollah Palangi[3]*

[1]Cholistan Institute of Biological Sciences, Cholistan University of Veterinary and Animal Sciences (CUVAS), Bahawalpur, Pakistan, [2]Department of Food Science and Technology, Cholistan University of Veterinary and Animal Sciences (CUVAS), Bahawalpur, Pakistan, [3]Department of Animal Science, Faculty of Agriculture, Near East University, Nicosia, Northern Cyprus, Türkiye

Introduction: Inflammatory skin disorders require effective topical therapies with minimal side effects. Clove (Syzygium aromaticum) is recognized for its potent anti-inflammatory, antimicrobial, and antioxidant properties, but it has a limited clinical use due to its highly volatile nature, poor solubility, and potential skin irritation at higher concentrations. This research aimed to develop and optimize clove oil nanoemulsion (CONE)-based topical cream, characterize its physicochemical properties, and evaluate anti-inflammatory efficacy using a mouse model.

Methodology & Results: CONE was prepared via ultrasonication and optimized using response surface methodology. The optimized CONE exhibited a mean droplet size of approximately 190 nm and Polydispersity Index of 0.08, with high entrapment efficiency (94.54%). GC-MS analysis confirmed eugenol as the major constituent. The nanoemulsion demonstrated strong antifungal activity. The minimum inhibitory concentration was 120 µl/mL. CONE significantly enhanced antioxidant capacity compared to clove oil. The cream was formulated by incorporating CONE into carboxymethyl cellulose (CMC) matrix and evaluated for stability, pH, morphology, and drug release. The cream maintains stability, favorable organoleptic properties, and sustained drug release, particularly at a 1 mL CONE concentration. Thirty adult male albino mice (30–40g) were used and randomly divided into six groups. Hematological parameters and C-reactive protein level further supported the anti-inflammatory efficacy topical cream, with marked improvements observed in treated groups. Histopathological analysis revealed re-epithelialization and diminished inflammatory infiltration.

Conclusion: CONE-based cream offers a promising, safe, and effective topical therapy for inflammatory skin conditions. The nanoemulsion formulation enhances clove oil's bioavailability, stability, and therapeutic potential, supporting further development for clinical and cosmetic applications.

KEYWORDS

anti-inflammatory, nanoemulsion, topical cream, drug release, sustainability

1 Introduction

Inflammatory skin disorders are a major health concern, often requiring long-term management with topical agents (1). Inflammation is the biological process the body develops in response to tissue damage or infection (2). It is a body's vascular and cellular reaction to an irritating incursion. It is well-defined by a combination of cardinal signs: swelling, redness, pain, and the symptom of infection or injury (3). In the absence of inflammation, infections, wounds, and tissue damage are not resolved (4). Conventional treatment modes of treating inflammatory dermatoses majorly rely on the use of corticosteroids and non-steroidal anti-inflammatory effects (5). All drugs used in treating various inflammatory diseases have long-term negative effects (6, 7). These limitations have prompted a growing interest in natural bioactive compounds.

As plant secondary metabolites, essential oils (EO) have recently emerged as therapeutics for inflammation and pain (8). The natural essentials oil are safe and effective substitutes to the standard curative treatments, such as clove oil. Clove is an aromatic flowering bud that is cultivated in various parts of the world for medical, culinary, and perfumery purposes (1, 9). *Syzygium aromaticum* contains approximately 15–20% of EO. Clove essential oil (CEO) is rich in phenolic compounds that have several biological properties, such as antibacterial, anti-inflammatory, antioxidant, analgesic, and insecticidal properties (10, 62). Clove oil supports wound healing by enhancing fibroblastic migration, wound healing, increasing angiogenesis, as well as alleviating scar formation (11). The bioactives can degrade when subjected to light, oxygen, variation in temperature, and moisture (12). As a solution to such instability, clove oil can be incorporated into nanoscale carrier systems hence maintaining its integrity and maximizing its delivery. Despite its therapeutic potential, the clinical application of clove oil in topical formulations is hampered by its volatility, poor aqueous solubility, and potential for skin irritation at higher concentrations (13).

Preparation of EOs as nanoformulations is a hopeful method to improve their action (14). Amongst the nanoformulations, nanoemulsions are highly considered because of the lower side effects and bioavailability, especially easier preparation (15, 16). NEs are biphasic clear dispersions that consist of an oil and water phase that are stably combined using surfactants/co-surfactants. Due to their droplet size, below 200 nm, such systems remain stable droplets against aggregation or creaming (17).

Effective topical delivery of nanoemulsions has some promising features, such as increased skin permeability and no irritation (18). The conversion of nanoemulsions to gels enhances the topical applications, physical stability, and heat resistance for EOs (19). Topical drug delivery is a critical factor in the therapeutic treatment of various cutaneous pathologies that include infectious dermatoses, cutaneous neoplasma, dermatitis, burn, inflammation, chronic wounds, as well as psoriasis (20). Nanoemulsion-based topical creams represent a more sophisticated approach to drug delivery. The diminutive droplet size significantly improves the solubility and bioavailability of poorly water-soluble drugs (21). Nanoemulsions enhance skin permeability and provide controlled release of the active ingredient constitutes a major advantage over conventional formulations (22). Consequently, nanoemulsion-based creams are increasingly being investigated for the delivery of a wide range of therapeutic agents, including antimicrobial, anti-inflammatory and antioxidant compounds (23). The aim of the conducted study was to design a topical cream based on nanoemulsions, to optimize and evaluate the characteristics of the topical cream that contains clove oil and has the aim of testing its anti-inflammatory properties in a mice model. The nanoemulsion will provide a novel, effective, and safe topical anti-inflammatory drug delivery system, which might make the best use of clove oil.

2 Materials and methods

Clove oil and canola oil were purchased from Karachi Essence, Lahore (Pakistan). Potato Dextrose Agar (PDA) and Tween80 were purchased from Sigma Aldrich (Saint Louis, MO, USA).

2.1 Preparation and optimization of nanoemulsion

Preparation and optimization of nanoemulsion was done by the ultrasonication method as reported by Jabbar et al. (24). The optimization process of CONE was performed by response surface methodology (RSM) in Box–Behnken Design (BBD) to improve the droplet size and Polydispersity Index (PDI). Tween80 aqueous solution (2.5% w/v) was prepared in deionized water at room temperature, followed by stirring for 30 min at 40 °C. Addition of clove oil (mixed phase 10%) and homogenized at 18000 rpm for 5 min using DH-1500 ultra turrax homogenizer. The crude emulsion was homogenized using an Ultra-Sonicator (UCD-1200, BIOBASE, Jinan, China) for 10 min at 50% power (30:30 s rest/work cycle). During ultrasonication, the samples were kept in a beaker containing ice water to minimize heat loss. The prepared nanoemulsion formulations were all kept at 4 °C until use for the experiments.

2.2 Characterization of nanoemulsion

Mean droplet size and PDI were determined by the dynamic light scattering (DLS) technique by diluting 200 times with fresh deionized water using zeta sizer Nano ZS 90 (25).

2.3 Gas chromatography–mass spectrometry (GC–MS) analysis

The clove oil was analyzed by GC–MS according to the method of Kelidari et al. (26), using a series of 7890A Network GC interfaced with a 5975C VL MSD with Triple-Axis Detector (Agilent Technologies, Santa Clara, CA, USA). A HP-5MS fused silica column was used for component separation, and the initial temperature was set at 40 °C for 1 min, and then the temperature was increased to the final temperature of 250 °C at a rate of 3 °C/min held for 90 min (80). Split-flow 10 mL/min with 6 mL/min septum purge, and 1 mL/min column flow. The helium gas was used as the carrier gas and it had a purity of 99.99%.

2.4 Transmission electron microscopy (TEM)

The morphological study of nanoemulsion droplets was thoroughly inspected through the use of digital transmission electron microscopy imaging. The CONE emulsion was deposited onto a carbon film laid upon a copper mesh utilizing a micropipette. It was then stained for contrast with a solution of 2% weight by volume phosphotungstic acid. Before analysis under the transmission electron microscope, the sample-coated mesh was permitted to thoroughly dehydrate in ambient conditions for a full day. Next, the TEM, operating at 100 KV, was employed to examine the stained specimen. This provided high-resolution images of droplet structure, allowing for a comprehensive analysis of NE morphology according to the methods outlined by Majeed et al. (27).

2.5 Entrapment efficiency of nanoemulsion

The entrapment efficiency of CONE was determined as described earlier by Majeed et al. (28), and Heydari et al. (29). Briefly, the nanoemulsions were mixed in distilled water under vigorous stirring for 10 min. The sample was centrifuged to get the supernatant, which contained unencapsulated essential oil. The sediment was mixed with water and later ethanol was added till further vortex for 15 min to achieve the inner essential oil content. The efficiency was calculated using the expression (Equation 1).

$$\text{Entrapment Efficiency} = \left[\frac{(\text{External} - \text{Internal})}{(\text{Total loaded})}\right] \times 100 \quad (1)$$

2.6 Formulation of cream

Carboxymethyl cellulose polymer (CMC) was selected for its frequent use in cosmetic fields (30). CMC powder (2 g) was dissolved in 100 mL distilled water, and stirring was conducted at 60 °C by a heater-stirrer (RTH-340, Robus Technologies, UK) for 45–60 min. The dissolved solution of CMC polymer was incorporated directly with different concentrations (w/v) of nanoemulsion and stirred for 10 min. Four different concentrations of clove oil nanoemulsion were used in the formulation of cream (500 µL, 750 µL, 1 mL, and 1.5 mL). Each concentration was added to 6 g of CMC solution. The formulated creams were evaluated for physical properties and further evaluation.

2.7 Organoleptic properties of cream

The appearance of the cream is judged by its color, smell, and texture (31).

2.7.1 pH of cream

The pH of the formulated cream was determined with a digital pH meter (32).

2.7.2 Cream separation

Cream (5 g) was centrifuged at 5000 rpm for 10 min at 25 °C (33).

2.7.3 Cream stability

The stability was tested in various conditions of the heating–cooling cycle (6 cycles): 45 °C (in incubator) and 4 °C (in refrigerator) for 48 h each cycle (34).

2.8 Entrapped drug release

An evaluation of the entrapped drug release of NE was conducted using UV spectroscopy. Ethanol was used to dissolve the best-formulated cream incorporating the CONE.

2.9 Antifungal efficacy

The agar-dilution method was applied to test the antifungal activity of CONE against *Aspergillus niger* and *Penicillium italicum*. The antifungal test was carried out according to the microdilution technique in 96-well plates, as reported earlier by Song et al. (35), with a few modifications. The examined levels of nanoemulsion were 20, 40, 60, 80, 100, 120, and 140 µL/mL. The fungal isolates were grown in potato dextrose agar (PDA) medium. The plates (96 wells) were incubated for 30 min at room temperature before 10ul of the fungal strains at 10^4 CFU/mL was added. Absorbance was measured at 340 nm. The time-kill graphs of fungi against CONE at their MIC were evaluated by following Majeed et al. (36). Time kills were performed at 0, 6, 12, 24, 36, 48, and 72 h by using the microdilution method in 96-well plates.

2.10 Antioxidant activity

2.10.1 DPPH radical capture assay

The antioxidant property of the CONE was evaluated by the DPPH method (2,2-diphenyl-1-picrylhydrazyl) (37). The CONE samples (10, 20, 40, 60, 80, 100 and 120 µL) were diluted in water to avoid aggregation. The CONE samples were added to 1 mL of methanolic DPPH solution (0.3 mmol) and incubated at 30 °C for 30 min in the dark; absorbance was measured at 517 nm on a UV–VIS spectrophotometer (T80, United Kingdom) (82). The scavenging rate was measured as the following Equation 2:

$$\text{Scavenging activity}(\%) = \left[\frac{(\text{Control}_a - \text{Sample}_a)}{\text{Control}_a}\right] \times 100 \quad (2)$$

Where, Control_a and Sample_a are the absorbance of control (DPPH solution) and samples, respectively. The methanolic DPPH solution (1 mL, 0.3 mmol) was used as a control sample.

2.10.2 ABTS radical scavenging

The ABTS 2,2′-azino-bis(3-ethylbenzothiazoline-6-sulfonic acid) radical scavenging activity was assessed according to the procedure that was described by Sridhar and Charles, (38), with slight alterations.

In a stock ABTS solution, equal quantities including those of 7 mM ABTS (aqueous) to 2.45 mM potassium persulfate (aqueous) were placed into a single container. The mixture was allowed to incubate at room temperature in the dark for 12–16 h. This was followed by the addition of 10–120 mm/L ascorbic acid (molecular weight 176.12 g/mol; used as standard) and 5, 10, 20, 40, 80, 100 and 120 µL of the sample and incubated under the aforementioned conditions until a time interval of 10 min was reached. One control contained 1 mL of ABTS solution together with 0.5 mL of distilled water. Absorbance was recorded at 734 nm and thereafter, percentage scavenging activity was determined according to the following Equation 3 (37):

$$\text{Inhibition}(\%) = \left[\frac{(\text{Control}_a - \text{Sample}_a)}{\text{Control}_a}\right] \times 100 \quad (3)$$

2.11 Animal

Male Albino mice, weighing between 30 and 40 g, were used for *in-vivo* study of the topical cream. The animals were housed under standard environmental conditions and experimental protocols approved by the Ethical Committee of Cholistan University of Veterinary and Animal Sciences Bahawalpur (ORIC-328). They were fed with a standard rodent diet and allowed to acclimatize for 2 weeks before the commencement of the experiment.

2.12 Diabetes induction

Diabetes was induced by following the method of Pakpahan et al. (39), with minor alteration. Before induction blood sugar level was measured. The tip of mice tail was cleaned with 70% alcohol then piercing with sterile lancet needle. A drop of blood was dripped on a sugar strip to measure the glucose level. Alloxan solution was administered orally (150 mg/kg) as described earlier by Oshkondali et al. (40). The mice were allowed to have access to food and water, as normal. Then stabilized for 7 days after alloxan solution induction. The levels of glucose of ≥250 mg/dL on day seven classify as diabetic (41), and hence qualify individuals to engage in the study of diabetes related experiment.

2.13 *In-vivo* experiment

Thirty Albino mice were used for *in-vivo* anti-inflammatory assay. Mice were randomly divided into six groups, with each group consisting of five animals. Mice were anesthetized using a cotton swab that had been dipped in chloroform until the mice were limp (39). The dorsal surface of each mice was shaved and cleaned with a sterile cotton swab. Inflammatory wound was created in this area to with sterile surgical blade, which was then treated according to the group-specific regimen. The progression of wound healing, inflammation reduction, and other relevant parameters was closely monitored.

The groups were categorized as follows: Control group (G_1), Diabetic model treated with market available cream (G_2), Diabetic model infected with *Staphylococcus aureus* treated with market cream (G_3), nanoemulsion incorporated topical cream treated group (G_4), Diabetic model treated with nanoemulsion incorporated topical cream (G_5) and Diabetic model infected with *Staphylococcus aureus* treated with nanoemulsion incorporated topical cream (G_6).

2.14 Hematological and histopathological assessment

For the hematological parameters, blood samples were collected in EDTA tubes (42). For histopathological analysis, animals were sacrificed and the skin was excised. The dorsal portion of mice skin was preserved in paraformaldehyde for checking skin tissues. Preserved skin tissues were sectioned using a microtome and stained with acidic dye (eosin) and basic dye (hematoxylin) for visualization under a microscope.

2.15 Molecular docking

Molecular docking analysis was performed to assess how eugenol might interact with inflammatory proteins like C-reactive protein (PDB ID: 7PKB) and Interleukin-1β (PDB ID: 9ILB). The structures for these proteins were retrieved from the RCSB PDB database[1] and the ligand was created from PubChem, Eugenol (PubChem ID: 3314). Each chemical structure chosen to participate in this study was taken from the PubChem database.[2] Molecular docking was done at the available online-based tool SwissDock provided by the Swiss Institute of Bioinformatics.[3] The ligand with the maximum binding energy was discarded and the one having the least binding energy thus was regarded as the ideal one to interact with the docking receptor. The visualization process involved presentation in the three-dimensional space through UCSF-Chimera version 1.17.3 (3D and solid surface) and creation of two-dimensional illustrations with the help of BIOVIA Discovery Studio Visualizer (version 4.5) (24).

2.16 Statistical analysis

For interpretation of results the datasets collected in the current experiment was statistical analyze using the One-way analysis of variance (ANOVA) using IBM SPSS Statistics, version 22. The data was represented by means and standard error (Means ± SE). The data was presented using (81) (Origin Lab Corporation, MA, USA).

3 Results

3.1 Preparation and optimization of NE

The CONE was systematically developed and optimized using Box–Behnken response surface design to assess the impact of four independent variables, oil concentration, Tween 80 concentration, sonication time and sonication power on droplet size and PDI. The optimization process revealed that increasing both emulsifier

1 https://www.rcsb.org/
2 https://pubchem.ncbi.nlm.nih.gov/
3 https://www.swissdock.ch/

concentration and sonication power significantly reduced droplet size and improved homogeneity. The optimal formulation, comprising 10% (v/v) clove oil, 2.5% (w/v) Tween 80, sonication time of 15 min and 50% sonication power, resulted in a NE with a mean droplet size of approximately 190 nm and a PDI of 0.08. These values reflect a uniform and kinetically stable nanoemulsion system, suitable for enhanced topical delivery applications.

3.2 Gas chromatography–mass spectrometry (GC/MS) analysis

The gas chromatographic analysis presented the retention time and peak areas of the major compound in CEO. The major compound is eugenol (58.92%). The retention time (21.30 min) and peak area of eugenol 892,342 au (arbitrary units) are shown in Figure 1.

3.3 Transmission electron microscopy (TEM)

The NE particles morphology and size of the optimized CONE were examined using TEM. It was indicated in Figure 2 that the core of each particle is lighter than the periphery, confirming the oil-in-water (O/W) nature of the NEs. The droplets were spherical, with a smooth surface and uniform dispersion. The droplets appeared well-dispersed without significant aggregation, suggesting good colloidal stability. The nanoemulsion droplet size ranged from 20 to 200 nm, with a mean value of 155.28 ± 7.99 nm as depicted in Figure 2b.

3.4 Entrapment efficiency

The optimal CONE was used to measure their entrapment efficiency by UV-spectrophotometry at the wavelength of 280 nm. CONE had an average entrapment efficiency of about 94.54% because of an effective formulation procedure and controllable oil dispersion in the NE matrix.

3.5 Properties of topical cream

Creams containing CONE were visually confirmed after being kept at heating–cooling conditions. The cream color and smell remained unchanged after the heating–cooling test compared with those before. The pH of cream containing NE before and after the heating–cooling test was found to be in the range of 6.5–8.0. The formulations NE cream immobilized kept pH values stable with few increases after the heating and cooling process. The resultant cream was stable with no separation. The properties of cream are shown in Table 1.

Various batches prepared were subjected to evaluation of organoleptic characters such as colour, odor, uniformity, physical stability, pH and spreadability. The most optimized formula was chosen according to the above parameters analysis and the release profile of the nanoemulsion. The optimized and stable formulation was then tested.

3.6 Sustain release of nanoemulsion in cream

In-vitro release studies of CONE incorporated topical cream formulations were performed using UV–Vis spectrophotometry. The release kinetics exhibited a biphasic trend with an initial burst release, followed by a sustained release pattern up to 72 h. Among all formulations (0.5, 0.75, 1 and 1.5 mL of CONE), only 1 mL formulation demonstrated the most favorable release behavior, balancing rapid initial diffusion with prolonged drug availability (Figure 3).

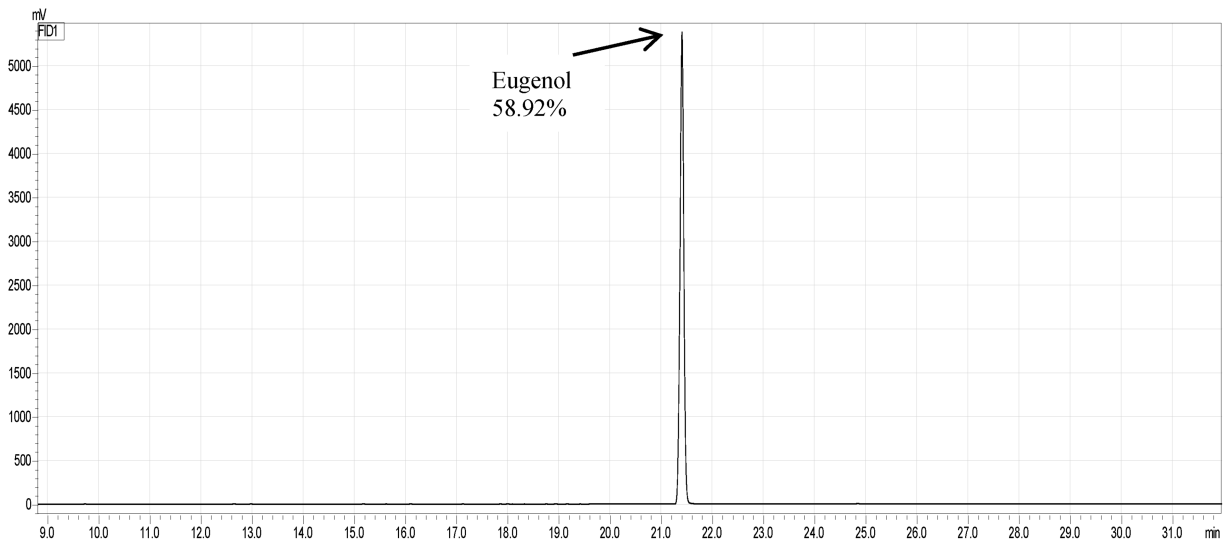

FIGURE 1
Gas Chromatography–Mass Spectrometry (GC/MS) analysis of clove oil.

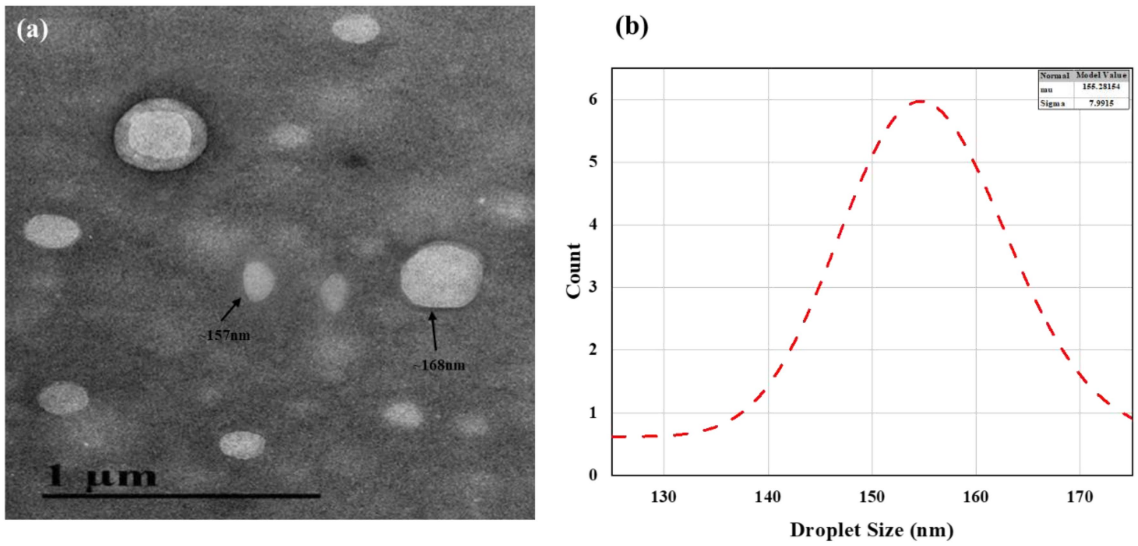

FIGURE 2
(a) Transmission Electron Microscope image of CONE; **(b)** Normal Distribution Model of Droplet size visualized by TEM micrograph.

TABLE 1 **Physical properties of cream embedded with clove oil nanoemulsion.**

Parameter	0.5 mL		0.75 mL		1 mL		1.5 mL	
	Before	After	Before	After	Before	After	Before	After
Appearance	Semisolid	Semisolid	Semisolid	Semisolid	Semisolid	Semisolid	Semisolid	Semisolid
Color	Cloudy white	No change	Cloudy white	No change	Cloudy white	No change	Cloudy white	No change
Smell	Characteristic	Characteristic	Characteristic	Characteristic	Characteristic	Characteristic	Characteristic	Characteristic
Texture	Smooth and consistent	Smooth and consistent	Smooth and consistent	Smooth and consistent	Smooth and consistent	Smooth and consistent	Smooth and consistent	Smooth and consistent
pH value	6.85	6.94	7.12	7.16	7.37	7.41	7.57	7.61
Separation	No	No	No	No	No	No	No	No
Stability	Stable	Stable	Stable	Stable	Stable	Stable	Stable	Stable

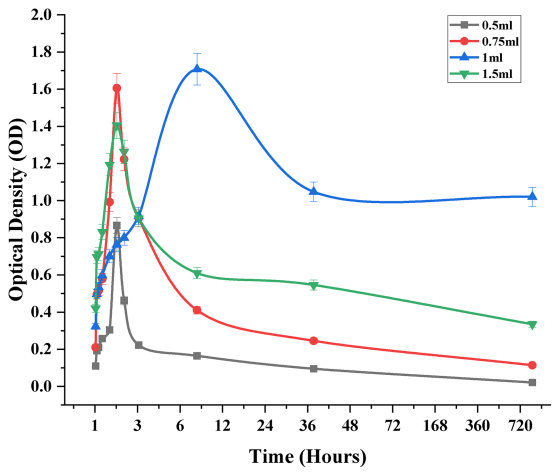

FIGURE 3
Drug release trend of clove oil nanoemulsion from cream after different time intervals.

The initial burst phase observed across all formulations is attributed to the rapid diffusion of surface-associated CEO molecules. However, 1 mL formulation exhibited a more controlled release trajectory, indicative of efficient entrapment and regulated diffusion from the cream matrix. In contrast, the 0.5 and 0.75 mL formulations displayed a sharp decline in drug release after the initial phase, suggesting premature depletion of the active compound and limited sustained release capacity. The 1.5 mL formulation showed a delayed onset of release with extended retention, potentially due to increased formulation viscosity or enhanced encapsulation hindering immediate diffusion.

At 24 and 48 h, 1 mL CONE cream maintained a steady release profile, whereas lower concentrations exhibited marked depletion. By 72 h, the 0.5 and 0.75 mL formulations approached complete release, while 1 mL formulation retained a therapeutically relevant concentration, confirming its superior sustained release characteristics. Although the 1.5 mL formulation also demonstrated prolonged retention, its lower initial release and delayed kinetics may necessitate further optimization to balance therapeutic efficacy

and diffusion control. The release data kinetic modelling showed that the Higuchi model was best able to describe the general release pattern which established diffusion-controlled mechanism. These findings suggest that 1 mL CONE concentration offers an optimal release profile for topical delivery, providing both immediate therapeutic action and extended drug retention, which are critical for effective anti-inflammatory outcomes.

3.7 Morphological study of cream

The morphological characteristics of the cream and carboxymethyl cellulose (CMC) were evaluated using compound microscopy, as illustrated in Figure 4. The CMC matrix exhibited a fibrous, thread-like morphology with irregular striations, indicative of its polymeric nature and its role in imparting structural integrity to the formulation (Figure 4a). Uniformly distributed circular formations were also observed, suggesting consistent dispersion. In contrast, the CONE-based cream displayed a morphology consistent with an O/W emulsion, characterized by numerous fine oil globules dispersed within a continuous aqueous phase as presented in Figure 4b. The absence of phase separation under microscopic observation confirms successful encapsulation of the oil phase and the formation of a stable NE-based cream system.

3.8 Antifungal activity

The promising potential of CONE was also highlighted as an effective antifungal agent. The antifungal assay was performed against *P. italicum* and *A. niger*. CONE strongly inhibits the growth of fungal strains as compared to their controls. Both the fungal strains showed almost the same trend and MIC (120 µL). It was observed that CONE strongly inhibits *P. italicum* as compared to *A. niger*. Figure 5 revealed that the fungal growth was reduced to almost 10^1 CFU/mL during the first 12 h and no significant growth was observed. While in the control group, the growth was significantly increased to 10^6 CFU/mL even after 6 h in the case of *A. niger* and it rose to 10^7 CFU/mL during 12 h. Later, it reduced to 10^6 CFU/mL till 72 h. While in the case of *P. italicum* control, maximum growth (10^7 CFU/mL) was observed after 24 h.

3.9 Antioxidant activity of CONE

The antioxidant potential of CEO and CONE was examined using the DPPH and ABTS radical scavenging assays. A dose-dependent increase in scavenging activity was observed for both CEO and CONE across a concentration range of 10 µL to 100 µL. However, the CONE consistently exhibited significantly higher scavenging efficiency compared to the pure CEO across all tested concentrations.

The results demonstrated that the CONE exhibited significantly enhanced antioxidant activity compared to the pure clove oil at all tested concentrations. At the highest concentration (100 µL), the NE achieved a maximum scavenging percentage of approximately 84%, while the unencapsulated clove oil showed about 47% scavenging activity as presented in Figure 6a. This enhancement may be attributed to the increased surface area, improved dispersion, and greater bioavailability of the active constituents in the nano-emulsified form. These findings suggest that nano-emulsification of CEO not only preserves but significantly improves its antioxidant efficacy, making it a promising candidate for therapeutic and cosmetic formulations where oxidative stress plays a central role. The result represented that at the highest concentration tested (100 µL), the CONE achieved a maximum scavenging activity of approximately 81%, while the corresponding value for CO was observed at around 30.3% (Figure 6b). This marked enhancement in antioxidant activity in the NE formulation may be attributed to the reduction of droplet size, which facilitates improved dispersion and solubility of active constituents such as eugenol. Additionally, the increased surface area of the NE droplets likely promotes more effective interaction with the ABTS radicals. *In-vivo* anti-inflammatory analysis.

The experimental study assessed the sequential progression of cutaneous inflammation in six groups (G_1–G_6) at multiple time points (1, 4, 8, 12, 16, and 21 days). On day 1, all groups exhibited significant inflammation, evidenced by pronounced redness, swelling, and skin lesions. By day 4, groups treated with CONE-based cream (G_4 and G_5) began to show improvement, with reduced redness and smaller lesion areas, while the control group and the group treated with a marketed dicloran gel (G_2 and G_3) continued to display persistent inflammation; G_6 showed moderate improvement, consistent with visual data. From day 8 onward, groups receiving CONE-based cream demonstrated marked healing, with significant reduction in redness and lesion size, whereas the control group remained largely unchanged, exhibiting ongoing severe inflammation. Groups G_2 and G_6 showed gradual but

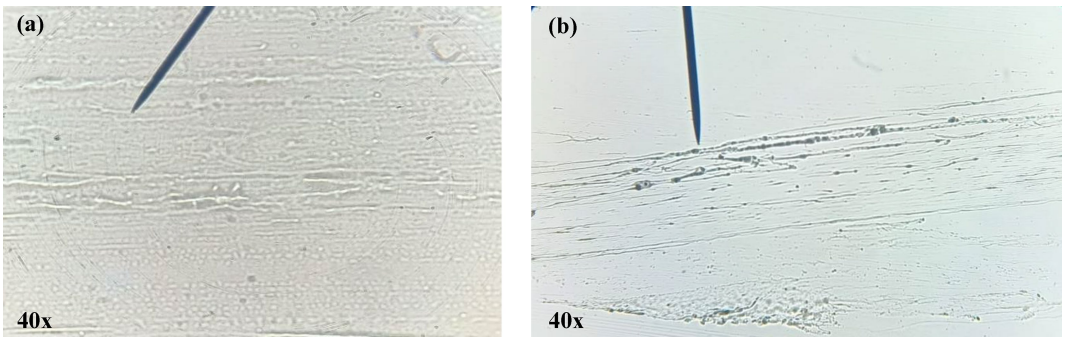

FIGURE 4
Microscopic examination of the polymer and CONE incorporated cream. **(a)** Carboxymethyl cellulose polymer, **(b)** CONE loaded cream.

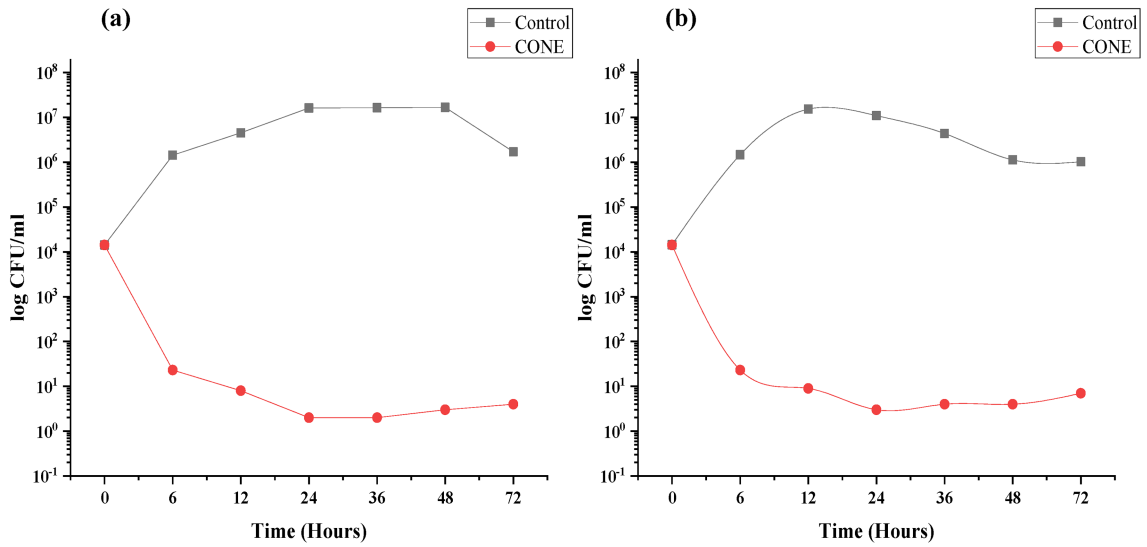

FIGURE 5
Time–kill plot for clove oil nanoemulsion (CONE). **(a)** *Penicillium italicum*; **(b)** *Aspergillus niger*.

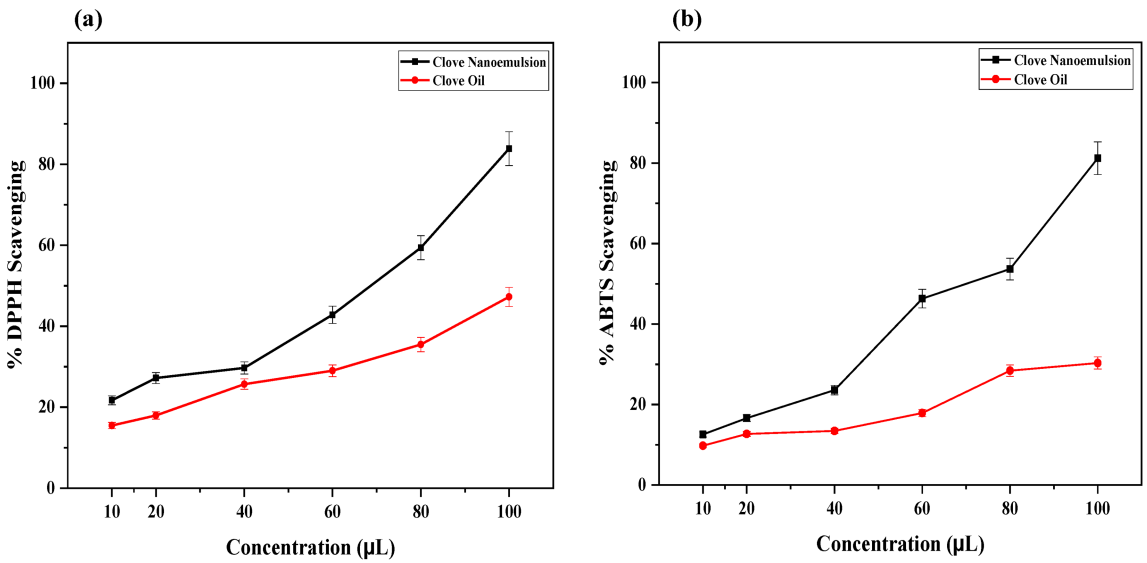

FIGURE 6
Antioxidant activities of clove essential oil and clove oil nanoemulsion **(a)** DPPH **(b)** ABTS. DPPH, (1,1-diphenyl picryl hydrazyl); ABTS, [2,2-azino-bis (3-ethylbenzothiazoline-6-sulfonic acid)].

less pronounced improvement. After day 21, animals in G_4 and G_5 exhibited almost complete skin healing with only faint residual marks, while the control group showed delayed recovery with lingering redness. Groups with severe inflammation due to *S. aureus* addition (G_3 and G_6) achieved moderate healing but retained evidence of tissue damage as presented in Figure 7.

3.10 Hematological analysis

Hematological profiling was performed to evaluate the systemic effects of CONE-based topical cream across six experimental groups: G_1 (control), G_2 (diabetic model + market cream), G_3 (diabetic + *Staphylococcus aureus* + market cream), G_4 (CONE cream only), G_5 (diabetic + CONE cream), and G_6 (diabetic + *S. aureus* + CONE cream). As summarized in Table 2, significant alterations in hematological parameters were observed among the groups.

White blood cell (WBC) counts were notably reduced in G_4 (5.15 ± 0.04) and G_5 (6.28 ± 0.02) compared to the other groups, potentially indicating an immunomodulatory or suppressive effect of the CONE-based formulation. A similar trend was observed in lymphocyte percentages, which were significantly lower in G_4 (72.83 ± 0.02) and G_5 (73.03 ± 0.06), suggesting modulation of immune cell populations. The monocyte and eosinophil (MID) counts were also decreased in G_4, G_5,

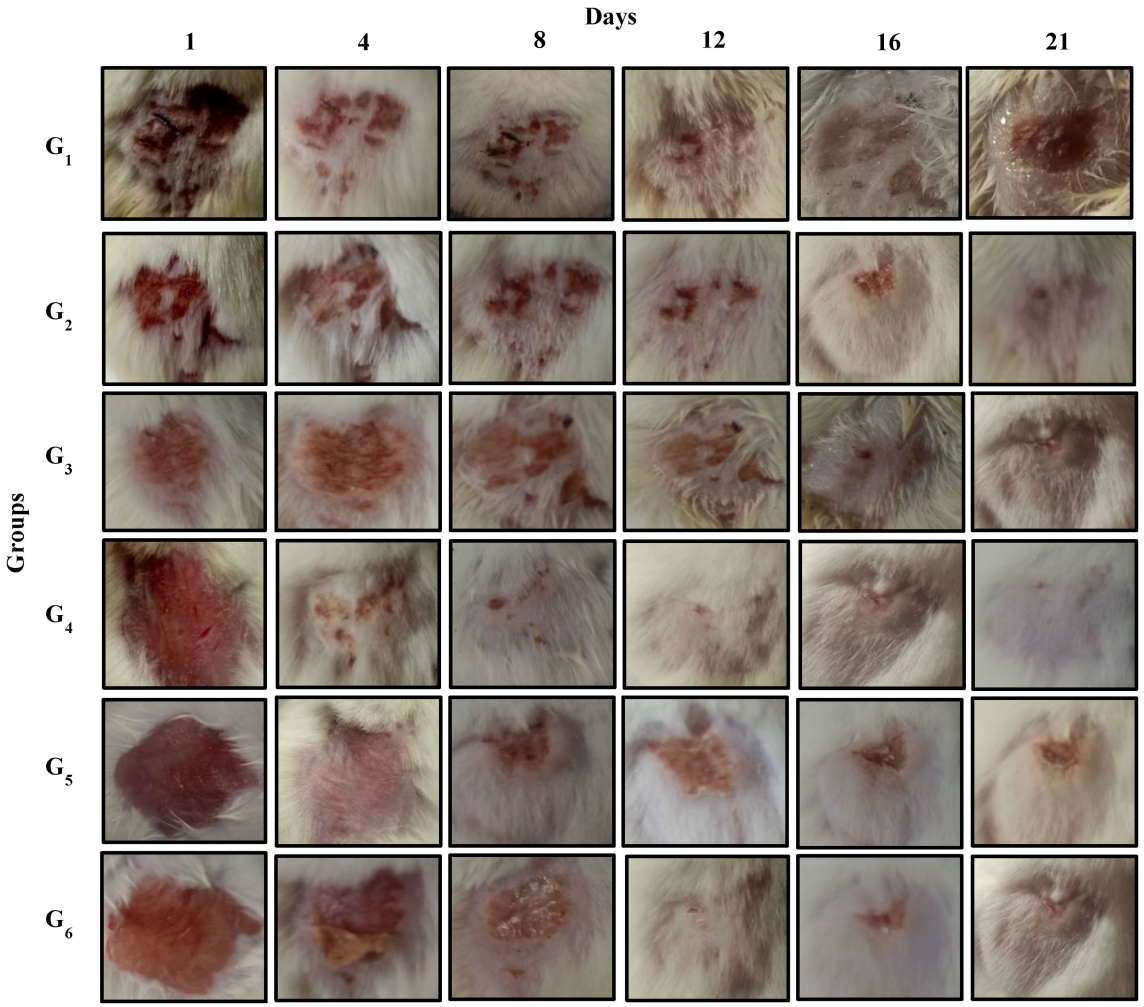

FIGURE 7
In-vitro trail images of inflammatory mice models at different days. Control group **(G_1)**; diabetic model treated with market available cream (dicloran gel) **(G_2)**; diabetic model infected with *S. aureus* treated with market cream **(G_3)**; CONE incorporated topical cream treated group **(G_4)**, diabetic model treated with CONE incorporated cream **(G_5)**; diabetic model infected with *S. aureus* treated with CONE incorporated cream **(G_6)**.

G_6, and G_3, implying altered leukocyte differentiation. Granulocyte (GR) percentages were significantly reduced in G_4 (9.24 ± 0.03) and G_6 (10.33 ± 0.02), further supporting immunological modulation by the nanoemulsion-based cream treatment.

Erythrocytic indices reflected substantial variation across groups. Red blood cell (RBC) counts were significantly elevated in G_4 (7.30 ± 0.26) and G_5 (5.88 ± 0.01), suggesting enhanced erythropoiesis. Hemoglobin (HGB) concentrations were also markedly increased in G_4 (135.22 ± 0.01) and G_5 (99.54 ± 0.02), while G_1 exhibited the lowest levels (65.35 ± 0.04). Hematocrit (HCT) was highest in G_5 (45.30 ± 0.01), indicating improved oxygen-carrying capacity. Mean corpuscular volume, mean corpuscular hemoglobin and mean corpuscular hemoglobin concentration were all significantly elevated in animals treated with nanoemulsion incorporated cream (G_4), further supporting improved erythrocyte quality and function following treatment.

Platelet indices also exhibited statistically significant differences. PLT was highest in G_1 and G_2, but significantly reduced in G_4 (681.27 ± 0.02) and G_5 (684.45 ± 0.03), possibly reflecting infection-related thrombocytopenia or platelet consumption. Mean platelet volume, plateletcrit and platelet distribution width (PDW) were significantly reduced in G_4, indicating altered platelet morphology and activation status. Collectively, these findings suggest that topical application of CONE modulates hematological parameters, including immune cell counts, erythropoietic markers and platelet indices. The observed variations indicate potential immunomodulatory and hematopoietic effects, warranting further mechanistic investigation.

3.11 C-reactive protein

The concentration of C-reactive protein (CRP), a key acute-phase inflammatory biomarker, was quantitatively evaluated in mouse serum using a UV–Vis spectrophotometer at 450 nm. Optical density (OD) values corresponding to CRP levels were recorded across all experimental groups (Figure 8). A normal value 0.435 ± 0.01 was recorded for healthy mice. Significantly elevated CRP levels were detected in inflammatory-induced and *Staphylococcus aureus*-infected groups, indicative of systemic inflammation. Interestingly, the highest CRP value was observed in the untreated control group, suggesting active inflammatory processes. Conversely, mice treated with the CONE-based cream (G_4) exhibited a

10.3389/fvets.2025.1716637

TABLE 2 Hematological parameters of different experimental groups (G1–G6).

Parameters	G_1	G_2	G_3	G_4	G_5	G_6
WBC	8.35 ± 0.05^{a}	8.33 ± 0.02^{a}	8.31 ± 0.02^{a}	5.15 ± 0.04^{c}	6.28 ± 0.02^{b}	8.27 ± 0.02^{a}
LYM%	87.37 ± 0.02^{a}	87.28 ± 0.03^{a}	87.17 ± 0.05^{a}	72.83 ± 0.02^{b}	73.03 ± 0.06^{b}	87.15 ± 0.01^{a}
MID%	8.29 ± 0.03^{a}	8.35 ± 0.03^{a}	7.24 ± 0.03^{b}	6.59 ± 0.01^{c}	7.25 ± 0.04^{b}	6.62 ± 0.03^{c}
GR%	18.54 ± 0.03^{a}	18.47 ± 0.03^{a}	17.54 ± 0.04^{b}	9.24 ± 0.03^{d}	17.56 ± 0.01^{b}	10.33 ± 0.02^{c}
RBC	4.35 ± 0.04^{d}	4.38 ± 0.01^{d}	4.82 ± 0.03^{c}	7.30 ± 0.26^{a}	5.88 ± 0.01^{b}	4.83 ± 0.03^{c}
HGB	65.35 ± 0.04^{e}	95.32 ± 0.02^{c}	95.35 ± 0.04^{c}	135.22 ± 0.01^{a}	99.54 ± 0.02^{b}	89.35 ± 0.04^{d}
HCT	37.27 ± 0.04^{d}	37.54 ± 0.03^{c}	38.36 ± 0.02^{b}	38.41 ± 0.03^{b}	45.30 ± 0.01^{a}	38.36 ± 0.02^{b}
MCV	53.72 ± 0.02^{d}	53.69 ± 0.01^{d}	54.48 ± 0.03^{b}	61.09 ± 0.04^{a}	54.45 ± 0.03^{bc}	54.40 ± 0.02^{c}
MCH	15.54 ± 0.04^{d}	18.34 ± 0.04^{c}	15.36 ± 0.02^{e}	20.10 ± 0.02^{a}	18.37 ± 0.03^{bc}	18.43 ± 0.04^{b}
MCHC	265.73 ± 0.03^{d}	267.17 ± 0.04^{c}	265.14 ± 0.03^{e}	302.45 ± 0.03^{a}	278.12 ± 0.02^{b}	267.13 ± 0.01^{c}
PLT	812.16 ± 0.04^{a}	812.20 ± 0.02^{a}	723.72 ± 0.02^{b}	681.27 ± 0.02^{d}	684.45 ± 0.03^{c}	723.68 ± 0.03^{b}
MPV	10.34 ± 0.05^{a}	9.81 ± 0.02^{bc}	9.77 ± 0.02^{cd}	6.42 ± 0.03^{e}	9.86 ± 0.02^{b}	9.73 ± 0.02^{d}
PCT	0.45 ± 0.03^{a}	0.36 ± 0.04^{d}	0.42 ± 0.02^{ab}	0.24 ± 0.02^{e}	0.38 ± 0.01^{cd}	0.42 ± 0.02^{ab}
PDW	18.9 ± 0.04^{a}	18.6 ± 0.03^{b}	18.9 ± 0.02^{a}	15.9 ± 0.02^{d}	16.4 ± 0.03^{c}	18.6 ± 0.03^{b}

Different superscript letters (a–e) within a row indicate statistically significant differences ($p < 0.05$).
WBC, white blood cell count; LYM, lymphocyte; MID, mid-sized cell; GR, granulocyte; RBC, red blood cell count; HGB, hemoglobin; HCT, hematocrit; MCV, mean corpuscular volume; MCH, mean corpuscular hemoglobin; MCHC, mean corpuscular hemoglobin concentration; PLT, platelet; MPV, mean platelet volume; PCT, plateletcrit; PDW, platelet distribution width.

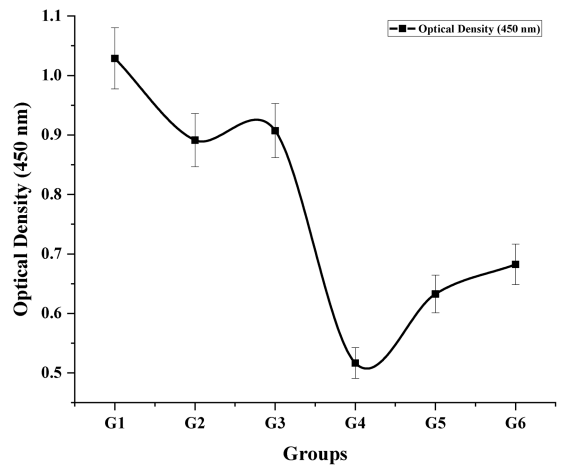

FIGURE 8
Optical density of C-reactive protein from serum of different mice groups.

substantial reduction in CRP levels, closely approaching baseline values. This reduction reflects the anti-inflammatory potential of the nanoemulsion formulation and supports its efficacy in attenuating systemic inflammatory responses *in-vivo*.

3.12 Histopathological analysis

After completion of the anti-inflammatory experiment, skin tissues from all groups were collected and subjected to histopathological examination using hematoxylin and eosin (H&E) staining. The histological analysis aimed to evaluate the extent of epidermal and dermal recovery, collagen organization, inflammatory infiltration, and tissue architecture preservation (Figure 9). Histological evaluation revealed pronounced epidermal and dermal disruption, characterized by thickened and dense infiltration of inflammatory cells in the control group (G_1). The diabetic group (G_2) treated with dicloran gel (marketed) exhibited partial epidermal restoration with thin, disorganized layers and moderate collagen disarray, along with persistent inflammatory infiltration. Hair follicles appeared sparse and atrophic.

The diabetic group infected with *S. aureus* and treated with market cream (G_3) displayed the most severe histopathological alterations, including epidermal erosion, dermal edema, extensive inflammatory infiltration, and collagen degradation. There was a high presence of polymorphonuclear cells, indicating acute inflammation and a lack of proper tissue healing. On the other hand, G_4: the group treated with CONE-based cream, showing significant improvement in histology. The epidermis showed good continuity and stratification, and the dermis revealed dense collagen bundles with few inflammatory infiltrates. The hair follicle was preserved, indicating that the formulation may have an initial healing potential. Diabetic group treated with CONE cream (G_5) showed marked epidermal hyperplasia, regular arrangement of cells, and senile cell presence with mild degree of dermal architecture. The hair follicles were excessive and morphologically normal. Likewise, in G_6 (diabetic + *S. aureus* + CONE cream), significant improvement in skin architecture was observed with re-established epidermal continuity, organized collagen deposition, and partial preservation of dermal appendages with mild remnant inflammation. Collectively, these findings confirm the therapeutic potential of the CONE-based cream in promoting epidermal and dermal regeneration, suppressing inflammation, and preserving skin integrity, even under diabetic and infectious conditions.

3.13 Molecular docking

The molecular docking analysis of eugenol with inflammatory protein targets revealed significant binding affinities and interaction patterns supporting its anti-inflammatory potential. It was observed

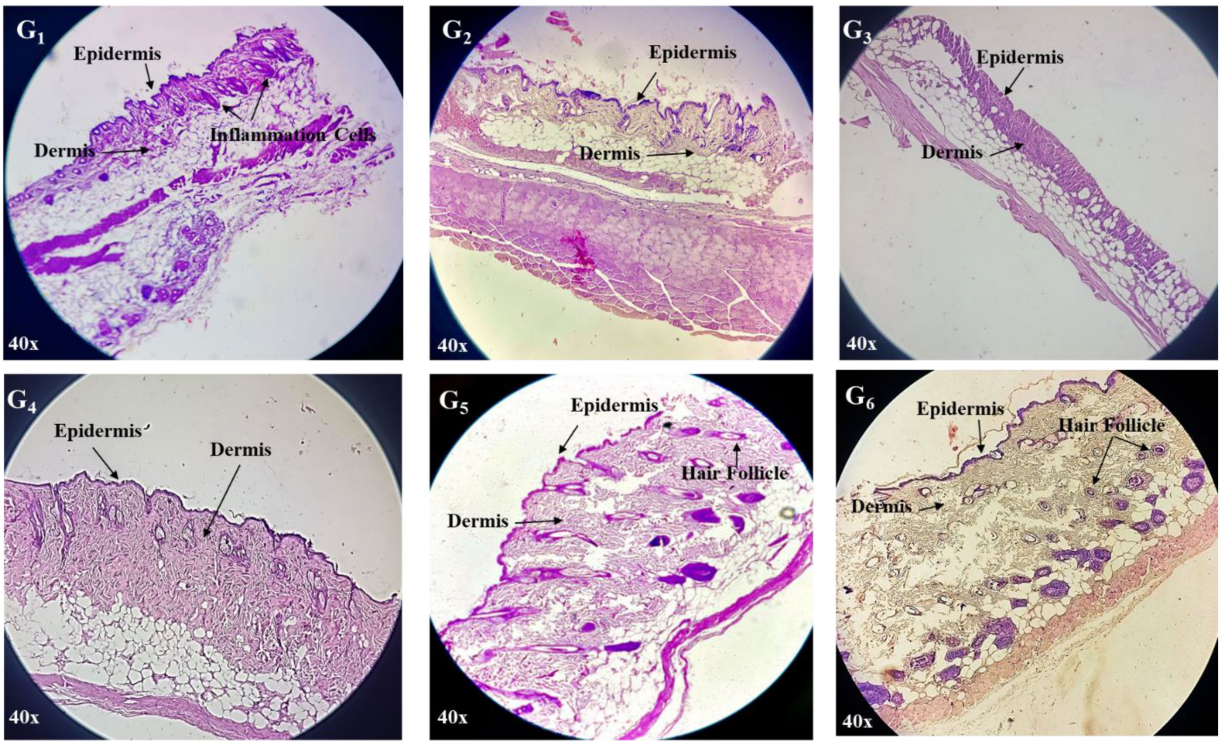

FIGURE 9
Histopathological examination of mice skin tissues. Control group **(G_1)**; diabetic model treated with market available cream (dicloran gel) **(G_2)**; diabetic model infected with *S. aureus* treated with market cream **(G_3)**; CONE incorporated topical cream treated group **(G_4)**, diabetic model treated with CONE incorporated cream **(G_5)**; diabetic model infected with *S. aureus* treated with CONE incorporated cream **(G_6)**.

that eugenol exhibited binding energies of approximately −4.7 kcal/mol with C-reactive protein (7PKB) and −4.9 kcal/mol with Interleukin-1β (9ILB). In case of CRP, eugenol engages in a π–π T-shaped interaction with PHE66 and π-alkyl interaction with LEU64, at distances of 6.52 Å and 4.77 Å, respectively. Stabilization is further supported by van der Waals contacts involving SER68, SER74, THR76, GLU81 and GLN150, anchoring the aromatic ring deep within the concave pocket reminiscent of the phosphocholine-binding site in CRP (Figure 10).

In Interleukin-1β (IL-1β; PDB ID: 9ILB), eugenol similarly achieved a favorable docked pose. A conventional hydrogen bond is formed with VAL41 (3.59 Å), accompanied by π-alkyl and alkyl contacts with LEU62 and VAL40, respectively. Notably, a distinct π-sulfur interaction with MET20 and additional π-alkyl interactions at distances between ~4.09 and 4.87 Å reinforce the binding. These combined interactions indicate a robust multi-mode binding paradigm within the IL-1β hydrophobic cavity (Figure 10).

4 Discussion

4.1 Optimization of NE

The CONE was optimized using response surface methodology, focusing on the effects of oil concentration, Tween 80, sonication time, and power on droplet size and PDI. The optimized formulation (10% v/v oil, 2.5% w/v Tween 80, 15 min sonication, 50% power) yielded the smallest droplet size (190 nm) and lowest PDI (0.08), indicating high stability and uniformity. Droplet sizes under 300 nm are known to enhance drug permeation (43), and the surfactant likely stabilized droplets by forming a compact interfacial film (44). Longer sonication time further reduced droplet size and PDI, likely due to enhanced cavitation effects, as supported by Ahmed et al. (45). When the PDI is smaller than 0.3, the nanoemulsion system has a narrow size distribution (46). The optimized NE showed PDI < 0.1, confirming narrow size distribution, which is suitable for topical delivery.

4.2 Entrapment efficiency

The present study demonstrated a high EE (94%) for CONE, aligning with previous reports on EO-based NE, where effective emulsification and optimized surfactant concentrations contribute to enhanced drug loading (47). The EE is primarily dependent on the solubility of the active, its compatibility with the constituents of the formulation. The poor aqueous solubility of CEO components might play in favor of encapsulation, which is further facilitated in the presence of surfactants and co-surfactants (48). Whereas those with very high levels of surfactants, such as emulsions with 74% Tween 80, can result in low entrapments, either by micellar solubilization, as has been reported in a few NEs and nano-emulgel (49).

4.3 Properties of topical cream

The organoleptic properties and pH of the prepared formulations are presented in Table 1. No evidence for phase separation or

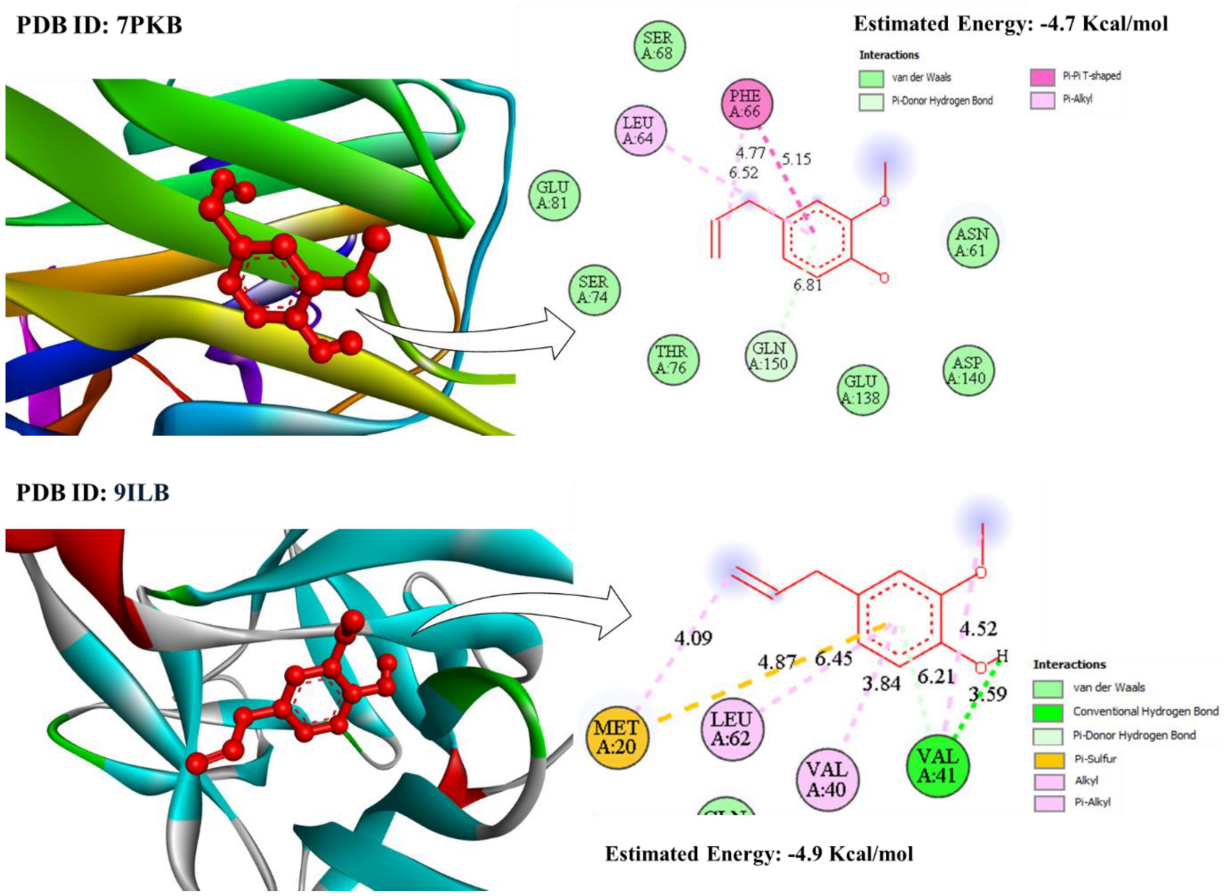

FIGURE 10
Molecular interactions between of eugenol and inflammatory proteins. PKB, C-reactive protein; 9ILB, Interleukin-1β.

inhomogeneity was noticed, which may be ascribed to the utilization of nonionic surfactants characterized by stability against ionic strength and pH adjustments (50). During the stability study, the preparations were microbiologically stable and had no variation in odor, attributable possibly to the emulsion's natural antioxidants and preservatives. The pH value is an important part of the stability and dermatological compatibility of topical formulations (51). The pH values of the prepared cream formulations were all in the compatible pH range of skin (4–7) (52), establishing that the products are suitable for topical application without any irritation.

4.4 Sustain release

In-vitro release studies are important preliminary investigations to gain knowledge on the *in-vivo* behavior of topical preparations, like release kinetics and mechanism. The *in-vitro* release pattern of CONE containing cream exhibited a typical biphasic one, as previously reported (53). Biphases kinetic profiles are commonly reported in lipid-based nanocarriers and nanoemulsions, where a burst phase can be observed at the onset of the therapy to ensure fast therapeutic delivery, and a further sustained phase to provide delayed availability to the drug (54). Droplet size, surfactant interfacial thickness, and drug-lipid interactions are some of the parameters that mediate the diffusion-controlled release stage. In the current study, the consistent release data with the Higuchi model proves that diffusion by the nanoemulsion-based matrix is the major force in release. This effect has been already described in polymeric and lipid nanoparticles, in particular with lipophilic and poorly water-soluble drugs, in which the matrix-controlled systems surpass traditional formulations to support long activity (55).

An initial burst release was seen at all the tested concentrations which resulted from the quick diffusion of clove oil, adsorbed on the surface of NE droplets. This was succeeded by the sustained release stage, controlled by the slowest release of drug due to diffusion from the lipid core that worked as a reservoir system. Such biphasic release profile can provide dual benefits of immediate availability of therapeutic moiety as well as a sustained effect, which is consistent with previous studies on nanoemulsion topical preparations (56).

Cream incorporated with 1 mL of CONE showed the best released pattern, although a burst release was observed after 72 h. Low concentrations CONE formulations (0.5 and 0.75 mL) which had a limited encapsulation, showed faster and burst release. On the other side the higher concentration of CONE (1.5 mL) showed irregular release pattern due to droplet agglomeration or saturation effects. The sustained and controlled release behavior of the 1 mL formulation indicates its suitability for extended dermal therapeutic efficacy (57,

58). This release mechanism that is controlled by diffusion ensures long retention of the active compound to the site of application; thus, therapeutic effectiveness is improved and offers less frequent reapplication. Comparable sustained release of eugenol loaded nanoemulsions have already been described by Ahmad et al. (59), explained by small, homogeneous droplets. Likewise, Aldeeb et al. (56) observed that an optimized release was obtained from citronellol nanoemulgels concerning the concentrations of the formulation, suggesting the importance of the parameters of formulation in controlling skin absorption. Taken together, these results establish the 1 mL CONE composition as being optimal for immediate and extended drug delivery.

4.5 Antifungal

CONE showed strong antifungal activity against *Penicillium italicum* and *Aspergillus niger*, causing significant inhibition of their growth compared to the control. The MIC values were similar for both fungal strains, demonstrating the broad-spectrum antifungal activity. Those results are consistent with those of Tomić et al. (60), who also documented comparable antifungal activities of essential oil nanoemulsion on *Cladosporium cladosporoides, Aspergillus fumigatus* and *Penicillium chrysogenum.* Fungal strains (*P. italicum* and *A. niger*) were chosen due to their importance as typical postharvest and opportunistic pathogens. In addition, the time-kill kinetics pattern indicated that CONE showed a quick and potent inhibition activity against *P. italicum*, which is acquiring fungicidal activity rather than fungistatic activity. This is also in agreement with Sim et al. (61), who highlighted the practical significance of the time-kill assays on *in-vitro* fungicidal potency of plant extracts at the MIC values.

4.6 Antioxidant assays

Nanoencapsulation has been confirmed by several studies to significantly enhance the antioxidant activity of natural products (62). This enhancement is achieved by improving the stability, bioavailability, and dispersibility of active components, protecting them from environmental degradation, and facilitating a greater interaction with free radicals due to the increased surface area at the nanoscale (63). In the present investigation, the antioxidant activity of CONE was tested using DPPH and ABTS radical scavenging. The free radical scavenging ability of CONE showed a dose-dependent increase and maximum DPPH inhibition (~84%) was observed at 100 µL, as compared to bulk clove oil 47%. These results were in agreement with those of Nagaraju et al. (37) also revealed 80% of DPPH radical scavenging activity at 100 µg/mL for clove oil nano emulsion. ABTS assay also showed 81% inhibition by CONE versus 30.3% by clove oil. On the whole, increased radical-scavenging activity of CONE suggests that nanoencapsulation greatly enhances the antioxidant activity of clove oil.

4.7 *In-vivo* anti-inflammatory activity

The *in-vivo* study reported that the topical creams incorporated with CONE significantly reduced skin inflammation and promoted wound healing in mice, even in diabetic and infected conditions. During the 21-days treatment period, the groups treated with CONE-based cream (G_4 and G_5) presented significant decreases in inflammatory area and were then in nearly complete remission. These results are better than a non-treated group and dicloran gel ones, confirming the higher efficiency of NE base. Another anti-inflammatory and regenerative aspect of clove oil was reported by Banerjee et al. (64), who detected decreased paw edema and increased wound closure in rats. Likewise, El-Zahaby et al. (11) found that the wound closure rate was enhanced by clove oil encapsulated nanostructured liquid crystals and showed the same result on wound healing in infected burn wounds. Mohamed et al. (65) demonstrated decreased pro-inflammatory cytokines and oxidative stress in clove oil nanoemulsion-treated mice.

Hematological examination showed raised RBC and HGB, while lowered WBC and platelet counts in CONE-treated groups. This reduction may be attributed to the anti-inflammatory and antioxidant actions of eugenol, the principal bioactive component of clove oil, which has been reported to inhibit the release of pro-inflammatory cytokines such as TNF-α, IL-1β, and IL-6 (66). By attenuating these mediators, eugenol can reduce leukocyte recruitment and proliferation, leading to stabilization of WBC levels during inflammation. Furthermore, the nanoemulsion delivery system enhances cutaneous penetration while minimizing systemic immune activation (67), thereby suppressing peripheral leukocytosis often seen in diabetic or infected models. Together, these effects may explain the lower WBC counts in G_4 and G_5 groups. Elgharib et al. (68), CEO restored hematological indices towards normal in the rats treated with cadmium chloride and supported its protective action against systemic toxicity. Similarly, Pandey et al. (10) stress that it is the context-dependent hematological effects of clove oil nanoemulsions that should be considered and further studied.

There were statistically significant differences in platelet indices in the experimental groups. The highest number of platelets (PLT) was seen in this case of G_1 and G_2, as compared to G_4 and G_5, which had significantly lower numbers. The platelet count decrease observed can be mechanistically explained by the fact that eugenol has been proven to have antiplatelet and antithrombotic effects, including platelet aggregation inhibition and thromboxane A_2 synthesis inhibition (69). As Wang et al. (70) state, eugenol disrupts the activity of cyclooxygenase (COX-1) to suppress the production of arachidonic acid and its further neutrophilization. Moreover, its antioxidant effect suppresses reactive oxygen species (ROS) (71), which is commonly the main initiator of platelet activation in the scenario of diabetes and inflammatory stress. The lower levels of PLT in G_4 and G_5 are, therefore, probably some sort of a normalization of hyperactive platelet activity as opposed to an expression of disease pathology of thrombocytopenia.

Histopathological examination of treated skin specimens showed normalization of the epidermal and dermal structure, decreased cellular infiltration in the inflammatory cells, and organized collagen deposition, proving the healing potential of the CONE incorporated cream. These findings support the previous report by El-Zahaby et al. (11), while the CONE-based cream promoted tissue regeneration and curbed infections. The bioactives of clove act as antioxidants, reducing oxidative stress and supporting the restoration of normal skin

structure (72). According to Banerjee et al. (64), a therapy via clove oil emulsion works effectively to achieve rapid wound healing, the skin layers, and production of collagen, which supports tissue repair. Similarly, Gul et al. (73) developed clove and olive oil NE to enhance skin penetration and tissue repair. Moreover, Mohamed et al. (65) also described histological improvement in systemic organs after treatment with CONE. Altogether, these results demonstrate the potential use of CONE to aid in skin regeneration through increased bioactive delivery to the wound site and reduction of oxidative damage.

4.8 Molecular docking

The molecular docking approach was used to explore the binding ability of eugenol to the major molecules participating in the human inflammatory process. *In-silico* studies indicated that eugenol tends to construct a stable complex with CRP and IL-1β, which underlies its anti-inflammatory activities. The docking of eugenol against CRP showed a favourable binding energy of −4.7 kcal/mol. CRP is a prototypical acute-phase reactant and a sensitive biomarker manifesting tight association with systemic inflammation; it also has direct pro-inflammatory actions such as complement activation and cytokine production (74). π–π T-shaped interaction with PHE66 and a π-alkyl interaction with LEU64 maintain the eugenol molecule in this important ligand-binding groove. The binding mode indicates that eugenol could be a competitive inhibitor that may obstruct the endogenous ligands binding and overlap with the inflammatory signaling of CRP, so as to play the role of inflammatory inhibitor (75). Notably, docking against 7PKB revealed π–π and π-alkyl interactions consistent with previously reported stabilization mechanisms for eugenol in inflammatory targets (e.g., COX-2, 5-LOX), where aromatic stacking with phenylalanine residues plays a dominant role in affinity enhancement (76).

Similarly, the simulation with Interleukin-1β (PDB ID: 9ILB), a primary cytokine driving fever and acute inflammation, showed a robust binding affinity (−4.9 kcal/mol). A conventional hydrogen bond with VAL41 provides directional stability, while hydrophobic contacts with LEU62 and VAL40 further secure the ligand in the protein's hydrophobic cavity. The presence of a π-sulfur interaction with MET20 further enhances binding stability, analogous to eugenol's interactions with PPARγ (77, 78), suggesting similar stabilization patterns. By occupying a key pocket on the IL-1β surface, eugenol could sterically hinder its interaction with the IL-1 receptor (IL-1R), thereby disrupting downstream pro-inflammatory signaling pathways such as NF-κB and MAPKs (79).

These molecular interactions provide a mechanistic rationale for eugenol's documented ability to ameliorate inflammation by modulating multiple signaling proteins (2). The docking outcomes with 7PKB and 9ILB demonstrate that eugenol can engage critical inflammatory enzymes via both hydrophobic and hydrogen bonding interactions. This supports the potential use of eugenol, particularly in nanoemulsion formulations, to intercept and suppress inflammatory pathways *in-vivo*.

5 Conclusion

This study confirms that CONE-incorporated cream is a promising approach for the treatment of skin inflammation. The optimized NE with small droplet size, low Polydispersity Index and high entrapment efficiency displayed strong antifungal, antioxidant and anti-inflammatory activity. *In-vivo* application of CONE based cream in mice model normalized hematological parameters, inhibited inflammatory cell infiltration, and re-epithelialization of tissues as confirmed by histopathology. The sustained drug release and stability of the cream also demonstrate its clinical relevance. Taken together, these data demonstrated that the clove oil encapsulated in nanoemulsion improves bioavailability and efficacy with reduced risk for irritation, which could facilitate its further development as a safe and effective topical treatment. This study also has some limitations, which include a small sample size ($n = 5$), a lack of formal power assessment, quantitative toxicity or irritation scoring, and dose–response assessment *in vivo*. These limitations in future research can be overcome by diversifying the size of animal groups, conducting toxicological tests, and systematic dose–response studies to make a more comprehensive spectrum of the safety and effectiveness of the formulation.

Data availability statement

The raw data supporting the conclusions of this article will be made available by the authors, without undue reservation.

Ethics statement

The animal study was approved by the methodology of this study was approved by the Ethical Committee of Cholistan University of Veterinary and Animal Sciences Bahawalpur (Date: 30-09-2024, No: ORIC-328). The study was conducted in accordance with the local legislation and institutional requirements.

Author contributions

AS: Data curation, Formal analysis, Writing – original draft. IB: Data curation, Investigation, Methodology, Project administration, Supervision, Writing – review & editing. ZF: Supervision, Writing – review & editing. HM: Supervision, Writing – review & editing. VP: Supervision, Writing – review & editing.

Funding

The author(s) declare that no financial support was received for the research and/or publication of this article.

Acknowledgments

The article was extracted from a Ph.D. thesis prepared by Ahsan Shafiq, under the supervision of Irfan Baboo, Zahid Farooq, Hamid Majeed and Valiollah Palangi.

Conflict of interest

The authors declare that the research was conducted in the absence of any commercial or financial relationships that could be construed as a potential conflict of interest.

Generative AI statement

The authors declare that no Gen AI was used in the creation of this manuscript.

Any alternative text (alt text) provided alongside figures in this article has been generated by Frontiers with the support of artificial intelligence and reasonable efforts have been made to ensure accuracy, including review by the authors wherever possible. If you identify any issues, please contact us.

Publisher's note

References

1. Ahmad, RM, and Ibrahim, OMS. Anti-inflammatory activity of clove (*Syzygium aromaticum*) oil extract against chronic inflammation in rat. *Adv Anim Vet Sci*. (2024) 12:77–84. doi: 10.17582/journal.aavs/2024/12.1.77.84

2. Pires Costa, E, Maciel dos Santos, M, de Paula, RA, da Silva, DA, Lopes, RP, Teixeira, RR, et al. Antioxidant and anti-inflammatory activity of eugenol, bis-eugenol, and clove essential oil: an in vitro study. *ACS Omega*. (2025) 10:31033–45. doi: 10.1021/acsomega.5c04146

3. Sharma, VM, and Jagdhane, VC. Role of leech therapy to encounter heel pain in associated conditions of retrocalcaneal bursitis, plantar fasciitis with tenosynovitis: a case study. *World J Pharm Res*. (2023) 9:686–94. doi: 10.20959/wjpr202011-18352

4. Medzhitov, R. The spectrum of inflammatory responses. *Science*. (2021) 374:1070–5. doi: 10.1126/science.abi5200

5. Ali, KA, Maity, A, Roy, SD, Pramanik, SD, Das, PP, and Shaharyar, MA. Insight into the mechanism of steroidal and non-steroidal anti-inflammatory drugs In: How synthetic drugs work: Academic Press (2023). 61–94. doi: 10.1016/B978-0-323-99855-0.00004-X

6. Bindu, S, Mazumder, S, and Bandyopadhyay, U. Non-steroidal anti-inflammatory drugs (NSAIDs) and organ damage: a current perspective. *Biochem Pharmacol*. (2020) 180:114147. doi: 10.1016/j.bcp.2020.114147

7. Hasan, HF. Evaluation of the effect of flavonoids isolated from *Spinacia oleracea* leaves on pituitary-adrenal ovarian axis in mice treated with doxorubicin. *J Adv Pharm Educ Res*. (2019) 9:74–9.

8. Aman, RM, Abu Hashim, II, and Meshali, MM. Novel clove essential oil nanoemulgel tailored by Taguchi's model and scaffold-based nanofibers: phytopharmaceuticals with promising potential as cyclooxygenase-2 inhibitors in external inflammation. *Int J Nanomedicine*. (2020) 15:2171–95. doi: 10.2147/IJN.S246601

9. El-Saber Batiha, G, Alkazmi, LM, Wasef, LG, Beshbishy, AM, Nadwa, EH, and Rashwan, EK. *Syzygium aromaticum* L. (Myrtaceae): traditional uses, bioactive chemical constituents, pharmacological and toxicological activities. *Biomolecules*. (2020) 10:202. doi: 10.3390/biom10020202

10. Pandey, VK, Srivastava, S, Dash, KK, Singh, R, Dar, AH, Singh, T, et al. Bioactive properties of clove (*Syzygium aromaticum*) essential oil nanoemulsion: a comprehensive review. *Heliyon*. (2024) 10:e20424. doi: 10.1016/j.heliyon.2023.e22437

11. El-Zahaby, SA, Wen, MM, Abdelwahab, IA, Shahine, YM, Abdelhady, SA, and Elbatouti, GA. Eco-friendly nanostructured liquid crystals loaded with clove oil as a sustainable approach for managing infected burn wounds. *AAPS PharmSciTech*. (2024) 26:15. doi: 10.1208/s12249-024-03009-z

12. Alanazi, AK, Alqasmi, MH, Alrouji, M, Kuriri, FA, Almuhanna, Y, Joseph, B, et al. Antibacterial activity of *Syzygium aromaticum* (clove) bud oil and its interaction with imipenem in controlling wound infections in rats caused by methicillin-resistant *Staphylococcus aureus*. *Molecules*. (2022) 27:8551. doi: 10.3390/molecules27238551

13. Kumar Pandey, V, Shams, R, Singh, R, Dar, AH, Pandiselvam, R, Rusu, AV, et al. A comprehensive review on clove (*Caryophyllus aromaticus* L.) essential oil and its significance in the formulation of edible coatings for potential food applications. *Front Nutr*. (2022) 9:987674. doi: 10.3389/fnut.2022.987674

14. Abedinpour, N, Ghanbariasad, A, Taghinezhad, A, and Osanloo, M. Preparation of nanoemulsions of *Mentha piperita* essential oil and investigation of their cytotoxic effect on human breast cancer lines. *BioNanoSci*. (2021) 11:428–36. doi: 10.1007/s12668-021-00827-4

15. Ghiasi, Z, Esmaeli, F, Aghajani, M, Ghazi-Khansari, M, Faramarzi, MA, and Amani, A. Enhancing analgesic and anti-inflammatory effects of capsaicin when loaded into olive oil nanoemulsion: an in-vivo study. *Int J Pharm*. (2019) 559:341–7. doi: 10.1016/j.ijpharm.2019.01.043

16. Maghbool, M, Khosravi, T, Vojdani, S, Chaijan, MR, Esmaeili, F, Amani, A, et al. The effects of eugenol nanoemulsion on pain caused by arteriovenous fistula cannulation in hemodialysis patients: a randomized double-blinded controlled cross-over trial. *Complement Ther Med*. (2020) 52:102440. doi: 10.1016/j.ctim.2020.102440

17. Esmaeili, F, Zahmatkeshan, M, Yousefpoor, Y, Alipanah, H, Safari, E, and Osanloo, M. Anti-inflammatory and anti-nociceptive effects of cinnamon and clove essential oils nanogels: an in vivo study. *BMC Complement Med Ther*. (2022) 22:143. doi: 10.1186/s12906-022-03619-9

18. Abbasifard, M, Yousefpoor, Y, Amani, A, and Arababadi, MK. Topical bee venom nano-emulsion ameliorates serum level of endothelin-1 in collagen-induced rheumatoid arthritis model. *BioNanoSci*. (2021) 11:810–5. doi: 10.1007/s12668-021-00871-0

19. Ghanbariasad, A, Azadi, S, Agholi, M, and Osanloo, M. The nanoemulsion-based nanogel of *Artemisia dracunculus* essential oil with proper activity against *Leishmania tropica* and *Leishmania major*. *Nanomed Res J*. (2021) 6:89–95. doi: 10.22034/nmrj.2021.01.010

20. Almuqbil, RM, and Aldhubiab, B. Bioadhesive nanoparticles in topical drug delivery: advances, applications, and potential for skin disorder treatments. *Pharmaceutics*. (2025) 17:229. doi: 10.3390/pharmaceutics17020229

21. Lal, DK, Kumar, B, Saeedan, AS, and Ansari, MN. An overview of nanoemulgels for bioavailability enhancement in inflammatory conditions via topical delivery. *Pharmaceutics*. (2023) 15:1187. doi: 10.3390/pharmaceutics15041187

22. Bodnár, K, Fehér, P, Ujhelyi, Z, Bácskay, I, and Józsa, L. Recent approaches for the topical treatment of psoriasis using nanoparticles. *Pharmaceutics*. (2024) 16:449. doi: 10.3390/pharmaceutics16040449

23. Iskandar, B, Liu, TW, Mei, HC, Kuo, IC, Surboyo, MDC, Lin, HM, et al. Herbal nanoemulsions in cosmetic science: a comprehensive review of design, preparation, formulation, and characterization. *J Food Drug Anal*. (2024) 32:428–58. doi: 10.38212/2224-6614.3526

24. Jabbar, M, Baboo, I, Majeed, H, Farooq, Z, and Palangi, V. Characterization and antibacterial application of peppermint essential oil nanoemulsions in broiler. *Poult Sci*. (2024) 103:104432. doi: 10.1016/j.psj.2024.104432

25. Moghimi, R, Aliahmadi, A, McClements, DJ, and Rafati, H. Investigations of the effectiveness of nanoemulsions from sage oil as antibacterial agents on some food borne pathogens. *LWT Food Sci Technol*. (2016) 71:69–76. doi: 10.1016/j.lwt.2016.03.018

26. Kelidari, HR, Moemenbellah-Fard, MD, Morteza-Semnani, K, Amoozegar, F, Shahriari-Namadi, M, Saeedi, M, et al. Solid-lipid nanoparticles (SLNs) containing *Zataria multiflora* essential oil with no-cytotoxicity and potent repellent activity against *Anopheles stephensi*. *J Parasit Dis*. (2021) 45:101–8. doi: 10.1007/s12639-020-01281-x

27. Majeed, U, Shafi, A, Shahbaz, M, Khan, KUR, Iqbal, KJ, Akram, K, et al. Assessment of growth inhibition of eugenol-loaded nano-emulsions against beneficial *Bifidobacterium* sp. along with resistant *Escherichia coli* using flow cytometry. *Fermentation*. (2023) 9:140. doi: 10.3390/fermentation9020140

28. Majeed, H, Bian, YY, Ali, B, Jamil, A, Majeed, U, Khan, QF, et al. Essential oil encapsulations: uses, procedures, and trends. *RSC Adv*. (2015) 5:58449–63. doi: 10.1039/C5RA06556A

29. Heydari, M, Amirjani, A, Bagheri, M, Sharifian, I, and Sabahi, Q. Eco-friendly pesticide based on peppermint oil nanoemulsion: preparation, physicochemical properties, and its aphicidal activity against cotton aphid. *Environ Sci Pollut Res*. (2020) 27:6667–79. doi: 10.1007/s11356-019-07332-y

30. Costa, EM, Pereira, CF, Ribeiro, AA, Casanova, F, Freixo, R, Pintado, M, et al. Characterization and evaluation of commercial carboxymethyl cellulose potential as an active ingredient for cosmetics. *Appl Sci*. (2022) 12:6560. doi: 10.3390/app12136560

31. Dhase, AS, Khadbadi, SS, and Saboo, SS. Formulation and evaluation of vanishing herbal cream of crude drugs. *Am J Ethnomed*. (2014) 1:313–8. doi: 10.22270/ajprd.v8i3.725

32. Afokoghene, AJ, Eziuzo, OS, and Lynda, NC. Antimicrobial investigation, formulation and evaluation of *Andrographis paniculata* aqueous herbal cream for topical application. *Res J Pharm Technol*. (2022) 15:3553–8. doi: 10.52711/0974-360X.2022.00596

33. Srirod, S, and Tewtrakul, S. Anti-inflammatory and wound healing effects of cream containing *Curcuma mangga* extract. *J Ethnopharmacol*. (2019) 238:111828. doi: 10.1016/j.jep.2019.111828

34. Leelapornpisid, P, Mungmai, L, Sirithunyalug, B, Jiranusornkul, S, and Peerapornpisal, Y. A novel moisturizer extracted from freshwater macroalga *Rhizoclonium hieroglyphicum* (C. Agardh) Kützing for skin care cosmetic. *Chiang Mai J Sci*. (2014) 41:1195–207. Available online at: http://epg.science.cmu.ac.th/ejournal/41

35. Song, R, Yan, F, Cheng, M, Dong, F, Lin, Y, Wang, Y, et al. Ultrasound-assisted preparation of exopolysaccharide/nystatin nanoemulsion for treatment of vulvovaginal candidiasis. *Int J Nanomedicine*. (2020) 15:2027–44. doi: 10.2147/IJN.S241134

36. Majeed, H, Liu, F, Hategekimana, J, Sharif, HR, Qi, J, Ali, B, et al. Bactericidal action mechanism of negatively charged food grade clove oil nanoemulsions. *Food Chem*. (2016) 197:75–83. doi: 10.1016/j.foodchem.2015.10.015

37. Nagaraju, PG, Sengupta, P, Chicgovinda, PP, and Rao, PJ. Nanoencapsulation of clove oil and study of physicochemical properties, cytotoxic, hemolytic, and antioxidant activities. *J Food Process Eng*. (2021) 44:e13645. doi: 10.1111/jfpe.13645

38. Sridhar, K, and Charles, AL. In vitro antioxidant activity of Kyoho grape extracts in DPPH and ABTS assays: estimation methods for EC_{50} using advanced statistical programs. *Food Chem*. (2019) 275:41–9. doi: 10.1016/j.foodchem.2018.09.040

39. Pakpahan, SE, Fadhilah, FR, Amalia, M, and Putri, EN. Topical hydrogel human amnion membrane for wounds healing in mice (*Mus musculus*) induced by diabetes. *Riset Informasi Kesehatan*. (2025) 14:194–203. doi: 10.30644/rik.v14i2.1013

40. Oshkondali, STM, Mahmoudy, E, Samira, F, Alacrouk, A, Abu, KM, Rashed, A, et al. Alloxan dose optimization to induce diabetes in albino mice and the determination of the induced diabetes type. *Saudi J Med Pharm Sci*. (2019) 5:813–6. doi: 10.36348/SJMPS.2019.v05i10.001

41. Hussain, F, Hafeez, J, Khalifa, AS, Naeem, M, Ali, T, and Eed, EM. In vitro and in vivo study of inhibitory potentials of α-glucosidase and acetylcholinesterase and biochemical profiling of *M. charantia* in alloxan-induced diabetic rat models. *Am J Transl Res*. (2022) 14:3824. Available online at: https://pmc.ncbi.nlm.nih.gov/articles/PMC9274573/

42. Toghyani, M, Gheisari, A, Ghalamkari, G, and Eghbalsaied, S. Evaluation of cinnamon and garlic as antibiotic growth promoter substitutions on performance, immune responses, serum biochemical and haematological parameters in broiler chicks. *Livest Sci*. (2011) 138:167–73. doi: 10.1016/j.livsci.2010.12.018

43. El-Dakroury, WA, Zewail, MB, and Amin, MM. Design, optimization, and in-vivo performance of glipizide-loaded O-carboxymethyl chitosan nanoparticles in insulin resistant/type 2 diabetic rat model. *J Drug Deliv Sci Technol*. (2023) 79:104040. doi: 10.1016/j.jddst.2022.104040

44. Zewail, MB, El-Gizawy, SA, Osman, MA, and Haggag, YA. Preparation and in vitro characterization of a novel self-nano emulsifying drug delivery system for a fixed-dose combination of candesartan cilexetil and hydrochlorothiazide. *J Drug Deliv Sci Technol*. (2021) 61:102320. doi: 10.1016/j.jddst.2021.102320

45. Ahmed, S, Gull, A, Alam, M, Aqil, M, and Sultana, Y. Ultrasonically tailored, chemically engineered and "QbD" enabled fabrication of agomelatine nanoemulsion; optimization, characterization, ex-vivo permeation and stability study. *Ultrason Sonochem*. (2018) 41:213–26. doi: 10.1016/j.ultsonch.2017.09.042

46. Pongsumpun, P, Iwamoto, S, and Siripatrawan, U. Response surface methodology for optimization of cinnamon essential oil nanoemulsion with improved stability and antifungal activity. *Ultrason Sonochem*. (2020) 60:104604. doi: 10.1016/j.ultsonch.2019.05.021

47. Kumar, A, Kanwar, R, and Mehta, SK. Development of phosphatidylcholine/tween 80-based biocompatible clove oil-in-water nanoemulsion as a green nanocarrier for controlled herbicide delivery. *Environ Pollut*. (2022) 293:118558. doi: 10.1016/j.envpol.2021.118558

48. Ullah, N, Amin, A, Farid, A, Selim, S, Rashid, SA, Aziz, MI, et al. Development and evaluation of essential oil-based nanoemulgel formulation for the treatment of oral bacterial infections. *Gels*. (2023) 9:252. doi: 10.3390/gels9030252

49. Nawaz, T, Iqbal, M, Khan, BA, Nawaz, A, Hussain, T, Hosny, KM, et al. Development and optimization of acriflavine-loaded polycaprolactone nanoparticles using Box–Behnken Design for burn wound healing applications. *Polymers*. (2021) 14:101. doi: 10.3390/polym14010101

50. Razzaq, FA, Asif, M, Asghar, S, Iqbal, MS, Khan, IU, Khan, SUD, et al. Glimepiride-loaded nanoemulgel; development, in vitro characterization, ex vivo permeation and in vivo antidiabetic evaluation. *Cells*. (2021) 10:2404. doi: 10.3390/cells10092404

51. Rehman, A, Iqbal, M, Khan, BA, Khan, MK, Huwaimel, B, Alshehri, S, et al. Fabrication, *in vitro*, and *in vivo* assessment of eucalyptol-loaded nanoemulgel as a novel paradigm for wound healing. *Pharmaceutics*. (2022) 14:1971. doi: 10.3390/pharmaceutics14091971

52. Baptista, S, Baptista, F, and Freitas, F. Development of emulsions containing L-ascorbic acid and α-tocopherol based on the polysaccharide FucoPol: stability evaluation and rheological and texture assessment. *Cosmetics*. (2023) 10:56. doi: 10.3390/cosmetics10020056

53. Gaber, DA, Alsubaiyel, AM, Alabdulrahim, AK, Alharbi, HZ, Aldubaikhy, RM, Alharbi, RS, et al. Nano-emulsion based gel for topical delivery of an anti-inflammatory drug: in vitro and in vivo evaluation. *Drug Des Devel Ther*. (2023) 17:1435–51. doi: 10.2147/DDDT.S407475

54. Dandamudi, M, McLoughlin, P, Behl, G, Rani, S, Coffey, L, Chauhan, A, et al. Chitosan-coated PLGA nanoparticles encapsulating triamcinolone acetonide as a potential candidate for sustained ocular drug delivery. *Pharmaceutics*. (2021) 13:1590. doi: 10.3390/pharmaceutics13101590

55. Baranda, ER, Santos, JS, Toledo, AL, and Barradas, TN. Design and characterization of stable β-caryophyllene-loaded nanoemulsions: a rational HLB-based approach for enhanced volatility control and sustained release. *Beilstein Arch*. (2025) 2025:36. Available online at: https://doi.org/10.3762/bxiv.2025.36.v181

56. Aldeeb, RAE, Ibrahim, SSA, Khalil, IA, Ragab, GM, El-Gazar, AA, Taha, AA, et al. Enhancing collagen based nanoemulgel for effective topical delivery of aceclofenac and citronellol oil: formulation, optimization, in-vitro evaluation, and in-vivo osteoarthritis study with a focus on HMGB-1/RAGE/NF-κB pathway, klotho, and miR-499a. *Drug Deliv Transl Res*. (2024) 14:3250–68. doi: 10.1007/s13346-024-01548-3

57. Algahtani, MS, Ahmad, MZ, and Ahmad, J. Nanoemulgel for improved topical delivery of retinyl palmitate: formulation design and stability evaluation. *Nano*. (2020) 10:848. doi: 10.3390/nano10050848

58. Soliman, WE, Shehata, TM, Mohamed, ME, Younis, NS, and Elsewedy, HS. Enhancement of curcumin anti-inflammatory effect via formulation into myrrh oil-based nanoemulgel. *Polymers*. (2021) 13:577. doi: 10.3390/polym13040577

59. Ahmad, N, Alam, MA, Ahmad, FJ, Sarafroz, M, Ansari, K, Sharma, S, et al. Ultrasonication techniques used for the preparation of novel eugenol-nanoemulsion in the treatment of wounds healing and anti-inflammatory. *J Drug Deliv Sci Technol*. (2018) 46:461–73. doi: 10.1016/j.jddst.2018.06.003

60. Tomić, A, Šovljanski, O, Nikolić, V, Pezo, L, Aćimović, M, Cvetković, M, et al. Screening of antifungal activity of essential oils in controlling biocontamination of historical papers in archives. *Antibiotics*. (2023) 12:103. doi: 10.3390/antibiotics12010103

61. Sim, JH, Jamaludin, NS, Khoo, CH, Cheah, YK, Halim, SNBA, Seng, HL, et al. In vitro antibacterial and time-kill evaluation of phosphanegold(I) dithiocarbamates, $R_3PAu[S_2CN(iPr)CH_2CH_2OH]$ for R = Ph, Cy and Et, against a broad range of gram-positive and gram-negative bacteria. *Gold Bull*. (2014) 47:225–36. doi: 10.1007/s13404-014-0144-y

62. Haro-González, JN, Schlienger de Alba, BN, Martínez-Velázquez, M, Castillo-Herrera, GA, and Espinosa-Andrews, H. Optimization of clove oil nanoemulsions: evaluation of antioxidant, antimicrobial, and anticancer properties. *Colloids Interfaces*. (2023) 7:64. doi: 10.3390/colloids7040064

63. Wang, S, Liu, Z, Tong, Y, Zhai, Y, Zhao, X, Yue, X, et al. Improved cancer phototheranostic efficacy of hydrophobic IR780 via parenteral route by association with tetrahedral nanostructured DNA. *J Control Release*. (2021) 330:483–92. doi: 10.1016/j.jconrel.2020.12.048

64. Banerjee, K, Madhyastha, H, Sandur, R, Nt, M, and Thiagarajan, P. Anti-inflammatory and wound healing potential of a clove oil emulsion. *Colloids Surf B Biointerfaces*. (2020) 193:111102. doi: 10.1016/j.colsurfb.2020.111102

65. Mohamed, HR, El-Shamy, S, Abdelgayed, SS, Albash, R, and El-Shorbagy, H. Modulation efficiency of clove oil nano-emulsion against genotoxic, oxidative stress, and histological injuries induced via titanium dioxide nanoparticles in mice. *Sci Rep*. (2024) 14:7715. doi: 10.1038/s41598-024-57728-1

66. Kakkar, A, Singh, H, Anand, A, Chopra, H, and Mishra, AK. Neuroprotective effects of eugenol in Alzheimer's disease: mitigating oxidative stress, inflammation and amyloid plaques. *Curr Pharm Des*. (2025). doi: 10.2174/0113816128373290250620054118

67. Rahaman, M, Basu, B, Ghosh, S, Dutta, S, Prajapati, B, and Kapoor, DU. Nanoemulsion-based therapies: a promising approach for managing psoriasis. *Biomed Mater Devices*. (2025):1–19. doi: 10.1007/s44174-025-00541-9

68. Elgharib, IM, Abdelhamid, FM, Elshopakey, GE, Sembawa, H, Albukhari, TA, Filimban, WA, et al. Therapeutic potential of clove oil in mitigating cadmium-induced hepatorenal toxicity through antioxidant, anti-inflammatory, and antiapoptotic mechanisms. *Pharmaceuticals*. (2025) 18:94. doi: 10.3390/ph18010094

69. Chang, Y, Hsia, CW, Chiou, KR, Yen, TL, Jayakumar, T, Sheu, JR, et al. Eugenol: a potential modulator of human platelet activation and mouse mesenteric vascular thrombosis via an innovative cPLA2-NF-κB signaling axis. *Biomedicine*. (2024) 12:1689. doi: 10.3390/biomedicines12081689

70. Wang, M, Dai, T, Li, S, and Wang, W. Eugenol suppresses the proliferation and invasion of TNF-α-induced fibroblast-like synoviocytes via regulating NF-κB and COX-2. *Biochem Biophys Res Commun*. (2022) 612:63–9. doi: 10.1016/j.bbrc.2022.04.074

71. Abdelmuhsin, AA, Sulieman, AME, Salih, ZA, Al-Azmi, M, Alanaizi, NA, Goniem, AE, et al. Clove (*Syzygium aromaticum*) pods: revealing their antioxidant potential via GC–MS analysis and computational insights. *Pharmaceuticals*. (2025) 18:504. doi: 10.3390/ph18040504

72. Sargsyan, T, Simonyan, HM, Stepanyan, L, Tsaturyan, A, Vicidomini, C, Pastore, R, et al. Neuroprotective properties of clove (*Syzygium aromaticum*): state of the art and future pharmaceutical applications for Alzheimer's disease. *Biomolecules*. (2025) 15:452. doi: 10.3390/biom15030452

73. Gul, U, Khan, MI, Madni, A, Sohail, MF, Rehman, M, Rasul, A, et al. Olive oil and clove oil-based nanoemulsion for topical delivery of terbinafine hydrochloride: in-vitro and ex vivo evaluation. *Drug Deliv*. (2022) 29:600–12. doi: 10.1080/10717544.2022.2039805

74. Amezcua-Castillo, E, González-Pacheco, H, Sáenz-San Martín, A, Méndez-Ocampo, P, Gutierrez-Moctezuma, I, Massó, F, et al. C-reactive protein: the quintessential marker of systemic inflammation in coronary artery disease—advancing toward precision medicine. *Biomedicine*. (2023) 11:2444. doi: 10.3390/biomedicines11092444

75. Zhou, HH, Tang, YL, Xu, TH, and Cheng, B. C-reactive protein: structure, function, regulation, and role in clinical diseases. *Front Immunol*. (2024) 15:1425168. doi: 10.3389/fimmu.2024.1425168

76. das Chagas Pereira de Andrade, F, and Mendes, AN. Computational analysis of eugenol inhibitory activity in lipoxygenase and cyclooxygenase pathways. *Sci Rep*. (2020) 10:16204. doi: 10.1038/s41598-020-73203-z

77. Anjum, NF, Shanmugarajan, D, Shivaraju, VK, Faizan, S, Naishima, NL, Kumar, BP, et al. Novel derivatives of eugenol as potent anti-inflammatory agents via PPARγ agonism: rational design, synthesis, analysis, PPARγ protein binding assay and computational studies. *RSC Adv*. (2022) 12:16966–78. doi: 10.1039/D2RA02116A

78. Kojasoy, V, and Tantillo, DJ. Impacts of noncovalent interactions involving sulfur atoms on protein stability, structure, folding, and bioactivity. *Org Biomol Chem*. (2023) 21:11–23. doi: 10.1039/D2OB01602H

79. Gojani, EG, Wang, B, Li, DP, Kovalchuk, O, and Kovalchuk, I. Anti-inflammatory properties of eugenol in lipopolysaccharide-induced macrophages and its role in preventing β-cell dedifferentiation and loss induced by high glucose-high lipid conditions. *Molecules*. (2023) 28:7619. doi: 10.3390/molecules28227619

80. Jabbar, M, Baboo, I, Majeed, H, Farooq, Z, Palangi, V, and Lackner, M. Preparation and characterization of cumin essential oil nanoemulsion (CEONE) as an antibacterial agent and growth promoter in broilers: a study on efficacy, safety, and health impact. *Animals*. (2024) 14:2860. doi: 10.3390/ani14192860

81. Pro, O. (2019). OriginLab: Northampton.

82. Martins, N, Barros, L, Dueñas, M, Santos-Buelga, C, and Ferreira, IC. (2015). Characterization of phenolic compounds and antioxidant properties of Glycyrrhiza glabra L. rhizomes and roots. *RSC Advances*. 5:26991–26997. doi: 10.1039/C5RA03963K

Glossary

CONE - clove oil nanoemulsion

CEO - clove essential oil

EO - essential oil

NE - nanoemulsion

PDI - Polydispersity Index

DLS - dynamic light scattering

TEM - transmission electron microscopy

GC–MS - gas chromatography–mass spectrometry

MIC - minimum inhibitory concentration

DPPH - 2,2-diphenyl-1-picrylhydrazyl

ABTS - 2,2′-azino-bis(3-ethylbenzothiazoline-6-sulfonic acid)

CMC - carboxymethyl cellulose

RBC - red blood cells

WBC - white blood cells

HGB - hemoglobin

HCT - hematocrit

MCV - mean corpuscular volume

MCH - mean corpuscular hemoglobin

MCHC - mean corpuscular hemoglobin concentration

PLT - platelets

MPV - mean platelet volume

PCT - plateletcrit

PDW - platelet distribution width

CRP - C-reactive protein

ANOVA - analysis of variance

RSM - response surface methodology

BBD - Box–Behnken Design

IL-1β - interleukin-1 beta

PDB - protein data bank

OD - optical density

UV–Vis - ultraviolet–visible spectroscopy

H&E - hematoxylin and eosin

frontiers | Frontiers in Veterinary Science

TYPE Original Research
PUBLISHED 21 January 2026
DOI 10.3389/fvets.2025.1728048

OPEN ACCESS

EDITED BY
Shuaiyu Wang,
China Agricultural University, China

REVIEWED BY
Yi Wu,
Yunnan Agricultural University, China
Xiaodong Xie,
Xinqiao Hospital, China
Xiuling Chu,
Liaocheng University, China

*CORRESPONDENCE
Kang Zhang
467863181@qq.com
Jianxi Li
lzjianxil@163.com

RECEIVED 19 October 2025
REVISED 07 December 2025
ACCEPTED 09 December 2025
PUBLISHED 21 January 2026

CITATION
Wang L, Zhang J, Xu G, Guo Z, Wang J, Huang L, Wei L, Wang L, Zhang K and Li J (2026) Linalool disrupts *Escherichia coli* biofilms via dual suppression of motility and adhesion.
Front. Vet. Sci. 12:1728048.
doi: 10.3389/fvets.2025.1728048

Linalool disrupts *Escherichia coli* biofilms via dual suppression of motility and adhesion

Lei Wang[1], Jingyan Zhang[1], Guowei Xu[1], Zhiting Guo[1], Jiamian Wang[1], Liping Huang[1], Lei Wei[1], Long Wang[2], Kang Zhang[1]* and Jianxi Li[1]*

[1]Traditional Chinese Veterinary Technology Innovation Center of Gansu Province, Key Laboratory of Veterinary Pharmaceutical Development of Ministry of Agriculture and Rural Affairs of China, Lanzhou Institute of Husbandry and Pharmaceutical Sciences of Chinese Academy of Agricultural Sciences, Lanzhou, China, [2]Zhengzhou Products Quality Inspection and Testing Center, Zhengzhou, China

Background: Bacterial biofilms, characterized by robust antibiotic resistance and involvement in chronic infections, present significant clinical challenges such as endometritis. While linalool as a natural extract exhibits potent antibiofilm properties, its precise mechanisms of action against *Escherichia coli* (*E. coli*) remain unclear.
Methods: The inhibitory effect of linalool on *E. coli* biofilm formation was evaluated using inhibitory curve analysis and scanning electron microscopy. The influence of linalool on flagella and fimbriae formation in *E. coli* biofilms was assessed through swarming and swimming motility assays, scanning electron microscopy, and qRT-PCR. Viable count assays and confocal laser scanning microscopy were employed to examine the suppression of *E. coli* adhesion to bovine endometrial epithelial cells by linalool. Furthermore, an *in vivo* rat intrauterine infection model with *E. coli* biofilms was established to investigate the anti-adhesion activity of linalool.
Results: *In vitro* assays demonstrated concentration-dependent biofilm inhibition by linalool, achieving 99% inhibition at 4 μL/mL, with structural disintegration confirmed through scanning electron microscopy. Mechanistically, linalool disrupted flagellar gene regulation, downregulating *fliA* and *motA* while upregulating *fliG* and *fliM*, and impaired both swarming and swimming motility. Simultaneously, it suppressed fimbriae-associated genes (*csgA, csgD*, and *fimH*), leading to 99% reduction in bacterial adhesion to bovine endometrial epithelial cells and the eradication of 95% of intrauterine biofilms *in vivo*.
Discussion: As a low-toxicity phytochemical, linalool exhibits a dual-action mechanism in inhibiting *E. coli* D5 biofilm formation by suppressing motility and blocking adhesion, representing a potent multitarget agent against biofilm-associated infections. Future studies should validate its pharmacodynamics and potential synergies with conventional antibiotics to facilitate clinical application.

KEYWORDS

adhesion blockade, *Escherichia coli* biofilm, linalool, motility inhibition, natural antimicrobial agent

1 Introduction

Bacterial biofilms, structured microbial communities encased in extracellular polymeric substances, exhibit remarkable resistance to antibiotics and host immune defenses, contributing to persistent infections and therapeutic failures in clinical settings (1). *Escherichia coli* (*E. coli*), a prevalent pathogen, forms resilient biofilms linked to respiratory infections, digestive disorders, and reproductive system diseases, presenting significant therapeutic challenges (2, 3). Current approaches, including high-dose antibiotics administration and physical biofilm removal, often

demonstrate limited efficacy and heightened risk of resistance development, emphasizing the urgent need for innovative therapeutic agents targeting biofilm-associated virulence mechanisms (4).

Natural products have reemerged as promising antibiofilm agents due to their multitarget potential and minimal risk of resistance development (5). Linalool, a monoterpene alcohol abundant in plant essential oils, exhibits broad-spectrum antimicrobial and anti-inflammatory properties (6–8). Recent studies have demonstrated its efficacy in inhibiting *Pseudomonas aeruginosa* biofilms by disrupting quorum sensing (9) and suppressing *Candida albicans* hyphal growth (10). However, its mechanism of action against *E. coli* biofilms, particularly concerning key virulence factors such as motility and adhesion, remains unexplored, presenting a critical gap in current knowledge.

Biofilm formation in *E. coli* is governed by two fundamental processes: (1) flagellum-driven motility, which facilitates surface colonization, and (2) fimbriae-mediated adhesion, essential for biofilm maturation (11). Flagellar assembly relies on key proteins such as FliG and FliM (rotor components) and MotA (stator complexes), while adhesion is mediated by curli and type I fimbriae, regulated by genes including *csgA*, *csgD*, and *fimH* (12, 13). Although phytochemicals such as cinnamomum and eugenol have been found to inhibit bacterial biofilm by inhibiting flagella protein synthesis and swarming motility or down-regulated fimbriae genes (14, 15), no compound has been reported to simultaneously disrupt both motility and adhesion in *E. coli* biofilms.

This study investigated the inhibitory mechanism of linalool on biofilms produced by the strong biofilm-forming strain *E. coli* D5 isolated from endometritis in dairy cows. Through a comprehensive approach integrating phenotypic assays, gene expression profiling, and *in vivo* models, linalool was demonstrated to disrupt biofilm formation via a dual mechanism: (1) dysregulation of flagellar gene networks, impairing motility, and (2) suppression of fimbriae biosynthesis, inhibiting bacterial adhesion. These findings not only elucidate linalool's unique mode of action but also underscore its potential as a multitarget therapeutic agent against biofilm-associated infections, particularly within intrauterine environments.

2 Materials and methods

2.1 Bacterial strains and growth conditions

This study utilized *E. coli* D5, a strain isolated from the uterine mucus of Holstein cows diagnosed with clinical endometritis. Its accession number in GenBank is PX494327. This strain, characterized by its strong biofilm-forming capacity, was preserved at the Lanzhou Institute of Husbandry and Pharmaceutical Sciences, Chinese Academy of Agricultural Sciences (CAAS). A green fluorescent protein (GFP)-tagged *E. coli* D5 strain was also maintained at the same institute. Additionally, *E. coli* ATCC 25922, sourced from the American Type Culture Collection, was included in this study. Both strains were cultured in nutrient broth medium at 37 °C for 24 h before experimental application.

2.2 Crystal violet assay for *Escherichia coli* biofilm quantification

The antibiofilm efficacy of linalool against *E. coli* strains D5 and ATCC 25922 was evaluated using crystal violet staining, following the protocol described by Stepanovic et al. (16). Overnight cultures were adjusted to a concentration of 3×10^7 CFU/mL in Luria-Bertani (LB) medium, and 100 µL aliquots were transferred to 96-well plates. Linalool (97%, Sigma) was added to an equal amount of dimethyl sulfoxide (DMSO) to mix well. Then the mixture was added to LB medium and mixed well, and then LB medium containing DMSO was used to dilute it in a two-fold manner to the required concentrations, maintaining the working concentration of DMSO in the solution at 1%. Linalool solutions (0.5, 1, 2, 4, 8, and 16 µL/mL) were added in equal volumes (100 µL per well), and incubation was conducted at 26 °C for 12 ~ 72 h. Following incubation, the medium was aspirated, and the wells were rinsed three times with phosphate-buffered saline (PBS, pH 7.4). After air-drying, biofilms were fixed in methanol (200 µL, 15 min), stained with 0.3% (w/v) crystal violet (200 µL, 5 min), and carefully washed. The bound stain was solubilized using 33% (v/v) glacial acetic acid (200 µL), and absorbance at 600 nm (n = 6 per group) was measured using the multi-mode reader (Synergy LX, BioTek, USA). Untreated bacterial suspensions served as controls, while sterile LB medium was used as a blank control.

2.3 Motility assays

The inhibitory effects of linalool on *E. coli* D5 motility were assessed through swarming and swimming assays. Swarming motility was evaluated following a modified protocol by Ranfaing et al. (17), whereas swimming motility was analyzed based on the method described by Li et al. (18) with slight modifications. The swarming medium contained 0.5% agar supplemented with 0.05% glucose, while the swimming medium consisted of 0.25% agar. Overnight cultures of *E. coli* D5 in LB medium were adjusted to a concentration of 4.5×10^8 CFU/mL. Linalool (0.25, 0.5, 1, 2, and 4 µL/mL) was incorporated into autoclaved molten media at 50 °C before solidification. Plates were centrally inoculated with 0.2 µL of the bacterial suspension and incubated at 37 °C for 24 h. Motility inhibition was quantified by measuring the diameters of the migration zones extending from the inoculation points.

2.4 Cell culture and bacterial adhesion assay

Bovine endometrial epithelial cells, isolated and maintained at the Lanzhou Institute of Husbandry and Pharmaceutical Sciences, CAAS, were cultured in DMEM/F12 medium supplemented with 10% fetal bovine serum under a 5% carbon dioxide (CO_2) atmosphere at 37 °C. Upon reaching 80% confluence, the cells were digested using 0.25% trypsin-ethylenediaminetetraacetic acid.

Adhesion assays were performed based on the methodology of Wultanska et al. (19), with modifications. Cells (2.5×10^5 cells/mL) were seeded in 24-well plates and cultured until reaching 90% confluence. Following three PBS washes, wells were co-incubated with *E. coli* D5 (1.5×10^7 CFU/mL) and linalool (0.5, 1, 2, and 4 µL/mL) for 2 h at 37 °C. Unattached bacteria were removed through two PBS washes. Adherent bacteria were lysed using 0.2% Triton X-100 for 10 min, serially diluted, plated on LB agar, and quantified after 24 h of incubation. Blank controls were included.

2.5 Confocal laser scanning microscopy (CLSM) for bacterial adhesion analysis

Bovine endometrial epithelial cells (5×10^5 cells/mL) were seeded onto confocal-grade glass-bottom dishes and cultured at 37 °C with 5% CO_2 until reaching 90% confluence. Following the aspiration of the culture medium and three PBS washes, the wells were incubated with GFP-tagged *E. coli* D5 (1.5×10^7 CFU/mL) and linalool (0.5 and 1 μL/mL) for 6 h under standard culture conditions. Following the additional three PBS washes, the cells were stained with Hoechst 33342 for 15 min in the dark, followed by another three PBS washes. Imaging was performed using CLSM (LSM 700, Zeiss, Germany). Untreated control samples were also included in the experiment for comparison.

2.6 Rat intrauterine bacterial adhesion assay

This study was approved by the Lanzhou Institute of Husbandry and Pharmaceutical Sciences, CAAS (Approval No. 2022–017). *E. coli* D5 biofilms were cultured at 26 °C for 48 h, subjected to ultrasonication (20 Hz, 1 min), thoroughly mixed, and centrifuged (4,000 × *g*, 10 min) before resuspension in sterile saline (10^{10} CFU/mL). Nulliparous female SD rats (230 ± 20 g, 9 weeks old; n = 6 per group) were anesthetized with inhaled isoflurane (4% for induction and 1.5 ~ 2% for maintenance) used by an animal anesthesia ventilator (R660, RWD Life Science Co., Ltd.). Then the rats were inoculated intrauterine with 0.1 mL of biofilm suspension. Tail elevation maintained for 2 ~ 3 min to prevent reflux.

At 24 h post-inoculation, the experimental rats were treated with intrauterine administration of linalool (0.05 mL/100 g·BW) under inhaled isoflurane anesthesia. The groups were divided as following: (1) blank control (saline perfusion), (2) model group (*E. coli* biofilm + saline), (3) vehicle control (*E. coli* biofilm + sweet almond oil), and (4) linalool treatment (25 μL/mL in sweet almond oil). After 24 h post-treatment, all rats were euthanized by an intraperitoneal injection of an overdose of sodium pentobarbital (15 mg/100 g·BW). Under aseptic conditions, the left uterine horns of rats in blank control group, model group and linalool treatment group were fixed in 2.5% glutaraldehyde for scanning electron microscopy (SEM). In contrast, the right horns of rats in all groups were washed with PBS, homogenized in 0.2% Triton X-100, serially diluted, and plated on blood agar. Bacterial loads (CFU/g tissue) were quantified following 24 h incubation at 37 °C. Inhibition ratios were calculated according to the following formula:

$$\text{Inhibition ratio} = \left[\begin{pmatrix} \text{bacterial loads of the model group} - \\ \text{bacterial loads of the experimental group} \end{pmatrix} / \text{bacterial loads of the model group} \right] \times 100\%.$$

2.7 SEM analysis of *Escherichia coli* biofilms

Biofilm structural analysis was conducted using SEM following the protocol described by Kang et al. (34). Overnight cultures of *E. coli* D5 were diluted to 3×10^7 CFU/mL in LB medium and aseptically transferred (500 μL/well) onto coverslips placed in 24-well plates. Linalool was co-administered at concentrations of 0, 4, and 8 μL/mL for *E. coli* D5 (500 μL/well). Subsequently, the plates were incubated at 26 °C for 24 h under static conditions.

To analyze the effects of linalool on bacterial flagella and fimbriae, *E. coli* D5 was exposed to 1 or 2 μL/mL linalool for 30 h, while the control group received no treatment. Cells were then washed three times with PBS (pH 7.4), fixed with 2.5% glutaraldehyde for 2 h, dehydrated through a graded ethanol series (30% ~ 100%, 15 min per step), subjected to critical point drying, sputter-coated with gold, and imaged by SEM (JSM-5600, JEOL, Japan).

Uterine tissues preserved in 2.5% glutaraldehyde were rinsed twice with ultrapure water rinsing (5 min each), dehydrated through a gradient ethanol series (30% ~ 100%, 10 min per step), mounted using conductive adhesive, coated with gold-sputtered, and SEM evaluation.

2.8 Real-time quantitative polymerase chain reaction (RT-qPCR)

Escherichia coli D5 cultures exposed to linalool (0, 1, and 2 μL/mL) were incubated at 26 °C for 24 h, following the procedure outlined in Section 2.2. Biofilms were ultrasonicated for 1 min, thoroughly mixed, and centrifuged at 8,000 × *g* for 10 min. The resulting pellets were washed three times with sterile PBS, and total RNA was extracted using the OMEGA bacterial RNA kit.

First-strand complementary DNA synthesis was performed using the PrimeScript™ reverse transcriptase kit. RT-qPCR analysis was performed on an Applied Biosystems QuantStudio 5 system with TB Green™ Premix Ex Taq™ II following the cycling conditions: 95 °C for 30 s (1 cycle), 95 °C for 5 s (40 cycles), and 60 °C for 30 s. Primers for target genes (*fliA, fliG, fliM, motA, fimH, csgA,* and *csgD*) and the reference gene (16S rRNA) (Table 1) were designed and synthesized by Sangon Biotech (Shanghai). Gene expression fold changes were calculated using the $2^{-\Delta\Delta Ct}$ method.

2.9 Data analysis

Statistical analyses were conducted using the Statistical Package for the Social Sciences software (version 25.0). Data are presented as mean ± standard deviation (SD). Group differences were evaluated using one-way ANOVA followed by Tukey's test. Statistical significance was defined as $p < 0.05$, while $p < 0.01$ was considered highly significant.

3 Results

3.1 Inhibitory effects of linalool on *Escherichia coli* biofilm formation

The antibiofilm activity of linalool against *E. coli* D5 and ATCC 25922 was evaluated using crystal violet staining (Figure 1). *E. coli* D5 biofilms co-cultured with linalool (0.25, 0.5, 1, 2, 4, and 8 μL/mL) for 12 ~ 72 h exhibited concentration- and time-dependent inhibition (Figure 1A). At 12 h, linalool at 2 ~ 8 μL/mL achieved 90% ~ 95% inhibition. Prolonged exposure (24 ~ 72 h) with 4 ~ 8 μL/mL linalool sustained inhibition above 95%, whereas 2 μL/mL demonstrated an efficacy of less than 70%. For the ATCC 25922 strain (Figure 1B), 2 μL/mL linalool consistently inhibited biofilm formation by more than 95% across all time points. In contrast, 1 μL/mL linalool exhibited suppression (82.53% at 12 h and 80.05% at 24 h), but its

effectiveness notably declined at 48 h (33.74%) and 72 h (46.88%). These findings indicated that 2 μL/mL linalool effectively inhibits biofilm formation in weak biofilm producers (ATCC 25922) and early-stage biofilm (12 h) in strong biofilm formers (D5). In contrast, higher concentrations (4 ~ 8 μL/mL) ensure sustained inhibition regardless of biofilm maturity.

TABLE 1 Primer sequences for target and reference genes.

Genes	Primer Sequences (5′–3′)	Gene size amplified (bp)
fliA	*fliA*-F: TTAGGGATCGATATTGCCGATT *fliA*-R: CGTAGGAGAAGAGCTGGCTGTT	70
fliG	*fliG*-F: GAGCTGACCGAAGTACTGAATG	120
	fliG-R: GGCTTCTTCCTGCTGAGTTT	
fliM	*fliM*-F: CAACCTGACCGGCGAATTTA	115
	fliM-R: GCGCCAGTTCTGATCTTCATTA	
motA	*motA*-F: TTGGAGCACTCTATCAACCCG	198
	motA-R: AGCGAAAACATCCCCATCTG	
fimH	*fimH*-F: CGTGCTTATTTTGCGACAGA *fimH*-R: AGGAATTGGCACTGAACCAG	166
csgA	*csgA*-F: GGTAACAGCGCTACTCTTGAT	119
	csgA-R: CGTTGACGGAGGAGTTAGATG	
csgD	*csgD*-F: AATCGCTGGCAATTACAGG	96
	csgD-R: CCGCTTCCATCATATCCAG	
16S	*16S*-F: CTGGAACTGAGACACGGTCC *16S*-R: GGTGCTTCTTCTGCGGGTAA	188

SEM analysis demonstrated structural disruption of 24-h biofilms following linalool treatment (Figure 2). Untreated *E. coli* D5 exhibited dense, multilayered architectures (Figure 2A). Exposure to 2 μL/mL linalool resulted in significant biofilm thinning and bacterial reduction (Figure 2B), while complete structural collapse was observed at 4 μL/mL, resulting in only fragmented cells (Figure 2C). These findings highlight linalool's ability to destabilize biofilm integrity through biomass reduction and ultrastructural degradation.

3.2 Linalool inhibits motility of *Escherichia coli* D5

The inhibitory effects of linalool on *E. coli* D5 motility were assessed using swarming and swimming assays (Figure 3). Swarming motility analysis (Figure 3A) revealed significant inhibition ($p < 0.05$) at 0.5 μL/mL linalool, with a progressive reduction in diameter at higher concentrations. Complete suppression of swarming was observed at 4 μL/mL linalool, indicating a dose-dependent inhibitory effect within the 0.25 ~ 4 μL/mL range.

Similarly, swimming motility assays (Figure 3B) exhibited significant suppression ($p < 0.01$) at 0.25 μL/mL linalool, with complete inhibition occurring at 2 μL/mL. A concentration-dependent inhibitor effect was observed across the 0.25 ~ 2 μL/mL linalool. These results confirmed linalool's effectively suppressed swarming and swimming motilities in *E. coli* D5 in a dose-dependent manner, with swarming inhibition requiring higher concentrations for complete suppression.

3.3 Linalool suppresses flagella and fimbriae formation in *Escherichia coli* D5 biofilms

The impact of linalool on flagella and fimbriae formation during biofilm development was assessed by treating *E. coli* D5 with linalool (0 ~ 2 μL/mL) for 30 h, followed by SEM analysis (Figure 4). Untreated controls exhibited abundant flagella and fimbriae, essential for bacterial motility and adhesion (Figure 4A). Exposure to 1 μL/mL linalool significantly reduced flagellar density and fimbriae length

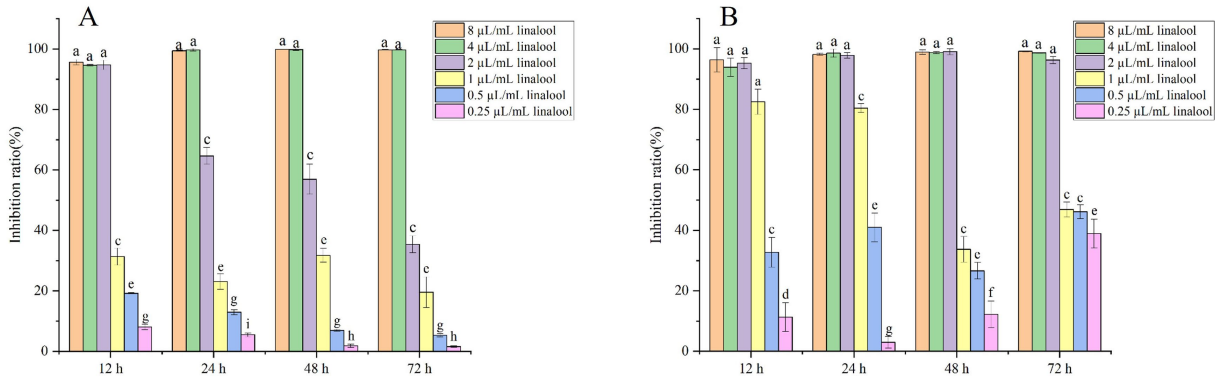

FIGURE 1
The inhibitory effect of linalool on *E. coli* biofilm: **(A)** *E. coli* D5; **(B)** *E. coli* ATCC25922. Data manifest the mean ± SD. Significant differences are indicated by different letters ($p < 0.05$ for adjacent letters; $p < 0.01$ for non-adjacent letters). $n = 3$.

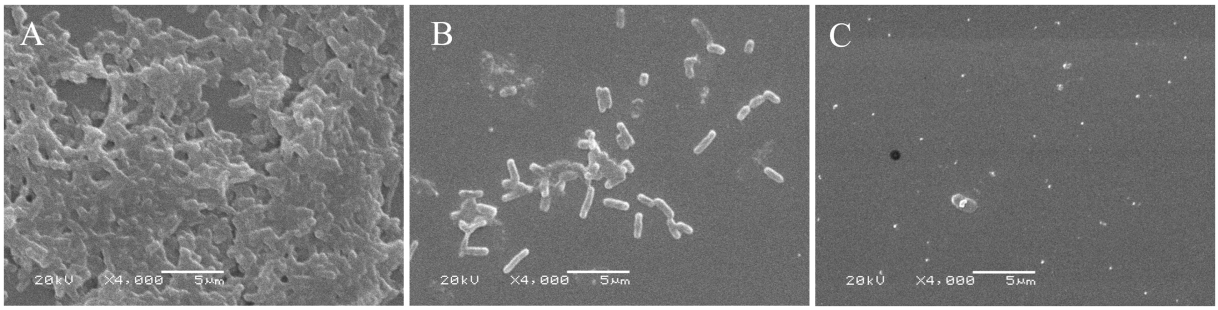

FIGURE 2
Scanning electron microscopy of *E. coli* biofilm treated by linalool for 24 h: **(A)** 0 μL/mL linalool against *E. coli* D5; **(B)** 2 μL/mL linalool against *E. coli* D5; **(C)** 4 μL/mL linalool against *E. coli* D5. The scale bars are 5 μm, $n = 3$.

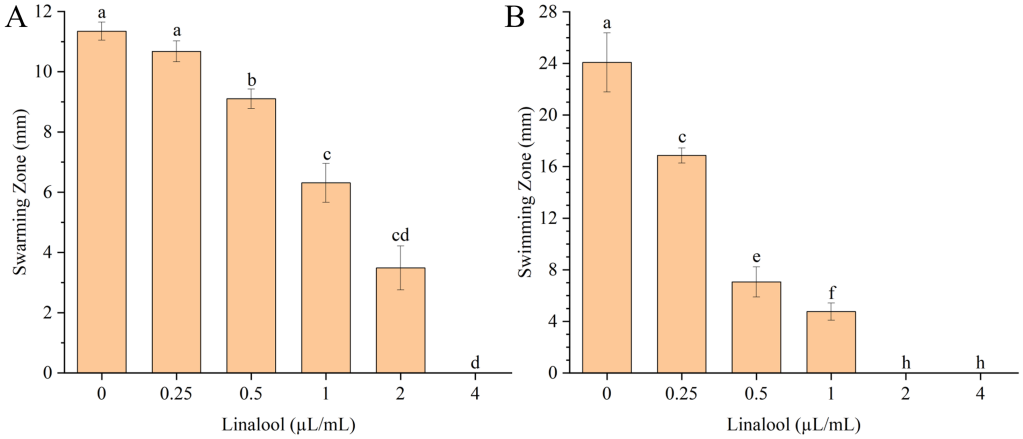

FIGURE 3
Effects of linalool on motilities of *E. coli* D5: **(A)** Swarming motility; **(B)** Swimming motility. Data manifest the mean ± SD. Significant differences are indicated by different letters ($p < 0.05$ for adjacent letters; $p < 0.01$ for non-adjacent letters). $n = 3$.

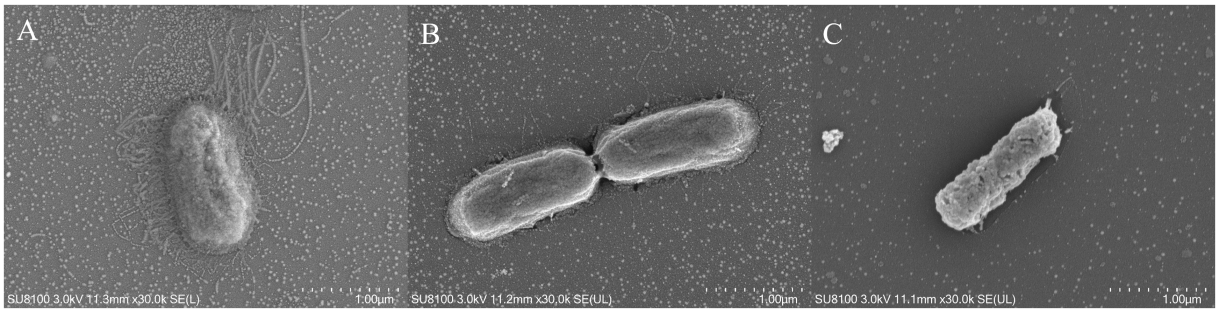

FIGURE 4
Scanning electron microscopy observation of the effect of linalool on bacterial flagella and fimbriae during the formation of biofilm in *E. coli* D5: **(A)** Control group; **(B)** 1 μL/mL linalool; **(C)** 2 μL/mL linalool. The scale bars are 1 μm, $n = 3$.

(Figure 4B). At 2 μL/mL linalool, complete structural elimination of flagella and fimbriae was observed, accompanied by cellular shrinkage and surface pitting (Figure 4C), indicating concentration-dependent ultrastructural disruption.

RT-qPCR analysis (Figure 5) demonstrated dose-dependent transcriptional regulation of key motility- and adhesion-related genes in *E. coli* D5 following linalool treatment. Flagellar rotor genes (*fliG* and *fliM*) were upregulated ($p < 0.05$) at 1 and 2 μL/mL linalool (Figure 5A). In contrast, the motility motor gene (*motA*) and the flagellar regulatory gene (*fliA*) were significantly downregulated at 2 μL/mL ($p < 0.05$). For adhesion-related genes (Figure 5B), linalool (1 ~ 2 μL/mL) downregulated the expression of curli-associated genes

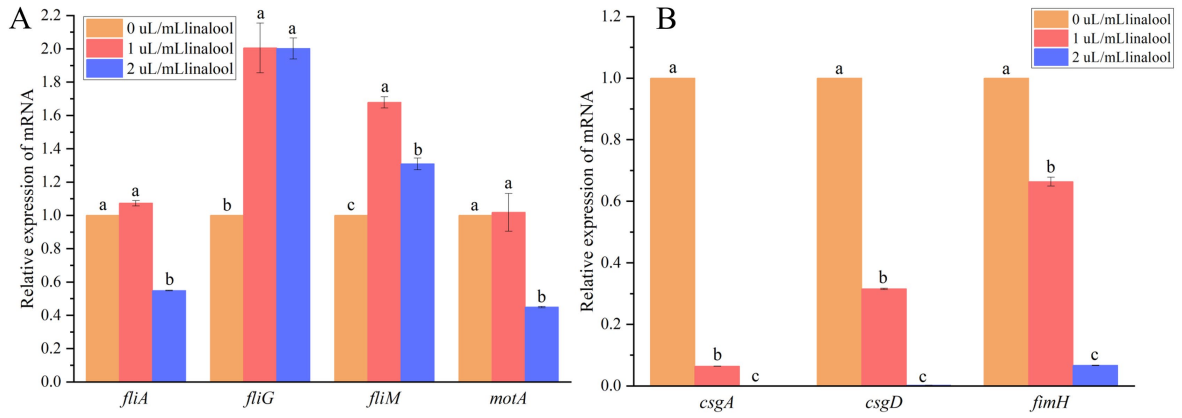

FIGURE 5
The effect of linalool on the relative expression levels of flagella and fimbriae mRNA during the formation of biofilm in *E. coli* D5: **(A)** Flagella related genes; **(B)** Fimbriae related genes. Data manifest the mean ± SD. Significant differences are indicated by different letters ($p < 0.05$ for adjacent letters; $p < 0.01$ for non-adjacent letters). $n = 4$.

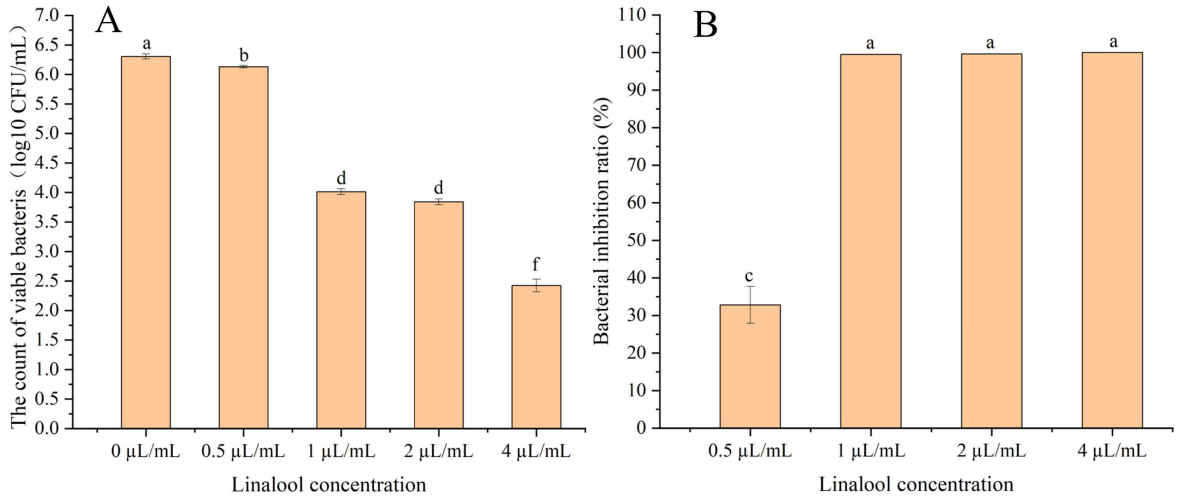

FIGURE 6
Effect of linalool on adhesion of *E. coli* D5 to endometrial epithelial cells of dairy cows: **(A)** The count of viable bacteria; **(B)** Bacterial inhibition ratio. Data manifest the mean ± SD. Significant differences are indicated by different letters ($p < 0.05$ for adjacent letters; $p < 0.01$ for non-adjacent letters). $n = 3$.

(*csgA* and *csgD*) and type I fimbriae gene (*fimH*) ($p < 0.05$). These transcriptional alterations align with the observed impairment in motility and adhesion, suggesting that linalool disrupts biofilm formation through dual inhibiting structural appendages and their regulatory pathways.

3.4 Linalool inhibits *Escherichia coli* D5 adhesion to bovine endometrial epithelial cells

Linalool significantly inhibited *E. coli* D5 adhesion to bovine endometrial epithelial cells in a concentration-dependent manner, as determined by viable count assays (Figure 6). Linalool at 0.5 μL/mL reduced adherent bacteria to 67.21% of the control level ($p < 0.05$). A marked suppression was observed at concentrations ≥ 1 μL/mL, with bacterial loads reduced to 5.13‰ (99.49% inhibition, $p < 0.01$), 3.46‰ ($p < 0.01$), and 0.13‰ (99.99% inhibition, $p < 0.01$) following treatment with 1, 2, and 4 μL/mL, respectively. Statistical comparison indicated significant differences between 0.5 and 1 μL/mL ($p < 0.01$) as well as 2 and 4 μL/mL ($p < 0.01$). In contrast, a statistically non-significant difference was observed between 1 and 2 μL/mL ($p > 0.05$) (Figures 6A,B).

CLSM analysis further supported these findings (Figure 7). Untreated controls exhibited dense GFP-tagged *E. coli* D5 adhesion (green fluorescence) surrounding Hoechst 33342-stained nuclei of endometrial epithelial cells of dairy cows (blue fluorescence) (Figure 7A). Linalool treatment (0.5 ~ 1 μL/mL) progressively reduced

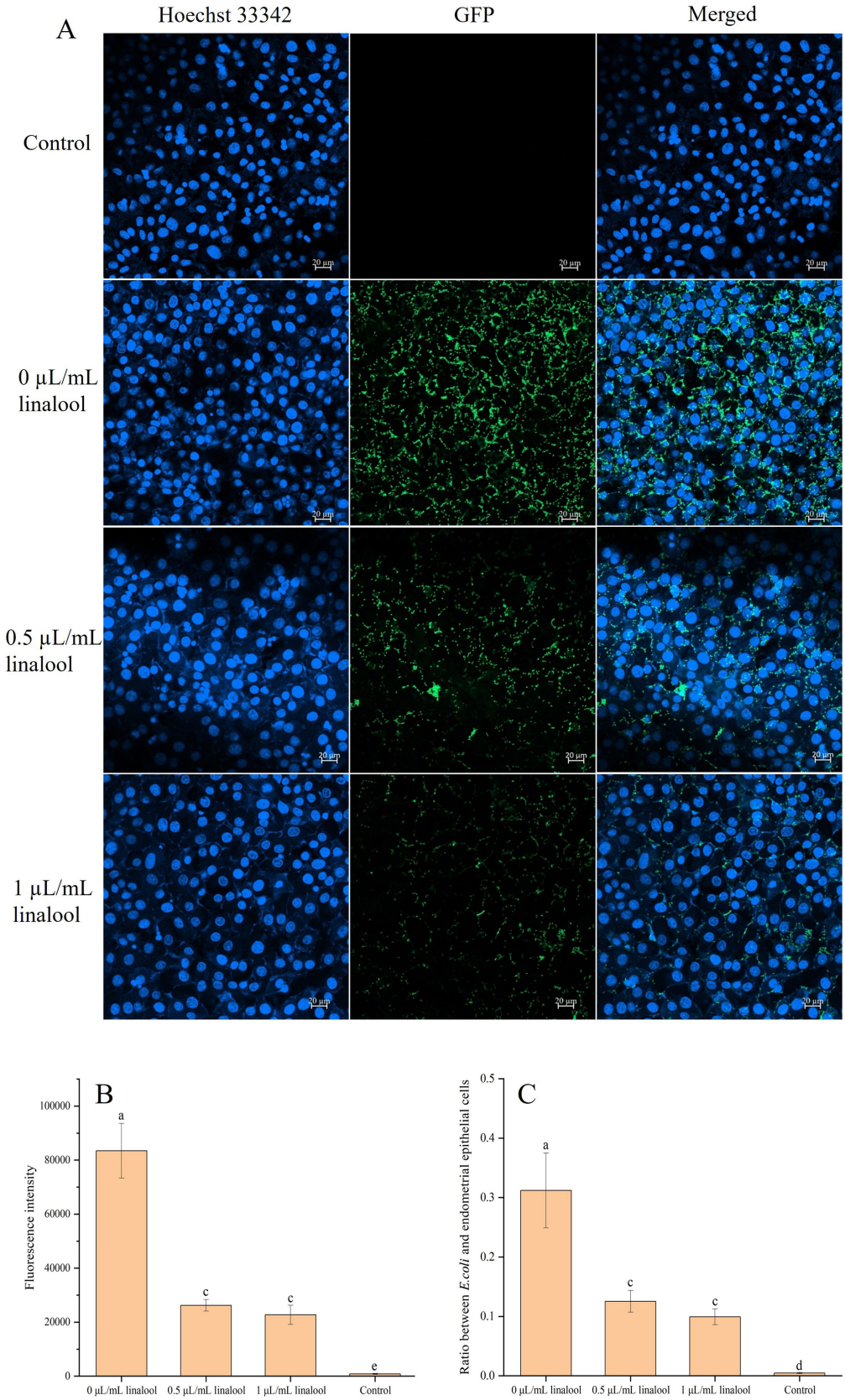

FIGURE 7
The inhibiting effect of linalool on *E. coli* D5 adhered on endometrial epithelial cells of dairy cows: **(A)** CLSM images; **(B)** Fluorescence intensity of *E. coli* D5; **(C)** Ratio between *E. coli* D5 and endometrial epithelial cells. Endometrial epithelial cells of dairy cows, blue; *E.coli* D5, green. The scale bars are 20 μm, $n = 3$. Data manifest the mean ± SD. Significant differences are indicated by different letters ($p < 0.05$ for adjacent letters; $p < 0.01$ for non-adjacent letters).

bacterial fluorescence intensity and ratios between *E. coli* D5 and endometrial epithelial cells (Figures 7B,C), confirming the suppression of linalool on bacterial adhesion.

3.5 Linalool inhibits Intrauterine *Escherichia coli* D5 adhesion in a rat model

The *in vivo* anti-adhesion efficacy of linalool was evaluated using a rat intrauterine infection model. *E. coli* D5 biofilms (10^{10} CFU/mL) were introduced into the uterine cavities, followed by 24-h treatment with 25 μL/mL linalool in a sweet almond oil carrier. Viable count assays demonstrated a significant bacterial load reduction, with linalool decreasing bacterial colonization to 4.77% of the model group ($p < 0.01$), whereas vehicle controls (sweet almond oil) retained 65.75% residual bacteria (Figure 8). Blank controls exhibited no detectable bacterial presence.

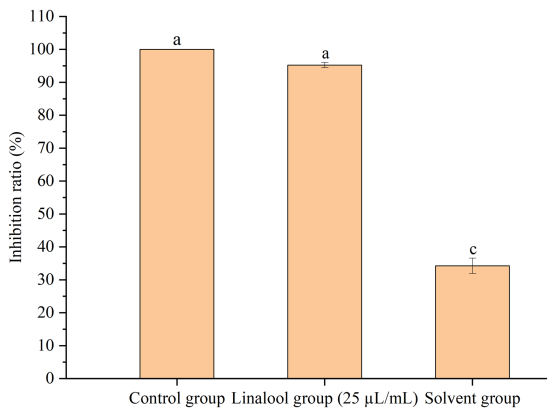

FIGURE 8
Inhibitory effect of linalool on the adhesion of *E. coli* D5 in rat uterus *in vivo* ($n = 6$) Notes: Data manifest the mean ± SD. Significant differences are indicated by different letters ($p < 0.05$ for adjacent letters; $p < 0.01$ for non-adjacent letters).

SEM analysis (Figure 9) revealed dense biofilm-like structures with stacked bacilli in the model group uteri. In contrast, linalool-treated uteri exhibited fragmented bacterial remnants without intact biofilms. These findings confirm the potent intrauterine anti-adhesion activity of linalool, exceeding vehicle efficacy by over 60% ($p < 0.01$), highlighting therapeutic potential against biofilm-associated uterine infections.

4 Discussion

Linalool, a monoterpenoid alcohol widely utilized in cosmetics, detergents, and food additives, exhibits diverse biological activities, including antimicrobial and anti-inflammatory properties (20). Despite its extensive applications, its antibiofilm mechanisms against *E. coli* remain unclear. Lahiri et al. (9) reported that linalool inhibits the protein and carbohydrate components of biofilm exopolysaccharide and quorum-sensing proteins in *P. aeruginosa*. Similarly, Shen et al. (21) demonstrated that linalool suppresses cell motility and reduces the production of exopolysaccharides and biofilm matrix proteins in *Bacillus amyloliquefaciens*. While these findings highlight the multifaceted antibiofilm effects of linalool, the precise mechanisms underlying its inhibition of bacterial motility and its impact on bacterial adhesion remain unclear. The present study elucidates a novel dual-action mechanism by which linalool disrupts *E. coli* D5 biofilms through motility suppression and adhesion blockade.

Biofilm initiation relies on surface attachment facilitated by flagellar motility (22). The flagellar apparatus, consisting of FliG/FliM rotor proteins and MotA/MotB stator complexes (12), enables both swimming (individual propulsion) and swarming (collective migration) (23). Treatment with 2 μL/mL linalool significantly downregulated *fliA* (flagellar transcriptional regulator) and *motA* (motor protein gene) while upregulating *fliG* and *fliM* (Figure 5A). This contradictory gene expression pattern, where structural components (*fliG* and *fliM*) enhanced while functional regulators (*fliA* and *motA*) were suppressed, possibly disrupts flagellar assembly kinetics. SEM analysis confirmed a dose-dependent reduction in

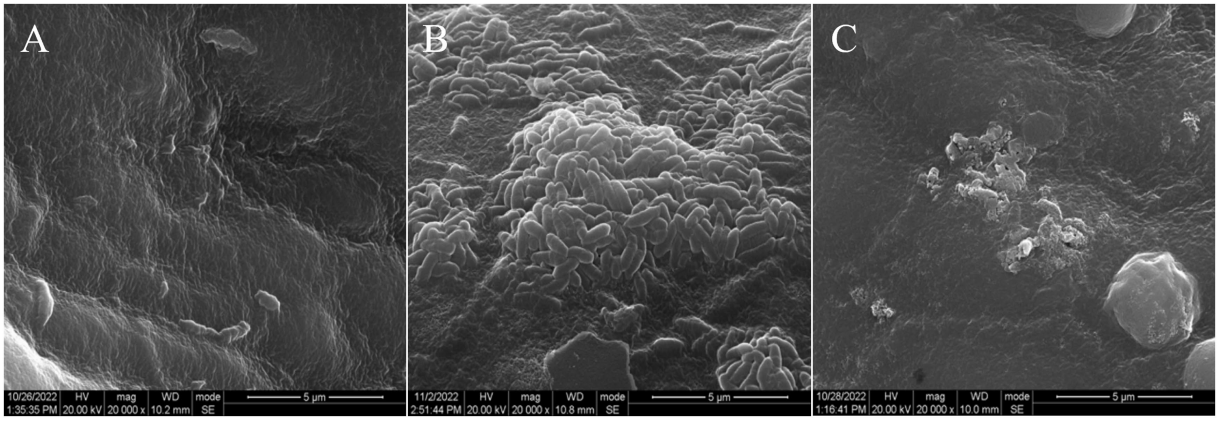

FIGURE 9
Scanning electron microscope image of *E. coli* in uterus of rat: **(A)** Blank control group; **(B)** Model group; **(C)** 25 μL/mL linalool group. The scale bars are 5 μm, $n = 3$.

flagellar structures (Figure 4C), corresponding with impaired swarming and swimming motility (Figure 3). This dual-phase interference suggests that linalool destabilizes flagellar integrity by disrupting the coordination between structural biosynthesis and functional maturation.

Fimbriae-mediated adhesion plays a crucial role in stabilizing surface colonization. Curli (*csgA* and *csgD*) and type I fimbriae (*fimH*) facilitate irreversible attachment and biofilm matrix consolidation (24, 35). Linalool treatment considerably suppressed the expression of relative genes such as *csgA*, *csgD*, and *fimH* (Figure 5B), aligning with previously reported phytochemical strategies. For example, Ginkgo extracts inhibited curli production (25), phloretin downregulated *csgAB* genes (26), and eugenol blocked *csgABDFG/fimCDH* expression (15). SEM analysis revealed fimbriae truncation at 1 μL/mL linalool (Figure 4B) and complete elimination at 2 μL/mL linalool (Figure 4C). These findings are consistent with the report demonstrating that inhibition of type I fimbriae impaired *E. coli* biofilm formation (27).

Notably, linalool significantly reduced *E. coli* D5 adhesion to biological substrates, including endometrial epithelium and uterus, which may be closely associated with decreased fimbriae. This finding aligns with a previous report by Sheng et al. (28), which demonstrated that curli fimbriae in *E. coli* O157: H7 enhance biofilm formation, epithelial cell invasion, and persistence in cattle. Additionally, prior studies have established that fimbriae abundance directly influences bacterial adherence (29, 30). Endometrial epithelial cells are the primary defensive barrier against pathogens within the maternal reproductive system. These cells detect intrauterine pathogens through Toll-like receptor-mediated recognition of bacterial components such as lipopolysaccharides, triggering pro-inflammatory cytokine production (31) and facilitating intercellular communication (32). Endometrial epithelial integrity is essential for critical reproductive functions, including embryo implantation and pregnancy maintenance. This study's findings highlight linalool's dual protective role: inhibiting bacterial adhesion to endometrial surfaces *in vitro* and eliminating intrauterine biofilms *in vivo*, promoting uterine health. This dual mechanism, characterized by impairment of bacterial motility and adhesion while preserving host tissue integrity, effectively disrupts biofilm formation and attenuates *E. coli* pathogenicity. However, cinnamaldehyde reduced the initial adhesion of bacteria and delayed the formation of biofilms rather than inhibiting flagellar-mediated motility (33). The specific inhibitory mechanism of linalool against the formation of *E. coli* biofilms demonstrates its potential as an anti-biofilm agent.

5 Conclusion

Linalool effectively combats *E. coli* D5 biofilms through a multimodal mechanism. It disrupts flagellar motility by modulating gene expression, specifically suppressing *fliA* and *motA* while upregulating *fliG* and *fliM*. Additionally, it inhibits fimbriae-mediated adhesion by downregulating *csgA*, *csgD*, and *fimH*, preserves endometrial epithelial integrity, reduced bacterial adhesion by more than 99.99% *in vitro*, and eliminated 95.23% of intrauterine biofilms *in vivo*. These findings underscore linalool's potential as a natural therapeutic agent against biofilm-associated infections, particularly within the urogenital tract, warranting further investigation into its synergistic effects with antibiotics and efficacy against multidrug-resistant strains.

Data availability statement

The datasets presented in this study can be found in online repositories. The names of the repository/repositories and accession number(s) can be found in the article/Supplementary material.

Ethics statement

The animal study was approved by the Lanzhou Institute of Husbandry and Pharmaceutical Sciences, CAAS (Approval No. 2022-017). The study was conducted in accordance with the local legislation and institutional requirements.

Author contributions

LeW: Conceptualization, Investigation, Writing – original draft. JZ: Methodology, Writing – review & editing. GX: Data curation, Software, Writing – review & editing. ZG: Visualization, Writing – review & editing. JW: Investigation, Writing – review & editing. LH: Validation, Writing – review & editing. LWe: Validation, Writing – review & editing. LoW: Writing – review & editing. KZ: Writing – review & editing, Methodology, Resources. JL: Funding acquisition, Writing – review & editing.

Funding

The author(s) declared that financial support was received for this work and/or its publication. This work was supported by the National Natural Science Foundation of China (32473082 and 31902316), Central Public-interest Scientific Institution Basal Research Fund (No. 1610322025003), Major scientific research tasks of the Science and Technology Innovation Project of Chinese Academy of Agricultural Sciences (CAAS-ZDRW202111), China Agriculture Research System (CARS-36-04), the Innovation Project of Traditional Chinese Veterinary Medicine and Clinical Science (25-LZIHPS-06), and Gansu province science and technology major special project (24ZDNA001).

Conflict of interest

The author(s) declared that this work was conducted in the absence of any commercial or financial relationships that could be construed as a potential conflict of interest.

Generative AI statement

The author(s) declared that Generative AI was not used in the creation of this manuscript.

Any alternative text (alt text) provided alongside figures in this article has been generated by Frontiers with the support of artificial

intelligence and reasonable efforts have been made to ensure accuracy, including review by the authors wherever possible. If you identify any issues, please contact us.

Publisher's note

All claims expressed in this article are solely those of the authors and do not necessarily represent those of their affiliated organizations, or those of the publisher, the editors and the reviewers. Any product that may be evaluated in this article, or claim that may be made by its manufacturer, is not guaranteed or endorsed by the publisher.

Supplementary material

The Supplementary material for this article can be found online at: https://www.frontiersin.org/articles/10.3389/fvets.2025.1728048/full#supplementary-material

References

1. Costerton, JW, Stewart, PS, and Greenberg, EP. Bacterial biofilms: a common cause of persistent infections. Science. (1999) 284:1318–22. doi: 10.1126/science.284.5418.1318

2. Croxen, MA, and Finlay, BB. Molecular mechanisms of *Escherichia coli* pathogenicity. Nat Rev Microbiol. (2010) 8:26–38. doi: 10.1038/nrmicro2265

3. Donlan, RM, and Costerton, JW. Biofilms: survival mechanisms of clinically relevant microorganisms. Clin Microbiol Rev. (2002) 15:167–93. doi: 10.1128/CMR.15.2.167-193.2002

4. Sharma, G, Sharma, S, Sharma, P, Chandola, D, Dang, S, Gupta, S, et al. *Escherichia coli* biofilm: development and therapeutic strategies. J Appl Microbiol. (2016) 121:309–19. doi: 10.1111/jam.13078

5. Abu Ghazal, TS, Schelz, Z, Vidacs, L, Szemeredi, N, Veres, K, Spengler, G, et al. Antimicrobial, multidrug resistance reversal and biofilm formation inhibitory effect of *Origanum majorana* extracts, essential oil and monoterpenes. Plants-Basel. (2022) 11:1432. doi: 10.3390/plants11111432

6. Altinoz, E, Oner, Z, Elbe, H, Uremis, N, and Uremis, M. Linalool exhibits therapeutic and protective effects in a rat model of doxorubicin-induced kidney injury by modulating oxidative stress. Drug Chem Toxicol. (2022) 45:2024–30. doi: 10.1080/01480545.2021.1894751

7. Maczka, W, Duda-Madej, A, Grabarczyk, M, and Winska, K. Natural compounds in the battle against microorganisms-linalool. Molecules. (2022) 27:6928. doi: 10.3390/molecules27206928

8. Wang, L, Wang, JM, Zhang, K, Zhang, JY, Cui, DA, Wang, JY, et al. Linalool as a potential agent for inhibiting *Escherichia coli* biofilm formation and exopolysaccharide production. BMC Vet Res. (2025) 21:235. doi: 10.1186/s12917-025-04681-4

9. Lahiri, D, Nag, M, Dutta, B, Dey, S, Mukherjee, D, Joshi, SJ, et al. Antibiofilm and anti-quorum sensing activities of eugenol and linalool from *Ocimum tenuiflorum* against *Pseudomonas aeruginosa* biofilm. J Appl Microbiol. (2021) 131:2821–37. doi: 10.1111/jam.15171

10. Manoharan, RK, Lee, JH, Kim, YG, Kim, SI, and Lee, J. Inhibitory effects of the essential oils -longipinene and linalool on biofilm formation and hyphal growth of *Candida albicans*. Biofouling. (2017) 33:143–55. doi: 10.1080/08927014.2017.1280731

11. Pratt, LA, and Kolter, R. Genetic analysis of *Escherichia coli* biofilm formation: roles of flagella, motility, chemotaxis and type I pili. Mol Microbiol. (1998) 30:285–93. doi: 10.1046/j.1365-2958.1998.01061.x

12. Zhao, K, Liu, M, and Burgess, RR. Adaptation in bacterial flagellar and motility systems: from regulon members to 'foraging'-like behavior in *E. coli*. Nucleic Acids Res. (2007) 35:4441–52. doi: 10.1093/nar/gkm456

13. Zuberi, A, Ahmad, N, and Khan, AU. CRISPRi induced of fimbriae gene (fimH) of a uropathogenic *Escherichia coli*: an approach to inhibit microbial biofilms. Front Immunol. (2017) 8:1552. doi: 10.3389/fimmu.2017.01552

14. Didehdar, M, Chegini, Z, Tabaeian, SP, Razavi, S, and Shariati, A. Cinnamomum: the new therapeutic agents for inhibition of bacterial and fungal biofilm-associated infection. Front Cell Infect Microbiol. (2022) 12:930624. doi: 10.3389/fcimb.2022.930624

15. Kim, YG, Lee, JH, Gwon, G, Kim, SI, Park, JG, and Lee, J. Essential oils and eugenols inhibit biofilm formation and the virulence of *Escherichia coli* O157:H7. Sci Rep. (2016) 6:36377. doi: 10.1038/srep36377

16. Stepanovic, S, Vukovic, D, Dakic, I, Savic, B, and Svabic-Vlahovic, M. A modified microtiter-plate test for quantification of staphylococcal biofilm formation. J Microbiol Methods. (2000) 40:175–9. doi: 10.1016/s0167-7012(00)00122-6

17. Ranfaing, J, Dunyach-Remy, C, Lavigne, JP, and Sotto, A. Propolis potentiates the effect of cranberry (*Vaccinium macrocarpon*) in reducing the motility and the biofilm formation of uropathogenic *Escherichia coli*. PLoS One. (2018) 13:e0202609. doi: 10.1371/journal.pone.0202609

18. Li, F, Cimdins, A, Rohde, M, Jaensch, L, Kaever, V, Nimtz, M, et al. DncV synthesizes cyclic GMP-AMP and regulates biofilm formation and motility in *Escherichia coli* ECOR31. MBio. (2019) 10:e02492–18. doi: 10.1128/mBio.02492-18

19. Wultańska, D, Paterczyk, B, Nowakowska, J, and Pituch, H. The effect of selected bee products on adhesion and biofilm of *Clostridioides difficile* strains belonging to different ribotypes. Molecules. (2022) 27:7385. doi: 10.3390/molecules27217385

20. An, Q, Ren, JN, Li, X, Fan, G, Qu, SS, Song, Y, et al. Recent updates on bioactive properties of linalool. Food Funct. (2021) 12:10370–89. doi: 10.1039/d1fo02120f

21. Shen, G, Yang, L, Lv, X, Zhang, Y, Hou, X, Li, M, et al. Antibiofilm activity and mechanism of linalool against food *spoilage Bacillus amyloliquefaciens*. Int J Mol Sci. (2023) 24:10980. doi: 10.3390/ijms241310980

22. Belas, R. Biofilms, flagella, and mechanosensing of surfaces by bacteria. Trends Microbiol. (2014) 22:517–27. doi: 10.1016/j.tim.2014.05.002

23. Wang, Y, Wu, Y, Niu, H, Liu, Y, Ma, Y, Wang, X, et al. Different cellular fatty acid pattern and gene expression of planktonic and biofilm state *Listeria monocytogenes* under nutritional stress. Food Res Int. (2023) 167:112698. doi: 10.1016/j.foodres.2023.112698

24. Cookson, AL, Cooley, WA, and Woodward, MJ. The role of type 1 and curli fimbriae of Shiga toxin-producing *Escherichia coli* in adherence to abiotic surfaces. Int J Med Microbiol. (2002) 292:195–205. doi: 10.1078/1438-4221-00203

25. Lu, L, Hu, W, Tian, Z, Yuan, D, Yi, G, Zhou, Y, et al. Developing natural products as potential anti-biofilm agents. Chin Med. (2019) 14:11. doi: 10.1186/s13020-019-0232-2

26. Lee, JH, Regmi, SC, Kim, JA, Cho, MH, Yun, H, Lee, CS, et al. Apple flavonoid phloretin inhibits *Escherichia coli* O157:H7 biofilm formation and ameliorates colon inflammation in rats. Infect Immun. (2011) 79:4819–27. doi: 10.1128/iai.05580-11

27. Wang, L, Keatch, R, Zhao, Q, Wright, JA, Bryant, CE, Redmann, AL, et al. Influence of type I fimbriae and fluid shear stress on bacterial behavior and multicellular architecture of early *Escherichia coli* biofilms at single-cell resolution. Appl Environ Microbiol. (2018) 84:e02343–17. doi: 10.1128/aem.02343-17

28. Sheng, H, Xue, Y, Zhao, W, Hovde, CJ, and Minnich, SA. *Escherichia coli* O157:H7 curli fimbriae promotes biofilm formation, epithelial cell invasion, and persistence in cattle. Microorganisms. (2020) 8:580. doi: 10.3390/microorganisms8040580

29. Jin, X, and Marshall, JS. Mechanics of biofilms formed of bacteria with fimbriae appendages. PLoS One. (2020) 15:e0243280. doi: 10.1371/journal.pone.0243280

30. McLay, RB, Nguyen, HN, Jaimes-Lizcano, YA, Dewangan, NK, Alexandrova, S, Rodrigues, DF, et al. Level of fimbriation alters the adhesion of *Escherichia coli* bacteria to interfaces. Langmuir. (2018) 34:1133–42. doi: 10.1021/acs.langmuir.7b02447

31. Herath, S, Fischer, DP, Werling, D, Williams, EJ, Lilly, ST, Dobson, H, et al. Expression and function of toll-like receptor 4 in the endometrial cells of the uterus. Endocrinology. (2006) 147:562–70. doi: 10.1210/en.2005-1113

32. Kaushic, C, Grant, K, Crane, M, and Wira, CR. Infection of polarized primary epithelial cells from rat uterus with *Chlamydia trachomatis*: cell-cell interaction and cytokine secretion. Am J Reprod Immunol. (2000) 44:73–9. doi: 10.1111/j.8755-8920.2000.440202.x

33. Yang, H, Dong, P, Huo, S, Nychas, GE, Luo, X, Zhu, L, et al. Deciphering the inhibitory mechanisms of cinnamaldehyde on biofilm formation of listeria monocytogenes and implement these strategies to control its transfer to beef surfaces. Food Res Int. (2025) 204:115946. doi: 10.1016/j.foodres.2025.115946

34. Kang, J, Liu, L, Wu, X, Sun, Y, and Liu, Z. Effect of thyme essential oil against Bacillus cereus planktonic growth and biofilm formation. *Appl. Microbiol. Biotechnol.* (2018) 102:10209–10218. doi: 10.1007/s00253-018-9401-y

35. Cohen, N, Zhou, H, Hay, AG, and Radian, A. Curli production enhances clay-E. coli aggregation and sedimentation. *Colloids Surf B Biointerfaces*. (2019) 182:110361. doi: 10.1016/j.colsurfb.2019.110361

Frontiers in Veterinary Science

Transforms how we investigate and improve animal health

The third most-cited veterinary science journal, bridging animal and human health with a comparative approach to medical challenges. It explores innovative biotechnology and therapy for improved health outcomes.

Discover the latest Research Topics

See more →

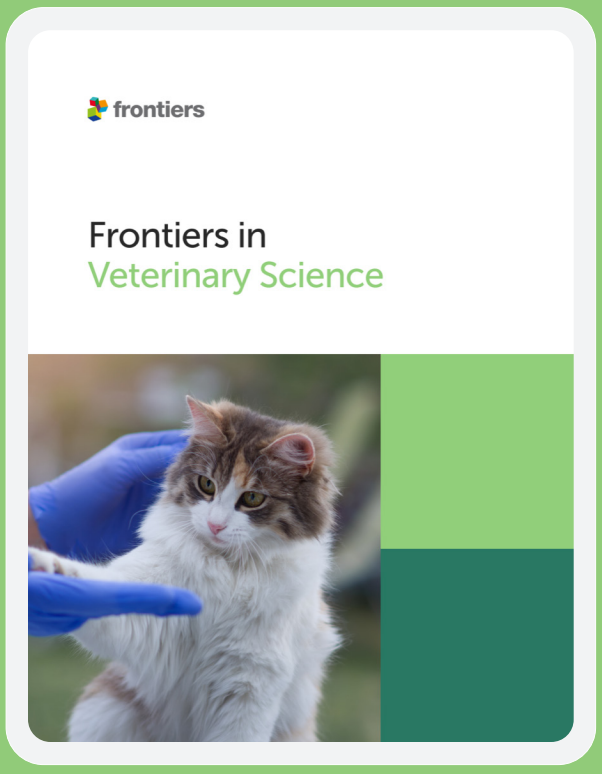

Frontiers

Avenue du Tribunal-Fédéral 34
1005 Lausanne, Switzerland
frontiersin.org

Contact us

+41 (0)21 510 17 00
frontiersin.org/about/contact